OBSERVATOIRE DE PARIS

SYSTÈMES DE RÉFÉRENCE TEMPS-ESPACE

UMR 8630 / CNRS

OBSERVATOIRE ROYAL DE BELGIQUE

Influence of geophysics, time and space reference frames on Earth rotation studies.

Influence de la géophysique et des systèmes de référence spatio-temporels sur les études de la rotation de la Terre.

JOURNÉES 2001 Π

SYSTÈMES DE RÉFÉRENCE SPATIO-TEMPORELS

Π BRUSSELS, 24-26 SEPTEMBER

OBSERVATOIRE DE PARIS

SYSTÈMES DE RÉFÉRENCE TEMPS-ESPACE

UMR 8630 / CNRS

61, Avenue de l'Observatoire – F75014 - PARIS

OBSERVATOIRE ROYAL DE BELGIQUE

avenue circulaire, 3, B-1180, Brussels, Belgium

Influence of geophysics, time and space reference frames on Earth rotation studies.

Influence de la géophysique et des Systèmes de référence spatio-temporels sur les études de la rotation de la Terre.

Actes publiés par
Edited by
N. CAPITAINE

JOURNÉES 2001 Π

SYSTÈMES DE RÉFÉRENCE SPATIO-TEMPORELS

Π BRUSSELS, 24-26 SEPTEMBER

ISBN 2 – 901057 – 46 - 2

JOURNÉES 2001

"Systèmes de référence spatio-temporels"

Scientific Organizing Committee:

A. Brzeziński, Poland; N. Capitaine (Chair), France; V. Dehant, Belgium; M. Soffel, Germany; J. Vondrák, Czech Republic; Y.A. Yatskiv, Ukraine

Local Organizing Committee:

A. Berger, C. Bruyninx, P. Defraigne, V. Dehant, O. de Viron, J. Jean, D. Mesmaker, P. Pâquet (Chair), S. Raynal, F. Roosbeek, B. Sépulchre, T. Van Hoolst, R. Warnant

Sponsored by:

La Banque Bruxelles Lambert (BBL)

Le Fonds National de la Recherche Scientifique (FNRS)

Les Services Scientifiques Techniques et Culturels du Ministère de la Politique Scientifique (SSTC)

Proceedings published by:

Observatoire de Paris

TABLE OF CONTENTS

PREFACE

The Journées 2001 "Systèmes de référence spatio-temporels", with the sub-title "Influence of geophysics, time and space reference frames on Earth rotation studies", have been organized from 24 to 26 September 2001 in Brussels (Belgium) jointly by the Royal Observatory of Belgium, the Institut d'Astronomie et de Géophysique G. Lemaître from the Catholic University of Louvain (UCL) and the Observatoire de Paris. These "Journées" have been the thirteen conference in this series organized in Paris from 1988 to 1992 and 1994, 1996, 1998 and 2000 and other European centres (Warsaw 1995, Prague 1997, Dresden 1999).

The organization of the Journées 2001 in Brussels results from a strong link between the Royal Observatory of Belgium and Paris Observatory and especially the Department of Fundamental Astronomy. The conditions of the meeting were especially comfortable thanks to the BBL which has kindly offered the availability of its building and facilities; the Proceedings are published thanks to the financial support of Paris Observatory.

The problems discussed during the meeting were related to various geophysical effects on Earth rotation such as geophysical fluids, tides, oceanic and atmospheric perturbations, as well as to the effects of time transfer, realization of time scales and terrestrial and celestial frames. This also includes the problem of sensitivity of the different techniques on observations of Earth rotation. Earth rotation studies have also been extended to other planets. The scientific programme was composed of the following sessions: I) Influence of geophysical and other effects on Earth's orientation; sensitivity of the observing systems, II) Geodesy and rotation of the other planets, III) Time and time transfer, IV) Local, regional and global terrestrial frames, station positions and their interpretation; influence of the geophysical fluids, tidal, ocean and atmospheric effects and V) Ephemeris and dynamical reference systems. We thank the Scientific Organizing Committee for its elaboration of the programme. Each session included invited papers and oral contributions and the poster session was introduced by short oral presentations.

There were approximately 80 attendants to these Journées from 18 different countries, 42 oral presentations have been given and there were about 20 posters. We thank here all the colleagues who attended these Journées and participated in the scientific discussions. In addition to the sessions, the participants had the opportunity to attend a lecture entitled "How astronauts would conduct a seismic experiment on the planet Mars" by Vladimir Pletser on the evening September 24. A special session was moreover organized in Louvain La Neuve on September 25, in which the G. Lemaître Prize was awarded to Kurt Lambeck, from the University of Camberra, who gave, at this occasion, a very interesting lecture on his contribution to geophysics.

These Proceedings are divided into five sections corresponding to the sessions of the meeting including, for each session, the invited talks, as well as oral and poster contributions which have been presented during the meeting, some of the papers being combined together in order to provide larger overview papers. The list of participants is given on pages viii and ix, the scientific program on pages x to xii. A Table of Contents and a Postface (giving the announcement for "Journées" 2003 in Bucharest, Romania) are given on pages v and vi and 281 respectively.

We thank all the authors of the papers who have sent their contribution in the required form and within the required deadline. We apologize for the unusual delay in the publication of these Proceedings due to the large amount of charges of the editor. We would like to thank the local organizing Committee for its very efficient work before and during the meeting, and especially Sophie Raynal, Julie Jean and Sonia Asselbergs. We are grateful to O. Becker for his technical help for the publication.

The organizers of the "Journées 2001"

P. PAQUET, N. CAPITAINE and V. DEHANT

Mars 2003

Liste des participants / List of Participants

BARRIOT *Jean-Pierre*, barriot@visto.com, *Observatoire Midi-Pyrénées*
BERGER *André*, berger@astr.ucl.ac.be, *U.C.L. Institut d'Astronomie et de Géophysique*
BIZOUARD *Christian*, bizouard@danol.obspm.fr, *Observatoire de Paris*
BOUALEM *Chemaa*, chemaa_b@yahoo.fr, *Institut National de Cartographie et de Teledetection*
BOUQUILLON *Sebastien*, seb@pluto.mtk.ac.nao.jp, *Observatoire de Paris*
BOURDA *Géraldine*, bourda@format.obspm.fr, *Observatoire de Paris*
BRETAGNON *Pierre*, pierre@bdl.fr, *Institut de mecanique celeste*
BRUYNINX *Carine*, Carine.Bruyninx@oma.be, *Royal Observatory of Belgium*
BRZEZINSKI *Alexander*, alek@cbk.waw.pl, *Space Research Centre Polish Academy of Sciences*
CAPITAINE *Nicole*, capitaine@obspm.fr, *Observatoire de Paris*
CARPANO *Stefania*, Carpano@oma.be, *Royal Observatory of Belgium*
CARPENTIER *Georges*, Carpentier@oma.be, *Royal Observatory of Belgium*
CHAPRONT *Jean*, jean-chapront@obspm.fr, *Observatoire de Paris*
COLL *Bartolomé*, bartolome.coll@obspm.fr, *Observatoire de Paris*
DAMLJANOVIC *Goran*, gdamljanovic@aob.bg.ac.yu, *Belgrade Astronomical Observatory*
DE MOUVEAUX *Pierre*, pierre@polaris-technologies.com,*Polaris Technologies - Bastia*
DE SAEDELEER *Bernard*, Bernard.Desaedeleer@fundp.ac.be, *FNDP - Namur*
DE VIRON *Olivier*, Olivier.deVIRON@oma.be, *Royal Observatory of Belgium*
DEBARBAT *Suzanne*, Suzanne.Debarbat@obspm.fr, *Observatoire de Paris*
DEFRAIGNE *Pascale*, Pascale.Defraigne@oma.be, *Royal Observatory of Belgium*
DEHANT *Veronique*, Véronique.Dehant@oma.be, *Royal Observatory of Belgium*
D'HOEDT *Sandrine*, sandrine.dhoedt@fundp.ac.be, *FNDP - Namur*
DICK *Wolfgang*, dick@iers.org, *Bundesamt für Kartographie und Geodäsie*
DIMARCQ *Noël*, noel.dimarcq@obspm.fr, *Observatoire de Paris*
ESCAPA *Alberto*, albesc@wmatem.eis.uva.es, *Universidad de Valladolid*
FEISSEL *Martine*, feissel@ensg.ign.fr, *Observatoire de Paris and Institut Geographique National*
FUKUSHIMA *Toshio*, Toshio.Fukushima@nao.ac.jp, *National Astronomical Observatory of Japan*
GAMBIS *Daniel*, daniel.gambis@obspm.fr, *Observatoire de Paris*
HEFTY *Jan*, hefty@cvt.stuba.sk, *Slovak University of Technology*
HENRARD *Jacques*, jacques.henrard@fundp.ac.be, *FNDP - Namur*
HUANG *Chengli*, clhuang@center.shao.ac.cn, *Shanghai Observatory*
KABELAC *Josef*, kabelac@inet.tpc.cz, *Czech Technical University*
KLIONER *Sergei*, Klioner@vcs.uvz.tn-dresden.de, *Lohrmann Observatory*
KOLACZEK *Barbara*, kolaczek@cbk.waw.pl, *Space Research Centre Polish Academy of Sciences*
KOSEK *Wieslaw*, kosek@cbk.waw.pl, *Space Research Centre Polish Academy of Sciences*
KUDLAY *Oleksandr*, kudlay@mao.kiev.ua, *Main Astronomical Observatory - Ukraine*
KUDRYASHOVA *Maria*, ai@astro.spbu.ru, *Astron. Inst. of St. Petersburg State University*
KUDRYAVTSEV *Sergey*, ksm@sai.msu.ru, *Sternberg Astron. Inst. of Moscow State University*
LAMBERT *Sebastien*, sabastien.lambert@obspm.fr, *Observatoire de Paris*
LE BAIL *Karine*, lebail@ensg.ign.fr, *ENSG/LAREG - Paris*
LEFFTZ *Marianne*, greff@ipgp.jussieu.fr, *Institut de Physique du Globe - Paris*
LEGROS *Hilaire*, hlegros@eost.u-strasbg.fr, *Ecole et Observatoire des Sciences de la Terre - Strasbourg*
LEMAITRE *Anne*, anne.lemaitre@fundp.ac.be, *FNDP - Namur*
MA *Chopo*, cma@virgo.gsfc.nasa.gov, *Goddard Space Flight Center*
MALKIN *Zinovy*, malkin@quasar.ipa.nw.ru, *Institut of Applied Astronomy - St. Petersburg*
MARCO CASTILLO *Francisco*, Jose marco@mat.uji.es, *Universidad Jaume I*
MARTINEZ USO *Maria José*, mjmartin@mat.upv.es, *Universidad Politécnica de Valencia*
MATHEWS *Piravonu*, mathews@imsc.ernet.in, *University of Madras - India*

MOREL *Laurent*, morel@oma.be, *Royal Observatory of Belgium*
NAWROCKI *Jerzy*, nawrocki@cbk.poznan.pl, *Astrogeodynamical Observatory Space Research Centre*
NOGAS *Pawel*, pnogas@cbk.pozman.pl, *Astrogeodynamical Observatory Space Research Centre*
NOTHNAGEL *Axel*, nothnagel@uni-bonn.de, *Geodetic Institute University Bonn*
PÂQUET *Paul*, P.Paquet@oma.be, *Royal Observatory of Belgium*
PASHKEVICH *Vladimir*, apeks@gao.spb.ru, *Central Astronomical Observatory - St.Petersburg*
PETIT *Gerard*, gpetit@BIPM.ORG, *BIPM*
PLETSER *Vladimir*, Vladimir.Pletser@esa.int, *ESTEC*
PONSAR *Stephanie*, Stephanie.PONSAR@oma.be, *Royal Observatory of Belgium*
PUGH *David*, dtp@mail.soc.soton.ac.uk, *Southampton Oceanographic Centre*
RICHTER *Bernd*, richter@iers.org, *Bundesamt für Kartographie und Geodäsie*
RIVOLDINI *Attilio*, Rivoldini@oma.be, *Royal Observatory of Belgium*
RON *Cyril*, ron@ig.cas.cz, *Astronomical Institute - Prague*
ROOSBEEK *Fabian*, Fabian.Roosbeek@oma.be, *Royal Observatory of Belgium*
ROTHACHER *Markus*, rothacher@bv.tum.de, *Forschungseinrichtung Satellitengeodaesie, TU Munich*
SAMMUNEH *Muhammad*, Ali sammuneh@ensg.ign.fr, *IGN/LAREG - Paris*
SCHUH *Harald*, hschuh@luna.tuwien.ac.at, *Univ. of Techno. Vienna Instit. of Geodesy and Geophys.*
SIDORENKOV *Nikolai*, sidorenkov@rhmc.mecom.ru, *Hydrometcenter of Russia - Moscow*
SLEEWAEGEN *Jacques*, Jacques.Sleewaegen@oma.be, *Royal Observatory of Belgium*
SMETS *Edouard*
SOFFEL *Michael*, soffel@rcs.uvz.tu-dresden.de, *Lohrmann Observatoire*
STAVINSCHI *Magda*, magda@roastro.astro.ro, *Astronomical Institute - Bucharest*
SUBERLAK *Vasyl*, suberlak@mao.kiev.ua, *Main Astronomical Observatory - Ukraine*
TEYSSANDIER *Pierre*, Pierre.Tyessandier@obspm.fr, *Observatoire de Paris*
TUPIKOVA *Irina*, tupikova@rcs.uvz.tu-dresden.de, *Lohrmann Observatoire*
URAS *Silvano*, uras@ca.astro.it, *Cagliari Astronomical Observatory*
VAN HOOLST *Tim*, Tim.Vanhoolst@oma.be, *Royal Observatory of Belgium*
VONDRAK *Jan*, vondrak@ig.cas.cz, *Astronomical Institute - Prague*
WARNANT *René*, Rene.Warnant@oma.be, *Royal Observatory of Belgium*
WEBER *Robert*, rweber@luna.tuwien.ac.at, *University of technology - Vienna*
WILLEMS *Sarah*, Sarah.Willems@oma.be, *Royal Observatory of Belgium*
YATSKIV *Ya*, yatskiv@mao.kiev.ua, *Main Astronomical Observatory - Ukraine*
YAYA *Philippe*, philippe.yaya@obspm.fr, *Observatoire de Paris*
YSEBOODT *Marie*, Marie.YSEBOODT@oma.be, *Royal Observatory of Belgium*
ZHU Sheng *Yuan*, zhu@dfd.dir.de, *GFZ - Germany*

JOURNÉES 2001 SYSTÈMES DE RÉFÉRENCE SPATIO-TEMPORELS

« *Influence of geophysics, time and space reference frameson Earth rotation studies* »

Scientific Organizing Committee : V. Dehant (Chair), A. Brzezinski, N. Capitaine, M. Soffel, J. Vondrak, Y. Yatskiv

Local Organising Committee : P. Pâquet (Chair), A. Berger, C. Bruyninx, P. Defraigne, V. Dehant, O. de Viron, J. Jean, D. Mesmaker, S. Raynal, F. Roosbeek,, B. Sépulchre, T. Van Hoolst , R. Warnant.

SCIENTIFIC PROGRAMME

Monday 24 September

Session 1.Influence of geophysical and other effects on Earth's orientation; sensitivity of the observing systems.

C.Ma : *The effect of reference frames on EOP estimates from VLBI.*

J.Vondrak, *C.Ron, D. Gambis,C.Bizouard and R.Weber* *: Combined celestial pole offsets from VLBI and GPS.*

Fukushima, **T.Shirai** : *Geophysical parameters estimated from VLBI nutation analysis.*

Ch.Huang, V.Dehant : *Effect of differential rotation on nutation and displacement fields of the Earth interior.*

P.M.Mathews and **P.Bretagnon** : *High frequency nutation.*

Z.Malkin : *A comparative analysis of the VLBI nutation series.*

M.Feissel, **M.Yseboodt**, **V.Dehant**, **O.de Viron** and **C.Bizouard** *: How much can we cheat the non-rigid Earth nutation theory to make it match VLBI results ?*

Ph.Yaya : *Combination of several geodetic techniques to determine earth orientation parameters.*

A.Brzezinski, N.Capitaine : *Lunisolar perturbations in Earth rotation due to the triaxial figure of the Earth: geophysical aspects.*

J.Nastula : *Atmospheric signals in polar motion excitation.*

C.Bizouard, S.Lambert : *Atmospheric and oceanic forcing in polar motion and length of day.*

N.Sidorenkov : *Chandler Wobble of the pole as part of the inter-annual oscillation of the atmosphere-ocean-Earth system.*

J.Nastula, B.Kolaczek and D.Salstein : *Variation of anomalies of atmospheric excitation function of polar motion in 1980-1999.*

W.Kosek, D.McCarthy and B.Luzum : *El Nino impact on polar motion prediction errors.*

O.Kudlay : *Atmospheric angular momentum irregularity effect on the Earth rotational eigenmodes.*

Session 2: Geodesy and rotation of the other planets

J.P. Barriot : *Netlander ionosphere and geodesy experiment on the planet Mars.*
A.Rivolidini, P.Defraigne, V.Dehant, T.Van Hoolst *: Free and forced response of a non-rigid Mars with an inner core. II. Numerical approach.*
M.Stavinschi, V.Mioc : *Earth effects of Mars' rotation on orbiter dynamics.*
O.de Viron, E.Van Den Acker, T.Van Hoolst, P.Defraigne, V.Dehant *: Comparison between the atmospheric forcing on Earth and Mars.*
T.van Hoolst, V.Dehant : *Tides of the planets Mars and Mercury.*
S.Bouquillon : *Mercury libration: first stage.*
G.Carpentier and F.Roosbeek : *Analytical developments of rigid Mercury nutation series.*
V. Pletser : *How astronauts would conduct a seismic experiment on the planet Mars*

Tuesday 25 September

Session 3: Time and time transfer

G.Petit : *The new IAU conventions for coordinate times and time transformations.*
B.Coll : *Physical relativistic frames.*
P.Teyssandier : *Relativistic theory of time and frequency transfer using the Synge's world-function.*
P.M.Mathews : *Time based on Earth rotation.*
N.Dimarcq : *Ultra stable clocks on board the international space station: the ACES project.*
P.Defraigne : *Time transfer with geodetic receivers.*
J.Nawrocki : *Polish atomic time scale, organization and results.*

Session 4: Local, regional and global terrestrial frames, station positions and their interpretation; influence of the geophysical fluids, tidal, ocean and atmospheric effects

R.Weber, C. Bruyninx, H.G. Scherneck, M. Rothacher, P.H. Anderson,T.F. Baker, T.van Dam : *Tidal effects in GPS/GLONASS data processing.*
J.Hefty : *Tidal variations of station coordinates observed in regional GPS permanent network.*
V.Suberlak : *Presentation of new SLR station "Golosiiv-Kiev".*
M.Greff-Lefftz : *LICODY: the dynamics of the fluid core from gravity signals.*

Poster presentation

Session1 :

H.Shuh, P.Varga, T.Seitz, J.Böhm, R.Weber, G.Mentes, Z.Zavoti : *Sub-semidiurnal variations of the EOP observed by space geodesy compared with other geophysical phenomena.*
S.Uras, A.Poma *: ERP and climate.*
M.Kudryashova *: Analysis of sub diurnal EOP variations.*
M.L. Bougeard, N. Rouveyrollis, D. Gambis : *A comparison study of EOF techniques in the determination of episodic terms in the 1999-2000 Polar Motion.*

Session2 :

M.Yseboodt :: *A simplified analytical formulation of the NEIGE orbiter/lander geodesy observable.*
V.Dehant *:: Comparison between the nutations of the planet Mars and the nutations of the Earth.*
V.Dehant *:: Free and forced response of a non-rigid Mars with an inner-core. I. Analytical approach.*

Session3 :

V.Zalutsky, V. Akulov, L. Kurisheva, N. Maksimovich : *About activity of the Russian Time-Frequency Service Siberian Metrological Center in the field of time metrology with the aid of GPS and GLONASS.*

Session4 :

Ch.Boualem : *Le projet : Système de référence de l'Afrique du nord "NAFREF".*
G.Damljanovic, M.S.De Biasi *: Classical astrometry longitude and latitude determination by using CCD technique.*
V.Zalutsky, K.Palamartchouk, L.Chirkov : *Impact of Irkutsk GPS/GLONASS station into supporting of the geodynamics phenomena monitoring networks.*

Session5 :

M.Castillo : *Monitoring reference systems: A try of global approach.*
M.J. Martinez Uso : *Comparison of analytical and geometrical methods of astrometric corrections in modern catalogues.*

Wednesday 26 September

Session 5: Ephemeris and dynamical reference systems

M.Soffel : *The new IAU resolutions concerning relativity: questions and answers.*
S.Klioner : *The Earth's rotation in the framework of GRT: rigid (multipole) models.*
A.Escapa , J. Getino, J.M Ferràndiz : *Application of Poincaré's formalism to the study of the free rotation of a three-layer Earth model.*
V.Pashkevich and G.Eroshkin : *High-Precision Numerical Theory of the Earth rotation : Main Principles of Construction and Results.*
N.Capitaine : *Theoretical considerations on precession and nutation referred to the GCRS.*
J.Chapront : *Contribution of Lunar Laser Ranging to metrology.*
P.Bretagnon : *Analytical solution of the Mars motion.*
S.Kudryavtsev : *Compact representation of spherical functions of Sun/Moon.*
A.Escapa , J.Getino , J.M.Ferràndiz *: Influence of the triaxiality of the non-rigid Earth on the J2 forced nutations.*

Session I)

INFLUENCE OF GEOPHYSICAL AND OTHER EFFECTS ON EARTH'S ORIENTATION: SENSITIVITY OF THE OBSERVING SYSTEMS

Introductory papers, oral communication and posters

INFLUENCE DE LA GEODÉSIE ET AUTRES PHÉNOMÈNES SUR LA ROTATION DE LA TERRE : SENSIBILITÉ AUX SYSTÈMES D'OBSERVATION

Exposés introductifs, communications orales et posters

THE EFFECT OF REFERENCE FRAMES ON VLBI EOP

C. MA
Space Geodesy Branch, NASA Goddard Space Flight Center
Goddard Space Flight Center, Greenbelt, MD, 20771, USA
chopo.ma@gsfc.nasa.gov

ABSTRACT

Only VLBI of the space geodesy techniques has the capability of directly linking the celestial and terrestrial reference frames while estimating all components of Earth orientation. The choice of frame definitions and the analysis configuration have significant effects on the EOP time series. In addition, VLBI solutions optimized for CRF or TRF or EOP do not produce the best results for the other aspects. An approach to an integrated analysis is outlined. Characteristics of the various space geodesy techniques and the IVS observing program for 2002 are described.

1. INTRODUCTION

The measurement of Earth orientation parameters (EOP) by VLBI has a history of two decades and is one of the principal reasons why VLBI was developed in as a space geodesy tool starting in the 1970s. The unique features of VLBI applicable to EOP monitoring are shown in table 1, but its actual use also depended on the development of instrumentation with sufficient precision of observation and modeling of sufficient completeness and accuracy as well as organizations and stations with a long term commitment to EOP. Changes in each of these factors and knowledge gained through experience and theoretical studies have paced the development and improvement of the EOP time series.

Table 1: Features of VLBI

Sensitivity to all Earth orientation parameters: x-pole, y-pole, UT1, $\Delta\varepsilon$, $\Delta\psi$
Direct access to quasi-inertial reference frame
Direct tie between celestial and terrestrial frames

2. REFERENCE FRAMES

Since EOP is the relationship between the terrestrial reference frame (TRF) and the celestial reference frame (CRF), it is instructive to describe how these frames have been realized in practice in the context of VLBI.

The CRF is conceptually realized by the fixed positions of a defined set of extragalactic radio sources. However, the set of radio sources used in EOP monitoring by VLBI has evolved considerably over time as shown in Figures 1A through 1E. Each figure shows the sources used most frequently during a five-year interval in all the geodetic/astrometric VLBI observing sessions. Since EOP sessions are the most common and other geodetic sessions use generally the same sources, these sources are the actual CRF in the relevant time interval. It can be seen that the number of "geodetic" sources has increased substantially since the beginning. The number was limited to the strongest sources at the outset by instrumental sensitivity and increased both as sensitivity improved and as the need for higher temporal resolution, i.e., more observations per hour, and higher density on the sky became clearer for better estimation of troposphere variations. In addition, the use of a larger number of sources in a given observing session permits a more robust schedule, a practical consideration since stations and sources do not always behave as expected. It should be noted that the choice of sources and the sequence of their (repeated) observation, i.e., the scheduling of a VLBI session, require deliberation, and scheduling algorithms have evolved along with instrumental and analytical capability.

The geodetic sources are only a small subset of the sources included in the ICRF and ICRF-Ext.1 catalogues. The majority of sources in these catalogues were observed only in astrometric sessions. The geodetic sources were and continue to be chosen from the strongest compact sources distributed as uniformly as practical over the sky. They are not necessarily ICRF defining sources, and they may even have a degree of position instability undesirable for the realization of the CRF, especially in the earliest years. As all aspects of VLBI have continued to evolve, the proper EOP analysis to take into account position variation for some sources and understanding the effect of such variations as well as changes in the set of geodetic sources are subjects of current studies. Two approaches could be to estimate different source positions at each epoch for such "unstable" sources or to model apparent proper motions.

The TRF is conceptually a set of station positions and velocities. As with the CRF, the actual stations used for EOP monitoring have changed as shown in Figures 2 and 3. ¿From the earliest one-baseline POLARIS network, the size of the individual networks, the number of active networks, and the temporal resolution of the EOP time series have fluctuated, sometimes increasing and sometimes decreasing. The changes were generally not for technical reasons but were related to the commitment and funding of the individual government agencies with interests in EOP for operational and scientific purposes. The U.S. National Geodetic Survey (NGS) and German Institut für Angewandte Geodäsie (IfAG) were early strong supporters of VLBI EOP monitoring, and the U.S. National Aeronautics and Space Administration (NASA) provided the initial and continuing technical expertise. The IRIS-A program, supported jointly by NGS and IfAG, was the primary source of VLBI EOP from 1984-1993. The U.S. Naval Observatory (USNO) initially began the NAVNET program to assure an EOP capability entirely under U.S. control but merged NAVNET with IRIS-A in 1993 under the U.S. National Earth Orientation Service (NEOS). Starting in 1997 the weekly NEOS program was complemented by several CORE networks to test the effects of varying the EOP network. VLBI EOP monitoring has been weakened in recent years by the withdrawal of NGS, which satisfies its statutory requirement for polar motion using GPS, and by decreased funding support at USNO and NASA. USNO fulfills its statutory responsibility for UT1 through weekly 24-hr sessions and daily 1-hr intensive sessions. The closure of the Richmond, Florida and Green Bank, West Virginia stations has been somewhat compensated by the addition of the Algonquin, Ontario station and regular participation of European stations, particularly Ny Ålesund in Spitsbergen.

As with the ICRF, the EOP network stations are a small subset of the VLBI TRF and ITRF2000. Similar questions about the proper modeling of particular stations and the effect of network changes over time and between sessions are being actively addressed. How well the VLBI EOP networks represent the orientation changes of the entire globe is related to the

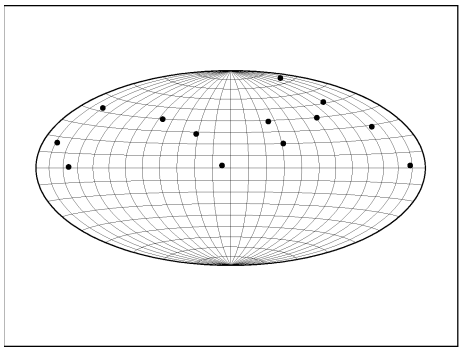

A. 13 sources, 1979–1983.

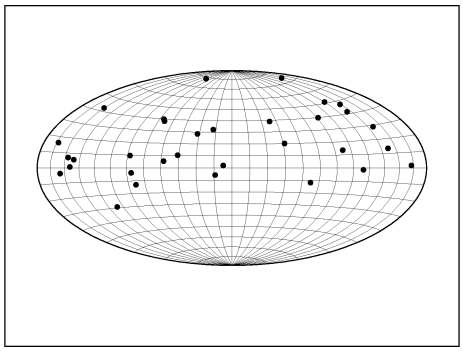

B. 32 sources, 1984–1988.

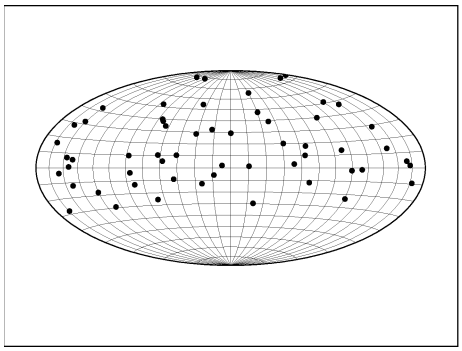

C. 57 sources, 1989–April 1993.

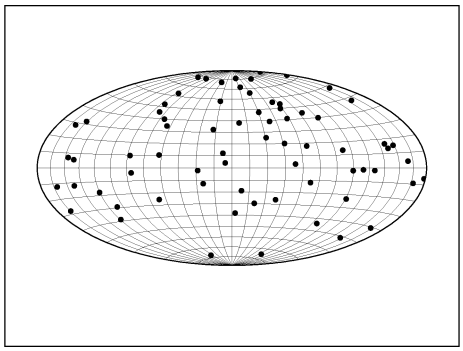

D. 70 sources, May 1993–1996.

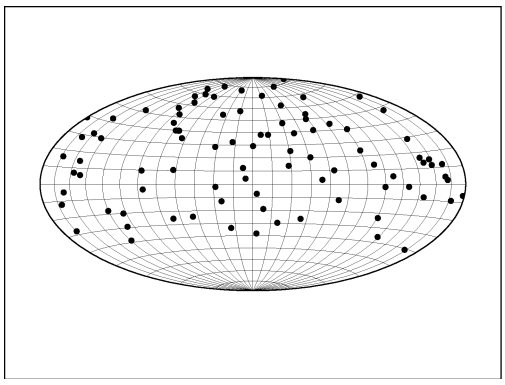

E. 92 sources, 1997–2001.

Figure 1: Progression of most commonly observed sources, 1979–2001.

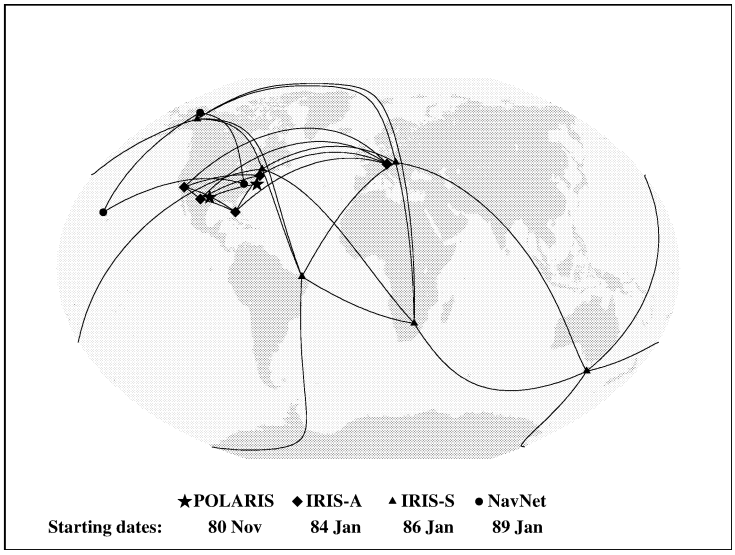

Figure 2: EOP networks–Polaris (1980-83), Iris-A (1984-93), Iris-S (1986-2001), Navnet (1989-93)

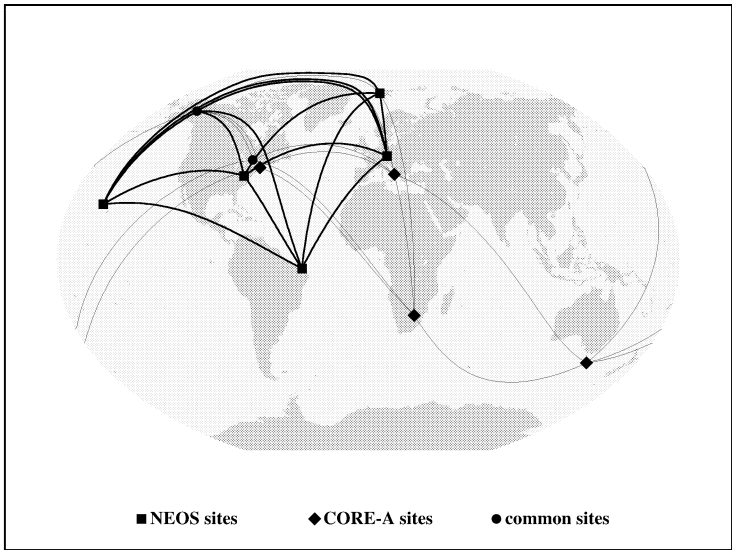

Figure 3: Neos and Core-A networks.

internal consistency and external datum of the TRF, but the results from the analysis of the VLBI EOP times series clearly show that considerable useful information is present.

It should be noted that there are some periods of exceptional quality, daily VLBI EOP measurements, particularly the fortnight of CONT94 in the beginning of 1994. Because of the personnel required at most VLBI stations, such extended periods of observation require a special effort. The stations also must be in the optimal operating condition, again requiring a special effort. Unfortunately the VLBI network performance has not been optimal recently because of lower funding in certain places. In addition, radio frequency interference from land and satellite transmissions is becoming a serious problem. While the Mark V recording system using PC disk drives will likely improve station reliability, interference may become a limiting factor in the dual-frequency ionosphere calibration.

3. OPTIMIZATION CONFLICTS

While the entire geodetic/astrometric VLBI data set can be used for analysis of the TRF, CRF and EOP, the reference frames for each and hence the analysis required have different individual purposes. A summary and some specific characteristics are shown in Table 2.

The ITRF2000 is a set of station position and velocities from various space geodetic techniques including VLBI. Such a construct is best served by using the longest time span to maximize the precision of the velocities and by treating all sites as moving linearly. Of particular interest are sites with collocated techniques to allow the integration of the TRF results from SLR, VLBI, GPS and DORIS. In reality some of the VLBI points show evidence of nonlinear movement, at least in some directions. Because of the temporal resolution from the EOP monitoring programs, these motions are most easily seen in the stations of the EOP networks, particularly Fort Davis, Texas and Green Bank, West Virginia. There may also be seasonal variations elsewhere that are not modeled. It should be mentioned that ITRF2000 was derived from analyses done in 2000, so the VLBI analysis configurations were state of the art for 2000.

The ICRF is a set of fixed source positions, formally only those for the 212 defining sources. (In the usual EOP analysis, the positions of all sources are held fixed at a priori values related to the ICRF or are treated as not changing with time.) For the CRF realization the most important considerations are to identify the sources whose positions are the most stable and reliable and to achieve the highest accuracy for their position estimates. An empirical test for stability is the time series of source positions, but generally only the geodetic sources have enough points for statistical analysis. The geodetic sources were not selected primarily for their CRF suitability, however. Astrometric sources are generally weaker radio emitters. Some of the astrometric sources may, in fact, be more stable in position, but with considerably fewer epochs of observation there may be insufficient data to decide. Since the relative positions of the sources in the sky are independent of the station positions, it is not necessary (and may even be deleterious) to estimate TRF positions and velocities in order get CRF information. Consequently, for example, it might be better to ignore the earliest VLBI data, which had a predominance of unstable sources (although this was not done in the ICRF and ICRF-Ext.1 analyses). If, however, TRF positions and velocities are not estimated, i.e., the station positions are estimated independently at each epoch, the terrestrial EOP components are not accessible. Finally, the ICRF analysis was done with the state of the art in 1995. Since the ICRF defining positions are now fixed, systematic modeling effects not included in the 1995 analyses are frozen. By 2000 and ITRF2000 the state of the art had progressed, particularly in modeling the troposphere, so there is a small degree of incompatibility between the ICRF and the VLBI analyses in ITRF2000 as well as an extended data set for the latter

The EOPs relate the CRF and TRF at a particular epoch. In reality the VLBI CRF and TRF at epoch are particular subsets of sources and stations, some of which may not be adequately

modeled by fixed source positions and linear station velocities, respectively. How to treat the imperfect sources and stations at epoch is now being discussed within and among the VLBI analysis groups.

More generally, the direct integration of TRF, CRF and EOP within a single VLBI solution requires a balancing of sometimes conflicting characteristics since the optimization of one aspect may weaken or discard another aspect. However, only VLBI among the space geodetic techniques has the potential of such an integrated solution independent of any other data. An integrated solution requires that at least some stations and sources be treated as moving linearly and fixed in space, respectively. Since there is a range of non-ideal behavior, it is not obvious that a clear distinction can be made that categorizes all sources and stations as ideal or non-ideal over the entire data span.

A conceivable approach, but rather laborious, might use several steps in creating the TRF and CRF followed by analysis of each session for non-ideal source or station behavior. The first step would be to define criteria for non-ideal behavior, perhaps from analyses of time series, to identify sources and stations that cannot be modeled by fixed positions and linear velocities, respectively. The next step would be to estimate TRF positions and velocities and CRF positions for the ideal stations and sources from independent optimized solutions while simultaneously estimating the positions of the non-ideal stations and sources at each relevant epoch. The third step would be to compute average station positions and velocities and average source positions for the non-ideal stations and sources from the resultant time series. Using the ideal and averaged TRF and CRF values, each session would be examined to determine which stations and sources deviated from their "correct" positions at that epoch by more than a specified amount, which might be epoch-dependent since the quality of the raw data has changed. Finally, in the integrated TRF/CRF/EOP solution, the TRF and CRF would be estimated for the ideal stations and sources while at each epoch EOP and the positions of any sources or stations behaving non-ideally at that epoch would be estimated.

Table 2: Desired Reference Frame for

TRF	CRF	EOP
maximum number of site positions and velocities	highest accuracy for positions of best sources	accurate TRF and/or CRF at observing epoch
long time span for precise velocity	minimize effects of network geometry and unstable sources	

4. DIFFERENCES BETWEEN SPACE GEODETIC TECHNIQUES

Table 3 shows characteristics of SLR, VLBI and GPS. The similarities and differences are rather heterogeneous. Certain particularities should be noted. While SLR is nominally continuous observing, most SLR stations do not observe all the time because of costs and weather. This also causes variation of the SLR network from day to day. The orbits of moving targets that define the celestial reference frame for satellite techniques must include VLBI UT1 for long

term stability. The huge number of GPS data effectively precludes frequent reanalysis of the entire data set with uniform modeling and elevation limits. Lower elevation limits permit better separation of troposphere and station vertical. At high latitudes, GPS observations also have a significant empty area at high elevations.

Table 3: Differences between Techniques

item	SLR	VLBI	GPS
data span	25 yr	20 yr	10 yr
observing	continuous	few/week	continuous
network size	few tens	usual 5-6, up to 20	several hundred
network variation	moderate	considerable	minimal
targets	few	50-80/day	24
target stability	moving	fixed	moving
analysis	consistent	consistent	evolved
troposphere	dry	dry + wet	dry + wet
elevation limit	high	low	medium

5. IVS OBSERVATIONS FOR THE FUTURE

Table 4 shows the integrated IVS (International VLBI Service for Geodesy and Astrometry) observing program in 2002 most directly related to EOP and TRF. Of particular interest is the inauguration of two 24-hr sessions per week for EOP monitoring with rapid processing. The networks are shown in Figures 4 and 5. The operational goal is to have EOP values within 15 days of observation. The two days replace the single NEOS day. Two separate baselines for 1-hr intensive UT1 measurements will provide redundancy and robustness. The proposed continuous 15-day period should provide data on the remaining discrepancies of the high frequency EOP variations from oceanic and atmospheric tides. The other sessions will tie the TRF together and provide a limited set of EOP with precision better than the weekly data.

Table 4: Proposed IVS Observing 2002

Two 24-hr sessions per week with rapid processing (IVS-R1, IVS-R4)
15-day period of continuous 24-hr observing
Two baselines for 1-hr UT1 intensives
Six VLBA sessions with large networks
Semimonthly 7 and 8-station 24-hr sessions

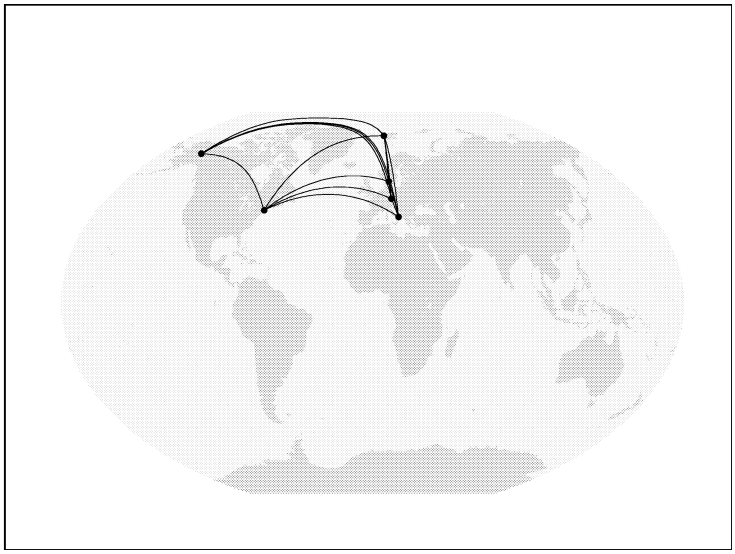

Figure 4: Sites in a representative IVS-R1 session.

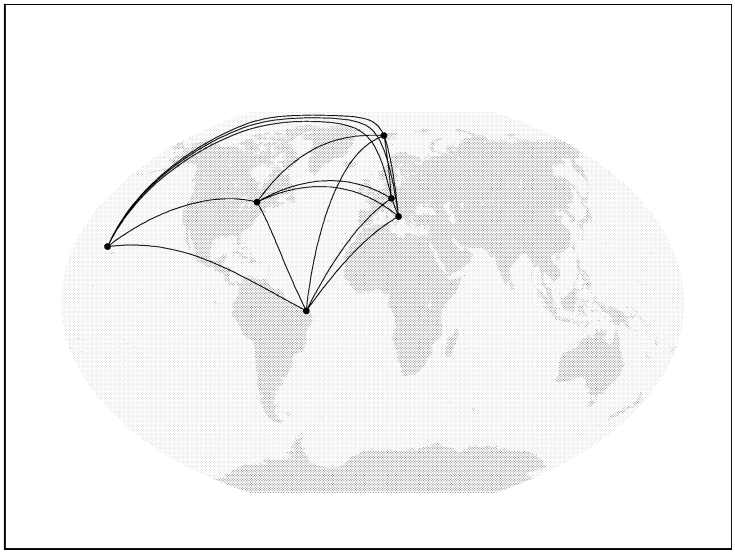

Figure 5: Sites in a representative IVS-R4 session.

COMBINED CELESTIAL POLE OFFSETS FROM VLBI AND GPS

J. VONDRÁK[1], C. RON[1], D. GAMBIS[2], C. BIZOUARD[2], R. WEBER[3]

[1]Astronomical Institute and Center for Earth Dynamics Research
Boční II, 141 31 Prague 4, Czech Republic
e-mail: vondrak@ig.cas.cz, ron@ig.cas.cz

[2]Observatoire de Paris, UMR8630
61, Avenue de l'Observatoire, 75014 Paris, France
e-mail: gambis@obspm.fr, christian.bizouard@obspm.fr

[3]Technical University Vienna
Gusshausstrasse 27-29, 1040 Vienna, Austria
e-mail: rweber@luna.tuwien.at

ABSTRACT. The recently proposed method of 'combined smoothing' is used to combine celestial pole offsets determined at the Institute of Applied Astronomy in St. Petersburg (from VLBI observations) with the celestial pole offset rates determined at the University of Berne (from GPS observations), in the interval 1997.0-2000.0. We demonstrated in our previous analyses that the latter series suffers from long-periodic systematic errors, with periods longer than a month, the most expressed period being about 60 days. Therefore, we removed the long-periodic part of celestial pole offset rates before the combination was made. The combined series is then compared on one hand to various solutions derived from the VLBI analysis centers and to recent theoretical precession-nutation models on the other hand. It is demonstrated that unbiased rms of the differences are typically in the range of 0.40 mas for both celestial pole offset components, the best agreement being found between combined smoothing and recently adopted precession-nutation theory IAU2000.

1. INTRODUCTION

When analyzing celestial pole offsets by modern space techniques, we usually use only the observations by Very Long-Baseline Interferometry (VLBI); satellite methods generally take over a model (either theoretical or based on VLBI observations) of precession-nutation, and determine only the remaining three Earth rotation parameters (polar motion, length-of-day). Recently, a new solution of celestial pole offset rates appeared based on Global Positioning System (GPS) observations (Rothacher et al. 1999). The recently developed method of 'combined smoothing' (Vondrák & Čepek 2000) is especially suitable to be used to combine the series of observed function values with their time derivatives, as demonstrated by Vondrák & Gambis (2000) or Vondrák & Čepek (2001). Here we shall concentrate on the use of this method in combining the celestial pole offsets with their rates, and on the comparison of the results with theoretical

precession-nutation models IERS96, IAU2000, and also with the IERS combined solution C04.

2. THE METHOD AND ITS PROPERTIES

Only the main philosophy of the method of combined smoothing is presented below since it was described in detail in the above cited papers.

Two series of observations are available, at unequally spaced epochs and with different weights: one with measured values of a function, one with measured values of time derivatives of the same function; the epochs of both series need not be identical. We are looking for two new series, defined at all n points with any observation, whose values lie on two relatively smooth curves satisfying three conditions:

- the first one must fit as close as possible to the first data series;
- the second one must fit as close as possible to the second data series;
- both curves must be tied by constraints assuring that the latter is the time derivative of the former.

To this end, we define the 'smoothness' S of the first curve (as the integral of its squared third derivative), the 'fitness' F (in the least-squares sense) of this curve to measured function values, the 'fitness' $\bar{F}$ of the second curve to measured time derivatives, and a set of linear constraints tying the two resulting curves. The solution that fulfills the condition

$$Q = S + \varepsilon F + \bar{\varepsilon}\bar{F} = \min. \tag{1}$$

is then sought, leading to a solution of the system of n linear equations with only 7 diagonals containing non-zero elements. Coefficients of smoothing ε, $\bar{\varepsilon}$ play the role of 'weights' and they have dimensions [time^{-6}], [time^{-4}], respectively.

From the tests made with simulated data (Vondrák et al. 2002), using numerous different combinations of ε, $\bar{\varepsilon}$, follow simple formulas for their optimal choice (in which $P_{\min}$ denotes the shortest significant period contained in the observed signal):

$$\varepsilon = \left(\frac{14.6}{P_{\min}}\right)^6, \quad \bar{\varepsilon} = \left(\frac{14.2}{P_{\min}}\right)^4 \qquad \text{if the density of both series is 1 day and} \tag{2}$$

$$\varepsilon = \left(\frac{12.6}{P_{\min}}\right)^6, \quad \bar{\varepsilon} = \left(\frac{16.9}{P_{\min}}\right)^4 \qquad \begin{array}{l}\text{if the density is 7 days for function values,}\\ \text{1 day for time derivatives.}\end{array} \tag{3}$$

These tests also revealed that the systematic errors in the observed derivatives having either stepwise or long-periodic character do not influence significantly the combined results; they are mostly absorbed in the residuals.

3. THE DATA USED AND THE COMBINED SOLUTION

Celestial pole offsets $\Delta\psi$, $\Delta\epsilon$ of the solution made at the Institute for Applied Astronomy (IAA) in St. Petersburg, Russia (IVS 2001) are used, and are combined with the rates $\Delta\dot{\psi}$, $\Delta\dot{\epsilon}$ determined by GPS at the Center for Orbit Determination in Europe (CODE), for the interval 1997.0–2000.0. The latter were shown to be able to deliver unique contributions to the nutation spectrum in the high frequency range, up to periods of 14 days (Rothacher et al. 1999, Weber 1996, 2001). The most recent tests (Ron & Vondrák 2001) revealed that GPS data suffer from large systematic errors for periods longer than about one month, the largest term having the period of about 60 days. The method of combined smoothing can remove these errors substantially, but not completely – about 10 per cent of them still 'leaks' into the final product.

Therefore, in this study the following approach is chosen:

- Long-periodic part of GPS data (containing periods 30 days and longer) is calculated by applying the filter (Vondrák 1977) with coefficient of smoothing $\varepsilon = 8 \times 10^{-5}\text{day}^{-6}$, and removed from the original data in order to keep only shorter periods.
- VLBI data are combined with the corrected GPS data, using combined smoothing procedure with coefficients of smoothing $\varepsilon = 30\text{day}^{-6}$, $\bar{\varepsilon} = 130\text{day}^{-4}$. These values were calculated from Eqs. (3), assuming there is no signal with periods shorter than 5–7 days.

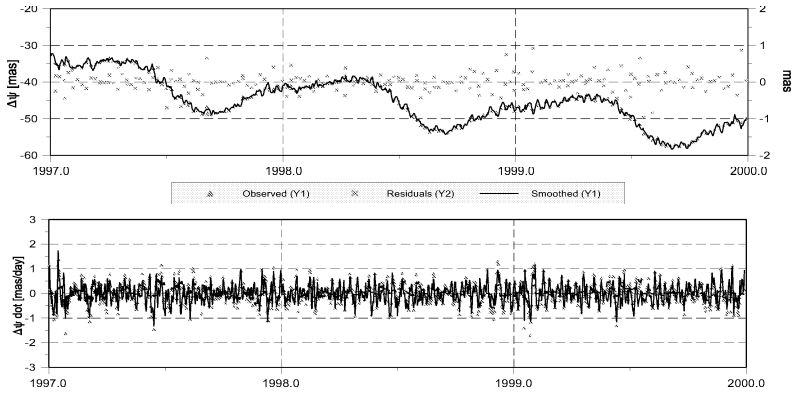

Figure 1: Combined smoothing of $\Delta\psi/\Delta\dot{\psi}$ from VLBI (IAA) and GPS (CODE).

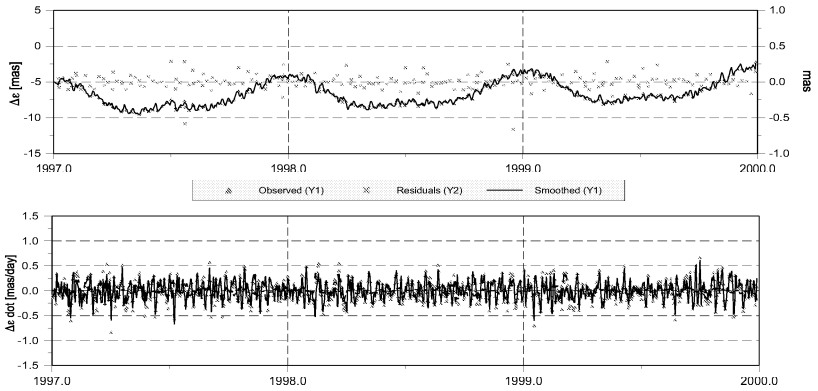

Figure 2: Combined smoothing of $\Delta\epsilon/\Delta\dot{\epsilon}$ from VLBI (IAA) and GPS (CODE).

The results for $\Delta\psi$, $\Delta\epsilon$ (referred to standard IAU 1976 precession and 1980 nutation theory) are depicted in Figs. 1 and 2, where the original observations are shown as triangles, smoothed values as full lines. Upper plots display the function values $\Delta\psi$, $\Delta\epsilon$, lower plots their rates $\Delta\dot{\psi}$, $\Delta\dot{\epsilon}$. Since the triangles cannot be distinguished from the full lines in upper plots, their differences (residuals) in function values are shown as crosses, in an enlarged scale (right axis). It is clear that the combined smoothed lines fit well to the observed values; our assumption on which we based our choice of coefficients of smoothing was probably correct, as can be seen from the comparison of *a posteriori* uncertainties computed from the residuals with their *a priori* values given by the analysis centers:

	a priori		*a posteriori*	
	$\Delta\psi \sin\epsilon$	$\Delta\epsilon$	$\Delta\psi \sin\epsilon$	$\Delta\epsilon$
VLBI [mas]	0.081	0.079	0.079	0.074
GPS [mas/day]	0.035	0.038	0.070	0.063

These values show that the *a posteriori* uncertainties are practically equal to their *a priori* values in case of VLBI observations. It is certainly not the case when GPS uncertainties are compared: the *a posteriori* values are about two times higher than the *a priori* values given by CODE. This ratio is however much lower than the one that we obtained with the original GPS celestial pole rates – it was about seven times larger as demonstrated by Vondrák et al. (2002). From this follows that most of the error budget in GPS celestial pole offset rates is contained in the long-periodic part that we here filtered out before the combination was made.

4. COMPARISON WITH OTHER RESULTS

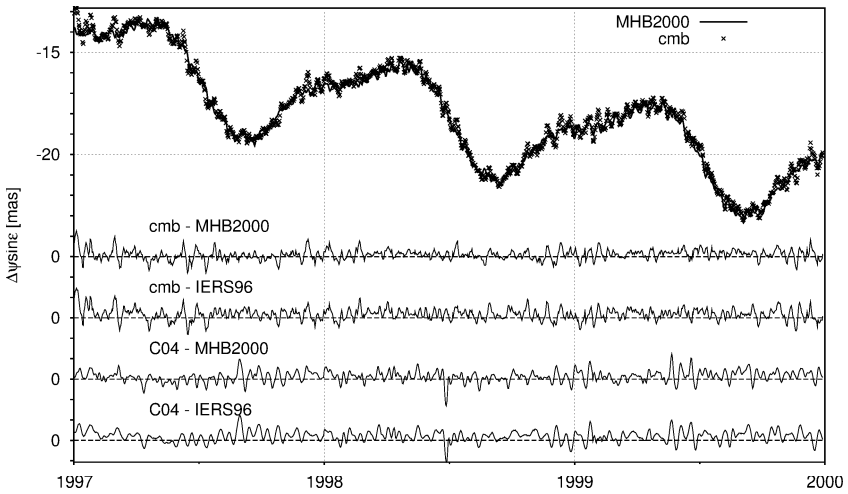

Figure 3: Comparison of combined values $\Delta\psi \sin\epsilon$ with MHB2000, IERS96 and C04.

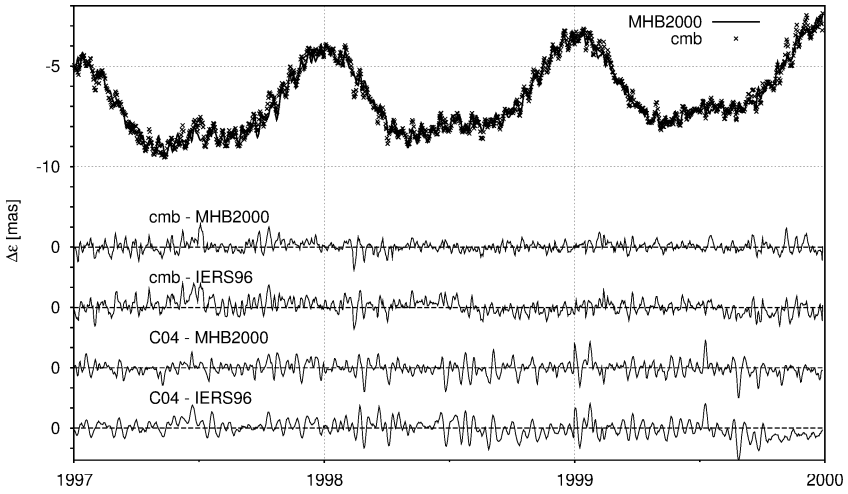

Figure 4: Comparison of combined values $\Delta\epsilon$ with MHB2000, IERS96 and C04.

The combined values are compared with two models of precession-nutation: the model MHB2000 (Mathews et al. 2001), recently adopted by the 24th IAU General Assembly as standard model with denomination IAU2000A that should be used as IAU standard after January 1, 2003, and the IERS 1996 Theory of precession-nutation (McCarthy 1996), whose transfer function between the rigid and non-rigid model of the Earth was estimated from past VLBI and LLR observations. In addition, the IERS standard combined solution C04, based on all available VLBI observations

at each epoch, is also used for comparison. The results of these comparisons for both components of celestial pole offsets $\Delta\psi \sin\epsilon$, $\Delta\epsilon$ are shown in Figs. 3 and 4, respectively.

In upper plots of both figures the VLBI/GPS combined solution is depicted as crosses, full lines represent the most recent (and presumably most accurate) theory MHB2000. Because the remaining two series (i.e., IERS96 and C04) are very close both to our combination and MHB2000, and therefore very difficult to distinguish one from the other, they are not given in these plots. Instead, the differences between the series cmb, C04 on one side and MHB2000, IERS96 on the other are displayed in lower plots. The best fit is apparently achieved between cmb and MHB2000. This is confirmed by the table below that displays the precise numbers for all the calculated differences (biases and uncertainties with and without biases are given), all in milliarcseconds (mas), from which it is clear that the smallest unbiased sigmas are achieved for the differences cmb–MHB2000 (first row):

	bias		σ		σ_{unbiased}	
	$\Delta\psi \sin\epsilon$	$\Delta\epsilon$	$\Delta\psi \sin\epsilon$	$\Delta\epsilon$	$\Delta\psi \sin\epsilon$	$\Delta\epsilon$
cmb – MHB2000	0.096	0.032	0.260	0.253	0.242	0.251
cmb – IERS96	0.179	0.045	0.329	0.340	0.276	0.337
C04 – MHB2000	0.125	−0.027	0.300	0.341	0.273	0.340
C04 – IERS96	0.210	−0.015	0.344	0.398	0.273	0.397

In order to find if there are some significant quasi-periodic differences between our combined solution and the model MHB2000, we made a spectral analysis of these differences, and compared the resulting periodogram with the one of the differences C04–MHB2000. The result is shown in Fig. 5, cmb-MHB2000 on the left and C04–MHB2000 on the right. One can see that there are practically no significant periods in the spectrum; the evident decrease of the amplitudes in short-periodic part of the spectrum is caused by the weak smoothing applied in the combination. The comparison of both spectra shows that the level of noise is lower in case of combined smoothing (cmb–MHB2000) than for the IERS standard combination (C04–MHB2000). General level of the noise is mostly lower than $50\mu as$.

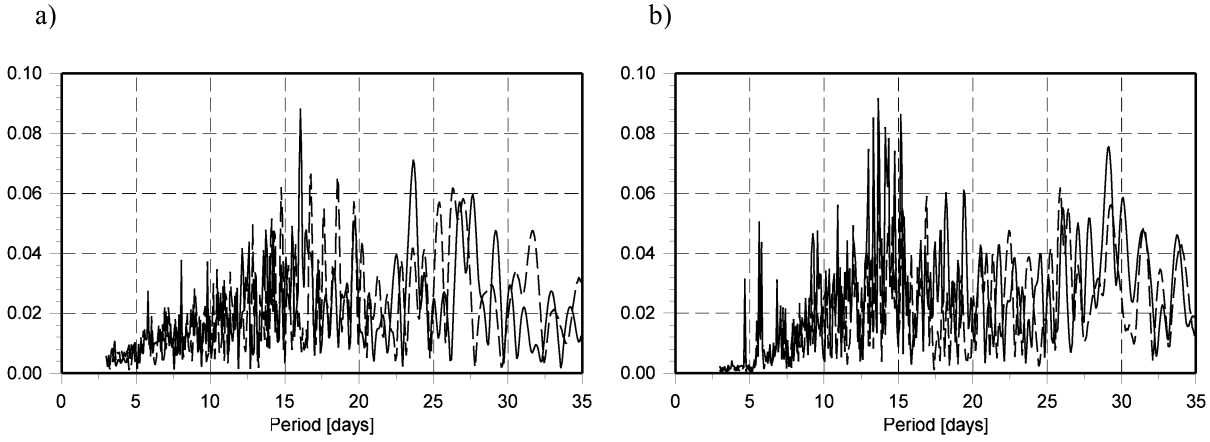

Figure 5: Periodograms of a) cmb–MHB2000 and b) C04–MHB2000. $\Delta\epsilon$ is given as full lines, $\Delta\psi \sin\epsilon$ as dashed lines, vertical scale is in milliarcseconds.

5. CONCLUSIONS

The method of combined smoothing is demonstrated to be a good tool to combine celestial pole offsets (observed by VLBI) with their rates (observed by GPS). Removing the long-periodic part

from GPS data before the combination helps improve the solution. Nevertheless, their formal *a priori* uncertainties are still about two times underestimated. The combination that we obtained in the interval 1997.0–2000.0 fits the new model of precession/nutation MHB2000A better than the standard IERS solution C04, which is confirmed also by spectral analysis. Therefore it seems that using the GPS information in combination with VLBI yields a better estimation of celestial pole offsets than using the VLBI observations alone, especially for periods shorter than a month. Consequently, the combined smoothing procedure will probably be used to produce the combined solution of the IERS Earth Orientation Parameters Product Center in future.

Acknowledgments. The grant No. LN005 awarded by the Czech Ministry of Education, Youth and Sports supporting this study is highly appreciated. This study used the solution iaao9907.eops provided by the International VLBI Service for Geodesy and Astrometry.

6. REFERENCES

IVS (2001) International VLBI Service products available at http://ivscc.gsfc.nasa.gov/service/products.html.

Mathews P.M., Herring T.A., Buffet B.A. (2001) Modeling of nutation-precession: New nutation series for nonrigid Earth, and insights into the Earth's interior. *J. Geophys. Res.*, in press

McCarthy D.D, ed. (1996) IERS Conventions (1996). *IERS Technical Note 21*, Observatoire de Paris

Ron C., Vondrák J. (2001) Mutual comparison of the combinations of Earth orientation parameters obtained by different techniques. *Poster presented at Symposium A*, IAG Scientific Assembly, Budapest, September 2001

Rothacher M., Beutler G., Herring T.A., Weber R. (1999) Estimation of nutation using the Global Positioning System. *J. Geophys. Res.* **104**, B3, 4835–4859.

Vondrák J. (1977) Problem of smoothing observational data II. *Bull. Astron. Inst. Czechosl.* **28**, 84–89.

Vondrák J., Čepek A. (2000) Combined smoothing method and its use in combining Earth orientation parameters measured by space techniques. *Astron. Astrophys. Suppl. Ser.* **147**, 347–359.

Vondrák J., Čepek A. (2001) On the use of the method of combined smoothing to combine EOP data from different techniques. In: N. Capitaine (ed.) *Journées 2000 Systèmes de référence spatio-temporels*, Observatoire de Paris, 252–259.

Vondrák J., Gambis D. (2000) Accuracy of Earth orientation parameters series obtained by different techniques in different frequency windows. In: M. Soffel & N. Capitaine (eds.) *Journées 1999 Systèmes de référence spatio-temporels & IX. Lohrmann-Kolloquium*, Observatoire de Paris, 206–213.

Vondrák J., Weber R., Ron C. (2002) Earth orientation parameters – combination of results obtained by different techniques. *Vistas for Geodesy in the New Millennium, Proc. IAG 2001 Scientific Assembly*, Springer Verlag, in press.

Weber R. (1996) Monitoring Earth orientation variations at the Center for Orbit Determination in Europe. *ÖZf Vermessung & Geoinformation* H3, 269–275.

Weber R. (2001) Estimation of nutation using the GPS. In: N. Capitaine (ed.) *Journées 2000 Systèmes de référence spatio-temporels*, Observatoire de Paris, 205–206.

GEOPHYSICAL PARAMETERS ESTIMATED FROM VLBI NUTATION ANALYSIS

T. FUKUSHIMA
National Astronomical Observatory
2-21-1, Ohsawa, Mitaka, Tokyo 181-8588, Japan
e-mail: Toshio.Fukushima@nao.ac.jp

ABSTRACT. By using the latest analysis of VLBI nutation observation (Shirai and Fukushima 2001b), we obtained new estimates of some geophysical parameters; (1) the period of FCN as -431.1 ± 0.4 sidereal days, (2) the Q-value of FCN as $(1.55 \pm 0.10) \times 10^4$, (3) the dynamical ellipticity of the whole Earth as $0.003273994 \pm 0.000000003$, (4) the Love number of the solid Earth as 0.2788 ± 0.0011, and (5) the phase lag of the solid Earth as 7.13 ± 0.23 degrees.

SUMMARY

First we developed a realistic model of Free Core Nutation (FCN) by taking into account the recent discovery of FCN excitations (Shirai and Fukushima 2001a, c). Next, based on the SOS formulation (Sasao *et al.* 1980), we obtained SOS transfer function with the geophysical constraints. By using these, we updated our previous phenomenological model (Shirai and Fukushima 2000b, c) and constructed a geophysically meaningful theory of the forced nutation of the non-rigid Earth (Shirai and Fukushima 2001b).

More specifically speaking, we adopted RDAN98 (Roosbeek and Dehant 1998) as the rigid Earth nutation theory. Next we convoluted it with the SOS transfer function by a numerical method of convolution in the time domain (Shirai and Fukushima 2000a). Then we readjusted the free parameters of the transfer function, which satisfy two geophysical constraints, by fitting the convoluted nutation theory to the latest VLBI observation of the nutation for the period 1979-2000 (McCarthy 2000) after subtracting the geodesic nutation (Fukushima 1991) and the determined FCN model (Shirai and Fukushima 2001c).

Through the examination of the dependence of residuals on the number of nutation terms, we truncated the series so as to contain only 194 terms. The resulting weighted root mean square of the residuals in complex form of nutation is 0.280 mas for the new nutation series, which is significantly smaller than 0.296 mas, that of the best empirical model, IERS96 (McCarthy 1996), which contains 381 terms.

Together with the geophysical parameters determined from the analysis, which are listed in the tables, we also obtained some astronomical parameters; (1) the corrections to the precession constants were determined as (-0.29856 ± 0.00030) ″/cy in longitude and (-0.02408 ± 0.00016) ″/cy in obliquity, respectively. (2) the correction to the CEP offsets at J2000.0 as (-0.042888 ± 0.000010) ″ in longitude and (-0.005171 ± 0.000010) ″ in obliquity, respectively.

Recently we constructed an entirely new precession formula based on thus obtained forced nutation models (Fukushima 2001).

Table 1: Parameters of Free Core Nutation

Reference	Period (sidereal day)	Q-value	Method
Wahr (1981)	-460.5	∞	Theory
Wahr and Bergen (1986)	-462.8	146000	Theory
Herring *et al.* (1986)	-433.2 ± 2.0	16129 (12195-23089)	VLBI
Richter and Zurn (1988)	-431.3 ± 3.7	3120 (2797-3433)	Gravimeter
Neuberg *et al.* (1987)	-431 ± 6	2758 (2222-3249)	Gravimeter
Mathews *et al.* (1991)	-457.1	∞	Theory
Cummins and Wahr (1993)	-437 ± 14	5722 (3035-49869)	Gravimeter
Sato *et al.* (1994)	-437 ± 15	6510 (3240-∞)	Gravimeter
Herring (1995)	-431.2	17161	VLBI
Dehant and Defraigne (1997)	-431.8	∞	Theory
Mathews *et al.* (2000)	-430.2 ± 0.2	19000	VLBI
Shirai and Fukushima (2000b)	-430.8 ± 0.6	16200 ± 1600	VLBI
Shirai and Fukushima (2001b)	-431.1 ± 0.4	15500 ± 1000	VLBI

Table 2: Dynamical Ellipticity

Reference	e (unit:10^{-3})	Method
Wang (1972)	3.245	Seisimic
Kinoshita (1977)	3.2740	Precession
Dziewonski and Anderson (1981)	3.247	Seismic
Nakiboglu (1982)	3.250	Seismic
Kinoshita and Souchay (1990)	3.2739567	Precession
Hartmann and Soffel (1997)	3.2737925	Precession
Souchay and Kinoshita (1997)	3.2737548	Precession
Bretagnon *et al.* (1997)	3.2737671	Precession
Roosbeek and Dehant (1998)	3.2737674	Precession
Mathews *et al.* (2000)	$3.28454034 \pm 0.00000049$	Nutation
Shirai and Fukushima (2001b)	3.273994 ± 0.000003	Nutation
Shirai and Fukushima (2001d)	3.2737914 ± 0.0000004	Nutation and Precession

Table 3: Love number

Reference	k_2	Phase Lag (^{o})	Method
Kozai (1968)	0.29 ± 0.03	5 ± 3	Satellite
Guinot (1974)	0.334 ± 0.005	N/A	UT1 (Mf)
	0.295 ± 0.011	N/A	UT1 (Mm)
Djurovic (1976)	0.343 ± 0.030	N/A	UT1 (Mf)
	0.301 ± 0.044	N/A	UT1 (Mm)
DE102 (1983)	0.29	2.656	LLR
Williamson and Marsh (1985)	0.330 ± 0.013	N/A	Satellite (Mf)
	0.252 ± 0.025)	N/A	Satellite (Mm)
DE405 (1997)	0.30	2.465	LLR
Shirai and Fukushima (2001b)	0.2788 ± 0.0011	7.13 ± 0.23	VLBI

REFERENCES

Bretagnon, P., Rocher, P., and Simon, J. L., 1997, *Astron. Astrophys.*, 319, 305

Cummins, P. R., and Wahr, J. M., 1993, *Geophys.J.R.Astron.Soc.* , 98, 2091

Dehant, V., and Defraigne, P., 1997, *J. Geophys.Res.* , 102, 27659

Djurovic, D., 1976, *Astron. Astrophys.*, 47, 325

Dziewonski, A. M., and Anderson, D. L., 1981, *Phys. Earth. Planet. Inter.*, 25, 297

Fukushima, T., 1991, *Astron. Astrophys.*, 244, L11

Fukushima, T., 2001, *Astron.J.* , submitted

Guinot, B., 1974, *Astron. Astrophys.*, 36, 1

Hartmann, T., and Soffel, M., 1994, *Astron.J.* , 108, 1115

Herring, T. A., 1995, *Hightlights of Astronomy*, 10, 222

Herring, T. A., Gwinn, C. R., and Shapiro, I. I., 1986, *J. Geophys.Res.* , 91, 8259

Kinoshita, H., 1977, *Celest. Mech.* , 15, 277

Kinoshita, H., and Souchay, J., 1990, *Celest. Mech.* , 48, 187

Kozai, Y., 1968, *Publ. Astron. Soc. Japan*, 20, 24

Nakiboglu, S. M., 1982, *Phys. Earth. Planet. Inter.*, 28, 302

Neuberg, J., Hinderer, J., and Zurn, W., 1987, *Geophys.J.R.Astron.Soc.* , 91, 853

Mathews, P. M., Buffett, B. A., Herring, T. A., and Shaprio, I. I., 1991, *J. Geophys.Res.* , 96, 8243

Mathews, P. M., Buffett, B. A., and Herring, T. A., 2000, *J. Geophys.Res.* , submitted

McCarthy, D. D., 1996, *IERS Technical Note 21*, 1

McCarthy, D. D., 2000, private communication

Richter, B., and Zurn, W., 1986, *The Earth's Rotation and Reference Frames for Geodesy and Geodynamics*, edited by Babcock, A., and Wilkins, G., 309

Roosbeek, F., and Dehant, V., 1998, *Celest.Mech.Dyn.Astr.* , 70, 215

Sasao, T., Okubo, S., and Saito, M., 1980, *Proc. IAU Symp.* No. 78, 165

Sato, T. *et al.*, 1994, *J. Geomag. Geoelectr.*, 46, 571

Shirai, T., and Fukushima, T., 2000a, *Astron.J.* , 119, 2475

Shirai, T., and Fukushima, T., 2000b, *Proc. IAU Coll.* No. 180, 223

Shirai, T., and Fukushima, T., 2000c, *Proc. of Journee 2000*, in press

Shirai, T., and Fukushima, T., 2001a, *J. Geod. Soc. Japan*, 47, 198

Shirai, T., and Fukushima, T., 2001b, *Astron.J.* , 121, 3270

Shirai, T., and Fukushima, T., 2001c, *Geophys. Res. Lett.*, 28, 3553

Shirai, T., and Fukushima, T., 2001d, *Highlights of Astronomy*, in press

Wahr, J. M., 1981, *Geophys.J.R.Astron.Soc.* , 64, 705

Wahr, J. M., Bergen, Z., 1986, *Geophys.J.R.Astron.Soc.* , 87, 633

Wang, C. Y., 1972, *J. Geophys.Res.* , 77, 4318

Williamson, R. G., and Marsh, J. G., 1985, *J. Geophys.Res.* , 90, 9346

IS THE DIFFERENTIAL ROTATION DETECTABLE FROM EARTH NUTATION ?

C. HUANG
Shanghai Astronomical Observatory, Chinese Academy of Sinica
80 Nandan Road, Shanghai 200030, P.R. China
e-mail: clhuang@center.shao.ac.cn

V. DEHANT
Royal Observatory of Belgium
Ave. Circulaire 3, 1180 Brussels, Belgium
e-mail: v.dehant@oma.be

ABSTRACT. In the past half decade, the possibility of a differential rotation between the inner core (IC) and the mantle (M) have been thoroughly studied from both geodynamo and seismological observations. In this paper, the effect on the Earth nutation and rotational modes of the possible differential rotation between the solid inner core, the fluid outer core and the mantle are calculated by numerical integration of the scalar equations of infinitesimal elastic-gravitational motion for a rotating, slightly elliptical Earth. We show that the effect of large differential rotation, compatible with the observation, according to several authors, can not be ignored in the nutation theory. The possibility to detect these differential rotations from the nutation observation is also discussed and shown to be at the present precision limit of the observations, even for large differential rotations . In the rotational modes, the motion equations in the Earth are used also to solve the eigenfrequencies of three eigen modes of the PREM Earth, i.e. the tilt-over mode (TOM), the Free Core Nutation (FCN) and the Free Inner Core Nutation (FICN), as well as their respective eigenfunctions in the particular case of differential rotation. For each eigen mode, we have obtained the displacement field, and in particular, the global rotational displacement and we have shown the differences in the amplitudes for the cases examined.

1. INTRODUCTION

It is usually considered that the three parts of the Earth, the solid inner core (IC), the fluid outer core (OC) and the mantle (M), rotate with the same mean angular velocity, $\Omega_0 = 7.292115\,10^{-5}$ rad/s i.e., 1 cycle per sidereal day.

Several years ago, Glatzmaier and Roberts (1995, 1996) suggested that, from their three-dimensional self-consistent geo dynamo, a super-rotation of the inner core relative to the mantle can be maintained by magnetic coupling between the inner core and an eastward thermal current in the fluid outer core, the differential rotation velocity of the inner core relative to the mantle being about 1 cycle/500 years, i.e. about 0.7°/year (eastward).

Less than one year later, several works reported, that differential rotation between the inner core and the mantle was indeed compatible with the observations (mainly seismological). For

example, Song and Richards (1996) reported a faster rotation of the inner core with respect to the mantle with 1 cycle per 300 years; Su et al. (1996) pointed out that the super-rotation velocity could be as fast as 3^o/year and so on... These reports from both geodynamo and seismological observations are sometimes controversial. Souriau and Poupinet (2000) have shown that the interpretation of seismic data in terms of differential rotation needs further caution. More and more people think that, e ven though the differential rotation exists, the velocity may not be so large, for example, may be less than $+0.2^o$/yr and may vary with time (Tromp, 2001). But none of them could definitely show the non-existence of a differential rotation between the inner core and the outer core or mantle. Using seismic normal modes, Vidale et al. (2000) found the differential rotation velocity to be about 0.1^o/year, Laske and Master (1999) and Laske et al. (2000) have found another value 0.0^o/year. A theoretical study of the gravitational interaction between the inner core and the mantle has lead Buffet and Glatzmaier (2000) also to a very small angular velocity of 0.02^o/year. So, the question of whether the differential rotations among the Earth's three parts are real, still remains an open question, while the present trend is that this differential rotation, if it exist, would be very small.

This controversial subject is nevertheless very interesting because the study of differential rotations would provide us with new insights to the Earth interior. For example, constraints in the dynamo motions underlying the geomagnetic field would be provided, and the flow models that can reproduce secular variation of the geomagnetic field and its reversals would be refined. The viscosity in the outer core may be obtained with a new value that, in turn, may provide new information on melting conditions and temperature in the outer core, and may refine the estimates of the heat flux across the core-mantle-boundary. Moreover, due to the new distribution of the angular momentum of the three parts of the Earth, the rotation axis of inner core may not track the spin axis in the precession of the equinox, and it may also influence the gravity field (Song and Richards, 1996). These are examples, but the existence of differential rotation opens new questions, one of them being its influence on the Earth's orientation.

Here, we are interested in an important sub-question, i.e., if there is a differential rotation in the Earth, doe s it result in observable changes in the Earth nutation? Or say, is it detectable from the nutation observations? This is an important question in the frame of nutation modeling because nutation observations are interpreted in terms of physics of the Earth's interior and the parameters involved in MHB2000 model (Mathews et al. 2001), which has been adopted by the IAU (International Astronomical Union), do not incorporate any differential rotation between the inner core and the rest of the Earth.

In the next section, the principle of the Earth nutation and its calculation is briefly reviewed; several cases of the differential rotations are hypothesized in Section 3; in Section 4, the results of the contribution to the main Earth nutation terms and the four Earth modes are presented, and the possibility to detect these differential rotations from the nutation observation is also discussed; finally, the displacement field associated with each case is computed and compared with the nominal case.

2. EARTH NUTATION AND ITS CALCULATIONS

Besides the polar motion and the length-of-day variation, the precession and nutation are another set of important parameters describing the orientation of the Earth rotation axis in space. They are caused by the gravitational attraction of the Sun, the Moon and the planets on the Earth's equatorial bulge. Precession is the secular part, while the nutation is the collection of the short-period components (in fact, the precession does also involve periods, but very long periods which can be considered as trends around J2000). In the nutation series, there is a discrete number of terms of periods from 2 days to 300 years, and all of these periods can be

expressed as linear combinations of fundamental arguments related to the orbits of the Sun, the Moon and the planets.

The rigid Earth nutation theory can nowadays be very accurate at the level of a few tens of micro-arc-second (μas), because it relays on celestial mechanics considerations and ephemer edes (Souchay et al., 1999; Bretagnon et al., 1998; Roosbeek and Dehant, 1998). The nutation theory for a more realistic Earth model (usually called non-rigid Earth) is not precise at that level. Residuals with respect to Very Long Baseline Interferometry (VLBI) observations are at the level of a tenth of milli-arc-second (μas) or even less (20 μas) for nutations of which the periods are less than a few year (see Dehant et al., 1999, for a complete review). There are several approaches for computing the non-rigid Earth nutations. For example, Shirai and Fukushima (2001) obtained a pure numerical nutation model fitted from VLBI observation ; Mathews et al. (1991, 2001) presented a semi-analytical model, which is the basis of the IAU2000A nutation model, in which several geophysical parameters are fitted from VLBI observation ; Getino and Ferrandiz (1999) apply the Hamilton method from the nutation study of rigid Earth. In the numerical integration approach used by Wahr (1981), Dehant and Defraigne (1997), Schastok (1997) and Huang et al. (2001), the so-called Earth Transfer Function (ETF) is computed for each nutation frequency. It is the response of the Earth to the gravitational force, integrated from a set of scalar equations of the infinitesimal elastic-gravitational motion for a rotating, slightly elliptical Earth, with appropriate boundary conditions as well as an appropriate a priori Earth model (density profile and rheological property profiles) (Dahlen, 1972; Smith, 1974). The non-rigid Earth nutation can then be obtained from the convolution of the ETF and a certain rigid Earth nutation model. In this numerical integration approach, some parameters of geophysical characters of the Earth interior are included, therefore geophysical informations may be obtained from comparing the nutation results with the modern precise observations (mainly VLBI), and then, these informations can be used, in return, to improve the Earth model and the nutation model. This numerical integration approach is also used in this work.

3. HYPOTHESES AND SIMULATIONS

When no differential rotation is considered, the mean velocities of all the three parts of Earth are considered to be equal to:

$$\Omega(r) = \Omega_0 = 2\pi/sid.day = 7.292115\ 10^{-5} radin/s$$

We suppose the rotation velocity throughout the Earth is a stepwise function as:

$$\Omega = \Omega(r) = \begin{cases} \Omega_0 + \delta\Omega_{IC} & (0 < r \leq r_{ICB}) \\ \Omega_0 + \delta\Omega_{OC} & (r_{ICB} < r \leq r_{CMB}) \\ \Omega_0 + \delta\Omega_M & (r_{CMB} < r \leq r_M) \end{cases} \quad (1)$$

where r_{ICB}, r_{CMB} and r_M are the radii of the inner core (of the Inner Core Boundary, ICB), the outer core (of the Core Mantle Boundary, CMB), and the mantle respectively.

So, in addition to the nominal case,

$$\delta\Omega_{IC} = \delta\Omega_{OC} = \delta\Omega_M = 0$$

we discuss the following three cases:

1. Only the inner core rotates differentially , so, $\delta\Omega_{OC} = \delta\Omega_M = 0$.

Case 1A: the inner core rotates faster than the other parts with 1^o/year eastward, which is the case of Song and Richards (1996);

Case 1B: the super-rotation velocity of the inner core is 5^o/year eastward, which can be considered as the maximum value found in the literature, deduced from present seismic observations;

2. Only the fluid outer core is hypothesized to rotate differentially, so, $\delta\Omega_{IC} = \delta\Omega_M = 0$.
Case 2A: if the change of the angular momentum of the inner core due to the differential rotation of the inner core of $\delta\Omega_{IC} = 5^o$/year is transferred to the outer core, then we can obtain by angular momentum conservation, from $\delta\Omega_{OC}C_{outer\ core} = \delta\Omega_{IC}C_{inner\ core}$, that $\delta\Omega_{OC}$ = 0.003^o/yr , where $C_{outer\ core}$ and $C_{inner\ core}$ are the principal polar moments of inertia of the outer core and inner core respe ctively.
Case 2B: the super-rotation velocity of the outer core is hypothesized to be $\delta\Omega_{OC}$ =+0.1 ^{o}/year (eastward).
3. There is no differential rotation among the three parts ($\delta\Omega_{IC} = \delta\Omega_{OC} = \delta\Omega_M = 0$). But in the history, mainly due to the dissipation by tidal friction, there is a secular deceleration, $\Delta\Omega_0/\Delta t = -5.5\ 10^{-22}$ (rad/s^2). So
Case 3A: 0.1 Million years ago, $\Omega = \Omega_0 + 3.1^o/year = (1 + 2.38\ 10^{-5})\Omega_0$;
Case 3B: 1 Million years ago, $\Omega = \Omega_0 + 31^o/year = (1 + 23.8\ 10^{-5})\Omega_0$. The simulation results are presented in the following section.

4. RESULTS AND DISCUSSIONS

4.1. Contribution to the main nutation terms

Table 1 gives the largest contribution of the differential rotation to the main nutation terms, and the unit is mas.

Table 1: The contribution of the differential rotation to main nutations (mas)

Case	$\delta\Omega_{IC}$	$\delta\Omega_{0C}$	$\delta\Omega_M$	$\Delta\psi^{ip}_{18.6yr}$	$\Delta\psi^{op}_{18.6yr}$	$\Delta\epsilon^{op}_{18.6yr}$	$\Delta\epsilon^{ip}_{18.6yr}$
1A	1	0	0	-0.01	0.	0.	+0.01
1B	5	0	0	-0.02	-0.01	0.	+0.01
2A	0	0.003	0	-0.03	0.	0.	+0.02
2B	0	0.1	0	-1.03	-0.02	0.	+0.53
3A	3.1	3.1	3.1	-0.24	-0.02	0.	+0.12
3B	31	31	31	-2.83	-0.23	-0.07	+1.49

Notes:
3A) $\Delta\psi^{ip}_{0.5yr}$ = -0.02, $\Delta\epsilon^{ip}_{0.5yr}$ = +0.01
3B) $\Delta\psi^{ip}_{0.5yr}$ = -0.17, $\Delta\psi^{op}_{0.5yr}$ = -0.02, $\Delta\epsilon^{ip}_{0.5yr}$ = +0.07, $\Delta\psi^{ip}_{1yr}$ = +0.02, $\Delta\psi^{op}_{13.66d}$ = -0.03, $\Delta\epsilon^{ip}_{13.66d}$ = +0.01

F rom these numbers, we can find the following considerations:
1) The differential rotations mainly influence the 18.6 year in-phase (ip) components of the nutations in longitude ($\Delta\psi$) and in obliquity ($\Delta\epsilon$); this provides a large contribution on the retrograde in-phase 18.6 year nutation;
2) The super-rotation of the inner core contributes to nutation, for a super-rotation velocity of 5^o/year, but the effect is very small: even for this large differential velocity, it contributes only to the $\Delta\psi^{ip}_{18.6yr}$ with 0.02 mas and $\Delta\epsilon^{ip}_{18.6yr}$ with 0.01 mas;
3) On the other hand, all results show that the importance of the outer core is obviously large: if the differential rotation velocity of the outer core is 0.1^o/year relative to the inner core and the mantle, it can influence $\Delta\psi^{ip}_{18.6yr}$ and $\Delta\epsilon^{ip}_{18.6yr}$ at the mas level and 0.5 mas level respectively. Again, the largest contribution is on the 18.6 year retrograde nutation. For the case of 2A, the effects of the differential velocity of 0.003^o/yr is similar to the effects of the case of 1B, i.e., $\delta\Omega_{IC}$

$= 5^o$/year, which was expected.
4) If a relative change in Ω_0 of 2 10^{-5} is considered, which was the case 0.1 million years ago, the associated 18.6 year nutation changes are $\Delta\psi^{ip}_{18.6yr} = 0.24$ mas and $\Delta\epsilon^{ip}_{18.6yr} = 0.12$ mas; while for the case of a relative change of 2 10^{-4}, which was the case of 1 million years ago, the changes of $\Delta\psi^{ip}_{18.6yr}$ and $\Delta\epsilon^{ip}_{18.6yr}$ can reach about 2.8 and 1.5 mas respectively. Again, this situation will correspond to a maximum change in the retrograde 18.6 year nutation. It must be noted that the changes in the amplitudes of the nutation do not incorporate the changes in the flattening associated with these changes in rotation.

As general conclusion, the values obtained in all simulations show im portant contributions to nutations, some times well above the actual precision of the observation (20 to 40 μas in the frequency domain). They show that for the level of differential rotation that we have chosen, the contributions can not be ignored in the nutation theory. The exageration done on purpose has pushed us to evaluate the actual possibilities for the differential rotations and the results are presented in Huang and Dehant (2001).

4.2. Influence on the normal mode periods

In all simulations, the influence of the differential rotation on the normal mode periods is also obtained (see Table 2). We have examined the Tilt-Over-Mode (TOM), which represents a steady rigid rotation of the body around an axis that does not coincide with the z-axis of the uniformly rotating reference frame. We have also examined the Chandler Wobble (CW), associated to the equatorial bulge of the Earth and related to the non-coincidence of the rotation axes and the mean polar moment of inertia l axes, the Free Core Nutation (FCN) and Free Inner Core Nutation (FICN), related mainly to gravitational and fluid pressure interactions at the CMB and ICB respectively.

Table 2: The influence of the differential rotation to normal mode periods (sidereal day)

Case	$\delta\Omega_{IC}$	$\delta\Omega_{0C}$	$\delta\Omega_M$	TOM	CW	FCN	FICN
normal	0	0	0	1-3.47 10^{-8}	-408.38	-457.67	+470.61
1A	1	0	0	1-2.90 10^{-8}	-408.38	-457.67	+472.40
1B	5	0	0	1-0.66 10^{-8}	-408.38	-457.66	+479.10
2A	0	0.003	0	1-3.21 10^{-8}	-408.38	-457.67	+470.61
2B	0	0.1	0	1+5.10 10^{-8}	-408.38	-457.52	+470.61
3A	3.1	3.1	3.1	1+2.361 10^{-5}	-408.39	-452.73	+475.92
3B	31	31	31	1+2.364 10^{-4}	-408.48	-412.67	+529.76

Notes of units:
1) for the $\delta\Omega_{IC}$, $\delta\Omega_{0C}$ and $\delta\Omega_M$, the unit is degree/year;
2) the unit of TOM and CW is sidereal day observed from the frame tied with the rotating Earth body, while the unit of FCN and FICN is sidereal day observed from the inertial space;
3) for the cases 3A and 3B, the unit is sidereal day.

In Table 2, the unit is degree/year for $\delta\Omega_{IC}$, $\delta\Omega_{0C}$ and $\delta\Omega_M$; the unit of TOM and CW periods is sidereal day observed in a frame tied with the rotating Earth, while the unit of FCN and FICN periods is sidereal day observed from the inertial space. It must be noted that the periods listed here are for an Earth in hydrostatic equilibrium (for that reason, there is about 30 days difference with the observed period for FCN). This does not prevent us to obtain the induced changes in the periods, which was the objective of this paper. For the cases 3A and 3B, the unit is sidereal day.

The period of the TOM is the spin period of the Earth and should accurately be one sidereal

day. This mode is not related to the internal constitution of the body. The result of this period from integration can serve as a check of the deformation theory and the numerical calculation (Smith, 1977; Rogister, 2001).

From Table 2, it can be seen that:

1) Due to the differential rotations in the interior, the period of the TOM can change from case to case but the changes are very small. In case 2B, its difference with 1.0 changes sign from minus to plus. The effects remain very small except when the global rotation is changing as in cases 3A and 3B.

2) The period of Chandler Wobble is not changed for the cases 1 and 2. This is because the CW represents the rotation of the instantaneous rotation axis about the axis of the polar principal moment of inertia, and the cases 1 and 2 do not change either the instantaneous rotation axis and have a negligible effect on the polar principal moment of iner tia. However, for the case 3, ignoring tidal friction on the polar principal moment of inertia, the rotation speed around the instantaneous rotation axis changes with 2.38 10^{-5} in case 3A and 23.8 10^{-5} in case 3B. This results in a change of the CW period with similar ratio.

3) The FCN period is quasi-diurnal (but larger than 1 day) in the terrestrial frame or about -460 (retrograde) day (for an Earth in hydrostatic equilibrium) in the inertial space. It is usually thought to depend mainly on the ellipticity of the core-mantle-boundary. For case 2B, in which the differential rotation speed between the outer core and the mantle reaches 0.1^o/year, the FCN period changes about 0.15 day.

4) Similar to the FCN, the FICN has a quasi-diurnal period but less than 1 day in the terrestrial frame. It is a prograde mode in the inertial space. Cases 1A and 1B indicate that the effects of the differential rotation of the inner core are dominant in the FICN. However, even though the possible dif ferential rotation (1^o/year, case 1A) of the inner core can change the period of FICN with about 2 days, it is still difficult to be seen from nutation because the FICN contributes to a very small amount to nutation (either the total nutation or the prograde annual nutation), and the free mode itself, contrary to the FCN, is not observed at the present-day precision of the observation.

4.3. The TOM, FCN and FICN eigenfunctions for the hypothesized differential rotations.

Here, we present the results about the eigenfunctions of the three modes: TOM, FCN and FICN.

We note $W_\ell m$ the toroidal displacement of degree ℓ and order m, while $U_\ell m$ and $V_\ell m$ are the spheroidal radial and spheroidal tangential displacements. Due to the Earth rotation and flattening, the displacement field in response of the Earth to a tidal potential of degree l and order m, is at the first order, a sum of spheroidal displacement (ℓ, m) $(\ell+2, m)$, $(\ell-2, m)$ and toroidal displacements $(\ell-1, m)$, $(\ell+1, m)$.

For the FCN, W_1^1 is very large in the outer core, decreases linearly there, jumps over the zero mean line at the CMB and increases linearly in the mantle. Although not changing linearly in the inner core, it decreases monotonously with similar trend as in outer core. It reflects that the FCN is the relative rotation between outer core and mantle. We think that the non-constant increase in the inner core is related to the starting solution at the center and is not real. The slops, i.e. the linear trends, S_{OC} and S_M, can be obtained from least square fit in outer core and mantle separately. Their ratio S_{OC}/S_M is about -7.8. U_2^1, V_2^1 and the non-linear part of W_1^1 are only 10^{-3} of the linear part of W_1^1 in the outer core.

For the FICN, the trends of W_1^1 in inner core and outer core are obviously reversed with a jump over the zero mean line at ICB, and the value in the inner core is about two-order of m agnitude larger than in the outer core. It shows that the FICN happens at ICB (where the displacement are maximum) and is mainly related to the inner core. The slop near the ICB

(representing the real slop due the initial solution problem), S_{IC}, can be compared with the slop in the outer core, S_{OC}; their ratio S_{IC}/S_{OC} is about +0.6.

Again, U_2^1, V_2^1 and the non-linear part of W_1^1 are only 10^{-3} of the linear part of W_1^1 in the inner core.

5. CONCLUSIONS

In the above sections, the contributions of the possible differential rotation between the three parts of the Earth's interior to the Earth nutation have been examined and the associated changes in the periods of four modes are calculated by using a numerical approach. The cases considered are rather extreme cases in order to see the order of magnitude of the effects. For the hypothesized cases presented, we have shown that the differential rotation, if large, can not be ignored in the modern nutation theory and observation. We have shown that, if they are large, it is possible to detect them from the nutation observation. We nevertheless believe that, considering the recent studies of the differential rotation of the inner core, the effects on nutations are at the limit of VLBI precision (20 mas) or less. In this paper, we have also shown that the amplitudes of the principal nutations (18.6 year nutations) may have changed as the global mean rotation has changed.

Acknowledgement: This work was performed mainly during the 6 month residence of C.L. Huang (HCL) at the Royal Observatory of Belgium (ROB), which was supported by the bi-lateral cooperation between the Services Federaux des Affaires Scientifiques, Techniques et Culturelles of Belgium and the Chinese Ministry of Science and Technology. HCL is indebted to Prof. Paul Paquet, the director of ROB, and Dr. Veronique Dehant, for their very kind helps during his stay in ROB, as well as many young coll eagues in ROB for their helps and discussions. This work is benefited from the discussions with Profs. W.J. Jin, X.H. Liao, R.S. Fu, Dr. T.V. Hoolst, Dr. O. de Viron. This work is also partly supported by the Project NSFC 10073015 and 10133010.

6. REFERENCES

Bretagnon P., Francou G., and Rocher P., 1998, SMART97: a new solution for the rotation of the rigid Earth, Astron. Astrophys., 329: 329-338.

Buffet B.A., 1996, Mechanism for decade fluctuations in the length od day, Geophys. Res. Lett., 23: 3803-3806.

Dahlen F.A., 1972, Elastic dislocation theory for a self-gravitating elastic configuration with an initial static stress field. Geophys. J. R. Astron. Soc., 28: 357-383.

Dehant V., Arias F., and Bizouard Ch., 1999, Considerations concerning the non-rigid Earth nutation theory. Celest. Mech. dyn. Astron., 72: 245-310.

Dehant V., and Defraigne P., 1997, New transfer functions for nutations of a non-rigid Eart h.. J. Geophys. Res., 102: 27659-27688.

Dehant V., et al., 1999, Considerations concerning the non-rigid Earth nutation theory, Celest. Mech. dyn. Astron., 72: 245-310.

Dziewonski A.D., and Anderson D.L., 1981, Preliminary Reference Earth Model. Phys. Earth planet. Inter., 25: 297-356.

Feissel M., Yseboodt M., de Viron O., Dehant V. and Bizouard C., 2001, How can we cheat

the non-rigid Earth nutation theory to make it match VLBI results? in: Journées 2001 Systèmes de Référence Spatio-Temporels, "Influence of geophysics, time and s pace reference frames on Earth rotation studies " Brussels, Belgium, 24-26 September 2001, this issue.
Getino J., and Ferrandiz, J.M., 1999, Accurate analytical nutation series. MNRAS, 306: L45-L49.
Glatzmaier G.A., and Roberts P.H., 1995, A three-dimensional self-consistent computer simulation of a geomagnetic field reversal, Nature, 377: 203-209.
Glatzmaier G.A., and Roberts P.H., 1996, Rotation and magnetism of Earth's inner core, Science, 274: 1887-1891.
Hide R, Boggs D.H., Dickey J.O., 2000, Angular momentum fluctuations within the Earth's liquid core and torsional oscillations of the core-mantle system, Geophys. J. Int., 143: 777-786.
Huang C.L., 2001, The scalar boundary conditions for the motion of the elastic Earth to second order in ellipticity, Earth, Moon, and Planets. 84: 125-141.
Huang C.L., Jin W.J., and Liao X.H. 2001, A new nutation model of non-rigid Earth with ocean and atmosphere. Geophys. J. Int., 146: 126-133.
Mathews P.M., Buffett B.A., and Herring T.A., 1991, Forced nutations of the Earth: Influence of inner core dynamics. I. Theory. J. Geophys. Res., 96(B5): 8219-8242.
Mathews P.M., Herring T.A., and Buffett B.A. 2001, Modeling of nutation-precession: New nutation series for non-rigid Earth, and insights into the Earth's interior. J. Geophys. Res., in press.
Rogister Y. 2001, On the diurnal and nearly diurnal free modes of the Earth, Geophys. J. Int., 144: 459-470.
Roosbeek F., and De hant V., g8, RDAN97: An analytical development of rigid Earth nutation series using the torque approach, Celest. Mech. dynamical Astron., 70: 215-253.
Schastok J., 1997, A new theoretical series for a more realistic model Earth. Geophys. J. Int., 130: 137-150.
Shirai T., and Fukushima T., 2001, Construction of new forced nutation theory of non-rigid Earth, Astron. J., 121: 3270.
Smith M.L., 1974, The scalar equations of infinitesimal elastic-gravitational motion for a rotating, slightly elliptical Earth. Geophys. J. R. Astron. Soc., 37: 491-526.
Smith M.L., 1977, Wobble and nutation of the Earth. Geophys. J. R. Astron. Soc., 50: 103-140.
Song X.D., and Richards P.G., 1996, Seismological evidence for differential rotation of the Earth's inner core, Nature, 382: 221-224.
Souchay J., Loysel B., and Kinoshita H., 1999, Corrections and new developments in rigid earth nutation theory: III. Final tables 'REN-2000' including crossed-nutation and spin-orbit coupling effects, Astro n. Astrophys. Suppl., 135: 111-131.
Souriau A., and Poupinet G., 2000, Inner core rotation: a test at the world wide scale, Phys. Earth Planet. Interior, 118: 13-27.
Su W.J., Dziewonski A.M., and Jeanloz R., 1996, Planet within a planet: rotation of the inner core of Earth, Science, 274: 1883-1887.
Tromp J., 2001, Inner-core anisotropy and rotation. Annu. Rev. Earth Planet. Sci., 29: 47-69.
Vidale J.E., Dodge D.A., and Earle P.S., 2000. Slow differential rotation of the Earth's inner core indicated by temporal changes in scattering. Nature, 405: 445-448.
Wahr J.M., 1981, The forced nutations of an elliptical, rotating, elastic and oceanless Earth. Geophys. J. R. Astron. Soc., 64: 705-727.

HIGH FREQUENCY NUTATIONS

P. M. MATHEWS
Department of Theoretical Physics, University of Madras
Guindy Campus, Chennai 600025, India
e-mail: mathews@imsc.ernet.in

P. BRETAGNON
Bureau des Longitudes URA 707 du CNRS,
77, Avenue Denfert-Rocherau, 75014 Paris, France
e-mail: pierre@bdl.fr

ABSTRACT. Expressions for the torques exerted by components of the tidal potential of any degree and order (n, m) are given and used to obtain the high frequency nutations excited, and the corresponding polar motions, as functions of frequency. Special features relating to different types of excitations are discussed, and a few examples of numerical results are shown.

1. INTRODUCTION

High frequency (HF) nutations are those with frequencies exceeding 0.5 cycles per sidereal day (cpsd). They appear in both prograde and retrograde diurnal, semidiurnal, $\cdots$ bands, which are bands of width 1 cpsd centered at ± 1, ± 2, $\cdots$, cpsd. They arise from the action of the tidal potential on geopotential coefficients $C_{l,k}, S_{l,k}$, with $k > 0$. Recent rigid Earth nutation series (e.g., Bretagnon et al. 1997, Roosbeek and Dehant, 1998, Souchay et al. 1999) include many diurnal and subdiurnal terms with coefficients up to ~ 15 μas in $\Delta\psi \sin\epsilon$ and $\Delta\epsilon$. Such nutations may no longer be ignored, since realistic uncertainties as low as 5 μas have already been attained in the estimation of many (low frequency) nutations: see Herring et al. (2001). A number of works focusing specifically on HF nutations have appeared more recently, e.g., Bretagnon (1999), and Roosbeek (1999) for the rigid Earth, Bizouard et al. (2000), Getino et al. (2001) and Brzeziński (2001) for the nonrigid Earth, and references therein. The Bizouard et al. (2000) results were obtained by applying (an early version of) the transfer function of Mathews et al. (2001) to the rigid Earth numbers from earlier works. This transfer function, constructed for the low frequency nutations, is not quite correct for HF nutations, but the differences are small in most cases, and the amplitudes of high frequency circular nutations are expected to be less than 20 μas. The numbers obtained by Getino et al. (2001) for semidiurnal nutations of the nonrigid Earth are consistent with the transfer function being essentially constant across the semidiurnal band; but the elementary physical reason for such a behaviour stays hidden behind the complexities of their Hamiltonian formalism. The treatment by Brzeziński (2001), while approximate, does offer useful insights.

We outline here a general treatment of HF nutations based on a generalization of the torque equations of Sasao et al. (1980) for the whole Earth and the fluid core. (Since amplitudes beyond about 20 μas are not expected, inner core effects and certain features of the more recent nutation theories, e.g., electromagnetic couplings, are ignorable when seeking an accuracy of 0.1 μas on the HF nutations.) Their expression for the torque is replaced by one appropriate to the potential that drives the nutations in the band of interest. Solution of the pair of coupled equations is elementary, once the torque is given. One sees almost trivially that the transfer function is essentially equal to the ratio of the moments of inertia of the whole Earth and the mantle for all HF nutations except for the prograde diurnals. The Chandler resonance is important in this exceptional case, which includes a secular wobble / polar motion term, as will be seen below.

2. WOBBLE, NUTATION, AND POLAR MOTION: KINEMATICAL RELATIONS

The complex nutation variable $\tilde{\eta}(t)$ defined by

$$\tilde{\eta}(t) \equiv \Delta\psi(t) \sin\epsilon + i\Delta\epsilon(t), \tag{1}$$

is related to the mantle wobble variable $\tilde{m}(t)$:

$$i\frac{d\tilde{\eta}(t)}{dt} = \Omega_0\, \tilde{m}(t)\, e^{i\Omega_0 t}, \tag{2}$$

with $\tilde{m}(t) = m_1(t) + i\, m_2(t)$, where $\Omega_0\, m_1$ and $\Omega_0\, m_2$ are the equatorial components of the Earth's angular velocity vector $\mathbf{\Omega}$ in the terrestrial frame, Ω_0 being the mean angular velocity. The *kinematical relation* (2), which holds independently of the Earth's structure and deformability properties, implies the correspondence

$$\tilde{m}(t) = \tilde{m}(\sigma)e^{i\sigma\Omega_0 t} \quad \leftrightarrow \quad \tilde{\eta}(t) = \tilde{\eta}(\nu)e^{i\nu\Omega_0 t} = -\tilde{m}(\sigma)e^{i\nu\Omega_0 t}/(1+\sigma), \qquad (\nu = 1+\sigma), \tag{3}$$

between a wobble of frequency $\sigma\Omega_0$ (σ cpsd) and its associated nutation. The case $\sigma = -1$ is an exception: it leads to a secular variation of $\tilde{\eta}(t)$, namely, precession:

$$\tilde{\eta}(t) = -i\tilde{m}(-1)\, \Omega_0 t. \tag{4}$$

An unfamiliar situation wherein $\tilde{m}(t)$ is proportional to t will be encountered in this work. This behaviour occurs when the tidal potential (and hence the torque which drives the wobble) is of zero frequency, as will be seen later. In this case, one finds from equation (2) that

$$\tilde{m}(t) = i\Omega_0 K t \quad \leftrightarrow \quad \tilde{\eta}(t) = K(1 - i\Omega_0 t)e^{i\Omega_0 t}. \tag{5}$$

In the representation adopted by the IAU for the transformation between terrestrial and celestial reference frames, only the low frequency part of the motion of the terrestrial pole in space is considered as nutation, while the high frequency part is viewed as "polar motion", namely, the motion of the celestial pole in the terrestrial frame. Polar motion is represented by

$$\tilde{p}(t) \equiv x_p(t) - iy_p(t) = -\tilde{\eta}(t)e^{-i\Omega_0 t} \tag{6}.$$

3. DYNAMICS: THE TORQUE AND EQUATIONS OF MOTION

The Cartwright and Tayler (1971) tidal potential of type (n, m) with frequency ω is

$$V_\omega^{(n,m)}(\mathbf{r}; t) = g_e H_\omega^{(n,m)}\, (r/a_e)^n\, \mathrm{Re}\, [\, \zeta_{n,m} Y_n^m(\theta, \varphi)\, e^{i\omega t}\,], \tag{7a}$$

$$Y_n^m(\theta,\varphi) = N_{n,m}\, P_n^m(\cos\theta)\, e^{im\lambda}, \qquad N_{n,m} = \left(\frac{2n+1}{4\pi}\frac{(n-m)!}{(n+m)!}\right)^{1/2}, \tag{7b}$$

where a_e is the Earth's equatorial radius, $g_e = GM_E/a_e^2$ (M_E being the Earth's mass), and $H_\omega^{(n,m)}$ is the tide height. (An initial phase has been ignored; it can be easily restored.) The frequency ω is confined, for given m, to the interval

$$0 \le \omega < (1/2)\Omega_0, \quad (m=0); \quad \text{and} \qquad (m-1/2)\,\Omega_0 < \omega < (m+1/2)\,\Omega_0, \quad (m>0). \tag{8}$$

The factor $\zeta_{n,m}$ is so defined that the real part in (7a) yields a cosine or a sine as appropriate:

$$\zeta_{n,m} = 1, \quad (n-m) \quad \text{even}; \qquad \zeta_{n,m} = -i, \quad (n-m) \quad \text{odd}. \tag{9}$$

The *torque* exerted by $V_\omega^{(n,m)}$ on the Earth has both prograde and retrograde frequencies,

$$\omega_p = \sigma_p\Omega_0 \equiv \omega \qquad \text{and} \qquad \omega_r = \sigma_r\Omega_0 \equiv -\omega, \tag{10}$$

respectively. The orgin of the torques and of the wobbles and nutations that they produce, as displayed in Table 1, may be seen from the expressions given below for the complex combination $\tilde\Gamma_\omega^{(n,m)} \equiv (\Gamma_{\omega,1}^{(n,m)} + i\Gamma_{\omega,2}^{(n,m)})$ of the equatorial components of the torque.

Table 1. Origin of high- and low-frequency nutations

TGP of type	Acting on	Produces: Wobbles	Produces: Nutations	For
$(n,0)$	$(C_{n,1}, S_{n,1})$	Low Frequency	Pro Diurnal	$n>2$
$(n,1)$	$C_{n,0}$	Ret Diurnal	Low Frequency	$n\ge 2$
$(n,1)$	$(C_{n,2}, S_{n,2})$	Pro Diurnal	Pro Semidiurnal	$n\ge 2$
$(n,2)$	$(C_{n,1}, S_{n,1})$	Ret Semidiurnal	Ret Diurnal	$n>2$
$(n,2)$	$(C_{n,3}, S_{n,3})$	Pro Semidiurnal	Pro Terdiurnal	$n\ge 3$
$(n,3)$	$(C_{n,2}, S_{n,2})$	Ret Terdiurnal	Ret Semidiurnal	$n\ge 3$

$$\tilde\Gamma_\omega^{(n,m)}(t) = \tilde\Gamma^{(n,m)}(\sigma_p)\; e^{i\sigma_p\Omega_0 t} + \tilde\Gamma^{(n,m)}(\sigma_r)\; e^{i\sigma_r\Omega_0 t}, \tag{11}$$

$$\tilde\Gamma^{(n,m)}(\sigma_p) = (i\Omega_0^2\bar A)\;(-1)^{m+1}\, G_{n,m}^{(+)}\, H_\omega^{(n,m)}\,[\,\zeta_{n,m}\,(C_{n,m+1} + iS_{n,m+1})\,], \quad (0\le m<n), \tag{12a}$$

$$\tilde\Gamma^{(n,m)}(\sigma_r) = (i\Omega_0^2\bar A)\;(-1)^{m}\, G_{n,m}^{(-)}\, H_\omega^{(n,m)}\,[\,\zeta_{n,m}^*\,(C_{n,m-1} - iS_{n,m-1})\,], \quad (1\le m\le n), \tag{12b}$$

$$\tilde\Gamma^{(n,0)}(\sigma_r) = -(i\Omega_0^2\bar A)\, G_{n,0}^{(+)}\, H_\omega^{(n,0)}\, \zeta_{n,0}^*\,(C_{n,1} + iS_{n,1}), \tag{12c}$$

$$G_{n,m}^{(-)} = \left(\frac{2n+1}{4\pi}\frac{(n+m)!}{(n-m)!}\right)^{1/2} \frac{g_e M_E}{2(2-\delta_{m,1})\Omega_0^2\bar A}, \qquad G_{n,m}^{(+)} = (n-m)(n+m+1)G_{n,m}^{(-)}. \tag{13}$$

$\bar A \equiv (A+B)/2$ is the mean equatorial moment of inertia. The range of values of σ_p and σ_r for each (n,m) may be found from (10) and (8).

As in Sasao et al. (1980), the dynamical equations consist of the coupled equations for the wobble $\tilde m$ of the mantle and the differential wobble $\tilde m_f$ of the fluid core relative to the mantle:

$$\left(\frac{d}{dt} - ie\Omega_0\right)\tilde m(t) + \frac{1}{\bar A}\left(\frac{d}{dt} + i\Omega_0\right)[\tilde c_3(t) + \bar A_f\tilde m_f(t)] = \frac{\tilde\Gamma(t)}{\bar A\Omega_0}, \tag{14a}$$

$$\left(\frac{d}{dt} + i\Omega_0\,(1+e_f)\right)\tilde{m}_f + \frac{d}{dt}\left(\tilde{m} + \frac{\tilde{c}_3^f(t)}{\bar{A}_f}\right) = 0, \tag{14b}$$

wherein $\bar{A}_f$ is the mean equatorial moment of inertia of the fluid core, e, e_f are the dynamical ellipticities of the whole Earth and of the fluid core (e.g., $e = C/\bar{A} - 1$), and $\tilde{c}_3(t), \tilde{c}_3^f(t)$ are complex combinations, $\tilde{c}_3 \equiv c_{1,3} + ic_{2,3}$ and $\tilde{c}_3^f \equiv c_{1,3}^f + ic_{2,3}^f$ of the indicated elements of their respective inertia tensors. Triaxiality terms on the left hand side of eqs. (14) have been suppressed but will be considered in the context of prograde semidiurnal nutations excited by the (2,1) potential, to which they make marginal contributions.

These equations may be solved for prograde wobbles by taking $\tilde{\Gamma}(t)$ to be the $e^{i\sigma_p\Omega_0 t}$ term of (11) together with (12a), and for retrograde wobbles, using the other term of (11) with (12b) or (12c) depending on the value of m.

In going over to the frequency domain, we generalize the expressions of Sasao et al. (1980) for $\tilde{c}_3$ and $\tilde{c}_3^f$ to potentials of arbitrary types (n, m):

$$\tilde{c}_3 = \bar{A}\,[\kappa(\tilde{m} - \tilde{\phi}\delta_{n,2}\delta_{m,1}) + \xi\tilde{m}_f], \qquad \tilde{c}_3^f = \bar{A}_f\,[\,\gamma(\tilde{m} - \tilde{\phi}\delta_{n,2}\delta_{m,1}) + \beta\tilde{m}_f\,], \tag{15}$$

wherein $\tilde{\phi}$, which is a dimensionless equivalent of H_ω, and $\tilde{m}, \tilde{m}_f$, are all viewed as functions of σ. The $\tilde{\phi}$ terms represent the contributions to $\tilde{c}_3$ and $\tilde{c}_3^f$ from the deformation due to the *direct* action of the tidal potential; they vanish for prograde frequencies (there being no prograde tidal waves), and for all $(n, m) \neq (2, 1)$ excitations (because of the spherical harmonic structure of the displacement fields produced). The other terms are due to centrifugal perturbations which are of the $(2, 1)$ type. Each of the compliance (deformability) parameters κ, ξ, γ, and β has a small complex and frequency dependent part when the effects of mantle anelasticity and ocean tides on deformations of the solid Earth are taken into account (see Mathews et al. (2001)). The frequency domain equations obtained from eqs. (14) are then, for all wobbles except the retrograde ones due to $(2, 1)$ potentials,

$$[\,(\sigma - e) + (1+\sigma)\kappa\,]\,\tilde{m}(\sigma) + (1+\sigma)(\xi + \bar{A}_f/\bar{A})\,\tilde{m}_f(\sigma) = \tilde{\Gamma}(\sigma)/(i\bar{A}\Omega_0^2), \tag{16a}$$

$$(1+\gamma)\,\sigma\,\tilde{m}(\sigma) + [\,1 + e_f + (1+\beta)\sigma\,]\,\tilde{m}_f = 0, \tag{16b}$$

where $\tilde{\Gamma}(\sigma)$ is $\tilde{\Gamma}^{(n,m)}(\sigma_p)$ of eq. (12a) or $\tilde{\Gamma}^{(n,m)}(\sigma_r)$ of eq. (12b) or (12c) according as σ is chosen as σ_p or σ_r. The absence of the $\tilde{\phi}$ terms causes the transfer function corresponding to eqs. (16) to differ from the $(2, 1)$ case.

4. WOBBLES DUE TO POTENTIALS OF TYPE (n, m)

For $(n, m) \neq (2, 1)$

Solution of eqs. (16) is almost trivially done. One obtains

$$\tilde{m}(\sigma) = \frac{X(\sigma)}{D(\sigma)}\,\frac{\tilde{\Gamma}(\sigma)}{i\Omega_0^2 A}, \tag{17}$$

where $D(\sigma)$ is the determinant 2×2 matrix of coefficients in (16), and $X(\sigma)$ is the coefficient $[1 + e_f + (1+\beta)\sigma]$ of $\tilde{m}_f(\sigma)$ in the second equation. As is well known,

$$D(\sigma) = (\bar{A}_m/\bar{A})(\sigma - \sigma_1)(\sigma - \sigma_2), \tag{18}$$

where $\bar{A}_m$ is the mean equatorial moment of inertia of the mantle, and σ_1 and σ_2 are, respectively, the Chandler wobble (CW) and free core nutation (FCN) resonance frequencies in cpsd:

$$\sigma_1 = \frac{A}{A_m}(e - \kappa) \quad \text{and} \quad \sigma_2 = -1 - \frac{A}{A_m}(e_f - \beta) \tag{19}$$

Now, both σ_1 and $|\sigma_2+1|$ are about 2×10^{-3}. It is evident then from (17) and (18) that $\tilde{m}(\sigma)$ will have a Chandler resonance for excitation by zonal ($m=0$) potentials for which $-1/2<\sigma<1/2$. The FCN resonance occurs if σ is in the *retrograde* diurnal band ($-3/2<\sigma<-1/2$), but the corresponding nutations, being of *low* frequencies, are not considered here. In all but these two bands, σ is close to $+1$ or ±2 or $\pm3,\cdots$, and hence,

$$\sigma-\sigma_1\approx\sigma,\quad \sigma-\sigma_2\approx\sigma+1,\quad X(\sigma)\approx\sigma+1,\quad D(\sigma)\approx(\bar{A}_m/\bar{A})\,\sigma(\sigma+1). \tag{20}$$

The approximation obtained by substituting these in (17) differs from $\tilde{m}_R(\sigma)$ of the rigid Earth only by the factor (A/A_m); thus the *transfer function* $T(\sigma)$ is very close to the constant (A/A_m).

In the case of the *low frequency wobbles* and the associated *prograde diurnal nutations* excited by zonal potentials $(n,0)$ for $n>2$, the value of κ becomes important because of its role in the Chandler resonance. (The $(2,0)$ and $(2,2)$ potentials do not produce any equatorial torque.) The complex anelasticity contribution to κ, which is strongly frequency dependent in the low frequency tidal band, is very relevant here. Its evaluation for frequencies down to about 1/7000 cpsd may be done as in Mathews et al. (2001) where certain subtle points involved are discussed in detail. Here we focus on the special case of excitation by the *zero frequency* term present in $(n,0)$ potentials with n even. The secular (or "fluid limit") values of the compliances have to be used for this constant term; for κ, the value may be shown to be e. The frequency domain equations do not apply then because the time dependence of $\tilde{m}(t)$ and $\tilde{m}_f(t)$ is secular, not periodic. Going back to the time domain equations (14), one finds, with $\kappa=e$, that

$$\tilde{m}(t)=i\Omega_0\,Kt,\quad \tilde{m}_f(t)=-K,\quad \text{with}\quad K=(A/A_m)K_R,\quad K_R=\tilde{\Gamma}(0)/(i\Omega_0^2A). \tag{21}$$

The solution $\tilde{m}_R$ for a *rigid* Earth is quite different, being just constant: $\tilde{m}_R=(K_R/e)$.

For prograde diurnal wobbles due to potentials of type $(2,1)$

Triaxiality terms which enter through the angular momenta $\mathbf{H}$ and $\mathbf{H}_f$ of the Earth and its fluid core are relevant here. They contribute the additional terms $-Z(d/dt+i\Omega_0)\tilde{m}^*$ to the left hand member of eq. (14a) and $-Z_f\,d(\tilde{m}^*+\tilde{m}_f^*)/dt$ to that of eq. (14b), where

$$Z=(B-A)e^{2i\alpha}/(2\bar{A})=(2M_Ea_e^2/\bar{A})(C_{2,2}+iS_{2,2})\quad\text{and}\quad Z_f=(B_f-A_f)e^{2i\alpha_f}/(2\bar{A}_f), \tag{22}$$

where $\alpha\approx-15^\circ$ is the longitude of the minor equatorial principal axis, and quantities with subscripts f pertain to the core. In the absence of any reliable estimate for the triaxiality of the core, we assume its order of magnitude to be no larger than that of the whole Earth, and take $\alpha_f=\alpha$. The frequency domain equations for the prograde wobbles may then be seen to be

$$[\,(\sigma_p-e)+(1+\sigma_p)\kappa\,]\,\tilde{m}(\sigma_p)+(1+\sigma_p)(\xi+\bar{A}_f/\bar{A})\,\tilde{m}_f(\sigma_p)=\tilde{\Gamma}^p/(i\bar{A}\Omega_0^2)+Z\tilde{m}^*(\sigma_r), \tag{23a}$$

$$(1+\gamma)\,\sigma_p\,\tilde{m}(\sigma_p)+[\,1+e_f+(1+\beta)\sigma_p\,]\,\tilde{m}_f(\sigma_p)=Z_f\sigma_p\tilde{m}^*(\sigma_r)+Z_f\sigma_p\tilde{m}^*(\sigma_r), \tag{23b}$$

where $\tilde{\Gamma}^p$ stands for (12a) with $(n,m)=(2,1)$: $\tilde{\Gamma}^p=(15/8\pi)^{1/2}(g_e\bar{A}/a_e^2)ZH_\omega^{(2,1)}$. Both $\tilde{m}^*(\sigma_r)$ and $\tilde{m}_f^*(\sigma_r)$ (with $\sigma_r=-\sigma_p$), which are the frequency domain versions of $\tilde{m}^*(t)$ and $\tilde{m}_f^*(t)$, are known from the well-studied theory of low frequency nutations associated with the *retrograde* diurnal wobbles (frequency σ_r); their contributions may be shown to be marginal in any case. Solution of eqs. (23) is straightforward.

5. NUTATIONS

Once the wobbles $\tilde{m}(\sigma)$ are determined for the desired frequency band, prograde or retrograde, the associated nutations are readily computed from eqs. (3) (or from (5) with K from

(21), in the special case $\sigma = 0$); and the polar motions may be obtained from (6). One finds from (1) and (6) that these alternative pictures are linked by the following relations among the coefficients of the sine and cosine parts (identified by superscripts s and c, respectively) of $\Delta\psi(t)$, $\Delta\epsilon(t)$, $x_p(t)$, and $y_p(t)$:

$$x_p^s = y_p^c = -\Delta\psi^s \sin\epsilon = \Delta\epsilon^c = \eta_I(\nu) \qquad -x_p^c = y_p^s = \Delta\psi^c \sin\epsilon = \Delta\epsilon^s = \eta_R(\nu), \tag{24}$$

where $\eta_R = \text{Re}\ \eta$, $\eta_I = \text{Im}\ \eta$. These relations hold for (prograde/retrograde) circular nutations, but not for the elliptical nutations obtained by combining the pair of nutations with frequencies ν and $-\nu$. For example, we find $(\Delta\psi^s, \Delta\psi^c, \Delta\epsilon^s, \Delta\epsilon^c)$ to be $(-34.2, -4.2, -1.7, 13.6)$ and $(0.6, -0.1, -0.0, -0.2)$ μas respectively, for the prograde and retrograde rigid Earth nutations (due to (3,0) and (3,2) potentials, respectively), of period 1.03505 day. They combine to give $(-34.8, -4, 3, -1.6, 13.4)$ μas for the elliptical nutation, in full agreement with the SMART series of Bretagnon et al. (1997). Our computations were based on the tidal amplitudes of Roosbeek (1996) and geopotential coefficients $C_{k,l}$ and $S_{k,l}$ listed in Bretagnon et al. (1997). The effect of the Chandler resonance is reflected in the amplitudes found for the pair of polar motion terms due to a single term of the (3,0) potential: For the +3231 day polar motion, $(x_p^s, y_p^s) = (-16.2, 1.8)$ μas for the nonrigid Earth and $(-9.5, 1.2)$ for the rigid; and for -3231 days, $(12.3, -1.6)$ and $(7.9, -1.0)$, respectively. The secular polar motion due to the constant term of the (4,0) tide is $(dx_p/dt, dy_p/dt) = (-3.8, -4.3)$ μas/yr.

Tables of nutations/polar motions, and details of the derivation of the expressions for the torque and of the treatment of low frequency polar motions will be presented elsewhere.

6. REFERENCES

Bizouard, C., M. Folgueira, and J. Souchay, 2000, Comparison of the short period rigid Earth nutation series, in *Proc. IAU Colloquium 178, "Polar motion: Historic and scientific problems"*, edited by S. Dick, D. McCarthy, and B. Luzum, ASP Conference Series, Vol. 208, pp. 613–617.

Bretagnon, P., 1999, Diurnal and subdiurnal nutations for a rigid Earth, in *Proc. Journées Systèmes de Référence Spatio-temporels 1998*, Paris Observatory, pp. 164–168.

Bretagnon, P., P. Rocher, and J-L. Simon, 1997, Theory of the rotation of the rigid Earth, *Astron. Astrophys.*, *319*, 305–317.

Brzeziński, A., 2001, Diurnal and semidiurnal terms of nutation: A simple theoretical model for a nonrigid Earth, in *Proc. Journées Systèmes de Référence Spatio-temporels 2000*, Paris Observatory, pp. 243–251.

Getino, J., J. M. Ferrandiz, and A. Escapa, 2001, Hamiltonian theory for the nonrigid Earth: Semidiurnal terms, *Astron. Astrophys.*, *370*, 330–341.

Mathews, P. M., T. A. Herring, and B. A. Buffett, 2001, Modeling of nutation-precession: New nutation series for nonrigid Earth, and Insights into the Earth's Interior, *J. Geophys. Res.*, in press.

Roosbeek, F., 1996, RATGP95: a harmonic development of the tide-generating potential using an analytical method, *Geophys. J. Int.*, *126*, 197–204.

Roosbeek, F., and Dehant, V., 1998, RDAN97: An analytical development of rigid Earth nutation series using the torque approach, *Celest. Mech.*, *70*, 215–253.

Roosbeek, F., 1999, Diurnal and subdiurnal terms in RDAN97 series, *Celest. Mech. Dyn. Astr.*, *74*, 243–252.

Souchay, J., B. Loysel, H, Kinoshita, and M. Folgueira, 1999, Corrections and new developments in rigid Earth nutation theory: III. final tables REN-2000 including crossed-nutation and spin-orbit coupling effects, Astron. Astrophys. Suppl. Ser., *135*, 111-131.

A COMPARATIVE ANALYSIS OF THE VLBI NUTATION SERIES

Z. MALKIN
Institute of Applied Astronomy RAS
nab. Kutuzova, 10, St.Petersburg 191187, Russia
e-mail: malkin@quasar.ipa.nw.ru

ABSTRACT. The paper presents results of investigation of systematic differences between VLBI nutation series AUSLIG, BKG, GSFC, IAA, USNO for period 1984–2001. It is found that rather large random and systematic differences exist between these series. In particular, systematic differences are found between nutation series obtained with CALC/SOLVE and OCCAM packages. In addition to the VLBI nutation series listed above, two combined EOP series EOP(IERS)C04 and NEOS for the same period were compared. Substantial random and systematic differences were found between these series, too. It is remarkable that these differences are small for epoch of VLBI sessions and increase between them. All series were also compared with the MHB2000 model.

1. INTRODUCTION

The goal of this paper is to make a preliminary comparison of the following VLBI series available in the IVS data base :

— 6 NEOS-A series (AUS, BKG1, BKG2, GSF, IAA, SPU1), 1993.3–2001.6;

— 5 "full series" (BKG1, BKG2, GSF, IAA, USN), 1984.0–2000.9.

AUS, IAA and SPU series are computed using various versions of the OCCAM package; BKG, GSF and USN series are obtained with CALC/SOLVE software.

In addition to these VLBI nutation series, two combined EOP series EOP(IERS)C04 and NEOS for a period 1984–2001 were compared.

All series were also compared with the MHB2000 model (version of May, 2001). Since this version is valid (in sense of interpolation of the FCN contribution for period 1979-2001.42, last points on the some plots below can be interpreted with caution due to errors of extrapolation.

2. NEOS-A SERIES

The mutual pair comparison of six VLBI nutation series obtained from processing of the NEOS-A observations (AUS, BKG1, BKG2, GSF, IAA, SPU1) has been performed. To make this comparison more strong, only epochs which are present in all series were selected for this analysis (unfortunately, only GSF and IAA series contain all NEOS-A data). As a result we have got 404 common epochs of 426 NEOS-A series observed during the period under consideration.

The result of comparison of the NEOS-A nutation series with the MHB nutation model is presented in Figure 1. One can see that all plots show some similar features. Evidently, this is a result of mismodelling the MHB2000, most probably one of the FCN components. On the

other hand, some dependence on software used can be also mentioned. Some details of the plot look similar for the series obtained with the same software.

Table 1: Annual term in differences between NEOS-A series.

	BKG1	BKG2	GSF	IAA	SPU1
			dPsi, μas		
AUS00001	150 ±41	140 ±41	166 ±37	24 ±44	52 ±43
BKG00001		18 ±38	31 ±34	174 ±42	99 ±41
BKG00002			29 ±35	163 ±42	89 ±40
GSF2001C				189 ±38	116 ±38
IAAO0106					75 ±44
			dEps, μas		
AUS00001	26 ±16	22 ±17	18 ±16	10 ±19	11 ±18
BKG00001		8 ±15	8 ±14	36 ±18	16 ±16
BKG00002			4 ±14	31 ±18	11 ±16
GSF2001C				28 ±17	9 ±15
IAAO0106					20 ±18

Differences between compared series were modelled as sum of linear trend and annual and semiannual terms. The trend parameters can be mainly explained by difference in TRF/CRF realizations used in various ACs. Analysis of seasonal terms may be more interesting. For example, Table 1 shows result of comparison of annual term in pair differences between six nutation series. One can see that differences between series obtained with the same software (GSF–BKG, AUS–IAA–SPU) are much smaller than differences between series obtained with different software. Obviously, this is an indication of systematic differences between two program packages or between ICRF-Ext.1 and individual CRF realizations that should be investigated more carefully to minimize their influence on the IVS combination.

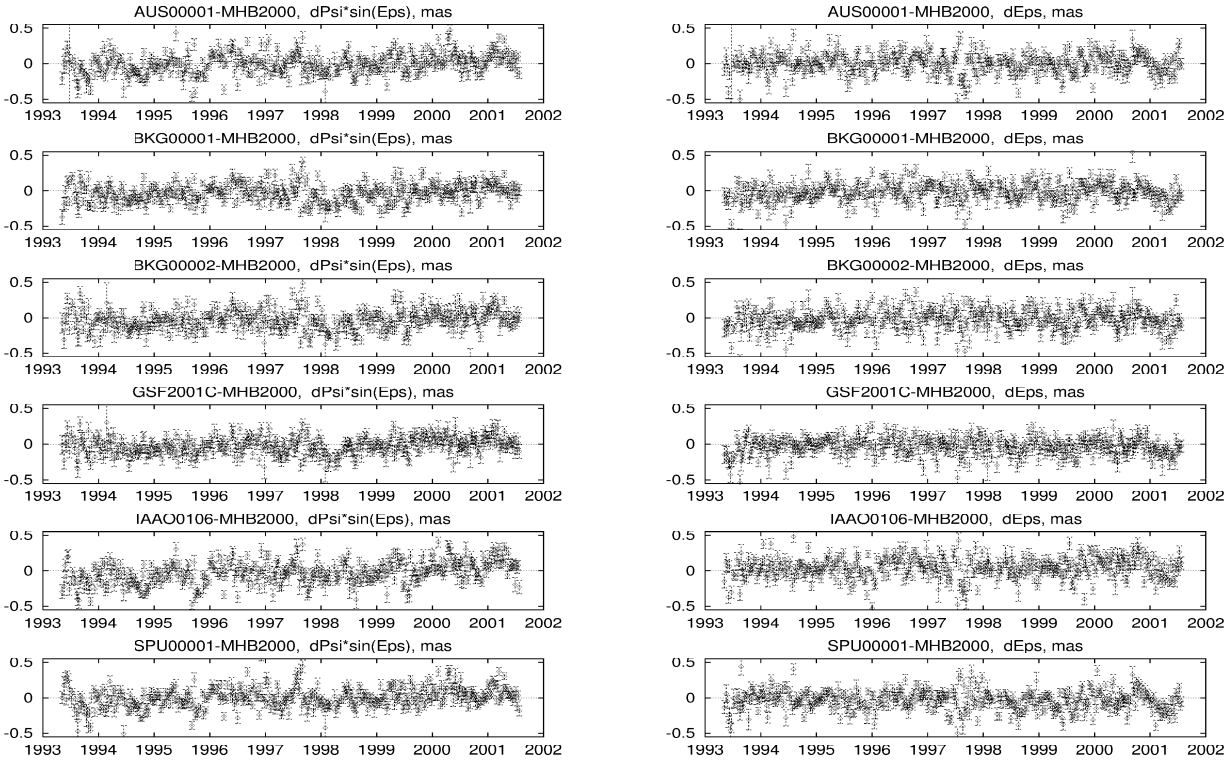

Figure 1: Differences between NEOS-A nutation series and the MHB2000 model.

3. FULL SERIES

Mutual comparison of five series (BKG1, BKG2, GSF, IAA, USN) obtained from various VLBI observing programs was made in analogous way as comparison of NEOS-A series. Again, we have chosen 1922 common epochs available in all compared series. Since there is only one full series (IAA) computed with OCCAM package, we did not compare dependence on software in detail, but it should be mentioned that seasonal term in differences between IAA and other series is much larger than in differences between the series obtained with CALC/SOLVE, which corresponds to data of Table 1.

Figure 2 shows dependence of formal error in nutation on number of observations used for computation of the nutation estimate. This dependence is very similar for all series. One can see that error does not decrease for number of observations greater than ≈2000.

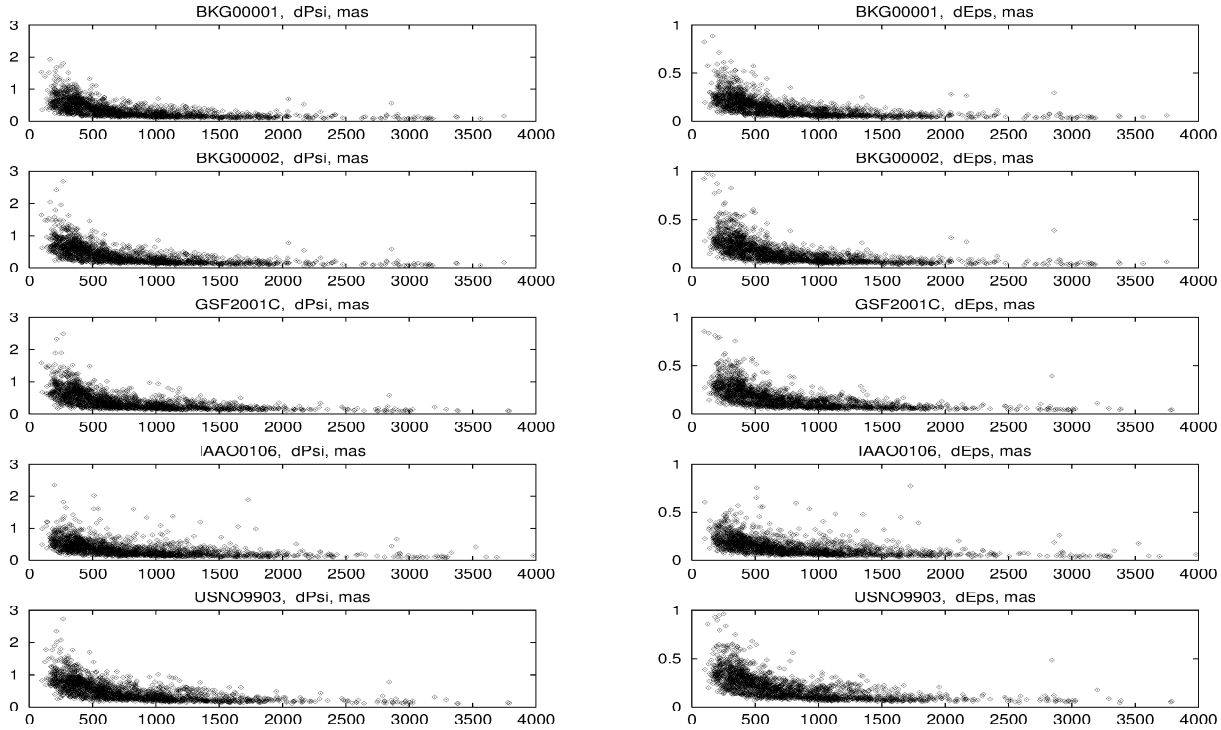

Figure 2: Dependence of formal error in nutation on number of observations.

The result of comparison of full series with the MHB2000 model is presented in Figure 3. Again, some similar details are present on all plots. Dependence on software is less evident than one for NEOS-A series. If we suppose that similar behavior of the differences between VLBI nutation series and the MHB2000 model are resulted from mismodelling, hopefully, this discrepancies can be eliminated with use more nutation series in adjustment of the model. On the other hand, these differences can be a result of some common error in the VLBI results, indeed.

4. COMBINED SERIES

Two combined series EOP(IERS)C04 and NEOS for the same period were also considered. The results are presented in Figure 4. Comparison with the MHB2000 model shows that NEOS

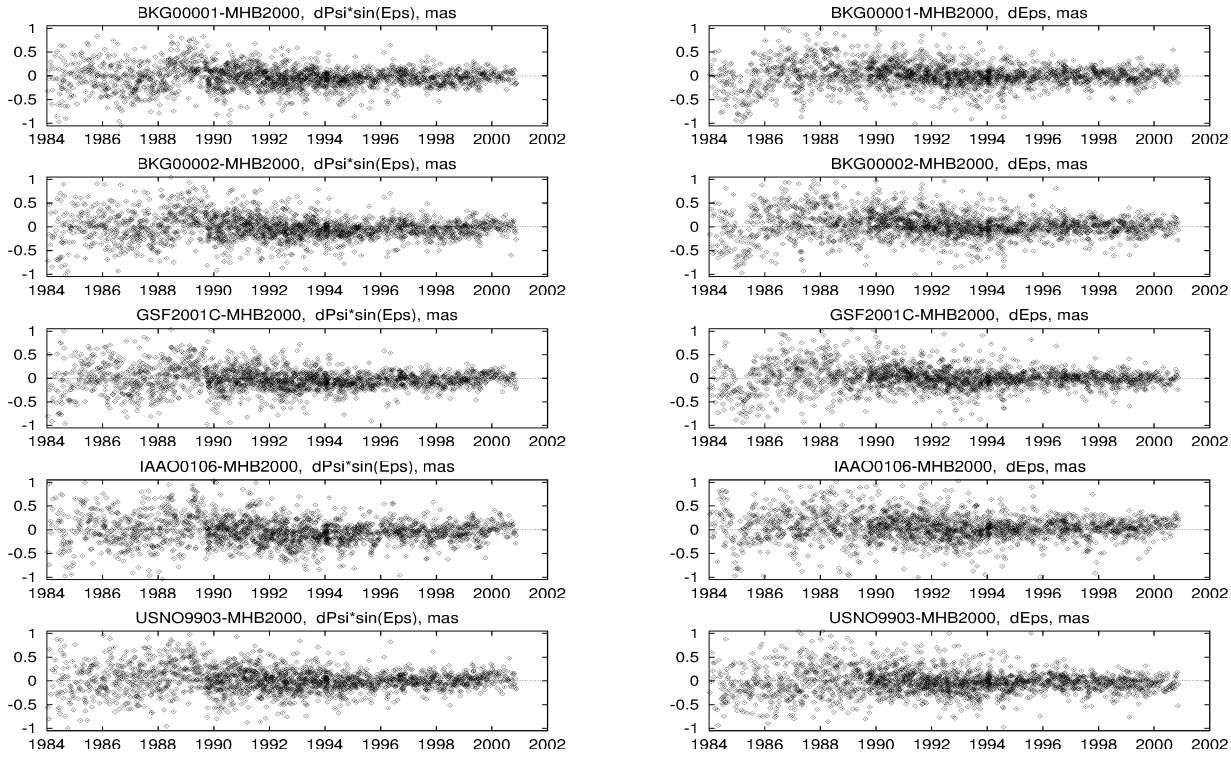

Figure 3: Differences between full nutation series and the MHB2000 model.

series is more consistent with the model It is also interesting that the C04 and NEOS series provide practically the same nutation values for epochs close to the NEOS-A observations and differ at interpolated epochs. This can be evidently explained by use of the IERS1996 model (which is still the official IERS model) during of computation of the C04 series.

5. FINAL REMARKS

It was also found (*e.g.* MacMillan & Ma, 2000, Sokolskaya & Skurikhina, 2000) that results of estimation of the nutation angles heavily depend on software used and network configuration. Table 2 summarizes the results obtained in these papers.

Dependence on network configuration means, in particular, that it may be rather difficult to obtain reliable estimate of principal nutation term with period 18.6 years because of replace of IRIS-A VLBI program by NEOS-A program which happened approximately in the middle of this nutation period.

Results of our investigations briefly described above show that rather large random and systematic differences exist between VLBI nutation (and not only nutation) series. Comparison of the nutation series derived from VLBI observations with the MHB2000 also shows significant systematic discrepancies common for all series. Time intervals where those are revealed often coincide with epochs of FCN or atmospheric disturbances found in (Fukushima & Shirai, 2001; Feissel *et al.*, 2001). Therefore, most of found systematic differences between the VLBI nutation series and MHB2000 maybe can be explained by mismodelling of the free core nutation contribution.

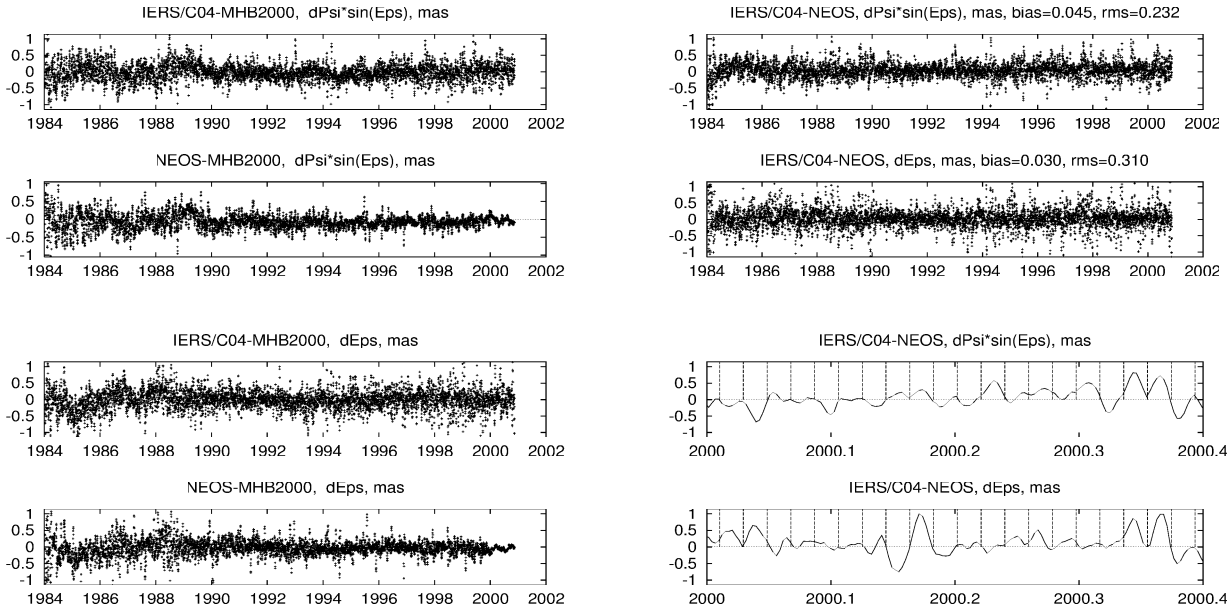

Figure 4: Differences between combined nutation series and comparison with the MHB2000 model. Differences C04-NEOS (on the right) are shown for whole period of comparison and for last several months to see more details. Vertical lines on the last two plots correspond to epochs of NEOS-A observations.

Table 2: NEOS-A – CORE-A differences, μas.

Software	CRS	EOP	Bias	σ_{NEOS}	σ_{CORE}	wrms
15 NEOS-A/CORE-A pairs with "nominal" set of stations						
ERA	IAA	$d\psi$	−180±297	367	325	1066
		$d\epsilon$	23±146	141	143	527
ERA	WGRF	$d\psi$	−88±269	367	305	967
		$d\epsilon$	−6±136	140	139	492
OCCAM	IAA	$d\psi$	186±116	200	202	412
		$d\epsilon$	−67±40	78	77	144
OCCAM	WGRF	$d\psi$	174±105	188	304	375
		$d\epsilon$	−107±33	72	120	119
CALC/ SOLVE	GSFC	$d\psi$	−242±60	202	172	265
		$d\epsilon$	90±23	82	64	109
63 NEOS-A/CORE-A pairs						
ERA	IAA	$d\psi$	249±129	375	320	978
		$d\epsilon$	−4±51	147	139	320
ERA	WGRF	$d\psi$	182±132	375	309	999
		$d\epsilon$	55±43	147	128	322
OCCAM	IAA	$d\psi$	166±60	261	247	455
		$d\epsilon$	13±23	95	90	174
OCCAM	WGRF	$d\psi$	186±63	258	267	485
		$d\epsilon$	9±25	94	103	193

3. REFERENCES

Fukushima, T., T. Shirai. Geophysical parameters estimated from VLBI nutation analysis. Journees 2001, Brussels, Belgium, Sep 24–26, 2001.

Feissel, M. *et al.* How much can we cheat the non-rigid Earth nutation theory to make it match VLBI results? Journees 2001, Brussels, Belgium, Sep 24–26, 2001.

MacMillan, D., C. Ma. Improvement of VLBI EOP Accuracy and Precision. In: N. R. Vandenberg, K. D. Baver (eds.), IVS 2000 General Meeting Proc., Koetzting, Germany, Feb 21–24, 2000, 247–251.

Sokolskaya, M. Ju., E. A. Skurikhina. Comparison of EOP Series Obtained from VLBI Observations. Trans. IAA, 2000, **5**, 45–57 (in Russian).

HOW MUCH MAY ONE "CHEAT" THE NON-RIGID EARTH NUTATION THEORY TO MAKE IT MATCH THE VLBI RESULTS?

M. FEISSEL
Observatoire de Paris (DANOF-UMR8630) and Institut Géographique National
61 Avenue de l'Observatoire, 75014 Paris (France)
e-mail: Feissel@ensg.ign.fr

O. DE VIRON, M. YSEBOODT, V. DEHANT,
Royal Observatory of Belgium
3, Avenue Circulaire, B-1180Brussels (Belgium)
e-mail: DeViron@oma.be; M.Yseboodt@oma.be; Veronique.Dehant@oma.be

C. BIZOUARD
Observatoire de Paris (DANOF-UMR8630)
61 Avenue de l'Observatoire, 75014 Paris (France)
e-mail: Christian.Bizouard@obspm.fr

ABSTRACT. Using comparisons of VLBI-observed precession and nutations with the MHB2000 model, we investigate the observed discrepancies under several viewpoints. Considering the internal consistency of the model, we show that frequencies of the free nutation modes are quite robust with respect to these discrepancies. We show that the variations in the atmospheric forcing of nutations associated with diurnal variations have amplitudes and dominant frequencies that vary with time. The possible contamination of VLBI results by apparent motions of the extragalactic radio sources may be a concern at low frequency, but stays small at the seasonal and free nutations frequencies.

1. INTRODUCTION

The variations of the orientation of Earth in space include the variations of the Earth rotation speed (length-of-day fluctuations), and the variations in the direction of the mean rotation axis in space (precession and nutations). Precession and nutations are mainly generated by the luni-solar attraction. The atmosphere and the ocean are responsible for time-varying excitations of some of the astronomical nutations. In addition, the fluid core and the solid inner core induce free nutation modes than can be excited and damped.

Observed precession and nutations are derived from Very Long Baseline Interferometry (VLBI) data. The VLBI observations are performed at stations whose positions are precisely known at the surface of the Earth (this includes taking account of plate tectonic motions and solid Earth tides). The VLBI data consist in delays between extra-galactical radio signal arrival times at the different stations. The Earth orientation parameters can be computed from these

measurements. The classical way to perform this computation is to consider that the celestial objects used to materialize the reference frame (International Celestial Reference Frame, ICRF) are fixed in space, and to use this fixed reference frame to observe the fluctuations of the Earth orientation in space.

Those VLBI-derived values are then compared with the output of theoretical models for precession and nutation, and the differences can be examined. In this paper, the reference nutation model is that derived by Mathews et al. (2001), referred to hereafter as MHB2000, that was adopted as the international conventional model by the International Astronomical Union in 2000.

The nutation models are built in three steps:

1. the precession/nutation for a rigid Earth is computed from astronomical considerations; these values deduced from high precision celestial ephemerides are known to better than a few (μas) microarcseconds;

2. a transfer function developed to account for the non-rigid Earth contributions is computed and convolved with the rigid Earth nutations; this transfer function involves physical properties of the Earth's interior, including resonance phenomena;

3. additionally, the effects of the external global geophysical fluids (atmosphere, ocean, hydrosphere) have to be considered; those effects include ocean tides, forcing by the atmosphere and hydrosphere, and ocean responding to the atmospheric forcing.

The VLBI-estimated nutation amplitudes and precession are then used to fit a few geophysical parameters in a physical nutation model. This modelling considers permanent internal effects, the S_1-atmospheric and oceanic influences being included through their mean values over the total span of VLBI observations (1980-2000). Such models give rise to residual discrepancies between theory and observation that are smaller than 100 μas (Mathews et al., 2001), while the statistical uncertainties of the VLBI-based parameters is of the order of 10 μas.

In order to check the robustness of the theory underlying the MHB2000 nutation model, we use the observed amplitude discrepancies for the largest nutation terms (18.6-year and annual) to perturb the model and investigate the stability of some geophysical parameters in the theory, namely the frequency of the Free Core Nutation (FCN) and of the Free Inner Core Nutation (FICN).

We study the effects of two possible causes for the observed discrepancies: (1) the variations in the atmospheric forcing (and potentially the oceanic forcing) of the nutations derived from actual observations (de Viron et al., 2001a, Yseboodt et al., 2001), and (2) the possible contamination of VLBI-derived nutation amplitudes by apparent motions of the extragalactic radio sources (Gontier et al., 2001).

2. HOW MUCH CAN ONE PERTURB THE NON-RIGID EARTH NUTATION THEORY AND STILL KEEP IT SELF-CONSISTENT?

The MHB2000 nutation theory is based on the fit of a physical model on the VLBI observed nutation amplitudes and phases, on the present knowledge of the Earth's interior, as well as on output of ocean tides models. The parameters of the Earth's interior appear in the nutation model through a transfer function that multiplies the rigid Earth nutation amplitudes. Except for the retrograde annual nutation, which period is close to the FCN resonance, the relative effect of the physical properties of the Earth's interior is small. Consequently, this effect can only be observed for the largest nutations, such as the semi-annual prograde and the 18.6-year ones, and for the retrograde annual nutation. We have thus tried to test how much the parameters of the

model would change and how well the theory would fit the VLBI results, taking into account revised atmospheric and oceanic effects. To investigate this effect we performed perturbation tests on the amplitudes of the largest nutation terms in MHB2000: applying the maximum and minimum corrections found in the analysis of the VLBI series described in section 4, we implemented the MHB2000 transfer function. We also added reasonable corrections accounting for the external fluid effects (see section 3) and tested the possible changes in the determined parameters. We considered the 13.6 days, the semi-annual, the annual and the 18.6 year prograde and retrograde nutations.

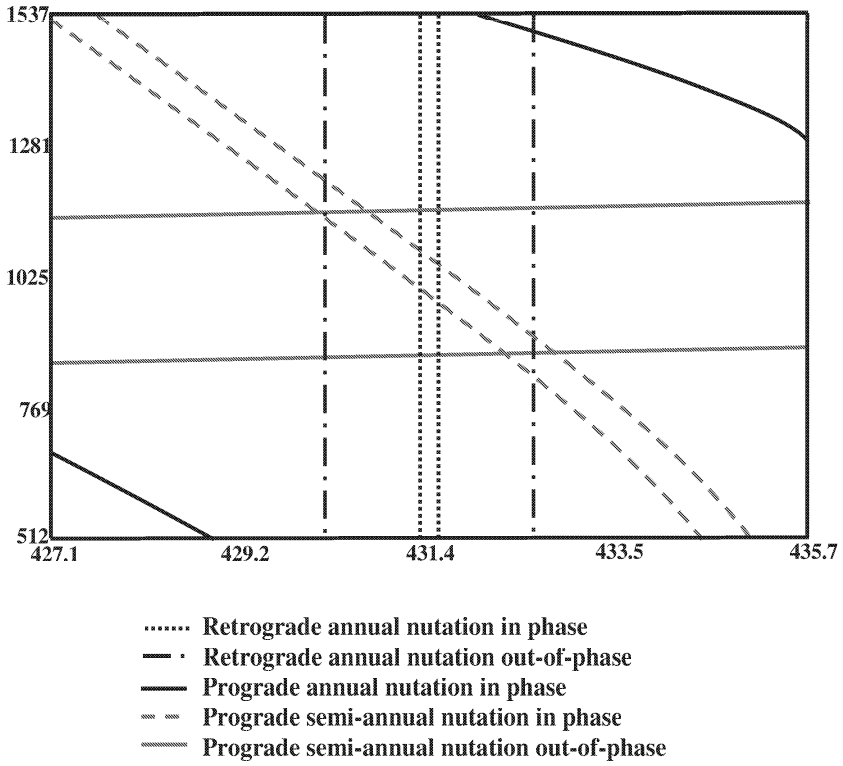

Figure 1: For each nutation, intervals in which the theoretical values of the FCN and FICN periods have values in agreement with the observed nutation; the intersection of all the intervals gives the solution for the periods of the FCN and FICN. Here the observations are assumed to be corrected for the atmospheric effects as computed by Yseboodt et al. (2001).

In figure 1, we show, for each considered nutation, the values for the periods of the FCN and FICN giving residuals smaller than the sum of the MHB2000 residuals and the maximum difference between the observed nutation series used in this paper, when the atmospheric effects are taken from Yseboodt et al. (2001). The intersection of those intervals corresponds to the values of the resonance period in agreement with the observed nutations at the required precision. The changes of the periods of free modes allowed by the results of our tests are very small with respect to MHB2000 and no change is still a solution. The constraints are quasi-exclusively given by the retrograde annual nutation and by the prograde semi-annual nutation. This is in perfect agreement with the qualitative discussion presented at the beginning of this section.

We also investigated the effect of unstability of the celestial reference frame studied in section 4. The results were very similar except for a small increase of the intervals of the possible resonance periods. These periods still remain very close to the MHB2000 values.

The corrections that are allowed are dictated by the precision and accuracy of the observation, the discrepancies between observation and theory, and the possible readjustment (within physical limits) of the fitted model. For the 18.6-year nutations and the semi-annual prograde nutation for instance, it is possible to accept changes by the theory at the few tens of μas level. For the retrograde annual nutation, it is possible to accept changes in the amplitude of about 80 μas, and still get the same values of the Earth interior parameters (at the 1-day level for the FCN and the 100-day level for the FICN).

3. EFFECTS OF ATMOSPHERIC VARIABILITY

The atmospheric angular momentum series, as provided by the IERS Special Bureau for the Atmosphere, are computed from several atmospheric global circulation models. They can be used to compute the atmospheric contributions to nutations. The most important contributions are on the annual prograde and retrograde components. At the prograde annual frequency, the forcing corresponds to the diurnal solar thermal effect on the atmosphere. At the retrograde annual term it corresponds to a seasonal modulation of the diurnal effect of the Sun, amplified by the resonance at the FCN frequency.

We used the wavelet analysis for studying the atmospheric excitation of the annual prograde and retrograde nutation, from the matter term and the wind term of the atmospheric angular momentum in a celestial reference frame. This is a complement to the study of Yseboodt et al. (2001). As shown in Yseboodt et al. (2001), the amplitude of the excitation is changing with time.

Dehant et al. (2002) show that the frequencies of the maximum excitation are not fixed at the S_1 and ψ_1 frequencies, but are changing with time. They find a range of about 30 days around the prograde annual frequency and about 100 days around the retrograde annual frequency. The time interval when the FCN amplitude is enhanced corresponds to atmospheric excitation with periods around the FCN period. Conversely, the observed retrograde annual amplitude is enhanced when the atmospheric excitation frequency is roughly annual. In the case of the prograde annual term, both the VLBI measurement and the estimate of the atmospheric excitation show stability with time.

4. VLBI ANALYSES OF PRECESSION AND NUTATION

As the modeling process considers only permanent or mean forcing, the comparison of VLBI results with the model is expected to exhibit signatures of time variable nutations, in particular at the annual frequency and at free modes frequencies, like the FCN and the FICN, with respective periods 430 days (retrograde) and 1025 days (prograde) in MHB2000. While the observed annual nutations are consistent in the mean with the MHB2000 ones, they show significant time variations around the mean. The time series of the FCN results show a distinct change in amplitude and phase in the late 1980's, changing from about 270 to 100 μas and less. The amplitude of the 1025-day term is of the order of 100 μas in the 1980's, and close to zero in the 1990's.

The first set of VLBI results that we consider are time series of the celestial pole offsets obtained by five analysis centres in global analyses covering 17 to 21 years (Table 1), that were submitted to the IERS in the recent years. The series of celestial pole offsets were analysed in the same conditions, looking on the one hand for differences in the low frequency terms (precession,

obliquity rate and 18.6-year term) and on the other hand for variable medium-frequency terms (annual and semi-annual forced nutation, 430d Free Core Nutation). In the following, we label "VLBI" the weighted mean of the results obtained from the analysis of the five series of $d\psi, d\epsilon$.

Table 1: The VLBI series of celestial pole offsets analysed

Institute	Series	Data span	No of points	Standard error (0.001")	Std. Dev. wrt MHB2000 (0.001")	No of sources
BKG	01 R 01	1984.0-2001.0	2273	0.19	0.22	578
GSFC	01 R 01	1980.0-2000.9	2696	0.27	0.23	552
IAA	01 R 01	1980.0-2001.2	2155	0.17	0.25	667
SHA	01 R 01	1980.0-2001.2	2735	0.24	0.23	675
USNO	99 R 03	1980.0-2001.0	2489	0.30	0.25	652

The second set of VLBI results that we consider are time series of source coordinates, estimated for each session in which the source was observed (Eubanks, 1999). The time variations of the right ascensions and declinations of 639 sources over 1980.0-1999.3 (150000 individual coordinates) are analysed by the least-square method to detect a possible contamination of the apparent celestial pole, either linear or with the main nutation periods. Would such signatures be found, additive corrections ΔCRF to the VLBI estimates of $d\psi, d\epsilon$ for the corresponding components might be considered.

The five time series of celestial pole offsets and the set of time series of source coordinates were analysed in parallel by the least-square method, over the same time intervals and with the same lists of unknown parameters, to determine linear and periodic corrections.

Table 2: Modeled and estimated values of trends in the celestial pole motion

Data	Precession corr. 0.001"/year		Obliquity rate 0.001"/year	
MHB2000	-2.997		-.255	
VLBI-MHB	.024	$\pm$ .002	.015	$\pm$ .002
ΔCRF	.010	$\pm$ .002	-.008	$\pm$ .001

Table 3: Modeled and estimated values of the 18.6-year nutation term. Unit: 0.001"

Span	Data	Prograde				Retrograde			
		In phase		Out of phase		In phase		Out of phase	
	MHB2000	-8024.775		1.433		-1180.459		-.105	
	MHB2000 residual	-.050	$\pm$ .027	.022	$\pm$ .026	-.038	$\pm$ .027	.072	$\pm$ .026
1980.0-2001.2	VLBI-MHB	-.028	$\pm$ .004	.021	$\pm$ .005	-.047	$\pm$ .005	.051	$\pm$ .003
1980.0-1999.3	ΔCRF	.029	$\pm$ .004	-.004	$\pm$ .005	.025	$\pm$ .004	-.006	$\pm$ .005

Table 2 gives the values of the precession correction and of the obliquity rate that are associated with the MHB2000 Nutation, the difference of the VLBI results with these reference values, and the estimated effect of source instability (ΔCRF). The latter is larger than 1/3 of the

VLBI correction. Applying it to the VLBI result would increase it in the case of the precession correction, and practically bring it to zero in the case of the obliquity rate.

Table 3 shows the results obtained for the 18.6-year term, with the addition of the "observed-model" residuals mentioned by Mathews et al. (2001). The discrepancies of the VLBI results with the MHB2000 values are statistically significant. The ΔCRF corrections are significant at the six-sigma level for the in phase components, and they have amplitudes comparable with the VLBI corrections (a factor of .3 to .6). The "ΔCRF" perturbations in the determination of time varying FICN, FCN or annual nutation were estimated to be smaller than 10 μas (Dehant et al., 2001)

5. CONCLUSION

We investigated several areas of possible perturbation in the observational and theoretical approaches. The study concentrated on the main forced terms (linear, 18.6-year, annual and semi-annual) and the free nutations of the fluid core and the solid inner core. The reference model used is MHB2000. The model of nutation has been shown to be very well constrained when considering the interior of the Earth. We determined precession and nutation corrections using five independent VLBI solutions. The amplitudes found are consistent among the analysis centres and with the MHB2000 values at the level of a few tens of μas. The perturbation due to instability of the radio sources was found to be negligible at the seasonal and free nutations periods. For the linear terms and the 18.6-year nutation, its amplitude (10-30 μas) is comparable to that of the observed discrepancies between VLBI results and the MHB2000 model. We have shown that significant time variations of the atmospheric excitation of nutations can be predicted, and are observed. The maximum of the energy of the atmosphere can even come very close to the Free Core Nutation Frequency. Near the FCN frequency, the response of the Earth gets amplified. This provides thus energy for explaining the changes in the free nutation amplitude observed by VLBI.

6. REFERENCES

Dehant, V., Feissel, M., de Viron, O., Ma, C., Yseboodt, M., Bizouard, C., 2002, "Possible causes perturbing the accurate modelling of nutation at the sub-milliarcsecond level. In preparation.

Eubanks, T.M., 1999, Private communication.

Gontier, A.-M., Le Bail, K., Feissel, M. and Eubanks, T.M., 2001, "Stability of the extra-galactic VLBI reference frame.", Astron. Astrophys. 375, 661.

Mathews, P.M., Herring, T.A., and Buffett, B.A., 2001, "Modeling of nutation-precession: new nutation series for nonrigid Earth, and insights into the Earth's interior, J. Geophys. Res., in press.

Yseboodt, M., de Viron, O., Chin, T.M., and Dehant, V., 2001, "Atmospheric excitation of the Earth nutation: Comparison of different atmospheric models.", J. Geophys. Res. (solid Earth), accepted.

COMBINATION OF GEODETIC TECHNIQUES TO DETERMINE THE EARTH ORIENTATION PARAMETERS

P. YAYA
DANOF/UMR8630-CNRS, Observatoire de Paris
61 avenue de l'Observatoire 75014 Paris - FRANCE
e-mail: philippe.yaya@obspm.fr

ABSTRACT. In the framework of the IERS Combination Research Centers, the Groupe de Recherche de Geodesie Spatiale (GRGS) from CNES has proposed to study the combination of five techniques (SLR, LLR, VLBI, GPS and DORIS) in order to obtain a global and homogeneous solution of the Earth Orientation Parameters (EOPs) : universal time UT1, pole motion and nutation corrections in longitude and obliquity, as well as stations coordinates. Advantages and inconvenient of three of these techniques (SLR,VLBI and GPS) are discused in terms of precision and resolution, and solutions for the EOPs are given. A combined solution is undertaken over three months and compared to the IERS products.

1. INTRODUCTION

Each geodetic technique has his own advantages and failings in the determination of precise geophysics parameters. Our motivation in this work is to exploit the benefit of each one of them to form the best possible combination to obtain precise parameters of the Earth rotation. In order to reach this goal, a preliminary work was undertaken last year. It concerned the comparison and the combination of Satellite Laser Ranging (SLR) and Very Long Baseline Interferometry (VLBI) (Yaya, 2000) over one month. The next step described in this paper consists in adding the Global Positioning System (GPS) technique, which now plays a significant role in the combination of individual series used to obtain IERS pole motion series. We also extend our time span to three months. For example, this has multiplied by four our number of VLBI session (from three to thirteen) and should give more reliable results.

2. DATA PROCESSING

2.1 Models and data

We adopt, as far as possible, the same models for all the techniques. They are either derived from GRSG GRIM5 gravity models or taken from IERS Conventions (McCarthy, 1996). With those environmental models, we will be able to process the distinct data, synthesized in figure 1.

SLR data come from Lageos1 and Lageos2 measurements. They can be found at CDDIS web site and range from 5 July 2000 to 26 September 2000. We analyzed approximately 2000 observations per week coming from about 30 stations, localised for the majority in the northern

hemisphere. The inherent bias coming from this unbalanced distribution should be solved by the combination.

For VLBI, we used all the "NEOS" data (USNO program) available between 1 July 2000 and 30 September 2000, *i.e.* thirteen principal 24-hour sessions, and four additionaly 24-hour sessions from the NASA "CORE" program. VLBI programs for Earth rotation are not continuously carried out, introducing problems for an optimum combination. The number of observations are about 1000 per session (half time less numerous than SLR observations) involving about 4 to 6 stations.

GPS data consist of about 700,000 observations (5 minute normal points) per week, from a main network of 40 stations collecting data from the 24 satellite constellation. The important number of GPS observation is able to compensate the relatively poor precision of the measurements.

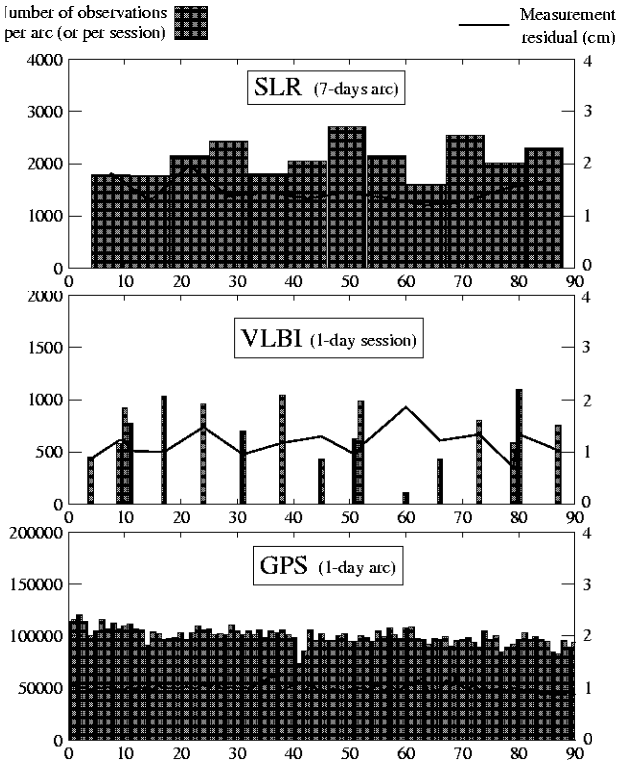

Figure 1: Number of observations and measurements residuals after GINS processing (abscissa : days from 1 July 2000)

2.2 Processing with GINS/DYNAMO software

GINS/DYNAMO was developed at CNES (the French spatial agency, in Toulouse) about twenty years ago. It was initially dedicated to earth satellite orbitography, giving also parameters related to gravity field, geophysics or Earth rotation. New routines have been implemented in the software in 1999 in order to process VLBI data (Meyer *et al.*, 2000). Although there is no

orbit integration for VLBI, the first results seemed to be encouraging in comparison with the JPL MODEST software.

Our software uses a classical least-square method to get the parameters, which are estimated by minimizing the differences (the residuals) between the observed and the calculated quantities. For satellite technique those quantities are the distances between a station and the satellite (in fact a time, changing in distance using a precise model of wave propagation). As for VLBI, the equivalent quantities are the time delays between two stations observing a same quasar.

The minimization of the residuals is done by GIN module, which finally gives a normal equation for each technique, with the partial derivatives of the parameters we want to solve for (orbital elements, as well as stochastic forces, tropospherics parameters, and, of course, the EOPs). The second module of our software, DYNAMO, is able to mix these equations, with a special weighting, to add new parameters if necessary, to reduce some of them, and to finally obtain the parameters we are interesting in, by inversion of the grouped normal equation.

3. RESULTS AND ANALYSIS

3.1 Processing results

The measurement residuals obtained by GINS module are shown in figure 1 for each technique, in comparison with the number of observations, showing some correlations between them, especially for VLBI where the number of observations is not as regular as the other technique.

The processing of SLR observations with GINS has proven itself for years at GRGS. The orbits residuals obtained for the 3-months period of this study have a root mean square (rms) of about 1.5cm for 7-day arcs, which is a common value for that kind of measurements.

As for VLBI, the usual value for the delay residuals rms - obtained with MODEST (JPL) or GLORIA (Gontier, 1992) - is about 40 picoseconds (ps) for a daily estimation. Our processing leads to the same value, between 30 and 60 ps, with a 40ps mean rms over the 3 months. We increased our precision by a factor 4, comparing to our last study (Yaya, 2000) thanks to a better estimation of tropospheric parameters (estimations each 2 hours). In figure 1 we convert our rms in distance value, multiplying them by the speed of light.

GPS has regular residuals during the test period : the range rms present a small variation around 1cm, which is a common number for range value. Our internal precision in then quite good. But the comparison of our orbits with IGS (International GPS Service) ones highlight clearly a lack of precision (about 10cm rms).

The three techniques present almost the same residuals, varying between 1 and 2 cm. This value is in accordance wih the precision we want to reach for the EOPs.

3.2 Results of EOPs estimates

Figure 2 compares, for each technique and for the combination, our daily series of pole motion and universal time with the reference IERS series EOPC04. SLR estimates present a usual rms *w.r.t* EOPC04 of 0.4 mas and no exageratted bias. For UT, we seem to detect a linear trend, althought satellite techniques are not adequate to estimate the Earth rotation rate (due to the correlation with the orbit node precession).

The GPS rms *w.r.t* EOPC04 is twice higher than those of other groups determining EOPs with GPS. It is surely due to the deficiency of precision in the orbits, as shown previously. This orbital trouble also probably causes the bias and trend in the estimates, especially for the Xp coordinate. We seems to observe a 2-months period signal in the Yp coordinate but further work need to be undertaken to confirm it. As SLR, GPS cannot precisely solve for UT1.

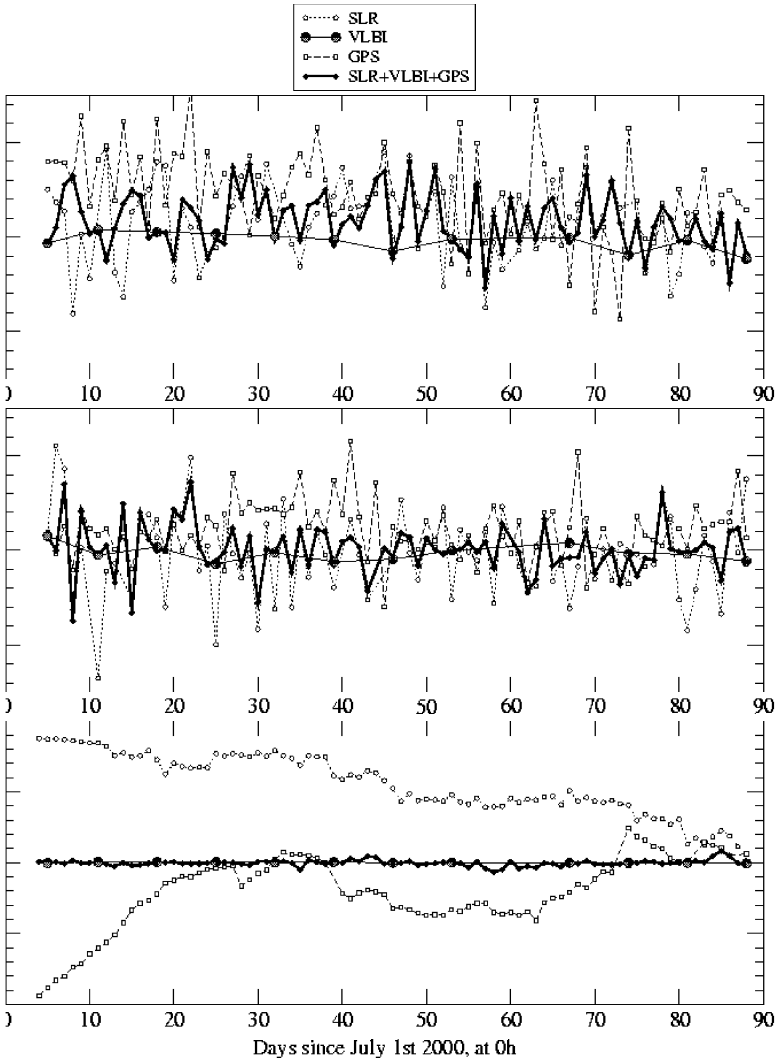

Figure 2: EOP differences between the IERS EOPC04 series and LAGEOS/VLBI solution series

Table 1: Comparison with EOP C04

		rms	bias	mean error
	SLR	0.45	0.12	0.14
Xp	VLBI	0.21	0.04	0.21
(mas)	GPS	0.47	0.49	0.08
	SLR+VLBI+GPS	**0.31**	**0.19**	**0.03**
	SLR	0.54	0.01	0.14
Yp	VLBI	0.16	-0.03	0.29
(mas)	GPS	0.37	0.22	0.08
	SLR+VLBI+GPS	**0.33**	**0.03**	**0.03**
UT	VLBI	0.17	0.02	0.14
(*0.1ms)	**SLR+VLBI+GPS**	**0.57**	**-0.14**	**0.03**

Concerning VLBI, the quality of the estimates are really excellent. The modelling of the measurement processing in GINS has been realized with success. Both pole coordinates and UT1 are determined with a great precision and a nice rightness. This is encouraging if we keep in mind that VLBI plays an important role in the IERS estimates of all EOPs, including nutation.

Finally, the results of the combination is shown in both table 1 and figure 2. We have applied a simple combination with the a-priori weights used in the GINS processing. DYNAMO software simply add the normal equation from each technique. The resulting series presents a stable (no bias) and a lower noise than the individual satellite series. Of course VLBI keeps its first rank due to its correspondance with a very-stable reference frame, but 7-days estimates introduce smoothness of the values.

4. CONCLUSION

This study has pointed out the advantage of combining VLBI to satellite techniques, such as GPS and SLR. The addition of other techniques like DORIS or LLR should improve our combination, or in the worst case would not introduce any regression of quality, as we just add some new measurements. The problem of weighting each technique with respect to others is a very important problem and will be our next step in our combination work. Nevertheless we could go further with the present data : for example, evaluate nutation will be a interesting test for VLBI goodness. We can also improve our final series quality with a combination processing of 24h and intensive VLBI sessions. Another way of study would be to estimate the stations positions, this could point out the problem of collocation, and maybe solve some of them. To conclude, our combination method seems to be very encouraging for the future and competitive in the framework of the Combination Research Centers studies.

6. REFERENCES

Gontier, A-M., 1992, PhD. at Paris Observatory "Earth Orientation by VLBI measurements"

Meyer, U., Charlot, P., Biancale, R., 2000, "GINS : a new multi-technique software for VLBI analysis", in IVS 2000 General Meeting Proceedings, Eds. N.R. Vandenberg and K.D. Baver, NASA/CP-2000-209893, p. 324-328

McCarthy D.D (ed.), 1996, IERS Conventions (1996), Observatoire de Paris

Shuygina, N.V., 1999, "Determination of the Earth Rotation Parameters from the Lageos SLR and VLBI data", in Actes des Journees 1999, p. 214-216

Yaya, P., 2000, "Comparison and combination of Lageos SLR and VLBI estimations for pole motion and universal time", in Actes des Journees 2000, p. 292-295

LUNISOLAR PERTURBATIONS IN EARTH ROTATION DUE TO THE TRIAXIAL FIGURE OF THE EARTH: GEOPHYSICAL ASPECTS

A. BRZEZIŃSKI[1] and N. CAPITAINE[2]

[1]Space Res. Centre, Polish Acad. of Sciences, Bartycka 18A, 00-716 Warsaw, Poland
e-mail: alek@cbk.waw.pl

[2]DANOF/UMR8630-CNRS
Observatoire de Paris, 61 avenue de l'Observatoire, 75014 Paris, France
e-mail: capitain@danof.obspm.fr

ABSTRACT. We derive an analytical solution for the lunisolar perturbations in polar motion and universal time due to the departures of the Earth's dynamical figure from the rotational symmetry. The underlying structural model of the Earth consists of two layers, an elastic mantle and a liquid core, which are not coupled to each other. We compute the parameters of the reference solution for the rigid Earth by using the satellite-determined coefficients of geopotential and the recent development of the tide generating potential. Finally, we estimate to which extent the amplitudes of perturbation can be modified by the contribution from the triaxiality of the core, on the basis of two different models of the core-mantle boundary shape.

1. INTRODUCTION

External lunisolar torque exerted on the triaxial figure of the Earth gives rise to small but not negligible, at a submilliarcsecond accuracy, variations in Earth rotation. The only components with amplitudes exceeding the level of 0.5 μas (microarcseconds) are the following:
– The prograde quasi-diurnal polar motion and quasi semidiurnal variations in the universal time UT1, corresponding to the $(2,2)$ component of the spherical harmonic expansion of geopotential. Here the label (l,j) means degree l and order j – see eq.(2) below.
– The long-periodic prograde and retrograde polar motion corresponding to the $(3,1)$ component of geopotential.
– Linear drift of the pole corresponding to the $(4,1)$ component of geopotential.

The first type of motion was described for the first time under the name "libration", because of "its generic similarity with the familiar libration of the Moon", and estimated by Chao *et al.* (1991), then corrected by Chao *et al.* (1996). This subject was later developed by Bretagnon (1998), Souchay *et al.* (1999), Brzeziński (2000; 2001), Bizouard *et al.* (2000; 2001), Getino *et al.* (2001), Molodensky and Groten (2001), Mathews and Bretagnon (this volume) and Escapa *et al.* (this volume). In part of these works the equatorial perturbation is considered as celestial motion, that is as prograde semidiurnal and diurnal nutation corresponding to prograde diurnal and long periodic polar motion, respectively. Here we apply the terrestrial representation, in agreement with the recently adopted definition of the Celestial Intermediate Pole (CIP); see (Brzeziński, 2001) for argumentation and (Brzeziński, 2000) for detailed description of the correspondence between the celestial and the terrestrial motion of the pole.

This paper is a continuation and an extension of the earlier works (Brzeziński, 2000; 2001) which were confined to the equatorial component of rotation. Here we derive also an analytical

solution for the spin component of rotation, expressed as variation of the universal time UT1. As before, we adopt a simple 2-layer model of the Earth comprising of an elastic mantle and a liquid core which are not coupled to each other. We compute the parameters of the reference solution for the rigid Earth by using the coefficients of the satellite-determined geopotential model JGM-3 recommended by the IERS Conventions (McCarthy, 1996) and of the recent development of the tide generating potential by Hartmann and Wenzel (1995). Finally, we estimate from the available models of the core-mantle boundary (CMB) shape to which extent our solution can be dependent on the triaxiality of the core.

2. DYNAMICAL MODEL

2.1. *Lunisolar torque on the triaxial Earth*

The torque $\vec{L}$ exerted on the Earth by the external point mass M_d (the Moon or the Sun) at the geocentric position $\vec{r}_d = (r_d \sin\theta_d \cos\lambda_d, r_d \sin\theta_d \sin\lambda_d, r_d \cos\theta_d)^T$, where r_d, θ_d, λ_d denote geocentric radius, co-latitude and longitude, can be evaluated as the negative of the torque on M_d due to the Earth, which yields the following expressions

$$L = L_1 + iL_2 = -i\, M_d \left(\frac{\partial U}{\partial \theta_d} + i \frac{\cos\theta_d}{\sin\theta_d} \frac{\partial U}{\partial \lambda_d} \right) e^{i\lambda_d}, \qquad L_3 = -M_d \frac{\partial U}{\partial \lambda_d}, \tag{1}$$

where $i = \sqrt{-1}$ denotes imaginary unit, $e^{i\lambda_d} = \cos\lambda_d + i \sin\lambda_d$ and U stands for the external gravitational potential of the Earth which can be conveniently expanded in spherical harmonics

$$U(\vec{r}) = \frac{GM}{r} \sum_{l=0}^{\infty} \sum_{j=0}^{l} \left(\frac{R_o}{r} \right)^l P_{lj}(\cos\theta)[C_{lj} \cos j\lambda + S_{lj} \sin j\lambda], \tag{2}$$

where M denotes the mass of the Earth, P_{lj} is the associated Legendre function of degree l and order j, and the (un-normalized) Stokes coefficients C_{lj}, S_{lj} are evaluated with reference to the radius of the Earth R_o (in the JGM-3 model the adopted value is $R_o = 6378136.3$ m).

The torque (1) can be expressed as an explicit function of time after using eq.(2) and taking into account the time dependence of r_d, θ_d, λ_d. The procedure developed by (McClure, 1974) yields the expressions involving coefficient of the tide generating potential $u(\vec{r})$

$$u(\vec{r}) = \frac{GM_d}{c_d} \sum_{l=2}^{\infty} \sum_{j=0}^{l} \left(\frac{r}{c_d} \right)^l P_{lj}(\cos\theta) \sum_s A_{ljs} \cos\left[\omega_{ljs} t + \beta_{ljs} + j\lambda + (l-j)\frac{\pi}{2} \right], \tag{3}$$

where c_d denotes the mean distance of the disturbing body and the potential is evaluated at the point with geocentric coordinates $\vec{r} = (r \sin\theta \cos\lambda, r \sin\theta \sin\lambda, r \cos\theta)^T$; see (Brzeziński, 2000) for description of the procedure. (Note that the available expansions of the tidal potential can use different normalizations

as that in eq.(3)). For a given degree l and order j the last summation extends over a set of the tidal frequencies ω_{ljs} (> 0) which are grouped around $j\Omega$, where Ω denotes mean value of the angular frequency of diurnal sidereal rotation. That is, for $j = 0, 1, 2, 3$ we have the long periodic, diurnal, semidiurnal and terdiurnal tides, respectively.

As it was argued by Chao *et al.* (1991), the nontrivial terms of the torque $\vec{L}$ start with degree $l = 2$ of geopotential U. The principal component of $\vec{L}$ is that expressing the retrograde quasi diurnal variation corresponding to the second degree zonal term U_{20}, which is responsible for the precession and long periodic nutation. This case will be not considered here because we are interested only in the effects associated with the triaxial structure of the Earth's inertia tensor, which in turn is expressed by the non-zonal terms U_{lj}, that is these corresponding to $j \neq 0$. Also the term U_{21} can be disregarded here because it vanishes if the terrestrial x_3-axis is aligned with the principal axis of inertia of the unperturbed Earth. Hence, the only second

degree term of geopotential expressing departures from the rotational symmetry of the Earth is the U_{22} term, and the corresponding torque will be considered later in details. Chao *et al.* (1991) neglected the higher degree terms of U because they are proportional to the powers of the factor R_o/r_d which is about 1/60 for the Moon and 1/23500 for the Sun, therefore diminish rapidly with l. This is true indeed but in case of the long periodic equatorial torques associated with the U_{31} and U_{41} terms of geopotential the resonant enhancement due to the proximity to the Chandler resonance can compensate the decrease of the torque magnitude. For this reason we will consider in Section 3 also the lunisolar equatorial torques associated with U_{31} and U_{41}.

2.2. *Lunisolar excitation of spin*

In the previous work (Brzeziński, 2001) we derived a solution for the lunisolar excitation of polar motion, associated with the triaxial figure of the Earth. Here we will perform a similar derivation for the spin component of rotation, expressed by the universal time UT1.

Assuming the sinusoidal axial torque on the elastic Earth

$$L_3 = L_{3,\sigma}\sin(\sigma t + \varphi_\sigma), \tag{4}$$

where $\sigma > 0, \varphi_\sigma$ denote the angular frequency and the phase of oscillation, we can derive the following solution for the observational quantity, the universal time

$$\Delta\mathrm{UT1} = \left(1 + \frac{4}{3}\frac{k_2}{k_s}\frac{C-A}{C}\right)^{-1}\frac{\kappa}{C\,\Omega}\iint L_3 dt^2 = \left(1 + \frac{4}{3}\frac{k_2}{k_s}\frac{C-A}{C}\right)^{-1}\frac{\kappa L_{3,\sigma}}{C\,\Omega\,\sigma^2}\sin(\sigma t + \varphi_\sigma + \pi), \tag{5}$$

where $\kappa = 0.997270$ is the conversion factor between the sidereal and solar time scales, C, A denote the principal axial and equatorial moments of inertia of the unperturbed Earth with assumed rotational symmetry, and $k_2 = 0.305$, $k_s = 0.94$ are the second degree tidal elastic and secular Love numbers. The factor in brackets accounting for the rotational deformations equals about 1.001 therefore has not important influence on the solution and will be disregarded here. Again, for the model of an elastic mantle and a liquid core which is not coupled to the mantle, the solution is obtained by replacing $L_{3,\sigma}, C$ by the mantle-referred counterparts $L^m_{3,\sigma}, C_m$. A final expression is

$$\Delta\mathrm{UT1} = \frac{\kappa L^m_{3,\sigma}}{C_m\Omega\,\sigma^2}\sin(\sigma t + \varphi_\sigma + \pi). \tag{6}$$

The corresponding solution $\Delta\mathrm{UT1}^r_\sigma$ for the rigid Earth which will serve us as reference for nonrigid Earth model, can be obtained by inserting in eq.(5) $k_2 = 0$.

3. SOLUTION FOR THE RIGID EARTH

In this section we will find explicit expressions for the lunisolar torques corresponding to particular terms of geopotential U, eq.(2), and for the corresponding perturbations in polar motion and UT1. We will also evaluate the amplitudes of the rigid-Earth solution by using the JGM-3 coefficients of geopotential and the tide-generating potential development of Hartmann and Wenzel (1995) referred to the standard epoch J2000.

3.1. *The (2,2) term of geopotential*

We find the following expression for the torque

$$L = 6\,\frac{GMM_dR_o^2}{c_d^3}\,D_{22}\sum_s A_{21s}e^{i\,(\omega_{21s}t+\beta_{21s}+2\lambda_{22})}, \tag{7a}$$

$$L_3 = -24\,\frac{GMM_dR_o^2}{c_d^3}\,D_{22}\sum_s A_{22s}\sin\left(\omega_{22s}t+\beta_{22s}+2\lambda_{22}\right), \tag{7b}$$

in which $C_{22} + iS_{22} = D_{22}(\cos 2\lambda_{22} + i\sin 2\lambda_{22}) = D_{22}e^{i2\lambda_{22}}$, and c_d denotes mean distance to the disturbing body; see (Brzeziński, 2001) for an interpretation of D_{22} and λ_{22}.

The corresponding solution for the rigid Earth, computed from equation (10) of Brzeziński (2001) and eq.(5) of this work with $k_2 = 0$, $\sigma_o = e\,\Omega$, $e = (C-A)/A$, takes the following form

$$p = -6\,\frac{GMM_dR_o^2}{c_d^3 A\,\Omega^2}\,D_{22}\sum_s \frac{A_{21s}e^{i\left(\omega_{21s}t+\beta_{21s}+2\lambda_{22}+\frac{\pi}{2}\right)}}{\left(\frac{\omega_{21s}}{\Omega}+1\right)\left(\frac{\omega_{21s}}{\Omega}-e\right)}, \tag{8a}$$

$$\Delta\mathrm{UT1} = 24\,\frac{\kappa GMM_dR_o^2}{c_d^3 C\,\Omega^3}\,D_{22}\sum_s \frac{A_{22s}\sin\left(\omega_{22s}t+\beta_{22s}+2\lambda_{22}\right)}{\left(\frac{\omega_{22s}}{\Omega}\right)^2}, \tag{8b}$$

As we mentioned in Sec. 2.1, $\omega_{21s} \approx \Omega$, $\omega_{22s} \approx 2\Omega$, therefore this solution express prograde quasi diurnal variation in polar motion p and quasi semidiurnal variation of UT1.

Table 1 and Table 2 give the amplitudes and phases of the largest terms of expansions (8a) and (8b), respectively. The convention applied for representing the arguments $\omega_s t + \beta_s$ as combination of the fundamental arguments is explained in Appendix.

Table 1: Prograde diurnal polar motion due to the action of the lunisolar tidal potential on the $(2,2)$ terms of geopotential, in (a) rigid Earth, (b) elastic Earth with rotationally symmetrical liquid core. Listed are all terms with amplitudes larger than 0.5 μas.

Fundamental arguments						Tidal wave			Polar motion			
l_m	l_s	F	D	$\hat{\Omega}$	$\hat{\Phi}$	Doodson number	Darwin symbol	Origin	Period day	Amp$^{(a)}$ μas	Amp$^{(b)}$ μas	Phase deg
−1	0	−2	0	−2	1	135.655	Q_1	M	1.119515	2.38	2.68	−120
0	0	−2	0	−1	1	145.545	⋯	M	1.075976	2.21	2.49	−120
0	0	−2	0	−2	1	145.555	O_1	M	1.075806	11.71	13.21	−120
−1	0	0	0	0	1	155.655	M_1	M	1.034719	0.87	0.98	60
0	0	−2	2	−2	1	163.555	P_1	S	1.002745	4.90	5.52	−120
0	0	0	0	0	1	165.555	K_1	M+S	0.997270	14.70	16.58	60
0	0	0	0	−1	1	165.565	⋯	M	0.997123	1.99	2.25	60
1	0	0	0	0	1	175.455	J_1	M	0.962437	0.78	0.88	60
Sum of all amplitudes > 0.01 μas (73 terms)										45.75	51.56	

Table 2: Semidiurnal variations of UT1 due to the action of the lunisolar tidal potential on the $(2,2)$ terms of geopotential, in (a) rigid Earth, (b) elastic Earth with rotationally symmetrical liquid core. Listed are all terms with amplitudes larger than 0.033 μs.

Fundamental arguments						Tidal wave			UT1			
l_m	l_s	F	D	$\hat{\Omega}$	$\hat{\Phi}$	Doodson number	Darwin symbol	Origin	Period day	Amp$^{(a)}$ 0.1μs	Amp$^{(b)}$ 0.1μs	Phase deg
−2	0	−2	0	−2	2	235.755	$2N_2$	M	0.537724	0.49	0.55	−30
0	0	−2	−2	−2	2	237.555	μ_2	M	0.536323	0.59	0.66	−30
−1	0	−2	0	−2	2	245.655	N_2	M	0.527431	3.56	4.01	−30
1	0	−2	−2	−2	2	247.455	ν_2	M	0.526084	0.67	0.76	−30
0	0	−2	0	−1	2	255.545	⋯	M	0.517564	0.67	0.75	150
0	0	−2	0	−2	2	255.555	M_2	M	0.517525	17.89	20.19	−30
1	0	−2	0	−2	2	265.455	L_2	M	0.507984	0.49	0.55	150
0	−1	−2	2	−2	2	272.556	T_2	S	0.500685	0.45	0.51	−30
0	0	−2	2	−2	2	273.555	S_2	S	0.500000	7.76	8.75	−30
0	0	0	0	0	2	275.555	K_2	M+S	0.498635	2.10	2.37	−30
0	0	0	0	−1	2	275.565	⋯	M	0.498598	0.63	0.71	−30
Sum of all amplitudes > 0.00067 μs (68 terms)										37.14	41.91	

Table 3: Long periodic polar motion due to the action of the lunisolar tidal potential on the $(3,1)$ terms of geopotential, in (a) rigid Earth, (b) elastic Earth with rotationally symmetrical liquid core. Listed are the terms with amplitudes larger than 0.5 μas.

Fundamental arguments						Tide	Polar motion					
						Doodson		Prograde			Retrograde		
l_m	l_s	F	D	$\hat{\Omega}$	$\hat{\Phi}$	number	Period day	Am.$^{(a)}$ μas	Am.$^{(b)}$ μas	Ph. deg	Am.$^{(a)}$ μas	Am.$^{(b)}$ μas	Ph. deg
-1	0	1	0	1	0	055.655	3231.50	9.62	16.21	-83	7.98	12.38	97
-1	0	1	0	0	0	055.665	2190.35	1.62	2.79	-83	1.22	1.87	97
0	0	1	-1	1	0	056.555	365.242	0.88	-1.28	-83	0.08	0.11	97
1	0	1	-2	1	0	057.455	193.560	2.84	2.10	97	0.64	0.81	97
0	0	1	0	2	0	065.545	27.4318	0.79	0.87	-83	0.71	0.82	-83
0	0	1	0	1	0	065.555	27.3216	15.28	16.75	97	13.72	15.88	97
0	0	1	0	0	0	065.565	27.2122	2.40	2.63	97	2.16	2.50	97
1	0	1	0	1	0	075.455	13.7188	1.16	1.29	97	1.22	1.40	97
Sum of all amplitudes > 0.01 μas (72 terms)								39.96	51.34		31.13	39.93	

3.2. *The (3,1) term of geopotential*

We find the following expression for the equatorial torque

$$L = i\,6\,\frac{GMM_dR_o^3}{c_d^4}\,D_{31}e^{i\lambda_{31}}\sum_s A_{30s}\sin\left(\omega_{30s}t+\beta_{30m}\right). \tag{9}$$

where $C_{31}+iS_{31}=D_{31}e^{i\lambda_{31}}$. The axial torque corresponding to U_{31} is not shown here because its amplitudes are below the adopted truncation level of 0.5 μas. As $|\omega_{30s}| \ll \Omega$, eq.(9) expresses the long periodic motion along the line of longitude $\lambda_{31}+\pi/2$.

The solution for polar motion of the rigid Earth is derived after applying the decomposition $i\sin\alpha = \left(e^{i\alpha}-e^{-i\alpha}\right)/2$ and using eq.(10) of Brzeziński (2001) with $k_2=0$, $\sigma_o = e\Omega$

$$p = 3\,\frac{GMM_dR_o^3}{c_d^4 A\,\Omega^2}\,D_{31}\sum_s\left[\frac{A_{30s}e^{i\left(\omega_{30s}t+\beta_{30s}+\lambda_{31}+\frac{\pi}{2}\right)}}{\left(\frac{\omega_{30s}}{\Omega}+1\right)\left(\frac{\omega_{30s}}{\Omega}-e\right)}+\frac{A_{30s}e^{-i\left(\omega_{30s}t+\beta_{30s}-\lambda_{31}-\frac{\pi}{2}\right)}}{\left(-\frac{\omega_{30s}}{\Omega}+1\right)\left(\frac{\omega_{30s}}{\Omega}+e\right)}\right]. \tag{10}$$

The amplitudes and phases of the largest terms of solution (10) are given in Table 3, while the underlying convention for expressing the arguments is described in Appendix.

For a given s the prograde and retrograde amplitudes are of similar size, at least for the most significant terms, therefore the corresponding constituent of the solution expresses the low frequency, highly elliptical motion of the pole.

3.2. *The (4,1) term of geopotential*

We find the following expression for the equatorial torque

$$L = -i\,10\,\frac{GMM_dR_o^4}{c_d^5}\,D_{41}e^{i\lambda_{41}}\sum_s A_{40s}\cos\left(\omega_{40s}t+\beta_{40s}\right). \tag{11}$$

where $C_{41}+iS_{41}=D_{41}e^{i\lambda_{41}}$. As in the case of the $(3,1)$ torque, we have the linear motion along the line of longitude $\lambda_{41}-\pi/2$.

An interesting feature of the corresponding solution for polar motion, first pointed out by Mathews (2000, presentation at the seminar of the Paris Observatory; see also his paper with Bretagnon in the present volume), is associated with the fact that this expansion contains a term for which $\omega_{s_o}t+\beta_{s_o}=0$, that is the constant torque

$$L_o = 10\,\frac{GMM_dR_o^4}{c_d^5}\,D_{41}e^{i\left(\lambda_{41}-\frac{\pi}{2}\right)}A_{s_o}. \tag{12}$$

The corresponding solution for the rigid Earth is a constant displacement of the pole

$$p_o = \frac{i\,L_o}{(C-A)\,\Omega^2} = 10\,\frac{GMM_dR_o^4}{(C-A)\,\Omega^2 c_d^5}\,D_{41}e^{i\lambda_{41}}A_{s_o}, \tag{13}$$

and in case of the elastic Earth a linear drift of the pole with

$$\dot{p}_o = \frac{L_o}{C\Omega} = 10\,\frac{GMM_dR_o^4}{C\Omega c_d^5}\,D_{41}e^{i\left(\lambda_{41}-\frac{\pi}{2}\right)}A_{s_o}; \tag{14}$$

see eq.(14) of Brzeziński (2001). Substitution yields $p_o = 0.67 \times e^{i\,221.5^o}\,\mu$as and $\dot{p}_o = 5.07 \times e^{i\,131.5^o}\,\mu$as/yr.

If we assume that the mantle is not coupled to the core, the drift increases by the factor of $C/C_m = 1.128$, which yields $\dot{p}_o = 5.72 \times e^{i\,131.5^o}\,\mu$as/yr. The drift is by almost 3 orders of magnitude smaller and has approximately opposite direction than the observed secular motion of the pole.

The solution for the periodical part of the torque can be derived in a similar way as that in the case $(3,1)$. We disregard this solution here because its largest term with period of 18.6 years has an amplitude of about 0.3 μas while other amplitudes do not exceed 0.03 μas.

4. MODELING THE RESPONSE OF NONRIGID EARTH

Eq.(11) of Brzeziński (2001) yields the following transfer coefficient between the periodical solution for the rigid Earth and that corresponding to the actual 2-layer model

$$\frac{p_\sigma}{p_\sigma^r} = \frac{\sigma-\sigma_r}{\sigma-\sigma_c}\,\frac{A}{A_m}\,\frac{L_\sigma^m}{L_\sigma}. \tag{15}$$

where we replaced $1+\frac{k_2}{k_s}e_m \approx 1.001$ by 1. In case of the prograde diurnal polar motion considered in Section 3.1, $\sigma \approx \Omega$ and the last expression can be further simplified by noting that the factor $(\sigma-\sigma_r)/(\sigma-\sigma_c)$ does not differ from 1 by more than about 1×10^{-3}.

The corresponding transfer coefficient for the spin component of Earth rotation is

$$\frac{\Delta\mathrm{UT1}_\sigma}{\Delta\mathrm{UT1}_\sigma^r} = \frac{C}{C_m}\,\frac{L_{3,\sigma}^m}{L_{3,\sigma}}. \tag{16}$$

In the transfer coefficients, equations (15) and (16), the factors $(\sigma-\sigma_r)/(\sigma-\sigma_c)$, A/A_m and C/C_m are known to the accuracy of the order of 1×10^{-3} or higher. Only the last factors, L^m/L, depending on the contribution to C_{lj}, S_{lj} from the core are largely uncertain. The usual assumption is the rotational symmetry of the core, which yields $L^m/L = 1$; see column (b) in Tables 1 to 3. In general case, however, there can be a non-negligible contribution to the observed Stokes coefficients from the triaxial shape of the core. We will describe here how this contribution can be estimated from geophysical models of the core-mantle boundary (CMB) shape, and compute its value from the available expansions of the CMB relief.

If the lateral heterogeneity of the CMB is expanded in spherical harmonics

$$\Delta r_{CMB}(\theta,\lambda) = \sum_{l=2}^{\infty}\sum_{j=0}^{l} P_{lj}(\cos\theta)[\Delta r_{lj}^c \cos j\lambda + \Delta r_{lj}^s \sin j\lambda], \tag{17}$$

the corresponding contribution to the Stokes coefficients from the core is

$$\Delta\begin{Bmatrix} C_{lj} \\ S_{lj} \end{Bmatrix} = \left[2.3 \times 10^6 (2l+1) 1.82^{(l+2)}\right]^{-1} \begin{Bmatrix} \Delta r_{lj}^c \\ \Delta r_{lj}^s \end{Bmatrix}, \tag{18}$$

Table 4: Contribution of the triaxial shape of the core to the Stokes coefficients, corresponding to the model of Defraigne *et al.* (1996) and of Morelli and Dziewonski (1987) (denoted DDW96, MD87).

degree	order	Model	CMB anomaly (metres)				Geopotential $\times 10^6$		JGM-3 values $\times 10^6$	
l	j		Δr^c_{lj}	σ	Δr^s_{lj}	σ	ΔC_{lj}	ΔS_{lj}	C_{lj}	S_{lj}
2	2	DDW96	309		−153		2.45	−1.21	1.5745	−0.9039
		MD87	187	±130	0	±130	1.48	0.0		
3	1	DDW96	152		−41		0.47	−0.13	2.1928	0.2680
		MD87	324	±225	−43	±225	1.01	−0.13		
4	1	DDW96	87		10		0.12	0.01	−0.5087	−0.4495
		MD87	209	±200	342	±190	0.28	0.05		

(Lambeck, 1988), where Δr should be expressed in metres.

We compute the numerical values corresponding to two different models of the CMB relief. The first one is that estimated from the inversion of travel-time residuals of waves reflected from and transmitted through the CMB, by Morelli and Dziewonski (1987). The second model is that corresponding to the mantle circulation theory developed by Defraigne *et al.* (1996). These two sets of estimates are compared in Table 4 to each other and to the satellite-determined values of the Stokes coefficients.

5. CONCLUSIONS

The lunisolar torque exerted on the triaxial figure of the Earth gives rise to minor, but not negligible at a submilliarcsecond accuracy, variations in both the equatorial component of Earth rotation (polar motion) and the axial component (UT1). We derived here an analytical solution for a simple model of the Earth comprising an elastic mantle and a liquid core, and taking into account all components of geopotential for which the corresponding effect exceeds the level of 0.5 μas. The amplitudes of the solution are proportional to the Stokes coefficients expressing triaxial figure of the Earth, namely these of degree/order of 2/2 for prograde diurnal polar motion and semidiurnal variation of UT1, and of 3/1, 4/1 for long periodic polar motion. The rigid Earth amplitudes which have been estimated here using the coefficients of the tide generating potential (Tables 1 to 3) are consistent at the submicroarcsecond level with previous results (Brzeziński, 2000) derived from the REN-2000 nutation theory of Souchay *et al.* (1999).

For the actual dynamical model of Earth rotation which assumes that the mantle is not coupled to the core, we should subtract from the satellite-determined values of the Stokes coefficients the contribution from the liquid core. This contribution depends on the shape of the core-mantle boundary which is known only from geophysical models. Our estimate based on

two different models of the CMB relief (Table 4) indicate that the contribution from the core can be of the same order as the total observed effect, but so far its estimate is largely uncertain.

Our investigations show that constraining the amplitudes of the lunisolar waves from the observations of polar motion and UT1 provides a direct mean for measuring the large-scale features of the CMB. However, prior to this we should remove from observations the oceanic and atmospheric perturbations with similar frequencies (Brzeziński, 2000), which have still too large uncertainties.

APPENDIX: Convention applied in Tables 1 to 3

High frequency polar motion $$\Delta p = \Delta x_p - i\Delta y_p = \sum_s a_s e^{i(\varphi_s+\pi)} e^{i\gamma_s(t)},$$

low frequency polar motion $$\Delta p = \Delta x_p - i\Delta y_p = \sum_s \left[a_s^+ e^{i(\varphi_s^+ +\pi)} e^{i\gamma_s(t)} + a_s^- e^{i(\varphi_s^- +\pi)} e^{-i\gamma_s(t)} \right],$$

universal time $$\Delta \mathrm{UT1} = \sum_s a_s \sin\left[\gamma_s(t) + \varphi_s\right].$$

where a_s, φ_s denote the amplitude and phase with the superscript $+/-$ labelling the prograde/retrograde term. The argument $\gamma_s(t) = \omega_s t + \beta_s$, in which ω_s denotes the angular frequency and $\beta_s(t)$ a quasi-constant phase - cf. eq.(3), is expressed using Woolard convention

$$\gamma_s(t) = k_1 l_m + k_2 l_s + k_3 F + k_4 D + k_5 \hat{\Omega} + k_6 \hat{\Phi}$$

in which l_m, l_s, F, D, $\hat{\Omega}$ denote the so-called "fundamental arguments", $\hat{\Phi} = \mathrm{GMST} + \pi$ and $k_1, \ldots, k_6$ are integer numbers; see (McCarthy, 1996) for detailed description of the arguments.

Acknowledgments. This research has been supported by Polish National Committee for Scientific Research (KBN) under grant No. 9 T12E 013 15. A.B. would like to acknowledge a grant received from the Paris Observatory, which covered his one month-long visit to P.O. in October'2000. We thank Pascal Defraigne for providing coefficients of the CMB spherical harmonic expansion.

REFERENCES

Bizouard Ch., Folgueira M. and Souchay J. (2000). Comparison of the short period rigid Earth nutation series, in. *Proc. IAU Colloquium 178*, Publications of the Astron. Soc. of the Pacific, Conf. Series, 613–617.

Bizouard Ch., Folgueira M. and Souchay J. (2001). Short periodic nutations: comparison between series and influence on polar motion, in. *Proc. Journees 2000 Systemes de Ref. Spatio-Temporels*, Paris Observatory, 260–265.

Bretagnon P. (1998). Diurnal and sub-diurnal nutations for a rigid Earth, in. *Proc. Journees 1998 Systemes de Ref. Spatio-Temporels*, Paris Observatory, 164–168.

Brzeziński A. (2000). Diurnal and sub-diurnal terms of nutation, in. *Proc. of IAU Colloquium 180*, U.S. Naval Observatory, 171–181.

Brzeziński A. (2001). Diurnal and subdiurnal terms of nutation: a simple theoretical model for a nonrigid Earth, in. *Proc. Journees 2000 Systemes de Ref. Spatio-Temporels*, Paris Observatory, 243–251.

Chao B. F., Dong D. N., Liu H. S. and Herring T. A. (1991). Libration in the Earth's rotation, *Geophys. Res. Letters*, **18**, No. 11, 2007–2010.

Chao B. F., Ray R. D., Gipson M. J., Egbert G. D. and Ma C. (1996). Diurnal/semidiurnal polar motion excited by oceanic tidal angular momentum, *J. Geophys. Res.*, **101**, No. B9, 20,151–20,163.

Defraigne P., Dehant V. and Wahr M. J. (1996). Internal loading of an inhomogeneous compressible earth with phase boundaries, *Geophys. J. Int.*, **125**, 173–192.

Getino J., Ferrándiz J. M. and Escapa A. (2001). Hamiltonian theory for the non-rigid Earth: Semidiurnal terms, *Astronomy & Astrophysics*, **370**, 330–341.

Hartmann T. and Wenzel H.-G. (1995). The HW95 tidal potential catalogue, *Geoph. Res. Lett.*, **22**, 3553-3556.

Lambeck K. (1988). *Geophysical geodesy: the slow deformations of the Earth*, Oxford University Press, New York.

McCarthy D. D. (ed.) (1996). IERS Conventions 1996, *IERS Technical Note 21*, Observatoire de Paris.

McClure P. (1973). Diurnal polar motion, *NASA Report X-592-73-259*,
Goddard Space Flight Center, Greenbelt, Md.

Molodensky S. M. and Groten E. (2001). Semidiurnal and long-period components in polar motion connected with the triaxiality of ellipsoid of inertia of the Earth and planets, *Studia geoph. et geod.*, **45**, 37–54.

Morelli A. and Dziewonski A. M. (1987). Topography of the core-mantle boundary and lateral homogeneity of the liquid core, *Nature*, **325**, 678–683.

Souchay J., Loysel B., Kinoshita H. and Folgueira M. (1999). Corrections and new developments in rigid Earth nutation theory: III. Final tables "REN-2000" including crossed-nutation and spin-orbit coupling effects, *A&A Suppl. Ser.*, **135**, 111–131.

ATMOSPHERIC EXCITATION FOR POLAR MOTION

J. NASTULA
Space Research Centre
Bartycka 18a, 00-716 Warsaw, Poland
e-mail: nastual@cbk.waw.pl

ABSTRACT

The interaction between the atmosphere and the underlying solid Earth causes important variations in all three components of the Earth's rotations vector on whole a range of different time scales. Some aspects of the atmospheric excitation of Earth rotation, such as seasonal oscillations, has a long history, but a more complete treatment of the subject has been possible for about two decades when several when several world's weather centers started regular estimations of the so called "effective angular momentum excitation functions". In this paper recent advances in the study of atmospheric influence on Earth rotation are reviewed. Emphasis is placed on those aspects which are a subject of our own investigations, such as regional contributions of the atmosphere to polar motion excitation. Recent estimations of oceanic excitation function of polar motion are also discussed.

1. INTRODUCTION

Earth rotation variations are excited either by: torque external to the Earth exerted by the Moon, the Sun, and the planets, or by geophysical processes leading to angular momentum exchanges between solid Earth and geophysical fluids like the atmosphere, ocean other parts of the hydrosphere.

Changes in the Earth's rotation are expressed as those in universal time UT1 and especially its temporal derivative, the length of day (LOD). Variations in the direction of the rotation axis are usually separated into polar motion, that is motion with respect to the Earth's crust, and nutation, that with respect to inertial space. The solid Earth and a geophysical fluid can be treated as a closed dynamical system in which angular momentum, a vector quantity, is conserved (Munk and Mac Donald, 1960). The variations of the angular momentum within the fluid component of the system therefore affect those of the solid Earth.

The interaction between the atmosphere, and the solid Earth is one of the most important sources changes the Earth's rotation vector and it occurs in a wide range of time scales. Perturbations in the axial LOD case, dominated by a strong seasonal oscillation and less regular fluctuations with variable period between 40 - 60 days the are excited by largely axisymetric wind fluctuations (see Munk and MacDonald, 1960; Lambeck, 1980; and Eubanks, 1993). Comparisons show that for periods from a few days to a few years the agreement between non-tidal variations of LOD and the wind component of axial atmospheric angular momentum reaches 0.2 mas, almost within the observational error. In the case of the equatorial component of Earth

rotation, the role of the atmosphere is not in such good agreement whether due to the data uncertainty as the participation of the other geophysical fluids principantly the ocean. The influence of the atmosphere on Earth rotation is currently expressed by an atmospheric excitation function often called the "effective atmospheric angular momentum" (EAAM) vector when its accounts for the effect of the Earth compressibility (Barnes et al., 1983).

In the paper we will review the types of atmospheric fluctuations responsible for polar motion, and note the regions at which the most important fluctuations occur in this context.

2. ATMOSPHERIC EXCITATION FUNCTIONS FOR POLAR MOTION

The angular momentum approach, as applied here, allows the solid Earth and atmosphere to be treated as a closed dynamical system in which angular momentum, a vector quantity, is conserved (Munk and MacDonald, 1960). Variations in the these components of atmospheric angular momentum force fluctuations in the equatorial components of the solid Earth angular momentum, impacting the motions of the pole. The atmospheric contributions to polar motion are computed using a formalism given by Barnes et al. (1983), including expressions for the equatorial EAAM. These χ_1^A and χ_2^A atmospheric functions consist of a pressure (P) term, closely equivalent the effect of air mass redistribution, and a wind (W) term, the effect of the relative motion of the atmosphere over the Earth. Additionally, if it is assumed that the oceans respond to the overlying atmospheric pressure completely isostatically, the so-called inverted barometer (IB) approximation is invoked., greatly reducing the impact of atmospheric fluctuations above the oceans. The IB effect is normally considered valid over most of the ocean in periods larger than a few days (Ponte at al., 1991).

EAAM functions can be evaluated from the gridded global fields of surface pressure and wind velocity at various heights, which are routinely produced by the world's major weather centers: U.S National Centers For Environmental Prediction (NCEP), United Kingdom Meteorological Office (UKMO), Japan Meteorological Agency (JMA) and European Centre for Medium-Range Weather Forecasts (ECMWF). Since 1989, the EAAM data sets have been determined, collected, archived, analyzed and distributed by the International Earth Rotation Service (IERS) Sub-bureau for Atmospheric Angular Momentum(Salstein et al., 1993) which became in 1998 the Special Bureau for the Atmosphere (SBA) in the Global Geophysical Fluids Center (IERS, 1989-1999). Operational EAAM data are characteristic of the specific system in use at the time of their production; they were sampled initially 2 times per day, but since every 1982 every 6 hours (Salstein et al., 1993). They are not homogeneous in time as a result of changes in the computational schemes and at times the atmospheric analyses circulation models, contain gaps, sometimes several weeks long. To mitigate the effects of such heterogencities, some meteorological centers have reanalyzed meteorological parameters assimilating in an optimal and consistent way past meteorological observations, from which EAAM functions have been determined. The longest series which is currently available from the SBA (IERS, 1992) is a more than 50-year-time series of 4-times daily, determined by Salstein and Rosen (1997) on the basis of results of the NCEP/NCAR reanalysis project (Kalnay et al., 1996).

3. CORRELATIONS BETWEEN ATMOSPHERIC AND GEODETIC EXCITATION FUNCTIONS OF POLAR MOTION

A standard method of estimation of atmospheric influence on polar motion is to derive first from geodetic observations of Earth rotation the corresponding so-called χ_1^G and χ_2^G geodetic excitation functions (that is the solution of the inverse problem, or deconvoluti on the polar motion series) which are then compared with the χ_1^A and χ_2^A geophysically observed excitation functions. This procedure usually makes use of the discrete approximation of the equations of

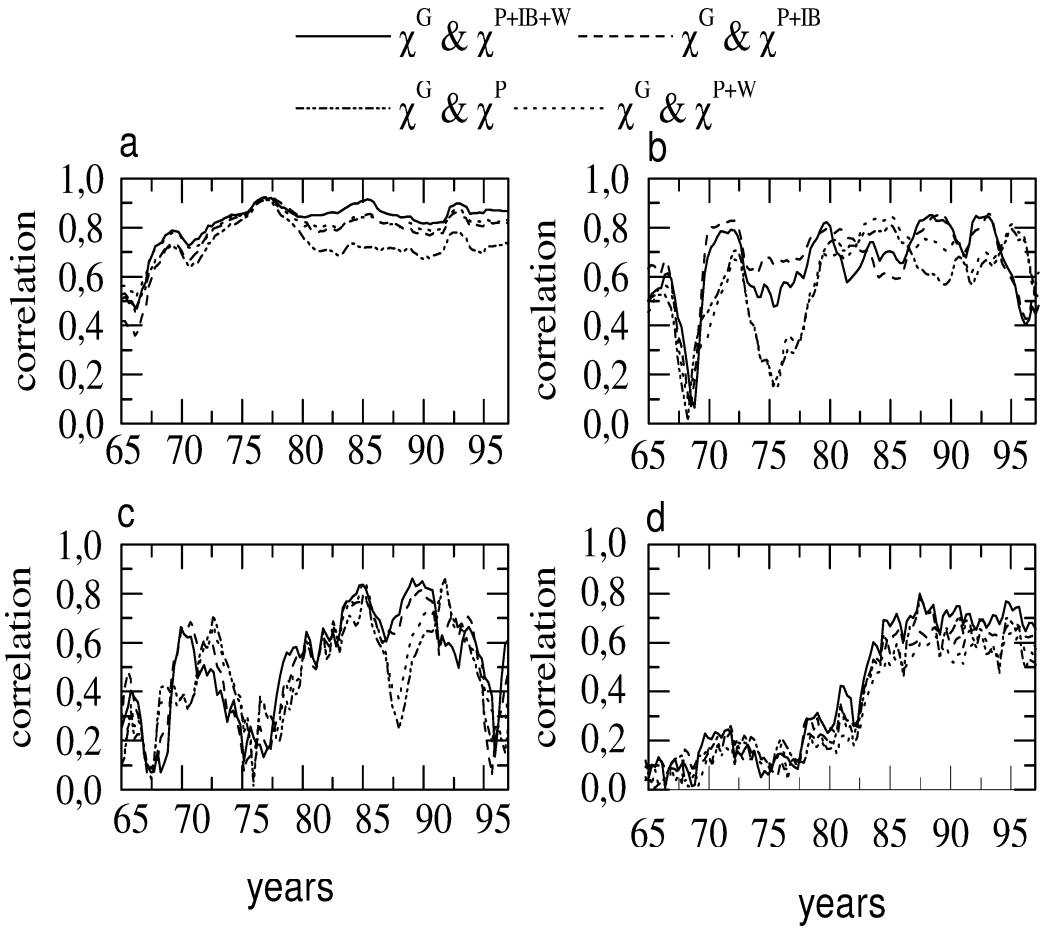

Figure 1: Correlation coefficients between the complex-valued equatorial components of geodetic and atmospheric excitation functions filtered by the use of the Butterworth filter into (a) 450-230 days, (b) 230-150 days, (c) 150-90 days, and (d) 90 -10 spectral bands, (Nastula, 2001).

Earth's rotation (Wilson, 1985). An alternative method described in detail by Brzeziński (1992) is to apply a Kalman filter for solving the inverse problem.

Polar motion and atmospheric circulation fluctuations occur on a variety of time scales. It is known that annual and semiannual oscillations in atmospheric circulation and in polar motion are linked(Munk and MacDonald, 1960, see also reviews by Eubanks, 1993 and references therein). Also fluctuations in polar motion on subseasonal time scales defined as periods shorter than 150 days, have been identified for a number of particular periods (Kołaczek, 1992; Kołaczek and Kosek, 1993; Kołaczek et al., 2000, Kosek, 1987) and tied to oscillations in EAAM (Eubanks et al., 1988; Kosek et al., 1995; Kuehne et al., 1993, Nastula, 1995; Nastula et al., 1997).

The correlation between geodetic and atmospheric excitation is related to the frequency. Additionally, when the correlation between atmospheric and geodetic excitation for polar motion is computed in a temporal windows, we note that the correlations are time-variable. Figure 1 shows an example of correlation coefficients between the geodetic and atmospheric excitation functions at four broad time scales, namely: annual (450-230 days), semi-annual (150-230 days), 120 days (90-150 days) and short period (10-90 days). The spectral bands are defined to give some insight into annual, semiannual, and subseasonal polar motion, although these cut-off periods are arbitrary. The subseasonal band is separated here between periods around 120 days

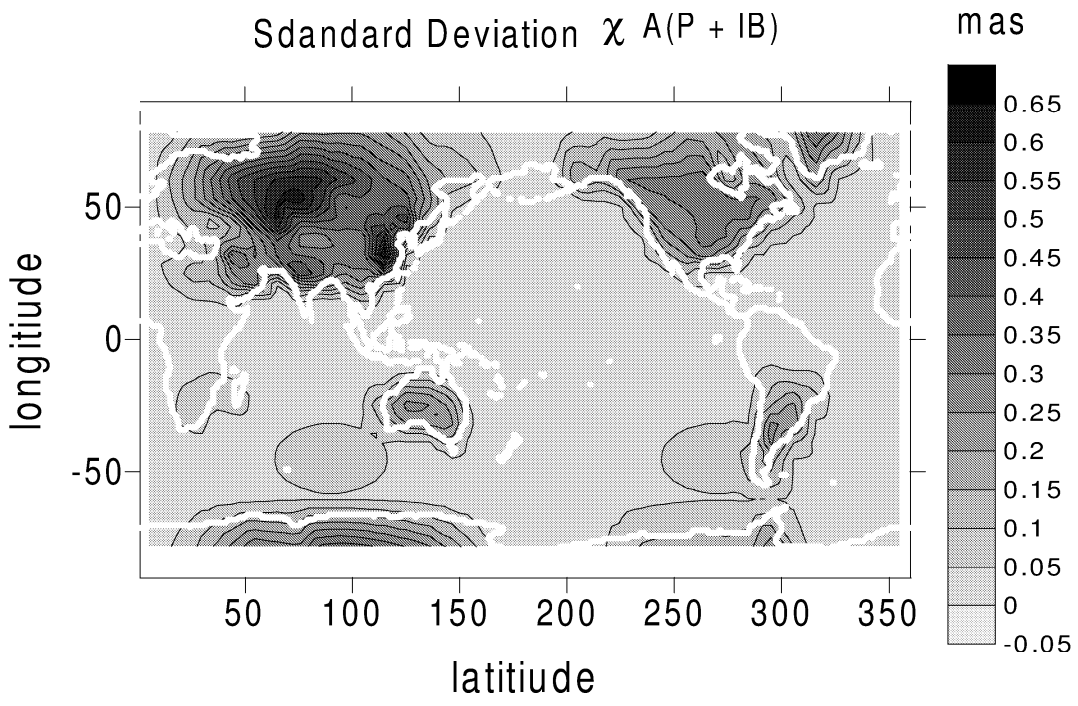

Figure 2: Map of standard deviation of amplitude of complex-valued atmospheric excitation function.

oscillations (terannual band) and shorter than 90 days (short period band). We see from Figure 1 that the correlation coefficient is most stable for the annual band; it has increased, moreover, since 1970. Given that the standard error of the difference equal to 0.26, correlation coefficients computed for various atmospheric terms and time periods are not significantly different in the case of annual oscillation. For the semiannual oscillation the correlation coefficient has significantly improved since 1975, for the pressure + IB and pressure terms and since 1985 for the wind term. In the case of the 120-day and short period oscillations the respective correlation coefficient has reached the values of 0.6 - 0.8 since 19 85. These earlier disagreements are likely due to less accurate polar motion and atmospheric excitation data (Nastula and Salstein, 1999). The correlation coefficients have been quite stable since 1970 for the annual and semi-annual bands. For the 120 days oscillation one can see two minima centred on 1987 and 1996. This drop of correlation might be connected with variations around the time of El Niño events (Nastula el al., 2002).

The significant correlation between atmospheric and geodetic excitation functions, especially in the latter period, was noted earlier, (Chao, 1993; Kuehne et al., 1993; Kosek et al., 1995; Nastula, 1995; Ponte et al., 1998). Modulation of the correlation coefficient was found by Kuehne et al. (1993), Kosek et al. (1995), Nastula (1995) for subseasonal oscillations and by Nastula and Kołaczek (2001) for seasonal and 120 days oscillations.

4. REGIONAL SIGNALS IN EXCITATION OF POLAR MOTION

Studies of variability in regional atmospheric excitation functions fields are necessary for understanding the processes involved, including a decomposition of the oceanic and atmospheric excitation into their regional values. The fluctuations of surface pressure over such areas as the North Atlantic, North Pacific, and the whole southern oceans strongly influence the global

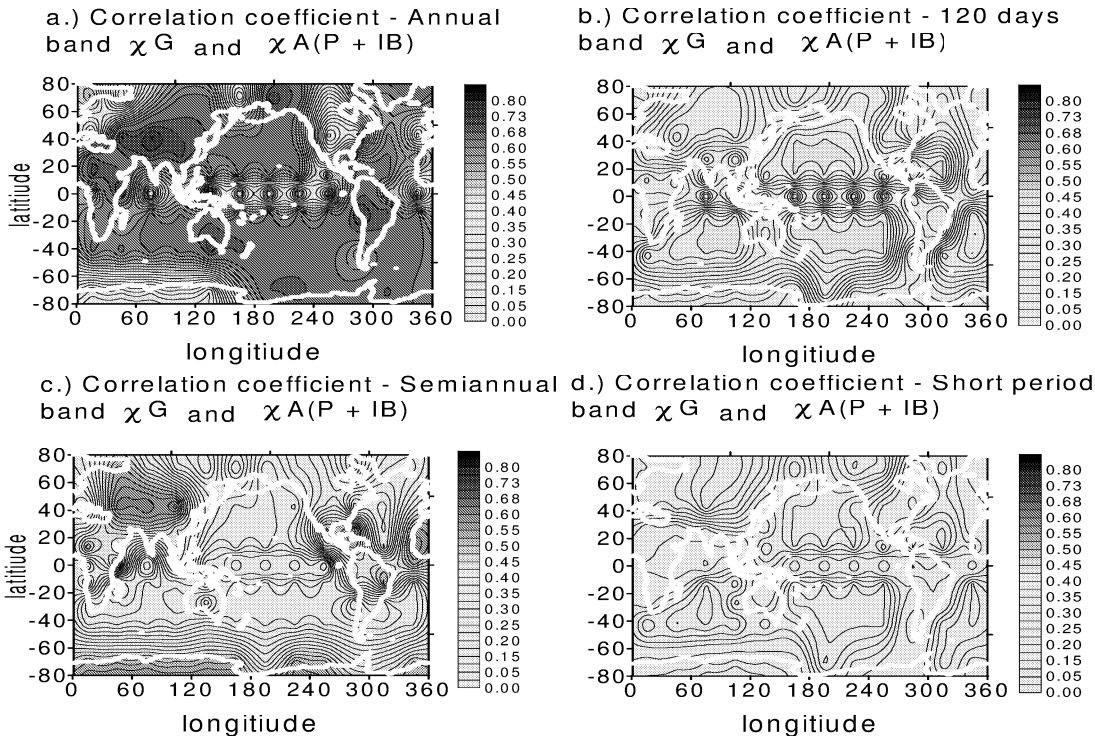

Figure 3: Maps of the correlation coefficient between χ^G geodetic and χ^{P+IB} regional values of polar motion atmospheric excitation function; filtered by the use of the Butterworth filter into (a) 450-230 days, (b) 230-150 days, (c) 150-90 days, and (d) 90 -10 spectral bands.

excitation functions for polar motion (Salstein and Rosen, 1989; Nastula, 1997, Nastula and Salstein 1999). However, as shown by Figure 2, when the inverted barometer (IB) correction is included, the spatial structure variations over the oceans is necessarily eliminated and so applying the IB correction to the pressure leads to the dominance of Eurasia and America instead, with nearly all Southern Hemisphere contributions unimportant (Nastula el al, 1997; Nastula and Salstein ,1999). It should be mentioned that regional atmospheric oscillations with maximum amplitudes are not always strongly correlated with polar motion variations. So, the sectors of the globe over which changes in atmospheric mass relate most importantly to global changes ought to be properly identified as having characteristics of maxima in common power, but also those of significant correlations.

Spatial patterns of regions that are significantly correlated to geodetic variations depend on spectral band (Nastula, 2001). Figure 3 shows an example of latitude-longitude maps of correlation coefficients between the geodetic excitation function and pressure+IB term of atmospheric excitation function. Similarly, as in the case of the global data, the maps are calculated from the data sets that have been filtered to include periods ranging from 230-450 days (annual), 150-230 (semi-annual), 90-150 days (120 days) and 10-90 days (short period).

For the case of annual band all correlation coefficients reach maximum values 0.7 - 0.8 over Tibet, Himalayas Mountains, Siberia, Gulf of Alaska and Greenland (Fig. 3). Correlation between semiannual polar motion and atmospheric excitation functions has dominated maxima over North Europe, Siberia, and Himalayas. Eurasia and North America dominate patterns of correlation coefficient for 120 days and short period cases. Correlation coefficients are lower than that for the annual and semiannual cases, however the addition of the IB correction increases the level of correlation above 0.4.

Wind contributions to regional excitation data (not shown here), however, were found to be

quite variable regionally and require a more careful interpretation to be useful in studying polar motion variations (Nastula, et al.,1997; Nastula, 2001). Regional variations of the wind term are significantly correlated with geodetic excitation function in case of annual oscillation only and have maxima over Himalayas and Rocky Mountains (Nastula, 2001).

The special importance of Eurasia for subseasonal excitation of polar motion is reconfirmed when modes of variability in the atmosphere are investigated by using Empirical Orthogonal Functions - EOF (see Preisendorfer, 1988) (Nastula and Salstein, 2000). For the case of pressure the two first complex modes contain patterns with strong variations over southern oceans, the Gulf of Alaska and North Pacific. The corresponding spatial pattern contains also a teleconnection between these regions of the Southern Hemisphere. The addition of the IB correction leads to the dominance of land areas, with Eurasia especially important. There are also some teleconnections with the Southern Hemisphere even in the IB case. The modes of pressure with IB terms of atmospheric excitation are more significant for polar motion excitation than those of non-IB pressure; however the non-IB modes may be an important indicator for atmospheric variations.

5. RAPID VARIATIONS OF POLAR MOTION

Increase of accuracy and resolution of the polar motion coordinates determined by the Global Positioning System (GPS) and Very Long Baseline Interferometry (VLBI), enables a study of rapid oscillations with periods of several hours (Schuh and Schmitz-Huebsch, 2000; Hefty et al., 2000; Rothacher et. al., 2001; Weber et al., 2000). The estimation of contribution of atmospheric signals to the excitation of the rapid variations of polar motion is made difficult by the scarceness high-resolution atmospheric data. Recently Weber et al. (2002) used a temporally dense set of pressure term of atmospheric excitation functions for polar motion, produced by the U.S. National Aeronautic and Space Administration (NASA) with a three-hours resolution for the year 1995. The spectra of the dense atmospheric data were compared with spectra of the geodetic excitation functions inferred from the GPS(CODE) polar motion series in the period 1997.5 trough 2001 with resolution of two hours. Oscillations at 8 and 12 hours are visible in both geodetic and atmospheric excitation of polar motion. Although detected with different time periods, amplitudes of oscillations of geodetic excitation functions are however considerably larger than those of the atmospheric excitation function. Thus, the atmospheric excitation does not appear to explain fully the amplitude variations of polar motion in this spectral range.

6. OCEANIC EXCITATION OF POLAR MOTION

The analysis of the atmospheric excitation functions should be complemented with similar analysis of the oceanic excitation functions (Ponte, 1997; Ponte and Stammer, 1999). Improvements in ocean modeling capabilities in recent years have made possible model calculations of OAM. Recent findings show that oceanic excitation, when added to atmospheric excitation leads to substantial improvements in the agreement with observed polar motion excitation at seasonal and intraseasonal periods (Fig. 4) (Ponte, 1997;, Ponte and Stammer, 1999; Nastula and Ponte, 2000).

Comparisons of regional atmospheric and oceanic excitation functions confirmed that oceanic excitation is very important source of polar motion excitation (Nastula et al., 2000; 2001). Bottom pressure variations in the ocean have comparable amplitudes to those of atmospheric pressure amplitude (with IB) over land masses. Oceanic currents have even larger amplitude than those of oceanic and atmospheric pressure regionally. Determining which oceanic regions are the most important for excitation of polar motion may also provide clues to the present accuracy of oceanic circulation models.

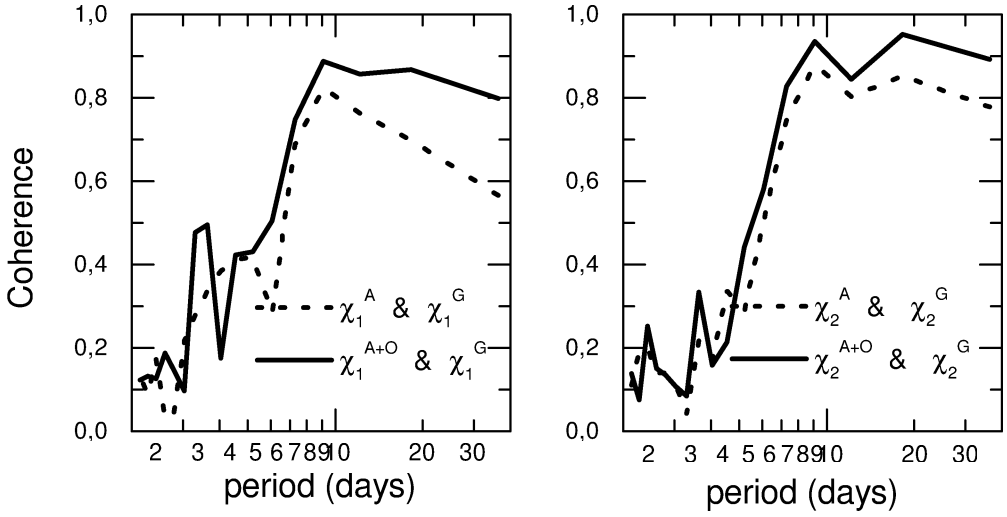

Figure 4: Coherence amplitude between χ^G and χ^A (dotted) and χ^G and χ^{A+O} (solid), (Nastula and Ponte, 1999). A=Atmospheric Pressure +IB + Wind, O = Oceanic Bottom Pressure + Motion.

The second main components polar motion besides the annual wobble, with relatively constant amplitude of about 90 mas is the 14-month free Chandler wobble whose amplitude varies about a about mean value 160 mas. Analysis of Wahr (1983), confirmed by recent studies based on the reanalyzes data sets of atmospheric pressured with the IB and wind (Brzeziński et al., 2002) show that the atmosphere, to a lesser extent provides about less than half of the necessary power to explain the Chandler wobbles.

The contribution of ocean angular momentum signals to the excitation of the Chandler wobble was expected to be an important part of the remaining discrepancy. Recently, determination of no tidal OAM has been attempted with the use of global ocean circulation models. Brzeziński and Nastula (2000) demonstrated that the OAM series of Ponte et al. (1998) is highly coherent with the no atmospheric excitation of the observed Chandler wobble signal. Gross (2000) concluded that during 1985 -1996 the Chandler wobble signal was excited by a combination of atmospheric and oceanic processes, with the dominant excitation mechanism being ocean-bottom pressure fluctuations. In studies Brzeziński and Nastula (2000) extended the analysis of Brzeziński et al. (2002) by using a 50-year time series of OAM estimated by Ponte and Stammer (1999) from a different model an data assimilation system. The spectral analysis of the OAM series shown that the ocean supplies a power of about $18 mas^2/cpy$ to the excitation of Chandler wobble, more than the atmospheric contribution (about $15 mas^2/cpy$) and only slightly less than the quantity required to explain the excitation power (about $20 mas^2/cpy$). However, the comparison between the 50-year AAM series with the inferred no atmospheric excitation shows significantly lower correlation and lower coherence at the Chandler frequency than estimations for period 1985 - 1996.

7 CONCLUSIONS

The atmosphere and ocean are the most important sources of polar motion excitation in the time scales from days to years. The lack of coherence between the polar motion excitation and joint forcing from atmosphere and ocean in the time scale from hours to days still awaits explanation. The oceanic excitation series still should be considered preliminary. Improvements

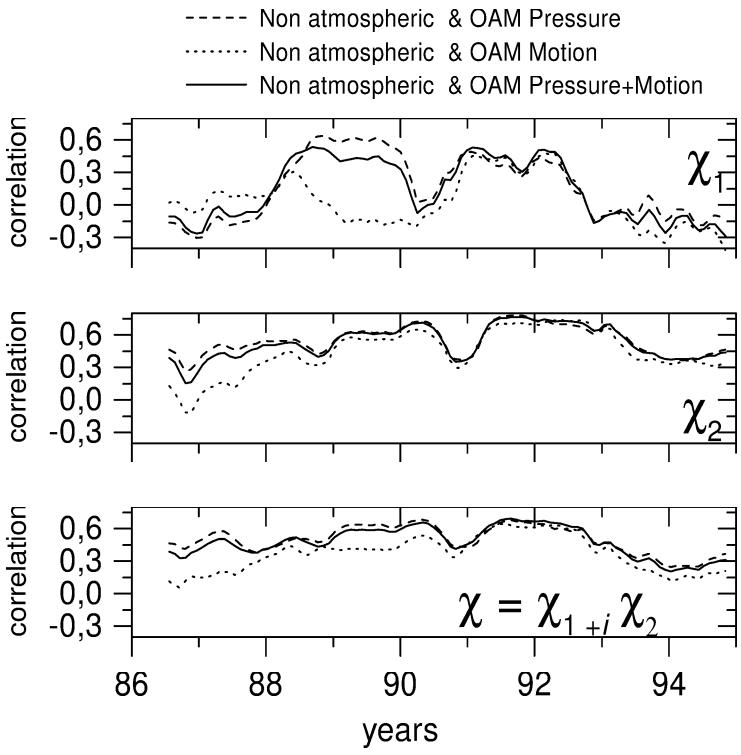

Figure 5: Time dependence of correlation between non-atmospheric and oceanic estimations of non seasonal polar motion excitation derived from a sliding window analysis.

in both the model and data assimilation system are expected in a near future. It may be that other sources of variability such as ground-water storage will have to be invoked.

8 ACKNOWLEGMENTS

The research reported here was supported by the Polish State Committee for Scientific Research through project /9T12E /0012. The author thanks D. A. Salstein from Atmospheric and Environmental Research Inc. for valuable comments on the manuscript.

9 REFERENCES

Barnes, R., T. H, R. Hide, A. A. White, and C. A. Wilson, 1983: Atmospheric angular momentum fluctuations, length-of- day changes and polar motion, Proc. R. Soc. Lond., A387, 31-73.

Brzeziński, A., 1992: Polar motion excitation by variations of the effective angular momentum functions: considerations concerning deconvolution problem, Manuscr. Geodet, 17, 3-20.

Brzeziński and J. Nastula, 2000: Oceanic excitation of the Chandler wobble, Adv. Space Res. in press

Brzeziński, A., J. Nastula, and R. M. Ponte, 2002: Oceanic excitation of the Chandler wobble using a 50-year time series of ocean angular momentum, International Association of Geodesy Symposia, Vol 125,Vistas for Geodesy in the New Millenium, Springer Verlag, 434 - 439.

Chao, B.F., 1993: Excitation of Earth's polar motion by Atmospheric Angular Momentum Variations, 1980-1990, Geoph. Res. Let., 20, 235-256.

Eubanks, T. M., 1993: Variations in the orientation of the Earth, in AGU Monograph, Con-

tributions of Space Geodesy to Geodynamics: Earth Dynamics, Smith and Turcotte eds., Geodynamics Series, 24, 1 - 54.

Eubanks, T. M., J. A. Steppe, J. O., Dickey, R. D. Rosen and D. A. Salstein, 1988: Causes of rapid motions of the Earth's pole, Nature, 334, 115 -119.

Gross, R. S., 2000: The excitation of the Chandler wobble. Geophys. Res. Lett., vol. 27, 2329-2332.

Hefty, J., M. Rothacher, T.Springer, and R.Weber, G.Beutler, 2000: Analysis of the first year of Earth Rotation parameters with a sub-daily resolution gained at the CODE processing center of the IGS. Journal of Geodesy, Vol. 74, 479-487.

International Earth Rotation Service (IERS), 1989-2001: IERS annual reports, Observatoire de Paris, Paris, France.

Kalnay, E., 1996: The NCEP/NCAR 40-year Reanalysis Project, Bull.Amer. Meteor. Soc., 77, 437 - 471.

Kołaczek, B., 1992: Variations of Short Periodical Oscillations of Polar Motion with Periods ranging from 10-140days. Report No. 419 Department of Geodetic Science and Surveying. The Ohio State university, Columbus, Ohio 43210-1247, Apr. 1992.

Kołaczek, B., and W. Kosek, 1993: Variations of 80-120 days oscillations of polar motion and Atmospheric Angular Momentum, Proc. 7th International Symposium "Geodesy and Physics of the Earth" IAG Symposium No. 112, Potsdam, Germany, Oct. 5-10, 1992. H. Montag and Ch. Reigber (eds.), Springer Verlag, 439-442.

Kołaczek, B., and W. Kosek, and H. Schuh, 2000: Short-period oscillations of Earth rotation, Proceedings of IAU Colloquium 178 Polar motion: Historical and scientific problems, 27-30 September, 1999, Cagliari, Italy, 2000, 533-544, ASP,USA.

Kosek, W., 1987: Computations of Short Periodical Variations of Pole Coordinates the Merit Campaign by the use of the Ormsby Filter and the Maximum Entropy Spectral Analysis with the Optimum filter length, Bulletin Geodesique, 61, 109-124.

Kosek, W., 1995:, Time Variable Band Pass Filter Spectrum of real and complex-valued polar motion series, Artificial Satellites, Planetary Geodesy, 30, 1, 27 - 43.

Kosek, W., J. Nastula, and B. Kołaczek, 1995: Variability of polar motion oscillations with periods from 20 to 150 days in 1979 -1991., Bulletin Geodesique, 69, 308-319.

Kuehne, J., T. S. Johnson, and C. R. Wilson, 1983: Atmospheric excitation of nonseasonal polar motion, J. Geophys. Res., 98, 19,973-19,978, 1993.

Lambeck, K.,1980: The Earth's Variable Rotation: Geophysical Causes and Consequences, Cambridge University Press.

Munk W., H., and G. J. F. MacDonald, 1960: The rotation of the Earth: A Geophysical Discussion, Cambridge Univ. Press.

Nastula, J., 1995: Short periodic variations of polar motion and hemispheric atmospheric angular momentum excitation functions in the period 1984 - 1992, Ann. Geophysicae, 13, 217 - 225.

Nastula, J., 1997: The regional atmospheric contributions to the polar motion excitation and EAAM functions, IAG Symposia, Vol. 117; Segawa et al. (eds.), Geoid and Marine Geodesy, Springer Verlag, 281 - 288.

Nastula, J., and R. M. Ponte, 1999: Further evidence of oceanic excitation of polar motion, Geophys . J. Int., 139, 123 - 130.

Nastula, J., and D. A. Salstein, 1999: Regional atmospheric momentum contributions to polar motion, J. Geophys. Res, 104, 7347 -7358.

Nastula, J., and D. A. Salstein, 2000: Modes of variability in high-frequencies atmospheric excitation for polar motion, IERS Technical Notes No 26, Paris France, 85 -90.

Nastula, J., and B. Kołaczek, 2001: Seasonal oscillations in regional oscillations of polar motion, in press Advances in Space Research.

Nastula, J., W. Kosek, and B. Kołaczek, 1997: Analyses of zonal atmospheric excitation functions and their correlation with polar motion excitation functions, Ann. Geophysicae, 15, 1439-1446. .

Nastula, J., R. M. Ponte , and D. A. Salstein, 2000: Regional signals in atmospheric and oceanic excitation of polar motion, in Proceedings of 178 IAU Colloquium Polar Motion: Historical and Scientific Problems, Cagliari Sardinia Italy, 463-472.

Nastula, J., R. M. Ponte, and D. A. Salstein, 2001: Regional high-frequency signals in atmospheric and oceanic excitation of polar motion, in press Advances in Space Research.

Nastula, J., B. Kołaczek, and D. A. Salstein, 2002: Variation of zonal anomalies of atmospheric excitation function for polar motion during 1983-1999, in this volume.

Ponte, R. M., 1997: Oceanic excitation of daily to seasonal signals in Earth rotation: Results from a constant-density numerical model, Geophys. J. Int., 130, 469 - 474, 1997.

Ponte, R. M., and D. Stammer, 1999: Role of ocean currents and bottom pressure variability on seasonal polar motion, J. Geophys. Res, 104, 23,393 - 23,409.

Ponte, R. M., D. A. Salstein, and R. D. Rosen, 1991: Sea level response to pressure forcing in a barotropic numerical model' J. Phys. Oceanogr., 21, No. 7, 1043-1057

Ponte, R. M., D. Stammer and J. Marshall,1998: Oceanic signals in observed motions of Earth's pole of rotation, Nature, 391, 476-479.

Preisendorfer, R. W., 1988: Principal component analysis in meteorology and oceanography", C. D. Mobley (eds.), Elsevier Science Publisher, Developments in Atmospheric Science, 17, 1988.

Rothacher, M., G. Beutler, R. Weber, and J. Hefty, 2001: High frequency Earth rotation variations from three years of Global Positioning System Data. JGR, Vol. 106, B7, 13711-13738.

Schuh, H., and H. Schmitz-Huebsch ,2000: Short period variations in Earth rotation as seen by VLBI. Surveys in Geophysics. 21, 499-520.

Salstein, D. A, and R. D. Rosen, 1989: Regional contributions to the atmospheric excitation of rapid polar motions, J. Geophys. Res., 94, 9971 - 9978, 1989.

Salstein, A. A., and R. D. Rosen, 1997: Global momentum and energy signals from reanalysis systems, paper presented at the 8th Conference on Climate Variations, Am. Meteorol. Soc., Long Beach, Calif., Feb. 2-7.

Salstein, D. A., D. M. Kann, A. J. Miller, and R. D. Rosen, 1993: The Sub-Bureau for Atmospheric Angular Momentum of the International Earth Rotation Service: a meteorological data center with geodetic applications, Bull. Amer. Meteor. Soc., 74, 67-80.

Wahr, J., M., 1983: The effects of the atmosphere and oceans on the earth's wobble and on the seasonal variations in the length of day-II. Results, Geophys. J. R. Astr. Soc., 74, pp. 451-487.

Weber, R., M. Rothacher, and G. Beutler, 2000: Contribution of the GPS to monitor Earth Orientation Parameters. IERS Technical Note. 28 Observatoire de Paris, 43-53.

Weber R., J. Nastula, B. Kołaczek, and D.A. Salstein, 2002: Analysis of rapid variations of polar motion determined by the GPS, International Association of Geodesy Symposia, Vol 125,Vistas for Geodesy in the New Millenium, Springer Verlag, pp 445-450.

Wilson, C. R., 1985: Discrete polar motion equations, Geophys. J.R.Astr. Soc., 80, 551-554.

ATMOSPHERIC AND OCEANIC FORCING IN POLAR MOTION AND LENGTH-OF-DAY

C. BIZOUARD, S. LAMBERT
DANOF/UMR8630-CNRS, Observatoire de Paris
61 avenue de l'Observatoire 75014 Paris - FRANCE
e-mail: christian.bizouard@obspm.fr

ABSTRACT. Besides the atmosphere, the oceans play an important part in the polar motion and length-of-day variations. Usual approach for quantifying this influence consists in computing the angular momentum of fluid layers, and then to compare them with the excitation, which can be infered from Earth's orientation data. Our study is devoted to this comparison, on the base of recent atmospheric and oceanic excitation series. We show that the add of oceanic excitation series to atmospheric ones better explains the polar motion and length of day. We focus on long periods (periods larger than 10 days) including seasonal terms and the Chandler term.

1. INTRODUCTION

The atmosphere plays a prominent part in the Earth's rotation changes. Until recently, the role of the oceans was poorly investigated because of the deficiency of data concerning its angular momentum at scales longer than a few days. Whereas diurnal and semidiurnal changes in OAM have been modelled from oceanic tidal models (these are the so-called Oceanic Tidal Angular Momentum or OTAM), more difficult is to take into account the currents taking place in the oceans as well as the influence of atmospheric forcing at the oceanic surface. From ocean global circulation model, Ponte (1998) has computed OAM series. Using these series Brzeziński and Nastula (2000) and Gross (2000) have shown that the joint effect of atmosphere and oceans matches better the polar motion, and more interesting that the additional power brought by oceans could better explain the source of the 433 days Chandler excitation.

Our aim is to validate these important results as well as to answer related questions. What is the improvement brought by the oceans at some specific seasonal term? Does the joint oceanic-atmospheric excitation better explain the LOD changes ? To which extent the correlation between observed excitation and geophysical excitation is improved ?

2. GEOPHYSICAL AND GEODETIC EXCITATION

This study deals with the so-called excitation functions of polar motion and LOD. The geophysical excitation functions, which are less-dimensional form of Atmospheric Angular Momentum (AAM) or Oceanic Angular Momentum (OAM), will be compared to the geodetic excitation functions, that is the observed excitation, which can be inferred from Earth Orientation Parameters (EOP). Let be p the complex-valued coordinate of the Celestial Ephemeris Pole (CEP) in

the terrestrial reference frame ($p = x - iy$) and ΔLOD the excess of length-of-day proportional to the time derivative of $UT1 - TAI$ (Universal time - Temps Atomique International). It can be shown (Barnes et al. 1983) that for processes at scales longer than a few days :

$$\begin{aligned} \chi_G &= p + \frac{i}{\sigma_{\rm cw}} \frac{{\rm d}p}{{\rm d}t} \\ \chi_{G,3} &= -\frac{\Omega}{2\pi k} \Delta LOD = \frac{d(UT1 - TAI)}{dt} \end{aligned} \tag{1}$$

where $\sigma_{\rm cw} = \frac{1}{433}(1 + \frac{i}{2Q})$ is the complex-valued frequency of the Chandler Wobble, known as a damping process of frequency of 0.8435 cycles per year and quality factor Q=170 according to Wilson and Vicente (1990), Ω is the nominal value of the Earth's angular velocity as adopted in the IERS numerical standards (IERS, 2001) and k is the ratio between the mean solar day and the sidereal day. The quantities χ_G and $\chi_{G,3}$ are the so-called geodetical excitation functions to be compared with the geophysical ones coming from the atmosphere χ_A and from the oceans χ_O.

We have used the effective atmospheric excitation functions time series computed by the National Center for Environmental Prediction/National Center for Atmospheric Research re-analysis project (NCEP/NCAR) and available at the Global Geophysical Fluids Center of IERS. These series cover the period from 1958.0 to 2001.0 and are sampled every 6 hours.

It is commonly assumed that oceans react as an Inverted-Barometer (IB) in front of a surface pressure change : the ocean surface is isostatically deformed in order that the weight of any column (water+air), at a planetary scale, remains unchanged at the oceanic bottom. The more the sea surface pressure fluctuation is long periodic, the more this process takes place in the redistribution of oceanic waters. Inverted-Barometer processes account for altimetric observations of the sea surface for time scales larger than 10 days. But how to take into account this behaviour of oceans in Earth's rotation ? Actually the IB hypothesis is equivalent to restrict the integration of the matter term of the AAM to the continents (de Viron and Dehant, 1999). By getting the so-called AAM-IB series, the atmospheric pressure fluctuations are taken into account in the combined atmospheric-oceanic effects. It has been shown that the AAM-IB series are more realistic, especially better correlated with geodetic observations. However by restricting the excitation to AAM-IB series, we do not deal with the wind forcing on the oceanic surface and oceanic currents.

Recently Ponte (1998, 1999, 2000) attempted to quantify these effects by using an ocean circulation model, and obtained corresponding OAM series. These series are sampled every 5 days (at 12h UTC) and cover the period from january 1985 to april 1996 and are available on the ftp server of the Global Geophysical Fluids Center of IERS. Contributions due to oceanic currents and ocean-bottom pressure changes have been computed separately by using an Oceanic General Circulation Model (OGCM). Note that atmospheric pressure has not been used to force this OGCM. In the following study, we will design the excitation from the atmosphere IB by χ_A and the excitation from the combined model of atmosphere IB and ocean by χ_{A+O}.

The AAM functions have been sampled at the same dates than the OAM series, from 1985.02 to 1996.30 : first, a low-pass Vondrák filter has been applied (half-cutting period of 5 days, 100% of the signal is passing for periods larger than 12 days, and 1% is allowed to pass for a period of 2 days) to remove the diurnal signal, and second, we have selected the data associated with the sampling of the oceanic series (each 5 days at 12h UTC).

Our geodetic excitation functions are based upon the C04 combined series produced by the IERS Earth Orientation Parameters Product Center (IERS EOP-PC, Paris Observatory). The C04 series gives daily averaged values (at 0h UTC) of the observed polar motion and UT1-UTC from 1962.0 to 2000.0, obtained by the combination of data from miscellaneous techniques (VLBI, GPS, SLR-LLR). In order to make C04 series consistent with the Ponte oceanic excitation

series, they have been interpolated from 1985.02 to 1996.30 at the dates of the OAM series. Then the geodetic excitation functions have been derived according to equation (1). The effects of zonal luni-solar tides bring an important contribution in UT1 series, and in turn has been removed. Equatorial tidal excitation, as modelled by Dickman (1993) and tabulated by Gross (1998) (9.12 days, 9.13 days, 13.63 days, 13.66 days, 27.56 days), has been removed from geodetic excitation functions.

Uncertainties on AAM and OAM are not provided, and are indeed very difficult to estimate because the AAM and OAM values are derived from circulation models. Mean accuracy of observed forcing $\Delta\chi_G$ can be roughly deduced from equation (1) where a derivative on three points is performed - mean uncertainty on polar motion (indifferently x-component or y-component) of C04 series is Δp=0.7 mas (over 1994-1995), mean uncertainty on UT1-TAI is 0.04 ms, as reported in IERS annual report (1999).

Table 1: Uncertainties of the excitation functions in milliarcsecond (mas).

	propagation of error		
	x	y	z
χ_G	10.50	10.50	0.04
χ_A	-	-	-
χ_{A+O}	-	-	-

3. COMPARISON OF ANNUAL AND SEASONAL TERMS IN GEOPHYSICAL AND GEODETIC EXCITATION

This first glance has been followed by least-square fits of seasonal terms of equatorial functions (annual, semi-annual and ter-annual). Any equatorial signal, χ_G,χ_A, χ_{A+O} is modelled as the sum of circular terms and a linear trend :

$$\chi = \sum_j A_j \mathrm{e}^{i\omega_j t} + at + b \tag{2}$$

where A_j is a complex amplitude. We have computed A_j under the form $A_j = M_j \mathrm{e}^{i\phi_j}$ where ϕ_j is the phase with respect to the reference epoch J2000.0 (january 1st 2000 at 12h UTC), ω_j the frequencies associated to the following circular periodic terms : annual prograde and retrograde terms (-1, 1 cpy), semi-annual prograde and retrograde terms (2, -2 cpy), ter-annual prograde and retrograde (3, -3 cpy).

Results are reported in Table 2. Adding OAM brings significant improvement of the balance between geodetic and geophysical excitations, except for the semi-annual retrograde oscillation. The prograde annual term of AAM-IB exhibits too much power with respect to the observed excitation, but the oceanic forcing reduces the relative offset from 30% to 10%. The annual retrograde amplitude undergoes ever better change, from 90% to 16%.

In all cases the phases are made considerably closer to that one of the geodetic excitation. This effect of OAM contribution is flagrant for 1 cpy, -3 cpy and 3 cpy. These results constitute already a proof of the influence of the oceanic angular momentum variations on polar motion.

We can now wonder weather such an influence is noticeable in axial excitation. As it has been done before, each axial function is modelled as the sum of harmonic components and a constant term :

$$\chi_3 = \sum_j A_j \cos(\omega_j t + \phi_j) + b \tag{3}$$

Table 2: Seasonal terms in equatorial excitation functions : amplitude (mas) and phase (degrees) with respect to epoch J2000.0.

cpy	χ_G		χ_A		χ_{A+O}	
	amplitude	phase	amplitude	phase	amplitude	phase
1	13.65 ± 0.37	-66.48 ± 19.18	16.56 ± 0.07	265.61 ± 3.00	10.63 ± 0.17	-77.94 ± 9.50
-1	7.55 ± 0.12	235.71 ± 4.74	14.71 ± 0.07	260.28 ± 1.18	7.99 ± 0.10	253.22 ± 2.50
2	5.72 ± 0.14	94.85 ± 1.08	3.22 ± 0.12	54.49 ± 4.33	2.81 ± 0.13	106.12 ± 3.04
-2	6.78 ± 0.04	126.93 ± 1.57	4.97 ± 0.03	108.87 ± 0.78	3.84 ± 0.04	138.80 ± 1.55
3	1.42 ± 0.06	232.06 ± 2.20	1.83 ± 0.03	-88.01 ± 0.10	2.15 ± 0.05	245.09 ± 1.54
-3	3.17 ± 0.08	214.90 ± 2.69	1.52 ± 0.06	229.12 ± 2.44	2.21 ± 0.06	222.36 ± 2.53

Table 3: Seasonal waves in axial excitation functions : amplitude (mas) and phase (degrees) with respect to epoch J2000.0.

cpy	χ_G		χ_A		χ_{A+O}	
	amplitude	phase	amplitude	phase	amplitude	phase
1	0.89 ± 0.04	-28.52 ± 1.16	0.87 ± 0.02	-32.40 ± 0.60	0.83 ± 0.02	-30.96 ± 0.60
2	0.66 ± 0.01	116.56 ± 0.23	0.56 ± 0.00	110.89 ± 0.09	0.56 ± 0.00	113.11 ± 0.10
3	0.12 ± 0.00	46.61 ± 0.15	0.11 ± 0.00	45.60 ± 0.07	0.11 ± 0.00	44.75 ± 0.08

where A_j is a real quantity, ϕ_j the phase with respect to january 1st 2000 at 12h UTC. Contribution for seasonal waves are reported in Table 3. As already shown by numerous studies, atmosphere is sufficient for accounting seasonal peaks of LOD fluctuations.

Comparison of geophysical and geodetic forcings is now extended to their whole spectra. Firstly the overall correlation of the geodetic excitation function and the geophysical ones has been computed on the span 1985.02-1996.30. Results are reported in Table 4. When looking at AAM-IB alone, we notice correlation of 0.38 for the x-component, 0.56 for the y-component. This dissimetry is probably associated to the fact that continental surface is prominent in the y direction (the y-axis is towards Asia). The oceans have a larger influence in the x direction (negative x-axis is facing the Pacific ocean). Indeed, when adding OAM to AAM series, the offset of correlation between x and y components is decreased, whereas both correlations become larger (up to 0.64). The correlation between axial component does not undergo significant changes when adding oceanic contribution, and remains at the level of 0.75.

Table 4: Global correlation between geodetic and geophysical excitation functions.

	x	y	z
Observed / AAM-IB	0.384	0.557	0.755
Observed / AAM-IB+OAM	0.526	0.636	0.755

The coherence between equatorial function excitations have been computed. It shows a global increase of the coherence by adding the oceanic excitation. The increase is larger for the prograde part of the signal and concerns especially the frequency band between -20 cpy and +20 cpy, around +1 cpy. At this frequency, before adding OAM effects, the coherence is about 0.2.

It grows at 0.6 with the OAM effects.

4. CONCLUSION

The non-tidal oceanic excitation is negligible in length of day variations. But the impact of the oceans is considerable for polar motion. In this case the correlation between geophysical and geodetic excitations is improved significantly by adding OAM to AAM. We notice that the budget of seasonal terms is almost closed except for the semi-annual amplitude. However for periods below 36 days (10 cpy) there is too much power in geophysical excitation with respect to the observed one.

6. REFERENCES

Barnes R.T.H., Hide R., White A.A., and Wilson C.A., 1983, Atmospheric angular momentum fluctuations, length-of-day changes and polar motion, *Proc. R. Soc. London*, **A 387**, 31–73.

Brzeziński A., 1994, Polar motion excitation by variations of the effective angular momentum function, II: extended model, *manuscripta geodaetica*, **19**, 157–171.

Brzeziński and Nastula, 2000, Investigations of the oceanic excitation of non-seasonal polar motion, to be published in *Proceedings COSPAR'2000 Scientific Meeting*, Advances in Space Research.

Dickman, 1993, Dynamic ocean-tide effects on Earth's rotation, *Geophys. Journal Int.*, **112**, 448-470.

Eubanks M., 1993, Interactions between the atmosphere, oceans and crust : possible oceanic signals in Earth rotation, *The orientation of the planet Earth as observed by modern space techniques*, edited by M. Feissel.

Gross R., 1998, Effects of long-period ocean tides on the Earth's polar motion, *progress in oceanography*,vol. **40**, No. 1-4, 385-397.

Gross R., The excitation of the Chandler Wobble, 2000, *Geophys. Res. Let.*, Vol. **27**, 15, 2329-2332.

IERS annual report, p. 125, 1999, Observatoire de Paris.

IERS, 2001, http://hpiers.obspm.fr/eop-pc/

Moritz and Mueller, *Earth rotation*, theory and Observation.

Ponte R.M., D. Stammer and J. Marshall, Oceanic signals in observed motions of the Earth's pole of rotation, 1998, *Nature*, vol. **391**, 476-479.

Ponte R.M. and D. Stammer, 1999, Role of ocean currents and bottom pressure variability on seasinal polar motion, *J. Geophys. Res.*, vol. **104**, 23393-23409.

Ponte R.P. and D. Stammer, Global and regional axial ocean angular momentum signals and length-of-day variations (1985-1996), *J. Geophys. Res.*, 2000, vol. **105**, 17161-17171.

de Viron O., Bizouard C., Salstein D., Dehant V., 1999, "Atmospheric torque on the Earth and comparison with the atmospheric angular momentum variations". *J. Geophys. Res.*, **104**, N3, p. 4835.

de Viron O. and V. Dehant, 1999, Earth's rotation and high frequency equatorial angular momentum budget of the atmosphere, *Surveys in Geophysics*, **20**, 441-462.

Wilson A., Vicente R., 1981, Estimates of Chandler's Component of Polar Motion as Derived from Various Data Sets, *Astron. Nachr.* **Bd 302 H 5**, 227-232.

CHANDLER WOBBLE AS PART OF THE INTER-ANNUAL OSCILLATION OF THE ATMOSPHERE-OCEAN-EARTH SYSTEM

N.S. SIDORENKOV
Hydrometcenter of Russia
11-13 Bolshoi Predtechenskii pereulok, MOSCOW, 123458
e-mail: sidorenkov@rhmc.mecom.ru

ABSTRACT. The power spectra of the pole coordinates, the El Nino/Southern Oscillation (ENSO) indices, the Quasi- Biennial Oscillation (QBO) in the zonal wind field of the tropical stratosphere and the effective atmospheric angular momentum function series are calculated. The presence of subharmonics of the Chandler period (1.2 years) and superharmonics of the lunar period (18.6 years) in the ENSO and QBO spectra are detected.

It is revealed that the power spectrum of the QBO and the series coordinates of the Pole have a similarity coefficient 2.

A model for the nonlinear nutation of the Earth - ocean - atmosphere system is constructed. In this model, the ENSO, acting at frequencies of combinational resonances, excites the Chandler wobble of the Earth's poles. At the same time, this wobble and long tide interacts with the nutation motions of the atmosphere and World Ocean.

ABBREVIATION: CW - Chandler Wobble, DT - Darwin-Tahiti, EAAM - Effective Atmospheric Angular Momentum, ENSO - El Nino–Southern Oscilation, QBO - Quasi-biennial Oscillation, SST - Sea-surface Temperature

1. INTRODUCTION

Despite a hundred years of investigation, the nature of the Chandler wobble of the poles (CW) remains unclear. The mechanism for its excitation is still actively discussed. Meteorological and seismic processes are most frequently considered as possible drivers of the CW. Most estimates suggest that the effect of the atmosphere is small. In our opinion, negative conclusions about the role of meteorological processes in exciting the CW have been reached for two different reasons. The first is the scarcity of meteorological observations in the Southern Hemisphere, where the ordered oscillations of air and water masses between the Pacific and Indian oceans (the El Nino Southern Oscillation, or ENSO) that swing the Earth take place (Sidorenkov 1992, 1997, 2000a). The second reason is the traditional use of linear oscillation theory for estimates, which is inadequate for describing these oscillations. Note that estimates of the excitation of the polar motion have usually been made near the principal resonance - the Chandler frequency (Wilson, Haubrich 1976; Vondrak, Pejovic 1988). However, in the Earth - ocean - atmosphere system exist nonlinear oscillations and excitation of the CWP occur primarily at combinational frequencies of the Chandler frequency (with periods of 2.4, 3.6, 4.8, and 6 years) (Sidorenkov

1992, 1997, 2000a), rather than at the principal resonant frequency.

Here, we present the results of our study of the power spectra of characteristics of oceanic and atmospheric processes. We also consider series of effective functions of the atmospheric angular momentum (EAAM). These spectra confirm the presence of subharmonics of the Chandler period and indicate the presence of superharmonics of the fundamental period of the Earth forced nutation (18.6 years). Generalization of these results suggests the existence of coordinated oscillation motions of the Earth, ocean, and atmosphere, which affect each other in a nonlinear way. We suggest that the wobble of the Earth's poles, the El Nino phenomenon in the ocean, the Southern Oscillation and Quasi-Biennial Oscillation in the atmosphere - currently studied as independent phenomena in different disciplines - should be treated collectively as a single phenomenon in connection with the nonlinear oscillation of the Earth-ocean-atmosphere system.

2. INITIAL DATA

A large number of indices have been devised to describe the ENSO phenomenon. We will use the Southern oscillation index (SOI). There is a continuous series of monthly averages of the SOI from 1866 to the present time (Sidorenkov 1991; Climate Diagnostics Bulletin; Allan et al. 1991).

Wright (Wright 1989) calculated series mean quarterly DT indices from 1851 to the present time in steps of three months (Wright 1989).

The QBO are characterized by mean zonal wind speed u in a layer between 19-31 km of the equatorial zone. We have series mean monthly u values spanning the period from 1954 to 2000 (Sidorenkov 2000b).

Thermal oscillations of the ocean are characterized by the sea surface temperature (SST) averaged over the most representative regions. The well-known series of monthly average SST indices for various Nino regions in the near- equatorial Pacific zone, the N.Atl and S.Atl regions in the Atlantic, the Tropics regions in three oceans, etc. Regrettably, these series are available only for the period from 1950 to the present.

Series of the components χ_i of the EAAM functions covering the period from 1958 to 2000 with a resolution of six hours are now available (Kalnay et al. 1996; Salstein and Rosen 1997).

3. SPECTRAL ANALYSIS

Sidorenkov (1997, 2000a) published analysis of a series of SOI values starting in 1866 and of DT indices starting from 1851. This revealed components with periods of about 6, 3.6, 2.8, and 2.4 years (and possibly 12 years as well).

In the current study, we calculated periodograms and power spectra for series of SOI values and SST anomalies for 1950 - 2000 (fig. 1). We also calculated the periodograms and power spectra of all daily averaged EAAM components χ_i^P and χ_i^w over the 42-year period. The table contains the results of our spectral analysis of all the series. The detected periods are given in the third column in order of decreasing spectral power.

Although the analyzed series of ENSO indices cover a relatively short time interval, the detected periods mainly coincide with those derived from 145- and 114-year series (Sidorenkov 1997,2000a). It is true, however, that a six-year period was detected in the 145- and 114-year ENSO series, while a 4.9- year period is indicated in the modern indices. Spectral analysis of series of the atmospheric angular momentum components χ_i^w (wind components) and χ_i^{Pib} (atmospheric pressure components with allowance for the inverted barometer effect) indicates the possible presence of superharmonics of the forced nutation period (4.7, 3.7, 3.1, 2.7, 2.3, 2.1, and 1.86 years). Some of these superharmonics are close to the 2.4-, 3.6-, 4.8-, and 6.0-year

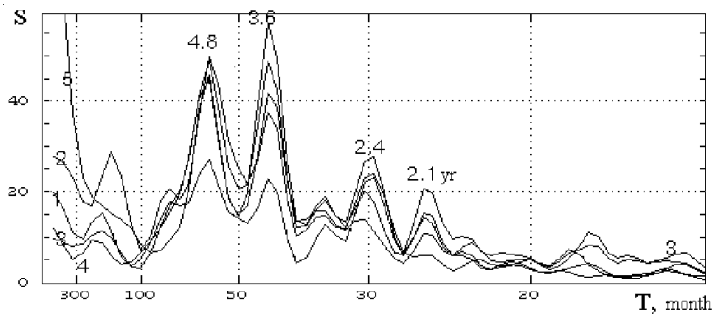

Figure 1: Spectra of oscillations of the SOI (1), Nino4 (2), Nino3.4 (3), Nino3 (4), and Tropics (5) indices. Oscillation periods (in months) and spectral densities (in arbitrary units) are plotted on the horizontal and vertical axes.

subharmonics of the Chandler period. Thus, our analysis of the atmospheric angular momentum components is consistent with the results obtained from analysis of the ENSO indices. However, series of atmospheric angular momentum components are still too short to reliably detect multi-year cycles.

The spectral - time diagrams of the SOI constructed in (Sidorenkov 1998), as well as wavelet and waveform analyses, show that the SOI cycles are unstable in time. After emerging at certain frequencies, the cycles can fade over some time interval and be excited again at other frequencies. For example, a six-year ENSO periodicity dominated until the middle of the 20th century, when it was replaced by a 4.9-year cycle (fig. 1).

The QBO power spectrum fully coincides with the power spectrum of the polar motion, if the frequency scale is doubled (fig.2) (Sidorenkov 2000b). In equatorial stratosphere the duration of all the Earth polar motion cycles is doubled.

Thus, all these investigations indicate the presence in the ENSO and QBO spectra of components 4.8, 3.6, 2.8, 2.4 that are approximately multiples of the Chandler period (1.2 years) and of the fundamental period of the Earth's forced nutation (18.6 years). The periods of superharmonics of the forced- nutation period are given in the last column of the table.

4. A MODEL FOR EXCITING FREE MOTION OF THE POLES

The redistribution of air and water masses between the Pacific and Indian oceans during the El Nino/Southern oscillation (ENSO) changes the components of the Earth's inertia tensor and shifts the position of the pole of the Earth's rotation. The excitation of the polar wobble can be estimated (Munk and Macdonald 1960) using the equation

$$\frac{i}{\underline{\sigma}}\frac{d\underline{m}}{dt} + \underline{m} = \underline{\Psi}. \qquad (1)$$

Here, $\underline{\sigma} = \sigma + i\beta, \sigma = 2\pi/T$, is the frequency of the free motion of the poles; $T = 1.2$ years is the Chandler period; β is the damping decrement; i is the square root of - 1; $\underline{m} = m_1 + im_2$ (m_1 and m_2 are the direction cosines of the Earth's instantaneous angular rotation vector); and $\underline{\Psi} = \chi_1 + i\chi_2$ (χ_1 and χ_2 are the components of the exciting function for the atmospheric angular momentum) (Munk and Macdonald 1960; Barnes et al. 1983).

Table 1: The dominant cycles of the ENSO and components of the EAAM.

Index	Region borders	Periods of cycles, year
SOI		4.9; 2.4; 3.6; 2.1
DT		5.8; 3.6; 2.8; 12; 2.4
QBO	$5°N - 5°S$ $0° - 360°$	4.8; 2.4; 2.0; 1.2; 1.0
$Nino4$	$5°N - 5°S$ $160°E - 150°W$	4.9; 3.6; 12; 2.4; 6.4
$Nino3.4$	$5°N - 5°S$ $170°W - 120°W$	4.9; 3.6; 2.4; 2.9;2.1
$Nino3$	$5°N - 5°S$ $150°W - 90°W$	3.6; 4.9; 2.1; 2.5; 2.9
$Nino1+2$	$0° - 10°S$ $90°W - 80°W$	3.6; 4.9; 6.4; 2.9; 2.1
$Tropics$	$10°N - 10°S$ $0° - 360°$	4.9; 3.6; 2.8; 2.4; 2.1
$N.Atl$	$5°N - 20°N$ $60°W - 30°W$	9.3; 3.6; 2.5; 2.1; 5.2
$S.Atl$	$0° - 20°S$ $30°W - 10°E$	12; 5.2; 2.3; 3.5
χ_1^w	$Globe$	2.7; 3.7; 1.86; 5.9; 2.4
χ_2^w	$Globe$	2.7; 3.1; 2.1; 1.8
χ_3^w	$Globe$	2.4; 3.7; 5.1
χ_1^{pib}	$Globe$	2.6; 3.7; 4.6; 1.7
χ_2^{pib}	$Globe$	2.4; 2.7; 5.9
χ_3^{pib}	$Globe$	5.1; 4.1; 2.3; 2.7
$18.6yr.$	superharmonics	6.2; 4.7; 3.7; 3.1; 2.7; 2.3; 2.1

The Chandler wobble of the poles is responsible for perturbations of the centrifugal potential and induces polar tide in the atmosphere and ocean. For example, the static polar tide in the ocean has the form (Munk and Macdonald 1960)

$$\zeta = -\frac{1+k-h}{g}\frac{\Omega^2 R^2}{2}\sin 2\theta(m_1\cos\lambda + m_2\sin\lambda), \tag{2}$$

where k and h are Love numbers, Ω is the magnitude of the Earth's angular rotation vector, θ is the colatitude, and λ is the longitude. In the atmosphere, the polar tide is described by the same expression, since

$$\Delta P = \int_0^{\zeta_a} \rho g dz, \tag{3}$$

but with a different amplitude. We should stress that the amplitude is a function of the polar deviation $\underline{m}$.

Analysis of tide records indicates a resonant spectral- density peak at period T (Munk and Macdonald 1960). A 14-month periodicity in the Atlantic subtropical circulation has repeatedly been noted (Lappo et al. 1990; Shuleikin 1965). By analogy with equations (2) and (3), we might expect that, in the case of linear interactions of nutation waves, the amplitude A of the exciting function $\underline{\Psi}$ for the atmosphere and the ocean must be a function of $\underline{m}$. However, the presence of subharmonics of the Chandler period (≈2.4, 3.6, 4.8, and 6.0 years) and superharmonics of the forced nutation period (≈2.3, 3.7, 4.7, and 6.2 years) in the ENSO and atmospheric angular momentum spectra indicate the nonlinear interaction of the forced and free nutation motions of the Earth, ocean, and atmosphere. Therefore, we assume that the amplitude A_k of each harmonic with number k of the exciting function $\underline{\Psi}$ has a power-law dependence on the value $\underline{m}$: $A_k = \mu_k \underline{m}^{\alpha_k}$, where α_k is a power law exponent different from unity and μ_k is a proportionality coefficient (Sidorenkov 1997, 2000a).

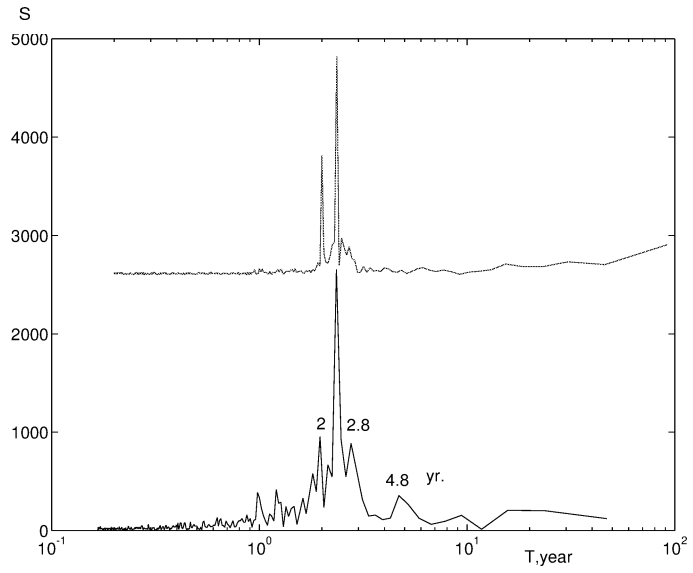

Figure 2: Power spectra of the QBO indices (bottom) and the coordinate x of the pole (top). For demonstrating the curves similarity on the plot x coordinate oscillation periods T and spectral densities S were calculated as $T = 2T_0$ and $S = 30 * S_0 + 2600$, where T_0 and S_0 are actual (initial) value.

Using this assumption, we can approximate the function $\underline{\Psi}$ by the sum of N harmonics:

$$\underline{\Psi} = \sum_{k=1}^{N} \mu_k \underline{m}^{\alpha_k} \exp[\omega_k i(t - t_{0k})] \approx \sum_{k=1}^{N} \mu_k \underline{m}^{\alpha_k} \exp(\omega_k i t). \tag{4}$$

Here, k is the number of the harmonic, ω_k is its frequency, and $\omega_k t_{0k}$ is the initial phase, which is set equal to zero. For subharmonics of the Chandler frequency, $\omega_k = \sigma/n_k$, where n_k =2, 3, 4, ... are subharmonic numbers.

We were not able to find a solution of equation (1) with the function $\underline{\Psi}$ in the form (4). Therefore, we simplified expression (4):

$$\underline{\Psi} = \underline{m}^{\alpha} \sum_{k=1}^{N} \mu_k \exp(\omega_k i t). \tag{5}$$

Then, the solution of equation (1) with the function $\underline{\Psi}$ given by (5) at $m(0) = m_0$ takes the form

$$\underline{m}(t) = \{\underline{m}_0^{1-\alpha} \exp[(1-\alpha)\underline{\sigma} i t] - i\underline{\sigma}(1-\alpha) \times \exp[(1-\alpha)\underline{\sigma} i t] \int_0^t \exp[(\alpha-1)\underline{\sigma} i \tau] \times$$
$$\times (\sum_{k=1}^{N} \mu_k \exp(\omega_k i \tau)) d\tau\}^{\frac{1}{1-\alpha}} = \{\underline{m}_0^{1-\alpha} \exp[(1-\alpha)\underline{\sigma} i t] +$$

$$+ \sum_{k=1}^{N} \frac{\mu_k (1-\alpha)\underline{\sigma}}{[(1-\alpha)\underline{\sigma} - \omega_k]} \times [\exp(i\omega_k t) - \exp[(1-\alpha) i \underline{\sigma} t]]\}^{\frac{1}{1-\alpha}}. \tag{6}$$

The first term in braces of (6) describes the free motion of the pole due to its initial deviation $\underline{m}_0$. The second term (first sum) describes the overall forced motion of the pole with the excitation frequencies ω_k. The third term (second sum) describes the polar motion caused by the function $\underline{\Psi}$ with the fundamental frequency $\underline{\sigma}$.

Expression (6) describes the result in the most general form. To make this equation easier to understand, we make the following simplifications: (a) We neglect the initial deviation of the pole; i.e., we set $\underline{m}_0 = 0$, and (b) we neglect damping; i.e., we set $\underline{\sigma} = \sigma$. In this case expression (6) takes the form

$$\underline{m}(t) = \{\sum_{k=1}^{N} \frac{\mu_k(1-\alpha)\sigma}{[(1-\alpha)\sigma-\omega_k]} \times [\exp(i\omega_k t) - \exp[(1-\alpha)i\sigma t]]\}^{\frac{1}{1-\alpha}} =$$

$$= \{\sum_{k=1}^{N} \frac{\mu_k(1-\alpha)\sigma}{i[\omega_k-(1-\alpha)\sigma]} 2\sin\frac{[\omega_k-(1-\alpha)\sigma]t}{2} \times \exp\frac{[\omega_k+(1-\alpha)\sigma]}{2} it\}^{\frac{1}{1-\alpha}}. \quad (7)$$

For $(1-\alpha)\sigma = \omega_k$, the term with number k in (7) is an indeterminate form of the type $0/0$. For subharmonics of the Chandler frequency, the exponent $\frac{1}{1-\alpha} = n_k$ is equal to a positive integer number ($n_k = 2, 3, 4, ...$). Let us suppose, for example, that $\omega_1 \to (1-\alpha)\sigma$. Then, the sine of the small angle in the first term of (7) can be replaced by the angle itself and will cancel from the numerator and denominator. All other terms (with numbers k = 2, 3, ..., N) remain unchanged, and we obtain

$$\underline{m}(t) = \{-\mu_1(1-\alpha)\sigma it\exp(i\omega_1 t) + \sum_{k=2}^{N} \frac{\mu_k(1-\alpha)\sigma}{[(1-\alpha)\sigma-\omega_k]}[\exp(i\omega_k t) - \exp[(1-\alpha)i\sigma t]]\}^{\frac{1}{1-\alpha}}. \quad (8)$$

The same result will be obtained if we formally evaluate the indeterminate form in (7) using L'Hopital's rule. The coefficient in the first exponential term increases with time t. All other terms have constant coefficients. Thus, at sufficiently large t, we can neglect all terms in braces except for the first.

In another time interval, a periodicity with frequency ω_k may dominate. In this case, analysis of the behavior of $\underline{m}$ gives a result similar to (8). Summing the resonant contributions from all terms, we obtain

$$\underline{m}(t) \approx \{\sum_{k=1}^{N}[-\mu_k(1-\alpha)\sigma it\exp(i\omega_k t)]\}^{\frac{1}{1-\alpha}} = \sum_{k=1}^{N}(\mu_k\omega_k)^{n_k} t^{n_k}\exp[i(\sigma t + \frac{3n_k\pi}{2})]. \quad (9)$$

Here, we took into account the relations $(1-\alpha)\sigma = \omega_k$, and $\frac{1}{1-\alpha} = n_k$.

Thus, for $\sigma = n_k\omega_k$, i.e., when the frequency of free oscillations of the pole is an integer multiple of the excitation frequency, a combinational resonance arises. The perturbing forces act synchronously with the proper oscillations of the Earth, giving rise to an intense swinging of the Earth about its rotation axis. The amplitude of the polar oscillations increases with time according to a power law (i.e., proportional to t^{n_k}), the more rapidly the lower the frequency of the subharmonic excitation component. Even low-power oscillations of the exciting function $\underline{\Psi}$ can lead to significant oscillations of the instantaneous angular rotation vector $\underline{m}$ of the Earth. As the amplitude of the polar oscillations increases, resistance leading to damping of the oscillation grows, so that an infinite increase of the amplitude becomes impossible.

5. CONCLUSIONS

The ENSO changes the components of the atmospheric inertia tensor and consequently excites motions of the Earth's poles. External actions from celestial bodies are superimposed on the internal stochastic oscillations of the atmosphere and the ocean. Some superharmonics (2.3,

3.7, 4.7, and 6.2 years) of the main component of the forced nutation motions of the atmosphere and ocean are near or equal to the subharmonics (2.4, 3.6, 4.8, and 6.0 years) of the period of free motion of the Earth's poles. Resonance excitation of the CWP occurs at these combinational frequencies.

It is revealed that the power spectrum of the QBO indices and the series coordinates of the Earth Pole have a similarity coefficient 2. In equatorial stratosphere the duration of all the Earth polar motion cycles is doubled.

Thus, the wobble of the Earth's poles, El Nino and La Nina oscillations in the ocean, the Southern oscillation and Quasi-Biennial Oscillation in the atmosphere are constituent parts of a single phenomenon - of the inter-annual oscillation of the Earth - ocean - atmosphere system.

ACKNOWLEDGMENT. The investigation was carried out under a financial support of the Russian Foundation for Fundamental Research, Grant No 99-02-16287.

7. REFERENCES

Allan, R. J., Nicholls, N., Jones P.D., and Butterworth, I.J., 1991, *J. Climate* **4**, 743.

Barnes, R. T. H., Hide R., White A.A. and Wilson C.A., 1983, *Proc. R. Soc. London,* Ser. **A 387**, 31.

Climate Diagnostics Bulletin. NOAA, Climate Prediction Center, Washington, D.C.

Kalnay E., Kanamitsu M., Kistler R., et al., 1996, *Bull. Am. Meteor. Soc.* **77**, 437.

Lambeck K., 1980, The Earth's Variable Rotation. Geophysical Causes and Consequences. Cambridge Univ. Press, Cambridge.

Lappo S. S., Gulev S. K. and Rozhdestvenskii A. E., 1990, Large-Scale Thermal Interaction in the Ocean - Atmosphere System and Energy-Active Areas of the World Ocean Gidrometeoizdat, Leningrad.

Munk W. H. and Macdonald G. J. F., 1960, The Rotation of the Earth, a Geophysical Discussion. Cambridge Univ. Press, Cambridge, 323.

Salstein D. A. and Rosen R. D., 1997, in Proc. Seventh Conference on Climate Variations (American Meteorological Society, Boston), 344.

Shuleikin V. V., 1965, *Izv. Akad. Nauk SSSR, Fiz. Atmos. Okeana.* **1**, 413 .

Sidorenkov N. S., 1991, *Tr. Gidromettsentra* **316**, 31.

Sidorenkov N. S., 1992, *Astron. Zh.* **69**, 905.

Sidorenkov N. S., 1997, *Astron. Zh.* **74**, 792.

Sidorenkov N. S., 1998, in Atlas of Time Variations of Natural, Anthropogeneous and Social Processes. Vol. 2. Cyclic Dynamics in the Nature and in Society (Nauchnyi Mir, Moscow), 274.

Sidorenkov N. S., 2000a, In "Polar Motion: Historical and Scientific Problems". ASP Conference Series **208**, S.Dick, D.D.McCarthy, and B.Luzum, eds. - P. 455-462.

Sidorenkov N. S., 2000b, *Tr. Gidromettsentra* **331**, 12.

Vondrak J. and Pejovic N., 1988, *Bull. Astron. Inst. Czechosl.* **39**, 172.

Wilson C. R. and Haubrich R. A., 1976, *Geophys. J. R. Astron. Soc.* **46**, 707.

Wright P.B., 1989, *Int. J. Climatol.* **9**, 33.

Yatskiv Ya. S. et al., 1976, *Itogi Nauki Tekhn., Ser. Astron.* 12.

VARIATION OF ZONAL ANOMALIES OF ATMOSPHERIC EXCITATION FUNCTION FOR POLAR MOTION DURING 1983-1999

J. NASTULA, B. KOLACZEK
Space Research Centre of the PAS,
Bartycka 18a, 00 716 Warsaw, Poland
e-mail: nastula@cbk.waw.pl; kolaczek@cbk.waw.pl
D. A. SALSTEIN
Atmospheric and Environmental Research Inc.,
Lexington, MA, USA
e-mail: dsalstei@aer.com

ABSTRACT
The pressure term of atmospheric excitation function for polar motion and monthly anomalies of its equatorial components χ_1 and χ_2 are computed in equal area belts for the 17 years from 1983 to 1999. The variance of the excitation maximizes in the middle to higher latitude belts of both hemispheres. In the case of equatorial component χ_1 of this excitation function there are distinct annual oscillations in the north. In the χ_2 component there are distinct disturbances in the south coinciding with La Nina phenomena in 1988, 1992, 1998. The variation in the overall amplitude of the excitation, from a combination of the χ_1 and χ_2 terms, maintains a distinctly annual oscillation in the north and La Nina disturbances in the south in its signature.

1. INTRODUCTION

Very high correlations between variations of Atmospheric Angular Momentum (AAM), length of day (LOD) and the El-Nino Southern Oscillation cycles are well known (Chao, 1989; Dickey et al., 1994, Dickey et al.; 1999; Eubanks et al., 1986; Gipson, 1999; Salstein et al., 1999). In the case of polar motion variations correlations with atmospheric excitation are not quite as strong. Maxima in the correlation coefficients are of the order of 0.8 but they are somewhat variable (Kosek et al., 1995; Kolaczek et al., 1999, 2000 a, b).

Anomalies of AAM wind term responsible for LOD variations computed in 46 equal area latitude belts from pole to pole for every day by Salstein et al. (1999) show distinctly disturbances related to the El Nino events of 1983 and 1987. Here zonal anomalies of equatorial components of the atmospheric pressure term, responsible for polar motion variations, over the last 17 years are investigated.

2. ANALYSIS AND RESULTS

Regional values of the atmospheric surface pressure excitation terms for polar motion, χ_1 and χ_2, pointing to the Greenwich and 90^oE meridians, respectively, have been computed in

3312 equal-area sectors from the NCEP/NCAR reanalysis AAM data since 1983. ¿From these data monthly anomalies of pressure atmospheric terms were calculated in 46 equal area latitude belts equivalent to those in Salstein (1999), but only those between 30 to 80 degrees are considered here. The absolute value of the anomaly amplitudes in that region are shown in Figure 1. Examining the modulus of these anomaly amplitudes provides a better way to detect the character of these variations. In the case of χ_1 in the Northern Hemisphere there are distinct annual variations, probably caused by continents, whose position is felt more by χ_1. In the case of χ_2 there are most distinct disturbances in the south coinciding with La Nina phenomena in 1988, 1992, 1998. The modulus of anomaly amplitudes of complex values of $\chi_1 + i\chi_2$ show these variations more distinctly in Figure 2. Introduction of the correction due to the inverted barometer (IB), however, tends to eliminate these variations. The modulus of the anomaly amplitudes of the combined term $\chi_1 + i\chi_2$ show also disturbances coinciding with mentioned La Nina phenomena, (Fig. 3).

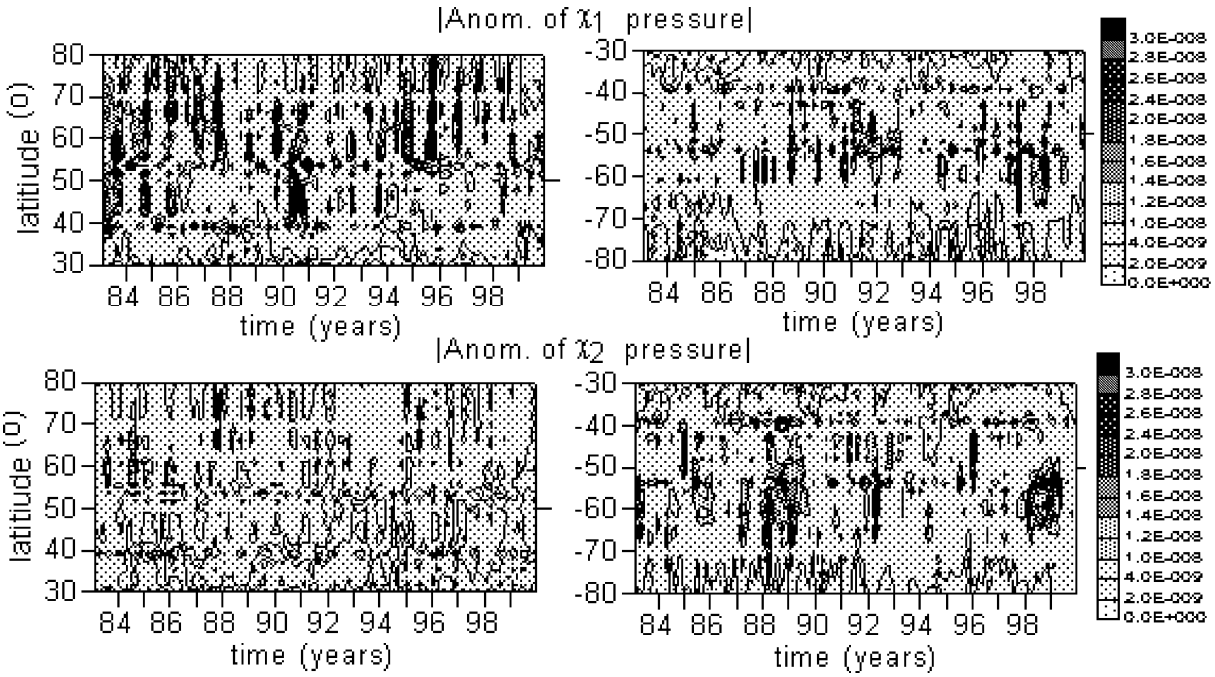

Figure 1. Modules of anomalous amplitude values of χ_1 and χ_2 components of AAM pressure term in equal area latitude belts for every month.

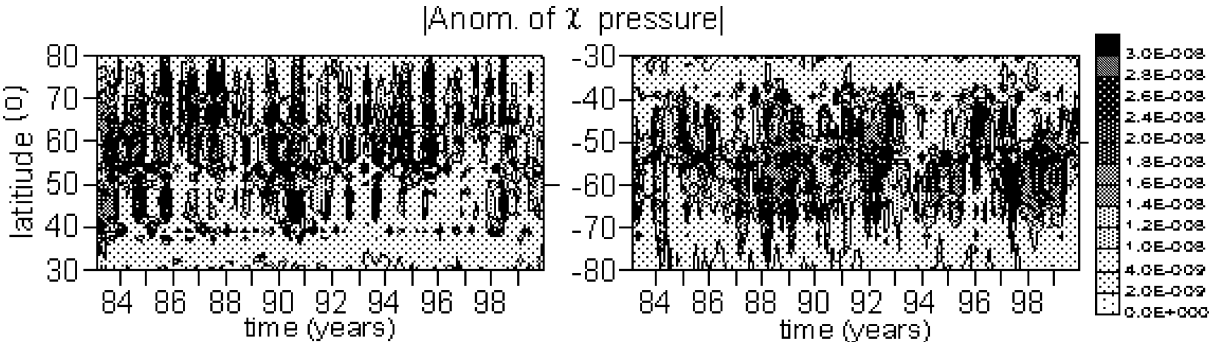

Figure 2. Modules of anomalous amplitude values of the complex, $\chi_1 + i\chi_2$ component of AAM pressure term in equal area latitude belts for every month.

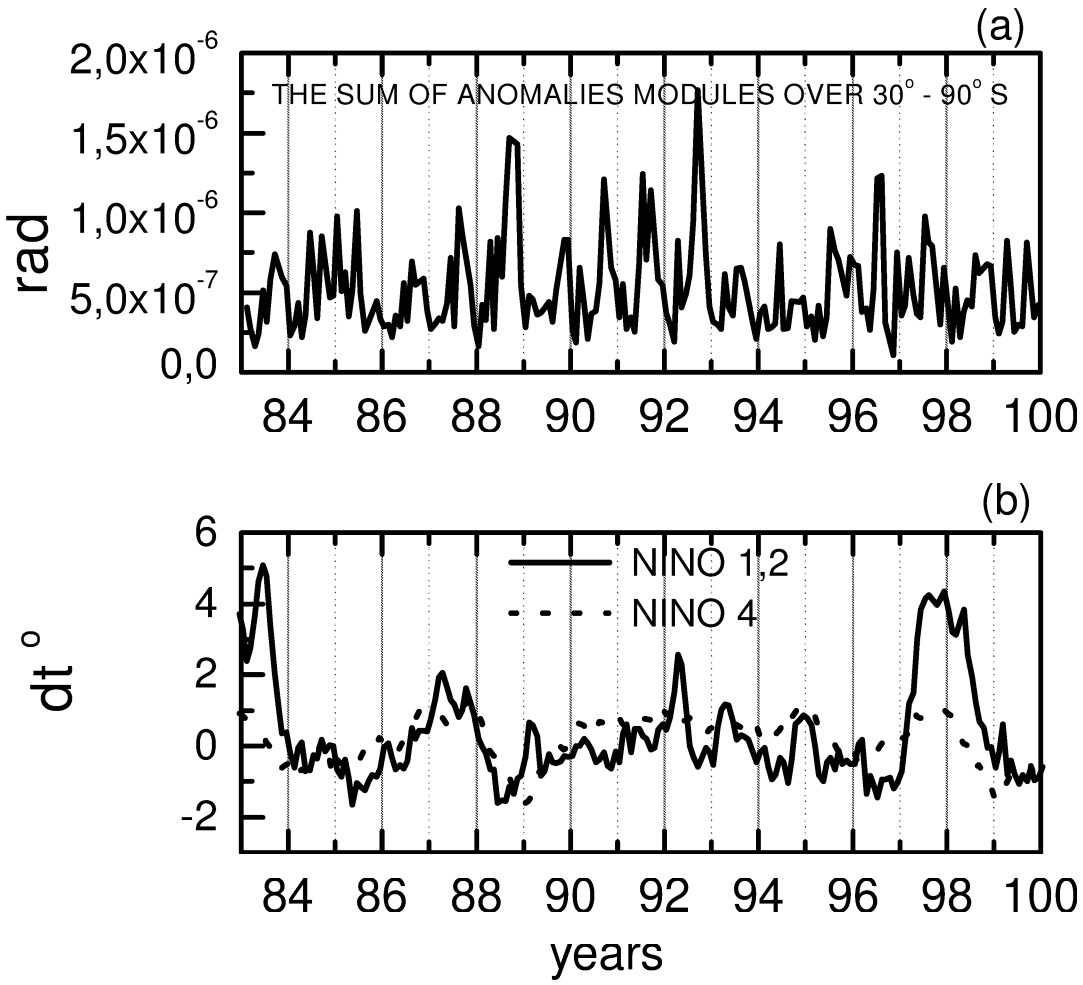

Figure 3. Comparison of (a) sum of anomaly amplitude modulus of $\chi_1 + i\chi_2$ pressure term with (b) Nino 1, 2 and Nino 4, related to sea-surface temperature in the eastern and central equatorial Pacific Ocean.

3. CONCLUSIONS

It is shown that anomalies of the pressure term of atmospheric excitation functions for polar motion have different patterns in the northern and in the southern hemispheres, with an annual pattern dominating the northern hemisphere, and a pattern related to the El Nino signal in the southern. For the modulus of the excitations, we note that years with La Nina events, the cold conditions in the eastern Pacific Ocean, a reduction in the anomalies of the excitation coefficients appears, from which we conclude that during La Nina, the forcing of polar motion by the atmosphere, particularly in the southern hemisphere, is reduced. The polar motion signals act rather differently that those noted for the axial component of Earth rotation, in which the anomalies of the wind term of atmospheric excitation function are strongly related to those of length of day, especially during all El Nino related events, including La Ninas. (Salstein et. al., 1999).

ACKNOWLEDGMENTS

The researches reported here were supported by the project of the Polish Committee Scientific Research, the Grant No. 9 T12E 009 13 and the NSF Grant Int. 9807014, and the NASA Earth Observing Program under Grant NAG5-9989.

4. REFERENCES

Chao B.F., 1989. Length of Day Variations Caused by El-Nino Southern Oscillation and Quasi Biennial Oscillation, Science, 243, 923-925.

Dickey, J.O., S.L. Marcus, R. Hide, T.N. Eubanks, and D.H. Boggs, 1994. Angular momentum exchange among the solid Earth, atmospheres and oceans: A case study of the 1982-1983 El Nino event, J. Geophys. Res. V. 99, No B12, Dec 10, pp 23921-2393.

Dickey, J.O., P. Gegout and S.L. Marcus, 1999. The 1997-1998 El Nino event: Insight via space geodesy, IERS TN 26, Observatoire de Paris, pp 29-32.

Eubanks, T.M., J.A. Steppe, and J.O. Dickey, 1986. The El Nino, the Southern Oscillation and the Earth's rotation, in Earth rotation, Solved and Unsolved Problems, NATO ASI Ser., Ser. C, 187, 163-186.

Gipson, J.M., and C. Ma, 1999. Signature of the El Nino in Length of Day as measured by VLBI, IERS Techn. Notes 26, Observatoire de Paris, pp. 17-23.

Kosek, W., J. Nastula, and B. Kolaczek, 1995. Variability of polar motion oscillations with periods from 20 to 150 days in 1979-1991, Bull. Geod. 69, 308-319.

Kolaczek B., M. Nuzhdina, J. Nastula and W. Kosek, 1999. El Nino impact on atmospheric and geodetic excitation functions of polar motion, IERS Technical Notes 26,Observatoire de Paris, pp. 23-28.

Kolaczek B., M. Nuzhdina, J. Nastula and W. Kosek, 2000. El Nino impact on atmospheric polar motion, JGR, Vol 105, No. B2, pp 3081-3087.

Salstein D.A., 1999. Atmospheric Angular Momentum during the 1997-98 El Nino event, . The impact of El Nino and other low-frequency signals on Earth rotation and global Earth system parameters, IERS TN 26, Observatoire de Paris, pp 13-16.

Salstein D.A., B. Kolaczek, and D. Gambis (Eds.), 1999. The impact of El Nino and other low-frequency signals on Earth rotation and global Earth system parameters, IERS TN 26, Observatoire de Paris.

VARIATIONS OF ANNUAL OSCILLATION PARAMETERS, EL NIÑO AND THEIR INFLUENCE ON POLAR MOTION PREDICTION ERRORS

W. KOSEK[1], D. D. McCARTHY[2], B. J. LUZUM[2]
[1]Space Research Centre, PAS, Warsaw, Poland,
[2]U.S. Naval Observatory, Washington D.C., USA.

1. INTRODUCTION

The error of short-term prediction of the pole coordinate data determined from space techniques is several times greater than their determination error, which is now of the order of 0.1 mas. The causes of such prediction errors are mainly due to irregular amplitudes and phases of the semiannual (Kosek and Kolaczek 1997) and shorter period oscillations (Kosek et al. 1995, 1998; Kosek 1997, 2000; Schuh and Schmitz-Hübsch 2000). Poor accuracy of short-term polar motion prediction can be also caused by the variable phase/period of the annual oscillation (Schuh et al. 2001a) which increase/decrease before the last 1997/98 El Niño event (Kosek et al. 2000, 2001). The Chandler phase/period variations at subseasonal time scale are more stable than the annual ones (Kosek et al. 2000, 2001).

In some of the prediction methods of polar motion, the parameters of harmonic functions including bias and drift were estimated and extrapolated into the future (Zhu 1981; McCarthy and Luzum 1991, 1996; Malkin and Skurikhina 1996). The polar motion was recently predicted using artificial neural networks (Schuh et al. 2001b), a nonlinear extended Kalman filter (Fernandez 2001) or by the autocovariance prediction applied to the pole coordinate data transformed into polar motion radius and angular distance (Kosek 2001). The current prediction method of polar motion data carried out in the IERS Rapid Service/Prediction Center is the least-squares extrapolation of a Chandler circle, annual and semiannual ellipses and a bias fit to the last 1 year of combined pole coordinate data (McCarthy and Luzum 1991). In this paper the same least-squares model is fitted to the last 1, 2,..., 6 years of combined pole coordinate data in order to determine the Chandler and annual amplitude and phase variations as well as to find the optimum model length for the prediction computation.

2. DATA

The analysis used USNO pole coordinate data (formerly referred to as NEOS data) in the years 1973.0 to 2001.6 with the sampling interval of 1 day (USNO 2001) and the monthly sea surface temperature anomalies Niño 1+2 in the years 1976.0 to 2001.6 from the Climate Prediction Center (NOAA 2001). The USNO series is based on a weighted cubic spline of multi-technique observational results corrected for possible bias and rate with respect to the IERS C04 series. The weights used in the combination are proportional to the inverse square of the estimated accuracy of input data.

3. ANALYSIS

Mis en forme

Implementing the least-squares model of the Chandler circle, annual and semiannual ellipses and the bias which is sliding along the whole data interval of pole coordinate data, it is possible to find the Chandler and annual amplitude and phase variations. Such variations were detected using the least-squares model fit to the 2, 3 and 4-year pole coordinate data sliding with a step of 7 days along the whole data interval from 1973.0 to 2001.6 (Fig. 1).

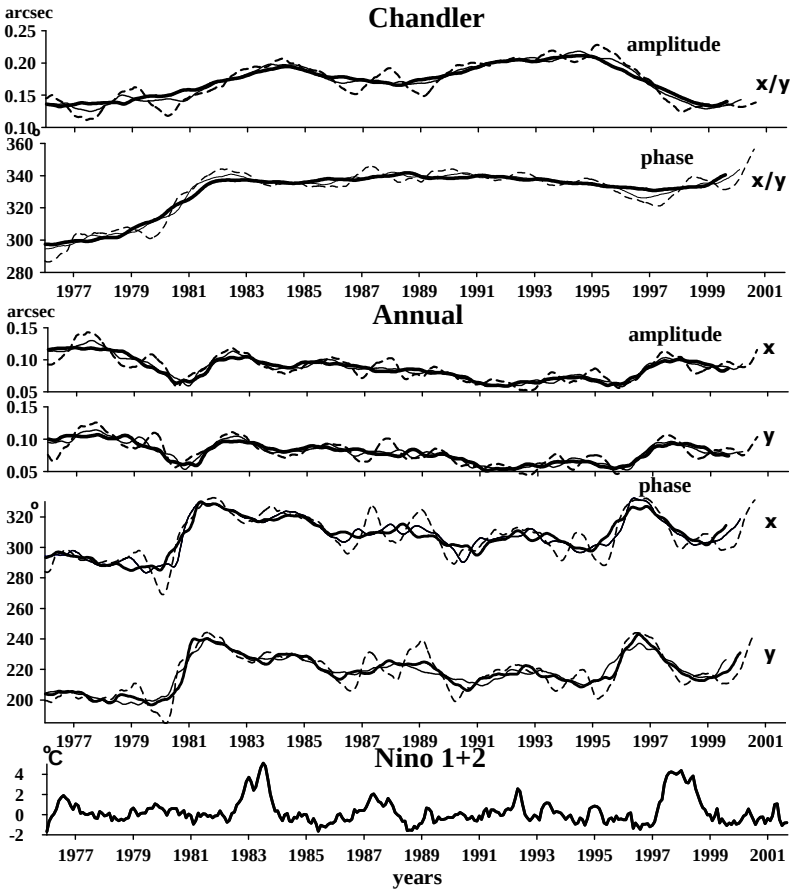

Fig. 1. The least-squares amplitudes and phases referred to the epoch 1976.060 (MJD=42800) of the Chandler and annual oscillations computed by the running 2 (dashed line), 3 (thin line) and 4-year (heavy line) boxcar windows and the Niño 1+2 data.

There are some increases of the annual oscillation amplitude just before or at the time of El Niño events in 1982/83 and 1997/98, respectively. After the 1980s, the amplitude of the annual oscillation was maximum during the time of the El Niño events in 1982/83 and in 1997/98, so it seems to be mostly correlated with the Niño 1+2 data. Before 1982 an increase of the phase of the Chandler oscillation of the order of 40° during 5 years can be seen and after that the variations of the phase of the Chandler oscillation are less than that of the annual oscillation. There are significant increases of the annual oscillation phase in the x and y pole

coordinate data of the order of 30°-40° before El Niño events in 1982/83 and 1997/98. Notice that the decrease of the phase values of the annual oscillation correspond to the maxima of El Niño events in 1982/83 and in 1997/98, so the first differences of the phase of the annual oscillation seem to be mostly correlated with the Niño 1+2 data.

The 1, 2 and 4-year least-squares extrapolation residuals of pole coordinate data were computed from the 1, 2, and 4-year series after subtracting the least-squares model data consisting of a Chandler circle, annual and semiannual ellipses and a bias (Fig. 2). These residuals were shifted by 7 days with respect to each other, then weighted by the trapezoid function and connected. The increase of the least-squares model length increases the amplitudes of the extrapolation residuals, and energetic oscillations of y extrapolation residuals usually have longer period oscillations than x extrapolation residuals.

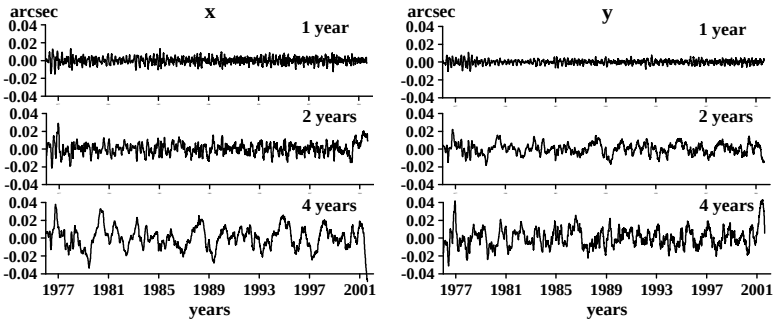

Fig. 2. Least-squares extrapolation residuals of x, y polar coordinates computed for the models with lengths of 1, 2 and 4 years.

Figure 3 shows the distance between the real and predicted pole positions from 1 to 90 days in the future as a function of starting prediction epochs and different lengths of pole coordinate data equal to 1, 2, 3, 4 and 6 years going into the least-squares model. Notice that when the length of the least-squares model increases, then the polar motion prediction errors increase too, and these errors became greater during the biggest El Niño events in 1982/83 and 1997/98. This suggests that there must be some relationship between the increase of polar motion prediction errors and the biggest El Niño events in 1982/83 and 1997/98. Big polar motion prediction errors before the 1980s were caused by less accurate polar motion data.

To check the relations between El Niño and the annual oscillation parameters, the correlation coefficients between the Niño 1+2 data and amplitude/phase variations of the annual oscillations were computed in the two time intervals 1980-2000 and 1990-2000 (Table 1). The least-squares amplitudes and phases were computed assuming the length of polar motion data going into the least-squares model was equal to 3 years. Notice that the absolute values of the correlation coefficients are significant at the 90% confidence level except the least-squares phase change data during the time interval of 1980-2000.

To estimate the relationship between El Niño and the polar motion prediction errors, the correlation coefficients between the Niño 1+2 data and mean polar motion prediction errors for 50 and 80 days in the future were computed (Table 1). The length of pole coordinate data going into the least-squares model was 3 years. Notice that these correlation coefficients are significant at the 90% confidence level except the polar motion prediction error at 80 days in the future computed during the time interval of 1980-2000.

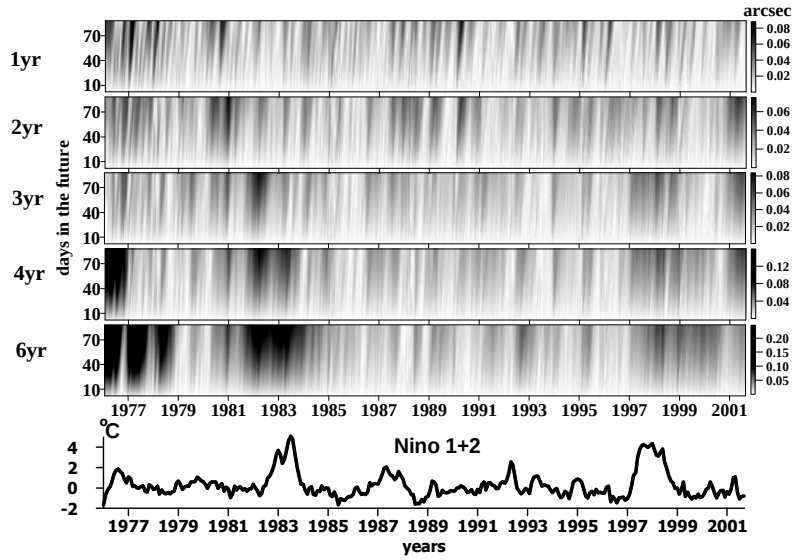

Fig. 3. The distance between the real polar motion position and that predicted by least-squares at different starting prediction epochs as a function of different lengths of the extrapolation models from 1 to 6 years. Niño 1+2 data are also shown.

Table 1. The correlation coefficient values between the Niño 1+2 data and the amplitudes/phase changes of the annual oscillation or the mean polar motion prediction error at 50 and 80 days in the future. * denotes correlation coefficients values significant at the 90% confidence level.

Time series / Time period	LS amplitude		LS phase-difference		Mean PM prediction error (days in the future)	
	x	y	x	y	50	80
Degrees of freedom → 1980-2000	26		36		26	24
	0.27*	0.28*	-0.20	-0.18	0.34*	0.25
Degrees of freedom → 1990-2000	13		18		13	12
	0.42*	0.44*	-0.35*	-0.32*	0.42*	0.46*

Figure 4 shows the mean prediction errors for polar motion as the mean error of the two errors estimated separately for x and y pole coordinate. These errors were estimated from the pole coordinate data in the time intervals of 1973.0 - 2001.6, 1984.0 - 2001.6 and 1984.0 - 1997.0 using different lengths of pole coordinate data equal to 1, 2,…, 6 years going into the least-squares model. Notice that during the first time interval of data the two biggest El Niño events in 1982/83 and 1997/98 occurred. During the second time interval of data there was only one El Niño in 1997/98, and during the third time interval of data no large energy El Niño events occurred. Notice that increasing the length of the pole coordinates data going into

the least-squares model increases the mean polar motion prediction errors. The polar motion prediction errors became larger when the time interval of polar motion data contain El Niño events.

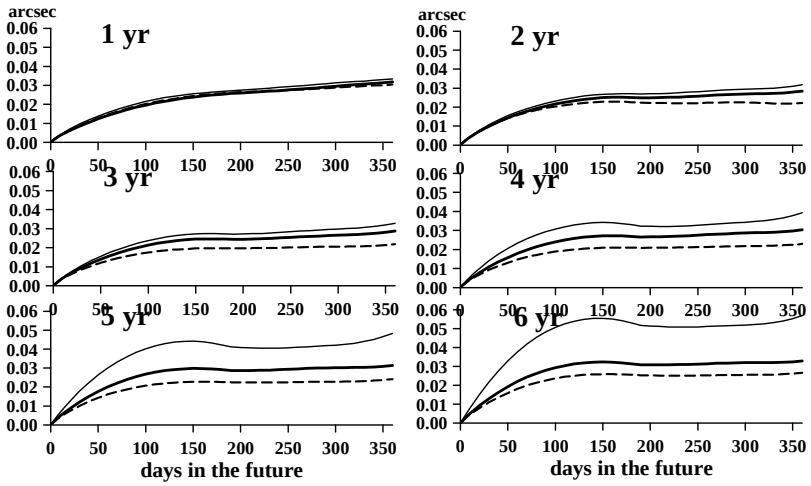

Fig. 4. Mean prediction errors for polar motion computed in 1973.0-2001.6 (thin line) (in the time period of the two biggest El Niño events in 1982/83 and 1997/98), in 1984.0-2001.6 (heavy line) (in the time period of the biggest El Niño event in 1997/98) and in 1984.0-1997.0 (in the time period between the two biggest El Niño events) as a function of least-squares model length of 1,2, …, 6 years.

4. CONCLUSIONS

-Poor accuracy of polar motion predictions can be caused by variable phase or period of the annual oscillation. There were two significant increases of the annual oscillation phase of the order of 30°-40° before the two biggest 1992/93 and 1997/98 El Niño events. The Chandler oscillation phase/period is more stable than the annual one and shows no significant correlation with El Niño events.

-The correlation coefficients between the 50- and 80-day predictions or amplitude/phase variations of the annual oscillation and the Niño 1+2 data are significant at the 90% confidence level.

-The increase of polar motion data length going into the least-squares extrapolation model increases the polar motion prediction errors, especially during the time of the biggest El Niño events in 1982/83 and 1997/98. Thus, it is advisable to choose a shorter least-squares extrapolation model lengths for polar motion prediction during the time of El Niño events.

Acknowledgments. This paper was supported by the Polish Committee of Scientific Research project No 8 T12E 005 20 under the leadership of Dr. W. Kosek. The authors thank Dr. J. Vondrák for fruitful scientific discussion.

5. REFERENCES

Fernandez L.I., 2001. Extended Kalman filtering for combining Earth rotation parameters time series, paper presented at the IAG'2001 Scientific Assembly in Budapest, Hungary, 2-7 Sep. 2001.

Kosek W., Nastula J., and Kolaczek B., 1995. Variability of Polar Motion Oscillations with Periods from 20 to 150 Days in 1979-1991, *Bull. Géod.*, **69**, 308-319.

Kosek W., 1997. Autocovariance Prediction of Short Period Earth Rotation Parameters, *Artificial Satellites, Journal of Planetary Geodesy*, Vol. **32**, *No. 2*, 75-85.

Kosek W. and Kolaczek B., 1997. Semi-Chandler and Semiannual Oscillations of Polar Motion. *Geophysical Research Letters*, Vol. **24**, No 17, 2235-2238.

Kosek W., McCarthy D.D., and Luzum B. 1998. Possible Improvement of Earth Orientation Forecast Using Autocovariance Prediction Procedures, *Journal of Geodesy* **72**, 189-199.

Kosek W., 2000. Irregular short period variations in Earth rotation, *IERS Technical Note* **28**, 61-64.

Kosek W., McCarthy D. D., and Luzum B. J., 2000. Prediction of complex-valued polar motion using the combination of autocovariance prediction and a least-squares extrapolation, paper presented at the EGS'2000 in Nice, France, 24-29 April, 2000.

Kosek W., 2001. Autocovariance prediction of complex-valued polar motion time series, accepted to *Advances of Space Research*.

Kosek W., McCarthy D.D., and Luzum B.J., 2001. El Niño impact on polar motion prediction errors., accepted to *Studia geophysica et geodetica*, 3rd Sep. 2001.

Malkin Z. and Skurikhina E., 1996. On Prediction of EOP, *Comm. IAA* **93.**

McCarthy D.D. and Luzum B.J., 1991. Prediction of Earth Orientation, *Bull. Géod.*, **65**, 18-21.

McCarthy D.D. and Luzum B.J., 1996. Path of the mean rotation pole from 1899 to 1994, *Geophys J. Int.* **125**, 623-629.

NOAA 2001. Climate Prediction Center – Data: Current Monthly Atmospheric and SST index values, http://www.cpc.ncep.noaa.gov/data/indices/

Schuh H. and Schmitz-Hübsch H., 2000. Short period variations in Earth rotation as seen by VLBI, *Surveys in Geophysics* **21**, 499-520.

Schuh H., Nagel S., and Seitz T., 2001a. Linear drift and periodic variations in long time series of polar motion, *Journal of Geodesy*, **74**, 701-710.

Schuh H., Ulrich M., Egger D., Müller J. and Schwegmann W., 2001b. Prediction of Earth orientation parameters by neural networks, submitted to *Journal of Geodesy*.

USNO, 2001. finals.all: all USNO EOP values since 12 Jan 1973 (with 1 year of predictions) http://maia.usno.navy.mil/

Zhu S. Y. 1981. Prediction of Earth rotation and polar motion, Reports of the Department of Geodetic Science and Surveying, *Report No.* **320**, Columbus, Ohio.

EARTH ORIENTATION PARAMETERS IRREGULARITY EFFECT ON ROTATIONAL EIGENMODES MODELLING.

O. KUDLAY
Main Astronomical Observatory of National Academy of
Sciences of Ukraine
03680, Golosiiv, Kyiv-127, Ukraine
e-mail: kudlay@mao.kiev.ua

ABSTRACT. Last Journees-2000 was reported about identification by two independent techniques - classical Lyapunov exponents method and recently modified by Korenberg Volterra-Wiener system analysis method (VWK), irregular variations in EOP series as chaotic ones . Here we present further investigation results of non-linear effects in EOP parameters by VWK . Some considerations are presented also about modification of theoretical approach to the Earth rotation modelling with Liouville equations .

Last Journees the situation was appeared when 2 different groups processing different EOP and AAM data by absolutely indepent methodes obtained positive results in nonlinear effects detection . Frede and Mazzega [3],[4] have analyzed 27 years long data set with one a day positions of polar motion , LOD and Atmospheric Angular Momentum by standard nonlinear techniques of correlation integral and Lyapunov exponents . Data filtered to store 0-100 day periods confidantly reveals the presence of chaotic signal with the next parameters : embedding space dimension 5-7, predictability horizon 10-18 days . Simply speaking this means that every process as in EOP or in AAM series must be described by 3 coupled equations which must give irregular trajectories with 10-18 days predictability interval (prediction error grows to observation r.m.s. during this time) . Filtration near Chandler peak showed that it is a regular process . Authors concluded that the atmosphere is a generator of chaotic signal which weakly non-linear Earth system reproduce in EOP seria .

Our work was based on application to variouse classical astrometry and modern techniques EOP and AAM data sets system analysis Volterra-Wiener method . The method was created by Volterra to study any complex system as a "black box" and recently modified by Korenberg to analyse systems by their own signal .It uses Taylor-like development of observation data in series of delayed argument degrees and calculate one-step-ahead prognosis with linear and nonlinear autocorrelations of the series itself . Procedure is performed for linear and non-linear prediction while we obtain for some delay and polinom degree values that minimize special information criterion . A standard Fisher test serves to reject with certain level of confidence the hyposesis that nonlinear model is no better than linear one as one-step-ahead predictor . For other mathematical details , please , see [1].

We analysed standard data length sets about 1000 points - too short for any nonlinear tech-

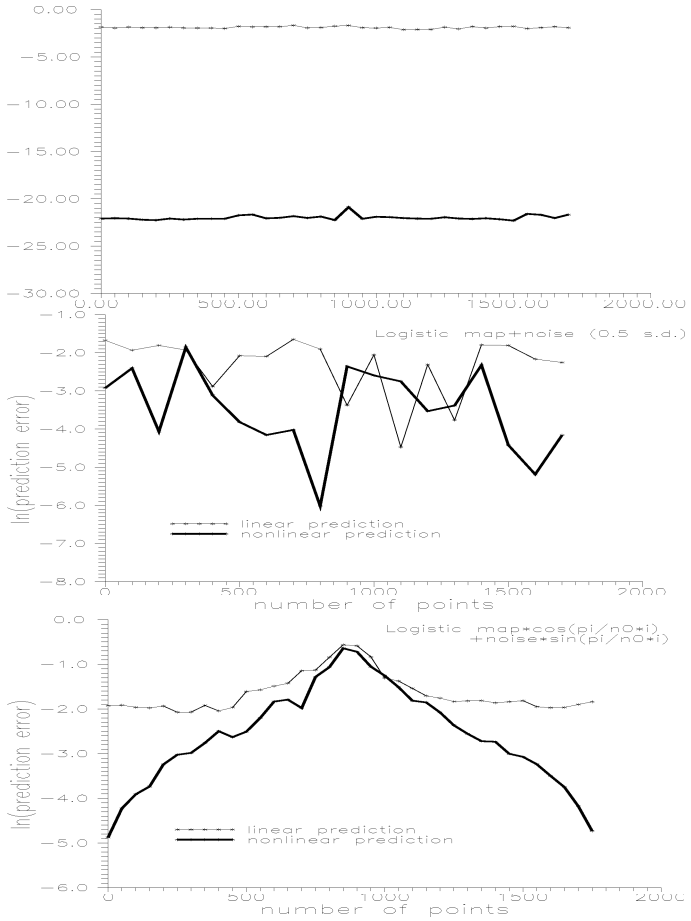

Figure 1: Prediction results for logistic map simulation.Top - Original chaotic signal,middle - chaos+noise, down - modulated chaos and noise

niques , having no spectral filtration or other data reduction , backed on studies of methode authors and found that historical LOD data from Morrison and McCarthy seria confirm chaoticity of the LOD process . Neither IPMS nor EOPC01 polar motion data revealed statistically significant chaotic signal presence but IPMS was close to the statistical criterion . Atmosphere's wind y-component occured positive , x- and y- components preassure terms were close to statistical criterion . So we considered AAM signal as marginally chaotic .

Afterwards considerations revealed that discrepancy could arise first of all due to : 1) different data sets and its preliminary reduction , 2) some properties of the VWK method , 3) indirect character of EOP and AAM observations which have a huge scope of preliminary reduction by various mathematical methods such as - interpolation, numerical integration, statistical approximation etc. Investigating limitation on data set length for VWK we found interesting phenomenon - if begine to analyse data from ultra short data length about 100 points increasing by every time the data length by the some number of points - then nonlinear superiority persist up to 300-400 points data length , and it failes for more data length . The hyposesis then was preposed that while data number increases some effects distort nonlinear prognosis of EOP signal by VWK . To test it we performed computer experiments with simulated chaotic data contaminated by various kind and level noises , time variations as chaotic and noise components and so on .

Let see for the beginning the situation with original chaotic signal (here it is so called logistic

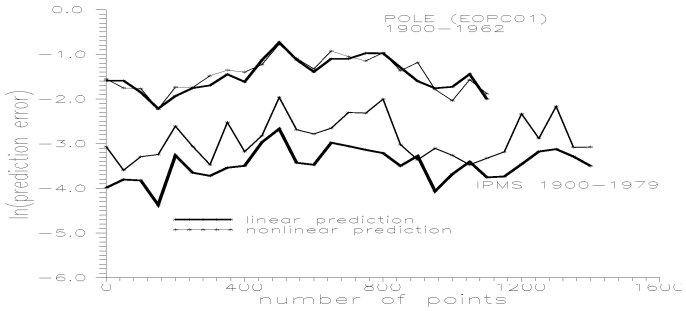

Figure 2: Prediction results for IPMS vs. EOPC01 polar motion data, bold line - nonlinear prognosis

map) - it is clearly seen (Fig 1.) that difference between linear and nonlinear prognosis error equals 15 orders of value , and both predictions are very stable . If we add the noise with an amplitude of 50 percent from chaotic signal r.m.s. - both prognoses become fluctuative and much closer one to each . If vary a noise amplitude with time by the sine law and chaotic signal by cosine then in the series center chaos will be absent and one can see how nonlinear response fall down to 0 here also . So , one can conclude that the method sensitively detects as chaos and noise variations even for strong noise contamination ,and the origin of VWK and Lyapunov exponent analysis descrepencies are due to more temporal sensitiviness of VWK . So, it was natural after that to repeat for the ultra short data length of the earlier processed seria . That was done with AAM data for 1999-2001 , IPMS polar motion data of Yumi & Yokoyama , EOPC01 pole and LOD data, Morrison & Stephenson and McCarthy & Babcock historical LOD data and gave the next results .

IPMS pole motion - is mostly nonlinear process during all the observation time . Pole of EOPC01 1900-1962 - do not contain any nonlinear signal . Please, compare 1900-1962 EOPC01 and IPMS predictability on the next Fig. 2 - it is seen the higher level of predictability as linear and nonlinear IPMS data for approximately the same time interval .

LOD EOPC01 1956-1999 : there is strange jump of linear predictability in the beginning of 70s , but any difference exists in both prognoses in other time . LOD of Morrison & Stephenson data give the indefinite result , LOD of McCarthy & Babcock - confidant nonlinear superiority .

Atmosphere : preassure z - (and all other preassure and wind) component - are linear values , wind x-component - time fluctuative but more or less nonlinear one, preassure x-component - strong nonlinear process .

To study the dipendence on the preliminary data reduction we simulate chaotic series processed by spline interpolation . An analysis showed that chaotic signal predictability drops by 10 orders of degree after interpolation . But from the other hand the same system but with strong noise contamination after interpolation improve prediction results and stabilize it . Interpolation of Morrison data really increases it's nonlinear predictability . So ,the conlusion is - influence of interpolation can be opposite depending on situation - making better or worse results . Further investigations are necessary to reveal all causes of the two methods descrepensies of course .

CONCLUSIONS

1. VWK method confidantly works with classical chaotic seria on ultra short data length samples about 100 points even under strong noise contamination . Its application to EOP and AAM data do not give such stability due to may be temporal variation of chaotic signal or its small frequency domaine extent or due to absence of preliminary filtration . In any way

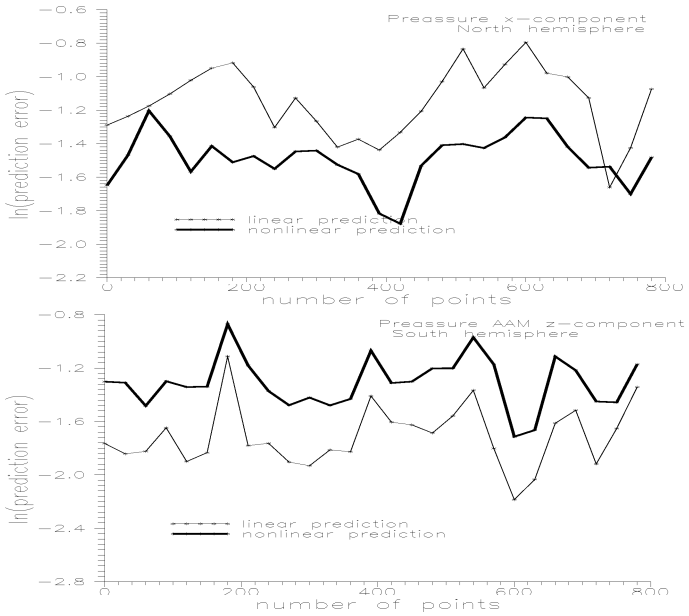

Figure 3: Preassure AAM x-term (top) vs. z-term (down) predictability , bold line - nonlinear prognosis

this fluctuative results confidantly confirm that x-,y-components of AAM are chaotic values but z-component is not such one .

2. IPMS and EOPC01 polar motion data are different, if IPMS contains chaotic signal , EOPC01 does not contain .Historical LOD data has fluctuative chaotic signal. Because of AAM z-component is not chaotic it can means that long term behavior of LOD may be ruled by ocean and liquid core or weakly non-linear Earth dynamical system do not only reproduce atmospheric chaotic signal but generate its own chaotic one .

3. Lyapunov exponents and VWK detection of wobble and ASM chaoticity hints that new non-linear theory of these modes need . This new theory have to take into account nonlinear terms in Louville equations expressed in variables which give the possibility to analyse the Earth dynamical system in phase space .

REFERENCES

[1] Barahona M., Chi-Sang Poon, *Detection of non-linear dynamics in short, noisy time series, Nature, 381, 215-217, 1996.* 1997 IERS Annual report, Observatoire de Paris, 1998.

[2] Yumi S., Yokoyama K., *Results of the international latitude service in a homogeneous system 1899.9-1979.0, Publ. of the Central Bureau of the International Polar Motion Service, 1980.*

[3] Frede V.,Mazzega P., *Detectability of deterministic non-linear processes in Earth rotation time-series. Embedding ,Geophys.J.Int, 137,551-564, 1999.*

[4] Frede V., Mazzega P., *Detectability of deterministic non-linear processes in Earth rotation time-series. Dynamics ,Geophys.J.Int, 137,565-579, 1999.*

SUB-SEMIDIURNAL VARIATIONS OF THE EOP OBSERVED BY SPACE GEODESY COMPARED WITH OTHER GEOPHYSICAL PHENOMENA

H. Schuh (1), P. Varga (2), T. Seitz (3), J. Böhm (1), R. Weber (1), G. Mentes (2), H. J. Závoti (2), M. Westerhaus (4)

(1) Institute of Geodesy and Geophysics, Vienna University of Technology, Austria
A-1040, Gusshausstrasse 27-29, Vienna
e-mail: hschuh@luna.tuwien.ac.at
(2) Geodetic and Geophysical Research Institute, Sopron, Hungary
(3) Deutsches Geodätisches Forschungsinstitut (DGFI), Munich, Germany
(4) Universität Karlsruhe, Germany

1. INTRODUCTION

In the last 20 years with the use of space geodetic techniques the influences of tides on the Earth orientation parameters (EOP) have been investigated. Most of the periods in length of day (LOD) or UT1-UTC, respectively, and polar motion (PM), related to lunisolar effects are as short as 24h and 12h, i.e. diurnal and semidiurnal variations. It is evident that meteorological processes also influence Earth rotation and polar motion in the band of periods between one year and some days but many details of interaction between atmospheric processes and Earth orientation are not clear yet. Both, simultaneous UT1-UTC and PM data series observed by GPS (Global Positioning System) as well as meteorological events were investigated in order to reveal common origins of the fluctuations and to discover facts which explain the interaction between atmosphere and the solid Earth. The time series were compared in time domain and analyzed in frequency domain by Fourier and wavelet analyses to search for similar periods.

2. SUB-SEMIDIURNAL PERIODS OF THE EOP

Figure 1 shows the polar motion time series observed by GPS from 1997.5 until 2001.0 with a resolution of 2 hours which was high pass-filtered, first. The Fourier spectra of the prograde (positive periods) and retrograde (negative periods) variations clearly reveal peaks with periods shorter than half a day at 8h, 6h, and 4.8h, i.e. at higher harmonics of a solar day. The wavelet scalograms plotted in figure 1 also contain maxima at these periods. It has been assumed that these periods are an artefact caused by resonances with the GPS satellite orbits. However, it is interesting to note that:
→ the retrograde variations are stronger than the prograde ones what is typical for the short period pole variations;
→ the retrograde 8h variation gets its maximum usually in January/February but almost disappears during the summer.
The observed time series of UT1-UTC from 1997.7-2001.0 (figure 2) also contains significant periods at 8h, 6h, and 4.8h; here the 6h variation is stronger than the other higher harmonics,

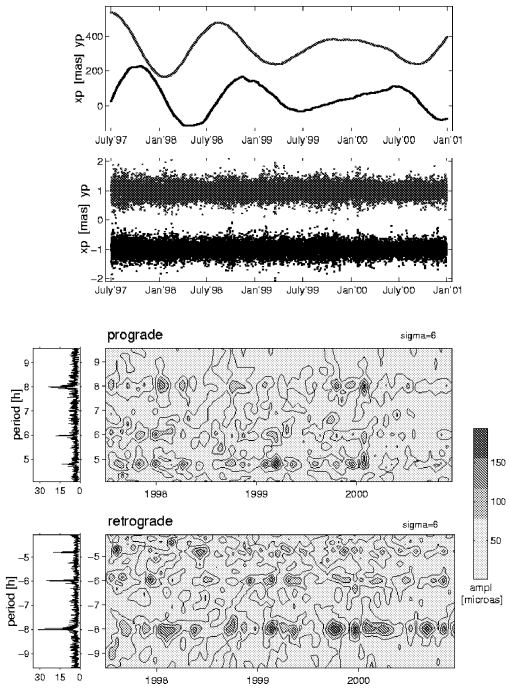

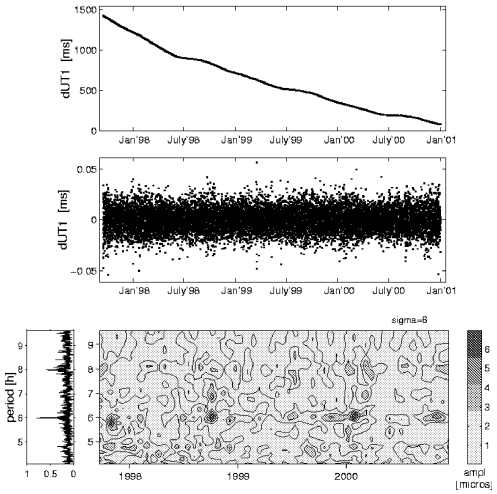

Fig. 1 (left) : Polar motion observed by GPS (upper panel), high-pass filtered (second panel from top) and Fourier spectra and wavelet scalograms for periods shorter than 10 hours (two lower panels)

Fig. 2 (right) : UT1-UTC derived from GPS observations (upper panel), high-pass filtered (central panel), Fourier spectrum and wavelet scalogram for periods shorter than 10 hours (lower panel)

again disappearing in summer. The 4.8 h variation is very weak.

3. SUB-SEMIDIURNAL PERIODS IN OTHER GEOPHYSICAL PHENOMENA

The very short periods at higher harmonics can also be seen in recordings of other geophysical phenomena as shown by several authors, e.g. Westerhaus (1996) or Polzer (1997). As an example the following geophysical data were analyzed by Fourier and wavelet methods:

→ air pressure at station Dokurcun, Turkey (figure 3).

→ air temperature at station BFO, Germany (figure 4).

4. DISCUSSIONS AND CONCLUSIONS

Sub-semidiurnal periods in the EOP corresponding to higher harmonics of a solar day can be seen in GPS observations. At present three explanations could be given for the sub-semidiurnal variations:

→ It is an artefact caused by resonances with the satellite orbits.

→ Sub-semidiurnal atmospheric tides and - to a less extent - ocean tides cause the corresponding sub-semidiurnal variations of the EOP.

→ The peaks which can be seen in the spectra are due to an asymmetric quasi-sinusoidal pattern which is repeated every 24 hours, e.g. in the air pressure and transmitted by atmospheric angular momentum into the observed EOP.

For a better understanding of the processes influencing our natural environment it is extremely

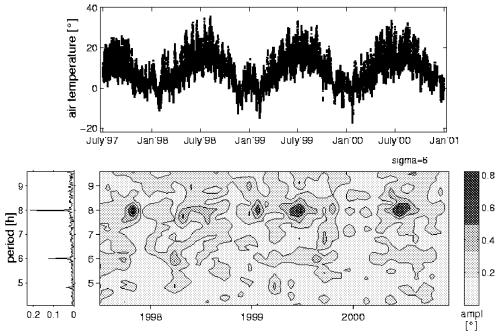

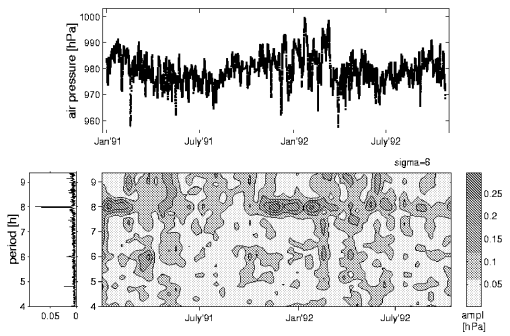

Fig. 3 (left) : Air pressure at Docurcun, Turkey
Fig. 4 (right) : Air temperature at Black Forest Observatory (BFO), Germany

important to know more on global meteorological conditions. An improved knowledge in this field would allow the estimation of the energy involved in different dynamical processes of geophysical fluids. A first comparison between sub-semidiurnal EOP-variations and corresponding periods in highly resolved atmospheric angular momentum (AAM) time series was published by Weber et al. (2001). On the observational side it can be expected that continuous VLBI measurements providing an independent control of the GPS results will help to answer the open questions.

5. REFERENCES

Polzer, G.: Analysis of Earth Tide Observations for the Determination of Core Resonance Parameters, ph.d. thesis, Universität Karlsruhe, 1997.

Westerhaus, M.: Tilt and Well Level Tides Along an Active Fault, Scientific Technical Report STR 96/05, GFZ, Potsdam, 1996.

Weber R., J. Nastula, B. Kolaczek, D.A. Salstein.: Analysis of Rapid Variations of Polar Motion Determined by the GPS. Proceedings of the IAG Scientific Assembly, Budapest, Sept. 2001.

ERP AND CLIMATE

A. POMA[1] and S. URAS[2]

[1]Osservatorio Astronomico di Cagliari
Poggio dei Pini, Str. 54, 09012 Capoterra (CA), Italy
e-mail: poma@ca.astro.it

[2] CNR - Istituto di Radioastronomia - Sez. di Cagliari
Poggio dei Pini, Str. 54, 09012 Capoterra (CA), Italy
e-mail: uras@ca.astro.it

1. INTRODUCTION

Various sources act via different mechanisms i.e. thermal (or thermodynamic), electromagnetic (or electrodynamic), and gravitational, over the three physical systems: atmosphere, ocean and solid Earth. The processes include atmospheric and ocean dynamics, telluric currents and geodynamics. Space age techniques have now achieved a high degree of accuracy in regular monitoring of the Earth's motion. International services give the total angular momentum of the Earth's atmosphere at a given time instant (allowing by this to investigate its correlation with the changes of the spin of the Earth). As regards this subject there is a great number of works concerning annual, semi annual and in general the so-called-seasonal variations (in both polar motion and LOD), confirming the atmosphere is the main excitation source for these fluctuations. At period longer than a few years, the relationship between meteorological processes and earth rotation parameters are less explained. At the same time scales, in fact, other geophysical effects may play an important role. Some climatic sources of decadal LOD fluctuations in LOD have been recognized (Salstein & Rosen 1986; Eubanks 1993). Recently Jochmann & Felsmann (2001) suggested the existence of climate cycles in long term variations of polar motion. But, in general, the question remains open. Requirements for progress in this field are strictly related to the problem of global climatic changes. We discussed below a possible relationship between ERP, ENSO and regional rainfall time series (Buffa & Poma 2000).

2. ERP AND CLIMATIC INDICES

Two of the major climatic indices of interannual variability in the atmospheric circulation are the El Niño-Southern Oscillation (ENSO) and the North Atlantic Oscillation (NAO). El Niño has been shown to have a direct and strong impact on the climate fluctuation in the tropical Pacific. The NAO (Hurrel 1996) is associated with changes in surface westerlies across the Atlantic onto Europe and characterizes a meridional oscillation in atmospheric mass. It accounts for more than 1/3 of the total variance of the sea level pressure field over the North Atlantic. There is a great number of works on the ENSO impact on LOD but recently some authors also investigated on the possible existence of a disturbance of polar motion during ENSO events (Frede & Mazzega 1999, Kolaczek et al. 1999). In figure 1-left we compared the Chandler x-component with a time series of rainfall recorded in Sardinia. Results seem to indicate the existence of a coupling in correspondence of the Chandler frequency. In the same figure a strong increase in amplitude of the cross-correlation signal may be also noticed in correspondence of

1951. In effect, it is well known that Chandler amplitude exhibits a large variation around 1950, while all Mediterranean area was strongly perturbed from a climatic point of view. However such results, in absence of any physical interpretation, should be used with much caution.

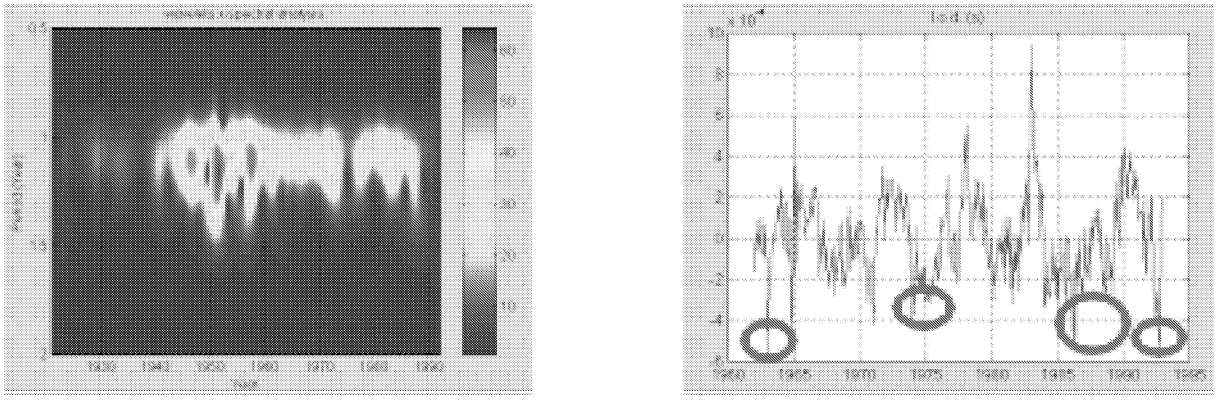

Figure 1: Sardinia local rainfall related to the Chandler x-component (left) and to the LOD (right).

As regards the LOD, a non-linear interaction between its seasonal variations and the ENSO phenomenon has been extensively reported in many papers (e. g. Gipson & Ma 1999). Changes in the atmospheric zonal winds determined by climate variations, may cause changes in the LOD by conservation of angular momentum. We analyzed the LOD with the aim to unveil the fingerprints of NAO in general circulation. In the figure 1-right we marked the LOD data corresponding to the dates of the last drought episodes in Sardinia. Dry periods seem to coincide with negative anomalies (decreases) in LOD. Note that positive anomalies of LOD and noticeable disturbances of polar motion typically occur during ENSO events, while to the negative phase of ENSO (La Niña) corresponds a negative anomaly in LOD. Spectral analysis shows that two concomitant frequencies are present in LOD and ENSO, corresponding to 3-4 and 2-2.5 years respectively. The 2-2.5 period in ENSO-LOD is generally explained in terms of a pattern of propagation of anomalies in zonal mean fields of atmospheric angular momentum across the globe. A lack of this signal in the NAO-LOD correlation should be accurately investigated in order to better understand teleconnections between NAO and ENSO.

3. REFERENCES

Buffa, F., & Poma A. 2000, On the Chandler periodicity (Polar motion, LOD and climate), in: Dick S., McCarthy D., Luzum B., (eds) Polar Motion: historical and scientific problems, IAU Colloquium 178, Cagliari, September 1999, Astronomical Society of the Pacific, San Francisco

Eubanks T.M. 1993, Interactions between the atmosphere, oceans and crust: possible oceanic signals in Earth rotation, in: M. Feissel (ed),: The Orientation of the Planet Earth as observed by Modern Space Tecniques, Pergamon Press

Frede, V., & Mazzega, P. 1999, Fluctuation of the Earth rotation and El Niño events, IERS Technical Note 26, 37

Gipson, J. M., & Ma, C. 1999, Signature of El Niño in the length of day as measured by VLBI, IERS Technical Note 26, 17

Hurrel, J. W. 1996, Geophys. Res. Lett., 665, 23

Jochmann, H., & Felsmann, E. 2001, J. of Geodesy, 74, 711-719

Kolaczek, B., Nuzhdina, M., Nastula, J., & Kosek, W. 1999, El Niño impact on atmospheric and geodetic excitations of polar motion, IERS Technical Note 26, 23

Salstein, D.A., & Rosen R.D. 1986, J. Climate and Applied Meteorology, 25,12,1870-1877

ANALYSIS OF SUB DIURNAL EOP VARIATION

M. KUDRYASHOVA, V. VITYAZEV, O. TITOV
Astronomical Institute of SPbU
Universitetskii pr., 28, Staryi Peterhof, Saint-Petersburg, Russia
e-mail: ai@astro.spbu.ru

ABSTRACT. The paper presents a study of the high frequency variations in the LOD and Polar motion series derived from the GPS observations. The initial time series have a 2 hour resolution and cover the time span from 1995 till 1998. Prior to spectral analysis the diurnal and semi-diurnal tidal effects have been eliminated from the data. The time variability of spectral lines at frequencies 3,4,5 cycle per day were thoroughly investigated by wavelet analysis. The wavelets clearly revealed that all the specific changes in the time dependent spectra coincide with the borders of the different segments of which the full time series under consideration had been constructed. It is concluded that the above mentioned oscillations are hardly connected with the Earth rotation and are most likely generated by processing of the GPS observation.

1. INTRODUCTION

A lot of geodesical and geophysical information may be derived from variations of the sub-diurnal Earth orientation parameters. In this connection the VLBI and GPS observations are of great importance. In the frames of Gipson and Eanes models the variations of Polar motion and length of day are comprised of several dozens of tidal terms. However, one may expect that other signals may be found in the range of periods from one hour up to several days.

Guided by this idea we made an analysis of a unique ERP data derived from GPS observations by the Center for Orbit Determination (CODE) [1]. These data form a continuous uninterrupted series of the LOD and of the Polar motion lasting 3.12 years (JD 49719-50859) with a time resolution as much as 2 hours. The first study of this data was presented by Rothacer and Beutler [1]. In particular, they reported the existence of non-tidal signals at the frequencies 3,4,5 cpd and posed the problem of their further study. The main goal of this paper is to clarify the nature of these harmonics.

2. METHODS OF ANALYSIS

We studied the post-fit residuals which were obtained after subtraction of all known harmonic components from initial data. They were: a) the tidal effects in the frame of Gipson model for LOD and Polar motion, b) the Chandler and annual components (for Polar motion only). The parameters of the Chandler and annual wobbles were derived from the data published by IERS for 1988- 2000.

The spectral properties of the residuals were studied by Fourier transform and by wavelet

transform with Morlet analyzing function [2].[3],[4].

3. RESULTS

First of all, we notice that the strong peaks near the frequencies $\nu = 1, 2$ cpd are still seen in the power spectra though the tidal effects in diurnal and semi-diurnal bands have been eliminated. Probably, such behavior may be explained by inconsistancy of Gipson model with GPS observations since this model was derived from VLBI data.

Now we are in position to describe the main item of our study, i.e. the frequency band from 2.5 till 5.5 cpd. Fourier spectra for series under consideration show three peaks at frequencies $\nu = 3; 4; 5$ cpd. It is clear, that these oscillations are beyond the Gipson model, and this is all what can be extracted from Fourier power spectra. To get more information we applied the wavelet technique [4] to the time series of LOD and x-, y- coordinates of Polar motion. Figure 1 exibit the wavelet spectrum of LOD (wavelet spectra of Polar motion series are analogous). The plot shows that the spectral lines at frequencies 3,4,5 cpd change their intensities with time. The crucial fact is that the wavelet spectrum for the first 636 days significantly differ from the spectrum from 637-th till 1140-th day. Actually, in the first part one can see the harmonic components at all mentioned frequencies (1-5 cpd), whereas the second part contains the harmonics at frequencies 1,2 cpd only (with noise at other frequencies). To our mind, the reason of this drastic change is connected with the changing of the orbit determination model for GPS satellites after 636-th day of observation [1].

Thus, we come to our main conclusion: since the time-dependent spectra reveal the date when at least two heterogeneous segments have been glued together, is naturally to suppose that the harmonics at frequencies 3,4,5 cpd are generated by processing of GPS observation, not by Earth rotation.

Acknowledgments The researches reported here were supported financially by Russian Foundation for Basic Research (grant 01-02-17070) and Russian Ministry of Education (grant E00-11.0-36).

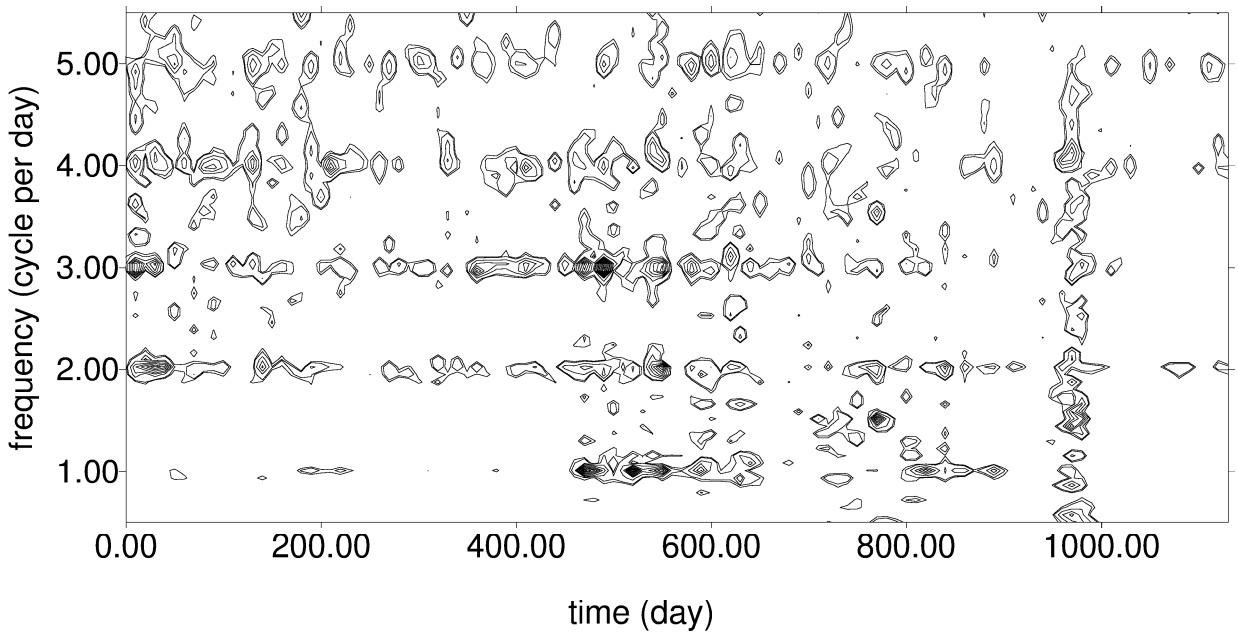

Figure 1: Wavelet spectrum of LOD series.

3. REFERENCES

[1] Rothacher M., et al. High-frequency Earth rotation variations from three years of GPS data. Submitted to *J. Geophys. Res.*in 1998.
[2] Grossman A., Morlet J., *SIAM J. Math. Anal.*, 15, 723, 1984.
[3] Vityazev V.V., The Gabor and Wavelet Analysis of the EOP in the system of HIPPARCOS. *Proc. JOURNEES 97*, Prague, pp. 149-152, 1997.
[4] Foster G., Wavelets for period analysis of unevenly sampled time series, *Astron. J.*, 1996, 112 (4), pp. 1709-1729

SINGULAR SPECTRUM ANALYSIS OF EPISODIC TERMS IN POLAR MOTION

M. BOUGEARD*,**, N. ROUVEYROLLIS**, D. GAMBIS**
(*) Université Lyon 1, UFR math., UMR 5028, 69100 Villeurbanne, France
(**) Observatoire de Paris, UMR 8630, IERS, France
e-mail: bougeard@hpopa.obspm.fr, nicolas.01@infonie.fr, gambis@obspm.fr

ABSTRACT

In this paper, we study the 1999-2000 Polar Motion series as derived from GPS (Weber, 2001; Rothacher, 2001) observations. On the basis of Functional Principal Analysis, we focus on the diurnal/subdiurnal variations. By applying the EOPSSA Matlab package developed at Paris Observatory, significant transient components are enlightened at periods of about 8, 12 and 24 hours.

1. INTRODUCTION

We focus on the sub-diurnal/diurnal polar motion variations, possibly inferred by non-linear processes in the atmosphere and oceans. We applied the Singular Spectrum Analysis (SSA) that allows spectral analysis and decompositions of experimental time series as shown in climatology papers (Vautard et al, 1992). It is a form of Principal Component Analysis in the time domain that provides data-adaptative filters and Functional Principal Components for describing the signal variability in terms of its lag-covariance structure. Section 2 presents EOPSSA, a Matlab computer package developed at Paris Observatory for SSA analysis. Its application to a 2-hour GPS Earth Rotation Parameters series is discussed in Section 3.

2. THE MATLAB COMPUTER PACKAGE EOPSSA

EOPSSA (Rouveyrollis, 2001) is a Matlab computer package for SSA analysis. It allows to identify and extract EOF components (trends, quasi-periodic or periodic oscillations) of a signal. Figure 1 shows the EOPSSA analysis window.

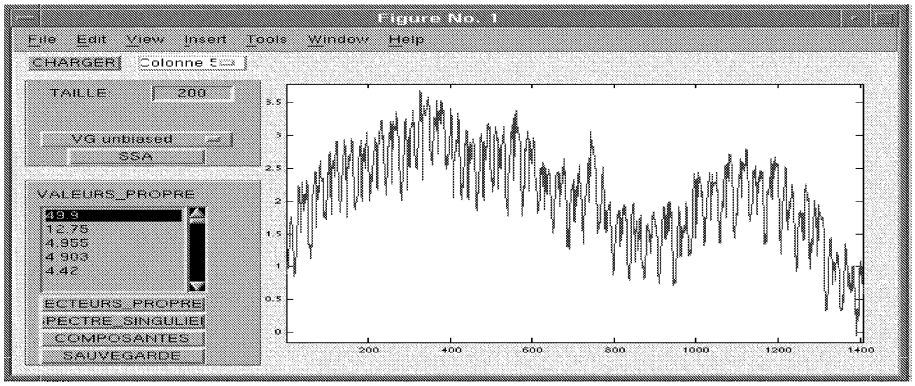

Figure 1 : EOPSSA main window showing LOD variations of IERS C04 solution

3. SSA ANALYSIS OF 1999-2000 GPS POLAR MOTION SERIES

We used the 2-hour GPS ERP-Series given on the 1999-2000 period; the series is the concatenation of the CODE subdaily 3-days series. Diurnal and subdiurnal variations induced by the oceanic excitation were removed (Ray et al., 1994). In order to keep variations smaller than a few days, a Vondrak filter (Vondrak, 1977) was applied.

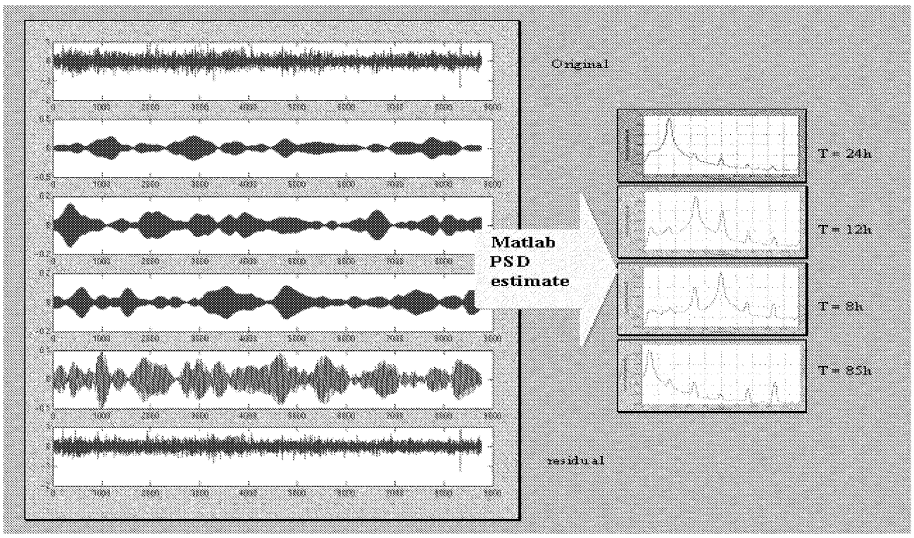

Figure 2 - Decomposition of the high-frequency signal. Significant components with periods of 12h and 24h appear. They might be in connection with an episodic oceanic excitation. 8-hour and 85-hour components not present in the oceanic model are also transiently appearing. At this point, more investigations are needed to state wether it is connected or not with oceanic S3 or M3 tides.

4. CONCLUSION

- The Singular Spectrum Analysis (SSA), widely used in climatic researches, is an efficient tool for signal decomposition.
- We have developed and implemented a SSA Graphic User Interface in Matlab environment.
- Episodic significant signals with signatures of 8h, 12h, 24h and 85h were identified on the 2-hour GPS series derived by Weber and Rothacher.
- Further studies are in progress to understand the reality and the origin of these components (oceans, atmosphere).

5. REFERENCES

Ray R.D., Steinberg D.J., Chao B.F., Cartwright D.E., 1994, Diurnal and semidiurnal variations in the Earth's rotation rate induced by oceanic tides., Science, V.264. pp 830-832.

Rouveyrollis N., 2001, Phd DESS, Lyon 1.

Rothacher M., 2001, personal communication.

Schoellhamer D. H., 2001, SSA for time series, Geophy. Res. Lett., vol 28, No 16, pp 3187-3190

Vautard R., Yiou P. and Ghil M., 1992, Singular Spectrum Analysis: a toolkit for short, noisy chaotic signals, Physica D, 58, 95-126.

Vondrak J., 1977, Bull. Astro. Czechoslovaquia, 28, 84.

Weber R., 2001, personal communication.

Session II)

GEODESY AND ROTATION OF THE OTHER PLANETS

Introductory papers, oral communication and posters

GEODESIE ET ROTATION DES AUTRES PLANETES

Exposés introductifs, communications orales et posters

THE NETLANDER IONOSPHERE AND GEODESY EXPERIMENT (NEIGE). COMPARISON BETWEEN THE NUTATIONS OF THE EARTH AND OF THE PLANET MARS.

V. DEHANT(1), J.P. BARRIOT(2), T. VAN HOOLST(1), P. DEFRAIGNE(1), M. YSEBOODT(1), and F. ROOSBEEK(1)
(1) Royal Observatory of Belgium
3 avenue Circulaire, B-1180 Brussels, Belgium
e-mail: dehant@oma.be
(2) Observatoire Midi-Pyrénées
14 avenue E. Belin, F-31400 Toulouse, France

ABSTRACT. The NEtlander Ionosphere and Geodesy Experiment (NEIGE) will be launched to the planet Mars in 2007. One of the objectives of this experiment is to get the nutations of Mars. The planets Earth and Mars are very similar. They both have precession and nutations. This paper compares the results and discusses the implications of their different interior structures. In particular, it is shown that the existence or absence of a liquid core, not yet proved for Mars, will be seen in the future observations performed by the NEIGE experiment.

1. DESCRIPTION OF NEIGE

In 2007, four similar landers will be sent to the planet Mars, in the frame of the NetLander mission set up by an European and American consortium (Harri et al., 1999). The small stations will operate on the surface of Mars for about one Martian year (687 days). Among the experiments on-board these four NetLanders, there will be a geodesy experiment called NEIGE (NEtlander Ionosphere and Geodesy Experiment) (Barriot et al., 2001). The NEIGE experiment will use the Doppler shifts of UHF and X-band radio links between the Netlander microstations on the Mars surface and an orbiter and between this orbiter and the Earth (at X-band). The NEIGE Experiment has two series of scientific objectives: (1) to determine Mars orientation parameters in order to obtain information about the interior of Mars and about the seasonal mass exchange between atmosphere and ice caps; and (2) to determine the total electron content (TEC) and the scintillation of radio signals in order to study the large- and small-scale structure of the ionosphere of Mars. These two sets of information will be derived from measurements of Doppler shifts.

From the observation of the variations in Mars' orientation in space, we will be able to determine the precession rate (long-term motion of the rotation axis around an axis perpendicular to the ecliptic; this determination would need also the use of Viking and Pathfinder data), the amplitudes of the main nutations (periodic motions of the rotation axis in space), the amplitudes of the seasonal components and the Chandler Wobble in the polar motion (motion of the rotation axis in a frame tied to the planet), and the rotation speed variations (length-of-day

variations). From precession and nutations, we will be able to give information about the core dimension, density and state, provided that the gravitational forcing is correctly known.

2. DESCRIPTION OF THE PRECESSION/NUTATIONS

Precession and nutations are due to the gravitational attraction of the Sun and the moon(s) acting on the whole planet. The other planets have a minor importance, but are taken into account when precise modeling is wanted. Due to the asymmetry of the planets (mainly flattening), there is a resulting torque that tends to re-orient the equator of the planet toward their orbital plane. Because the Earth and Mars are rotating, they react to this torque like a gyroscope, and their rotation axes describe a large motion in space around the perpendicular to the their orbital plane, called precession.

Due to the fact that the Earth, Mars, the Sun, the Moon, Phobos and Deimos, and the other planets are not fixed with respect to each others, periodic motions in space are generated in addition to the large precessional motion, with periods related to the orbital periods of the perturbing and perturbed bodies (such as annual and semi-annual periods from the main perturbing body, the Sun). These periodic motions in space are called nutations.

A first step in the evaluation is to compute these nutations considering that the planets are rigid. See Section 3 for the Earth and 4 for Mars.

In a second step, the non-rigid response of the planets to the forcing is computed. This response must account for the deformability of the planet and also, the potential presence of a liquid core (to be proved for Mars). See Section 5 for the Earth and 6 for Mars. We have computed the nutations of the planets Earth and Mars using particular rheology profiles and allowing a liquid as well as a solid core for Mars.

For the Earth, the nutations are modeled very precisely (< 100 μas (microarcsecond)) because the profiles of the rheological properties and the radii of the different layers are well known, and because we have high precision observations from which parameters can be fitted.

For Mars, we don't know yet the details of the interior of the planet, e.g. we do not know the exact dimension of the core, and we do not have any nutation data yet.

3. RIGID EARTH NUTATIONS

The nutations of the Earth as a rigid body have been computed very accurately by Souchay and Kinoshita (1997), Roosbeek and Dehant (1998), and Bretagnon et al. (1998). The first team has been working using the Hamiltonian approach, and the two others, using the torque approach. In these computations, different second order effects are taken into account. Direct and indirect effects of the planets, nutation on the nutation effect, and the J_2-tilt effect are presently taken into account in the computation of the nutations of a rigid Earth. For details about these contributions, see Dehant et al. (1999).

4. RIGID MARS NUTATIONS

The nutations of Mars, considered as a rigid body, have been computed with a very high precision (Bouquillon and Souchay, 1999, Roosbeek, 1999). The method used is the direct computation of the torque acting on Mars from the gravitational interactions with the other bodies of the planetary system, mainly with the Sun. The main inaccuracy in the amplitudes of nutations for a rigid Mars is related to the uncertainty in the dynamical flattening of the planet. This last parameter has been computed from precession observation and degree-two gravity field (J_2) observation (Folkner et al., 1997), obtained from Viking and Pathfinder data. The

most important nutation is the prograde semi-annual nutation (343 days). This nutation has almost the same amplitude as the corresponding prograde semi-annual nutation of the Earth (182 days). The reason why they have the same amplitude relies in the fact that the mean distance between Mars and the Sun is about twice the mean distance between Earth and the Sun, and the flattening of Mars is about twice the flattening of the Earth. The nutations coming from the gravitational attractions form Phobos and Deimos are very small.

5. NON-RIGID EARTH TRANSFER FUNCTION FOR NUTATIONS

The contribution of the planet non-rigidity to nutations are accounted for by means of transfer functions. The present-day transfer functions for the non-rigid Earth nutation account for the fact that the Earth is an ellipsoid, that it is rotating, that there exist an inner core, a liquid outer core, and a solid inelastic mantle. In the model, the Earth is not considered to be in hydrostatic equilibrium. Because the Earth has a liquid core, there exists a normal mode called the Free Core Nutation (FCN), which is related to the fact that the Core-Mantle Boundary (CMB) is ellipsoidal and deformable. Due to the FCN, there is a resonance in the nutation amplitude. This resonance mainly affects the annual retrograde nutation. Additionally, large amplitude nutations far away from the resonance can also feel the influence of the resonance. This is the case for the prograde and retrograde 18.6 year nutations and the prograde semi-annual nutation.

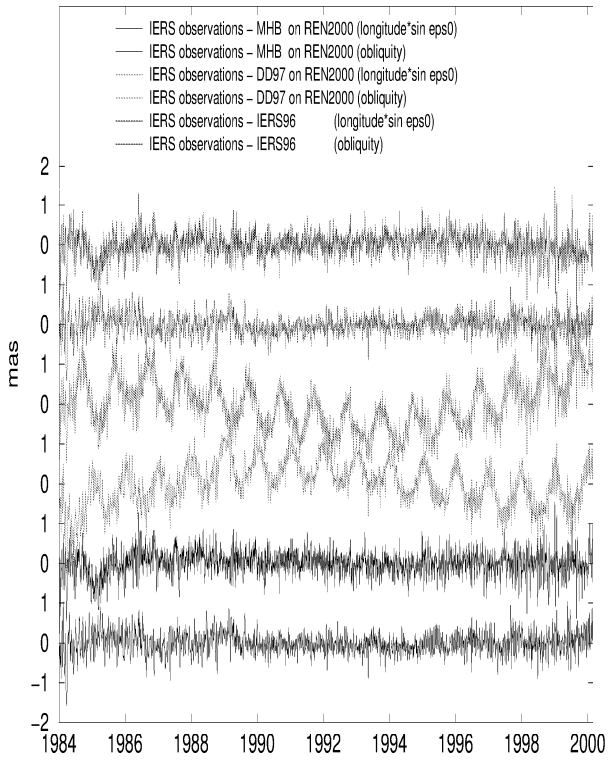

Figure 1: Residuals between the VLBI observed nutation and nutation models for the Earth. The first two curves are residuals for the IERS 1996 model (see McCarthy, 1996), the two middle curves are residuals for the numerical integration model of Dehant and Defraigne (1997), and the two last curves are residuals for MHB2000 model of Mathews et al. (2001).

Empirical models (such as the two first curves in Figure 1, Herring, 1996, see McCarthy, 1996), and geophysical model (such as the MHB2000 shown in the two last curves in Figure 1, Mathews et al., 2001) are in good agreement with the VLBI observations (the residuals are shown

in the figure). These models incorporate a FCN resonance which accounts for dissipation at the CMB. Numerical integration models, while incorporating non-hydrostatic CMB topography, do not incorporate any dissipation at the core-mantle boundary and need still improvement (such as the DD97 shown in the two middle curves in Figure 1).

The model MHB2000 has been adopted by the IAU in 2000. It incorporates mantle inelasticity, CMB non-hydrostatic topography, dynamical flattening in agreement with the precession constant, and an electromagnetic torque at the CMB, as well as at the ICB (Inner Core Boundary). Resonances to the Chandler Wobble, the FCN and the Free Inner Core Nutation (FICN, this mode is due to the fact that the Earth has a solid inner core within the liquid outer core, and that the Inner Core Boundary (ICB) is ellipsoidal and deformable) are considered. Constant atmospheric and tidal ocean effects on nutations are considered. Residuals with respect to VLBI data are of the order of a few 10 μas in the frequency domain. The physical parameters such as the electromagnetic coupling at the CMB and ICB are adjusted using VLBI observations. This provides the scientific community with important constraints on the magnetic field amplitude at these boundaries (see Dehant and Mathews, 2002).

6. NON-RIGID MARS TRANSFER FUNCTION FOR NUTATIONS

In order to be able to compute Mars' transfer function for nutations, it is necessary to know some of the properties of the interior of the planet. Figure 2 shows a comparison of the interior of Mars and of Earth.

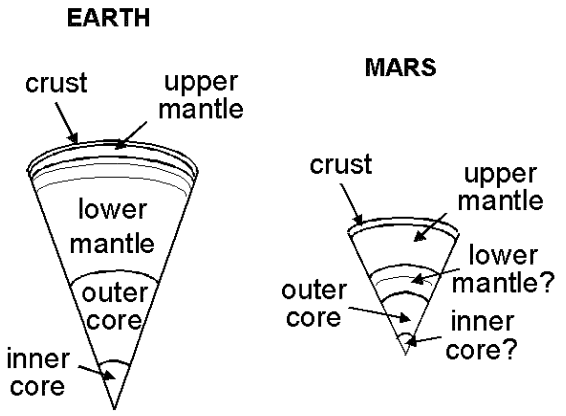

Figure 2: Comparison between the interiors of the Earth and of Mars.

Mars has a radius of about the half of the Earth mean radius. The dimension of the core of Mars is about the dimension of the Earth's inner core. We know its dimension approximately from the observed moment of inertia (1500km +/- 200km) as derived from Viking and Pathfinder data (Folkner et al., 1997). The composition of the core has been deduced from modeling using the SNC meteorites composition. The state of the core is not known with certainty; most models predict a completely liquid core. A completely solid core is also a possibility. The existence of a solid inner core is possible, too. The FCN exists only if Mars has a liquid core. The FICN exists only if Mars has a solid inner core within a liquid outer core. Consequently, different possibilities must be considered when computing non-rigid Mars nutations: with and without resonance at the FCN, with and without resonance at the FICN. The presence of a potential

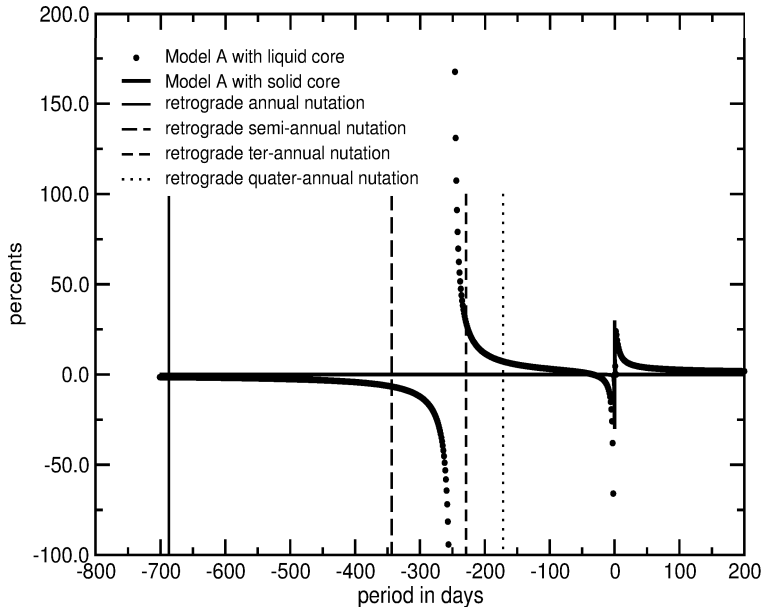

Figure 3: Transfer function of the planet Mars when a liquid core is considered and when a solid core is considered.

inner core and thus of a resonance at the FICN is treated in detail in separated papers of this volume (Dehant et al., 2002, and Rivoldini et al., 2002). The different possibilities for the core are detailed in Dehant et al. (2000). If there is a liquid core in Mars, there would be a resonance at a period of about -256 days corresponding to the FCN. This is particularly important for the retrograde semi-annual (-343 days) and ter-annual (-229 days) nutations. We present in Figure 3 the relative non-rigid contribution to the nutation amplitudes, as a function of the period.

If the core is liquid, the FCN resonance is visible, even in the prograde part of the spectrum. In particular, there is an important effect on the largest nutation, the prograde semi-annual nutation at 343 days; the difference between the non-rigid Mars transfer function with and without liquid core is at the level of 1% at that frequency, which corresponds to about 5 mas (milliarcsecond) on the amplitude of that nutation. The resonance period is highly dependent on the core dimension, and on the non-hydrostatic contribution which could be important as seen from the existence of Tharsis and the associated geoid anomalies. These results are discussed in Dehant et al. (2000).

The expected precision of the NEIGE experiment is below 5 mas, which will, for example, allow us to answer the question about the state of the Martian core. For that purpose, we will deduce the annual, semi-annual, ter-annual, quater-annual nutation amplitudes from the Doppler shift measurements.

7. CONCLUSIONS

Both Earth and Mars have nutations from which the observations can provide information on the interior of the planets. The most important nutation of Mars is the prograde semi-annual nutation; its amplitude is about the same as the corresponding one for the Earth. The moons of Mars, Phobos and Deimos, do not contribute with a high level to the nutational motions, while for the Earth, the 18.6 year nutations (period of the node of the Moon), are the largest nutations.

Present-day VLBI data obtained on Earth are unprecedented high precision data which has allowed to constrain very well the Earth's interior properties e.g. the outer core and inner core

flattenings, the coupling at the CMB and ICB. A very precise nutation model, MHB2000, has been adopted by the IAU in 2000. In the future, the NEIGE experiment will allow us to obtain precise nutation of the planet Mars, and so, e.g. to better constrain the core dimension, and to determine the state of the core and the eventual existence of an inner core.

REFERENCES

Barriot J.-P., Dehant V., Folkner W., Cerisier J.-C., Ribes A., Benoist J., Preston R., Van Hoolst T. et Warnant R., 2001, The NetLander Ionosphere and Geodesy experiment, in: Proc. Journées Systèmes de Référence 2000, Paris, France, ed. N. Capitaine, pp 196-198.

Bretagnon, P., Francou, G., Rocher, P., and Simon, J.-L., 1998, SMART97: a new solution for the rotation of the rigid Earth, *Astron. Astrophys.*, 329, pp 329-338.

Bouquillon, S., and Souchay, J., Precise modeling of the precession-nutation of Mars, Astron. Astrophys., 345, 282-297, 1999.

Dehant V. and Defraigne P., 1997, New transfer functions for nutations of a non-rigid Earth, *J. Geophys. Res.*, 102, pp 27,659-27,688.

Dehant V., Arias F., Bizouard Ch., Bretagnon P., Brzezinski A., Buffett B., Capitaine N., Defraigne P., de Viron O., Feissel M., Fliegel H., Forte A., Gambis D., Getino J., Gross R., Herring T., Kinoshita H., Klioner S., Mathews P.M., McCarthy D., Moisson X., Petrov S., Ponte R.M., Roosbeek F., Salstein D., Schuh H., Seidelmann K., Soffel M., Souchay J., Vondrak J., Wahr J.M., Weber R., Williams J., Yatskiv Y., Zharov V. et Zhu S.Y., 1999, Considerations concerning the non-rigid Earth nutation theory, *Celest. Mech. Dyn. Astr.*, 72, 4, pp 245-310.

Dehant V., Defraigne P. et Van Hoolst T., 2000, Computation of Mars' transfer function for nutation tides and surface loading, *Phys. Earth planet. Inter.*, 117, pp 385-395.

Dehant V., M. Greff-Lefftz, H. Legros, T. Van Hoolst, P. Defraigne, and O. de Viron,2002, Free and forced response of a non-rigid Mars with an inner-core. I. Analytical approach, in: *Proc. 'Journées des Systèmes de Référence Spatio-temporels 2001'*, Observatoire Royal de Belgique, sept. 2001, ed. Capitaine N., this issue.

Dehant and Mathews, 2002, Information about the core from Earth nutations, in: 'Core dynamics, structure and rotation', *AGU Monograph*, accepted.

Folkner, W.M., Yoder, C.F., Yuan, D.N., Standish, E.M., Preston, R.A. 1997, Interior structure and seasonal mass redistribution of Mars from radio tracking of Mars Pathfinder, *Science*, 278, 1749-1752.

Harri, A.-M., Marsal, O., Leppelmeier, G.W., Lognonné, P. Glassmeier, K.-H., Angrilli, F., Banerdt, B., Barriot, J.P., Bertaux, J.-L., Berthelier, J.J., Calcutt, S., Cerisier, J.C., Crisp, D., Dehant, V., Di Pippo, S., Giardini, D., Guerrier, D., Jaumann, R., Kumpulainen, K., Langevin, Y., Larsen, S., Menvielle, M., Musmann, G., Polkko, J., Pommereau, J.P., Runavot, J., Schumacher, W., Siili, T., Simola, J., and Tillman, J.E., Network Science Landers for Mars, Advances in Space Research, 23(11), 1915-1924, 1999.

Herring T.A., Gwinn C.R. and Shapiro I.I., 1986, Geodesy by Radio Interferometry: Studies of the Forced Nutations of the Earth. 1. Data Analysis, *J. Geophys. Res.*, 91, B5, pp 4745-4754.

Mathews P.M., Buffett B.A., and Herring T.A., 2001, Modeling of nutation-precession: new

nutation series for nonrigid Earth, and insights into the Earth's interior, *J. Geophys. Res.*, in press.

McCarthy D.D., 1996, IERS Conventions. *IERS Technical Notes*

Rivoldini A., P. Defraigne, V. Dehant, et T. Van Hoolst, 2002, Free and forced response of a non-rigid Mars with an inner-core. II. Numerical approach, in: *Proc. 'Journées des Systèmes de Référence Spatio-temporels 2001'*, Observatoire Royal de Belgique, sept. 2001, ed. Capitaine N., this issue.

Roosbeek F. and Dehant V., 1998, RDAN97: an analytical development of rigid Earth nutation series using the torque approach, *Celest. Mech. Dyn. Astr.*, 70, pp 215-253.

Roosbeek, F., 1999, Analytical developments of rigid Mars nutation and tide generating potential series, *Celest . Mech. Dyn. Astr.*,75, 287-300.

Souchay J. and Kinoshita H., 1997, Corrections and new developments in rigid Earth nutation theory: II. Influence of second-order geopotential and direct planetary effect, *Astron. Astrophys.*, 318, pp 639-652.

FREE AND FORCED RESPONSE OF A NON-RIGID MARS WITH AN INNER-CORE. NUMERICAL APPROACH.

A. RIVOLDINI, P. DEFRAIGNE, V. DEHANT, T. VAN HOOLST
Royal Observatory of Belgium
3, Avenue Circulaire
B-1180 Bruxelles
Belgium
e-mail: rivoldini@oma.be

ABSTRACT.

If the planet Mars contains a liquid core and a solid inner core, there is, in addition to the Free Core Nutation (FCN, existing only if the core is liquid) the Free Inner Core Nutation (FICN). The FCN is known to have a frequency in the retrograde band of the forced nutation frequencies. The FICN is in the prograde nutation frequency band. Inside the planet Mars, it is presently not known if there exists an inner core, and what would be the dimension of this inner core. Consequently, it is necessary to examine the impact of the presence of an inner core on the nutations of Mars. We use a numerical integration method, integrating from the center up to the surface. We have implemented our numerical code in order to compute the FICN as well as the forced nutations that may feel the resonance due to their proximity to the mode.

1. INTRODUCTION

The present knowledge of the interior of Mars is sparse and relies mainly on a few observational constraints. This is about to change in the future due to the NEtlander Ionospheric and Geodesic Experiment (NEIGE) (Barriot et al., 2001). The NEIGE experiment will be part of the NEtlander mission planned for 2007. Four identical landers will be sent to Mars, all of them will contain a coherent transponder which will be in communication with an orbiter connected via radio-links to the Earth. The Doppler shifts associated with the variations of Mars' orientation in space will be measured, and will provide us, for the first time, with measurements of the variations of length-of-day, of polar motion, and of precession and nutations (see Dehant et al., 2002, this issue). The determination of these rotation parameters will improve our knowledge of the interior structure of Mars, and in particular the knowledge about the state of the core. If the core is fluid there exists a normal mode called FCN which induces a resonance in the nutations, that will be visible in the NEIGE measurements. Moreover, a inner-core induces another normal mode called FICN with a corresponding resonance in the nutations.

The present models of Mars' interior, such as those of Sohl and Spohn (1997), are obtained from extrapolation of the Earth's internal structure, from chemical composition derived from the SNC meteorites and constraints such as the chondritic Fe/Si ratio or the precession rate (and

consequently the polar moment of inertia) determined form the Viking and Pathfinder missions. Nevertheless those models cannot resolve the uncertainties related to the core's dimension the core's state and the possible existence of an inner core. Both the liquid and the solid configuration can be consistent with the observational constraint that the Martian dipole magnetic field is very weak or non-existent compared to that of the Earth. Also the thermodynamical state of the iron alloy, with a composition incorporating iron and a light element (14 wt%) sulfur, favors a liquid core and no inner-core, but the percentage of light elements is controversial and a slightly smaller value would allow for inner-core formation.

In this paper we compute the free and forced response of a non-rigid Mars as function of the inner-core size. The inner-core size is varied from 0 km (without inner-core) to approximately 1470km (fully solidified core).

The paper is organized as follows. In Section 2, the basics of nutation and normal mode theory are reviewed, specifically the resonances induced by the free core nutation (FCN) and the free inner-core nutation (FICN), which both exist only if the core is liquid and the second only exists if the inner-core is present. In Section 3 the equations and the interior structure involved in our numerical modeling are discussed. In Section 4 we display the results, namely the influence of the inner-core size on the amplitude of the transfer function. Then we compare the transfer function for a planet with a 900 km and a 1100 km inner-core size to a configuration without inner-core.

Finally the last section is be devoted to discussion and concluding remarks.

2. NUTATIONS OF MARS.

Nutations of a planet are periodic changes of the orientation of the rotation axis with respect to an inertial frame. These motions are due to the gravitational torque acting on the equatorial bulge of the flattened planet. This torque can be computed from the tidal potential which essentially depends on the relative position of the planet with respect to the Sun, the moon(s) and the other planets.

The computation of the nutational motions of the rotation axis is done in two steps. First the nutation series for a rigid planet is derived (Roosbeek, 2000), then the non-rigid effects on nutation are calculated with the help of a transfer function, for each frequency of this series . The transfer function is defined as the ratio of the nutation amplitudes for a non-rigid planet to the nutation amplitude for a rigid planet considered at the same frequency (Dehant et al, 2000).

The most important normal modes for nutations are (see Figure 1):

- the Chandler Wobble related to a rotation of the instantaneous rotation axis around the axis of greatest polar principal moment of inertia; it has long period and is prograde in a frame tied to the planet
- the free core nutation (FCN) related to a relative rotation of the liquid core instantaneous rotation axis with respect to that of the mantle; it is diurnal in a frame tied to the planet and has a retrograde long period in space.
- the free inner-core nutation (FICN) related to a relative motion of the instantaneous rotation axis of the inner-core with respect to that of the liquid core and the mantle; it is diurnal in a frame tied to the planet and has a prograde long period in space.

The influence of Mars' interior (mantle and core) on the CW and on the FCN have been investigated by Van Hoolst et al (2000 a,b) and Defraigne et al (2001). The present paper is more concerned with the effect of a possible inner core on the FCN and on the FICN.

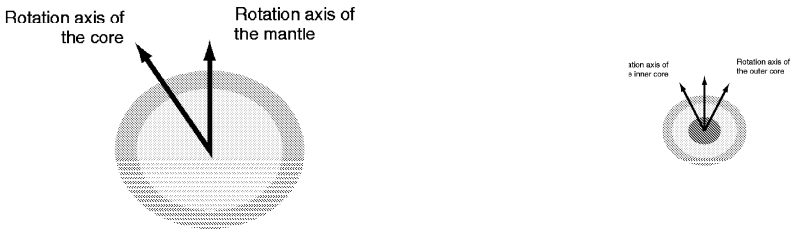

Figure 1: Definitions of the FCN and of the FICN

3. NUMERICAL MODELING.

In our approach we consider the linearized equations of motion of a small displacement for a rotating elliptical planet

$$\begin{aligned} \rho_0 \frac{d^2\overline{u}}{dt^2} + 2\rho_0\,\overline{\Omega}_0 \wedge \frac{d\overline{u}}{dt} &= \rho_0\,\overline{F}_e - \rho_0\,\overline{\nabla} W_1 + \overline{\nabla}\cdot\underline{\overline{T}} + \rho_0\,(\overline{\nabla}\cdot\overline{u})(\overline{\nabla}W_0) \\ &- \rho_0\,\overline{\nabla}(\overline{u}\cdot\overline{\nabla}W_0) - \rho_0(\overline{\Omega}_0 \wedge (\overline{\Omega}_0 \wedge \overline{r})). \end{aligned}$$

They contain the tidal forcing $\overline{F}_e$, the initial and the Eulerian gravitational potential (W_0,W_e), the rotational contribution like the Coriolis and centrifugal potential ($\overline{\Omega}$ is the rotation vector), the Cauchy stress-strain tensor $\underline{\overline{T}}$ and the initial density ρ_0. Those parameters are related by the Poisson equation,

$$\Delta(W_1 + \phi_1^{cf}) = -4\pi\,G\,\overline{\nabla}\cdot(\rho_0\overline{u}),$$

which relates the change of the Eulerian gravitational (W_1) and the Eulerian centripetal (ϕ_1^{cf}) potentials to the local density change and the stress-strain relation,

$$\underline{\overline{T}} = \lambda(\overline{\nabla}\cdot\overline{u})\,\underline{\overline{1}} + \mu(\overline{\nabla}\underline{u} + (\overline{\nabla}\underline{u})^T),$$

where λ and μ Lamé are the parameters.

This system of coupled partial differential equations is first shifted into phase space and then expanded in generalized spherical harmonics to give a system of 10 linear ordinary differential equations of first order. Numerical integration and application of the boundary conditions, supplemented by a density profile and the values of the rheological properties of the martian interior give for each generalized spherical harmonic a set of frequency dependent solutions, consisting of the values of the displacement, of the potentials and of the stress-strain tensor for each radius from the center to the surface. Due to an apparent singularity at the origin, the numerical integration is done from the surface of a small initial sphere to the surface of the planet. An analytical solution is used for the initial sphere (Gilbert et al, 1960).

The martian core modeling is done essentially in four steps (see figure 2). At a given temperature and at fixed concentrations of iron and a light element, the core is completely liquid. The core will remain in this state with decreasing temperature until the liquidus curve is reached somewhere in the core. This happens first at the center, and liquid iron starts to precipitate to the center forming a growing solid inner core. The concentration of iron in the liquid core decreases with the iron precipitation going on until the eutectic point is reached. At this point the alloy of iron and a light element starts to freeze and build a layer around the iron kernel. With decreasing temperature this layer grows until the core is fully solidified.

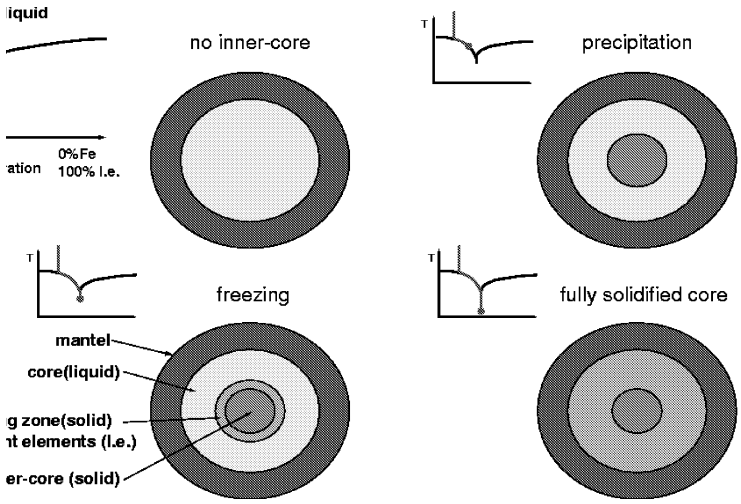

Figure 2: Core modeling

4. RESULTS

The transfer function as a function of inner-core radius and period, for Mars, is shown in figure 3. The inner-core size varies from a small 100 km to 1400 km. The FCN is in the retrograde frequency-band and its period stays at a more or less constant value of 270 days for an inner-core size up to 1000 km, the precipitation regime. After a 1000 km inner-core size, when freezing of light elements around the inner-core occurs, the FCN period starts decreasing until it reaches a value around 188 days for an almost completely solid core.

During the precipitation regime, the FICN period, which is in the prograde frequency band, is increasing from 360 days at 100 km with growing inner-core size to 600 days at 1000 km. After precipitation, in the freezing regime a further increase in kernel size makes the period of the FICN decrease until it reaches a value of 200 days for a kernel size of 1400 km.

Figure 4 and figure 5 show the influence of an inner-core of 900 km and 1100 km on the transfer function. As the FICN is prograde, mainly the prograde nutations will be influenced. For a 900 km inner-core the FICN is located close to the prograde annual nutation frequency. Increasing the inner-core size to 1100 km decreases the FICN frequency to a value near the semi-annual nutation frequency.

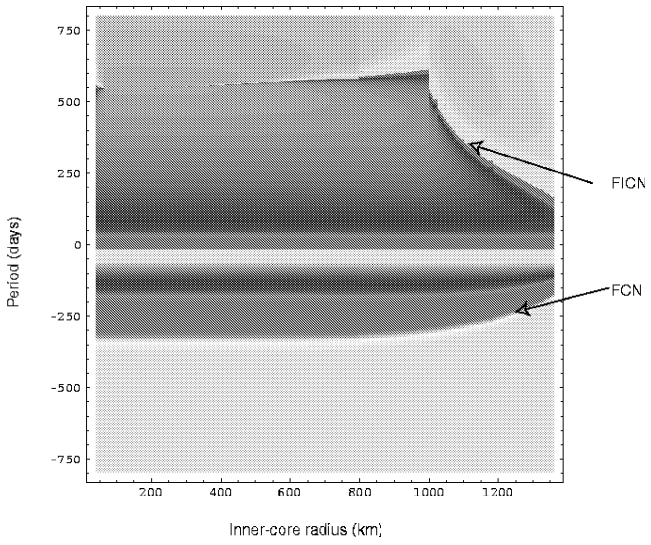

Figure 3: B-Ratio of Mars as a function of inner-core radius

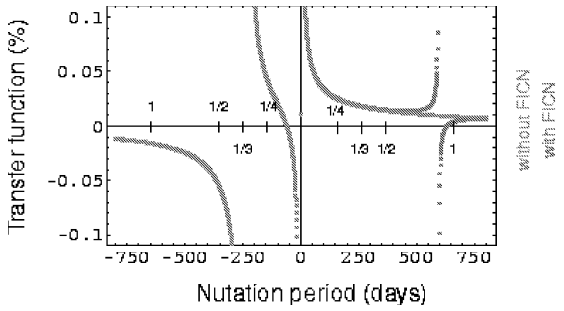

Figure 4: Influence of a 900 km inner-core on the transfer function

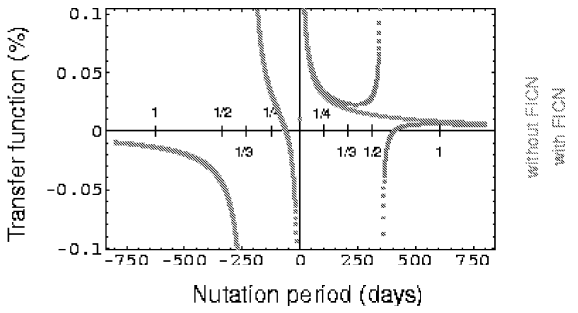

Figure 5: Influence of a 1100 km inner-core on the transfer function

5. CONCLUSIONS

The Free Core Nutation FCN and the Free Inner Core Nutation FICN periods dependend on the inner core dimension. For an iron-rich alloy composition with 14 wt% of light element sulfur, they can vary from short periods to 280 days for the FCN and to 600 days for the FICN. The FCN and the FICN may be observed from resonances in nutations excited by the Sun (and to a smaller extend by Phobos and Deimos). Their observation by the NEtlander Ionosphere and Geodesy Experiment (NEIGE), in the framework of the NetLander mission, will allow to infer properties of the mantle, the core, and of a possible inner core. In particular, the geophysical properties such as the dimensions and the physical state of the core will be determined from the resonances.

6. REFERENCES

Barriot J.P., Dehant V., Folkner W., Cerisier J.-C., Ribes A. and Benoist J.e al, 2001, "The NetLander ionosphere and geodesy experiment (NEIGE)", *Advance Space Res.*, 28(8), pp 1237-1249.

Dehant V., Van Hoolst T., and Defraigne P., 2000, "Comparison between the nutations of the planet Mars and the nutations of the Earth.", *Survey Geophys.*, 21, 1, pp. 89-110.

Defraigne P., Dehant V., and Van Hoolst T., 2000, "Steady state convection constrained by Tharsis, the geoid and the precession constant.", *Planetary and Space Sciences*, 49, pp. 501-509

Gilber F. and Backus G., 1960, "Elastic-Gravitational Vibrations of a Radially Stratified Sphere", *Dynamics of Stratified Solids*, ed. by Herrman, pp. 82-95

Roosbeek F., "Analytical developments of a rigid Mars nutation and tide generating potential series", *Celest. Mech.*, 2000

Sohl F.and Spohn T., 1997, "The interior structure of Mars: implications from SNC meteoroids", *J. Geophys. Res.*, 102, pp. 1613-1636

Van Hoolst T., Dehant V., and Defraigne P., 2000a, "Sensitivity of the Free Core Nutation and the Chandler Wobble to changes in the interior structure of Mars.", in: Proc. SEDI meeting, Session 8: 'Deep interior of terrestrial planets', Tours, France, July 1998, *Phys. Earth planet. Inter.*, 117, pp. 397-405.

Van Hoolst T., Dehant V., and Defraigne P., 2000b, "Chandler Wobble and Free Core Nutation for Mars.", *Planet. Space Sc.*, 48, 12-14, pp. 1145-1151.

EFFECTS OF MARS' ROTATION ON ORBITER DYNAMICS

V. MIOC and M. STAVINSCHI
Astronomical Institute of the Romanian Academy
Str. Cuţitul de Argint 5, RO-75212 Bucharest, Romania
e-mail: vmioc@aira.astro.ro, magda@aira.astro.ro

ABSTRACT. Of first importance in the theoretical study of a spacecraft motion, in view of a cosmic flight, is the modelling of as much perturbing effects as possible; this contributes essentially to a better knowledge of the trajectory.

This paper deals with the influence of Mars' rotation on the dynamics of an orbiter via rotation and oblateness of its atmosphere (considered separately from the general atmospheric drag). For the density distribution, the nominal density profile proposed by Sehnal is adopted. As regards the orbiter dynamics, one considers only initially circular trajectories lying entirely in the altitude range 100-1000 km.

Using a method proposed by Zhongolovich, that uses the argument of latitude as independent variable (allowing in this way the study of circular orbits), the first order difference between the nodal period of the orbiter and the corresponding Keplerian period is analytically determined. The first order changes of five independent osculating orbital elements (the classical set of six without the dynamical one) along one nodal period are determined, too. All analytic results are translated in terms of physical motion. The evolution of the radius vector and the related change of the nodal period prove to be closely related to the initial orbital inclination.

1. INTRODUCTION

While studying theoretically the motion of a spacecraft, in view of a cosmic flight, of first importance is the modelling of as much perturbing effects as possible. Better known the influence of the various perturbing factors is, and better known the trajectory of the cosmic vehicle will be.

Among the effects that act on the motion of a planetary orbiter, we dwelt upon the planet's rotation. Its influence can be tackled from many standpoints, considering for instance: the noncentrality of the gravitational field given by the second zonal harmonic, the relativistic effect of the quadrupole momentum, the Lense-Thirring effect, the atmospheric rotation and/or oblateness (due, obviously, to the planet's rotation).

In the sequel we approach the last situation for the concrete case of Mars. The perturbed motion of an orbiter in the Martian atmosphere was first studied analytically by Sehnal and Pospišilová (1988). Using the data provided by Moroz et al. (1988), they modelled the density distribution by the law

$$\rho = \exp(a_{1j} + a_{2j}/h), \quad j \in \{1, 2, 3\}, \tag{1}$$

where the numerical value of the density ρ results in kg/m^3 for the altitude h above Mars'

surface expressed in km. The constants a_{1j}, a_{2j} are separately determined for the minimal ($j = 1$), nominal ($j = 2$), and maximal ($j = 3$) density profiles. In the nominal model used by us for numerical estimates, Sehnal (1990) gave $a_{12} = -37.936$, $a_{22} = 2376.1$. Expression (1) is valid for the altitude range 100 km $\leq h \leq$ 1000 km.

The quoted papers did not considered the atmospheric rotation and oblateness. Further analytic approaches took into account these effects (e.g. Mioc et al. 1991), but imbedded in the general atmospheric drag effect, and only for orbital elements, or went deeper in the Martian atmospheric drag problem, but without considering rotation and oblateness (Mioc and Radu 1991b). The subject that interests us here is the way in which the separate influence of the rotation and oblateness of Mars' atmosphere could affect the motion of an orbiter.

We shall study the respective perturbations in both the nodal period

$$T_\Omega = \int_0^{2\pi} (dt/du)du, \tag{2}$$

and the orbital elements

$$y \in Y = \{p, \Omega, i, q = e\cos\omega, k = e\sin\omega\}. \tag{3}$$

Here u = argument of latitude, p = semilatus rectum, Ω = longitude of ascending node, i = inclination, e = eccentricity, ω = argument of periastron (all with respect to a frame originated in Mars' mass centre, whose fundamental plane is the Martian equatorial plane.

We study the orbiter motion within the following physical and dynamical framework:

(i) the atmosphere rotates with the same angular velocity ($\omega_M = 6.124$ rad/day) as Mars, and is oblate (the surfaces of equal density having the same oblateness $\eta = 0.0065$ as the planet);

(ii) the initial orbit lies entirely in the range of heights 100-1000 km above Mars' surface;

(iii) the initial orbit is circular ($e_0 = e(t_0) = 0$, which implies $q_0 = 0$, $k_0 = 0$).

2. BASIC EQUATIONS

Under the influence of any perturbing factor depending on a small parameter ε, the orbiter motion undergoes a perturbing acceleration (of radial, transverse, and binormal components denoted by R, T, N, respectively).

We have chosen the nodal period as basic time interval. Accordingly, let us describe the motion via the Newton-Euler equations written with respect to the argument of latitude (*cf.* Mioc and Stavinschi 1995, 1997):

$$\begin{aligned}
dp/du &= 2(\gamma/\mu)r^3T,\\
d\Omega/du &= (\gamma/\mu)r^3[\sin u/(p\sin i)]N,\\
di/du &= (\gamma/\mu)r^3(\cos u/p)N,\\
dq/du &= (\gamma/\mu)\{(r^2\sin u)R + r^2[r(q+\cos u)/p + \cos u]T + r^3[k\cos i\sin u/(p\sin i)]N\},\\
dk/du &= (\gamma/\mu)\{-(r^2\cos u)R + r^2[r(k+\sin u)/p + \sin u]T - r^3[q\cos i\sin u/(p\sin i)]N\},\\
dt/du &= (\gamma/\sqrt{\mu p})r^2.
\end{aligned} \tag{4}$$

where $\gamma = [1 - r^2\dot{\Omega}\cos i/\sqrt{\mu p}]^{-1}$, μ = Mars' gravitational parameter ($\mu = 0.426503 \times 10^{14}$ m^{3}s^{-2}), and r = planetocentric radius vector.

Using the method proposed by Zhongolovich (1960) for a wholly different model, the variation of the nodal period can be expressed as $\Delta T_\Omega = \sum_{i=1}^4 J_i$, with

$$J_1 = (3/2)\sqrt{p_0/\mu}\int_0^{2\pi}(1 + q_0\cos u + k_0\sin u)^{-2}\Delta p du,$$

$$
\begin{aligned}
J_2 &= -2p_0\sqrt{p_0/\mu}\int_0^{2\pi}(1+q_0\cos u+k_0\sin u)^{-3}\Delta q\cos u du,\\
J_3 &= -2p_0\sqrt{p_0/\mu}\int_0^{2\pi}(1+q_0\cos u+k_0\sin u)^{-3}\Delta k\sin u du,\\
J_4 &= \int_0^{2\pi}\{\partial[r^4\dot{\Omega}\cos i/\mu p]/\partial\varepsilon\}\varepsilon du,
\end{aligned}
\tag{5}
$$

in which the subscript "0" means (as above) the initial values, whereas the changes $\Delta y = y - y_0$, $y \in Y$, after the interval $[u_0, u]$ are determined from

$$
\Delta y = \int_{u_0}^{u}(dy/du)du, \quad y \in Y, \tag{6}
$$

under the condition (natural and not restrictive) that the orbital parameters experience small perturbations over one revolution.

Since our intention is to consider here only initially circular orbits ($q_0 = 0$, $k_0 = 0$, $p_0 = r_0$), expressions (5) reduce to

$$
\begin{aligned}
J_1 &= (3/2)\sqrt{p_0/\mu}\int_0^{2\pi}\Delta p du,\\
J_2 &= -2p_0\sqrt{p_0/\mu}\int_0^{2\pi}\Delta q\cos u du,\\
J_3 &= -2p_0\sqrt{p_0/\mu}\int_0^{2\pi}\Delta k\sin u du,\\
J_4 &= (p_0^3/\mu)\cos i_0\int_0^{2\pi}(\partial\dot{\Omega}/\partial\varepsilon)\varepsilon du.
\end{aligned}
\tag{7}
$$

For sake of simplicity, in the sequel we shall drop the subscript "0" for the initial values of (3) and functions of them. Every further subscript "0" (except u_0) is a simple notation and does not refer to initial values. Actually, every quantity in the right-hand side of (4) or (7) that does not depend on u will be considered constant over one revolution, and equal to its value for $u = u_0$.

3. EQUATIONS OF MOTION

Let us consider only the influence of Mars' atmospheric rotation (oblateness entailed) on the orbiter motion. In this case, the components of the perturbing acceleration, for an initially circular trajectory, reduce to (*cf.* Mioc and Radu 1991a):

$$
\begin{aligned}
R &= 0,\\
T &= \rho\delta\sqrt{\mu p}\omega_M\cos i,\\
N &= -\rho\delta\sqrt{\mu p}\omega_M\sin i\cos u,
\end{aligned}
\tag{8}
$$

where δ stands for the drag parameter (ballistic coefficient) of the orbiter.

Now we have to express the density as a function only of u. By $h = r - R_M(1 - \eta\sin^2\varphi)$, where $R_M = 3380$ km is the mean equatorial radius of Mars, $\varphi =$ latitude, and $\sin\varphi = \sin i\sin u$, we get $h = p - R_M(1 - \eta\sin^2 i + \eta\sin^2 i\sin^2 u)$, hence the density expression (1) becomes

$$
\rho = \exp\left[a_{12} + \frac{a_{22}}{(p - R_M + \eta R_M\sin^2 i)(1 - W\cos^2 u)}\right], \tag{9}
$$

where $W = \eta R_M \sin^2 i/(p - R_M + \eta R_M \sin^2 i)$. Condition (ii) easily leads to $W_{\max} = 0.15$, therefore we have to first order in W:

$$\rho = \alpha \exp(\beta \cos^2 u), \tag{10}$$

with $\alpha = \exp[a_{12} + a_{22}/(p - R_M + \eta R_M \sin^2 i)]$, $\beta = a_{22}W/(p - R_M + \eta R_M \sin^2 i)$. A straightforward computation shows that β does not exceed 3; consequently, we shall expand (10) as

$$\rho = \alpha \sum_{n=0}^{8} (\beta^n/n!) \cos^{2n} u. \tag{11}$$

Having in view the fact that the perturbations of $y \in Y$ are small over one revolution, and taking into account Zhongolovich's (1960) method, we easily get the expressions of the first five equations (4) for our case:

$$\begin{aligned}
dp/du &= 2\alpha p^3 \sqrt{p/\mu}\delta\omega_M \cos i \sum_{n=0}^{8} (\beta^n/n!) \cos^{2n} u, \\
d\Omega/du &= -\alpha p^2 \sqrt{p/\mu}\delta\omega_M \sum_{n=0}^{8} (\beta^n/n!) \cos^{2n+1} u \sin u, \\
di/du &= -\alpha p^2 \sqrt{p/\mu}\delta\omega_M \sin i \sum_{n=0}^{8} (\beta^n/n!) \cos^{2n+2} u, \\
dq/du &= 2\alpha p^2 \sqrt{p/\mu}\delta\omega_M \cos i \sum_{n=0}^{8} (\beta^n/n!) \cos^{2n+1} u, \\
dk/du &= 2\alpha p^2 \sqrt{p/\mu}\delta\omega_M \cos i \sum_{n=0}^{8} (\beta^n/n!) \cos^{2n} u \sin u.
\end{aligned} \tag{12}$$

4. RESULTS

By (7), the integrals (6) must be performed only for p, q, and k. Performing them with the integrands provided by the corresponding equations (12), we get

$$\begin{aligned}
\Delta p &= -Zp \left[u + \sum_{n=0}^{8} (\beta^n/n!) \left(P_n u + \frac{1}{2n} \sum_{j=0}^{n-1} P_{nj} \cos^{2n-2j-1} u \sin u \right) - F_1^0 \right], \\
\Delta q &= Z \left[\sum_{n=0}^{8} \frac{\beta^n}{n!(2n+1)} \sum_{j=-1}^{n-1} Q_{nj} \cos^{2n-2j-2} u \sin u - F_2^0 \right], \\
\Delta k &= -Z \left[\sum_{n=0}^{8} \frac{\beta^n}{n!(2n+1)} \cos^{2n+1} u - F_3^0 \right],
\end{aligned} \tag{13}$$

where we abridged $Z = 2\alpha p^2 \sqrt{p/\mu}\delta\omega_M \cos i$, and

$$\begin{aligned}
P_n &= \frac{(2n-1)!!}{2^n n!}, \quad n = 1, 2, ...; \\
P_{n0} &= 1, \quad P_{nj} = \frac{(2n-1)(2n-3)...(2n-2j+1)}{2^j (n-1)(n-2)...(n-j)}, \quad j = \overline{1, n-1}; \\
Q_{n,-1} &= 1, \quad Q_{nj} = \frac{2^{j+1} n(n-1)...(n-j)}{(2n-1)(2n-3)...(2n-2j-1)}, \quad j = \overline{0, n-1},
\end{aligned} \tag{14}$$

while F_s^0, $s = \overline{1,3}$, stands for the value of the whole expression (function of u) preceding it inside the square brackets, for $u = u_0$.

Substituting (13) in (7), and performing the integrations, we find $J_1 \neq 0$ (see its expression below), $J_2 = 0$, $J_3 = 0$. As regards J_4, using the last equation (4) and the second equation (12), then performing the last integral (7), in which α plays the role of the small parameter, we get $J_4 = 0$. So, we obtain the first order difference between the nodal period and the corresponding Keplerian period:

$$\Delta T_\Omega = 6\pi\alpha(p^4/\mu)\delta\omega_M \cos i \left[\pi \sum_{n=0}^{8} (\beta^n/n!)P_n - F_1^0\right]. \tag{15}$$

To end, we give the variations of the orbital elements (3) over one nodal period. Replacing (12) in (6), then integrating between 0 and 2π, and keeping, by abuse, the same notation Δy, $y \in Y$, for these changes, we obtain

$$\begin{aligned} \Delta p &= 4\pi\alpha p^3\sqrt{p/\mu}\delta\omega_M \cos i \sum_{n=0}^{8} (\beta^n/n!)P_n, \\ \Delta\Omega &= 0, \qquad \Delta q = 0, \qquad \Delta k = 0, \\ \Delta i &= -2\pi\alpha p^2\sqrt{p/\mu}\delta\omega_M \sin i \sum_{n=0}^{8} (\beta^n/n!)P_{n+1}. \end{aligned} \tag{16}$$

5. CONCLUSIONS

Examining formulae (15) and (16), we can draw some conclusions concerning the physical behavior of the orbiter:

5.1. Since $\Delta q = \Delta k = 0$, the initially circular orbit returns to a circular shape after one nodal period.

5.2. Since Δp contains $\cos i$, multiplied by a positive quantity, after one nodal period, the new orbital radius, compared to the initial one, will be greater if the initial orbit is direct ($i < \pi/2$), equal for a polar orbit ($i = \pi/2$), and smaller for a retrograde orbit ($i > \pi/2$).

5.3. Since $\Delta\Omega = 0$, the node comes back to its initial position after one nodal period.

5.4. Since Δi contains $\sin i$, multiplied by a negative quantity, after one nodal period the inclination becomes smaller: a direct initial orbit will be shifted towards an equatorial one, whereas a retrograde initial orbit will be shifted towards a polar one.

5.5. By 5.2, the nodal period, compared to the corresponding Keplerian period, is greater for direct initial orbit, equal for the polar case, and smaller for retrograde motion.

Two general conclusions, as regards the techniques we used, can also be formulated:

5.6. The use of the argument of latitude as independent variable allows the study of the perturbations in the period for very low eccentric orbits (even circular, as we considered). Such a study is impossible if one of the anomalies is taken as independent variable.

5.7. Our results are valid only under the hypotheses (i)-(iii) formulated in Section 1, and only in a first order approximation with respect to the small parameter α. However, they constitute a sufficiently real departure point for further refinements.

6. REFERENCES

Mioc, V., Radu, E.: 1991a, *Bull. Astron. Inst. Czechosl.*, **42**, 298.
Mioc, V., Radu, E.: 1991b, *Bull. Astron. Inst. Czechosl.*, **42**, 395.

Mioc, V., Blaga, C., Radu, E.: 1991, *Europhys. Lett.*, **16**, 327.
Moroz, V. I., Izakov, M. N., Linkin, V. M.: 1988, *Inst. Kosm. Issled. AN SSSR*, Preprint No. 1449.
Sehnal, L..: 1990, *Bull. Astron. Inst. Czechosl.*, **41**, 107.
Sehnal, L., Pospišilová, L: 1988, *Astron. Inst. Czechosl. Acad. Sci.*, Preprint No. 75.
Zhongolovich, I. D.: 1960, *Byull. Inst. Teor. Astron.*, **7**, 521.

COMPARISON BETWEEN THE ATMOSPHERIC FORCING ON EARTH AND MARS

O. DE VIRON, E. VAN DEN ACKER, T. VAN HOOLST, P. DEFRAIGNE, V.DEHANT
Royal Observatory of Belgium
Avenue circulaire, 3, B-1180 Brussels, Belgium
e-mail: o.deviron@oma.be

ABSTRACT. The interaction between the Earth and its atmosphere is the main cause for the fluctuations in the Earth's rotation and, in particular, for the variations of the Earth's rotation rate. For Mars, the effect of the atmosphere and of the ice caps is also the major contributor to rotation fluctuation. In this paper, we compare the interaction between each planet and its fluid layer, by analyzing both the variation of the angular momentum of the fluid layer and the interaction torques. The differences and similarities for both planets are discussed in terms of the global dynamics of the atmosphere.

1. INTRODUCTION

The rotation of the Earth is not constant in time; its angular velocity presents fluctuations, which are associated with variations of the length-of-day. In addition, the positions of the rotation axis in the Earth and in the inertial frame change with time, generating polar motion and precession-nutation. The global geophysical fluids (atmosphere, core, ocean) are responsible for the major part of these fluctuations. The planet Mars also has an atmosphere, though much lighter (mean atmospheric pressure of 760 Pa). This atmosphere is mainly composed of CO_2 and has a dynamics very different from the Earth's atmosphere. In particular, due to the huge temperature differences at the Martian surface, about half of the atmosphere condensates in very large polar ice caps during the winters. As expected, variations of the Martian rotation are associated with these large scale mass displacements .

To investigate the effects of the fluid layers on the planet rotation, the so-called atmospheric angular momentum approach is commonly used: in the Newtonian framework, the angular momentum (AM) of any isolated system is conserved. Considering the fluid+planet system as isolated, the knowledge of the change of the fluid layer AM gives all the information about the change of AM of the planet, and thus the rotation of the planet is totally constrained. The AM of the fluid layer is classically divided into two parts: the matter term, corresponding to a rigid rotation of the fluid with the planet, and the motion term, corresponding to the relative angular momentum of the fluid with respect to the Earth. In the case of the Earth, this method has successfully been applied in a lot of papers, as Barnes et al. [1982], for example. It has also been used to compute the effect of Mars' atmosphere and ice cap in several studies, see Cazenave and Balmino [1981], Chao and Rubincam [1990], Defraigne et al. [1999], or Van den Acker et al. [2001]. An alternative approach is known as the torque approach. It consists in an evaluation of

the fluid effect on Earth rotation by a direct computation of the interaction torque. This torque is classically divided into three parts, a pressure torque acting on the topography, a gravitational torque due to the interaction between the heterogeneities of mass inside the planet and the fluid, and a friction torque due to the relative velocity of the fluid. For the equatorial component, the effect of the equatorial bulge is very important. It appears through the pressure torque and the gravitational torque acting on the ellipsoidal geopotential of the Earth. As they are proportional (and partially canceling each other), they are computed together, as the ellipsoidal torque, using, as in Bell [1994]

$$\vec{\Gamma}_{\text{Ellips.}} = \vec{\Omega} \wedge \vec{H}_{\text{matter}} \tag{1}$$

where $\vec{\Gamma}_{\text{Ellips.}}$ is the ellipsoidal torque, $\vec{\Omega}$ is the Earth mean rotation vector, and $\vec{H}_{\text{matter}}$ is the matter term of the AM of the fluid layer.

In Section 2, we will compare some general characteristics of Mars and Earth that are relevant for the computation of the atmospheric effect on the rotation. Section 3 will be devoted to the comparison of the AM of the fluid layers, and their effect on the annual fluctuation of Martian rotation. In Section 4, we will discuss the atmospheric torque on Earth and Mars, and we will conclude in Section 5.

2. GENERAL CHARACTERISTICS OF EARTH AND MARS

Mars is about twice smaller than the Earth (radius=3390km). Mars' principal moment of inertia is about $3 \cdot 10^{36} kg\, m^2$ ($8 \cdot 10^{37} kg\, m^2$ for the Earth). The atmosphere is much lighter, with a mean surface atmospheric pressure of 760 Pa (100 000 Pa for the Earth). The mean gravity is 3.7 $m\, s^{-2}$ for Mars. The mean length-of-day of Mars (24.66 hours) is close to that of the Earth. A rough evaluation of the relative size of the effects of the fluids on Mars' and Earth's length-of-day, at equivalent dynamics gives an effect of Mars' atmosphere + ice cap on the length-of-day about 25 times smaller than the atmosphere + ocean effect on Earth.

Actually, the effect is only about 6 times smaller. This difference mainly comes from a different dynamics. We will not discuss here those differences in detail, they are analyzed in Dehant et al. [2001]. The main differences are the following:

- A large proportion of the Mars' atmosphere condensates/sublimes in the large polar ice caps of Mars, in relation with the seasonal cycle in the solar heating. Consequently, there is a large change in the fluid mass repartition with a seasonal frequency.
- The gravitational potential at the surface of Mars is much more irregular than at the Earth surface.
- There exists oceans at the Earth surface, which, due to the associated huge thermal inertia, have a large impact on the Earth climate. There is no such large "damping effect" at the Martian surface.
- There are large dust storms at the Mars' surface.
- The orbit of Mars is much more eccentric than the Earth orbit. For this reason, the length of the season is not the same for the northern and southern hemisphere (the summer is longer for the Northern hemisphere; the winter is longer for the Southern hemisphere).

As we will see, all those differences have a direct impact on the effect of the atmosphere on the Earth rotation.

3. INTERACTION PLANET-ATMOSPHERE BY THE ANGULAR MOMENTUM APPROACH

Figure 1 shows the effect of the atmosphere + ocean of the Earth and atmosphere + ice caps of Mars on the annual variation of the length-of-day, showing the matter term and wind term of the AM for each. It can be seen that the results are totally different, as the fluctuation of the Earth fluid AM is mainly associated with changes in the fluid motion (nearly only fluctuation of the wind) whereas, for Mars, it is mainly due to a change in the distribution of the Mass (atmosphere + ice caps). For the polar motion (Figure 2), the motion and matter terms are at the same order of magnitude for Earth, but the motion term are still much smaller for Mars. This first important difference is associated with the fact that there is a large change in the mass distribution associated with the CO2 condensation/sublimation process on Mars.

There exists also dust storms at the Martian surface,of which the effect on the Martian rotation can be very important (see Van den Acker et al., 2001).

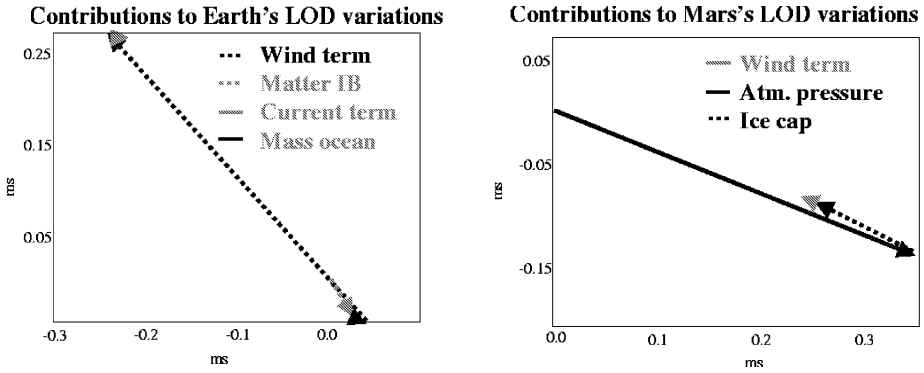

Figure 1: Effect of fluid layer on the length-of-day of Earth (left) and Mars (right)

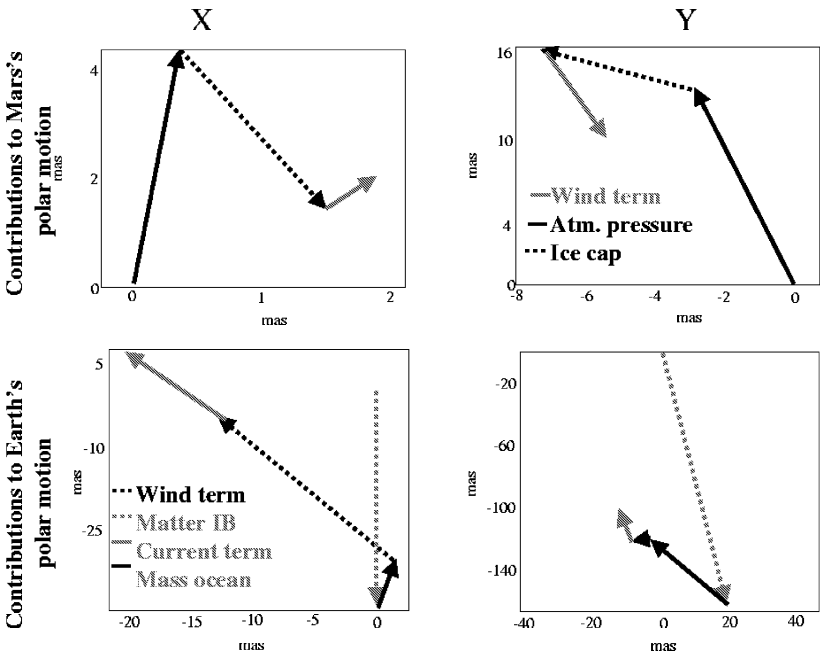

Figure 2: Effect of fluid layer on the polar motion of Earth (left) and Mars (right)

4. INTERACTION PLANET-ATMOSPHERE BY THE TORQUE APPROACH

For lod, it is well known that, for the Earth, the friction torque dominates the annual signal. It has been shown in de Viron et al. [2001] that this signal is mainly associated with the friction on the Indian Ocean. Figure 3 shows the repartition of the effect between the different torques on the length-of-day variation. Unlike what is observed for the Earth, the gravitational torque is not negligible on Mars. This is due to the large irregularities of the geoids. Figure 4 shows the equatorial components. As is known (see de Viron et al. [1999], for instance), the ellipsoidal torque dominates the equatorial torque acting on the Earth. This is not the case for the Y component of the torque acting on Mars. On Earth, the presence of oceans imposes a geometry in the surface pressure that generates a large ellipsoidal torque at all the frequencies. The absence of oceans at the Martian surface explains why no such pressyre distribution exixsts on Mars. As for LOD, the gravitational torque (non-ellipsoidal) is much larger for Mars than for the Earth.

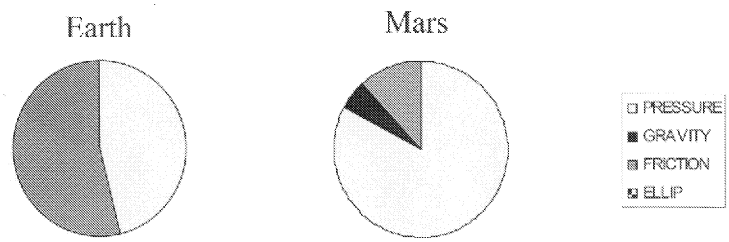

Figure 3: Effect of fluid layer on the polar motion of Earth (left) and Mars (right)

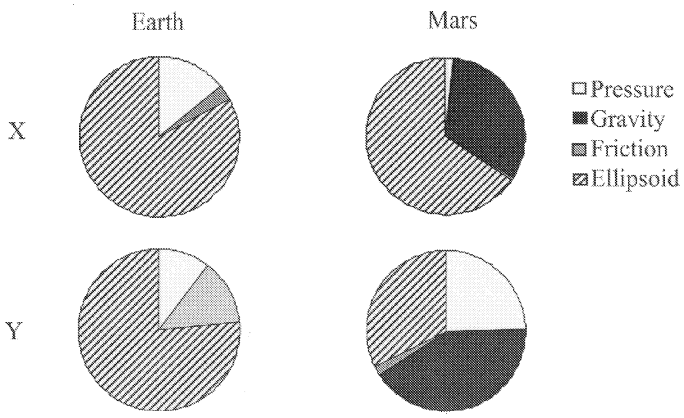

Figure 4: Torque causing variation of the Earth (left) and Mars (right) polar motion

5. CONCLUSIONS

The dynamics of both atmospheres are very different. The presence of the oceans at the Earth's surface is a source of important stability in the Earth atmosphere. As Mars does not have oceans, there is no such stability. The condensation/sublimation process at the Martian surface is associated with huge mass motion. Consequently, the change of the mass repartition dominates the variation of the AM of the fluid layer, whereas, on Earth, the fluctuation of the wind (mainly the westerlies) is the major cause of AM fluctuation. The atmosphere+ice cap of Mars, though much lighter than on Earth, is a source of rotation variation nearly as large as

the one on Earth. The dust storms at the Martian surface are also a source of large change in Mars' rotation. The effect of the ocean on the Earth rotation is also shown by this comparison to have a large indirect impact, as the ocean have a very important role in the global dynamics of the Earth's atmosphere.

6. REFERENCES

Barnes, R. T. H., R. Hide, A. A. White, and C. A. Wilson, Atmospheric angular momentum fluctuation, length-of-day changes and polar motion, *Proc. R. Soc. London, Ser. A*, *387*, 31-73.

Bell, M. J., Oscillations in the equatorial components of the atmosphere's angular momentum and torques on the Earth's bulge, *Q. J. R. Meteorol. Soc., 120*, 195-213, 1994.

Cazenave A., Balmino G., Meteorological effects on the seasonal variations on the rotation of Mars, *Geophys. Res. Lett.*, 8(3), 245-248, 1981.

Chao B. F., Rubincam D. P., Variations of Mars' gravitational field and rotation due to seasonal CO_2 exchange, *J. Geophys. Res.*, 95, B9, 14755-14760, 1990.

Defraigne, P., O. de Viron, V. Dehant, T. Van Hoolst, and F. Hourdin, Mars rotation variations induced by atmospheric CO2 and winds. *J. Geophys. Res.*, 105:, E10, pp 24563-24570, 2000.

Dehant, V., O. de Viron, T. Van Hoolst, P. Defraigne and O. Karatekin, Comparison between the fluid effect on Earth's rotation and on Mars rotation, in preparation

de Viron, O., C. Bizouard, D. Salstein, and V. Dehant, Atmospheric torque on the Earth and comparison with atmospheric angular momentum variations, *J. Geophys. Res.*, *104*, 4861-4875, 1999.

de Viron, O., J.O. Dickey and S.L. Marcus, Annual Atmospheric Torques: Processes and Regional Contributions, accepted for publication in *Geophysical Research letters.*

Van den Acker, E., T. Van Hoolst, O. de Viron, P. Defraigne, V. Dehant, F. Forget, and F. Hourdin, Influence of the winds and of the CO_2 mass exchange between the atmosphere and the polar ice caps on Mars' orientation parameters, submitted to *J. Geophys. Res.*.

TIDES ON THE PLANETS MARS AND MERCURY

T. VAN HOOLST, V. DEHANT
Royal Observatory of Belgium
3 avenue Circulaire, B1180 Brussels, Belgium
e-mail: v.dehant@oma.be

ABSTRACT We have calculated tides on Mars and Mercury. In particular for Mars, we have used Roosbeek's tidal potential to calculate tidal displacements and gravity var iations. The tides are mainly caused by the Sun, the natural satellites Phobos and Deimos contribute about 8% and 0.08%, respectively. The Martian tidal displacements are about 1 centimeter and the tidally induced gravity changes on Mars are of the order of 1 μGal. These findings are important in the frame of the future geophysical experiment Netlander, which will measure station positions and gravity variations. For Mercury, the tidal signals are about 100 times larger, making future tidal measurements very interesting since they would offer the possibility to better determine the interior structure of this planet. The large tidal signal compared to Mars is caused by the proximity of Mercury to the Sun.

1. INTRODUCTION

Mars has no large natural satellites and due to its larger distance from the Sun and smaller radius, the ratio of the tidal potential U_T caused by the Sun on Mars to that on the Earth can be estimated as $(R_{\rm M}/R_{\rm E})^2(d_{\rm M}/d_{\rm E})^3 \approx 0.08$. Here, R and d denote mean radius and distance to the Sun, and subscripts M and E stand for Mars and Earth. Mercury has no natural satellites and the Sun is the only solar system body that causes important tides. Mercury's radius is almost 40% of the Earth's radius, and its mean distance to the Sun is also almost 40% of the Earth's mean distance to the Sun. Therefore, the tidal potential caused on Mercury by the Sun is about 2.5 times larger than the solar tidal potential on Mars.

The tidal potentials on Mars and Mercury induce periodic changes in station positions, lead to gravity variations that can be measured by a lander on the surface, and cause variations in the external gravitational potential fields of Mars and Mercury. The surface displacements can be estimated by the displacements of the equipotential surfaces near the surface of the planet, which are given by the ratio of the tidal potential to the gravity. For Mars, this gives tidal displaceme nts of about 3 cm, for Mercury of about 1 meter. The tidal contribution to surface gravity can be estimated as $2U_T/R$ and gives $\approx 1\mu$Gal for Mars and ≈ 0.3 mGal for Mercury.

Present technologies allow the determination of the position with an accuracy of a few centimeters, and of the measurement of gravity below 1 μgal. Tidal studies on Mars and Mercury can thus be undertaken. Tides can be extremely useful for better determining the interior structure of planets, as will be explained below. For Mars, several experiments of the space missions to Mars depend on accurate position or gravity determinations. The NetLander mission (Harri et al. 2000), which is planned to be launched in 2007, has a seismology experiment (SEIS)

and a geodesy experiment (NEIGE). Both experiments could be used to measure the tides on Mars.

2. TIDAL CALCULATIONS

Tides occur at various frequencies connected to the rotation of the planet and the periodically changing re lative positions between the planet and the bodies causing the tides. As for the Earth, the main tides of Mars and Mercury lie in diurnal, semi-diurnal, and long-period bands. Here, diurnal and subdiurnal have to be understood as with respect to the day of the planet defined by its rotation period about its axis. For Mars, a day is only slightly longer than on Earth, but on Mercury it is about 58 times longer. In addition to these period bands, Mars has also important tides with periods below half a day connected with Phobos, which revolves around Mars in about 8 hours.

A tidal potential for Mars has been calculated by Roosbeek (2000). For Mercury, a tidal potential has recently been calculated. These potentials form the starting point for tidal calculations as they give the gravitational forcing that is applied to the planets decomposed into periodic series.

Tidal displacements, gravity variations and external potential variations describe different reactions to the tidal forcing. They depen d on the interior of the planets. We have used different models of the interior structure of Mars and Mercury. We especially considered models with different core radii. These radii are not well known presently. For Mars, the core radius is believed to be between about 1300 and 1700 kilometers (see Van Hoolst et al 2000, for the models), for Mercury, the core radius is estimated as 1860km $\pm$ 100km. For Mars, it is moreover not known with certainty whether its core is (partly) liquid or not.

The reaction of planets to a gravitational forcing is most conveniently described by Love numbers. We have calculated Love numbers h and k for tidal displacements and external potential variations respectively. We also determined the so-called gravimetric factor δ for gravity variations. The tidal signals have then been calulated as a function of time for the different models.

3. RESULTS

For Mars, Love number h is about 0.2, three times smaller than th e values of 0.6 for the Earth. Love number k is about 0.1, also three times smaller than the Earth value. The reasons for the smaller Love numbers are that Mars is a smaller planet and that the liquid core is relatively smaller. The core radius is about 45 % of the planet's radius, compared to 55 % for the Earth.

Love numbers h are larger for a liquid core than for a solid core and increase when the core radius increases. For example, increasing the core radius by 200 km (about 14 %) increases the second-degree Love number $h^{(0)}$ by 25 %, and changing to a solid core decreases the second-degree Love number by 29 %. The Love numbers h, and therefore also the tidal displacements, are thus very sensitive to the dimension and state of the core. Love numbers k show a similarly large dependence on the core.

The tidal station displacements have been calculated by using expressions for a flattened planet as given in Mathews et al. (1995) and Dehant et al. (1999). All three components of th e displacement stay below 1 cm, and the radial component is about twice the tangential components. The NEIGE experiment to be sent to Mars in 2007 will determine positions of the NetLanders with an accuracy of about 5 cm (Barriot et al 2001). The tidal displacements fall below this threshold and can therefore not be observed with this experiment. However,

station position measurements can be corrected for the calculated tidal displacements before interpreting the results in terms of other time-varying phenomena such as nutations, polar motion, or length-of-day variations.

The external potential variations have been calculated according to an expression given in Dehant et al. (1999) for an ellipsoidal planet. For a satellite at an altitude of several hundred kilometers, the relative tidally induced potential variations are of the order of 10^{-8}. Atmospheric variations linked to the CO_2 cycle have an effect on satellites that is of the same order of magnitude (Smith et al. 1999), which is at the limit of dectectibility.

Also the gravitational acceleration of the attraction on Mars changes due to the direct attraction of the Sun, Phobos, and Deimos, to the gravitational attraction of the mass redistribution induced by the tides, to the change in station position, and to the accelerations induced by the tides (see Dehant et al. 1999). All these contributions appear in the definition of the gravimetric factor, which is defined as the ratio between the body tide signal measured by a gravimeter along the vertical and the gradient of the external potential along the perpendicular to the reference ellipsoid (see also Dehant et al. 1999).

We have calculated the gravimetric factors for all the tidal waves considered and computed the gravity variations. It was found that especially the gravity variations induced by Phobos are geophysically important. Although they are an order of magnitude smaller than the solar induced gravity variations, they do not suffer from the thermal effect which leads to a much higher noise level at the solar tides than at the Phobos tides. According to simulations of Lognonné et al. (1996), for long enough observation series, Phobos induced tides can be observationally determined with a precision of 1 nGal. The main ($l = 2, m = 2$) wave has an amplitude of 0.453μGal, two orders of magnitude above the measurement precision. Due to the high sensitivity to the core, precise gravity measurements of the main degree 2, order 2 Phobos induced tide can therefore yield important information on the core. As an example, we derived that a change in core radius of about 60 km corresponds to a 1 nGal change in amplitude of the gravimetric tidal signal.

For Mercury, the Love numbers h and k are about 0.8 and 0.4, respectively. These large values compared to Earth are a result of the large (partially liquid) core of Mercury. Mercury is believed to have a large core of about 1860 km, compared to a total radius of 2440 km. The core is assumed to be mostly solid with the uppe r few hundred kilometers liquid. We studied the sensitivity of the Love number k, which gives the external potential variations, to the core radius. Wu et al. (1995), using numerical simulations, showed that an orbiter-lander system with current technologies, can determine Love number k with a precision of 0.01. Using a set of Mercury models with varying core radius, we found that a change of 0.2 in k corresponds to a change of 120 km in our models. For a change in k corresponding to the Wu et al. (1995) measurement accuracy of 0.01, this gives a change in radius of only 6km. Evidently then, the extent of Mercury's core, presently derived with an error of $\pm$ 100 km, could be improved by a tidal experiment.

REFERENCES

Barriot, J.-P., Dehant, V., Cerisier, J.-C., Folkner, W., Rhibes, A., Benoist, J., Van Hoolst, T., Warnant, R., Defraigne, P., Preston, R.A., Romans, L., Wu, S., and Wernik, A.W., NEIGE: NetLander Ionosp here and Geodesy Experiment, Advances in Space Research 28(8), 1237-1249, 2001.

Dehant, V., Defraigne, P., and Wahr, J.M., Tides for a convective Earth, J. Geophys. Res.

104, 1035-1058, 1999.

Harri, A.-M., Marsal, O., Leppelmeier, G.W., Lognonné, P., Glassmeier, K.-H., Angrilli, F., Banerdt, W.B., Barriot, J.-P., Bertaux, J.-L., Berthelier, J.J., Calcutt, S., Cerisier, J.-C., Crisp, D., Dehant, V., Di Pippo, S., Giardini, D., Guerrier, D., Jaumann, R., Kumpulainen, K., Langevin, Y., Larsen, S., Menvielle, M., Musmann, G., Polkko, J., Pommereau, J.P., Runavot, J., Schumacher, W., Siili, T., Simola, J., and Tillman, J.E., Network Science Landers for Mars, in: Proc. of COSPAR Meeting, Session BO.4 on 'Return to Mars', Advances in Space Research 23(11), 1915-1924, 1999.

Lognonné, Ph., Gagnepain Beyneix, J., Banerdt, W.B., Cacho, S., Karczewski, J.F., and Morand, M., Ultra broad band seismology on InterMarsNet, Planet. Space Sci. 44, 1237-1249, 1996

Mathews, P.M., Buffett, B.A., and Shapiro, I.I., Love numbers for a rotating spheroidal Earth: New definitions and numerical values, Geophys. Res. Lett. 22, 579-582, 1995

Roosbeek, F., Analytical developments of rigid Mars nutation and tide generating potential series, Celest. Mech. Dyn. Astr. 75, 287-300, 2000

Smith, D.E., Zuber, M.T., Haberle, R.M., Rowlands, D.D., and Murphy, J.R., The Mars seasonal CO_2 cycle and the time variation of the gravity field: A general circulation model simulation, JGR 104, 1999

Sohl, F., Spohn, T., The interior structure of Mars: implications from SNC meteorites, JGR 102, 1613-1635, 1997.

Van Hoolst, T., Dehant, V., Defraigne, P., Sensitivity of the Free Core Nutation and the Chandler Wobble to changes in the interior structure of Mars, PEPI 117, 39 7-405, 2000.

Wu, X., Bender P.L., and Rosborough G.W., Probing the interior structure of Marcury from an orbiter plus single lander, J. Geophys. Res., 100, 1515-1525, 1995.

MERCURY LIBRATION: FIRST STAGE

S. BOUQUILLON
National Astronomical Observatory of Japan
Tokyo To Mitaka Shi Osawa 2-21-1
e-mail: seb@pluto.mtk.nao.ac.jp

ABSTRACT. This is a first step to obtain a precise analytical model of Mercury rotation. We consider the plane problem: Angular Momentum, Axis of Figure and axis perpendicular to Mercury orbit are a same axis. We study the librations of the rotation of Mercury around its spin-orbit resonance 3/2 caused by the Sun and by the indirect effect of the other planets.

1. INTRODUCTION

The construction of a precise model of the Mercury rotation is justified by two spacecraft projects: the Mission Bepi Colombo of E.S.A. and the Messenger mission of N.A.S.A.

The plane problem could seem too simpler to obtain an accurate model of Mercury rotation but the conditions of rotation of Mercury are very close to this state : The observations of the rotation of Mercury by radar ranging data with an accuracy around 0.7 degree (De Vries and Harmon, 1994) are not precise enough to makes it possible to differentiate angular momentum and axis normal to the orbit of Mercury. Moreover, as the rotation of Mercury is probably in a "Cassini's state" the mean value of its obliquity could be estimated between 10 and 1 minutes of arc (Peale, 1988). The angle between the axis of figure and the angular momentum of Mercury is also probably very close to zero as for most celestial bodies. (All these effects will be considered as some small perturbations to the plane problem in a second note.)

If we name $A < B < C$ the principal moment of inertia of Mercury, the quantity $(C-A)/C = (2.3 \pm 1.1) \times 10^{-4}$ and $(B-A)/C = (1.2 \pm 0.7) \times 10^{-4}$ (Anderson, 1987) are not well known. So we must keep them as explicit parameters in our solution.

We use as orbital solution of Mercury, the analytical solution VSOP87 in rectangular coordinates with respect to the dynamical ecliptic and equinox J2000.0 (Bretagnon, 1988). The relative precision of this ephemeride with the JPL's numerical one is around 29.d-10 radian during one century (Private communication, Bretagnon).

2. VARIABLES

We study the relative position between the direction of the Sun (look from Mercury) and the direction of the Axis of minimum moment of inertia ($\vec{A}$) of Mercury.

In this study, the orbital plane of Mercury at J2000.0 (=Mercury Equator) is the reference plane. The position of this plane with respect to the ecliptic and equinox J2000.0 is given by two constant angles :

• Ω is the angle between the equinox J2000.0 and the ascending node of the reference plane with respect to the ecliptic J2000.0.

• i is the inclination of the reference plane with respect to the ecliptic J2000.0.

We choose as origin on the reference plane the position of the perihelion at J2000.0. localized by the longitude ω. The values of these constants are:

$$\begin{aligned} \Omega &= 48^o.3308932 \\ i &= 7^o.0049863 \\ \omega &= 257^o.45611895 \end{aligned}$$

The position of the Sun is given by:

• The longitude λ of the Sun measured from the perihelion of the Sun at J2000.0 along the reference plane.

• The latitude δ of the Sun with respect to the reference plane. ($\delta \simeq 0$)

The position of Mercury axis of minimum moment of inertia $\vec{A}$ (forced to stay in the reference plane) is given by the longitude g whose variations are the aim of this work. g is measured from the perihelion. The conjugated momentum of g is the angular momentum of Mercury G. All these variables are summarized in figure (1)

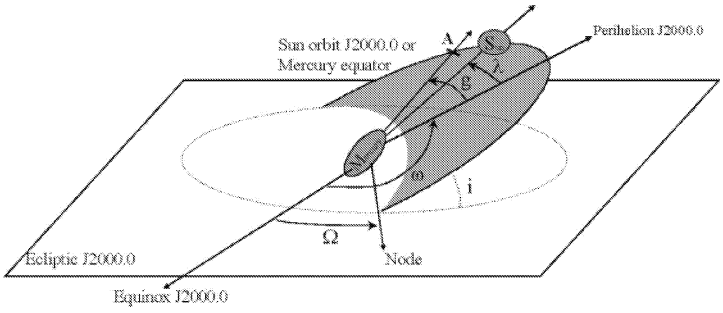

Figure 1: Variables

In the next part we need to have the Sun's position with respect to the Axis of minimum moment of inertia and looked from Mercury center of Mass. That is to say the rectangular coordinates of the Sun in the system $R = (O, \vec{A}, \vec{B}, \vec{C})$ which $\vec{A}$ is the unit vector in the same direction as the axis of minimum moment of Inertia A, $\vec{C}$ In the same direction as the axis of maximum moment of inertia C and $\vec{B}$ in the same direction as the axis of intermediate moment of inertia B.

The ephemeride VSOP87 for the orbital motion of Mercury give us Mercury rectangular coordinates (x_1, x_2, x_3) with respect to the dynamical ecliptic and equinox J2000.0. (x_1, x_2, x_3) are given in the following form :

$$x_i = \sum_j t^{b_j} \times [C_j \cos\theta_j + S_j \sin\theta_j] \qquad (1)$$

$$where \qquad \theta_j = \eta_{j,1}\lambda_1 + \eta_{j,2}\lambda_2 + \eta_{j,3}\lambda_3 + \eta_{j,4}\lambda_4 + \eta_{j,5}\lambda_5 + \eta_{j,6}\lambda_6 + \eta_{j,7}\lambda_7 + \eta_{j,8}\lambda_8$$

b_j, C_j, S_j and $\eta_{j,1..8}$ are some constants (C_j, S_j are real and b_j, $\eta_{j,1..8}$ are integer). $\lambda_{1..8}$ are the eight mean longitudes of the planets (Mercury, Venus, Earth, Mars, Jupiter, Saturn, Uranus, Neptune).

With the help of rectangular coordinates (x_1, x_2, x_3) of Mercury we are able to determinate the rectangular coordinates (X_s, Y_s, Z_s) of the Sun in the system $R = (O, \vec{A}, \vec{B}, \vec{C})$

$$\begin{pmatrix} X_s &=& r\cos\delta\cos(\lambda - g) \\ Y_s &=& r\cos\delta\sin(\lambda - g) \\ Z_s &=& r\sin\delta \end{pmatrix} = M_3(\omega - \Omega + g) \times M_1(i) \times M_3(\Omega) \begin{pmatrix} -x_1 \\ -x_2 \\ -x_3 \end{pmatrix} \quad (2)$$

Where M_1 is the matrix of rotation around the first axis of the system and M_3 is the matrix of rotation around the third axis of the system.

We use to manipulate these series a program based on Broucke's works (Broucke, 1980).

3. HAMILTONIAN

The Hamiltonian of the plane problem could be written like that:

$$K_1 = \frac{G^2}{2C} + \alpha\frac{a^3}{r^3}P_2(\sin\delta) + \beta\frac{a^3}{r^3}P_2^2(\sin\delta)\cos(2\lambda - 2g) + \Lambda_t \quad (3)$$

$where$

$$\frac{\alpha}{C} = \left(\frac{\kappa^2 M_S}{a^3}\right)\frac{2C - A - B}{2C} = \left(\frac{n^2}{1+\mu}\right)J_2\frac{MR^2}{C} = n^2 * (1.85 \pm 0.8) \times 10^{-4}$$

$$\frac{\beta}{C} = \left(\frac{\kappa^2 M_S}{a^3}\right)\frac{A - B}{4C} = -\left(\frac{n^2}{1+\mu}\right)C_{2,2}\frac{MR^2}{C} = n^2 * (-3.08 \pm 1.5) \times 10^{-5}$$

Where

• κ^2 is the gravitational constant, M_S and M are respectively the mass of the Sun and the mass of Mercury, μ is equal to M/M_S, $A < B < C$ are the principal moment of inertia of Mercury, a is the Semi-major Axis, r is the distance between Mercury and the Sun and (λ,δ) are respectively the longitude and the latitude of the Sun with respect to Mercury J2000.0 orbit ($\delta \simeq 0$).

• Λ_t is the conjugated momentum of time.

• (g, G) are the canonical variables defined in section 2.

The spherical harmonics $P_2(\sin\delta)$ and $P_2^2(\sin\delta)\cos(2\lambda - 2g)$ could be written with rectangular coordinates of the Sun (X_s,Y_s,Z_s) of section 2.1

$$P_2(\sin\delta) = \frac{3}{2}\sin^2\delta - \frac{1}{2} = \frac{3}{2}\left(\frac{Z_s}{r}\right)^2 - \frac{1}{2} \simeq -\frac{1}{2}$$

$$P_2^2(\sin\delta)\cos(2\lambda - 2g) = 3\cos^2\delta\cos(2\lambda - 2g) = \frac{3}{r^2}(X_s^2 - Y_s^2)$$

By this way we can write the Hamiltonian K_1 according to the time and to the variables g and G. But the rotation of Mercury is known as a 3/2 spin-orbit resonance case. So we have to introduce the angle of libration θ instead of the angle g. So we make the following canonical transformation:

$$\left\{\begin{array}{cc} g & G \\ t & \Lambda_t \end{array}\right\} \; ------> \; \left\{\begin{array}{cc} \theta = g - 3/2\bar{\lambda} & \tilde{G} = G - G_0 \\ t & \Lambda_t + G_0 G \end{array}\right\} \quad (4)$$

Where $\bar{\lambda}$ is the linear part of λ (that is to say the mean anomaly) and $G_0 = 3/2\dfrac{\dot{\bar{\lambda}}}{C}$ is constant.

4. RESONANCE PERIOD (T_R) OF θ

As we study the planar case, the latitude of the Sun with respect of the reference plane is zero. So we can simplify the Hamiltonian like that:

$$K = \frac{G^2}{2C} + 3\beta\frac{a^3}{r^3}\cos(2\lambda - 2g)$$

with : $\dfrac{\beta}{C} = n^2 * (-3.08 \pm 1.5) \times 10^{-5}$

If we expand $\dfrac{a^3}{r^3}\cos(2\lambda - 2g)$ according to $\theta = g - \dfrac{3}{2}\bar{\lambda}$ and to the first order of eccentricity e, we obtain:

$$K = \frac{G^2}{2C} + 3\beta\left[\cos(2\theta + \bar{\lambda}) - \frac{e}{2}\cos(2\theta + 2\bar{\lambda}) + \frac{7e}{2}\cos(2\theta)\right]$$

In this expression, we keep only the secular and long periodic terms. Moreover as θ is a small angle, we can write $cos(2\theta) = 1 - \theta^2$. K becomes:

$$K_s = \frac{G^2}{2C} - 21\beta e\theta^2$$

We can transform this Hamiltonian in an Hamiltonian of an Harmonic oscillator (for the method see Moons' Thesis) and so we work out the expression of resonance period of θ : T_R

$$T_R = \frac{2\pi}{\sqrt{-42\dfrac{\beta}{C}e}} \in [11\ \ years,\ \ 21\ \ years]$$

5. VARIATION OF g

With the help of the ephemerides VSOP87 of Mercury (Bretagnon, 1988), we write λ and $\dfrac{a^3}{r^3}$ as Fourier series whose arguments are linear combinations of the eight mean longitudes of planets $\lambda_{1..8}$ (Mercury,..., Neptune). With these series, we can write the Hamiltonian K as :

$$K = K_s + K_p$$

where K_s is the simplified Hamiltonian studied just before and K_p the other perturbation terms due to the effect of the Sun and the indirect effect of the other planets.

We use the method of Lie transformation to get the variation Δg of g. We use the following convention to write the series Δg : For each term T_j of the Hamiltonian K_p, we look the period of its argument θ_j.

• If the period of the argument is not too close to the resonance period T_R:

$$\Delta g = \sum_j \gamma^{b_j} \times [C_j \cos\theta_j + S_j \sin\theta_j]$$

Where θ_j is the argument ($\theta_j = \eta_{j,1}\lambda_1 + \eta_{j,2}\lambda_2 + \eta_{j,3}\lambda_3 + \eta_{j,4}\lambda_4 + \eta_{j,5}\lambda_5 + \eta_{j,6}\lambda_6 + \eta_{j,7}\lambda_7 + \eta_{j,8}\lambda_8$), b_j is a positive integer smaller than 20, C_j and S_j are real coefficients in second of arc and γ is the following parameter:

$$\gamma = \left[\frac{C_{22}}{1 \cdot 10^{-5}}\right]^{1/4}$$

• If the period of the argument is close to the resonance period T_R:

$$\Delta g = \sum_j \frac{n_j + \alpha_j \times n_{R_0}}{n_j + \alpha_j \times \gamma^2 n_{R_0}} \times \gamma^{b_j} \times [C_j \cos\theta_j + S_j \sin\theta_j]$$

Where n_j is the mean motion of the argument θ_j, α_j is an integer equal to -1 or 1 and n_{R_0} is the mean motion corresponding to the resonance period T_R with $C_{22} = 1 \cdot 10^{-5}$.

$$n_{R_0} = 23.2319696095 \quad (^o/year)$$

Moreover we have put the secular terms of second order of this mean motion in table 1 : ($n_l = \gamma^2 n_{l_0} + \sum_j \gamma^{b_j} \times C_j$ with C_j are in degrees by year)

j	C_j	b_j
2	0.0048952450	6
3	0.0000046864	10
4	0.0000000406	8
5	0.0000000219	12
6	0.0000000039	4

Table 1: *secular terms of second order of* n_l

The resulting series for Δg are presented in the following tables 2 and 3 (C_j and S_j in second of arc and the period of the argument θ_j is indicated in years.

The table 2 shows the terms not to close to the resonance. This table contains only the 29 first terms bigger than 1 second of arc. The complete series (159 terms, terms bigger than 1×10^{-3}) could be asking to the author.

The table 3 shows the terms close to the resonance. This table contains 14 terms bigger than 1×10^{-3}.

6. REFERENCES

Anderson, J.D. and al.: 1987, *Icarus* **71**, 337. Bretagnon, P.: 1988, *Astron. Astrophys.* **202**, 309. Broucke,R.A.,1980 *A Fortran-System for the Manipulation of Symbolic Poisson Series with Application to Celestial Mechanics*, Institute for advanced Study in Orbital Mechanichs,Univ.Texas. De Vries, C.H. and Harmon, J.K.: 1994, *American Astonomical Society Meeting* **185**, 43.13. Moons, M.:1981,*thèse de doctorat*, Facultés Universitaires Notre-Dame de la Paix, Namur. Peale, S.J.: 1988, *Mercury.* Tucson, AZ, University of Arizona Press p461-493.

j	s_j	b_j	$\eta_{j,1}$	$\eta_{j,2}$	$\eta_{j,3}$	$\eta_{j,4}$	$\eta_{j,5}$	$\eta_{j,6}$	$\eta_{j,7}$	$\eta_{j,8}$	period	C_j	S_j
1	0	4	1	0	0	0	0	0	0	0	0.241	-21.1743	4.7078
2	0	10	1	0	-10	11	0	0	0	0	1618.795	14.6458	-8.4619
3	0	8	1	0	-10	11	0	0	0	0	1618.795	-14.6423	9.0356
4	0	10	0	0	0	0	2	-5	0	0	-883.270	.3173	12.6704
5	0	8	0	0	0	0	2	-5	0	0	-883.270	-.5768	-12.6603
6	0	8	5	-14	2	0	0	0	0	0	319.434	10.4630	-8.4428
7	0	10	5	-14	2	0	0	0	0	0	319.434	-10.1315	8.3054
8	0	12	1	0	-10	11	0	0	0	0	1618.795	-9.7656	5.2584
9	0	6	1	0	-10	11	0	0	0	0	1618.795	9.7583	-6.4054
10	0	12	0	0	0	0	2	-5	0	0	-883.270	-.0962	-8.4520
11	0	6	0	0	0	0	2	-5	0	0	-883.270	.6246	8.4307
12	0	6	5	-14	2	0	0	0	0	0	319.434	-7.1777	5.7695
13	0	12	5	-14	2	0	0	0	0	0	319.434	6.5216	-5.4728
14	0	14	1	0	-10	11	0	0	0	0	1618.795	4.1859	-2.0894
15	0	4	1	0	-10	11	0	0	0	0	1618.795	-4.1800	2.9082
16	0	14	0	0	0	0	2	-5	0	0	-883.270	.0124	3.6240
17	0	4	0	0	0	0	2	-5	0	0	-883.270	-.4032	-3.6071
18	0	4	5	-14	2	0	0	0	0	0	319.434	3.1489	-2.5770
19	0	14	5	-14	2	0	0	0	0	0	319.434	-2.6919	2.3251
20	0	4	2	0	0	0	0	0	0	0	0.120	.9698	2.0714
21	0	8	0	0	0	0	0	0	0	2	82.385	-1.4132	-1.8603
22	0	10	0	0	0	0	0	0	0	2	82.385	1.1915	1.5685
23	0	6	0	0	0	0	0	0	0	2	82.385	1.0519	1.3847
24	0	4	2	-5	0	0	0	0	0	0	5.664	1.2703	1.3836
25	0	8	2	-5	0	0	0	0	0	0	5.664	1.0040	1.0936
26	0	10	1	0	-4	0	0	0	0	0	6.575	-.6600	-1.0656
27	0	10	2	-5	0	0	0	0	0	0	5.664	-.9762	-1.0633
28	0	16	1	0	-10	11	0	0	0	0	1618.795	-1.0466	.4813
29	0	2	1	0	-10	11	0	0	0	0	1618.795	1.0441	-.7675

Table 2: *Series* Δg

j	s_j	b_j	$\eta_{j,1}$	$\eta_{j,2}$	$\eta_{j,3}$	$\eta_{j,4}$	$\eta_{j,5}$	$\eta_{j,6}$	$\eta_{j,7}$	$\eta_{j,8}$	period	C_j	S_j
1	-1	2	0	0	0	0	0	2	0	0	14.729	-2.2000	-4.5972
2	-1	2	0	0	0	0	1	0	0	0	11.862	1.7011	1.5905
3	-1	2	5	-14	2	0	0	0	0	0	319.434	.0000	.1027
4	1	2	2	-7	3	0	0	0	0	0	-13.427	.0524	-.0684
5	-1	2	0	0	0	0	0	1	0	0	29.457	.0540	.0413
6	-1	2	0	0	0	0	0	3	0	0	9.819	.0519	-.0201
7	-1	2	1	-5	4	0	0	0	0	0	40.859	.0059	-.0427
8	-1	2	0	0	0	0	2	-3	0	0	14.978	-.0420	-.0361
9	1	2	0	0	0	0	2	-7	0	0	-14.487	.0082	-.0222
10	-1	2	0	0	0	0	0	0	2	0	42.010	.0103	.0174
11	-1	2	0	0	0	0	2	-2	0	0	9.929	.0022	.0039
12	-1	2	0	0	0	0	1	-1	0	0	19.859	.0000	.0035
13	1	2	0	0	0	0	1	-5	0	0	-11.705	.0000	-.0019
14	-1	2	0	0	0	0	3	-5	0	0	12.023	.0016	.0000

Table 3: *Series* Δg

ANALYTICAL DEVELOPMENT OF RIGID MERCURY NUTATION SERIES

G. CARPENTIER and F. ROOSBEEK
Royal Observatory of Belgium
Avenue Circulaire, 3 – 1180 Brussels – Belgium
e-mail: g.carpentier@oma.be – f.roosbeek@oma.be

ABSTRACT. In this paper, series of rigid Mercury nutations are computed. The method used is based on the calculation of the forces produced by the Sun on the rigid Mercury. In order to take into account the indirect effects coming from the orbit perturbations of Mercury, we used the ephemerides VSOP87 (Bretagnon and Francou, 1988). Due to non negligeable difference between the principal moment of inertia A and B in the case of Mercury, we compute also the triaxiality terms in addition to the main problem. With a truncation level of 10^{-3} mas (milliarcsecond), related to the present-day precision of the Mercury precession constant, 149 terms in longitude ($\Delta\psi \sin\varepsilon$) and 142 terms in obliquity ($\Delta\varepsilon$) are computed. The value of the dynamical flattening used is $H_D = \frac{(C-A)}{C} = 2.3\ 10^{-4}$ (Anderson et al., 1987).

1. INTRODUCTION

Theoretical nutations for a nonrigid model of Mercury are computed from a convolution of rigid Mercury nutation amplitudes with a transfer function accounting for geophysical parameters influencing Mercury's response. The present paper is concerned with the rigid part. The method is similar to the one developed in Roosbeek and Dehant (1998). This method is based on an analytical computation of the forces produced by the Sun on the rigid Mercury.
In the case of Mercury, the effect of the triaxiality (difference between the moment of inertia A and B) is not negligeable, contrarily for example, to the case of the planet Mars (Roosbeek, 1999b). This is why, in this paper, we have also added a contribution coming from the triaxiality to the main problem. The method used for this triaxiality part is similar to the one developed in Roosbeek (1999a).
Furthermore, the triaxiality is also very important in the case of Mercury because the corresponding terms are in the same frequency band as the terms coming from the main problem, contrarily to the planets Mars (Roosbeek, 1999a) or to the Earth (Roosbeek and Dehant, 1998). Indeed, for Mercury, the rotation period corresponds approximately to 2/3 of the revolution period (59 days and 88 days respectively). So, the triaxiality terms, which are terms for which the period is a multiple of the rotation period, are in the same frequency band as the main terms.

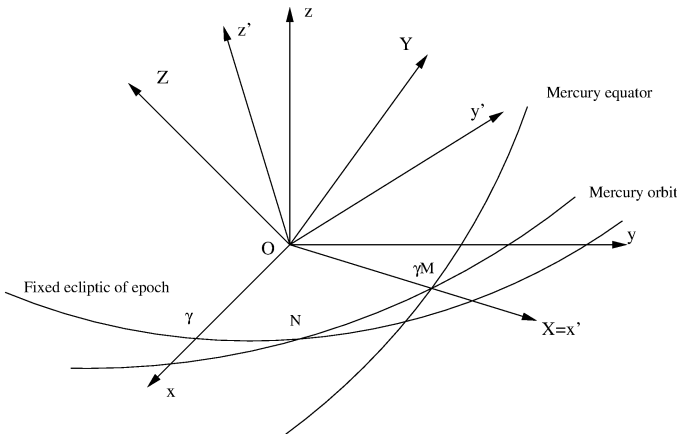

Figure 1: Ω_M and θ_M are the angles corresponding to the arcs (γ_N) and $(N\gamma_M)$, ε_M is the inclination of Mercury equator on Mercury orbit and i_M is the inclination of Mercury orbit in the fixed ecliptic of epoch. γ_M is the intersection between Mercury equator and Mercury orbit plane like γ is the intersection between Earth equator and ecliptic, in the case of the Earth.

2. CONSTANTS AND EPHEMERIDES

The series computed in this paper are referred to the ecliptic and equinox of J2000.0 of Mercury. The reference frame is formed by the axes (X, Y, Z), where (OX, OY) is the Mercury equatorial plane with the X axis in the direction of the ascending node (γ_M) of Mercury equator on Mercury orbit plane (see Figure 1). For the solar ephemerides, we use the VSOP87 series (Bretagnon and Francou, 1988). These series give the positions of the eight planets taking into account all the mutual perturbations between them.
For each triplet of coordinate (X, Y, Z), the solution is written as:

$$\begin{pmatrix} X \\ Y \\ Z \end{pmatrix} = \sum_i (S_i \sin f_i + C_i \cos f_i) \qquad (1)$$

where S_i and C_i are the amplitudes and f_i is a linear combination of fundamental arguments (Mean longitudes of the 9 planets and mean Mercury sidereal time).
The constants that we have used in our computation are presented in Table 1. They come from the IERS Conventions (McCarthy, 1996), from Anderson et al. (1987), from Vilas et al. (1988) and from Simon et al. (1994). The value of θ_M has been provided to us by J. Chapront (personal communication, 2001)

3. THEORY

We split the computation of Mercury nutation series in two parts: (1) the main problem coming from the direct effect of the Sun and (2) the triaxiality problem coming from the difference between the moment of inertia A and B.
All the equations are written for the angular momentum axis of Mercury. At our level of precision, the nutation series of the three axis, the angular momentum axis, the rotation axis, and the figure axis, are the same. So, strictly speaking, the series developed here correspond to the nutation of any of the three axis. Briefly (for more details, see Carpentier and Roosbeek

Item	Recommended value	Comments
ε	$0.12°$	Vilas et al
$\frac{C-A}{C}$	$2.3\ 10^{-4}$	Anderson et al
J_2	$6.0\ 10^{-5}$	Anderson et al
$c_{2,2}$	$1.0\ 10^{-5}$	Anderson et al
$s_{2,2}$	0	Anderson et al
GM_S	$1.327124\ 10^{20} m^3/s^2$	IERS 1996
Ω_R	$1.24\ 10^{-6} rad/s$	Vilas et al
Ω_M	$48°.330893$	Simon et al
θ_M	$62°.9651$	Chapront
i_M	$7°.004986$	Simon et al
ε_M	$0°.12$	Vilas et al

Table 1: Constants and physical parameters.

(2002)), the nutation equations for the main problem are expressed as:

$$\begin{aligned} \frac{d(\Delta\psi)}{dt} &= \frac{1}{C\Omega_R}\frac{1}{\sin\varepsilon_M}\frac{GM_B}{d^3}(C-A)\frac{3}{2}\sin 2\delta\sin\alpha \\ \frac{d(\Delta\varepsilon)}{dt} &= -\frac{1}{C\Omega_R}\frac{GM_B}{d^3}(C-A)\frac{3}{2}\sin 2\delta\cos\alpha \end{aligned} \tag{2}$$

For the triaxiality part, the equations are:

$$\begin{aligned} \frac{d\,(\Delta\psi_{tr})}{dt} &= \frac{1}{C\Omega_R}\frac{1}{\sin\varepsilon}\frac{GM_B}{d^3}(C-A)\left\{ \begin{array}{l} 6\cos\delta\sin\delta\sin\alpha\left(\begin{array}{l} \frac{c2,2}{J_2}\cos 2H \\ -\frac{s2,2}{J_2}\sin 2H \end{array}\right) \\ +6\cos\delta\sin\delta\cos\alpha\left(\begin{array}{l} \frac{c2,2}{J_2}\sin 2H \\ +\frac{s2,2}{J_2}\cos 2H \end{array}\right) \end{array}\right. \\ \frac{d\,(\Delta\varepsilon_{tr})}{dt} &= \frac{1}{C\Omega_R}\frac{GM_B}{d^3}(C-A)\left\{ \begin{array}{l} -6\cos\delta\sin\delta\cos\alpha\left(\begin{array}{l} \frac{c2,2}{J_2}\cos 2H \\ -\frac{s2,2}{J_2}\sin 2H \end{array}\right) \\ +6\cos\delta\sin\delta\sin\alpha\left(\begin{array}{l} \frac{c2,2}{J_2}\sin 2H \\ +\frac{s2,2}{J_2}\cos 2H \end{array}\right) \end{array}\right. \end{aligned} \tag{3}$$

with the following link to the ephemerides (X, Y, Z):

$$\begin{aligned} X &= d\cos\delta\cos\alpha \\ Y &= d\cos\delta\sin\alpha \\ Z &= d\sin\delta \end{aligned} \tag{4}$$

Note that the hour angle of the perturbing body is expressed in function of the fundamental arguments by: $H = \chi - \alpha - 180°$, where χ is the mean Mercury sidereal time.

4. FIGURES AND COMPARISON WITH THE EARTH

In order to display the nutations series graphically, we plot a time prediction of $\Delta\psi\sin\varepsilon$ covering 2.8 years (Figure 2) and we compare with a time prediction covering 20 years for the Earth (Figure 3). The contribution of the main terms is plotted in plain line while the triaxiality contribution is plotted in dashed line. The rigid Earth nutations series are the RDAN97 series

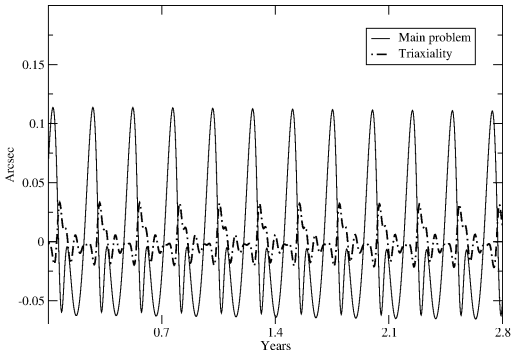

Figure 2: Time prediction of $\Delta\psi \sin\varepsilon$ of Mercury on a 2.8 years time span

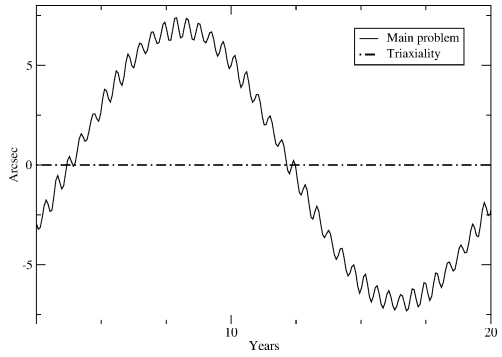

Figure 3: Time prediction of $\Delta\psi \sin\varepsilon$ of the Earth on a 20 years time span (series RDAN97)

(Roosbeek and Dehant, 1998).

As we can see on the plain lines, the Mercury series are dominated by a wave with a period of 88 days and an amplitude of 0".06. This can be compared to the main 18.6 years wave for the Earth which has an amplitude of about 6".6. We can see clearly that in the case of Mercury, the triaxiality terms are relatively more important as for the Earth; they are of the same order as the main terms.

A Fast Fourier Transform (FFT) of the previous Figures is also provided in the Figures 4 and 5. Like for the previous graphs, the contribution of the main terms is plotted in plain lines while the triaxiality contribution is plotted in dashed lines. We see clearly on these Figures that in the case of Mercury, the main and the triaxiality terms are in the same frequency band, contrary to the Earth's case.

We summarize this comparison between the Earth and Mercury on the Table 2. The differences in amplitude between main and triaxiality terms can be explained by the value of c_{22}/J_2. This value is equal to 0.1 in the case of Mercury and 0.001 in the case of the Earth. The differences in frequency between main and triaxiality terms can be explained by the values of the rotation and revolution periods for the Earth and Mercury as written in Table 3.

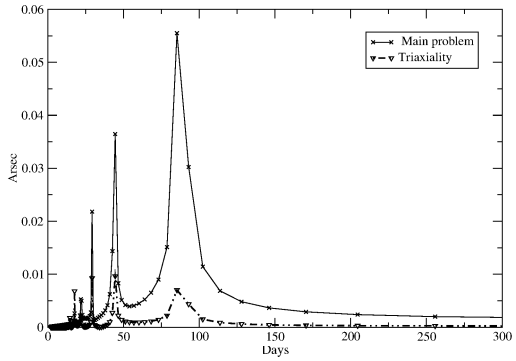

Figure 4: Fast Fourier Transform (FFT) of the nutations $\Delta\psi \sin\varepsilon$ of Mercury (Figure 2).

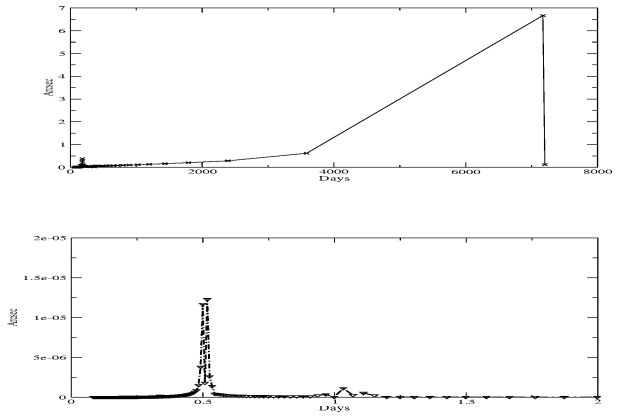

Figure 5: Fast Fourier Transform (FFT) of the nutations $\Delta\psi \sin\varepsilon$ of the Earth (Figure 3).

$\Delta\psi \sin\varepsilon$	main problem		triaxiality	
	greatest term	period	greatest term	period
Earth	$\sim$ 6.6"	18.6 years	$\sim$ 12 μas	0.5 day
Mercury	$\sim$ 0.06"	88 days	$\sim$ 0.01"	44 days

Table 2: Comparison Earth - Mercury

	Revolution	Rotation
Earth	365.25 days	1 day
Mercury	88 days	59 days

Table 3: Rotation and revolution period

5. CONCLUSION

The rigid Mercury nutations series developed here are computed with an analytical method that was used previously by Roosbeek and Dehant (1998) for the Earth. The truncation level has been set to 10^{-3} mas. The ephemerides used are the VSOP87 for the effect of the Sun.
As we can see from the previous Figures, these series are very different to the Earth's series. This is due to the fact that the triaxiality effect plays an important role in the case of Mercury while it is nearly negligeable for the Earth. This comes from the coupling effect between revolution and rotation of Mercury.
Including both the main and the triaxiality effects in our computation lead to series of 149 terms in longitude and 142 terms in obliquity.

6. AVAILABILITY

The RMEAN01 series are available by the anonymous FTP system at omaftp.oma.be , directory dist/astro/roosbeek/, files rmean01*.

7. ACKNOWLEDGMENTS

Dr. J. Chapront is gratefully acknowledged for providing the software GREGOIRE used in this work to compute the series.

8. REFERENCES

Anderson F.D.: 1987, The Mass, Gravity Field and Ephemeris of Mercury., *Icarus.* **Vol. no. 71**, pp. 337–349

Bretagnon P. and Francou G.: 1988, VSOP87: Planetary theories in rectangular and spherical variables, *Astron. Astrophys.* **Vol. no. 202**, pp. 309–315

Carpentier G. and Roosbeek F.: 2002, Analytical Development of Rigid Mercury Nutation Series, submitted to *Celest. Mech.*

Chapront J.: 2001, Personal communication

McCarthy D.: 1996, IERS Conventions, *IERS Tech. Note,* **Vol. no. 21**, 95 pp.

Roosbeek F.: 1999a, Diurnal and Subdiurnal Terms in RDAN97 Series, *Celest. Mech.* **Vol. no. 74**, pp. 243–252

Roosbeek F.: 1999b, Analytical Developments of Rigid Mars Nutation and Tide Generating Potential Series, *Celest. Mech.* **Vol. no. 75**, pp. 287–300

Roosbeek F. and Dehant V.: 1998, RDAN97: An analytical development of rigid Earth nutation series using the torque approach, *Celest. Mech.* **Vol. no. 70**, pp. 215–253

Simon J.L., Bretagnon P., Chapront J., Chapront-Touzé M., Francou G. and Laskar J.: 1994, Numerical expressions for precession formulae and mean elements for the Moon and the planets, *Astron. Astrophys.* **Vol. no. 282**, pp. 663–683

Vilas F., Chapman C.R. and Matthews M.S.: 1988, Mercury, *The University of Arizona Press.*

HOW ASTRONAUTS WOULD CONDUCT A SEISMIC EXPERIMENT ON THE PLANET MARS

V. PLETSER [1], P. LOGNONNE [2], V. DEHANT [3]

[1] Manned Spaceflight and Microgravity Directorate, ESTEC, European Space Agency (ESA)
P.O. Box 299, NL-2200 AG Noordwijk, The Netherlands; E-mail: Vladimir.Pletser@esa.int

[2] Space and Planetary Geophysics Dept, Institute of Geophysics of Paris (IPGP), 4, avenue de Neptune, F-91107 Saint Maur des Fossés, France; E-mail: Lognonne@ipgp.jussieu.fr

[3] Time, Earth Rotation and Space Geodesy Dept, Royal Observatory of Belgium (ROB), 3, avenue Circulaire, B-1180 Bruxelles, Belgium; E-mail: v.dehant@oma.be

ABSTRACT. During the Summer 2001 Flashline Mars Arctic Research Station (M.A.R.S.) campaign in Devon Island, Nunavut, Canada, the crew of the second rotation conducted a geophysics experiment aiming at assessing the feasibility of an active seismology method to detect subsurface water on Mars. A crew of three deployed a line of 24 sensors. Reflected and refracted signals produced by mini-quakes generated by a sledge hammer were recorded by a seismograph. The experiment was conducted three times, once in a dry run and twice during simulated Extra-Vehicular Activities (EVA) on the edge of the Haughton crater, allowing a three dimensional characterization of the subsurface ground to a depth of several hundred meters. Data were recorded for later detailed processing. A third EVA attempt inside the crater had to be aborted because of the poor weather and terrain conditions. Despite this failed attempt, a large amount of results were collected. Several operational lessons were learned from conducting this experiment under simulated EVA conditions. This paper presents the experiment and the methodology used, reviews the experiment performance and summarizes the results obtained and the operational lessons learned.

1. INTRODUCTION

The Mars Society [1] is a non-profit private organization whose purposes are "to further the goal of the exploration and settlement of the Red Planet by broad public outreach to instill the vision of pioneering Mars; by supporting ever more aggressive government funded Mars exploration programs around the world; and by conducting Mars exploration on a private basis." In this framework, The Mars Society has established the Flashline Mars Arctic Research Station (M.A.R.S.) in Devon Island, Nunavut, North of Canada, at a latitude of 75 degrees North, well in the Arctic Circle. The Flashline MARS station is situated on the edge of the Haughton crater [2] which was formed by the impact of a large meteorite 23 millions years ago. The strange geology and ecology of this site and the harsh climatic conditions make this part of the Earth surface as close as one could expect to a Martian environment, except for the presence of a breathable atmosphere. Arctic wild life, including polar bears, is the only sign of life on this island. The

interest in using this Mars analog on Earth was recognized by NASA several years ago. Several research programs were initiated by the NASA Ames Center and the SETI Institute under the umbrella of the NASA-Haughton Mars Project (HMP) [3].
During the Summer 2001, the MARS Flashline Research Station supported an extended international simulation campaign of human Mars exploration operations. Six rotations of six person crews spent from four to ten days each at the MARS Flashline Research Station. International crews, mixed in gender and in professional qualifications, conducted various tasks as a Martian crew would do including scientific experiments in several fields (Geophysics, Geology, Biology, Psychology, ...). One simulation campaign goal was to assess the operational and technical feasibility of sustaining a crew in an autonomous habitat, while conducting a field scientific research program. Operations were conducted as they would be during a Martian mission, including Extra-Vehicular Activities (EVA) with specially designed unpressurized suits.
Water on the surface of Mars exists in its solid form in the polar caps, but can not exist in its liquid form due to the low Martian atmospheric pressure. However, it is suspected that liquid water could exist under the surface possibly as underground pockets or trapped in rocks. Detecting liquid water under the Martian surface at a depth accessible to a human crew (from several to a few hundreds meters) is important for two main reasons. First, under the adage "Find the water, and you may find life", detecting liquid water would increase the chances of finding evidence of past or present life, possibly in a bacterial form somehow similar to terrestrial extremophile bacteria. Second, water detected close to first human settlement on Mars could help to sustain the human crew presence and operations in terms of consumption and fuel generation.
To prepare for this kind of operation, one of the experiments during the Flashline MARS Summer 2001 campaign was proposed by Dr P. Lognonné (*Institut de Physique du Globe de Paris*, IPGP), Dr V. Dehant (Royal Observatory of Belgium, ROB) and Dr V. Pletser (ESA). This experiment "Subsurface water detection by seismic refraction" aimed at assessing the feasibility of conducting an active seismology experiment to detect the potential presence of subsurface water. It can, together with a Ground Penetrating Radar, provide a sounding of the subsurface allowing to identify conductive liquid (e.g. salty water) from rocks or non conductive liquids (e.g. liquid CO_2).
A line of 24 seismometer sensors was deployed in several directions on the surface of the edge of the Haughton crater to record seismic signals generated by a mini-quake, somehow similar to experiments conducted on the Moon [4]. The seismic instrumentation was provided by the IPGP. Signals were recorded for later analysis to extend the characterization of the Haughton crater structure by supporting Scientists of the IPGP and the ROB.
This experiment can be seen as a possible continuation of the future automatic Seismology and Gravimetry experiment (SEIS) aimed at characterizing the deep internal structure of Mars and of its direct subsurface, to search for the presence of water. This SEIS experiment [5] will be conducted by teams of IPGP, ETHZ (Switzerland), JPL (USA) and ROB Scientists during the NETLANDER mission, a cooperative program between France, Germany, Finland, Belgium and the USA, to be launched in 2007.

2. METHOD, INSTRUMENTATION AND PREPARATION

The proposed geophysics experiment relies on the general principle of the seismic refraction method, in which a wave generated by a seismic event and propagating in the ground is reflected on and refracted along the interface between two underground media. Reflected and refracted signals are recorded by a set of seismic sensors connected to a seismograph. The analysis of the recorded signals allows to separate the signal reflected and refracted components. To characterize the underground media, only the refracted components are considered for detailed analysis, providing information on the propagating speed, the depth and geometry of the interface and the nature of the encountered media. More details can be found in [6-8].
24 seismic sensors, called geophones, were installed every four meters in linear array, called a geophone flute. The geophone line was connected via data cabling to a Seismograph Acquisition System (SAS) (Terraloc Mark 6 Seismograph [9]). Mini-quakes were generated by using either a sledge hammer on a metallic plate or a geophysical thumper gun.

The experiment was conducted in several steps, involving ten successful test shot recording in stacking mode for each of six test configurations in the selected area. SAS recordings were started by a trigger geophone installed close to the source seismic event. Three test configurations required the line of 24 geophones to be installed in one direction, the other three test configurations required the geophone line to be installed in the perpendicular direction. The three test configurations differed by the location of the trigger geophone and the quake source:
- Test 1 : trigger geophone and quake source placed in the middle of the geophone line,
- Test 2 : trigger geophone and quake source placed at one extremity of the geophone line, and
- Test 3 : trigger geophone and quake source placed at the other extremity of the geophone line.

Recorded signals were viewed on the SAS screen display between the shots to assess the acquisition and the quality of the recorded signals. After completion of the tests, data were transferred to floppy disks for later detailed analysis.
All seismic equipment was lent by the IPGP Laboratory. One of the Investigators, who lead the field operations at the Flashline MARS Station, was trained in using the instrumentation at the Geophysical Research Centre of Garchy, France, one month prior the Flashline MARS campaign. Step-by-step nominal and off-nominal troubleshooting procedures were prepared and rehearsed. The instrumentation was packed in three containers and shipped to Canada for delivery to the NASA HMP Base Camp on Devon Island. A GPS system and shot shells were available at the Flashline Mars station. The equipment total mass of 130 kg however could be reduced to a few tens of kg and is therefore compatible with payload constraints of future Mars missions.

3. CONDUCTING THE EXPERIMENTS

The experiment program conducted by the second rotation crew is summarized in Table 1.

TABLE 1: EXPERIMENTS CONDUCTED BY THE ROTATION 2 CREW (10 - 17 July 2001)

Geophysics:	Subsurface water detection on Mars by active seismology *Dr P. Lognonne, M. Diament (IPGP, Paris Univ., F), Dr V. Dehant (Belgium Royal Observatory, Brussels, B), Dr V. Pletser (ESA)*
Biology:	Search for fossils and evidence of microbial life *Dr C. Cockell (British Antarctic Survey, UK)*
Radio-Biology:	Deployment of radiation dosimeters, during 1 EVA *Dr C. Cockell (British Antarctic Survey, UK)*
Human Factors	Time dependent occupation of habitat volume by a human crew of six in isolation *Dr W. Clancey (NASA Ames, USA)* Human factors and habitability assessment *Drs J. Novak, E. Morphew, J. Connolly (NASA-JSC Crew Station Branch, USA)* Needs assessment of psychosocial support to individuals in a space simulation in an extreme environment *Pr. J. Lapierre (Quebec Univ., CDN)* Assessment of water consumption of a Mars human crew of six *Mr R. Zubrin (The Mars Society)*

Regarding the geophysics experiment, the operations of geophone line deployment and quake generation with a sledge hammer are mildly physically demanding in normal conditions. However, it was not known a priori whether the experiment would be feasible under EVA conditions and with operators wearing simulated Martian EVA suits.
A first dry run was conducted in the afternoon of Tuesday 10 July, before the rotation 2 crew entered into the Flashline Mars Habitat. The three instrumentation containers were transported in a trailer pulled by an All Terrain Vehicle (ATV). A three person team deployed the 24 geophone flute line in the Haynes Ridge plain, on the edge of the Haughton crater, a few hundred meters away from the Mars Habitat. This deployment direction was approximately perpendicular to the

crater rim. This dry run was to verify the instrumentation and to train the other crew members who would be involved in the experiment during future EVA's. A single point was measured with the trigger geophone and the seismic source located in the middle of the geophone line.
During the second EVA, a three member EVA crew conducted the seismic experiment during a four hour EVA in poor weather conditions (rain and wind); see Figure 1. The 24 geophone flute line was deployed in the Haynes Ridge plain, in front of the Flashline MARS Habitat. The geophone flute was laid in a South-South-East direction, approximately parallel to the Haughton crater rim. This direction was chosen perpendicular to the direction of the flute laid in the previous dry run trial. Three tests were conducted with the trigger geophone triggered by quakes created by sledge hammer shots. . Three tests were conducted with the trigger geophone and the sledge hammer shots at the middle of the geophone flute (Test #1) and at the flute both extremities (Tests #2 and 3). Locations were measured using a hand-held GPS receiver. The geophones were tested individually and automatically prior to conducting the first Test and were found in functioning conditions. In order to improve the signal to noise ratio, tests were conducted in a stacking mode with ten hammer shots for each test. Data were recorded and logged in the SAS for later data treatment and assessment in the Flashline MARS Habitat to obtain first results.

Figure 1: EVA crew member K. Quinn hits the sledge hammer under the rain during the second EVA on 12 July, while V. Pletser operates the SAS under monitoring of R. Zubrin; the Mars Habitat is visible in the background (Photo V. Pletser).

The third three hour EVA took place on Saturday 14 July to deploy radio-biology dosimeters at Breccia Hill and Trinity Lake inside the Haughton crater. While on EVA with the ATV's, four other potential locations for deployment of the seismic experiment were visited, respectively close to Trinity lake, at the bottom of a small valley at the intersection of two small rivers, on the inside rim of the crater, and on the crater external rim. The fourth EVA expedition on Sunday 15 July was a scouting EVA to find other potential locations to deploy the seismic experiment into the Von Braun Planitia, a few km away from the Flashline Mars Habitat and the NASA-HMP Base Camp. It was hoped to conduct the geophysical sounding of a pingo (a mass of water ice in the ground), but it was not sure if there were any at a reachable distance with ATV's. Two potential locations were found which were not too muddy nor covered by too many loose pebbles and

rocks. After assessing the merits and disadvantages of the several locations visited, taking into account the potential seismic interest, the access possibilities of ATV's with the 130 kg instrumentation trailer, the terrain conditions (rather muddy in some places due to severe rains in previous days and weeks), it was decided that the fifth EVA of Monday 16 July would take place in the Haughton crater. It would be the most ambitious EVA planned, with deployment of the geophone flute in two perpendicular directions in the Haughton crater, and with six series of measurements, including ten shots with the sledge hammer in stacking mode and one with the geophysical thumper gun at each of the six locations. Four EVA crewmembers left for the crater in the morning. While inside the Haughton crater, the trailer with the 130 kg instrumentation got stuck in the Arctic mud to a depth of half a meter. More than one hour was spent pulling the trailer out with the other ATV's (see Figure 2). In view of the exhaustion of all crew members and the degrading terrain conditions, it was decided to abort the EVA and to return to the Habitat. On the way back, the instrumentation trailer got stuck a second time in the mud and was salvaged again only after quite some time. This EVA lasted eventually three and half hours, unfortunately without any results.

Figure 2: EVA crew members R. Zubrin and V. Pletser pushing the instrumentation trailer out of the mud in the Haughton crater during the fifth EVA of 16 July (Photo Discovery Channel).

The sixth and last EVA took place on Tuesday 17 July and lasted two and half hours. It was again a three person EVA to deploy the geophone flute in the Haynes Ridge plain, in front of the Flashline MARS Habitat, at the same location of the deployment during the second EVA. The geophone flute was laid in a direction perpendicular to the one of the second EVA, approximately perpendicular to the Haughton crater rim, i.e. the same direction as for the dry run of Tuesday 10 July. Three tests were again conducted as previously and locations were measured using a handheld GPS. This final series of measurements allowed a complete characterization of the three dimensional underground structure of the Haynes Ridge plain in front of the Mars Habitat. After completion of the test, data were recorded and transferred to diskettes for later analysis. All equipment was packed into the transport containers, for the return shipment on the evening return flight of the same day.

4. FIRST RESULTS

The location of the geophone flute laid down during the second EVA of Thursday 12 July were as follows (within GPS precision and related to the WGS84 ellipsoid):

4 m mark at N 75 deg. 25.871, W 89 deg. 50.067, 240 m elevation
96 m mark at N 75 deg. 25.847, W 89 deg. 49.894, 242 m elevation
Shot (Test #1) at N 75 deg. 25.859, W 89 deg. 49.976, 253 m elevation
Shot (Test #2) at N 75 deg. 25.872, W 89 deg. 50.075, 260 m elevation
Shot (Test #3) at N 75 deg. 25.846, W 89 deg. 49.881, 256 m elevation

A first analysis in the Mars Habitat of data obtained for this run with a sampling interval of 100 micro-s and a number of samples of 2048, showed the following results:

1. For all test configurations, the average underground velocity of the signal was approximately 2600 m/s. (See Figure 3)

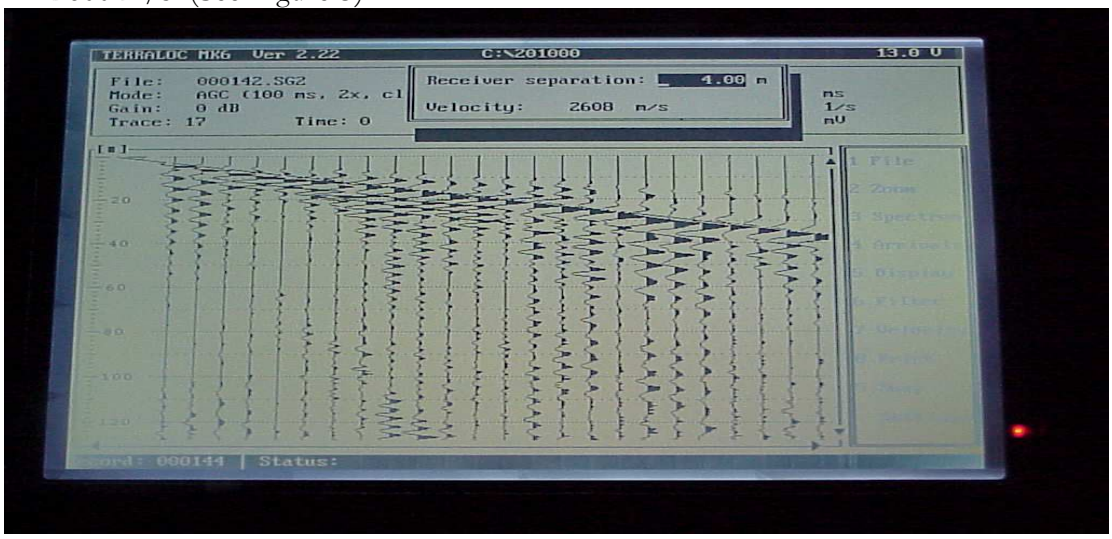

Figure 3: View of the SAS screen during first data analysis in the Habitat. An average velocity of 2600 m/s is found (Photo V. Pletser)

2. The spectrum analysis for each geophone signal for the three tests showed the following ranges of maximum frequency peaks :
   Test #1: 135 Hz (channel 18) to 405 Hz (Channel 17)
   Test #2: 121 Hz (channel 22) to 443 Hz (Channel 7)
   Test #3: 67 Hz (channel 3) to 409 Hz (Channel 17)
3. Sounding extended to vertical depths in excess of 550 m, a depth likely greater than drill which might be foreseen on Mars in the few next decades. A deeper sounding could easily be reached by using safe explosive sources, either shot shell or binary storage explosives.
4. The first refracted signal recorded in Test #1 was returned after 70 milliseconds, consistent with an approximate position of an interphase at a depth of 90 m.

No underground water was detected in the Haynes Ridge plain, despite the rainy conditions prevailing at the surface. Average velocities of wave transmission for water are catalogued between 1450 and 1500 m/s for liquid water and between 3300 and 3800 m/s for ice. The average velocity deduced from test results is consistent with Calcium Carbonate and Dolomite (catalogued range: 1200 to 7000 m/s), which is commonly found in this area [10]. A more detailed analysis of the results is in process to further characterize the underground structure of the Haughton crater rim.

5. OPERATIONAL LESSONS LEARNED

During the three EVA's dedicated to the deployment of this seismic experiment, and two other scouting EVA's to search for potential experiment locations, several observations could be made from an operational view point. These are believed to be important lessons learned that should be

considered when planning future missions to Mars and preparing scientific expeditions on the surface of Mars by the first human crews.

5.1 OPERATOR SKILLS

To successfully conduct a field scientific experiment requires among other things expert knowledge, training, adequate and working instrumentation and favorable weather and terrain conditions. This is an obvious statement. However, a multidisciplinary crew, like those who would eventually be sent to Mars, would be composed of scientists and engineers in different scientific and technical fields. Being an expert in his own field, a crew member needs also to be trained at an adequate field working level in other disciplines. In this respect, the dry run conducted before entering the Mars Habitat on Tuesday 10 July proved to be more than helpful in reviewing the instrumentation and in training other crew members to use the instrumentation and to follow the experiment procedures.

This specific experiment required the installation of 24 geophone sensors, the deployment of more than hundred meters of cabling, more than 50 data electrical connections in the appropriate order, the keying in of the appropriate settings in the SAS computer, and the testing of all sensors and connections before eventually conducting the experiment itself. All the installation, laying out and preparation of the instrumentation took more than 80% of the time, with the remaining less than 20% of time needed for the experiment performance itself. It is therefore of paramount importance to properly prepare, optimize and discuss all operations during briefing prior to starting the EVA. It means also that in the field, the location of the experiment needs to be properly assessed and decided by the relevant discipline experts having the necessary scientific and field know-how. It is therefore crucial for the relevant scientific and technical disciplines to be represented among the crew members and for properly qualified scientists to be selected as part of the human crews for these planetary missions.

The experiment performance under EVA conditions was very physically demanding. Crew members at the end of EVA's were quite exhausted, not only due to physical activities while wearing EVA suits, such as transporting heavy equipment, walking over long distances carrying part of the instrumentation, handling the sledge hammer, and so on, but also due to riding the ATV's with EVA suits and overheating despite the ambient Arctic Summer conditions (with temperatures ranging between 5 and 10 deg. C). This has a direct consequence on the choice of conditions for the several month interplanetary travel between Earth and Mars. An interplanetary flight under microgravity conditions would have well-known debilitating effects on the musculo-skeletal system to a point where a human crew after landing on Mars could no longer be engaged in physically demanding scientific activities like this seismic experiment. Therefore, the Mars mission scenario should foresee either some sort of artificial gravity system in the design of the interplanetary spacecraft for the Earth-Mars leg of the mission, even at a partial earth gravity level, e.g. a Martian gravity level of 0.38 g, or appropriate counter-measures to delay or minimize the microgravity debilitating effects on the human body.

5.2 EVA AND SUPPORTING TECHNICAL EQUIPMENT COMMUNICATIONS IN DEGRADED MODE

During field operations, communications among EVA crew members and between EVA crew members and the base (the Mars Habitat in this case) are of paramount importance, for safety reasons first, but also to properly conduct the experiment. A portable radio system allowed communication among EVA crew members themselves and with the Habitat base. Unfortunately, this portable radio system failed regularly and on nearly all EVA's due to either battery problems (insufficiently charged, or loosing their charge because of cold temperatures), or accidental disconnection of cabling due to falls or arm movements, or stuck buttons, or to improperly set or shifting gain. When this happened, communications between crew members were conducted either verbally through helmets when in close range, or with hand signals at further range. During the experiment performance, at more than one instance, arm signals were also nominally used between the SAS operator and the sledge hammer operator to signal stand-by for acquisition (one arm raised) and ready for acquisition (both arms raised).

• Impaired vision

When wearing the EVA suit helmet, vision was impaired in particular conditions in three cases. The first one occurred while setting up the SAS on the second EVA of Thursday 12 July in poor weather conditions (rain and wind). The SAS screen visibility was impaired by straylight and multiple reflections inside the spherical helmet, further aggravated by rain drops on the helmet. In normal conditions, the screen brightness is sufficient to neglect straylight and multiple reflection, but this incident showed the importance of improving the visibility of the helmet material and shape. A flat transparent surface in front of the face (or at least a portion with a larger curvature radius) could be considered to improve the helmet in this respect.
The second case was mud partially covering the helmet impairing sometimes drastically the vision. During the fifth aborted EVA, nearly all EVA crew members fell several times in the mud. Their helmets were covered to various extents by mud. Wiping them with gloves (also covered in mud) was obviously ineffective. This was also true to a lesser extent during other EVA's while raining; wiping helmets with dirty or dusty gloves resulted also in muddy strains across the helmet vision field. This could have resulted in safety issues, especially while riding ATV's at the end of EVA's. Rain and mud would obviously not be a problem on the surface of the planet Mars. However, this situation experienced several times is relevant for Martian wind and dust, that could eventually cover the helmet of a Martian EVA suit. A system should be designed such as to allow cleaning of the external surface of the helmet in the vision field of the EVA crew member, either with a special brush mounted on the arm of the EVA suit, or a system of several transparent layers adherent to the helmet external surface that could be peeled off by the EVA crew member.
The third case, more common, was fogging of the inside surface of the helmet due to perspiration or exhalation. Ejection of water by the mouth after taking a sip from the drinking outlet valve was effective to wash out the helmet inside surface. For further EVA's, a fine layer of liquid soap was smeared on the helmet inside surface prior to EVA's, which was sufficiently efficient.

• Downward vision in the sagittal plane

The helmet design provided a nearly 180 deg. vision in the horizontal plane and a more than 90 deg. vision angle in the sagittal plane, from slightly below the horizontal plane upward. This angle meant that it was impossible to look at one's own chest, where some of the controls for the radio were mounted. It was also difficult to look at the suit pockets. Although difficult to be implemented, the design requirement for an EVA helmet should be to provide a larger downward vision angle in the sagittal plane as close as possible to that of normal vision.

• Rear vision

Rear vision was also extremely difficult, especially while riding ATV's. To look behind oneself while walking or standing, an EVA crew member had to turn the torso, which was not easy with bulky EVA suits, or to turn completely on himself. This obviously is not possible while riding ATV's. The situation could be improved by mounting rear view mirror(s) on the ATV's, or, better, installing a mirror on the arm of the EVA suit, like it was done with a handheld mirror and some sticky tape. The design of arm mirror actually exists on orbital EVA suits used by Russian cosmonauts and US astronauts on the Mir and the ISS space stations.

• A Martian GPS system ?

For the purpose of this seismic experiment, the use of a handheld GPS system proved to be very useful. A similar GPS system could be considered for future Mars missions. The installation of piggyback GPS systems on presently considered Martian spacecrafts that once in orbit around the planet, would create a simplified Martian GPS constellation. This would greatly enhance the safety of the first human crews and ease their field operations and expeditions.

5.3 ERGONOMY OF INSTRUMENTATION WITH EVA SUIT COMPATIBLE INTERFACES

The instrumentation (geophones, data cabling, SAS, handheld GPS) used for this seismic experiment was designed to be used on earth in normal field conditions and not adapted for use with EVA suit gloves. Several ergonomic problems were encountered, although these have most likely already been foreseen and solved by space mission managers and designers.
The use of bulky gloves caused difficulties for the following categories of operations:
(1) pushing keys on SAS keyboard and on handheld GPS, activating switches, activating radio push button, opening and closing locks and manipulating handles on transport containers;

(2) plugging and unplugging certain connectors (requiring turning a security ring on the connectors), adjusting rotating radio gain buttons;
(3) unrolling and rolling data electrical cables;
(4) writing with pens, manipulating diskettes for data back-ups, holding procedure booklets and turning pages (especially when raining).
Turn-around solutions were found each time and implemented, but often at the cost of carrying extra equipment and extending the operation time. The obvious solution to category 1 operations was to use an extra tool (e.g. screwdriver) to activate keys on keyboards and switches. One crew member improved the idea by taping a small screwdriver on her index finger to push keys on her handheld GPS. Radio push buttons were too small to be properly activated with one gloved finger and resulted often in a two hand operation to bring the button box in the vision field to ascertain that the button was properly depressed.
The solution for category 2 operations was to use another tool (pliers) to turn connectors, especially those not having space around them, being too close to other connectors or box edges to allow manipulation with gloved fingers. Adjusting the rotating radio gain button was found difficult and resulted often in a loss of radio contact; no solution could be found.
Regarding the third category, the rolling of several tens of meters of electrical cables was difficult as the cables would get entangled and create knots. No specific solutions were found, other than patience and the extra time needed to undo knots in the cables.
No solution was be found for the fourth category, other than avoiding these operations and relying on logging data and results either by radioing to base (but not often possible due to radio contact failures) or copying them in memories of the SAS and the handheld GPS computers.
It was found also that it was easier to have the tools that one crew member would need carried in another crew member's suit pocket, as vision of the own suit pockets was very limited.
Finally, it was found that the time allocated for each sequence of steps was longer than anticipated, even with an EVA correction factor of 2 or 3. However, certain sequence of steps were found shorter than anticipated while others were much longer than expected, e.g. for those operations involving EVA operators walking to install instrumentation. Furthermore, certain sequence of settings on the SAS could have been automated or implemented as default choices.

6. CONCLUSIONS

This simulation campaign was extremely productive scientifically and technically. The multidisciplinary and multicultural aspects of the crew members were definitely an enrichment and it was extremely rewarding to work and interact in such a high level environment.
The goal of the proposed experiment was achieved, i.e. to demonstrate the feasibility of conducting a seismic experiment in extreme conditions. It was proven possible to conduct this physically demanding scientific task under EVA conditions similar to those that human crews would encounter on the planet Mars. Despite the one failed attempt due to specific terrestrial weather conditions, it was shown also that the implementation of the seismic refraction method is feasible by EVA crew members in an extreme environment such as the Arctic and that it could be envisaged for future human missions to the planet Mars to detect subsurface water.
Water was not found in the area chosen for measurements, but a large amount of data on the underground structure of the Haynes Ridge plain at the Haughton crater rim was obtained and is still under analysis. A first assessment of the recorded data showed results consistent with the already known underground structure, i.e. mainly Calcium Carbonate and Dolomite rocks.
From an operational viewpoint, several lessons were learned and were presented above in order to improve design of EVA suits and of instrumentation to be used by crew members. Based on observations during the simulated EVA's, suggestions were also made regarding Martian mission concepts and scenarios. It is hoped that these comments and suggestions would be considered for further simulation campaigns and eventually for the first human Mars mission.

7. ACKNOWLEDGEMENTS

Drs P. Lognonne (IPGP), M. Diament (IPGP) and V. Dehant (ROB) are acknowledged for the preparation of the experiment proposal and for conducting the initial field training. Mr C. Cavoit and the technical team of the *Centre de Recherches Geophysiques* of Garchy, France, is acknowledged for supporting the initial field training. The *Institut de Physique du Globe de Paris* is acknowledged for the scientific instrumentation loan and for its shipment to Canada. The Mars Society intervention is acknowledged for the shipment inside Canada. Regarding field operations, the help of MIT Geologist K. Quinn and of Mr R. Zubrin was invaluable. The other crew members W. Clancey, C. Cockell, S. Braham contributed also to the experiment success.
Me4675

8. REFERENCES

[1] The Mars Society, http://arctic.marssociety.org/
[2] D. Scott, Z. Hajnal, "Seismic signature of the Haughton structure", *Meteoritics* **23**, 239-247, 1988.
[3] NASA-HMP, http://www.arctic-mars.org/
[4] P. Lognonné, B. Mosser, "Planetary seismology", *Surveys in Geophysics* **14**, 239-302, 1993.
[5] P. Lognonné, D. Giardini, B. Banerdt, J. Gagnepain-Beyneix, A.Mocquet, T. Spohn, J.F. Karczewski, P. Schibler, S. Cacho, W.T. Pike, C. Cavoit, A. Desautez, J. Pinassaud, D. Breuer, M. Campillo, P. Defraigne, V. Dehant, A. Deschamp, J. Hinderer, J.J. Lévéque, J.P. Montagner, J. Oberst, "The NetLander Very Broad band seismometer", *Planet. Space Sc.* **48**, 1289-1302, 2000.
[6] V. Ballu, "Initiation aux methodes de prospection geophysique: Gravimetrie, Magnetisme, Prospection electrique, Sismique refraction", *CIES, Academie de Paris*, 1995.
[7] D. Palmer, "The Generalized Reciprocal Method of Seismic Refraction Interpretation", *Society of Exploration Geophysicists*, ISBN 0-931830-14-1, 1980.
[8] B. Sjogren, "Shallow Refraction Seismics", *Chapman and Hall*, ISBN 0-412-24210-9, 1984.
[9] "Terraloc Mark 6 Seismograph, Users Manual and Technical Manual", Part no 9133 0011 90 (2), ABEM Instrument AB, Sweden, 1994.
[10] V. Pletser, P. Lognonne, M. Diament, V. Ballu, V. Dehant, P. Lee, R. Zubrin, "Subsurface Water Detection on Mars by Active Seismology: Simulation at the Mars Society Arctic Research Station", Abstract 7018, *Conference on the Geophysical Detection of Subsurface Water on Mars*, Lunar and Planetary Institute, Houston, 6-10 August 2001.

A SIMPLIFIED ANALYTICAL FORMULATION OF THE NETLANDER IONOSPHERE AND GEODESY EXPERIMENT ORBITER/LANDER OBSERVABLE

M. YSEBOODT[1], J.P. BARRIOT[2], V. DEHANT[1]
[1] Royal Observatory of Belgium, avenue Circulaire, 1180 Bruxelles, Belgium.
[2] Observatoire Midi-Pyrénées, UMR 5562/GRGS, 14 av. Belin, 31400 Toulouse, France
E-mail: m.yseboodt@oma

The NetLander Mission that will be launched to Mars in 2007, will deploy a network of four similar micro-stations on the planet surface to observe the atmosphere and the internal structure of Mars by means of nine geophysical instruments, including the NEtlander Ionosphere and Geodesy Experiment (NEIGE). The geodesy part of this experiment consists in analysing the Doppler shifts of a radio-signal transmitted between (1) the landers and the orbiter (data relay) and (2) the orbiter and the Earth in order to obtain the Mars orientation parameters. By monitoring the polar motion, variations in the rotation rate or in the length-of-day (lod), precession and nutations, we will be able to obtain information about the Martian internal structure. See Dehant, Barriot et al, 2002, this issue.

The NEIGE Doppler observable q between the data relay orbiter and one lander on Mars' surface can be analytically modeled in a simplified way by looking at the instantaneous projection of the velocity difference between the satellite and the lander on the satellite-lander line. The hypotheses used are: (1) an instantaneous propagation, (2) no ionospheric perturbation of the signal, (3) no gravity field and no other forces acting on the satellite. The expression for the Doppler observable has been linearized in the first order in the small quantities X, Y and ξ which are linked to the geophysical rotation parameters.

We have to express the lander and satellite coordinates and velocities in the same frame. In order to go from a Martian Reference Frame to an Inertial Reference Frame, we use the rotation matrix $\mathbf{M}$ depending on the five Martian Orientation Parameter (MOP): nutation and precession, polar motion and sidereal time. This matrix can be divided in two parts $\mathbf{M} = \mathbf{M_{Reg}}\ \mathbf{M}_\infty$:

- a regular matrix $M_{Reg} = R_z(-\psi_R)R_x(I_R)R_z(-\phi_R)$ that includes all the constants and linear contributions of each rotation angle I_R (the obliquity), ϕ_R (the rotation angle) and ψ_R (the precession angle) and
- an infinitesimal matrix M_∞, which includes the periodic irregularities: the polar motion (x_P, y_P), the nutations (δI, $\delta\psi$) and the variation of the length-of-day ($\delta\phi$).

This infinitesimal matrix can be expressed using three parameters (X, Y, ξ) only, instead of the five MOP. The link between X, Y, ξ and the MOP is :

$$\begin{aligned} X &= x_P + \sin I_R \cos\phi_R\, \delta\psi - \sin\phi_R\, \delta I \\ Y &= y_P + \sin I_R \sin\phi_R\, \delta\psi + \cos\phi_R\, \delta I \\ \xi &= -\cos I_R\, \delta\psi - \delta\phi \end{aligned}$$

This formulation in X, Y, ξ gives simpler expressions for the matrix $\mathbf{M}$, for the rotation vector and finally for the Doppler observable q. We considered a precessing orbit for the data relay (J_2 term).

There are lander-orbiter configurations for which visibility is not possible. For example, if the lander latitude is larger than 27° and for a circular equatorial 400 km orbit, the orbiter is always under the lander horizon. The effect of such configurations can be seen on the upper left corners of the graphs in Fig. 1 where the contribution is strictly equal to 0.

The expression of the Doppler observable as function of X, Y and ξ allows us to understand how the geophysical information appears in the signal. We have studied different lander locations and changed the orbital parameters of the data relay, in order to see how the signature in the Doppler observable of the geophysical phenomena under study can be maximized (accounting for the visibility/non-visibility of the lander by the orbiter).

The quantities plotted in Fig. 1 are the contributions to the Doppler observable of different (or all) geophysical parameters. These contributions have been computed by evaluating the difference between the Doppler observable with and without the geophysical contents (the perturbations on the MOP models are: for nutations, changes on the transfer function parameters corresponding to perturbation up to 12 mas, for polar motion, to 50 mas perturbation, for UT, to 300 mas perturbation). We have scaled the results by 0.1 mm/s, which is the nominal precision of NEIGE. The configurations that maximizes the 3 geophysical effects (Nutation, UT and

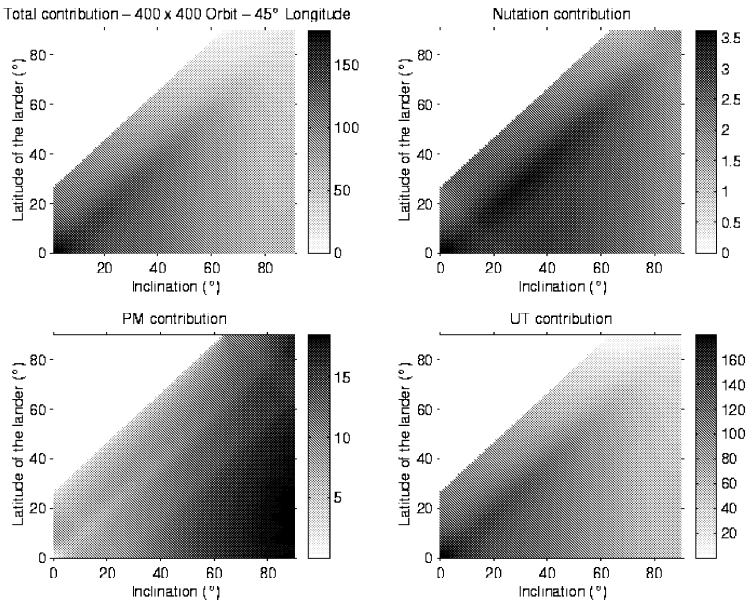

Figure 1: Total contribution (upper left graph) to the Doppler Observable and Nutation (upper right), Polar Motion (PM, lower left) and Sidereal Time (UT, lower right) contributions as function of the orbiter inclination and the lander latitude. The statistical quantity plotted is the quadratic mean of the temporal series when there is visibility (0.1 mm/s). The orbit is a circular 400km-high orbit

PM) are different. But the NEIGE experiment focuses rather on nutation and UT, which have similar signatures on the Doppler signal. The local maxima for the nutation contribution are reached if the lander latitude is almost equal to the orbit inclination, while the maximum for the PM contribution occurs for a large orbit inclination. The best configuration to get a large UT signature corresponds to both lander latitude and orbit inclination below 10°. These graphs are independent of the lander longitude.

FREE AND FORCED RESPONSE OF A NON-RIGID MARS WITH AN INNER-CORE. I. ANALYTICAL APPROACH

V. DEHANT
Royal Observatory of Belgium
3 avenue Circulaire, B1180 Brussels, Belgium
e-mail: v.dehant@oma.be

M. GREFF-LEFFTZ
Institut de Physique du Globe de Paris, France

H. LEGROS
Ecole et Observatoire de Physique du Globe de Strasbourg, France

T. VAN HOOLST, P. DEFRAIGNE, O. de VIRON
Royal Observatory of Belgium

1. INTRODUCTION

We know that Mars had a magnetic field and thus that there was a liquid core at that time (3.9 Gyr B.P.). It is generally believed that Mars has presently a liquid core: the expected core composition (iron + 14% of light element sulfur) favours a liquid core and no inner core. Nevertheless, the percentage of light element is controversial and a smaller value would allow for inner core formation.

The absence of intrinsic global magnetic field of Mars at present (results from Mars Global Surveyor, Acuna et al., 1999, Science 284, 790-793) indicates other possibilities such as the following ones: (1) Mars would be between two magnetic reversals (controversial), (2) the motion in the conducting core would be unable to generate a strong magnetic field, (3) the magnetic field could be shielded by the iron rich mantle, and (4) a completely solid core is also a possibility.

If Mars has a liquid core, there exists a normal mode called the Free Core Nutation (FCN); this mode is diurnal in a frame tied to Mars and has a long retrograde period in the inertial frame. And if Mars has a solid inner core, there exists an additional normal mode called the Free Inner Core Nutation (FICN); this mode is also diurnal in a frame tied to Mars and has a long prograde period in the inertial frame. Both modes appear as a resonances in the motion of the rotation axis of Mars in space (nutations).

Whatever the interior of Mars is, Mars has a normal mode called the Chandler Wobble (CW), due to its equatorial bulge. If Mars has a solid inner core within a liquid outer core, there is an additional normal mode called the Inner Core Wobble (ICW). Both modes have long periods in a frame tied to Mars.

These four modes induce resonance effects in nutations and polar motion. Consequently, it is necessary to examine the impact of the presence of an inner core on the nutations of Mars and of the polar motion of this planet. This will allow us to derive a strategy to interpret the

nutations (which will be observed with the NetLander geodesy experiment NEIGE) in terms of information about the core of Mars. The observation by NEIGE of a possible ICW resonance in polar motion would provide us with complementary information.

2. ADJUSTEMENT OF THE LIQUID CORE AND SOLID INNER CORE DENSITIES, AND COMPUTATION PROCEDURE

We first considered an analytical approach. We computed the resonant response of an ellipsoidal and rotating planet composed of three homogeneous incompressible layers (the inner core, the liquid core and the mantle). We solved the angular momentum budget equations for these three layers, considering coupling mechanisms at the inner core-outer core boundary (ICB) and at the core-mantle boundary (CMB); the deformations and mass redistribution within the planet are accounted for by using a Love numbers formalism. A numerical approach has been used by Rivoldini et al. (2001, this issue).

The growth of the inner core is modeled as follows:
- at the beginning, the inner core is created by precipitation of the iron contained in the liquid core and thus has the density of the pure solid iron;
- after the eutectic point is reached, the inner core grows by solidification (freezing) of the liquid outer core and thus the newly formed outer layers have the same concentration in light element as the liquid core.

3. COMPUTATION OF THE NORMAL MODE FREQUENCIES AND OF THE NUTATION AND POLAR MOTION TRANSFER FUNCTION

First, we compute analytically the frequencies of the modes for the different radii of the inner core. Then, we compute the transfer function for nutation (usually called the B_{ratio}) for different radii of the inner core, as well as the transfer function for polar motion for different radii of the inner core. Our computations were based on the rheological properties deduced from Sohl and Spohn's model (1997, J. Geophys. Res. 102, 1613-1635) (for the mantle and the core dimension) and on surface densities of iron and sulfur re-evaluated at the core pressure and temperature (also taken from Sohl and Spohn, 1997).

The normal mode periods depend very much on the inner core radius. The FICN period ranges from 100 or less to 250 days in the freezing case, and to 600 days in the precipitation case; the FCN period ranges from 100 or less to 280 days in both, the freezing and precipitation cases. The ICW can vary from a few hundred days to about one hundred of years. Our results show that the ICW period could have a period very close to the annual period, which is excited by the sublimation/condensation process of the CO_2 (atmosphere and ice caps).

The experiment NEIGE aims at obtaining the orientation parameters of the planet Mars from Doppler measurements between the landers and an orbiter and between the orbiter and the Earth (see Barriot et al., 2001, this issue).

From the orientation parameters determined by NEIGE, it will be possible to determine polar motion, length-of-day and precession/nutations.

The CW and ICW induce resonances in polar motion at frequencies close to the atmospheric excitation (condensation/sublimation of ice caps). Their observation will allow to infer properties of the mantle and of the inner core.

The FCN and FICN induce resonances in nutations excited by the Sun (and to a smaller extent by Phobos and Deimos). Their observation will allow to infer properties of the outer core and of the inner core. In particular, the dimensions and physical state of the core can be determined from the resonance(s), and the existence of an inner core could possibly be seen.

THE NEW IAU'2000 CONVENTIONS FOR COORDINATE TIMES AND TIME TRANSFORMATIONS

G. PETIT
Bureau International des Poids et Mesures
Pavillon de Breteuil 92312 Sevres Cedex France
e-mail: gpetit@bipm.org

ABSTRACT. At its 2000 General Assembly, the International Astronomical Union has adopted a set of Resolutions that provide a consistent framework for defining the barycentric and geocentric celestial reference systems at the first post-Newtonian level. This paper describes in some detail the two Resolutions that define time coordinates and allow to realize time transformations. New clock technology and space missions will necessitate the application of this framework for time and frequency measurements in the solar system.

1. INTRODUCTION

In its 1991 General Assembly the International Astronomical Union (IAU) explicitly adopted the general theory of relativity as the theoretical framework for the definition and realization of space-time reference frames (IAU, 1991). Barycentric and geocentric coordinate time scales and the relativistic transformations between them were defined, together with procedures for their realization. In section 2, we recall the content of the IAU 1991 resolution A4 dealing with the definition of reference systems, time coordinates and time transformations, and we expose some of the limitations of this framework.

The IAU Working Group on Relativity in Celestial Mechanics and Astrometry (RCMA), since 1994, and the BIPM/IAU Joint Committee on relativity for space-time reference systems and metrology (JCR), since 1997, have worked to provide an extension of the IAU'1991 framework at the first post-Newtonian level (Soffel, 2000; Petit, 2000). This work resulted in a set of Resolutions passed at the IAU 2000 General Assembly. The complete text of the Resolutions may be found in IAU publications (or see `http://danof.obspm.fr/IAU_resolutions/Resol-UAI.htm`) and a complete explanatory supplement may be found in (Soffel et al., 2001). The new IAU'2000 framework is specified in Resolutions B1.3(2000) "Definition of barycentric celestial reference system and geocentric celestial reference system" and B1.4(2000) "Post-Newtonian potential coefficients". In Section 3 of this paper, we focus on the two Resolutions which deal with time transformations and the definition of coordinate times, namely Resolutions B1.5(2000) "Extended relativistic framework for time transformations and realization of coordinate times in the solar system" in section 3.1 and B1.9(2000) "Re-definition of Terrestrial Time TT" in

section 3.2.

2. THE IAU'1991 FRAMEWORK AND ITS LIMITATIONS

The IAU resolution A4 (1991) contains nine recommendations, the first five of which are directly relevant to our discussion.

In the first recommendation, the metric tensor for space-time coordinate systems $(t, \mathbf{x})$ centered at the barycenter of an ensemble of masses is recommended in the form

$$\begin{aligned} g_{00} &= -1 + \frac{2U(t,\mathbf{x})}{c^2} + \mathcal{O}(c^{-4}), \\ g_{0i} &= \mathcal{O}(c^{-3}), \\ g_{ij} &= \delta_{ij}\left(1 + \frac{2U(t,\mathbf{x})}{c^2}\right) + \mathcal{O}(c^{-4}). \end{aligned} \tag{1}$$

where c is the speed of light in vacuum ($c = 299792458$ m/s), U is the sum of the gravitational potentials of the ensemble of masses and of a tidal potential generated by bodies external to the ensemble, the latter potential vanishing at the barycenter. The algebraic sign of U is taken to be positive. This recommendation recognizes that space-time cannot be described by a single coordinate system. The recommended form of the metric tensor can be used not only to describe the barycentric reference system (BRS) of the whole solar system (which is called BCRS where C stands for Celestial since the IAU'2000 Resolutions), but also to define the geocentric reference system (GRS) centered in the center of mass of the Earth, which is now called GCRS. In analogy to the GRS, a corresponding reference system may be defined for any other body of the Solar system.

In the second recommendation, the origin and orientation of the space coordinate grids for the solar system (BRS) and for the Earth (GRS) are defined. Notably it is specified that the space coordinate grids of these systems should show no global rotation with respect to a set of distant extragalactic objects. It also specifies that the SI (International System of units) second and the SI meter should be the physical units of proper time and proper length in all coordinate systems. It states in addition that the time coordinates should be derived from an Earth atomic time scale.

The third recommendation defines TCB (Barycentric Coordinate Time) and TCG (Geocentric Coordinate Time) – the time coordinates of the BRS and GRS, respectively. The recommendation also defines the origin of the times scales (their reading on 1977 January 1, $0^{\mathrm{h}}\,0^{\mathrm{m}}\,0^{\mathrm{s}}$ TAI ($JD = 2443144.5\,TAI$) must be 1977 January 1, $0^{\mathrm{h}}\,0^{\mathrm{m}}\,32.184^{\mathrm{s}}$) and declares that the units of measurements of the coordinate times of all reference systems must be coincide with the SI second and SI meter. The relationship between TCB and TCG is given by a full 4-dimensional transformation

$$TCB - TCG = c^{-2}\left[\int_{t_0}^{t}\left(\frac{v_E^2}{2} + U_{ext}(t,\mathbf{x}_E(t))\right)dt + v_E^i r_E^i\right] + \mathcal{O}(c^{-4}), \tag{2}$$

where x_E^i and v_E^i are the barycentric coordinate position and velocity of the geocenter, $r_E^i = x^i - x_E^i$ with x^i the barycentric position of the observer, and $U_{ext}(t,\mathbf{x}_E(t))$ is the Newtonian potential of all solar system bodies apart from the Earth evaluated at the geocenter.

In the fourth recommendation another time coordinate, Terrestrial Time (TT), is defined for the GRS. It differs from TCG by a constant rate only

$$TCG - TT = L_G \times (JD - 2443144.5) \times 86400, \qquad L_G \approx 6.969291 \times 10^{-10}, \tag{3}$$

so that the unit of measurement of TT agrees with the SI second on the geoid. TT represents an ideal form of TAI, the divergence between them being a consequence of the physical defects of atomic clocks.

The fifth recommendation states that the former dynamical barycentric time TDB may still be used where discontinuity with previous work is deemed to be undesirable.

Because of the form of the metric (1) in the IAU'1991 framework, time transformations and the realization of coordinate times in the barycentric system are not specified at the c^{-4} level, i.e. at a level of a few parts in 10^{16} in rate. The new IAU'2000 framework allows to remove this limitation. Nevertheless, within the IAU'1991 approximation, constants L_B and L_C were introduced in notes to the Recommendation 3 (1991) to express the mean rates between time scales as

$$\begin{aligned} TCB - TDB &= L_B \times (JD - 2443144.5) \times 86400, \\ & \quad L_B \approx 1.550505 \times 10^{-8}, \text{ and} \\ TCB - TCG &= L_C \times (JD - 2443144.5) \times 86400 + v_E^i r_E^i / c^2 + P, \\ & \quad L_C \approx 1.480813 \times 10^{-8}, \end{aligned} \tag{4}$$

where P represents periodic terms. Since JD is not specified to be a particular time scale, these constants were not properly defined so that confusion appeared in their usage. This point was adressed in Resolution B1.5(2000) by defining $< TCG/TCB >= 1 - L_C$ and $< TT/TCB >= 1 - L_B$, where $<>$ means a sufficiently long term average taken at the geocenter. The actual computation of L_C and L_B requires the integration of solar system ephemerides and the specification of an averaging duration, and this process may be applied to the utmost accuracy, after a choice of ephemerides and averaging duration. For example Irwin and Fukushima (1999) determined $L_C = 1.48082686741 \times 10^{-8} \pm 2 \times 10^{-17}$. However, because no unambiguous definition may be provided for L_B and L_C, these constants should not be used in formulating time transformations when it would require knowing their value with an uncertainty of order 1×10^{-16} or less.

Another problem arising from the situation before IAU'1991 is that the barycentric dynamical time TDB did not have a good definition. This could have been corrected by turning a specific value of L_B into a defining constant thus providing in retrospect a good definition of TDB. It was not felt necessary to address explicitly this point in a recommendation.

3. TIME COORDINATES IN THE IAU'2000 FRAMEWORK

For practical applications concerning time and frequency measurements in the solar system, it is necessary to consider a conventional model for the realization of time coordinates and time transformations. This model should be chosen so that i) its accuracy is significantly better than the expected performance of clocks and time transfer techniques, ii) it is consistent with the general framework of IAU Resolutions B1.3 and B1.4 (2000) and may readily be used with existing astrometric quantities, e.g. solar systems ephemeris. The second condition has been ensured by explicitly deriving the developments from the general framework of IAU Resolutions B1.3 and B1.4, using the same conventions and notations.

Regarding the first condition, accuracy limits to be used in the developments were derived in a straightforward way. At present the best accuracies are reached by Cs-fountain clocks at about one part in 10^{15} in fractional frequency (Lemonde et al., 2001; Weyers et al., 2001), with a frequency stability characterized by a standard Allan deviation of order $\sigma_y(\tau) = 4 \times 10^{-14} \tau^{-1/2}$ for an integration time τ in seconds. In the near future, high accuracy laser cooled Rb clocks (Bize et al. 1999) and space-borne Cs clocks are expected to reach accuracies of a few parts in 10^{17} in fractional frequency and stabilities of order $\sigma_y(\tau) = 1 \times 10^{-14} \tau^{-1/2}$, with τ in seconds.

The uncertainty in the time transformations should induce errors that are always lower than the expected performance of these future clocks. Including a factor 2 as safety margin, we therefore conclude that time coordinates and time transformations should be realized with an uncertainty not larger than 5×10^{-18} in rate or, for quasi-periodic terms, not larger than 5×10^{-18} in rate amplitude and 0.2 ps in phase amplitude.

For the spatial domain of validity of the transformations, we note that projects like SORT (Solar Orbit Relativity Test) plan to fly high accuracy clocks to within 0.25 AU of the Sun, but it turns out that formulations valid there will also be valid at a few solar radii from the Sun which is therefore the lower limit for the distance to the barycenter that has been considered. In the geocentric system locations from the Earth's surface up to geostationary orbits ($|\mathbf{X}| < 50000$ km) have been considered.

3.1 Resolution B1.5(2000): Extended relativistic framework for time transformations and realization of coordinate times in the solar system

Following Resolutions B1.3(2000) and B1.4(2000), the metric tensor in the BCRS is expressed as

$$\begin{aligned} g_{00} &= -(1 - \tfrac{2}{c^2}(w_0(t,\mathbf{x}) + w_L(t,\mathbf{x})) + \tfrac{2}{c^4}(w_0^2(t,\mathbf{x}) + \Delta(t,\mathbf{x}))) \\ g_{0i} &= -\tfrac{4}{c^3} w_i(t,\mathbf{x}) \\ g_{ij} &= \left(1 + \tfrac{2w_0(t,\mathbf{x})}{c^2}\right) \delta_{ij} \end{aligned} \tag{5}$$

where $(t \equiv TCB, \mathbf{x})$ are the barycentric coordinates, $w_0 = G \sum_A M_A / r_A$, with the summation carried out over all solar system bodies A, $\mathbf{r}_A = \mathbf{x} - \mathbf{x}_A$, $r_A = |\mathbf{r}_A|$, and where w_L contains the expansion in terms of multipole moments, as defined in Resolution B1.4(2000) and references therein, required for each body. In many cases the mass-monopole approximation ($w_L = 0$) may be sufficient to reach the above mentioned uncertainties but this term should be kept to ensure the consistency in all cases. The values of masses and multipole moments to be used may be found in IAU or IERS documents (IERS, 1996), but care must be taken that the values are in SI units (not in so-called TDB units or TT units). The vector potential $w^i(t,\mathbf{x}) = \sum_A w^i_A(t,\mathbf{x})$ and the function $\Delta(t,\mathbf{x}) = \sum_A \Delta_A(t,\mathbf{x})$ are given later.

From (5) the transformation between proper time and TCB may be derived. It reads:

$$\mathrm{d}\tau/\mathrm{d}TCB = 1 - \frac{1}{c^2}\left(w_0 + w_L + \frac{v^2}{2}\right) + \frac{1}{c^4}\left(-\frac{1}{8}v^4 - \frac{3}{2}v^2 w_0 + 4v^i w^i + \frac{1}{2}w_0^2 + \Delta\right) \tag{6}$$

To reach the uncertainty mentioned earlier, it is sufficient to express the vector potential $w^i_A(t,\mathbf{x})$ of body A as

$$w^i_A(t,\mathbf{x}) = G\left[\frac{-(\mathbf{r}_A \times \mathbf{S}_A)^i}{2r_A^3} + \frac{M_A v^i_A}{r_A}\right] \tag{7}$$

where $\mathbf{S}_A$ is the total angular momentum and v^i_A is the coordinate velocity of body A. As for the function $\Delta_A(t,\mathbf{x})$ it is sufficient to express it as

$$\Delta_A(t,\mathbf{x}) = \frac{GM_A}{r_A}\left[-2v_A^2 + \sum_{B \neq A}\frac{GM_B}{r_{BA}} + \frac{1}{2}\left(\frac{(r^k_A v^k_A)^2}{r_A^2} + r^k_A a^k_A\right)\right] + \frac{2Gv^k_A(\mathbf{r}_A \times \mathbf{S}_A)^k}{r_A^3} \tag{8}$$

where $r_{BA} = |\mathbf{x}_B - \mathbf{x}_A|$ and a^k_A is the coordinate acceleration of body A.

Evaluating the Δ_A-terms for all bodies of the solar system, we find that $|\Delta_A(t,\mathbf{x})|/c^4$ may reach at most a few parts in 10^{17} in the vicinity of Jupiter and about 1×10^{-17} close to the

Earth. Presently, however, for all planets except the Earth, the magnitude of $\Delta_A(t,\mathbf{x})/c^4$ in the vicinity of the planet is smaller than the uncertainty originating from its mass or multipole moments so that it is practically not needed to account for these terms. Nevertheless, when new astrometric observations allow to derive the mass and moments with adequate uncertainty, it will be necessary to do so. In any case, for the vicinity of a given body A, only the effect of $\Delta_A(t,\mathbf{x})$ is needed in practice, i.e., the effect of $\sum_{B\neq A}\Delta_B(t,\mathbf{x})$ is smaller than our accuracy specifications. For a clock in the vicinity of the Earth, to be compared with other clocks in the solar system or to TCB, it may thus be needed to account for $\Delta_E(t,\mathbf{x})/c^4$. Also, in these formulas, the terms in $\mathbf{S}_A$ are needed to reach the mentioned uncertainty only for Jupiter ($S\approx 6.9\times 10^{38} m^2 s^{-1} kg$) and Saturn ($S\approx 1.4\times 10^{38} m^2 s^{-1} kg$), in the immediate vicinity of these planets.

Similarly, the transformation between TCB and TCG may be written as

$$\begin{aligned} TCB - TCG = c^{-2}\left[\int_{t_0}^{t}\left(\frac{v_E^2}{2}+w_{0ext}(\mathbf{x}_E)\right)dt + v_E^i r_E^i\right] \\ -c^{-4}[\int_{t_0}^{t}\left(-\frac{1}{8}v_E^4-\frac{3}{2}v_E^2 w_{0ext}(\mathbf{x}_E)+4v_E^i w_{ext}^i(\mathbf{x}_E)+\frac{1}{2}w_{0ext}^2(\mathbf{x}_E)\right)dt \\ -(3w_{0ext}(\mathbf{x}_E)+v_E^2/2)v_E^i r_E^i] \end{aligned} \tag{9}$$

where t is TCB and where the index ext refers to all bodies except the Earth. This equation is composed of terms evaluated at the geocenter (the two integrals) and of position dependent terms in r_E, with position dependent terms in higher powers of r_E having been found to be negligible. The first integral may be computed from existing planetary ephemeris (Fukushima, 1995; Irwin and Fukushima, 1999). Since, in general, the planetary ephemeris are expressed in terms of a time argument T_{eph} which is close to TDB, rather than in terms of TCB, the first integral will be computed as

$$\int_{t_0}^{t}\left(\frac{v_E^2}{2}+w_{0ext}(\mathbf{x}_E)\right)dt = \left[\int_{t_{eph_0}}^{t_{eph}}\left(\frac{v_E^2}{2}+w_{0ext}(\mathbf{x}_E)\right)dt_{eph}\right]/(1-L_B)\,. \tag{10}$$

Terms in the second integral of (9) are secular and quasi periodic. They amount to $\sim 1.1\times 10^{-16}$ in rate ($\mathrm{d}TCB/\mathrm{d}TCG$) and primarily a yearly term of ~ 30 ps in amplitude (i.e. corresponding to periodic rate variations of amplitude $\sim 6\times 10^{-18}$). Terms in $\Delta_{ext}(t,\mathbf{x})$ that would appear in this integral are negligible in the vicinity of the Earth where this formula is to be used. Besides the position dependent terms in c^{-2} which may reach several microseconds, position dependent terms in c^{-4} (the last two terms in (9)) are not negligible and reach, for example, an amplitude of 0.4 ps ($\sim 3\times 10^{-17}$ in rate) in geostationary orbit.

Thus Resolution B1.5(2000) provides all necessary information to treat future space missions carrying high accuracy cold atoms clocks. Applications considered are e.g. the frequency comparison of two clocks in two different locations in the solar system or the realization of TCB from an Earth atomic time scale. When the accuracy specified in Resolution B1.5 will be deemed insufficient, formulas extending those given above should be re-derived from resolutions B1.3 and B1.4.

3.2 Resolution B1.9(2000): Re-definition of Terrestrial Time TT

Evaluating the contributions of the higher order terms in the metric of the geocentric reference system (Resolution B1.3), it is found that the IAU'1991 framework with the metric of the form (1) is sufficient for time and frequency applications in the GCRS in the light of present and foreseeable future clock accuracies. In particular a choice of gauge and of the state of rotation of the GCRS (kinematically or dynamically non-rotating) does not influence the time

and frequency application at the given level of accuracy (Note however that the IAU framework has specified GCRS to be kinematically non-rotating). Nevertheless, in applying the IAU'1991 formalism, some care needs to be taken when evaluating the Earth's potential at the location of the clock specially when accuracy of order 10^{-18} is required (Klioner, 1992; Wolf and Petit, 1995; Petit and Wolf, 1996).

Presently, the time scale of reference for all practical matters on Earth is Terrestrial Time TT or one of the scales realizing it and differing by some time offset (e.g., TAI, UTC, GPS-time). TT was defined in IAU Resolution A4 (1991) as: "a time scale differing from the Geocentric Coordinate Time TCG by a constant rate, the unit of measurement of TT being chosen so that it agrees with the SI second on the geoid". According to the transformation between proper and coordinate time, this constant rate is given by $\mathrm{d}(TT)/\mathrm{d}(TCG) = 1 - U_g/c^2 = 1 - L_G$, where U_g is the gravity (gravitational + rotational) potential on the geoid.

Some shortcomings appeared in this definition of TT when considering accuracies below 10^{-17}. First, the uncertainty in determination of U_g is of order 1 $\mathrm{m^2\,s^{-2}}$ or slightly better (Groten, 2000). Second, even if it is expected that the uncertainty in U_g improves with time the surface of the geoid is difficult to realize (so that it is difficult to determine the potential difference between the geoid and the location of a clock). Third, the geoid is, in principle, variable with time. Therefore it was decided to desociate the definition of TT from the geoid while maintaining continuity with the previous definition. The constant L_g was turned into a defining constant with its value fixed to $6.969290134 \times 10^{-10}$ to ensure the continuity with the current best estimation of U_G/c^2, from the value $U_G = 62636856$ $\mathrm{m^2\,s^{-2}}$ provided by the International Association of Geodesy Special Commission 3 (Groten 2000).

Thus Resolution B1.9 will allow to use the full potential of future high accuracy clocks on board terrestrial satellites to realize TT.

4. REFERENCES

Bize S. et al., *Europhys. Lett.* **45** (5), 558 (1999)

Fukushima T., *Astron. Astrophys.*, **294**, 895 (1995)

Groten E., *Proc IAU Colloquium 180*, 337 (2000)

IAU, Transactions of the International Astronomical Union, **XXIB** (edited by J.Bergeron), Dordrecht, Kluwer (1991)

IERS Conventions, International Earth Rotation Service Technical Note 21 (ed. by D.D.McCarthy), Observatoire de Paris (1996)

Irwin A., Fukushima T., *Astron. Astrophys.*, **348**, 642 (1999)

Klioner S.A., *Celest. Mech. Dyn. Astr.*, **53**, 81 (1992)

Lemonde P. et al., in: Frequency Measurement and Control, Luiten A.N. ed., Springer (2001)

Petit G., Wolf P., *IEEE Trans.* **IM 46**, 2, 201 (1996)

Petit G., *Proc. IAU Colloquium 180*, 275 (2000)

Soffel M., *Proc. IAU Colloquium 180*, 283 (2000)

Soffel M. et al., *Astron. J.*, in preparation (2001)

Wolf P., Petit G., *Astron. Astrophys.*, **304**, 653 (1995)

Weyers S. et al., *Metrologia* **38**, 4, 343-352, (2001)

ACKNOWLEDGEMENTS

The contributions of members of the BIPM/IAU Joint Committee on Relativity (which may be found at `http://www.bipm.org/WG/CCTF/JCR/jcrsccor.html`) are gratefully acknowledged, with special thanks to my colleague Peter Wolf.

PHYSICAL RELATIVISTIC FRAMES

B. COLL
DANOF/UMR8630-CNRS
Observatoire de Paris, 61 avenue de l'Observatoire, 75014 Paris, France
e-mail: bartolome.coll@obspm.fr, http://coll.cc

ABSTRACT. The concept of relativistic positioning system is introduced and the project SYPOR, aiming for its application to the Galileo navigation system, is sketched.

1. INTRODUCTION

Coordinate systems are the basic pieces for the construction of reference systems and, consequently, of reference frames. There is an abundant literature on them, but they are always considered from partial points of view. This is true both, in newtonian physics as well as in relativity. Moreover, an extended idea pretends that there is no essential differences between newtonian and relativistic coordinate systems.

It is clear that further thought, based in larger points of view, needs to be given to this subject. To provide incentives in this direction, I will begin here with a fairly basic presentation of the different classes of coordinate systems admitted by both, newtonian and relativistic space-times. This is the subject of Section 2.

Able to coincide in newtonian physics, reference systems and positioning systems are necesarily disjoint objects in relativity. The notion of relativistic positioning systems, their basic properties and their simple possibilities of construction are presented in Section 3.

The idea of the project SYPOR appear then clearly: to give to the constellation of satellites of the future GALILEO navigation system the status of a *primary relativistic positioning system for the Earth*. Points concerning this idea, and a simple version of an important control result are briefly sketched in Section 4.

Some ideas and results on this subject come from a long collaboration with Ll. Bel, J.J. Ferrando, J.A. Morales and A. Tarantola.

2. CAUSAL CLASSES OF COORDINATE SYSTEMS

In newtonian space-time, one uses to take coordinate systems in which one coordinate line is generated by a clock and the other three, more or less directly related to rods, lie in the absolute three-dimensional space at every instant. The space-time line generated by the clock, because transverse to this space at any instant, is called *time-like*, and those determined by the rods, because belonging to it, are called *space-like*; the corresponding coordinate systems are said of *type* **teee**.

But coordinate systems other than the above ones may also be taken. For example, those

Figure 1: A coordinate system is usually related to a clock and three rods.

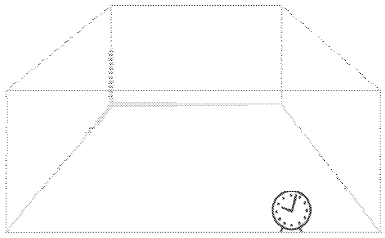

constituted by four separated megaphones shouting at every instant the time of a clock in a region of the space (the gap at every point between their messages, due to the sound's velocity, allow to locate the point in the space-time). It can be seen that now the corresponding four coordinate lines are *time-like* lines; these coordinate systems are said of *type* **tttt**.

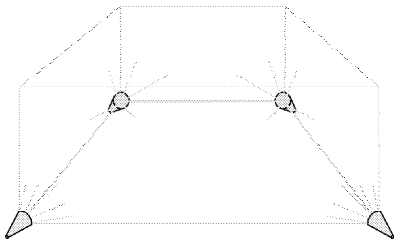

Figure 2: Coordinate systems may also be realized by means of four megaphones shouting at every instant the time of a clock.

Coordinate systems of types **teee** and **tttt** are said to belong to different *causal classes*[1]. Thus, a simple and natural question arises: *how many causal classes of coordinate systems exist in Newtonian space-time?*

The fact that this natural question has never been asked shows the above mentioned partial character of the studies made up to now on coordinate systems, reference systems and reference frames. The answer is here presented to information only, as a mean to emphasize the differences between Newtonian and relativistic coordinate systems.

This answer says that *there exist twelve disjoint causal classes of Newtonian coordinate systems*, according to Table I. In this table, t's and e's denote respectively time-like and space-like causal characters, and italic, roman and capital styles denote respectively coordinate hypersurfaces, coordinate lines and coordinate surfaces (or covectors, tangent vectors and planes rspectively). A class is represented by the set $\{\mathbf{xxxx}; \mathbf{XXXXXX}; \mathbf{xxxx}\}$ of the causal characters of the coordinate ingredients of a coordinate system. The six surfaces or planes of every class $\mathbf{X_1X_2X_3X_4X_5X_6}$ are subtended respectively by the four hypersurfaces $\mathbf{x_1}$, $\mathbf{x_2}$, $\mathbf{x_3}$, $\mathbf{x_4}$ in the following order: $\mathbf{X}_1 = \mathbf{x_1} \wedge \mathbf{x_2}$, $\mathbf{X}_2 = \mathbf{x_1} \wedge \mathbf{x_3}$, $\mathbf{X}_3 = \mathbf{x_1} \wedge \mathbf{x_4}$, $\mathbf{X}_4 = \mathbf{x_2} \wedge \mathbf{x_3}$, $\mathbf{X}_5 = \mathbf{x_2} \wedge \mathbf{x_4}$, $\mathbf{X}_6 = \mathbf{x_3} \wedge \mathbf{x_4}$.

What causal classes correspond in relativity to these twelve classes? The absolute lack of intuition about the answer evidence the need of further thought on this subject: *in relativity there exist one hundred and ninety nine causal classes of coordinate systems* (Coll and Morales, 1992, Coll 2000). They are given in Table II, where now $\boldsymbol{l}$, $\mathbf{l}$ and $\mathbf{L}$ stand respectively for light-like coordinate hypersurfaces, lines and surfaces.

On these one hundred and ninety nine different ways of locating points of our neighbourhood, only *two* have been significantly considered in the literature: the "classical" one, $\{\mathbf{teee}; \mathbf{TTTEEE}; \mathbf{teee}\}$, and, for theoretical considerations, the "null" ones, $\{\mathbf{llee}; \mathbf{TLLLLE}; \mathbf{llee}\}$, associated to some radiative problems. The reference systems belonging to all the other *nine hundred and ninety seven* classes remain essentially unexplored[2] .

[1]For the notion of causal class in relativity, see (Coll and Morales, 1992).

[2]Reference systems with light-like coordinate lines were considered in Coll, 1985; for their causal duals, i.e. with light-like coordinate hypersurfaces, see Coll 2000 and also Hehl 2001.

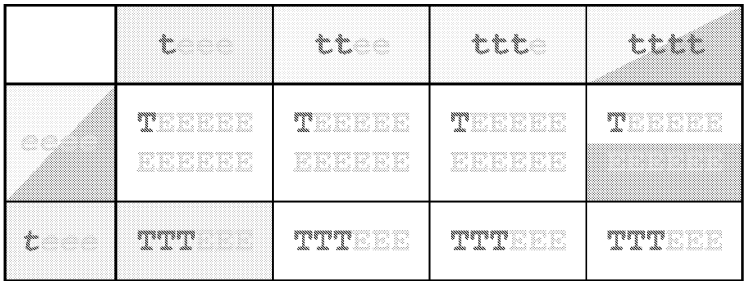

TABLE I: The twelve causal classes of reference systems of Newtonian physics.

Perhaps the origin of this sort of cultural alienation is the fact that our vision of the world is, due to many historical reasons, too polarized in the evolution point of view of the space-time. A plausible vision, of course, but a very particular one in the set of the almost two hundred other points of view... Our group *Systèmes de Référence Relativistes* of the DANOF is particularly concerned by the study of coordinate systems with potential interest in astronomy and physics, watever be their character, usual or unusual.

3. POSITIONING SYSTEMS

One of the reasons that make coordinate systems important in practice is the fact that they allow *to situate points of a region with respect to one observer* (usually located at the origin); this function gives rise to *reference systems* (resp. *reference frames*). But another important reason for their use is that they allow *to indicate to every point its position* (with respect to them); this gives rise to *positioning systems* (resp. *positioning frames*).

In Newtonian theory, coordinate systems may be constructed in such a way that both functions be simustaneously accomplished. In relativity, nevertheless, this is not possible by a sole coordinate system. Thus, in relativity we are led to consider separately both, reference systems (resp. reference frames) and positioning systems (resp. positioning frames). We are here interested in positioning systems.

In relativity, positioning systems are intended to have three important properties, namely those of being *generic*, *free* and *immediate*.

* A relativistic positioning system is *generic* for a given class of space-times if the underlying coordinate system exists in *any* space-time of this class. For example, cartesian systems are not generic but for (the class of) the sole flat space-time; harmonic systems are generic for the whole class of all space-times.

* It is *free*, or *gravity-free*, if their (physical) construction does not need the knowledge (measure) of the gravitational field (space-time metric). For example, harmonic systems are not free.

* It is *immediate* if every point of its space-time domain may know its coordinates without delay, in real time. For example, the inertial system constructed by an inertial observer by means of two-way signals is not immediate.

An important epistemic result is that the set of generic, free and immediate relativistic positioning systems constitute a little class of systems. The simplest one of the class consists of four free falling clocks (satellites) broadcasting their proper times.

The coordinate systems associated to these positioning systems are thus such that their coordinate hypersurfaces are constituted by the loci of equal proper time of every satellite. They are thus null hypersurfaces. According to Table II, all these coordinate systems belong

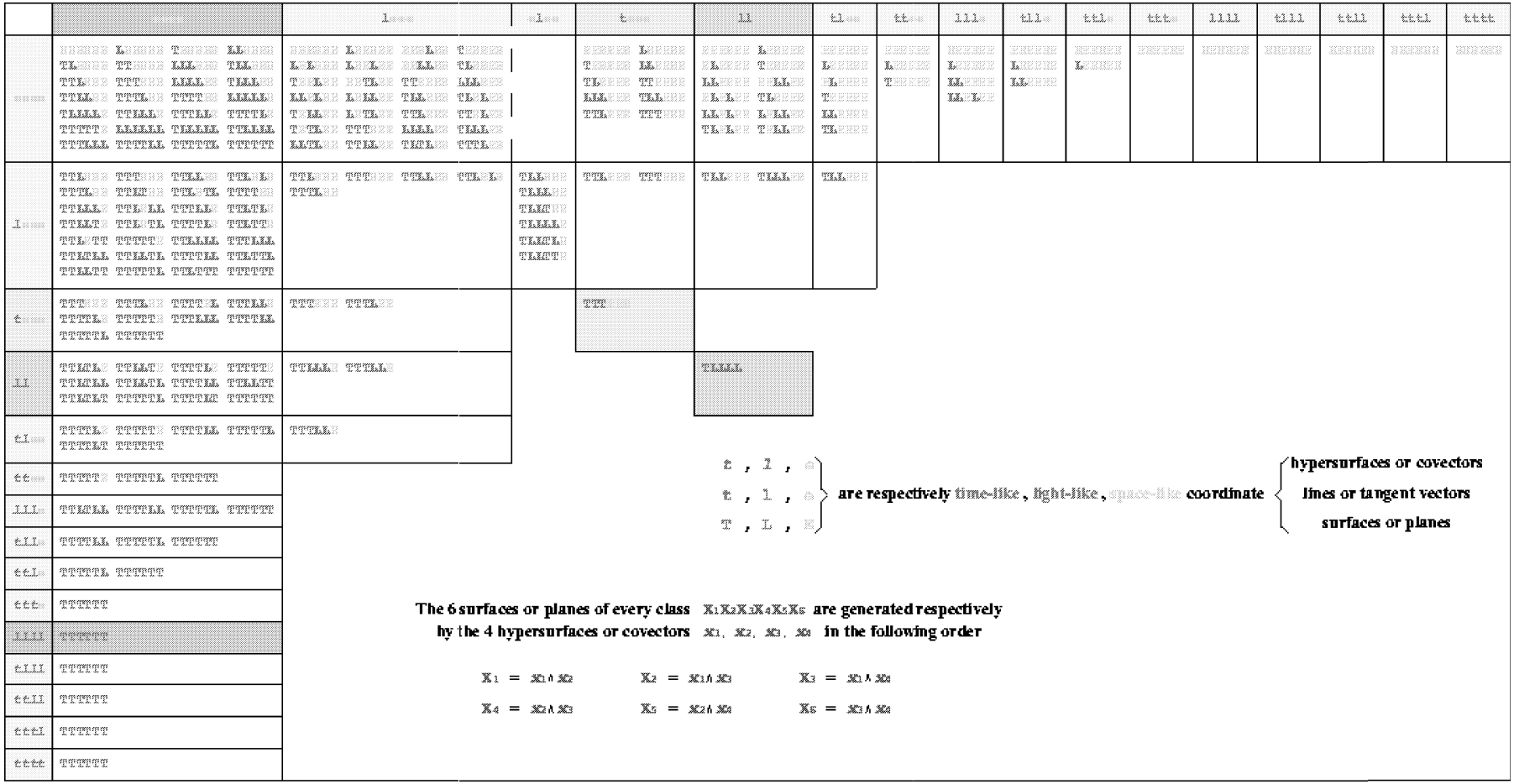

TABLE II: The 199 causal classes of reference systems of relativistic physics.

Figure 3: The location of points by an observer using two-way signals does not constitute an immediate system.

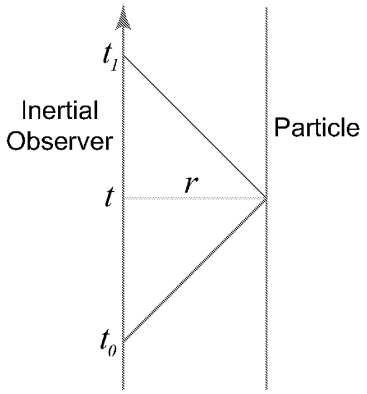

to a sole causal class, namely that of the form $\{\mathbf{llll}; \mathbf{TTTTTT}; \mathbf{eeee}\}$, a very unusual one (for them, all coordinates, like the usual time coordinate, "flow" whatever the observer). A two dimensional representation would have the aspect shown in figure 4.

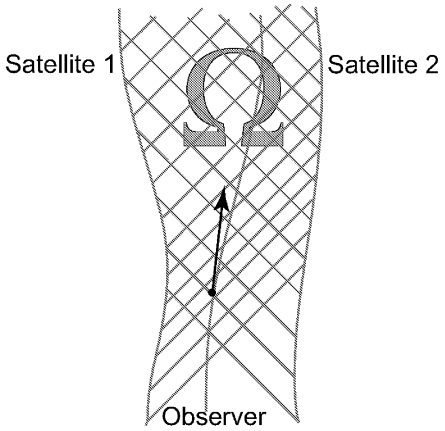

Figure 4: Two satellites broadcasting their proper time by means of electromagnetic signals constitute a relativistic positioning system

4. THE PROJECT *SYPOR*

All usual coordinate systems on the Earth are Newtonian. But constellations of satellites broadcasting their proper times are, of own right, relativistic physical systems. Rather than to flatten them directly against an approximate Newtonian model, it is better to treat conceptually them as principal objects.

The objective of the project SYPOR[3] is to endow the Earth with a relativistic positioning system. More precisely, it aims to use the constellation of satellites of the future GALILEO navigation system as an immediate, generic, free and primary relativistic positionning system for the Earth.

Every four neighbouring satellites of the constellation generate a *local chart*, the constellation defining then the *primary atlas* of local charts for the surrounding area of the Earth.

Newtonian cartographic or geocentric coordinates become in the project secondary coordinate systems, to be defined with respect to this primary atlas attached to the constellation. This defining task concerns the control segment of the navigation system, which must invert its usual reading, its function being not now to determine the position of the satellites with respect

[3]Presented at the CNES"appel à idées" of September 2001

to some terrestrial coordinates but to define these last ones with respect to the constellation of satellites.

In order to complete the primary character of the constellation, one has i) to endow every satellite with a device sending its proper time to the neighbouring satellites (autonomy of control and internal conformation), ii) to endow at least four satellites of a device for orientation with respect to the ICRF (autonomy of control and external orientation), and iii) to endow every satellite of a device broadcasting over the Earth its *proper coordinates*, i.e. not only its proper time, but the proper times received from the neighboring satellites (guarantee of *public character*, defining completely the system and allowing authorized users to evaluate the precision of the system at every instant).

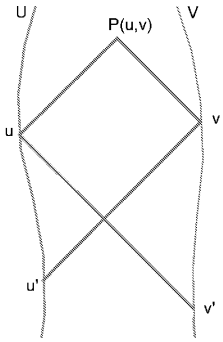

Figure 5: For any observer receiving the coordinates of the satellites, the reference frame is completely defined.

Finally, to close this survey, we shall present a two-dimensional simplified version of the complete definition of the system. In the coordinate system $\{u, v\}$ generated by the proper times of the satellites U and V, any observer receives at every instant (u, v) of its trayectory, the coordinates (u, v') of U and the coordinates (v, u') of V. These sets of values up to the instant P define, in the coordinate system $\{u, v\}$, the trayectories $\Phi(u, v) = 0$ and $\Psi(u, v) = 0$ of the satellites U and V respectively. One can then show the following result:

Theorem (Coll-Morales-Tarantola): *In a two-dimensional space-time, let U and V be two arbitrary satellites emitting respectively their proper times u and v and their reciprocal ones u' and v'. Let $\Phi = 0$ and $\Psi = 0$ be respectively the equations of their trayectories, obtained from the sent data. Then, in the coordinate system $\{u, v\}$ so generated, the space-time metric tensor g is given by*

$$g \;=\; \frac{1}{2}\,\Phi'_u\,\Psi'_v\,du \otimes dv \;.$$

This information is all what one can expect to know from a primary system of coordinates, so it is complete. Observe that, in terms of these proper times u and v, the expression is independent not only of the velocities of the satellites in their constellation (relative velocities), but also of the velocity of the user with respect to the constellation.

5. REFERENCES

Blagojević, M., Garecki, J., Hehl, F.W., Obukhov, Yu. N. (2001), Real null coframes in general relativity and GPS type coordinates, to appear in Phys. Rev.,; also in http://fr.arxiv.org, gr-qc/0110078 .

Coll, B. (1985), in *Trobades Cientifiques de la Mediterranea*, Actes dels ERE 85, Servei de Pub. de l'E.T.S.E.I.B., Barcelona, p. 29-38; English translation in http://coll.cc .

Coll, B. (2001), in Reference Frames and Gravitomagnetism, Proc. of the Spanish Relativistic Meeting EREs 2000, World Scientific p 53-65; also in http://coll.cc .

Coll, B. & Morales, J. A. (1992), Int. Jour. Theo. Phys., **31**, p 1045-62.

RELATIVISTIC THEORY OF TIME AND FREQUENCY TRANSFERS USING THE SYNGE'S WORLD-FUNCTION

P. TEYSSANDIER
SYRTE/UMR 8630-CNRS
Observatoire de Paris, 61 avenue de l'Observatoire, F-75014 Paris, France
E-mail: pierre.teyssandier@obspm.fr

B. LINET
Laboratoire de Mathématiques et Physique Théorique, UMR 6083-CNRS
Université François Rabelais, F-37200 Tours, France
E-mail: linet@celfi.phys.univ-tours.fr

ABSTRACT. We outline a general procedure to determine the influence of the mass and spin multipoles on the time and frequency transfers in the gravitational field of an isolated, axisymmetric rotating body. Our method is based on the world-function, as developed by Synge in general relativity.

1. INTRODUCTION

In recent years, it has appeared that significant improvements in the accuracy of time-keeping could be realized by installing laser cooled atomic clocks in space (Spallicci et al. 1997). For instance, for ESA's ACES mission, the expected time-keeping accuracy is about 10^{-16} in fractional frequency. Then a fully relativistic treatment of time and frequency transfers between a satellite and a terrestrial station is necessary. An almost complete general-relativistic theory have been recently extended up to the order $1/c^3$ in (Blanchet et al. 2001), justifying the results previously given in (Ashby 1998) without a detailed calculation. In (Blanchet et al. 2001), however, some terms in $1/c^3$ due to the quadrupole moment J_2 of the Earth are not calculated in detail and the effects in $1/c^4$ due to the intrinsic angular momentum of the Earth are only the subject of a rough estimate. Furthermore, the problems are treated within the limited framework of general relativity, thus preventing a thorough discussion of new tests of gravitational theories.

Our main purpose here is to outline a procedure enabling to determine systematically the influence of the mass and spin multipole moments of an axisymmetric, rotating body on the time/frequency transfers. Detailed calculations for the mass, the quadrupole moment and the intrinsic angular momentum will be given in (Linet and Teyssandier 2002).

Our results are established within the weak-field, post-Newtonian approximation of the metric theories of gravity, using the ten-parameter Nordtvedt-Will PPN formalism (Will 1981). We assume that the photons ensuring the transfers follow null geodesics. We suppose that space-time is covered by a global quasi-Cartesian coordinate system $(x^\mu) = (ct, \mathbf{x})$. The metric $g_{\mu\nu}$ is assumed to be stationary. The signature is $(+ - - -)$.

In order to perform the calculation of the time and frequency transfers between two points $x_A = (ct_A, \mathbf{x}_A)$ and $x_B = (ct_B, \mathbf{x}_B)$ connected by a light ray, we have to solve the following problems:

i) to calculate the coordinate time transfer $t_B - t_A$ as a function of $\mathbf{x}_A$ and $\mathbf{x}_B$;

ii) to determine the vectors tangent to the light ray at x_A and x_B. Solving this latter problem is indeed indispensable to calculate the frequency shift between x_A and x_B.

The methods generally employed to study the problems related to the propagation of light in a gravitational field require the solution of the null geodesic equations: see, e.g., (Klioner 1991, Kopeikin 1997, Kopeikin and Schäfer 1999, Kopeikin and Mashhoon 2001) for investigations in the linearized, weak-field limit of general relativity. However, the method of the world-function developed in (Synge 1964) spares the trouble of integrating the geodesic equations and constitutes a powerful tool to determine the time transfer and the frequency shift between two points in space-time. This is this method that we use here. It is noteworthy that the world-function would also be very convenient for modelling space missions devoted to measuring astrometric positions and parallaxes with a very high accuracy, like DIVA (Bastian et al. 1996) or GAIA (Perryman et al. 2001).

2. THE WORLD-FUNCTION $\Omega(x_A, x_B)$

Consider two points x_A and x_B in an arbitrary space-time. We assume that x_A and x_B are connected by a single geodesic path Γ. The Synge's world-function is defined by $\Omega(x_A, x_B) = \frac{1}{2}\varepsilon[s_{AB}]^2$, where s_{AB} is the geodesic distance between x_A and x_B and $\varepsilon = 1, 0, -1$ for timelike, null and spacelike geodesics, respectively.

The utility of the world-function for our purpose comes from the two following properties.

i) Two points x_A and x_B are linked by a light ray if and only if the condition

$$\Omega(x_A, x_B) = 0 \tag{1}$$

holds. The time transfer can therefore be determined when $\Omega(x_A, x_B)$ is known, since we can obtain $x_B^0 - x_A^0$ as a function of x_A^0, $\mathbf{x}_A$ and $\mathbf{x}_B$ from (1).

ii) The covariant components of the vector $p^\alpha = dx^\alpha/d\lambda$ tangent to the geodesic Γ at the points x_A and x_B are respectively given by

$$(p_\alpha)_A \equiv \left(g_{\alpha\beta}\frac{dx^\beta}{d\lambda}\right)_A = -\frac{\partial\Omega}{\partial x_A^\alpha}\,, \quad (p_\alpha)_B \equiv \left(g_{\alpha\beta}\frac{dx^\beta}{d\lambda}\right)_B = \frac{\partial\Omega}{\partial x_B^\alpha}\,, \tag{2}$$

where λ is any affine parameter of Γ such that $\lambda_B - \lambda_A = 1$.

Thus, if $\Omega(x_A, x_B)$ is known, the vectors tangent to the geodesic Γ connecting two points x_A and x_B can be calculated at x_A and x_B without integrating the differential equations of the geodesic curves.

In this paper, we restrict our attention to stationary space-times. The world-function is then of the form $\Omega(x_B^0 - x_A^0, \mathbf{x}_A, \mathbf{x}_B)$ and condition (1) may be equivalently written as a formula giving the coordinate time transfer

$$t_B - t_A = \pm\,\mathcal{T}^{\pm}(\mathbf{x}_A, \mathbf{x}_B)\,, \tag{3}$$

where the sign + (resp. −) corresponds to a photon travelling from $\mathbf{x}_A$ to $\mathbf{x}_B$ (resp. $\mathbf{x}_B$ to $\mathbf{x}_A$). We call $\mathcal{T}^{\pm}$ the time transfer function. It is worth noticing that $\mathcal{T}^{-}(\mathbf{x}_A, \mathbf{x}_B) = \mathcal{T}^{+}(\mathbf{x}_B, \mathbf{x}_A)$.

It is easily seen that the 4-vectors defined by their covariant components

$$(l_0^{\pm})_A = 1, \quad (l_i^{\pm})_A = \pm c \frac{\partial}{\partial x_A^i} \mathcal{T}_{\pm}(\mathbf{x}_A, \mathbf{x}_B)\,, \tag{4}$$

$$(l_0^{\pm})_B = 1, \quad (l_i^{\pm})_B = \mp c \frac{\partial}{\partial x_B^i} \mathcal{T}_{\pm}(\mathbf{x}_A, \mathbf{x}_B) \tag{5}$$

are tangent to the light ray at x_A and at x_B, respectively . Furthermore, these tangent vectors correspond to an affine parameter such that $l_0^{\pm} = 1$ along the ray.

The time transfer function $\mathcal{T}^{\pm}(x_A, x_B)$ is clearly involved in the determination of the frequency shift of an electromagnetic signal between a source located at x_A and a receiver located at x_B. Indeed, denote by ν_A the proper frequency of the source moving with the unit 4-velocity $u_A^{\mu} = (dx^{\mu}/ds)_A$ and by ν_B the frequency as measured by the receiver moving with the unit 4-velocity $u_B^{\mu} = (dx^{\mu}/ds)_B$. One has the well-known formula (Synge 1964)

$$\frac{\nu_A}{\nu_B} = \frac{u_A^{\mu}\,(l_{\mu}^{+})_A}{u_B^{\mu}\,(l_{\mu}^{+})_B}\,, \tag{6}$$

where $(l_{\mu}^{+})_A$ and $(l_{\mu}^{+})_B$ are given by Eqs. (4) and (5), respectively.

3. ISOLATED, AXISYMMETRIC ROTATING BODY

We consider here the gravitational field of an isolated, axisymmetric rotating body. We assume that the matter constituting the body is a perfect fluid in a stationary state. We use the Nordtvedt-Will post-Newtonian formalism (Will 1981) involving ten parameters $\beta, \gamma, \xi, \alpha_1, ..., \zeta_4$. We suppose that the quasi-Cartesian coordinate system covering space-time is a non rotating one. The center of mass O is taken as origin of the spatial axes and is assumed to move with a constant velocity $\mathbf{v}_r$ [4] relative to the universe rest frame. We choose the axis of symmetry as the x^3-axis and we assume that the body is slowly spinning around Ox^3 with a constant angular velocity $\boldsymbol{\omega}$, so that the coordinate velocity $\mathbf{v} = d\mathbf{x}/dt$ of an element of the fluid is given by $\mathbf{v}(\mathbf{x}) = \boldsymbol{\omega} \times \mathbf{x}$.

Then, with a convenient choice of the gauge, the metric reads at the order $1/c^3$

$$g_{00} = 1 - \frac{2}{c^2} U + O(4)\,, \quad g_{ij} = -\left(1 + \frac{2\gamma}{c^2} U\right) \delta_{ij} + O(4)\,, \tag{7}$$

$$\{g_{0i}\} = \frac{2}{c^3}\left[(\gamma + 1 + \frac{1}{4}\alpha_1)\mathbf{W} + \frac{1}{4}\alpha_1 \mathbf{v}_r\, U\right] + O(5)\,, \tag{8}$$

where U and $\mathbf{W}$ respectively obey the equations

$$\nabla^2 U = -4\pi G \rho^*\,, \quad \nabla^2 \mathbf{W} = -4\pi G \rho^* \boldsymbol{\omega} \times \mathbf{x}\,, \tag{9}$$

G being the Newtonian gravitational constant and ρ^* the conserved mass density [5].

Since all the $O(2)$ and $O(3)$ perturbations of the metric are linear in G, the world-function $\Omega(x_A, x_B)$ may be written up to the order $1/c^3$ in the form found by Synge in the linearized, post-Minkowskian approximation (Synge 1964). Putting $\mathbf{R}_{AB} = \mathbf{x}_B - \mathbf{x}_A$ and $R_{AB} = |\mathbf{R}_{AB}|$,

[4] This velocity is denoted by $\mathbf{w}$ in (Will 1981).

[5] See (Will 1981). Note that the Newtonian-like potential U differs from the potential W used in the more general work (Linet and Teyssandier 2002) only by terms of order $1/c^2$.

we get

$$\Omega(x_A, x_B) = \frac{1}{2}\left[(x_B^0 - x_A^0)^2 - R_{AB}^2\right] + \Omega^{(1)}(x_A, x_B) + O(4)\,, \tag{10}$$

where the perturbation $\Omega^{(1)}(x_A, x_B)$ may be written as

$$\Omega^{(1)}(x_A, x_B) = \Omega_U^{(1)}(x_A, x_B) + \Omega_{\mathbf{W}}^{(1)}(x_A, x_B) + \Omega_{\mathbf{v}_r}^{(1)}(x_A, x_B)\,, \tag{11}$$

with

$$\Omega_U^{(1)}(x_A, x_B) = -\frac{1}{c^2}\left[(x_B^0 - x_A^0)^2 + \gamma R_{AB}^2\right]\int_0^1 U(\mathbf{x}(\lambda))d\lambda\,, \tag{12}$$

$$\Omega_{\mathbf{W}}^{(1)}(x_A, x_B) = \frac{2}{c^3}(\gamma + 1 + \frac{1}{4}\alpha_1)(x_B^0 - x_A^0)\mathbf{R}_{AB}\cdot\int_0^1 \mathbf{W}(\mathbf{x}(\lambda))d\lambda\,, \tag{13}$$

$$\Omega_{\mathbf{v}_r}^{(1)}(x_A, x_B) = \frac{1}{2c^3}\alpha_1(x_B^0 - x_A^0)(\mathbf{R}_{AB}\cdot\mathbf{v}_r)\int_0^1 U(\mathbf{x}(\lambda))d\lambda\,, \tag{14}$$

the integrals being taken along the curve $\mathbf{x}(\lambda) = (\mathbf{x}_B - \mathbf{x}_A)\lambda + \mathbf{x}_A$, $0 \leq \lambda \leq 1$.

¿From (10)-(14), we get the following expression for the time transfer function defined by (3):

$$\mathcal{T}_{\pm}(\mathbf{x}_A, \mathbf{x}_B) = \frac{1}{c}R_{AB} + \frac{1}{c^3}(\gamma + 1)R_{AB}\int_0^1 U(\mathbf{x}(\lambda))d\lambda \tag{15}$$
$$\mp\frac{2}{c^4}\mathbf{R}_{AB}\cdot\left[(\gamma + 1 + \frac{1}{4}\alpha_1)\int_0^1 \mathbf{W}(\mathbf{x}(\lambda))d\lambda + \frac{1}{4}\alpha_1\mathbf{v}_r\int_0^1 U(\mathbf{x}(\lambda))d\lambda\right] + O(5)\,.$$

Using a method of integration developed in (Buchdahl 1979), we find that the integrals in (12)-(14) may be written as

$$\int_0^1 U(\mathbf{x}(\lambda))d\lambda = G\int\rho^*(\mathbf{x}')F(\mathbf{x}', \mathbf{x}_A, \mathbf{x}_B)d^3\mathbf{x}'\,, \tag{16}$$

$$\int_0^1 \mathbf{W}((\mathbf{x})(\lambda))d\lambda = G\int\rho^*(\mathbf{x}')F(\mathbf{x}', \mathbf{x}_A, \mathbf{x}_B)\boldsymbol{\omega}\times\mathbf{x}'d^3\mathbf{x}'\,, \tag{17}$$

where $F(\mathbf{x}, \mathbf{x}_A, \mathbf{x}_B)$ is a kernel function defined by

$$F(\mathbf{x}, \mathbf{x}_A, \mathbf{x}_B) = \frac{1}{R_{AB}}\ln\left(\frac{|\,\mathbf{x} - \mathbf{x}_A\,| + |\,\mathbf{x} - \mathbf{x}_B\,| + R_{AB}}{|\,\mathbf{x} - \mathbf{x}_A\,| + |\,\mathbf{x} - \mathbf{x}_B\,| - R_{AB}}\right)\,. \tag{18}$$

In what follows, we put $r = |\mathbf{x}|$ and we call θ the angle between $\mathbf{x}$ and Ox^3. We denote by r_e the radius of the smallest sphere centered on O and containing the body (for celestial bodies, r_e is the equatorial radius). Since we use the multipole expansions of the potentials to determine the r.h.s. of (16) and (17) outside the body, we suppose that all points $\mathbf{x}$ of the straight line joining $\mathbf{x}_A$ and $\mathbf{x}_B$ are such that $|\mathbf{x}| > r_e$.

When $r > r_e$, U and $\mathbf{W}$ may be respectively expanded in multipole series of the form

$$U(\mathbf{x}) = \frac{GM}{r}\left[1 - \sum_{n=2}^{\infty} J_n\left(\frac{r_e}{r}\right)^n P_n(\cos\theta)\right]\,, \tag{19}$$

$$\mathbf{W}(\mathbf{x}) = \frac{G\mathbf{S}\times\mathbf{x}}{2r^3}\left[1 - \sum_{n=1}^{\infty} K_n\left(\frac{r_e}{r}\right)^n P'_{n+1}(\cos\theta)\right]\,. \tag{20}$$

Here the P_n's are Legendre polynomials; $M = \int\rho^*(\mathbf{x}')d^3\mathbf{x}'$ is the sum of the rest masses of the particles constituting the perfect fluid; coefficients J_n are Newtonian-like mass multipole

moments; $\mathbf{S}$ is the intrinsic angular momentum of the rotating body ($\mathbf{S} = I\boldsymbol{\omega}$, I being the momentum of inertia about the x^3-axis); coefficients K_n coincide up to $1/c^2$ terms with the spin multimole moments introduced and calculated in (Teyssandier 1977 and 1978). Note that $M, ..., J_n, ..., \mathbf{S}, ..., K_n, ...$ correspond up to terms of order $1/c^2$ to generalized Blanchet-Damour multipole moments (Blanchet and Damour 1989, Damour, Soffel and Xu 1991).

We show elsewhere (Linet and Teyssandier 2002) that (16) and (17) may be respectively written as

$$\int_0^1 U(\mathbf{x}(\lambda))d\lambda = GM\left[1 - \sum_{n=2}^{\infty} \frac{1}{n!} J_n r_e^n \frac{\partial^n}{\partial z^n}\right] F(\mathbf{x}, \mathbf{x}_A, \mathbf{x}_B)\Big|_{\mathbf{x}=0}, \tag{21}$$

$$\int_0^1 \mathbf{W}(\mathbf{x}(\lambda))d\lambda = -\frac{1}{2} G\mathbf{S} \times \nabla\left[1 - \sum_{n=1}^{\infty} \frac{1}{n!} K_n r_e^n \frac{\partial^n}{\partial z^n}\right] F(\mathbf{x}, \mathbf{x}_A, \mathbf{x}_B)\Big|_{\mathbf{x}=0}. \tag{22}$$

Inserting (21) and (22) in (12)-(14) and (15) yields the multipole structure of the world-function and of the time transfer function, respectively.

Thus, the explicit calculation of the influence of the mass and spin multipole moments on the time and frequency transfers comes down to straightforward differentiations of the kernel function defined by (18).

3. REFERENCES

Spallicci, A. et al. 1997, Class. Quantum Grav. **14**, 2971.
Blanchet, L., Salomon, C., Teyssandier, P. and Wolf, P. 2001, Astron. Astrophys. **370**, 320.
Ashby, N. 1998, IEEE International Frequency Control Symposium, 320.
Linet, B. and Teyssandier, P. 2002, in preparation.
Will, C.M. 1981, *Theory and Experiment in Gravitational Physics* (Cambridge University Press).
Klioner, S.A. 1991, Sov. Astron. **35**, 523.
Kopeikin, S.M. 1997, J. Math. Phys. **38**, 2587.
Kopeikin, S.M. and Schäfer, G. 1999, Phys. Rev. D **60**, 124002.
Kopeikin, S.M. and Mashhoon, B. 2001, *preprint* gr-qc/0110101.
Synge, J.L. 1964, *Relativity: The General Theory* (North-Holland).
Bastian, U. et al. 1996, Astron. Nachr. **317**, 281.
Perryman, M.A.C et al. 2001, Astron. Astrophys. **369**, 339.
Buchdahl, H.A. 1979, Aust. J. Phys. **32**, 405.
Teyssandier, P. 1977, Phys. Rev. D **16**, 946.
Teyssandier, P. 1978, Phys. Rev. D **18**, 1037.
Blanchet, L. and Damour, T. 1989, Ann. Inst. H. Poincaré Phys. Théor. **50**, 377.
Damour, T., Soffel, M. and Xu, C. 1991, Phys. Rev. D **43**, 3273.

TIME BASED ON EARTH ROTATION

P. M. MATHEWS
Department of Theoretical Physics, University of Madras
Guindy Campus, Chennai 600025, India
e-mail: mathews@imsc.ernet.in

ABSTRACT. We examine the expression for the Earth's instantaneous angular velocity vector in terms of the Earth orientation parameters employed in the characterization of the transformation between the celestial and terrestrial reference frames, and confirm that the stellar angle, on which the definition of UT1 recently adopted by the IAU is based, is indeed the time integral of the component of the angular velocity vector in the direction of the Celestial Intermediate Pole (CIP). We consider also a different conceptual basis for a measure of time based on Earth rotation—a "World Time" (WT) which, unlike UT1, stays strictly in synchronism with the apparent motion of the Sun as seen from the Earth despite the precession of the Earth's axis, and is therefore most appealing as a time scale for civil use. Unlike UT1 based on the stellar angle, WT depends only on the instantaneous values of the Earth orientation parameters. It cannot, however, replace UT1, which is needed for the investigation of geophysical mechanisms responsible for variations in the Earth's rotation rate.

1. INTRODUCTION

The definition of UT1 is based on the angle through which the Earth rotates about a specified axis. Variability of the direction of the Earth's rotation axis, in space and relative to the Earth, makes it a nontrivial task to characterize precisely the most appropriate angle (about what axis? from what origin?), and to relate it to the Earth orientation parameters measured, e.g., by very long baseline interferometry (VLBI).

The definition adopted by the International Astronomical Union in 2000 relates UT1 to the stellar angle θ based on the concept of the "nonrotating origin" (Guinot, 1979) on the instantaneous equator associated with the celestial intermediate pole. In the decomposition of the transformation between the celestial and terrestrial reference frames (CRF and TRF) into polar motion, axial rotation about the CIP, and nutation-precession, θ appears in combination with s and s' of Capitaine et al. (1986), which are time integrals of quantities characterizing the paths of the CIP in the CRF and the TRF.

Possible alternative definitions of an origin have been considered and their relative merits discussed by Fukushima (2001).

However, the concept of an origin is not needed at all for expressing the Earth's angular velocity vector $\mathbf{\Omega}$ in terms of the celestial and terrestrial position coordinates (X, Y) and $(x_p, -y_p)$ of the CIP, the angle of rotation χ around the CIP, and the time derivatives of these quantities. One of our objectives here is to show explicitly, *without any reference to any origin*, that the

integral of the expression for the component of $\boldsymbol{\Omega}$ in the direction of the CIP does coincide with the stellar angle θ.

The use of an intermediate pole (the Celestial Ephemeris Pole or the recently adopted CIP) has been believed for long to be necessary for the estimation of the low frequency "polar motion" in the terrestrial frame. However, as has been shown by Mathews and Herring (2000), one could very well eliminate the intermediate pole and use the pole of the TRF itself as the reference pole (thereby making $x_p = y_p = 0$) and still estimate the polar motion from the high frequency part that would then be present in X and Y. The feasibility of such estimation has been demonstrated by Bizouard et al. (2000) from an analysis of simulated data. The stellar angle would then be simply the integral of the angular velocity component Ω_3 in the direction of the pole of the TRS which is essentially along the symmetry axis of the ellipsoidal Earth. The zonal tidal deformations and ocean tides which give rise to UT1 variations are symmetric about the third (polar) axis, and hence it is Ω_3 that is directly linked to UT1 variations. Therefore it would be most logical to use the angle θ defined as $\int \Omega_3 dt$, rather than the θ defined with reference to the CIP (a notional pole with no physical existence) as the basis for defining UT1.

A second objective of this paper is to introduce a different measure of time, also based on Earth rotation, which stays synchronized with the apparent motion of a suitably chosen celestial body in the sky (a fixed star/quasar), as viewed from the precessing, nutating, and rotating Earth. The "World Time" (WT) is obtained from the angle of rotation so defined, by taking account of the motion of the Sun relative to the fixed stars. WT would be strictly synchronous with the motion of the Sun in the sky, and a day of WT would be the interval between successive meridian crossings of the Sun. UT1, on the other hand, cannot remain in phase with the mean solar day on account of precession, as noted by Capitaine et al. (1986). It appears therefore that WT would be best suited for civilian use, while UT1 is undoubtedly the scale of choice for the study of geophysical phenomena affecting the angular velocity of Earth rotation.

2. TRANSFORMATION FROM CRF TO TRF, AND KINEMATIC RELATIONS

The transformation to the terrestrial reference frame from the space-fixed celestial one is

$$T = W^{-1}(x_p, y_p)\, R(\chi)\, S(X, Y), \tag{1}$$

where

$$W = \begin{pmatrix} 1 - x_p^2/2 & x_p y_p/2 & -x_p \\ x_p y_p/2 & 1 - y_p^2/2 & y_p \\ x_p & -y_p & 1 - (x_p^2 + y_p^2)/2 \end{pmatrix}, \qquad R = \begin{pmatrix} \cos\chi & \sin\chi & 0 \\ -\sin\chi & \cos\chi & 0 \\ 0 & 0 & 1 \end{pmatrix}, \tag{2}$$

$$S = \begin{pmatrix} 1 - FX^2 & -FXY & -X \\ -FXY & 1 - FY^2 & -Y \\ X & Y & 1 - F(X^2 + Y^2) \end{pmatrix} \tag{3}$$

with $F = (1 + Z)^{-1}$, $Z = (1 - X^2 - Y^2)^{1/2}$. The matrix S transforms the celestial frame into one with its third axis in the direction of the CIP, R rotates the transformed frame around the CIP, and W^{-1} takes the third axis of the rotated frame into the third axis of the terrestrial frame.

The kinematic relations connecting the terrestrial components of the angular velocity vector $\boldsymbol{\Omega}$ to the Earth orientation parameters are encompassed in the matrix equation

$$M = \frac{dT}{dt} T^{-1} = \left(\frac{dW^{-1}}{dt} W\right) + W^{-1} \left(\frac{dR}{dt} R^{-1}\right) W + (W^{-1} R) \left(\frac{dS}{dt} S^{-1}\right) (W^{-1} R)^{-1}, \tag{4}$$

M is the antisymmetric matrix with elements

$$M_{2,3} = \Omega_1 \equiv \Omega_0 m_1, \quad M_{3,1} = \Omega_2 \equiv \Omega_0 m_2, \quad M_{1,2} = \Omega_3 \equiv \Omega_0(1 + m_3). \tag{5}$$

On evaluating the right hand member of eq. (2), one obtains

$$\Omega_1 = L_{23} + L_{12}x_p - (1/2)(L_{23}x_p - L_{31}y_p)x_p - \dot{y}_p - (1/2)(x_p\dot{x}_p + y_p\dot{y}_p)y_p, \tag{6a}$$

$$\Omega_2 = L_{31} - L_{12}y_p + (1/2)(L_{23}x_p - L_{31}y_p)y_p - \dot{x}_p - (1/2)(x_p\dot{x}_p + y_p\dot{y}_p)x_p, \tag{6b}$$

$$\Omega_3 = L_{12}[1 - (1/2)(x_p^2 + y_p^2)] - (L_{23}x_p - L_{31}y_p) - (1/2)(y_p\dot{x}_p - x_p\dot{y}_p), \tag{6c}$$

where Ω_0 is the mean angular velocity of Earth rotation and

$$L_{23} = -L_{32} = (\dot{X} + \Delta_X)\sin\chi - (\dot{Y} + \Delta_Y)\cos\chi, \tag{7a}$$

$$L_{31} = -L_{13} = (\dot{X} + \Delta_X)\cos\chi + (\dot{Y} + \Delta_Y)\sin\chi, \tag{7b}$$

$$L_{12} = -L_{21} = \frac{d\chi}{dt} + \Delta_3, \tag{7c}$$

with

$$\Delta_X = X(X\dot{X} + Y\dot{Y}), \quad \Delta_Y = Y(X\dot{X} + Y\dot{Y}), \quad \Delta_3 = (Y\dot{X} - X\dot{Y})/(1 + Z). \tag{8}$$

3. ANGULAR VELOCITY AND THE STELLAR ANGLE

How directly is the stellar angle related to the angular velocity?

Consider first the component $\mathbf{\Omega}\cdot\mathbf{e}$ of the angular velocity vector in the direction of the CIP. The unit vector $\mathbf{e}$ in this direction has components x_p, $-y_p$, $(1 - x_p^2 - y_p^2)^{1/2}$. Evaluation of $\mathbf{\Omega}\cdot\mathbf{e}$ with the help of eqs. (6) is then straightforward. One finds that a number of cancellations take place, leading to the end result:

$$\mathbf{\Omega}\cdot\mathbf{e} = \frac{d\chi}{dt} + \Delta_3 + \frac{1}{2}\left(y_p\frac{dx_p}{dt} - x_p\frac{dy_p}{dt}\right). \tag{9}$$

Integration of the above equation from an epoch t_0 up to t yields

$$\int_{t_0}^{t} \mathbf{\Omega}(t')\cdot\mathbf{e}(t')dt' = \chi(t) - \chi_0 + \int_{t_0}^{t}\Delta_3(t')dt' + \frac{1}{2}\int_{t_0}^{t}\left(y_p(t')\frac{dx_p(t')}{dt'} - x_p(t')\frac{dy_p(t')}{dt'}\right)dt'. \tag{10}$$

On taking note of the expression given in eq. (8) for Δ_3, one recognizes readily that the last two integrals in (10) are the quantities s and $-s'$, respectively, of Capitaine (1990). Thus

$$\int_{t_0}^{t} \mathbf{\Omega}(t')\cdot\mathbf{e}(t')dt' = \chi(t) - \chi_0 + s - s'. \tag{11}$$

To see the connection of this result with the stellar angle θ, observe that in the notation of Capitaine, the transformation from the CRF to the TRF is

$$T = W(t)R(t)NP(t), \tag{12}$$

where the quantities in (12) go over to the following quantities in (1):

$$W(t)R_3(-s') \to W^{-1}(x_p, y_p), \quad R_3(s')R(t)R_3(-c_0 - s) \to R(\chi), \quad R_3(c_0 + s)NP(t) \to S(X, Y), \tag{13}$$

where $R_i(\alpha)$ is a rotation about the ith axis through the angle α. Since $R(t)$ is $R_3(\theta)$ and our $R(\chi)$ is simply $R_3(\chi)$, it follows that

$$\chi = \theta - (s + c_0) + s'. \tag{14}$$

On comparing this result with eq. (11), we obtain explicit confirmation that the stellar angle θ is the time integral of the component of the angular velocity vector in the direction of the CIP:

$$\theta(t) = \int_{t_0}^{t} \mathbf{\Omega}(t') \cdot \mathbf{e}(t') dt' + \chi_0 + c_0. \tag{15}$$

If the pole of the TRF were used as the reference pole as proposed by Mathews and Herring (2000), eliminating the intermediate pole (CIP), then x_p and y_p would vanish, W in eq. (4) would reduce to the unit matrix, and all terms in eqs. (6) involving x_p or y_p (or either of their derivatives) would drop out. The relation (15) would simply get replaced by

$$\theta(t) = \int_{t_0}^{t} \Omega_3(t') dt' + \chi_0 + c_0. \tag{16}$$

The derivation of this result would go through exactly as before, but with the simplifications mentioned above. It is to be noted, however (Mathews and Herring, 2000) that parts with diurnal and higher frequencies will now be present in X and Y:

$$X(t) = X_0(t) + \sum_{n \neq 0} [X_n(t) \cos(n\Omega_0 t) - Y_n \sin(n\Omega_0 t)] \tag{17a},$$

$$Y(t) = Y_0(t) + \sum_{n \neq 0} [X_n(t) \sin(n\Omega_0 t) + Y_n \cos(n\Omega_0 t), \tag{17b}$$

with the spectrum of every $X_n(t)$ and $Y_n(t)$, $(n \neq 0)$, confined to low frequencies $(-\Omega_0/2$ to $\Omega_0/2)$. The roles earlier played by x_p and y_p will be mimicked now by X_1 an Y_1.

The real distinction between (15) and (16) consists in the physical significance of the angle θ. In the former case, it is the cumulative angle of rotation about an axis which has no physical existence. (In fact, inasmuch as its definition depends in an essential manner on a separation between low and high frequency components of its motion, the CIP is nonlocal in the time variable.) On the other hand, θ in (16) is the rotation about the Earth's symmetry axis, which is indeed the axis of reference for the zonal tides which give rise to UT1 variations. Therefore, it would be most logical, in principle, to use this θ in defining UT1. However, there is no possibility, at present, of computing the stellar angle defined through (16) because the procedure envisaged in the work of Mathews and Herring (2000) for representing the spectral content of the Earth orientation parameters in different spectral bands is yet to be implemented in software for the analysis of space geodetic data.

4. TIME SYNCHRONIZED TO THE MOVEMENT OF STARS IN THE SKY

For the definition of such a time scale, one needs to specify a reference star. Rather than select a particular physical object, we represent the direction of the "reference star" by the point Σ_0 in the direction of x-axis of the currently adopted CRF. Define a sidereal time by the Greenwich hour angle (GHA) of this space-fixed point. The unit vector in the direction of Σ_0 has the coordinates $(T_{1,2}, T_{1,2}, T_{1,3})$ in the terrestrial frame. So the GHA of Σ_0 is

$$(GHA)_{\Sigma_0} = -\text{arc tan}(T_{1,2}/T_{1,1}). \tag{18}$$

This angle provides a measure of time, $(GST)_{\Sigma_0}$, that directly reflects the positions of stars in the sky.

Since the transformation matrix T is expressed in terms of the EOP through eq. (1), this time measure is in terms of the *instantaneous* values of the EOP. No integration over time is involved, unlike in the case of UT1.

The solar time WT will be related to $(GHA)_{\Sigma_0}$ in the same manner as UT1 is related to the stellar angle θ.

5. REFERENCES

Bizouard, Ch., N. Capitaine, A. M. Gontier, and P. M. Mathews, 2000, Practical realization of the CEP through VLBI data processing, in Proc. Journées Systèmes de Référence Spatio-temporels 1999, p. 51, Observatoire de Paris.

Capitaine, N., 1990, The celestial pole coordinates, *Celest. Mech. Dyn. Astr.*, *48*, 127–143.

Capitaine, N., 2000, Definition of the celestial ephemeris pole and the celestial ephemeris origin, in *Proc. IAU Colloquium 180*, edited by K. J. Johnston, D. D. McCarthy, B. J. Luzum, and G. H. Kaplan, pp. 153–163, USNO, Washington, DC.

Capitaine, N., B. Guinot, and J. Souchay, 1986, *Celest. Mech.*, *39*, 283–307.

Fukushima, T., 2001, Global rotation of the nonrotating origin, *Astron. J.*, *122*, 482–486.

Guinot, B., 1979, Basic problems in the kinematics of the rotation of the Earth, in *Time and the Earth rotation*, edited by D. D. McCarthy and J. D. Pilkington, Reidel, Dordrecht.

Mathews, P. M., and T. A. Herring, 2000, On the reference pole for Earth orientation, and UT1, in *Proc. IAU Colloquium 180*, edited by K. J. Johnston, D. D. McCarthy, B. J. Luzum, and G. H. Kaplan, pp. 164–170, USNO, Washington, DC.

ULTRA STABLE CLOCKS ON BOARD THE INTERNATIONAL SPACE STATION : THE ACES PROJECT

CH. SALOMON(1), N. DIMARQ(2), A. CLAIRON(3), G. SANTARELLI(3), P. LAURENT(3), P. LEMONDE(3), P. UHRICH(3), L.G. BERNIER(4), G. BUSCA(4), P. THOMANN(4), E. SAMAIN(5), P. WOLF(6), F. GONZALEZ(7), PH. GUILLEMOT(7), S. LEON(7), F. NOUEL(7), C. SIRMAIN, S. FELTHAM(8)

(1) Laboratoire Kastel-Brossel
(2) Laboratoire de l'Horloge Atomique
(3) Laboratoire Primaire du Temps et des Fréquences
(4) Observatoire Cantonal de Neuchâtel
(5) Observatoire de la Côte d'Azur - CERGA
(6) Bureau International des Poids et Mesures
(7) Centre National d'Etudes Spatiales
(8) European Space Agency - ESTEC

The ACES project aims at operating a cold atom clock (PHARAO) and an hydrogen maser (SHM) on board the International Space Station. The expected clock performance are a frequency stability of 10^{-16} over 10 days and an accuracy at the level of 10^{-16}. The launch is scheduled in 2005 and the mission duration will be between 18 months and 3 years.

For characterization and utilization purposes, ACES space clocks will be compared to ground clocks with a microwave Time and Frequency (T/F) link specially designed to reach the 10^{-16} level (time stability better than 10 ps over 1 day).

The main scientific objectives of ACES concerning T/F metrology and fundamental physics will be presented : measurement of the gravitational red shift, search for possible drift of the fine structure constant, test of special relativity, improvement of atomic time scales...Detrimental effects which perturb time comparisons between distant clocks will be discussed and possible concepts for the ACES microwave links will be described.

TIME TRANSFER WITH GEODETIC GPS RECEIVERS

P. DEFRAIGNE, C. BRUYNINX
Observatoire Royal de Belgique
3, Avenue Circulaire, B-1180 Brussels, Belgium
e-mail: p.defraigne@oma.be

ABSTRACT. The classical time transfer method used to realize the TAI (International Atomic Time) is based on the common view technique, with GPS observations collected by C/A (Course Acquisition) code receivers. However, the geodetic GPS receivers have the advantage of providing additionally P (Precise) code and carrier phase data, which can be used to compare the internal receiver clocks with a very high precision. This paper presents the possibilities and limitations of the geodetic GPS receivers for time and frequency transfer applications.

1. INTRODUCTION

The International Atomic Time scale (TAI) is computed by the Bureau International des Poids et Mesures (BIPM) from a set of atomic clocks distributed in about 40 time laboratories over the world. Each laboratory 'k' maintains a local realization of UTC called UTC(k), to which all the clocks of the laboratory are reported. In order to compare remote clocks for the computation of TAI, time receivers (which are C/A code receivers) are installed in the time laboratories. These receivers are connected to the 1 pps (pulse per second) signal delivered by UTC(k), and an internal software computes, following a given procedure as recommended by the CCTF (Allan and Thomas, 1994), the clock offsets between UTC(k) and GPS time as realized by each satellite for conventional tracks appearing in the international BIPM tracking schedules. When comparing clocks located at several thousands km from each other, the precision of this technique is of a few nanoseconds.

Geodetic GPS receivers have the advantage of providing additionally P code and carrier phase data, with a noise level significantly smaller than the noise on the C/A code. However, most of these receivers do not allow a direct link between their internal clock signal and the external clock used to steer the receiver frequency. These receivers resynchronize their internal clock on GPS time after each tracking interruption, and this with an uncertainty of 1 microsecond. This induces a clock discontinuity at each tracking interruption. Some geodetic receivers, especially designed to be also suitable for time transfer, like the Ashtech Z-XII3T, are steered by an external clock frequency and synchronize their internal clock on the 1pps signal provided by the same external clock, so that the receiver internal clock is directly a mirror of the external clock. In this way, there are no clock discontinuities associated with tracking interruptions as is the case with classical geodetic receivers.

The use of geodetic receivers for time and frequency comparisons fits with the main goals of the IGS-BIPM pilot project (Ray, 1999). These are, first, to allow a comparison of frequency standards ("clocks") with higher stability than the classical common view with C/A code. A

second objective is to use GPS in order to get an improved availability of accurate time and frequency comparisons. On the one hand, the TAI has a very good long term stability, but is available only after several weeks. On the other hand, the IGS can provide with a 2-day delay a time scale with a very good short-term stability. This will be steered to TAI in order to ensure the long-term stability. This IGS time scale is realized from the IGS clock combinations, i.e. satellite and receiver clock offsets (Kouba and Springer, 2001; Senior et al., 2001), based on time transfer between IGS receiver and/or satellite clocks, and it is computed from the combination of code and phase observations. In the present study, we show the advantage of using geodetic GPS receivers like the Ashtech Z-XII3T, involved in IGS, to establish the link between the IGS clock combinations (satellite and receiver clock offsets) and TAI.

2. FREQUENCY TRANSFER USING GPS CARRIER PHASES

The noise level of the carrier phase observable is about 100 times smaller than the corresponding noise level on the code observable. For this reason, the carrier phases have been used since '80 for different geodetic applications requiring very high precision. During the last years, the potential of GPS carrier phases for time transfer was recognized and demonstrated by different authors (Overney et al., 1998, Larson et al., 1999, Bruyninx et al., 2000). The phase observable is given as

$$P_p^i = -f(\tau_p^i + \Delta t_p - \Delta t^i) + (\Phi_0^i - \Phi_{0p}) + N_p^i \tag{1}$$

where τ_p^i is the travel time (including the atmospheric effects), Δt_p and Δt^i are the receiver and satellite clock offsets, Φ_{0p} and Φ_0^i are the receiver and satellite initial phases, and N_p^i is the phase ambiguity, which is constant during one track if there is no tracking interruption. The clock offset between two receivers p and q, written as Δt_{pq}, is obtained from the single difference

$$P_p^i - P_q^i = -f(\tau_p^i - \tau_q^i + \Delta t_{pq}) + (\Phi_{0p} - \Phi_{0q}) + N_p^i - N_q^i \tag{2}$$

Due to the unknown phase ambiguities, it is not possible to determine the absolute value of Δt_{pq}. The carrier phase observable can thus only be used for frequency transfer, i.e. for the determination of the time evolution of Δt_{pq}. The absolute value of the clock offset will be determined using the code observables. A combined analysis using both carrier phase and code observations is necessary to obtain both the absolute value of the clock offset, with a precision limited by the code noise level (some nanosecond), and a very precise determination of the frequency transfer.

The comparison of very stable frequency standards over short time intervals using code observables does not give sufficiently precise results. Consequently, the stability of the frequency standards is deteriorated by this comparison technique. Recent tests have shown that the carrier phase frequency transfer allows to compare clocks with a stability of some parts in 10^{16} at a period of 1 day. This is illustrated in Figure 1 where the frequency transfer has been performed between two Hydrogen masers located in Brussels and Westerbork (about 290 km far from Brussels). The modified Allan deviation of this frequency transfer is reported in the right part of Figure 1; it corresponds exactly to the Allan deviation characterizing the Hydrogen masers. This indicates that the carrier phases are a very powerful tool for the frequency transfer between stable frequency standards because their noise level is smaller than the noise level of the clocks compared. This fits perfectly within the first goal of the IGS-BIPM pilot project as described in the introduction.

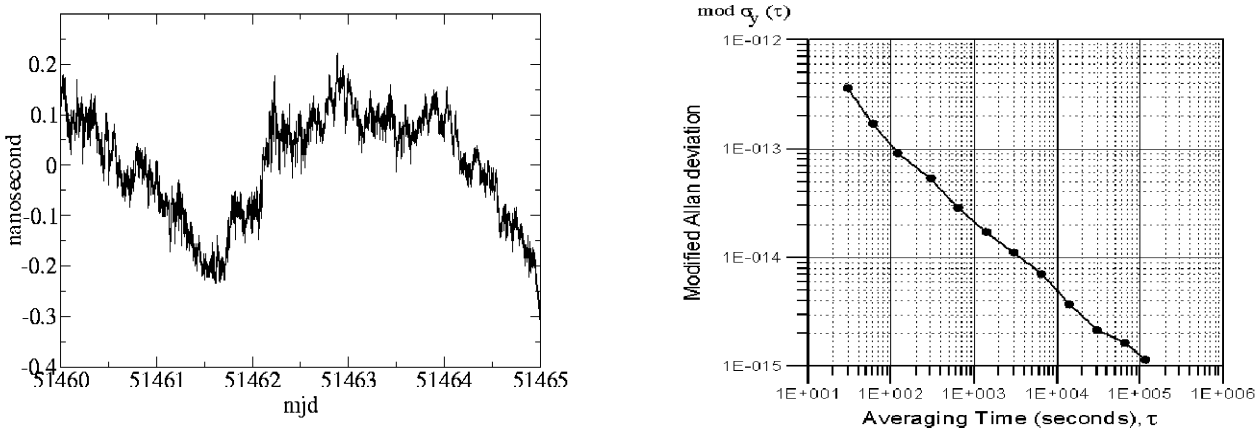

Figure 1: (left) Frequency transfer between the two Hydrogen masers located in Brussels and Westerbork, computed from carrier phase analysis. (right) Stability of the signal presented in the left part of the figure, as given by the modified Allan deviation, as a function of the averaging time.

3. LINK BETWEEN TAI AND IGS CLOCK PRODUCTS

The link between TAI and the IGS clock products can be established from time transfer between atomic clocks operating within both the IGS and time communities. Furthermore, we developed the idea to use the same GPS receiver for both applications, TAI and IGS. As explained in the introduction, most of the geodetic GPS receivers used with IGS synchronize their internal clock on GPS time, and provide a discontinuous time scale in case of tracking interruption. However, when using the Ashtech Z-XII3T, of which the internal clock is driven by an external clock frequency and is synchronized on its 1pps signal, the receiver clock will be continuous and directly linked to the external clock. So, using this receiver for time transfer applications allows a direct time transfer between the external clocks, which is not the case for the classical geodetic receivers for which the link between the receiver clock and the external clock is not constant, or even cannot be precisely determined.

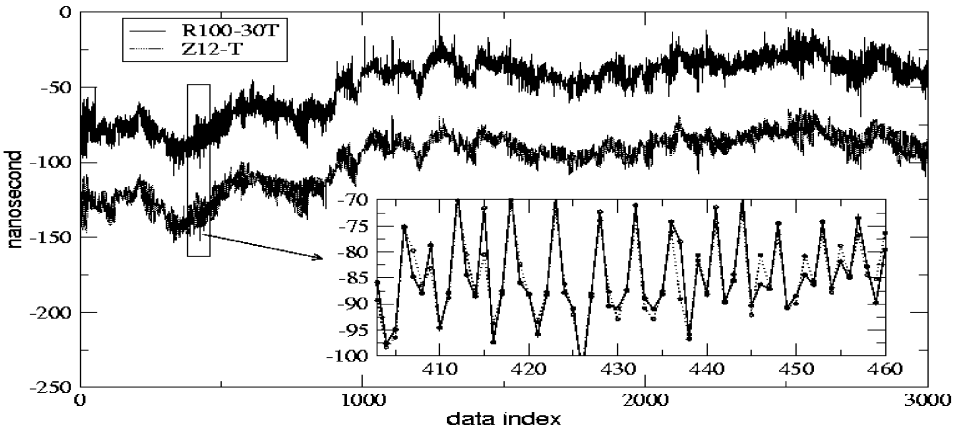

Figure 2: Figure 2. Figure 2. Comparison between the CCTF results (UTC(ORB)-GPS time) computed by the R100-30T receiver and the RINEX-based CCTF deduced from the Ashtech Z-XII3T receiver after shifting one curve by 50 ns for better visibility (only in the zoom).

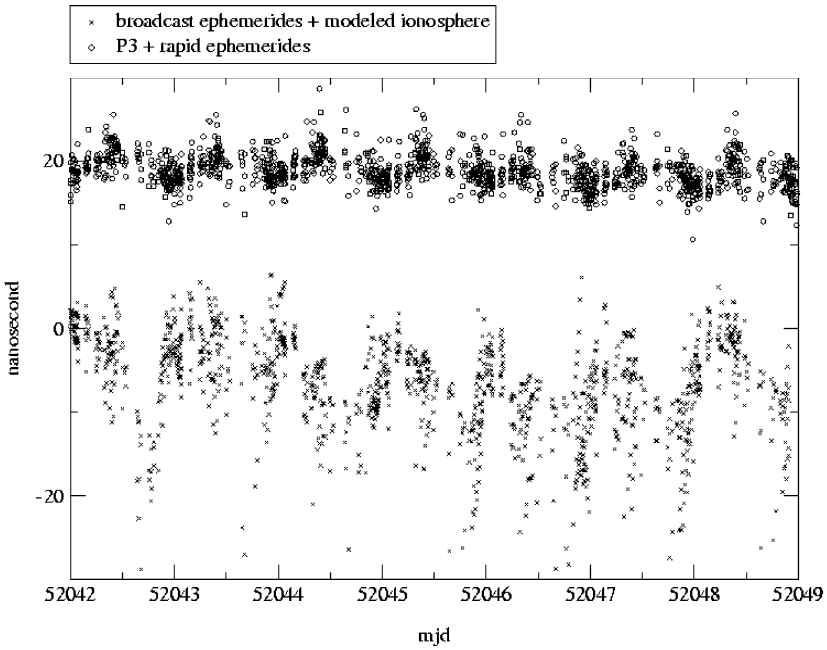

Figure 3: Figure 3. Time transfer between two hydrogen masers, located in Brussels and second at USNO (Washington), when using the classical CCTF procedure (i.e. broadcast ephemerides and broadcast ionospheric model) and when using the modified CCTF procedure, (i.e. using the P3 code and the IGS rapid orbits). The offset between the two signals has been introduced to allow better visibility.

In order to use the geodetic GPS receiver Ashtech Z-XII3T for time transfer to TAI, we developed a software (Defraigne and Bruyninx, 2001) which constructs, from the RINEX observation files, the CCTF files needed for TAI. This software follows exactly the procedure recommended by the CCTF (Allan and Thomas, 1994) for the computation of the clock offsets between UTC(k) and GPS time as realized by each satellite for conventional tracks appearing in the international BIPM tracking schedules. This procedure uses the C/A code observations, and, in order to obtain the clock offset between the laboratory clock and GPS time, corrects them for the geometric delay (computed with antenna coordinates and broadcast satellite ephemerides), ionospheric and tropospheric delays, sagnac effect, periodic relativistic effect associated with the satellite orbit, L1-L2 group delay, satellite clock offset with respect to GPS time, receiver hardware delay, antenna and local clock cable delays. Figure 2 shows the comparison between the CCTF results (corresponding to UTC(ORB)-GPS time) obtained with a time receiver R100-30T from 3S-Navigation, and with our software applied to the RINEX observation files from the geodetic GPS receiver Ashtech Z-XII3T. The differences between both are at the noise level.

We also proposed to modify the classical CCTF procedure in order to use the additional observations provided by the geodetic GPS receivers. Firstly, the P codes which are given in the RINEX files for the two GPS frequencies L1 and L2, and which are called P1 and P2, can be combined into the so-called 'ionospheric-free' code observable P3. This combination exploits the frequency dependence of the ionospheric delay in order to cancel it out. In this P3 code, the ionospheric delay is therefore absent, while the ionospheric correction proposed in the CCTF procedure for the C/A code is based the Klobuchar ionospheric model which corrects only one part of the ionospheric delay, because it cannot represent and hence correct the effects of the random part of the ionospheric activity. Secondly, we also replace the broadcast ephemerides with the "rapid orbits" as computed by IGS in differate time (after a time delay of about 2

days). Figure 3 shows the time transfer between two Hydrogen masers, the first one located Brussels and the second one located at USNO (Washington), when using the classical CCTF procedure and when using the modified CCTF procedure, i.e. using the P3 code and the IGS rapid ephemerides.

If the same receiver is involved within both IGS and TAI, we have access to its clock offset with respect to the IGS clock products and with respect to TAI. In the case of the Ashtech Z-XII3T receiver, we have therefore simultaneously the clock offset of the external clock with respect to the IGS clock products and with respect to TAI. If we apply this setup in several stations we will finally be able to determine, with very high precision, the link between the IGS clock products and the TAI.

Note that in order to know the absolute offset between these clocks and the two time scales (IGS and TAI), all the delays due to propagation of the signal inside the GPS antenna, cables and receiver must be precisely determined. This stresses the need of perfectly calibrated installations. A calibration campaign for the determination of antenna and receiver hardware delays of receivers ZXII-T is presently organized under the initiative of the BIPM (Petit et al., 2001).

4. CONCLUSIONS

We have shown that the geodetic GPS receivers are very good tools for precise frequency transfer with GPS. However, in order to determine the absolute offsets, the frequency transfer obtained from carrier phase analysis must be complemented by the code observations. The IGS time products are based on a combined analysis of code and phase observations. The link between these IGS clock products and the international atomic time scale TAI requires several calibrated IGS receivers, driven by atomic clocks also contributing to TAI.

5. REFERENCES

Allan, D.W., and C. Thomas, "Technical directives for standardization of GPS time receiver software", Metrologia 31, PP. 69-79, 1994.

Bruyninx, C., Defraigne, P., Dehant, V. and Paquet, P., "Frequency transfer using GPS acrrier phases: influence of temperature variations near the receiver", IEEE Trans. on UFFC, 47, 522-525, (2000).

Defraigne, P., and C. Bruyninx, 2001, " Time Transfer for TAI using a geodetic receiver, An Example with the Ashtech Z-XIIT", GPS Solutions, in press.

Kouba, J., and T. Springer, " New IGS Station and Satellite Clock Combination", GPS Solutions, issue 4(4), in press, 2000.

Larson, K. and Levine J., 1999, Carrier-phase time transfer, IEEE Trans. On UFFC, 46, pp. 1001-1012.

Overney, F., Prost, L., Dudle, G., Schildknecht, T., Beutler, G., Davis, J., Furlong, J. and Hetzel, P., GPS time transfer using geodetic receivers (GeTT): Results on European baselines, Proc. 12th EFTF, Milan, 1998.

Petit, G., Z. Jiang, P. Uhrich, F. Taris, "Differential calibration of Ashtech ZXII-T receivers for accurate time comparisons", Proc. 15th EFTF, pp. 164-166, 2001.

Ray, J.R., "IGS/BIPM time transfer project", GPS Solutions, 2(3), pp. 37-40, 1999.

Senior, K., Koppang, P., Matsakis, D. and Ray, J., 2001, D eveloping an IGS time scale, Proc. IEEE/EIA Int. Freq. Control Symp., 2001.

Session IV)

LOCAL, REGIONAL AND GLOBAL TERRESTRIAL FRAMES, STATION POSITIONS AND THEIR INTERPRETATION; INFLUENCE OF THE GEOPHYSICAL FLUIDS, TIDAL, OCEAN AND ATMOSPHERIC EFFECTS

Introductory papers, oral communication and posters

REPÈRES TERRESTRES LOCAUX, REGIONAUX ET GLOBAUX, POSITIONS DES STATIONS ET LEUR INTERPRÉTATION, INFLUENCE DES FLUIDES GÉOPHYSIQUES, DES MARÉES, DES OCÉANS ET DES EFFETS ATMOSPHÉRIQUES

Exposés introductifs, communications orales et posters

TIDAL EFFECTS IN GPS/GLONASS DATA PROCESSING

R. Weber[1], Carine Bruyninx, H.G. Scherneck, M. Rothacher,P.H. Andersen, T.F. Baker, T. van Dam

[1]Institute of Geodesy and Geophysics, TU-Vienna, Gusshausstr.27-29,A-1040 Vienna, Austria, email: rweber@luna.tuwien.ac.at

1. INTRODUCTION

Considering the present quality of modelling satellite orbits the microwave space-techniques GPS and GLONASS are in principle sensitive to a variety of tidal effects. This holds especially for GPS, claiming an almost unbelievable orbit precision level of about 5cm. This paper covers in principle the results of the IAG/ETC Working Sub-Group 6/4, *Solid Earth tides in space geodetic techniques-GPS/GLONASS*. We discuss the list of tidal signals which have to be considered in GNSS data processing, followed by a survey on how different Analysis Center of the IGS handle these effects. Furthermore we briefly touch upon the still unsolved problem how to treat the permanent tide and conclude with remarks on future perspectives.

2. GPS/GLONASS ORBIT MODELLING AND ORBIT CONSISTENCY

In order to achieve ultimate accuracy in processing GPS data in postprocessing or near-realtime mode it has become common practice to pick up IGS precise or rapid orbits, available at various data centers. Nowadays these ephemerides, obtained as a weighted combination of up to eight IGS Analysis Center submissions, are a quasi standard for a large number of applications. According to the Terms of Reference the ultimate goal of the IGS is 'to provide a service to support geodetic and geophysical research activities, through GPS data and data products'. All IGS products are based on tracking data from a real global permanent station network shown in figure 1.

Various improvements in GPS orbit modelling over the past years led to a current orbit precision level of a few centimeters. To evaluate the real accuracy of these ephemerides we may compare the microwave results with orbit calculations based on a different technique, in particular on laser data (two GPS satellites carry laser reflectors). Both solutions still agree at the 5cm level. This level of precision asks for taking into account a number of tidal effects and for looking very careful at the consistent handling of these effects to avoid systematic differences between the various Analysis Center solutions.

GLONASS orbits, on the other hand, are currently not of a quality comparable to the GPS ephemerides. This is caused by a less populated tracking network (about 35 stations) as well as a smaller number of satellites. Nevertheless, orbits are at the 25cm precision level but heavily constrained to the GPS frame. In the near future the situation might improve considerable because of scheduled launches of new satellites as well as new strategies in orbit modelling within the IGLOS-Pilot Project of the IGS.

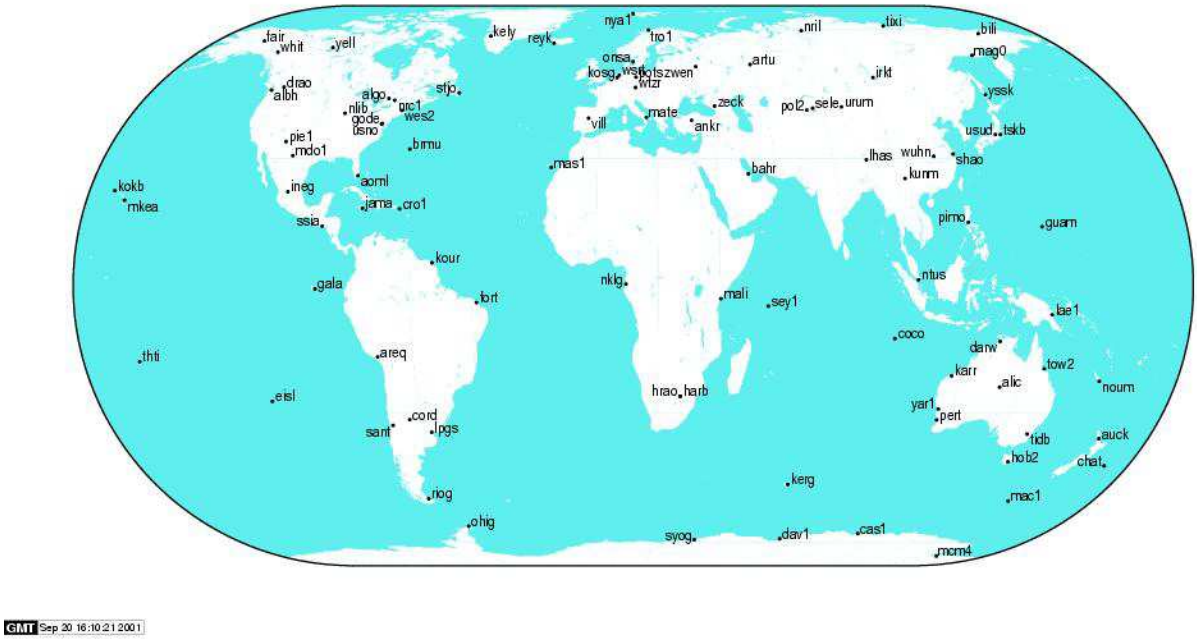

Figure 1 : IGS Global Tracking Network, status September 2001

3. TIDAL EFFECTS TO BE CONSIDERED IN THE GPS/GLONASS DATA PROCESSING

In the first place **local site displacements** due to **solid earth tides** and **ocean loading** have to be taken into account. The effect of solid earth tides is discussed extensively in (McCarthy , 1996). Application of the given equations describe the radial motion as well as the transverse diplacements at the 1mm level. A two step procedure is recommended, accounting in step one for motions by means of nominal real love numbers h and l common to all degree 2 tides. The second step corrects for the frequency dependence of these numbers (diurnal band, long periods). An improved precision demands in addition the calculation of displacements due to degree 3 tides. Movements induced by ocean loading may reach the range of a few centimeters in the vertical (Scherneck, 1996) based on the models FES94 (Le Provost et al., 1994), CSR4.0 (Eanes and Bettadpur,1999), or, alternatively GOT99.2 (Ray, 1999). Displacements are available now for almost all global stations of the IVS, ILRS, IGS, DORIS services.

Although **atmosphere loading** may cause vertical diplacements of several (up to some tens of) millimeters, an adequate correction is not applied by the IGS Analysis Centers at the moment (see list below). This goes together with the discussion about the reliability of the available models and the question at which periods the inverted/non-inverted barometer assumption for the response of the oceans due to changes in air pressure is valid.

As part of the **orbit model**, the **tidal forces** are most conveniently described as variations in the standard geopotential coefficients. The tidal contributions are expressible in terms of the potential Love number k. Modelling the solid earth tides usually starts with frequency independent Love numbers up to degree and order 3. Subsequently frequency dependent corrections are applied for

up to 34 constituents. The effects of ocean tides are also incorporated by periodic variations in the Stokes' coefficients. Coefficients used in GPS orbit modelling were obtained in most cases from the UT CSR3.0 (Eanes et al., 1996) ocean tide height model or from the model of Schwiderski (Schwiderski, 1983).

Ocean and atmosphere tides induce a motion of the coordinate frame of tracking stations of all satellite techniques relative to the Earth's center of mass. Viewed from the rigid crust-fixed frame, the motion of the coordinate system origin is known as 'geocenter-motion' and the tidal induced components as '**geocenter tides**'. Presently, these centimeter-size motions may not be seen in GPS/GLONASS analyses, thinking of the current accuracy of the orbits. However, in SLR the terms are clearly resolvable and in order to foster a uniform data processing for all techniques, these variations should be taken into account.

Ocean tides (matter and motion terms) induce variations in the axial (LOD) as well as in the equatorial **earth rotation components** (polar motion) in three frequency bands: semidiurnal, diurnal and long-periodic. The former can be monitored very precisely by satellite techniques like GPS. Apriori correction for daily and subdaily tidal variations in the Earth rotation and polar motion by means of the Ray model (Ray, 1996; 8 constituents) has become standard in IGS data processing since 1997.

See below (Table 1) an overview (extract from the analysis center log files available at the IGS Central Bureau System: Dec 2001) is given of how the different IGS analysis centers correct for tidal effects. At first glance the results of this survey look not very homogeneous, but we should keep in mind that testing and applying different models is an essential step for innovation. Also, in a few cases, this information might not mirror the current situation. An update, if necessary, has been requested by this Working Group.

	CODE	EMR	ESOC	GFZ	JPL	NOAA	SIO	USNO
Solid Earth Displacement Force	Model IERS96 nominal h_2 / l_2 0.6078/0.0847 +corrections frequ. indep. Love's Nr: $k_2 = 0.300$	Williams frequ. indep. Love's Nr: $k_2 = 0.300$	Model IERS92 nominal h_2 / l_2 0.609/0.085 $dh_2(K1)$:-0.089 frequ. depend.; Wahr model; nominal $k_2 = 0.300$	Model IERS92 nominal h_2 / l_2 0.609/0.085 $dh_2(K1)$:-0.089 frequ. depend.; Wahr model; nominal $k_2 = 0.300$	Model IERS00 nominal $k_{2(0-2)}$ 0.299/0.3/0.302 $k_{3(0-3)} = 0.093$ +34 frequ.dep. corrections	Model IERS96 nominal h_2 / l_2 0.6067/0.0844 +corrections frequ.depend.; Wahr model; nominal $k_2 = 0.300$	Model IERS92 nominal h_2 / l_2 0.609/0.085 $dh_2(K1)$:- 0.089 frequ. indep. Love's Nr: $k_2 = 0.300$	Williams nominal $k_{2(0-2)}$ 0.299/0.3/0.302 $k_{3(0-3)} = 0.093$ +34 frequ.dep. corrections
Perm. Tide Displacement Force	not removed applied	no info	no info	not removed applied	no info	not removed applied	no info	no info
Pole Tide	applied IERS96 mean m1/m2 0.033/0.331	applied	not applied	applied IERS92	applied IERS00	applied IERS96	not applied	applied
Ocean Loading Displacement Force	Scherneck UT CSR	Scherneck UT CSR	Scherneck Schwiderski	Pagiatakis Schwiderski	Scherneck UT CSR + TEG-2B data	Ray/Schrama Ray/Schrama	not applied UT CSR	Pagiatakis UT CSR + TEG-2B data
Atmosphere Loading	not applied	not applied	not applied	not applied	not applied	not applied	not applied	not applied

Table 1: Tides related part of the Analysis Strategy Summaries of the IGS ACs (December 2001)

4. TREATMENT OF THE 'PERMANENT TIDE PROBLEM' WITHIN GPS/GLONASS DATA PROCESSING

Basically, in order to allow intercomparison and combination of the solutions of different techniques the recommendation is that every technique handles the permanent tide in the same way.

The current working standard is to subtract a permanent tide from the individual ((quasi-) instantaneous) observations of the station position. The amplitude of this permanent tide displacement is governed by the elastic Love numbers at semi-diurnal frequencies. An additional simplification implies is that a spherical earth is a sufficient model for this tide and that linear superposition holds. The model taken into account contains the full effect of the solid earth tides, but using unfortunately the nominal (semidiurnal,diurnal) Love-number ($h_2 \approx 0.60$) for the secular part (instead of the secular Love-number 1.94).

A zero-tide definition including a permanent tide in a fluid approximation could be chosen to derive a physically plausible tide-free reference frame. However, no independent observation method exists which could uniquely separate the permanent tidal flattening of the earth from the rotational flattening without additional assumptions (finite elasticity in the crust for instance) which are again difficult to verify contemplating the fact that we deal with an infinite-time response.

There is a recommendation of the IAG to work on the Earth's crust. This implies, that the correction of the permanent tide should not be applied. We have to apply the nominal correction not taking into account the secular term.

If station positions have to be expressed on the 'tide-free' crust, they must be corrected for the complete response of the earth to tidal force. Thus, again we have to apply the nominal correction and afterwards account for the difference between the semidiurnal and the secular Love number. Both proposals (recommendations) are satisfying the scientific point of view but they are in conflict with the present practice.

Analysis experts insist on their 'working position', because it would be extremely dangerous to change the convention. If the transition has to be performed, each site coordinate file would have to be firmly ear-marked as to what definition is implied. Also, during the transition phase incompatible versions of analysis procedures and subroutines might coexist. Therefore, it appears viable to (continue to) stipulate the implication of a purely conventional permanent elastic tide in the computed tide displacement of a station in the reduction of space geodetic observations.

If in future more exact formulations of tide displacements come about (which would employ the frequency response method based on a harmonic expansion of the tide potential in the tradition of Doodson), we propose to

(1) exclude the zero-frequency term delivered by this method, and
(2) include instead the conventional zero-frequency term.

With sufficient accuracy, this term is

u = -0.6026 * 0.19844 * (1/2)(3\sin^2 \theta -1)
v = -0.0831* 0.19844 * (3/2)\sin(2\theta)

where u is vertical and v north displacement in meters, and theta is the geocentric latitude. The numbers in front are the basic Love numbers of the 1996 Conventions, and the second factor is the amplitude coefficient. In the IERS Standards (McCarthy, 1992) these quantities were h_2 = 0.6090, l_2 = 0.0852 and the amplitude coefficient was 0.19841.

In order not to introduce jumps in station coordinates each time the response parameters are changed, the tide model must recreate the original permanent tide.

5. THE DETERMINATION OF TIDAL PARAMETERS

Last but not least we should discuss the capability and limitations of the microwave satellite techniques to investigate tidal effects (including oceanic and atmospheric tides) and to determine tidal parameters ?

First of all we may distinguish between longer periods and the diurnal/subdiurnal band. In terms of periods of several days and more three formal approaches can be considered :

(1) Do not correct for the long period solid earth tides within the data analysis, but correct for ocean (and atmospheric) loading. Then, the 13.66 days, 27 days and one year periods will show up in the residuals. This should allow to extract information about the Love numbers for these frequencies for the solid earth tides (using the known tide generating potential).

(2) Correct in the data analysis as completely as possible for the solid earth tides (and for atmospheric loading), extract ocean loading from residuals.

(3) Correct in the data analysis as completely as possible for the solid earth tides and correct for ocean loading, extract atmospheric loading from residuals.
Preliminary results using Precise Point Positioning (PPP) as well as differencing schemes when processing regional continuous GPS networks show that atmospheric loading effects are somewhat attenuated (in Scandinavia effects are found that are a factor of three smaller than predicted using load convolution methods; the inverted barometer assumption does not seem to be the critical factor). Together with earlier results (van Dam, Herring, 1994), the resolution of atmospheric loading effects is expected at the 1-3 mm level (implying that vertical motion is better resolved than horizontal).

In terms of daily and subdaily periods we may conclude that:

(1) studying (ocean) tidal effects from a series of 2-hourly ERP values, based on 3 years of data of the global GPS network of the IGS, has shown (Rothacher et al., 2000) that tidal amplitude models, currently available from VLBI, SLR, GPS and Altimetry, agree within

$10\,\mu as$ in Polar Motion and $1\,\mu s$ in UT1.

(2) On the other hand, tides with periods close to 12 and 24 hours (S1, $\psi 1$; K1, S2, K2) seem to be biased because of orbit errors. The residual spectrum, that remains after removal of the main tidal terms contains non-tidal signals up to $50\,\mu as$ in polar motion and $3\,\mu s$ in UT1. These effects might be due to the resonance effect (12 sidereal hours revolution period of the GPS satellites) or, alternatively, due to atmospheric or oceanic normal modes. To add GLONASS data seems to be a very promising way to overcome some model deficiences. First of all, the revolution period of $11^h\ 15^m$ is not in resonance with earth rotation and, moreover, the increased orbital inclination reduces the impact of along track orbit errors on LOD estimates.

6. PERSPECTIVES

Future perspectives are of course closely tied to modelling improvements in the non-gravitational forces acting on the satellites and to tropospheric effects. Another important point is the impact of improved ocean loading tides (altimetry models) on orbits and subsequently on the ERP estimation or for the accurate determination of water vapour from GPS measurements. Advantages of analyzing data from different satellite navigation systems were discussed above. Last but not least the steady increase of available ERP and station coordinate time series involves decreasing formal errors in the derived tidal parameters.

7. REFERENCES

Baker, T.F., Curtis D.J., Dodson A.H., 1995
Ocean Tide Loading and GPS
GPS World, March, pp.54-59.

Bos,M.S., Baker T.F., 2000
Ocean tides and loading in the Nordic Seas,
Memoirs of National Institute of Polar Research (Japan), Special Issue, No.54.

Eanes R.J., S.V. Bettadpur, 1996,
The CSR 3.0 global ocean tide model,
Center for Space Research, Techn. Memorandum,CSR-TM-96-05.

Eanes R.J., S.V. Bettadpur, 1999,
The CSR 4.0 global ocean tide model

Kouba J., T. Springer, 1999
Analysis Activities,
International GPS Service; IGS Annual Report 1998, pp.13-17,
IGS Central Bureau, JPL.

Le Provost C., M. Genco, F. Lyard, P. Incent, P. Canceil, 1994,
Spectroscopy of the world ocean tides from a finite element hydrological model,
JGR, Vol. 99, pp. 24777-24798.

McCarthy D.D. (editor), 1992,
IERS Standards,
IERS Technical Note 13, Observatoire de Paris.

McCarthy D.D. (editor), 1996,
IERS Conventions,
IERS Technical Note 21, Observatoire de Paris.

Ray R.D., 1996,
Tidal Variations in the Earth's Rotation,
in 'IERS Conventions', McCarthy D.D. (editor)
IERS Technical Note 21, pp. 76-77, Observatoire de Paris.

Ray R.D., 1999,
A Global Ocean Tide Model from TOPEX/POSEIDON Altimetry:GOT99.2

NASA/TM-1999-209478; National Aeronautics and Space Administration,
Goddard Space Flight Center, Greenbelt,MD.

Rothacher M., G. Beutler, R. Weber, J. Hefty, 2000,
High Frequency Earth Rotation Variations from three Years of Global Positioning System Data,
Submitted to the Journal of Geophysical Research.

Scherneck, H.G., 1991,
A parameterized solid earth tide model and ocean tide loading effects for global geodetic baseline measurements,
Geophys. J. Int., 106, pp. 677-694.

Scherneck, H.G., 1996,
Site displacement due to ocean loading,
McCarthy D.D.(editor): IERS Technical Note 21,.pp. 52-56.

Scherneck H.-G., J.M. Johansson, F.H. Webb, 2000,
Ocean Loading Tides in GPS and Rapid Variations of the Frame Origin,
in Schwarz K.P. (editor): Geodesy beyond 2000, The Challenges of the First Decade,
IAG Symposia, Volume 121,Springer, pp. 32-40.

Schwiderski,E., 1983,
Atlas of Ocean Tidal Charts and Maps
Marine Geodesy, Vol. 6, pp.219-256

Van Dam T.M., T.A. Herring, 1994,
Detection of Atmospheric Pressure Loading using Very Long Baseline Interferometry Measurements, JGR, Vol.99, pp.4505-4517.

Van Dam T.M., G. Blewitt, M.B. Heflin, 1994,
Atmospheric Pressure Loading Effects on GPS Coordinate Determinations,
JGR, Vol.99, pp.23939-23950.

Weber R., 1999,
The Ability of the GPS to Monitor Earth Rotation Variation
in 'Acta Geodaetica et Geophysica Hungarica',
Vol. 34, Number 4, pp. 457 – 473, Akademiai Kiado, Budapest.

TIDAL VARIATIONS OF STATION COORDINATES OBSERVED IN REGIONAL GPS NETWORK

J. HEFTY
Department of Theoretical Geodesy, Slovak University of Technology
Radlinského 11, 813 68 Bratislava, Slovakia
hefty@cvt.stuba.sk

ABSTRACT. One-year interval of GPS permanent network observations in Central Europe was analyzed with intention to investigate the short-term oscillations in time series of station positions. In spectra of diurnal and semi-diurnal bands the constituents with tidal periods dominate. The relation to ocean loading effects and other phenomena is discussed.

1. INTRODUCTION

The permanent monitoring of GPS satellites allows to detect both the long-term and short-term variations of geocentric position of observing sites. While the long-term behaviour of station coordinates time series is frequently analyzed in connection with plate motions, regional geodynamics and seasonal local variations, the short-term oscillations of position are studied only rarely. One of the reasons for high-frequency variations in the observed station position could be associated with local tidal displacements. In the processing of phase GPS observations using the Bernese GPS software Version 4.2 (BV42, Hugentobler et al., 2001) the station displacements due to solid Earth tides are modeled according to the IERS Conventions (McCarthy, 1996). In this paper we will examine the time series of station coordinates with intend to detect residual short-period oscillations with tidal frequencies. The observed variations could be associated with ocean tidal loading effects (Hatanaka et al., 2001), atmospheric loading effects, local heterogeneities and non-tidal phenomena with frequencies related to tidal spectrum like troposphere and ionosphere mismodeling and orbit determination biases.

Our analysis uses one-year interval time series from routine processing of Central Europe GPS permanent network performed at Slovak University of Technology (Hefty & Kártiková, 2000). The network covers the area from Baltic Sea to Mediterranean and Black Sea. It comprises 15 sites separated from 150 to 500 km (the distribution of sites is visible on figures in parts 3 and 4 of the paper). Only the differential variations of 3D positions can be observed as the individual network solutions are referenced to one selected site (in our case Graz) with heavily constrained position. Each network solution yields independent set of coordinates of all sites. The time resolution of network solutions is 3 hours, it allows for separation of main tidal constituents in the diurnal and semi-diurnal bands.

2. REGIONAL NETWORK OF PERMANENT GPS STATIONS IN CENTRAL EUROPE

Since January 2000 is at the Slovak University of Technology (SUT) in Bratislava routinely analyzed network of selected GPS permanent stations operating in the region of Central Europe. The main reason of the analysis is preparation of time series of station coordinates suitable for geodynamical investigations in the region. The processing procedure follows the general rules adopted for EUREF Permanent Network analysis. However the main difference is that besides the daily network solutions at SUT also alternative network solutions for 3-hour intervals are performed.

The main parameters of the processing are summarized in Table 1. We will further analyze the one-year interval of data from network consisting of 15 stations. The whole period from DOY 001 to DOY 366, year 2000, was processed by the unique strategy. The only one change was in DOY 100, when the method of reduction of local troposphere effects for 3-hour intervals was altered.

Software	Bernese GPS Software Version 4.2
Celestial reference frame	Satellite orbits and satellite clocks - CODE solution, EOPs from IERS solutions
Terrestrial reference frame	ITRF97, reference point GRAZ constrained to 0.0001 m
Sampling rate of observations	30 s
Interval for coordinate estimates	Standard strategy: one set of coordinates for each 24 h UT, alternative strategy: coordinate estimates for 3 h intervals
Minimum elevation	5°
Ionosphere modeling	Regional model derived from iono-free linear combination $L3$
Troposphere modeling	Apriori model of Saastamoinen, stochastic parameters estimated from 24-hour sessions for 2-hour intervals. Troposphere handling for 3-hour coordinate estimates: Until DOY 100, troposphere parameters for 1.5-hour intervals After DOY 100, troposphere parameters taken from 24-hour solutions.
Ambiguity resolution	Each independent baseline resolved by QIF strategy, ambiguities for 3-h intervals adopted from 24-h solution
Tidally induced station displacements	Solid Earth tides according to IERS Conventions, ocean loading corrections - not introduced

Table 1: Main parameters of processing the Central European GPS permanent network at SUT Bratislava

Results of the processing are the coordinate time series transformed to Cartesian local horizontal system with North-South, West-East and Up components. The example of resulting series for the site Jozefoslaw is shown in Fig. 1. In the plotted data the long-term linear trend due to Eurasian plate motion was removed. The time series of all three coordinate components are influenced by various perturbing phenomena like individual or group outliers, seasonal and short-term variations and occasional jumps, sometimes of unknown origin. The effect of change in the troposphere modeling after DOY 100 is clearly visible. The utilization of zenith delays obtained from 24-hour processing significantly reduced the scatter in the height component. In the first step all the series were homogenised by statistical testing, excluding outliers, estimating and correcting the jumps. Finally the series were submitted to high frequency filtering using the Vondrák (1969) smoothing procedure.

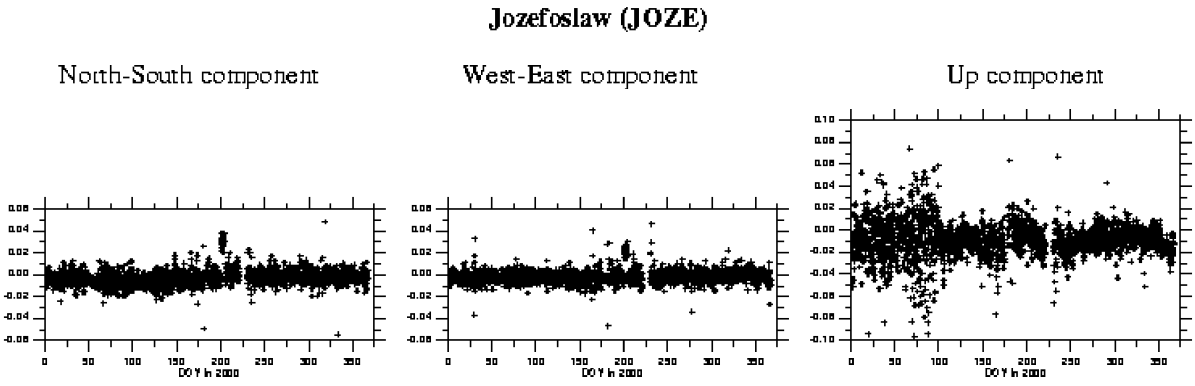

Figure 1: Time series of horizontal coordinates and height for site Jozefoslaw, linear trend due to Eurasian plate motion was removed. The y-scales are in meters.

All the other sites were treated by the same procedure. Note that the coordinate variations in the series reflect the difference between short-term oscillations of the site analyzed and the short term oscillations of the reference site Graz.

3. ANALYSIS OF TIME SERIES OF STATION COORDINATES IN DIURNAL AND SEMI-DIURNAL BANDS

The one-year intervals of three coordinates components of each of 14 sites in the network were submitted to spectral analysis (except Graz as it was kept fixed during the whole analyzed period). We applied the least-squares spectral analysis procedures because of lot gaps in the series due to observation breaks and outliers exclusions. As an example of resulting spectra we show the horizontal coordinates components of the site Borowiec. Because we are interesting in the tidal frequencies, Fig. 2 shows detailed spectra in the diurnal and semi-diurnal bands. The dominance of tidal periods is clearly visible. The main components have amplitudes from 0.5 up to 1 mm with uncertainties 0.15 mm.

Spectra of horizontal components of other sites have similar behaviour like the Borowiec site. In most of series the semi-diurnal K_2, S_2 and M_2 as well as the diurnal S_1, P_1 and O_1 dominate. We stress that the observed values represent the differential oscillations of the sites analyzed with respect to reference site Graz. The GPS observations were corrected in the course of processing with BV42 for the solid Earth's tides. So the observed effects reflects the residual variations in horizontal position due other phenomena like ocean loading effects, atmosphere loading, troposphere modeling, etc.

Fig. 3 shows distribution of horizontal amplitudes of two semi-diurnal waves S_2 and K_2. The amplitudes are obtained as combination of North-south and West-east components. We stress that S_2 and K_2 components are significant in spectra of all analyzed sites. The increase of amplitudes from Graz to marginal sites of the network is clearly visible, mainly for S_2 constituent.

In the spectra of vertical component the dominance of tidal periods is not so pronounced, the uncertainties of main tidal terms are up to 0.4 mm. It is worth to mention that the shape of the spectra of vertical component changed if only the data after DOY 100 were taking into account. Due to lower homogeneity we will not use the vertical data in further analysis in this paper.

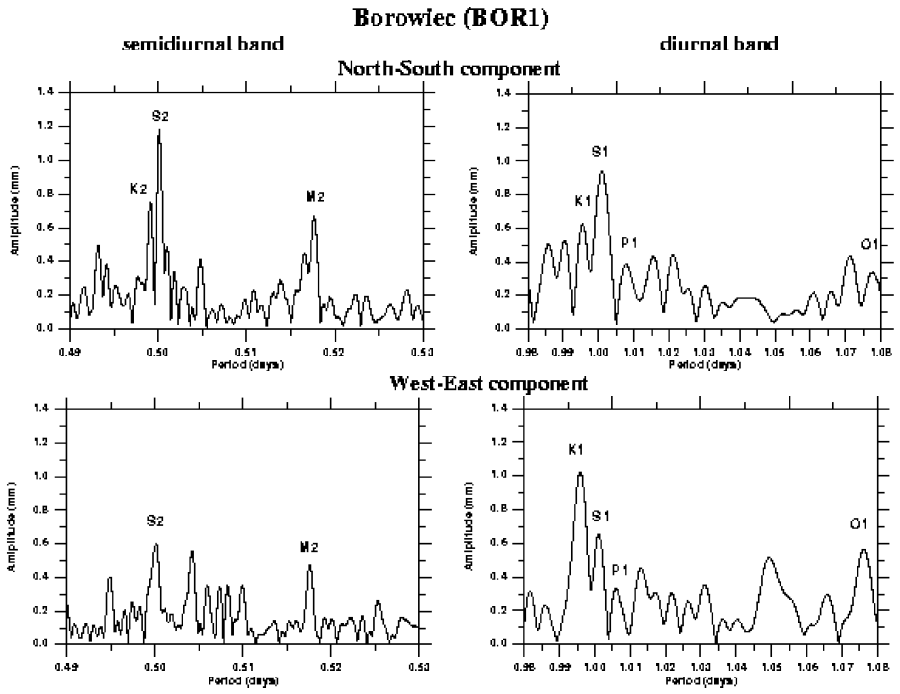

Figure 2: Spectra of Borowiec (BOR1) horizontal coordinates in semi-diurnal (left side) and diurnal (right side) bands.

4. COMPARISON OF OBSERVED VARIATIONS WITH OCEAN LOADING MODEL

The main known systematic influences not included in the processing of GPS data are the tidal ocean loading effects. We will compare the amplitudes obtained from spectral analysis of GPS time series in the above mentioned procedure, with the ocean model of Schwiderski (1981). The amplitudes and phases of diurnal and semi-diurnal tidal waves were obtained using the computation procedure for ocean loading corrections offered by Astronomical Institute of University in Berne (Schaer, 2001). Our GPS analysis reflects only the differential variations with respect to Graz. It means that also the modeled amplitudes of ocean tides have to be expressed as relative quantities to reference site Graz.

In Fig. 4 is plotted the distribution of amplitudes of M_2 tidal wave. Left side of the graph shows the GPS amplitudes and the right side the amplitudes of ocean loading. The disagreement of the two graphs is evident. The surprising fact is that the more than 4 mm amplitude predicted for Sarajevo (SRJV) is not reflected in the GPS data. Also the GPS M_2 amplitudes on other sites do not match the ocean model. Fig. 5 shows the amplitude distributions the observed GPS and modeled ocean O_1 tide. Also in this case the disagreement is clearly visible. It is worth to mention that the ocean loading amplitudes of S_2 and K_2 are negligible when comparing to observed effects in GPS data in Fig. 3.

The above mentioned results indicate that the observed up to 1.5 mm oscillations with tidal frequencies could not be associated with Schwiderski ocean loading model. The other candidates for explanation of observed variations are, besides the mismodeling of ocean tides, the non-tidal phenomena. The S_1 and S_2 could be connected with troposphere modeling, e.g. correlations of troposphere parameter estimates on close observing sites. Variations with K_1 and K_2 frequencies are closely related to orbit modeling effects and nutation representation. The most suitable for verification of ocean modeling are M_2 and O_1 frequencies, however the results in Figs 4 and 5 indicate problems with Schwiderski ocean loading model in the Central European region.

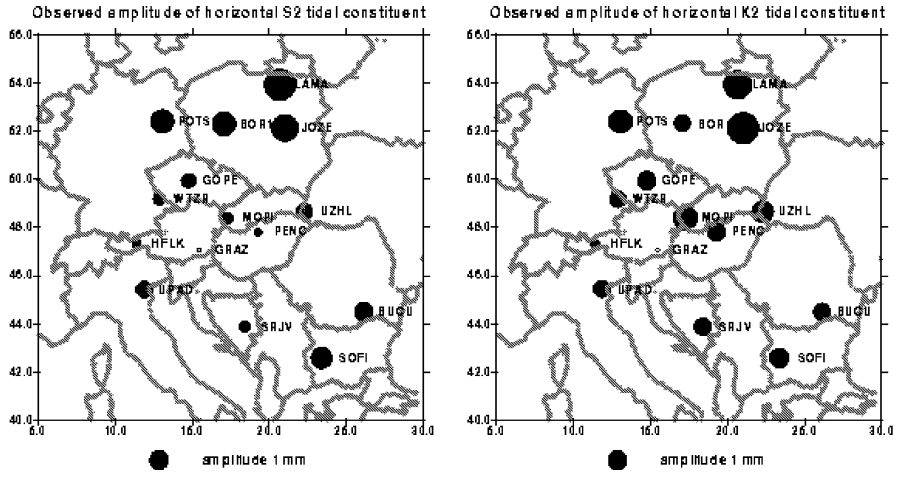

Figure 3: Observed amplitudes of horizontal constituents with semi-diurnal tidal frequencies. Left map - distribution of amplitude of S_2, right map - distribution of amplitude of K_2.

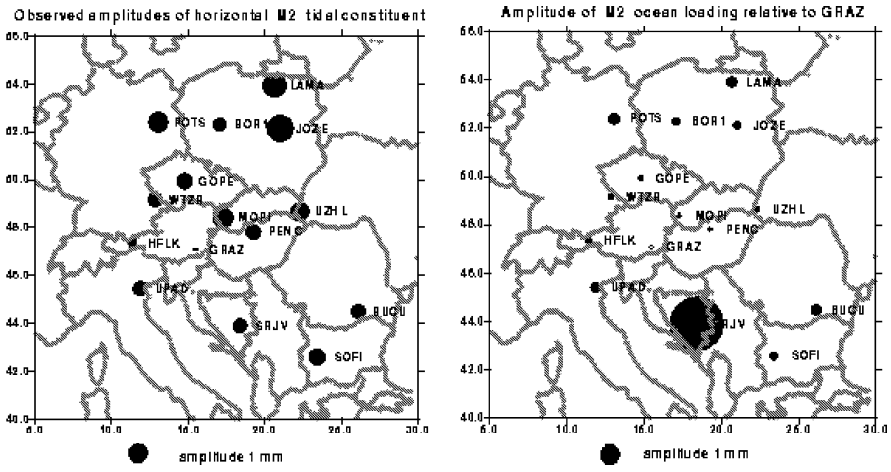

Figure 4: Amplitudes of M_2 tidal wave. Left map - distribution of GPS derived amplitudes, right map - distribution of amplitudes of ocean loading model.

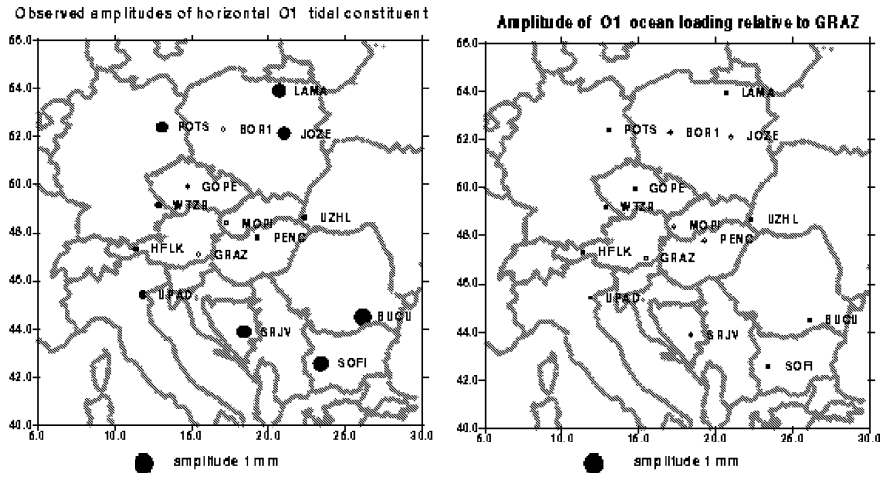

Figure 5: Amplitudes of O_1 tidal wave. Left map - distribution of GPS derived amplitudes, right map - distribution of amplitudes of ocean loading model.

5. CONCLUSIONS

We showed that the permanent regional GPS network analysis allows for experimental detection of periodic variations with tidal frequencies. One-year interval of data allowed to separate terms with up to 1.5 mm amplitudes and with 0.2 - 0.4 mm uncertainties. Due to referencing of the network solution to one selected point only the differential phenomena can be observed. Significant periodic oscillations with K_2, S_2, M_2, K_1, S_1, O_1 and P_1 were detected at most of the stations. Comparison of the observed values with ocean loading effects shows larger amplitudes than can be explained by the Schwiderski ocean model. The further research has to be concentrated on amplitude and phase estimates, indirect effects modeling, aliasing effects studies and comparisons with other tidal ocean models.

Acknowledgements: Author thanks to the Grant Agency of Slovak republic VEGA (grant No. 1/8252/01) for supporting this work.

REFERENCES

Hatanaka, Y. et al. (2001) "Detection of Tidal Loading Signal from GPS Permanent Array of GSI Japan", *Journal of the Geod. Soc. of Japan* **47**, 187-192.

Hefty, J., Kártiková, H., 2000 "The network of permanent GPS stations in Central Europe and its significance for geodynamic research and realization of geocentric reference frame". Proc. of the Institute of Geodesy and Cartography, Bratislava, (in Slovak).

Hugentobler, U., Schaer, S., Fridez, P. (eds), 2001, "Bernese GPS Software Version 4.2", Astronomical Institute, University of Berne, Berne.

McCarthy, D.D.(ed.), 1996, "IERS Conventions", IERS Technical Note 21, Observatoire de Paris, Paris.

Vondrák, J., 1969, "A contribution to the problem of smoothing observational data", *Bull. Astron.Czech.* **20**, 349-355.

Schaer, S., 2001, "Automatic service for computing BLQ tables", BSW Electronic Mail 0134. Astronomical Institute, University of Berne.

Schwiderski, E.W., 1981,"Ocean Tides. Part I. Global Ocean Tidal Equations. Part II. Hydrodynamical Interpolation Model", *Marine Geodesy* **3**, 161.

SLR STATION "GOLOSIIV-KIEV": CURRENT STATE AND ACTIVITY.

O. BOLOTINA, Yu. GLUSHCHENKO, M. MEDVEDSKIJ, M. PERETYATKO, V. SUBERLAK, D. YATSKIV.
Main Astronomical Observatory of Ukrainian National Academy of Sciences
27 Akademika Zabolotnogo St., 03680 Kyiv, Ukraine
e-mail : suberlak@mao.kiev.ua

ABSTRACT.

Satellite laser ranging station "Golosiiv-Kiev". O. Bolotina, Yu. Gluschenko, M. Medvedskij, N. Peretyatko, V. Suberlak, D. Yatskiv. Basic characteristics of the satellite laser ranging station "Golosiiv-Kiev" (SLR) are presented. The principle of operation and the field system software of the station are described. The properties of satellite tracking system and the realization of measurements calibration are indicated. The results and the analysis of observations and accuracy estimations of distance measurements are adduced. The coordinates of the SLR station reference point are improved on the basis of LAGEOS-1 and LAGEOS-2 observations for the period 24.01.2001-17.06.2001. The results of comparing of coordinates obtained with the SLR method and calculated on the basis of geodetic measurements and analysis of their differences are shown.

1. INTRODUCTION

A Satellite Laser Ranging Station "Golosiiv-Kiev" of the Main Astronomical Observatory (MAO) of the National Academy of Sciences of Ukraine was founded in 1985 for participating in ukrainian and nternational SLR networks. The station was designed for determining distances between a satellite and the station reference point (the point of the telescope axes intersection) in a uniform time scale. Due to some technical and economical problems the station was not in operation up to the 1996. The new team of researchers and engineers was organized in 1996 to put the station into the experimental operation. The experimental ranging of the satellites was started on April 1, 1997. The routine ranging are carring out since January 2000, and the results are sending to the Eurolas Data Center at DGFI.

2.INSTRUMENTATION AND BASIC CHARACTERISTICS

The SLR station "Golosiiv-Kiev" general block-scheme is shown on the Fig. 1. Its main systems are:

- laser
- transmitting–receiving system:
  - photodetectors of transmitted–received signals.
  - subsystem of the optical martching of the telescope with the laser and the photodetectors;
- operation system of the telescope:
  - telescope,
  - step-motor drivers,
  - position sensors of the telescope (encoders);
- data measuring system;
- time and frequency service;
- visual controlling system:
  - guide of the telescope,
  - CCD camera.

All system of the station are operated by two personal computers. To main characteristics of the station are [6]:

- single-shot RMS — 7.2 cm
- range of measuring of distances up to satellites — 750–8300 km
- frequency of the laser pulses — 10 Hz
- telescope:
  - optical system — focus Coude
  - primary mirror — 1 m diameter
  - secondary mirror — 25 cm diameter
  - field of view — 120 x 120 (arcsec)
  - equivalent focal distance — 21 m
  - mount — Alt–Azimuthal
  - pointing accuracy — 20″
- laser:
  - wavelength — 532 nm
  - pulse energy — 0.01–0.03 mJ
  - pulse width — 0.4 ns
  - controlled change of a laser beam divergence on the telescope output — 8–60”
- time service — GPS and rubidium frequency standard

3. MEASUREMENT OF DISTANCES UP TO THE SATELLITES

The process of satellites ranging starts with preparation of search ephemeris. For the pointing and the tracking of a satellite by the telescope satellite's azimuth and altitude are determined by a software which designed at the Texas University and adapted for the station by local team [5]. For this purpose GFZ predictions in the reference format IRV obtained through Internet are used.

For successful realization of a satellite ranging the precise pointing on a satellite and its tracking is necessary during session of observation. For this purpose a real-time software is used. To point the telescope on a satellite with hight accuracy a mount errors model is used. It provides accuracy of pointing about 20 arcsec. The specially designed automatic system of the stars observation is used for definition of parameters of the mount errors model.

Developed real-time software is used for ranging control and measuring of distances up to satellites. The main task of the software is measuring propagation time of a laser pulse up to a

satellite and back using for this purpose basic hardware

All measurements are necessary to refer to an unified reference point of the station, which is the intersection point of telescope's rotation axes. For this purpose a pre- and post calibration on the external target is used. The error of calibration measurements is about 8 cm.

For post–processing analysis of the satellites ranging results a software designed by SLR Borowiec team (Poland) is used [4]. This software allows to separate useful measurements from noise, to conduct processing of calibrations results, to determine and to take into account range and time biases, to estimate an internal error of results, to carry out cataloguing the data. Obtained files of normal points in the reference format are transmitted through Internet to Eurolas Data Center.

4. RESULTS AND ACCURACY OF THE SATELLITE LASER RANGING

The results of the satellite ranging are time delays of a laser pulse propagation referred to the stations reference point, value of a calibration constant and its accuracy, moments of launching laser pulses, preasure, temperature, humidity for a ranging period.

Since 1997 the regular night observations of 9 low orbital satellites are carried out. In 1999 the station was registered in ILRS Network and obtained the codes:

NAME	Golosiiv–Kiev
CDP	1824
IERS DOMES NUMBER	1235
MARK	S001
PLATE	EURA

Since 2000 the results of observations are transmitted to EDC. Since 2001 the ranging of Lageos–1 and Lageos–2 are carried out.

On the Fig. 2 and Fig. 3 the satellites ranging results for the period January – July 2001 are adduced. The quantity of passes and obtained normal points are shown. In total for this period 414 passes were made and 5213 normal points were obtained.

On the Fig. 4 the results of processing by the Center of Space Researches of the Texas University of LAGEOS satellites ranging for this period are adduced. The single–shot RMS is 7.2 cm, the RMS of normal points is 1.1 cm, the short–period range bias stability equals 48 cm accordinly to this Center.

5. DETERMINING OF THE COORDINATES OF THE SLR STATION "GOLOSIIV–KIEV" ON THE BASIS OF LAGEOS–1 AND LAGEOS–2 OBSERVATIONS

The coordinates of the SLR–station 1824 reference point were calculated on the basis of Lageos-1 and Lageos–2 satellites observations. Data from 21 Jan 2001 till 17 Jun 2001 were used. 219 Lageos–1 and 50 Lageos–2 observations were obtained during this period.

The software "Kiev–Geodynamics 5.2" was used for this purpose. The standard models and algorithms for SLR data processing at the MAO SLR data analysis center were applied [3].

The SLR observations of 117 stations were used [7]. The initial coordinates of the new stations 1824 ("Golosiiv–Kiev") and 7355 ("Urumqi") were taken from SSC(CSR)95L01 solution and the initial coordinates of another 115 stations were taken from SSC(GAOUA)00L01 solution.

The following values of the station coordinates were received in SSC(GAOUA)00L01 system:

$$(\overrightarrow{R^{gao}_{1824}})_{slr} = \{3512989.463, 2068968.664, 4888817.296\}$$

The coordinates of 97 SLR stations which are common in SSC(GAOUA)00L01 and ITRF97 solutions [1] were analysed to obtain the parameters of transformation between these terrestrial

systems. The following coordinates of the SLR station in ITRF97 were obtained:

$$(\overrightarrow{R^{itrf}_{1824}})_{slr} = \{3512989.469, 2068968.669, 4888817.281\}$$

This result was compared with another deternimaiton of the coordinates of the SLR station 1824 referense point. The hight–accuracy local (LOC) geodetic measurements (GEO) of the SLR–station reference point coordinates $(\overrightarrow{R^{loc}_{1824}})_{geo}$ and permanent GPS-station (GLSV) $(\overrightarrow{R^{loc}_{glsv}})_{geo}$ were considered as initial data for this purpose.

The ITRF97 coordinates of the GLSV-station from GPS technique $(\overrightarrow{R^{itrf}_{glsv}})_{gps}$ were used for determination [2] of the transformation matrix M between local system and ITRF97. The following equation was considered as a basic:

$$\left[(\overrightarrow{R^{itrf}_{1824}})_{gps} - (\overrightarrow{R^{itrf}_{glsv}})_{gps}\right] = M \times \left[(\overrightarrow{R^{loc}_{1824}})_{geo} - (\overrightarrow{R^{loc}_{glsv}})_{geo}\right]$$

The following coordinates of the SLR–station 1824 reference point on the basis of GPS–determination and geodetic measurements were obtained in ITRF97:

$$(\overrightarrow{R^{itrf}_{1824}})_{gps} = \{3512989.738, 2068968.942, 4888817.813\}$$

The comparison of the coordinates of the SLR–station 1824 reference point obtained on the basis of SLR-technique $(\overrightarrow{R^{itrf}_{1824}})_{slr}$ and GPS-technique $(\overrightarrow{R^{itrf}_{1824}})_{gps}$ demonstrates some inconsistent: the absolute difference between them is equal to 0.656 m. The cause of the existance of this difference was not detected completely.

There was assumed that difference can be partially caused by the calibration error which influences on the satellite observations. Such error 6 cm between calculated and used in software for calibration values as detected. The differences of the $(\overrightarrow{R^{itrf}_{1824}})_{slr}$ and $(\overrightarrow{R^{itrf}_{1824}})_{gps}$ can be occured by discrepancy between the orientation of the coordinate systems realized by SLR–technique and GPS–technique observations too.

The redetermined coordinates of the SLR–station reference point on the basis of SLR–technique were used for laser ranging Lageos–1 and Lageos–2 through the period from 29 Jun 2001 to 28 Jul 2001. The improving of the satellites tracking system was not detected because of insignificant differ (about 0.01 arcsec) between of the used before improving and the new values of the station's latitude and longitude.

6. CONCLUSION

The regular night observations of 9 low orbital satellites and Lageos–1, Lageos–2 are carried out at the SLR station "Golosiiv-Kiev".

In 1999 the station is registered in ILRS network and has CDP code 1824.

The single–shot RMS of ranging results is 7.2 cm, the RMS of normal points is 1.1 cm, the short–period range bias stability equals to 48 cm.

The coordinates in ITRF97 system of the SLR station "Golosiiv–Kiev" reference point obtained on the basis of 269 passes of Lageos–1 and Lageos–2 during the period 21 Jan – 17 Jun 2001 are:

$$(\overrightarrow{R^{itrf}_{1824}})_{slr} = \{3512989.469, 2068968.669, 4888817.281\}$$

References

[1] *C. Boucher, Z. Altamimi, P. Sillard* IERS TECHNICAL NOTE 27. The 1997 International Terrestrial Reference Frame (ITRF97).–1999.–P. 91.

[2] *Denis D. McCarthy* IERS Conventions (1996).–1996.–95 p.

[3] *S. Rudenko* Terrestrial Reference Frame Realization From the Analysis of 15-year LAGEOS–1 & LAGEOS–2 SLR World Network data//In: "Proceedings of the international workshop on GEodetic Measurements by the collocation of Space Techniques ON Earth", Tokyo, Japan, January, 25-28, , 1999.–Tokyo.–1999.–'. 201-207.

[4] *Schillak S, Butkiewicz E.* Software of the BOROWIEC-2 SLR system//Artificial Sattelites.–1996.–Vol.31.–No 3.–P. 71-80.

[5] *Schutz, B.E., Tapley, B.D., Eanes, R.J., Cuthbertson, B.* LAGEOS Ephemeris Predictions, Proc. of the 4th International Workshop on Laser Ranging Instrumentation, Austin, Texas, pub. by Geodetic Institute, Univ. of Bonn, Oct. 12-16.–1981.–145 p.

[6] *D. Ya. Yatskiv,M. M. Medvedskij, V. R. Suberlyak, M. M. Peretyatko* Kyiv laser ranging station: report on the experimental operation 1997-1998//Preprint of the Main Astronomical Observatory of the NAS of Ukraine.–MAO-98-6E.–Kyiv.–1998.–15 c.

[7] ftp://ftp.csr.utexas.edu/pub/slr/weekly/stations_information

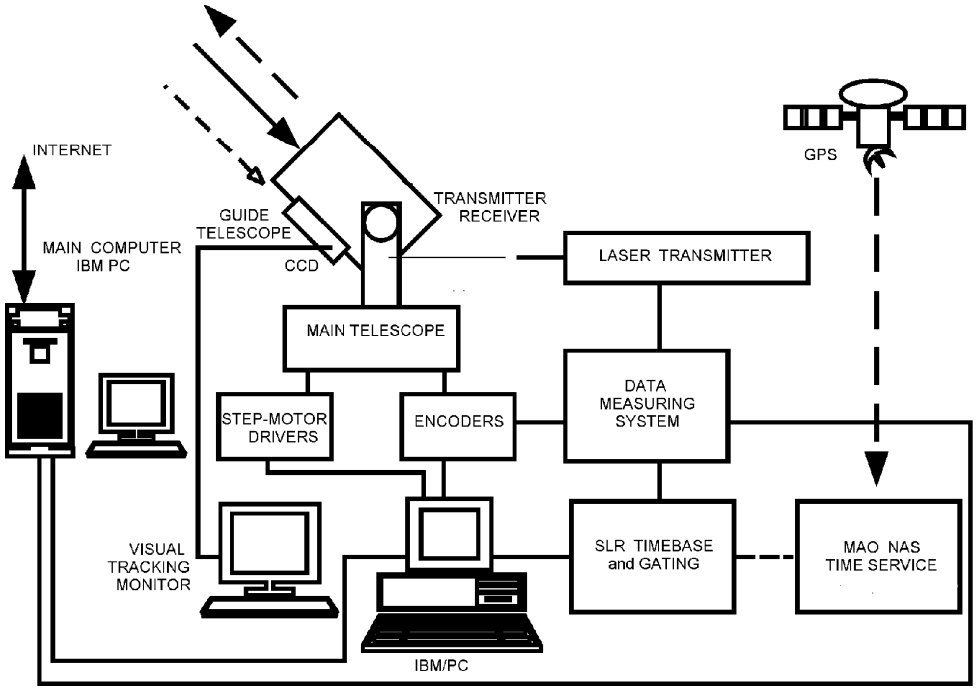

Figure 1: The SLR station "Golosiiv–Kiev" general block–scheme.

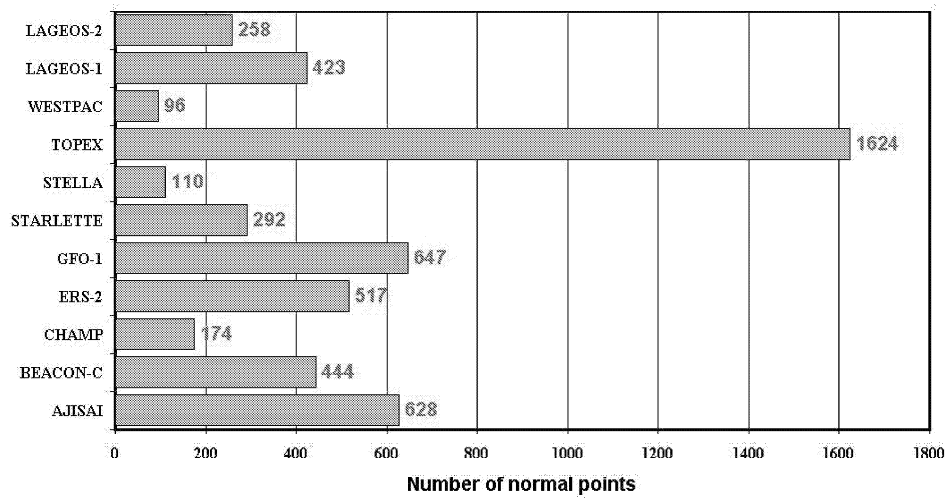

Figure 2: Normal points summary at the period Jan 2001–Aug 2001. Total points – 5213

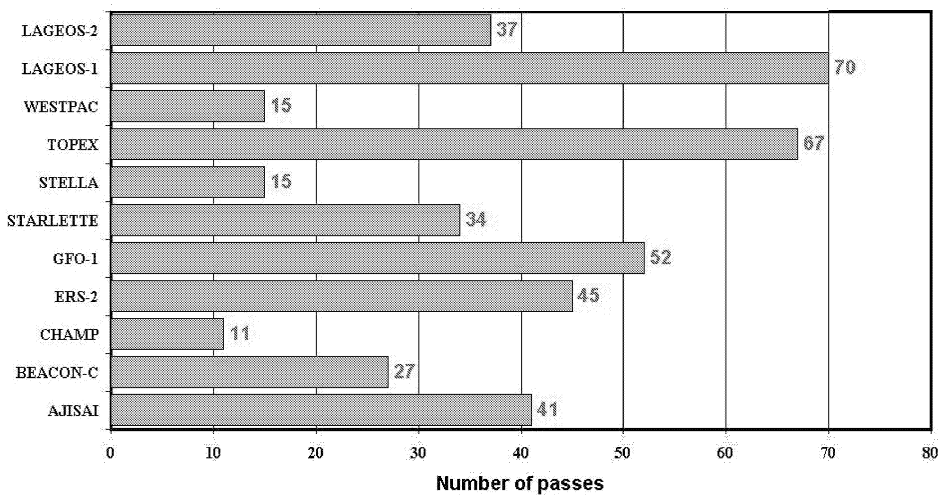

Figure 3: Pass summary at the period Jan 2001–Aug 2001. Total passes – 414.

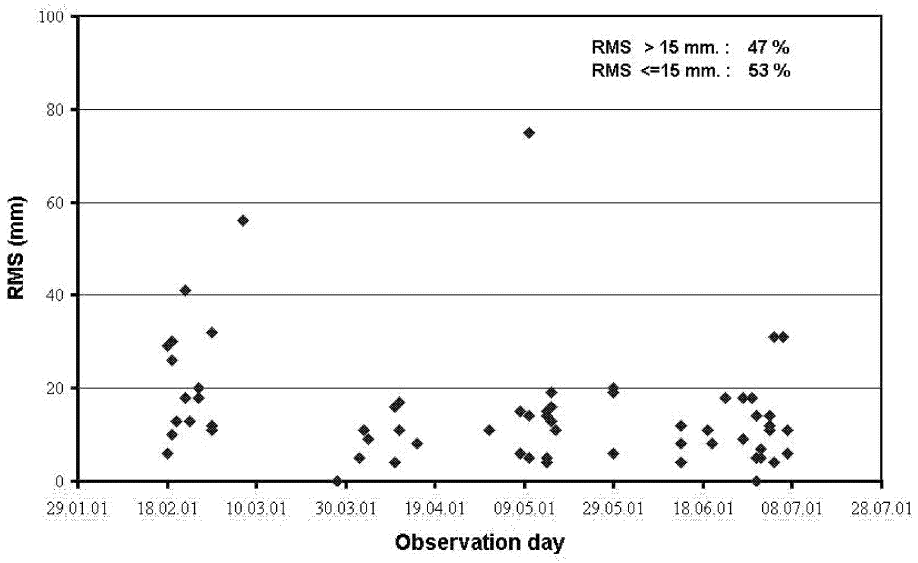

Figure 4: Normal points RMS of the LAGEOS satellites.

LICODY : THE DYNAMICS OF THE FLUID CORE FROM GRAVITY SIGNALS

M.GREFF (1), V. DEHANT (2), P. LOGNONNÉ (1), T. VAN HOOLST (2) and H. LEGROS (3).

(1) Institut de Physique du Globe de Paris, Paris, France.
(2) Observatoire Royal de Belgique, Bruxelles, Belgique.
(3) Institut de Physique du Globe de Strasbourg, Strasbourg, France.

Abstract

LICODY (Laser Interferometry for Core and Oceans DYnamics) is a project of mission to discover the dynamics of the Earth's liquid part: liquid iron core and water ocean.
The primary objective of this project is to study the dynamics of the Earth's liquid core and solid inner core from the time variations of very small global gravitational signals (from hundred seconds to decade time scales), with, in particular, the detection of rotational eigenmodes, the oscillation modes of the core, the Slichter modes, the seismic modes and, if possible, the motions within the core and the differential rotation of the inner core.
The secondary objective will be the monitoring of the gravity signals associated to the hydrology, oceanography and atmosphere.
These signals will be derived from laser measurements of perturbations between the relative position of several (3-4) satellites.

Scientific Objectives

The primary objective of the mission will be the determination of the structure of the core and its dynamics. The Earth's core is almost transparent for seismology and only the radial profile of P waves velocities, and to a lesser extend the density, are known. Many properties such as the Brunt-Vaissala frequency and the lateral density variations are not known. The main reason is related to the fact that only two of the gravity and core modes, and possibly the Slichter mode, have been so far detected. In contrast, about a thousand of modes, sensitive to the 3D elastic structure of all solid parts of the Earth, were detected and used to built tomographic models of the Earth. The bulk liquid core of the Earth remains one of the most mysterious parts of our planet, and the magnetic field is mainly constraining the flow at the surface of the core. We describe here all the modes that will be searched by the mission.

Rotational eigenmodes

The four rotational eigenmodes of the Earth are theoretically well known (see Figure 1). The

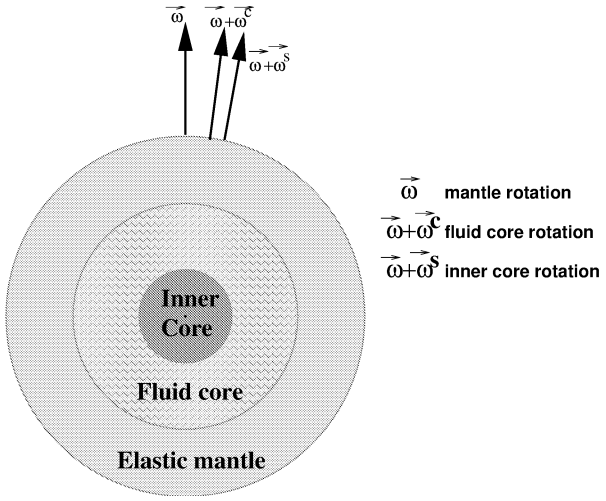

Figure 1: Rotational eigenmodes of the Earth: the Chandler Wobble (CW, motion of the Earth's rotation axis with respect to the figure axis of the mantle), the Nearly Diurnal Free Wobble (NDFW, also called the Free Core Nutation, FCN, related to the fluid core), the Free Inner Core Nutation (FICN, nearly diurnal eigenmode related to the inner core), and the inner core wobble (motion of the rotation axis of the inner core with respect to its figure axis).

Chandler wobble and the Free Core Nutation (FCN) have been extensively investigated and observed using geodetic and gravimetric measurements. The only way that information can be provided on the Free Inner Core Nutation (FICN) using these measurements is via the resonance effect on long period nutations. This effect is however very small and is partly hidden by oceanic and atmospheric effects on the observed frequencies. The rotational eigenmode itself has never been observed. The FICN resonance strength is weak due to the small size of the inner core. Superconducting gravimeters have failed to observe the FICN resonance because of the atmospheric noise around its period. The observation of this mode may however be possible by using diurnal gravity-induced perturbations on the satellites as they are almost not influenced by the local atmospheric noise.
It will provide information about different geometrical and physical parameters within the deepest Earth's interior. As a matter of fact, its period depends on the dynamical flattening and the density jump at the ICB (Inner Core Boundary), on the deformations of the ICB induced by the various rotational potentials, on the gravitational coupling between the inner-core and the mantle, on the magnetic friction and on the inner viscosity (Figure 2-a). This mode is damped because of the magnetic friction and of the inner-core viscosity (Figure 2-b). Consequently, the observations of the period and the quality factor of the FICN could involve informations on the amplitude of the radial component of the magnetic field at the ICB and on the effective viscosity of the inner core.

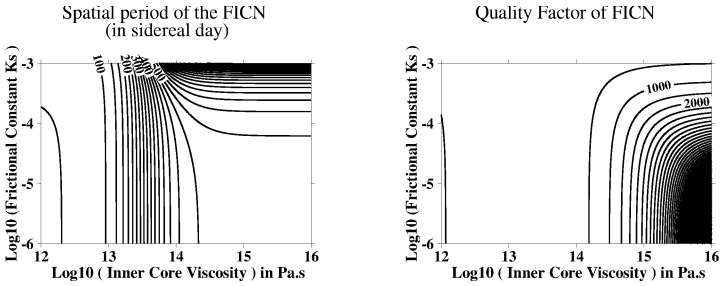

Figure 2: Spatial period and quality factor of the FICN. K_s is proportional to the square of the radial component of the geomagnetic field; for details see Greff, Legros and Dehant (2000)

As an example, our computations (Greff, Dehant and Legros, 2001) have shown that the possible range of viscosity and magnetic field in the inner core corresponds to a change of about 10 nanogals in the gravity perturbations induced by the tidal wave K_1 (the precession) at the Earth surface. We have plotted in Figure 3-a and 3-b the components in-phase and out-of-phase of the gravity perturbations induced by this wave.

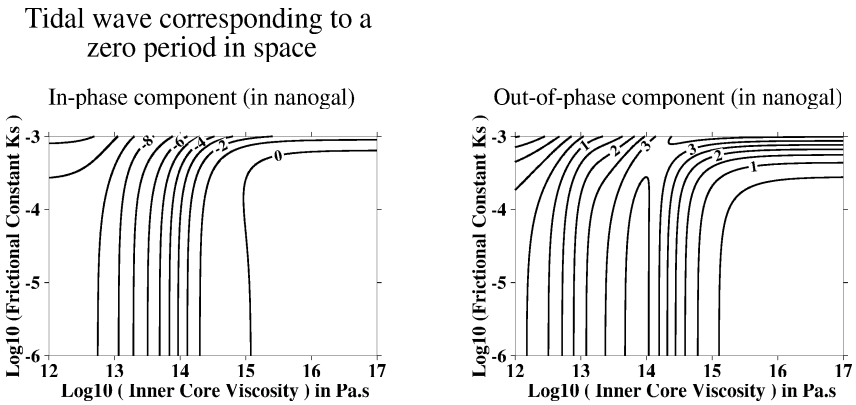

Figure 3: Components in-phase and out-of-phase of the gravity perturbations (in nanogal) induced by the tidal wave K_1 (Precession)

Oscillation modes of the core

The gravito-inertial modes of the fluid core depend on the gravity, on the density and its gradient, and on the compressibility, through the Brunt-Vaissala frequency. This parameter is related to the dynamical stability or instability of the fluid outer core. Observing their periods will allow us to constrain the rheological parameters and the core dynamics. The excitation mechanisms of these modes are not well identified; they include earthquakes, small-scale turbulence within the core, magnetic jerks, atmosphere pressure and winds, as well as ocean pressure and currents. The observation of the amplitudes of the core modes will allow to test the excitation models.

Seismic modes of the core and the mantle

The seismic modes of both core and mantle (see Lognonné and Clévédé, 2002) ranging from about one hundred of seconds to almost one hour can also be detected. The knowledge of their periods is important for determining the rheological properties of the mantle and the core. Observations of their excitation after earthquakes is provided by broad-band seismometers. Due to the high precision of our experiment we will be able to improve the measurement of splitting and to detect modes never observed before. The observation through the gravity signal related to mass redistribution will also strongly increase our sensitivity to lateral density variations in the deep mantle.

Slichter modes

The observation of the Slichter modes (three translational motions of the inner core with periods between 2 and 6 hours, corresponding to the spheroidal mode 1S1) has been claimed to be detected by the superconducting gravimeter community. But this observation is controversial and in particular the periods computed and observed are still under discussion. The experiment will allow to observe them.

The periods of the Slichter modes depend on the density jump and on the viscosity at the inner core boundary. Their observation will thus constrain these parameters and allow us to obtain information about the boundary conditions at the ICB very important for geodynamo investigations, as well as thermodynamic models.

Motions within the core

Density perturbations associated with decadal motions in the fluid core are presently only constrained by the secular variation of the surface magnetic field. This is a however a constraint for the flow only at the core mantle boundary, which moreover assumes some strong physical

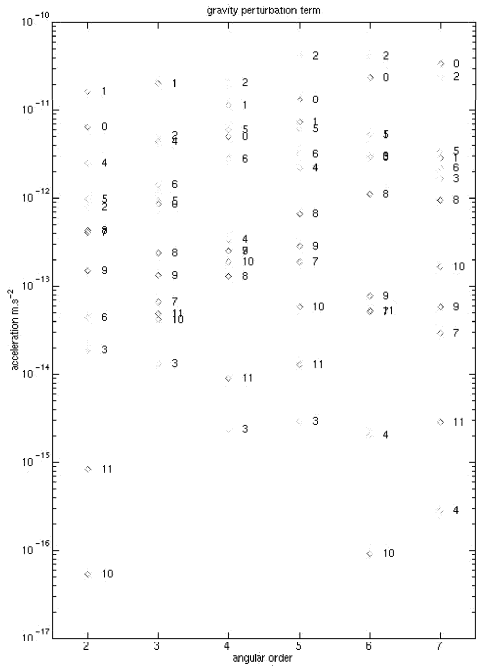

Figure 4: Amplitude of seismic modes following theory and estimates of Lognonné (1991) for a deep magnitude 7 quakes. The amplitude corresponds only to the gravity perturbation

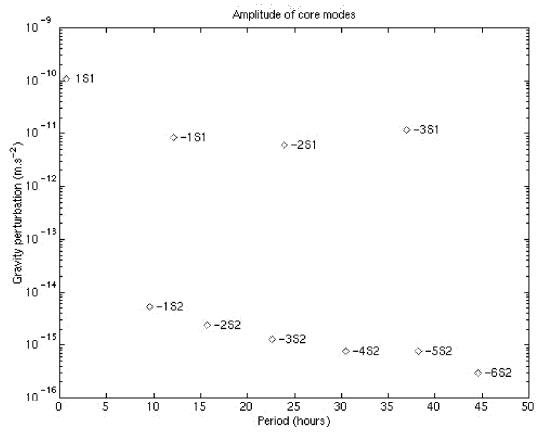

Figure 5: Amplitude of Slichter mode and core gravity modes following theory and estimates of Crossley (1988) for a magnitude 9 shallow Earthquake comparable with the Chili 1960 quake (depth=25 km). Deep quakes with magnitude 8 may excite the core modes with a-priori comparable amplitudes. Core modes have a priori very high Q (very likely much higher than 1000), enabling stack and amplification by a factor of Q of the amplitude spectral density

hypotheses. There is a gravitational potential induced by these density perturbations which varies at decadal and secular time scales. The precision reached by our experiment will allow to observe this trend and to provide information on the core dynamics. Additionally, very rapid motions within the fluid core, which are not detectable from the geomagnetic data because of the so-called 'skin depth' related to the conductivity of the lower mantle, can be detected by our gravitational measurements.

Secondary Objectives

Due to the extreme sensitivity of the mission, the measurement of the temporal variations of the gravity such as those due to slow, seasonal and annual variations in the ocean, ground-water, soil-moisture levels, changes in the masses of the Antarctic and Greenland ice sheets, will be possible. These scientific objectives could be seen in the continuation of the GRACE and GOCE mission. The LICODY mission, due to its improved sensibility, will be able to continue, after the end of the GRACE mission, the monitoring of the global mass redistribution of the Earth related to climatic effects and the global warming.

Technical concepts

LICODY is based on several (at least three) satellites performing laser interferometry inter-satellite links. The space-crafts will be around the Earth on a circular polar orbit. The time-depending lateral variations of the gravity field will perturb in a different way the trajectory of each satellite. Consequently, the distance satellite-satellite will oscillate with frequencies obtained by combining the orbital frequency of the satellite and the eigenfrequencies of the Earth. The distance measurements between two satellites will be performed by optical interferometry. This technique is close to the one utilized for the LISA (Laser Interferometry Space Antenna) mission, which aims at the detection of gravity waves (more information on LISA can be found at http://lisa.jpl.nasa.gov). Preliminary studies have shown that the LISA system is able to detect distance variations with a resolution of 20 pico-m/Hz.
Assuming LISA type of performances, preliminary calculations for LICODY show that the corresponding noise in displacement is produced by a time gravity variation of less than 10^{-16} m.s^{-2} in the core modes frequency bandwidth for degrees (in the spherical harmonics expansion) less than five. Very likely, the main difficulties in the detection of core modes with such a system will be related to the implementation of the LISA system on an orbiting satellite. The altitude of the satellites must be compatible with the LASER link. The most difficult technical part of the mission seems related to the design of the optical system and attitude control system enabling the Laser interferometry to be operational between two Earth orbiting satellite with a noise compatible with LISA performances
A minimum of 5 years is necessary to achieve several (5-10) high magnitude deep quakes which are strong sources for the excitation of core modes. 10 years are however optimum.
The orbit of such a mission must be studied in detail, in order to achieve the best sensitivity at low angular order enabling the desired duration of the mission.

References

Crossley, D.J., 1988, The excitation of core modes by Earthquakes, Geophysical Monograph 46, 41-50.
Greff-Lefftz, M., Legros, H., and Dehant, V., 2000. Influence of the inner core viscosity on the rotational eigenmodes of the Earth.*Phys. Earth Planet. Int.*, 122, vol 3-4, 187-203.
Greff-Lefftz, M., Dehant, V., and Legros, H., 2001. Effects of inner core viscosity on gravity changes and spatial nutations induced by luni-solar tides. *Phys. Earth Planet. Int.*, in press.
Lognonné, P., 1991. Normal modes and Seismograms in an anelastic rotating Earth., *J. Geophys. Res.*, 96, 20309-20319.
Lognonné, P., and Clévédé, E., 2002. Chapter 37: Normal modes of the Earth and Planets, Handbook on Earthquake and Engineering Seismology, IASPEI Centennial Publications, H. Kanamori, P. Jennings and W. Lee editors, in press.

CLASSICAL ASTROMETRY LONGITUDE AND LATITUDE DETERMINATION BY USING CCD TECHNIC

G. DAMLJANOVIĆ (1,3), M.S. DE BIASI (2), and G. GERSTBACH (3)
(1) Astronomical Observatory (AOB)
Volgina 7, 11160 Belgrade, Yugoslavia
e-mail: gdamljanovic@aob.bg.ac.yu
(2) Facultad de Ciencias Astronómicas y Geofísicas (UNLP)
Paseo del Bosque s/n, 1900 La Plata, Argentina
Consejo Nacional de Investigaciones Científicas y Técnicas (CONICET), Argentina
e-mail: debiasi@fcaglp.unlp.edu.ar
(3) Vienna University of Technology (TU Wien)
Institute of Geodesy and Geophysics (IGG), Dept. of Advanced Geodesy
Gusshausstrasse 27-29, A-1040 Wien, Austria
e-mail: ggerstb@luna.tuwien.ac.at

ABSTRACT. At the AOB, it is the zenith-telescope (D=11 cm, F=128.7 cm, denoted by BLZ in the list of Bureau International de l'Heure - BIH), and at Punta Indio (near La Plata) it is the photographic zenith tube (D=20 cm, F=457.7 cm, denoted by PIP in the list of BIH). At the AOB there is a CCD camera ST-8 of Santa Barbara Instrument Group (SBIG) with 1530x1020 number of pixels, 9x9 mikrons pixel size and 13.8x9.2 mm array dimension. We did some investigations about the possibilities for longitude (λ) and latitude (φ) determinations by using ST-8 with BLZ and PIP, and our predicted level of accuracy is few 0."01 from one CCD zenith stars processing with Tycho-2 Catalogue. Also, astro-geodesy has got new practicability with the CCDs (to reach a good accuracy of geoid determination via astro-geodesy λ and φ observations). At the TU Wien there is the CCD MX916 of Starlight Xpress (with 752x580 pixels, 11x12 mikrons, 8.7x6.5 mm active area). Our predicted level of accuracy for λ and φ measurements is few 0."1 from one CCD MX916 processing of zenith stars, with small optic (20 cm focus length because of not stable, but mobile instrument) and Tycho-2. A transportable zenith camera with CCD is under development at the TU Wien for astro-geodesy subjects.

1. ASTROMETRY AND ASTRO-GEODESY WITH CCD TECHNIC

Nowadays, there are big possibilities for astrometry by using the good quality optic with modern computer and Charge Coupled Device (CCD) technic. Here, we put our attention to the BLZ and PIP instruments. Both were in the list of BIH and participated with their observations to take a part in new "Earth orientation parameters 1899.7-1992.0 in the ICRS based on the HIPPARCOS reference frame" (Vondrák et al. 1998). For the PIP with CCD, the process of measurement is the PZT's one, just to remove the observations by photo plate and to adapt CCD. If we fix the tube of BLZ in the zenith direction and follow PZT's process of

observations we can use BLZ (with CCD) for λ and φ determinations. Both instruments can be full-automatic ones. The features of CCD astronomy can be found in (Martinez and Klotz 1998) and the manuals (Santa Barbara Instrument Group 1994, Starlight Xpress Ltd. 1999).

The Tycho-2 (at ICRS reference system) is an astrometric reference catalogue with positions (the precise is 60 mas for all stars), proper motions (2.5 mas/yr, precise) and two-colour photometric data for about 2.5 million brightest stars in the sky. Only 4% stars are without proper motion data. The star density is about 150 stars/sq.deg. for $b = 0°$ (50 for $b = \pm 30°$, and 25 for $b = \pm 90°$) and V is near 11.5 mag (with 90% completeness).

The sky field of BLZ with ST-8 (1."44/px for both axis, x and y) is $37'$x$25'$, and $10'$x$7'$ for PIP. With BLZ and Tycho-2 we can "catch" about 20 stars or few stars with PIP. It is enough to reach few 0."01 accuracy of λ and φ. The accuracy of PIP can be double than BLZ's one because of better optic. The standard error of unit weight (for λ and φ determination with BLZ/PIP) was about 0."15 by using visual (for BLZ) and photo plate (for PIP) observations. It means, our predicted accuracy (for BLZ and PIP with one CCD image procedure) is quite good and open new possibilities for astrometry with CCD technic.

In geodesy, the rapid measurement of the direction of vertical has three goals: (a) the geoid determination by Vertical Deflection (VD) profiles, (b) the terrestrial network reduction to a geodetic ellipsoid, and (c) the inversion of VDs to determine density structures of the Earth's crust. The necessary accuracy of λ and φ is $\pm 0."3$ (c) - $\pm 1"$ (a). Usual, it is the simultaneous λ and φ observation by small Zeiss astrolabes (about 15 star transits $60°$ during 1 hour) or zenith cameras. The geoid projects in flat countries mainly use gravimetry. Observation time is very short, but to get high geoid accuracy 200-500 points per 1000 km3 are necessary, whereas astrogeodesy requires only 10-20 VD points (Gerstbach 1997). Therefore in alpine countries, the astrogeoid is much more effective than gravimetry. At the TU Vienna, a special research project "CCD in astro-geodesy" started in 1999, sponsored by ÖNB. In the first 2 years Olympus CCD cameras were used with the Zeiss astrolabe (4/20 cm) and Kern theodolite DKM3a (7/40 cm). The accuracy was $\pm 1"$ (Gerstbach 2000), but the measuring time was not shorter than visually one. Therefore, we continue to develop the small zenith camera. We test the astro-camera MX916. The zenith camera has a teleobjective 1:4/20cm. Near Vienna, the MX916 pictures with 5^s exposures show the stars up to 12^{th} magnitude. The camera was turned manually. The relation turning axis - vertical is measured by two levels at the camera turning plate. The field of view is about 1.5x2°. First tests show 20-50 stars (faintest not used). The accuracy is less than 2" with 10 Hipparcos stars and 1" with 20 Tycho stars. Combining 4 images and Tycho-2 we expect $\leq \pm 0."5$ of the vertical direction. In 2002/3, we hope the geodetic zenith camera will be used for geoid profile densification in Austria to improve the geoid from ± 3 cm to ± 1 cm.

2. REFERENCES

Gerstbach, G.: 1997, How to get an European Centimeter Geoid ("astro-geological geoid"), Physics and Chemistry of the Earth 21/4, Lindau/London, 343-346.

Gerstbach, G.: 2000, CCD und Astro-Geodäsie, Geowiss. Mitt. 50, TU Wien, 45-57.

Martinez, P., Klotz, A.: 1998, A Practical Guide to CCD Astronomy, Cambridge University Press, reprinted 2000.

Santa Barbara Instrument Group: 1994, CCD Camera Operating Manual for the Model ST-7 and ST-8.

Starlight Xpress Ltd.: 1999, MX916 CCD system, user handbook.

Vondrak, J., Pesek, I., Ron, C., Cepek, A.: 1998, Earth orientation parameters 1899.7-1992.0 in the ICRS based on the HIPPARCOS reference frame, Astron. Inst. of the Academy of Sciences of the Czech R., Publ. No. 87.

VARIATIONS IN THE ORBITAL ELEMENTS OF ASTEROIDS INDUCTED BY THE COMPARISON HIPPARCOS-FK5

M.J. MARTINEZ[1], J.A. LOPEZ[2], F.J. MARCO[2]
[1]Universidad Politecnica de Valencia
[2]Universidad Jaume i de Castellon
[1] Camino de Vera S/N. 46022 Valencia. Spain
[2] Campus de Riu sec. 12004 Castellon. Spain
mjmartin@mat.upv.es, lopez@mat.uji.es, marco@mat.uji.es

ABSTRACT. In the last years the old reference system, based in the FK5 fundamental catalogue, has been replaced by the new fundamental system, initially based in the Hipparcos catalogue. The FK5 catalogue is included in Hipparcos, but some bias between them are to be expected. The bias may be summed up by the existence of infinitesimal rotation. They induct corrections to the angular elements of the asteroids referred to these catalogues.

1. CORRECTION MODEL

The 1st of January 1998 the old reference system, materialized by the old FK5, was replaced by the new reference system, initially materialized by the Hipparcos Catalogue for optical wavelength. The resulting reference system is consistent with the FK5 except for the existence of infinitesimal rotations. The correction model from with we compute the system rotations is based in the minimization of the O-C residuals. Basically, we consider the differences $\Delta\alpha_C = \alpha_C - \alpha_F$ and $\Delta\delta_C = \delta_C - \delta_F$, where with the C subindex we denote the coordinates obtained from a catalog which we suppose that contains systematic errors and with the subindex F we denote the coordinates obtained after removing the systematics errors of C and after applying an infinitesimal transformation given by a matrix R:

$$R = \begin{bmatrix} 1 & \Delta\xi & \Delta\eta \\ -\Delta\xi & 1 & \Delta\varepsilon \\ -\Delta\eta & -\Delta\varepsilon & 1 \end{bmatrix} \tag{1}$$

so the corrections model results:

$$\begin{aligned} \Delta\alpha_C \cos\delta &= \Delta\xi\cos\delta + \Delta\eta\sin\alpha\sin\delta - \Delta\varepsilon\cos\alpha\sin\delta \\ \Delta\delta_C &= \Delta\eta\cos\alpha + \Delta\varepsilon\sin\alpha \end{aligned} \tag{2}$$

Applying to this model a mean squares method we obtain a normal system of equations given

by:

$$A \begin{bmatrix} \Delta\xi \\ \Delta\eta \\ \Delta\varepsilon \end{bmatrix} = \overrightarrow{b} \tag{3}$$

with

$$A = \begin{bmatrix} \cos^2\delta & \frac{1}{2}\sin\alpha\sin(2\delta) & -\frac{1}{2}\cos\alpha\cos(2\delta) \\ \frac{1}{2}\sin\alpha\sin(2\delta) & \sin^2\alpha\sin^2\delta+\cos^2\delta & \frac{1}{2}\sin(2\alpha)\cos^2\delta \\ -\frac{1}{2}\cos\alpha\cos(2\delta) & \frac{1}{2}\sin(2\alpha)\cos^2\delta & \cos^2\alpha\sin^2\delta+\sin^2\delta \end{bmatrix} \tag{4}$$

and the independent term is the vector:

$$\overrightarrow{b} = \left(\Delta\alpha\cos^2\delta, \frac{1}{2}\Delta\alpha\sin\alpha\sin(2\delta)+\Delta\delta\cos\alpha, -\frac{1}{2}\Delta\alpha\cos\alpha\sin(2\delta)+\Delta\delta\sin\alpha\right)^t \tag{5}$$

2. VARIATIONS IN THE ANGULAR ELEMENTS OF ASTEROIDS INDUCED BY THE SYSTEM ROTATIONS

Let us consider the vectors h and p, which are, respectively, the normal to the orbital plane of the asteroid vector and the vector in the direction of the periaster and let Δh and Δp the corresponding incremental vectors. The composition of the matrix (1) with the transformation P into equatorial coordinates provides the equation:

$$\begin{aligned} R^t P(-\varepsilon)\, h &= P(-\varepsilon)\,[h+\Delta h] \\ R^t P(-\varepsilon)\, p &= P(-\varepsilon)\,[p+\Delta p] \end{aligned} \tag{6}$$

The application of the previous formulas to obtain variations of the angular elements of the asteroids gives the following relationships:

$$\begin{aligned} \Delta i &= \Delta\xi\sin\Omega\sin\varepsilon - \Delta\eta\sin\Omega\cos\varepsilon + \Delta\varepsilon\cos\Omega \\ \Delta\Omega &= \Delta\xi(\cos\varepsilon+\cos\Omega\cot i\cos\varepsilon) + \Delta\eta(\sin\varepsilon-\cos\Omega\cot i\cos\varepsilon) \\ &\quad -\Delta\varepsilon\sin\Omega\cot i \\ \Delta w &= [-\Delta\xi\cos\Omega\sin\varepsilon + \Delta\eta\cos\Omega\cos\varepsilon + \Delta\varepsilon\sin\Omega]\csc i \end{aligned} \tag{7}$$

Given the numerical values of the rotational parameters relating both systems from [2] and applying the formulas (7) the corrections to the angular elements of the asteroids give the following results (in arc seconds, No represents the number of the asteroid):

Table 1:

N^o	1	2	3	4	6	7	11	18	25	39	40
Δi	-.003	.020	.020	.005	.015	.003	.012	.018	.016	.019	.002
$\Delta\Omega$	.130	.027	.037	.178	.072	.009	.220	.076	-.005	.064	.290
Δw	-.003	.002	.003	.004	.009	-.004	.009	.008	-.010	.007	.001

Addittionally, we have calculated the values of partial derivatives of the elements with respect the initial ones following the perturbed elements method explained in [1] and the same derivatives with respect to the initial elements corrected according with Table1.

3. REFERENCES

Marco,F.J., López J.A., Martínez, M.J. 1997. *Cel. Mech.* 68.193.

Mignard, F., Froeschlé M. "Global and local bias in the FK5 from the Hipparcos data" *Astron.Astrophys.* 354, 732-739. (2000)

Session V)

EPHEMERIS AND DYNAMICAL REFERENCE SYSTEMS

Introductory papers, oral communication and posters

EPHÉMÉRIDES ET SYSTÈMES DE RÉFÉRENCES DYNAMIQUES

Exposés introductifs, communications orales et posters

SOME QUESTIONS CONCERNING THE NEW IAU RELATIVISTIC FRAMEWORK

M. SOFFEL, S.A. KLIONER
Lohrmann Observatory, Dresden Technical University
01062 Dresden, Germany

ABSTRACT. Some particular questions concerning the new IAU2000 relativistic resolutions are discussed. The relation of the BCRS metric and the well known PPN form of the metric is shown. The relation of the BCRS-GCRS coordinate transformations and the Lorentz transformation is discussed. The multipole expansions of the local gravitational potentials of the Earth are discussed and justified.

1. INTRODUCTION

It is clear that the new IAU resolutions on relativity, being rather complicated, require some additional comments and explanations. A detailed explanatory supplement is presently in preparation by the IAU Working Group on General Relativity in Celestial Mechanics, Astrometry and Metrology (WG RCMAM). It is the long-term task of the WG RCMAM to show how these recommendations have to be used in the 'models' for various kinds of observations (VLBI, SLR, LLR, radar ranging, positional observations, etc.). This paper is devoted to a brief review of some of the most important questions concerning the new IAU resolutions.

Let us note from the very beginning that most of the relativistic models currently in use are already in full agreement with the new resolutions, though the languages might sound a bit different at first glance. No conceptual modifications of the present models are excepted. Two examples: the so-called Einstein-Infeld-Hoffmann equations of motion that form the basis of modern solar system ephemerides (such as the JPL planetary ephemerides) can be derived from the resolutions (see, e.g., Damour, Soffel, Xu (1991) for more details). These equations of motion contain the masses M_A of the various solar system bodies. How M_A can be written as integral over body A is irrelevant for practice since their numerical values will be determined from observational data. Another example is the VLBI model published in the IERS Conventions (1992). This "consensus" VLBI model is based on a number of the relativistic VLBI models published by several authors and is in agreement with the resolutions. Further implementation of the new relativistic IAU framework could result in some changes of the models as soon as higher accuracy is required.

2. BARYCENTRIC CELESTIAL REFERENCE SYSTEM

The Barycentric Celestial Reference System (BCRS) is intimately related with the ICRS in the sense that an ICRF catalogue of quasar positions is meaningful only in combination with the

metric tensor of the BCRS. The Geocentric Celestial Reference System (GCRS) is actually that system in which the gravitational field of the Earth and also the Earth's rotation parameters should be defined. Note, that the difference between the BCRS and the GCRS is not only the origin but there is a complicated space-time transformation between these two systems. The word "celestial" in the names of these two reference systems means that both reference systems are non-rotating with respect to remote stars (i.e., these reference systems do not rotate with the Earth).

The metric tensor of the BCRS with coordinates $x^\mu = (ct, x^i)$ is written in the form

$$\begin{aligned} g_{00} &= -1 + \frac{2w}{c^2} - \frac{2w^2}{c^4} + \mathcal{O}(c^{-5}), \\ g_{0i} &= -\frac{4}{c^3} w^i + \mathcal{O}(c^{-5}), \\ g_{ij} &= \delta_{ij} \left(1 + \frac{2w}{c^2}\right) + \mathcal{O}(c^{-4}) \end{aligned} \tag{1}$$

with

$$w(t, \mathbf{x}) = G \int d^3x' \frac{\sigma(t, \mathbf{x}')}{|\mathbf{x} - \mathbf{x}'|} + \frac{1}{2c^2} G \frac{\partial^2}{\partial t^2} \int d^3x' \, \sigma(t, \mathbf{x}') |\mathbf{x} - \mathbf{x}'|, \tag{2}$$

$$w^i(t, \mathbf{x}) = G \int d^3x' \frac{\sigma^i(t, \mathbf{x}')}{|\mathbf{x} - \mathbf{x}'|}. \tag{3}$$

Here σ and σ^i are the gravitational mass and current densities, respectively. The Einstein field equations in the harmonic gauge fixed by the resolutions for the metric (1) read

$$\left(-\frac{1}{c^2}\frac{\partial^2}{\partial t^2} + \Delta\right) w = -4\pi G\sigma, \tag{4}$$

$$\Delta w^i = -4\pi G \sigma^i. \tag{5}$$

They fix the potentials w and w^i completely only together with the boundary conditions

$$\lim_{\substack{r \to \infty \\ t = \text{const.}}} w = 0\,, \tag{6}$$

$$\lim_{\substack{r \to \infty \\ t = \text{const.}}} w^i = 0\,, \tag{7}$$

requiring that space-time described by the BCRS is considering to be asymptotically flat.

Let us stress that the metric (1) with (2)–(3) fully agrees with the one that can be found in standard textbooks (e.g., Misner et al., 1973; Will 1993). To show this explicitly one has to consider matter to consist of an ideal fluid for which the metric in Will (1993) is valid (in the IAU form of the metric no assumptions or simplifications for the model of matter is used). In this ideal fluid model we encounter variables like ρ (rest mass density), $\mathbf{v}$ (the velocity of fluid elements), p (pressure), Π (internal specific energy) and a potential U

$$U(t, \mathbf{x}) \equiv G \int \frac{\rho(t, \mathbf{x}')}{|\mathbf{x} - \mathbf{x}'|} d^3x' \tag{8}$$

and we can express our densities σ and σ^i as

$$\sigma = \rho\left(1 + \frac{1}{c^2}\left[\Pi + 2\mathbf{v}^2 + 2U\right]\right) + 3\frac{p}{c^2} + \mathcal{O}(c^{-4}) \tag{9}$$

$$\sigma^i = \rho v^i + O(c^{-2})\,. \tag{10}$$

After a transformation to harmonic coordinates the 'traditional form' of e.g., g_{00} reads:

$$g_{00} = -1 + \frac{1}{c^2}\left[2U + 4\Phi_1 + 4\Phi_2 + 2\Phi_3 + 6\Phi_4\right] \tag{11}$$

$$-\frac{2}{c^4}U^2 + \frac{1}{c^4}\chi_{,tt} \tag{12}$$

with

$$\Phi_1 \equiv \int \frac{\rho' v'^2}{|\mathbf{x} - \mathbf{x}'|}\, d^3x', \tag{13}$$

$$\Phi_2 \equiv \int \frac{\rho' U'}{|\mathbf{x} - \mathbf{x}'|}\, d^3x', \tag{14}$$

$$\Phi_3 \equiv \int \frac{\rho' \Pi'}{|\mathbf{x} - \mathbf{x}'|}\, d^3x', \tag{15}$$

$$\Phi_2 \equiv \int \frac{p'}{|\mathbf{x} - \mathbf{x}'|}\, d^3x' \tag{16}$$

and

$$\chi(t, \mathbf{x}) \equiv -G \int \rho' |\mathbf{x} - \mathbf{x}'|\, d^3x'\,. \tag{17}$$

By means of the relations of densities with the fluid variables we find e.g.,

$$w = U + 2\Phi_1 + 2\Phi_2 + \Phi_3 + 3\Phi_4 - \frac{1}{2c^2}\chi_{,tt} + O(c^{-4})$$

and the two forms of g_{00} coincide completely. It is also trivial to check that the same is true for all other components of the metric. Note that Will (1993) derives the metric tensor not only within General Relativity, but within the so-called PPN formalism which represent an phenomenological scheme covering certain classes of alternative metric theories of gravity. In the PPN formalism various theories (including General Relativity) are characterized by several numerical parameters which can be fitted from observations. Let us also note that the BCRS, GCRS, the transformation between them and various kind of the equations of motion have been derived in Klioner & Soffel (2000) in the framework of the PPN formalism. For the limit of general relativity all the formulas given in that publication become equivalent to those derived in the framework of the new IAU resolutions.

One might think of a split of g_{00} into "Newtonian" and "post-Newtonian" pieces, i.e., $w = $'Newtonian potential' $U +$' relativistic corrections', but this way of thinking is not adequate. The better approach is to define adequate parameters of a theory (masses etc.) whose values can be derived from observational data. Those parameters are defined in the full relativistic context and it makes no sense to split them into unobservable pieces. E.g., physically meaningful relativistic potential coefficients have been defined by a multipole expansion of w,

and not of U (the so-called Blanchet-Damour multipole moments, which are used in Resolution B1.4).

3. THE BCRS-GCRS TRANSFORMATION AND THE LORENTZ TRANSFORMATION

Here we would like to stress the relation between the rather complicated BCRS-GCRS coordinate transformation given in Resolution B1.3 and the well-known Lorentz transformation. If we neglect all gravitational fields and acceleration terms then the BCRS-GCRS transformation as given in the IAU Resolution B1.3 can be re-written in the form:

$$T = t - \frac{1}{c^2}\left[\frac{1}{2}v^2\,t + \mathbf{v}\cdot(\mathbf{x}-\mathbf{v}\,t)\right] + \frac{1}{c^4}\left[-\frac{1}{8}v^4\,t - \frac{1}{2}v^2\,\mathbf{v}\cdot(\mathbf{x}-\mathbf{v}\,t)\right] + \mathcal{O}(c^{-5}), \tag{18}$$

$$\mathbf{X} = \mathbf{x} - \mathbf{v}\,t + \frac{1}{c^2}\left(\frac{1}{2}\mathbf{v}\,(\,\mathbf{v}\cdot(\mathbf{x}-\mathbf{v}\,t)\,)\right) + \mathcal{O}(c^{-4}). \tag{19}$$

Since all acceleration terms were neglected we employ here that the BCRS position of the Earth is given by $\mathbf{x}_E = \mathbf{v}\,t$ and $\mathbf{v} = \text{const}$. Regrouping the terms in this transformation one gets ($\beta = |\mathbf{v}|/c = \text{const}$)

$$T = t\left(1 + \frac{1}{2}\beta^2 + \frac{3}{8}\beta^4\right) - \left(1 + \frac{1}{2}\beta^2\right)\frac{\mathbf{v}\cdot\mathbf{x}}{c^2} + \mathcal{O}(c^{-5}), \tag{20}$$

$$\mathbf{X} = \mathbf{x} - \left(1 + \frac{1}{2}\beta^2\right)\mathbf{v}\,t + \frac{1}{2}\frac{\mathbf{v}\,(\mathbf{v}\cdot\mathbf{x})}{c^2} + \mathcal{O}(c^{-4}). \tag{21}$$

This, however, is nothing but a Lorentz transformation from Special Theory of Relativity (e.g., Weinberg, 1993)

$$T = \gamma\,t - \gamma\,\frac{\mathbf{v}\cdot\mathbf{x}}{c^2},$$

$$\mathbf{X} = \mathbf{x} - \gamma\,\mathbf{v}\,t + \frac{(\gamma-1)}{v^2}(\mathbf{v}\cdot\mathbf{x})\mathbf{v} \tag{22}$$

in the corresponding approximation since

$$\gamma \equiv (1-\beta^2)^{-1/2} = 1 + \frac{1}{2}\beta^2 + \frac{3}{8}\beta^4 + \mathcal{O}(\beta^6)\,. \tag{23}$$

The terms containing w_{ext} and w^i_{ext} in the full BCRS-GCRS transformation result from the fact that one wants the GCRS to be Lorentzian ($G_{\alpha\beta} = \text{diag}(-1,+1,+1,+1)$) at the geocenter. Finally there are acceleration terms that are related with inertial effects and indicate that the GCRS is only a local system whose coordinates make sense only for distances smaller than $c^2/a_E \sim 500$ pc.

4. MULTIPOLE EXPANSIONS OF THE GRAVITIONAL POTENTIALS IN THE GCRS

Although the expansion of the local potential W_E of the Earth in Resolution B1.4 looks Newtonian, W_E obviously is a full post-Newtonian potential. This is possible since the mass

M_E and the potential coefficients C_{lm}^E and S_{lm}^E that appear in the expansion from Resolution B1.4

$$W_{\rm E} = \frac{GM_{\rm E}}{R}\left[1+\sum_{l=2}^{\infty}\sum_{m=0}^{+l}\left(\frac{R_{\rm E}}{R}\right)^l P_{lm}(\cos\theta)(C_{lm}(T,R)\cos m\phi + S_{lm}(T,R)\sin m\phi)\right] \quad (24)$$

are themselves full post-Newtonian quantities. These quantities are defined by the corresponding Blanchet-Damour mass multipoles of the Earth. E.g., the mass M_E is formally given by (Σ and Σ^a are the corresponding mass and mass current densities defined in the GCRS)

$$M_E = \int_E d^3X\Sigma + \frac{1}{6c^2}\frac{d^2}{dT^2}\left[\int_E d^3X\mathbf{X}^2\Sigma\right] - \frac{4}{3c^2}\frac{d}{dT}\left[\int_E d^3X X^a\Sigma^a\right], \quad (25)$$

but such a formal expression is not needed for practice, unless one really wants to relate the high-precision value for the mass of the Earth derived from, e.g., the SLR observations, to geophysical data and models concerning the distribution of density, pressure, etc. inside the body of the Earth.

Actually the full post-Newtonian expansion for W_E has additional second time derivative terms as in

$$C_{lm}^E \to C_{lm}^E - \frac{1}{2(2l-1)}\frac{R^2}{c^2}\frac{d^2}{dT^2}C_{lm}^E \quad (26)$$

and a gauge term

$$\frac{4}{c^2}\frac{\partial}{\partial T}\Lambda\,. \quad (27)$$

This full expansion can be found, e.g., in Theorem 6 of Damour, Soffel, Xu (1991). The 2nd time derivative terms are a factor $(v_{\rm rot}/c)^2 \simeq 10^{-12}$ times smaller than non-axisymmetric terms ($C_{22}^E \simeq 5\cdot 10^{-6}$, $S_{22}^E \simeq 3\cdot 10^{-6}$). The Λ-term does not enter equations of motion and produce effects smaller than 10^{-18} in the transformations between proper time of an observer and TCG or TCB. That is why these additional terms are not mentioned in the resolutions.

The expansion of W_E^a given in Resolution B1.4

$$W_E^a(T,\mathbf{X}) = -\frac{G}{2}\frac{(\mathbf{X}\times\mathbf{S}_E)^a}{R^3} \quad (28)$$

is also related with further approximations. In the full PN expression for W_E^a also given, e.g., in Theorem 6 of Damour, Soffel, Xu (1991) we also encounter first time derivative terms of the mass moments or potential coefficients. The leading term is of order $|C_{22}^E|MR^2\Omega$ and therefore smaller than the spin term by a factor determined by C_{22}^E. Since the Earth is almost axisymmetric and slowly rotating these terms are negligible. Note that the expression for W_E^a is required only in post-Newtonian terms of equations of motion and coordinate transformations, and, therefore, needs to be calculated with moderate accuracy only.

There are interesting additional relativistic terms that have been neglected. In relativity the set M_L^E of mass-moments is not enough to characterize the gravitational field outside the Earth. One needs an additional set of spin moments S_L^E. In our PN scheme S_L appear only to Newtonian order. We studied rigid models with

$$\mathbf{\Sigma} = \Sigma(\mathbf{\Omega}\times\mathbf{X})\,. \quad (29)$$

For these models one gets

$$S_L = C_{dL}\Omega^d \tag{30}$$

with

$$C_{dL} = -M_{dL} + \frac{l+1}{2l+1}\delta_{d<c_l} N_{L-1>}\,, \tag{31}$$

where

$$M_L \equiv \int_E \Sigma \hat{X}^L\, d^3X, \tag{32}$$

$$N_L \equiv \int_E \Sigma \mathbf{X}^2 \hat{X}^L\, d^3X\,, \tag{33}$$

and the angle brackets "$< \ldots >$" as well as the caret "$\hat{}$" indicates a symmetrization and removal of traces of all indices involved. In a first model we considered a homogenous ($\Sigma = $const.) and spherical Earth with radius R. For $l = 1$ one finds

$$C_{ab} = \delta_{ab}\left(\frac{2}{5}MR^2\right) \tag{34}$$

and

$$C_{bL} = 0 \quad \text{for} \quad l > 1\,. \tag{35}$$

Then we considered a more complicated problem: a rigidly rotating oblate spheroid with polar radius A, equatorial radius C and angular velocity $\mathbf{\Omega} = (0, 0, \Omega)^T$. One finds that for all even l

$$S_L = 0,\ l = 2k\,. \tag{36}$$

For $l = 1$ we get

$$S_3 = \frac{2}{5}MA^2\Omega, \tag{37}$$

and for $l = 3$ (up to symmetries of S_{abc})

$$S_{113} = S_{223} = -S_{333}/2 = \eta\,\Omega \tag{38}$$

with

$$\eta = \frac{4MA^4}{175}\frac{A^2 - C^2}{A^2}\,. \tag{39}$$

From this we conclude that even the largest higher-order spin term (S_{abc}) in the metric is at least 10^{-4} times smaller than the S_a term leading to the well known Lense-Thirring effects, which are themselves tiny (e.g. the Lense-Thirring precession of a gyroscope on board of a low-flying Earth satellite is of order $0.2''$ per year). That is the reason why higher spin-moments are not mentioned in the resolutions.

The reason to express the vector potential W_E^a in terms of the spin and not in terms of an angular velocity of the Earth is a conceptual one. The spin-moments of a body play a similar role in relativity as the potential coefficients. Even for black holes there is no problem to define the spin vector. Angular velocity is conceptually a rather complicated quantity in GRT where rigid bodies do not exist. Nevertheless the spin is needed here only to Newtonian order and we

can determine $\mathbf{S}_E$ from an angular velocity (all advanced models of Earth nutation contain a solution also for the Earth's spin).

5. REFERENCES

Damour, T., Soffel, M., Xu, C., 1991, Physical Review D, **43**, 3273

Klioner, S.A., Soffel, M. (2000): Relativistic Celestial Mechanics with PPN Parameters. Physical Review D, **62**, ID 024019

Misner, C., Thorne, K., Wheeler, 1973, Gravitation, Freeman, San Francisco

Weinberg, S., 1972, Gravitation and Cosmology, John Wiley & Sons, New York

Will, C., 1993, Theory and experiment in gravitational physics, Cambridge university press, Cambridge

EARTH'S ROTATION IN THE FRAMEWORK OF GENERAL RELATIVITY: RIGID MULTIPOLE MOMENTS

S.A. KLIONER, M. SOFFEL, Ch. XU, X. WU
Lohrmann Observatory, Dresden Technical University
01062 Dresden, Germany

ABSTRACT. A set of equations describing the rotational motion of the Earth relative to the GCRS is formulated in the approximation of rigidly rotating multipoles. The external bodies are supposed to be mass monopoles. The derived set of formulas is supposed to form the theoretical basis for a practical post-Newtonian theory of Earth precession and nutation.

1. INTRODUCTION

The relation between the International Celestial Reference System (ICRS) and the corresponding terrestrial one (ITRF) is a central problem of astrometry, geodesy and related disciplines. From a theoretical point of view this requires not only a precise determination of the ICRS and the ITRS, but also a detailed modelling of Earth's rotation. Due to the high accuracy requirements it is obvious that all of these problems have to be formulated in Einstein's theory of gravity, at least in its first post-Newtonian approximation. Until now most Newtonian treatments of Earth's rotation are based upon some highly accurate rigid body theory such as SMART97 (Bretagnon *et al.*, 1998) and add effects from elasticity, the atmosphere, the oceans, the core etc. in a perturbative manner. Actually, the concept of a rigid body is very powerful in Newton's theory where the three fundamental axes, the total angular momentum or spin axis, the rotation axis and the figure axis, can be introduced without efforts. Unfortunately rigid bodies with an internal velocity field of the form $\mathbf{v} = \omega \times \mathbf{x}$ in general do not exist in General Relativity. Nevertheless one might introduce a certain class of models, where the time behavior of potential coefficients, moments of inertia tensor, etc. is completely determined by some quantity $\omega(\mathbf{T})$. We call such models "rigidly rotating multipole" models.

The aim of this paper is to summarize a set of formulas describing the rotational motion of the Earth with respect to the Geocentric Celestial Reference System (GCRS) in the approximation of rigidly rotating multipole moments. The GCRS is defined in the post-Newtonian approximation of General Relativity by the IAU Resolution B1.3 adopted at the 24th General Assembly of the IAU (Manchester, 2000) and published in the IAU Information Bulletin No. 88 (see also erratum in Bulletin No. 89). Full text of this Resolution can be also found at `http://danof.obspm.fr/IAU_resolutions/Resol-UAI.htm`. The approximation of rigidly rotating multipoles used in this paper is a phenomenological model which allows one to simplify the mathematical description of rotational motion almost to the level of Newtonian theory. Likely, the model of rigidly rotating multipoles is not consistent with general relativity in the sense that there is no physical equation of state and local conditions of matter that will support

the model. However, a theory of motion within this model can be used as a first approximation to be refined later by methods of perturbation theory. Within this model the accuracy of the given formulas is not worse than 0.1 μas.

2. POST-NEWTONIAN EQUATIONS OF ROTATIONAL MOTION

The post-Newtonian equations of rotational motion of the Earth relative to the Geocentric Celestial Reference System (GCRS) can be derived from the metric tensor of the GCRS (Voinov, 1988; Damour, Soffel, Xu, 1993; Klioner, 1996) in the form

$$\frac{d}{d\,TCG}\,S^a = L^a + \mathcal{O}(c^{-4}). \tag{1}$$

where S^a is the post-Newtonian spin defined as an explicit integral over the body of the Earth

$$S^a = \varepsilon_{abc}\int_V X^b\,p^c\,d^3X + \mathcal{O}(c^{-4}). \tag{2}$$

Here,

$$p^a = \Sigma^a\,\left(1+\frac{4}{c^2}\,W\right) - \frac{1}{2c^2}\,G\,\Sigma\int_V \Sigma^b(T,\mathbf{X}')\,\frac{7\,\delta^{ab}+n^a n^b}{|\mathbf{X}-\mathbf{X}'|}\,d^3X' + \mathcal{O}(c^{-4}), \tag{3}$$

$$n^a = \frac{X^a - X'^a}{|\mathbf{X}-\mathbf{X}'|}, \tag{4}$$

and Σ and Σ^a are defined by the components of the energy-momentum tensor in the GCRS, $\mathcal{T}^{\alpha\,\beta}$, as $\Sigma = \mathcal{T}^{\alpha\,\alpha}$ and $\Sigma^a = \mathcal{T}^{0a}$. W is the potential appearing in the metric tensor of the GCRS. This definition of spin was first derived by Fock (1955) and thoroughly discussed in, e.g., Damour, Soffel and Xu (1993). The right-hand side of (1) represent the post-Newtonian torque which can be represented as

$$L^a = \sum_{l=0}^{\infty}\,\frac{1}{l!}\,\left(\varepsilon_{abc}\,M_{bL}\,G_{cL} + \frac{1}{c^2}\,\frac{l+1}{l+2}\,\varepsilon_{abc}\,S_{bL}\,H_{cL}\right) + \frac{d}{d\,TCG}\widetilde{S}^a. \tag{5}$$

Here M_L and S_L are the Blanchet-Damour mass and spin multipole moments characterizing the Earth, and G_L and H_L for $l \geq 2$ are the gravitoelectric and gravitomagnetic tidal moments of the external gravitational field experienced by the Earth. The moments M_L are equivalent to the set of coefficients C_{lm} and S_{lm} in the conventional expansion of the gravitational potential of the Earth in terms of spherical functions. Explicit formulas for G_L within the adopted model will be given below. The moment H_a describes the inertial forces induced by the rotation of the GCRS relative to the locally inertial reference system (these forces appear because the GCRS is defined to be kinematically non-rotating with respect to the BCRS):

$$\Omega^a_{\rm iner} = \frac{1}{2c^2}\,H_a = -\frac{3}{2\,c^2}\,\varepsilon_{aij}\,v^i_E\,\frac{\partial}{\partial x^j}w^{\rm ext}(\mathbf{x}_E) + \frac{2}{c^2}\,\varepsilon_{aij}\,\frac{\partial}{\partial x^j}w^i_{\rm ext}(\mathbf{x}_E) - \frac{1}{2\,c^2}\,\varepsilon_{aib}\,v^i_E\,G_b, \tag{6}$$

where v^i_E is the barycentric velocity of the Earth, $w^{\rm ext}(\mathbf{x}_E)$ and $w^i_{\rm ext}(\mathbf{x}_E)$ are the external BCRS potential evaluated at the geocenter, and G_a is the acceleration of the geocenter with

respect to the geodetic motion (all these quantities are defined and briefly explained in the IAU Resolution B1.3). The quantity $\Omega^a_{\rm iner}$ represent the angular velocity of precession of the GCRS with respect to the locally inertial axis. This relativistic precession consist of geodetic, Lense-Thirring and Thomas precessions (the three terms in (6), respectively) and amounts to $\sim 1.92''$ per century plus periodic terms with maximal amplitudes of 0.15 mas. It is easy to estimate that $|\Omega^a| < 3.1 \cdot 10^{-15}$ s^{-1}.

The last term in (5) represent a total time derivative and can be in principle included in the definition of the post-Newtonian spin S^a as suggested by Damour, Soffel and Xu (1993). Here we prefer to retain the definition of S^a to be (2)–(4). An explicit formula for $\widetilde{S}^a$ is given by Eqs. (2.14)–(2.16) of Damour, Soffel, Xu (1993). Numerical estimates of this term and the way to cope with it will be published elsewhere.

3. POST-NEWTONIAN ANGULAR VELOCITY AND TENSOR OF INERTIA

In order to be able to discuss the rotational motion of the Earth it is not sufficient to consider only the time dependence of the spin S^a described by (1). In classical Newtonian (Eulerian) theory of a gyroscope the concepts of a figure axis, tensor of inertia and an angular velocity of the body play a central role and one expects the introduction of corresponding quantities in a relativistic framework to be very fruitful.

Different approaches leading to the same results are possible. Both restricted rigid body models (Thorne, Gürsel, 1983; Soffel, 1994) and a theory of post-Newtonian Tisserand axes for a deformable body (Klioner, 1996) allows one to derive the same definition of the post-Newtonian tensor of inertia and split the post-Newtonian spin S^a defined by (2)–(4) in the Newtonian-looking way

$$S^a = C^{ab}\,\omega^b, \tag{7}$$

where C^{ab} is the post-Newtonian tensor of inertia and ω^b is the angular velocity of rotation of the post-Newtonian Tisserand axes (Klioner, 1996).

The explicit formula for C^{ab} as an integral over the volume of the Earth is given in Klioner (1996). Although the definition of C^{ab} contains a number of explicit relativistic terms usually we do not compute C^{ab} from the distribution of density, pressure, etc. within the Earth, but determine the values of C^{ab} from observations (as numerical parameters of the models). Therefore, for practical purposes we can simply use the fact that the spin S^a can be represented in the form given in (7).

4. RIGIDLY ROTATING MULTIPOLE MOMENTS

Up to now the tensor of inertia C^{ab} and the multipole moments of the Earth's gravitational field M_L and S_L were considered as arbitrary functions of time. In Newtonian theory of Earth's rotation a rigid Earth plays a very important role as a first order approximation. This rigid model i) crucially simplifies the mathematical description of the rotational motion and ii) is not too far from reality, so that the effect of non-rigidity can be than added to the model by means of perturbation theory. The reason why the rigid body model substantially simplifies the rotational equations of motion is that both the mass multipole moments $M_L^{\rm Newt}$ and the tensor of inertia $C^{ab}_{\rm Newt}$ rotate rigidly with the same angular velocity. In other words there exist a rigidly rotating reference system $Y^a = P^{ab}(T)\,X^a$, where $P^{ab}(T)$ is some time-dependent orthogonal matrix, where both $M_L^{\rm Newt}$ and $C^{ab}_{\rm Newt}$ are constant. Moreover, in Newtonian theory one can easily prove

that the time dependence of matrix $P^{ab}(T)$ defines the same angular velocity which appears in the Newtonian analog of (7). All this can be proved starting from the fundamental assumption that the velocity $\mathbf{v}$ of matter inside the body is described by a rigid rotation $\mathbf{v} = \omega \times \mathbf{X}$.

It is well known that in general relativity it is impossible to define a rigid non-isolated body in a self-consistent way even in the first post-Newtonian approximation (see, e.g., Thorne, Gürsel, 1983). However, we can *assume* the same nice properties of the relativistic tensor of inertia C^{ab} and multipole moments M_L and S_L that we had in Newtonian theory. Thus, we define the model of rigidly rotating multipole moments by means of a series of *assumptions*:

$$C^{ab} = P^{ac}\, P^{bd}\, \overline{C}^{cd}, \quad \overline{C}^{cd} = \text{const} \tag{8}$$

$$M_{a_1 a_2 \ldots a_l} = P^{a_1 b_1}\, P^{a_2 b_2} \ldots P^{a_l b_l}\, \overline{M}_{b_1 b_2 \ldots b_l}, \quad \overline{M}_{b_1 b_2 \ldots b_l} = \text{const}, \quad l \geq 2, \tag{9}$$

$$S_L = C^{bL}\, \omega^b, \quad l \geq 2, \tag{10}$$

$$C^{b a_1 a_2 \ldots a_l} = P^{bd}\, P^{a_1 c_1}\, P^{a_2 c_2} \ldots P^{a_l c_l}\, \overline{C}_{d c_1 c_2 \ldots c_l}, \quad \overline{C}_{d c_1 c_2 \ldots c_l} = \text{const}, \quad l \geq 2, \tag{11}$$

where $P^{ab}(T)$ is the orthogonal matrix related to ω^a by the kinematical Euler equations

$$\omega^a(T) = \frac{1}{2}\, \varepsilon_{abs}\, P^{db}(T)\, \frac{d}{dTCG}\, P^{dc}(T). \tag{12}$$

Note that we *assume* that ω^a in (10) and (12) is identical with ω^a from (7). We *assume* also that to bring $\overline{C}^{ab}$ into a diagonal form one more *time-independent* rotation is required. The matrix $P^{ab}(T)$ can be parametrized by three Euler angles ψ, θ, φ, and the time-derivatives of these angles define the angular velocity of rotation according to (12). Relations (10)–(11) for the higher spin moments S_L, $l \geq 2$ and for C_{iL} are only necessary to Newtonian accuracy since they appear only in relativistic terms of (5).

Let us stress again that in Newtonian theory one one can derive (7) and (8)–(12) from the fundamental property of rigidity of the body $\mathbf{v} = \omega \times \mathbf{X}$. On the contrary, in general relativity we define the model by *assuming* the properties of C^{ab}, M_L and S_L without further restrictions of the local flow of matter.

The experience of Newtonian models of Earth's rotation shows that the phenomenological model (8)–(12) can be used as a first-order approximation for a description of the global rotational motion of the Earth. As in Newtonian theory, such a model serves as a basis for considering the effects of non-rigidity in the rotational motion of the Earth.

5. FURTHER SIMPLIFYING ASSUMPTIONS

A number of additional simplifying assumptions will be adopted here. Some of these assumptions are justified by numerical estimations of the corresponding terms in the equations of rotational motion of the Earth.

- It is natural to assume that the GCRS is defined in such a way that the mass dipole M_a of the Earth vanishes (this assumption is actually supported by the IAU Resolution B1.4 in (IAU, 2001)), i.e. the origin of the GCRS is assumed to agree with the post-Newtonian center of mass of the Earth.

- In order to numerically estimate the influence of the terms in the right-hand side of (5) produced by S_L with $l \geq 2$ (and for that purpose only!) let us consider the following model for the matter of the Earth

$$\Sigma^a = \Sigma\, \varepsilon_{abc}\, \omega^b\, X^c. \tag{13}$$

Since we want to numerically estimate post-Newtonian terms it is sufficient to consider (13) as a Newtonian assumption of a rigidly rotating body. Substituting (13) into the definition of S_L for $l \geq 2$ one can prove that

$$S_L = C_{aL}\, \omega^a, \tag{14}$$

$$C_{aL} = -M_{aL} + \frac{l+1}{2l+1} \delta_{a<b_l} N_{L-1>}, \tag{15}$$

where the moments M_L and N_L to Newtonian order read

$$M_L \equiv \int_E \Sigma\, \hat{X}^L\, d^3X, \tag{16}$$

$$N_L \equiv \int_E \Sigma\, \mathbf{X}^2\, \hat{X}^L\, d^3X. \tag{17}$$

Here the angle brackets "$< \ldots >$" as well as the caret "$\hat{}$" indicate symmetric and tracefree (STF) part of the corresponding expression. Eqs. (14)–(16) allow one to estimate the torque $\delta \dot{S}^a \Big|_{S_L}$ due to S_L, $l \geq 2$ as

$$\left(\frac{|\delta \dot{S}^a|}{|S^a|} \right) \Bigg|_{S_L} \sim \max(|J^E_{l+1}|, |J^E_{l-1}|) \cdot \sum_A \frac{GM_A}{c^2} \frac{v_{EA}}{r^2_{EA}} \left(\frac{R_E}{r_{EA}} \right)^{l-1} < 10^{-20}\, \mathrm{s}^{-1}. \tag{18}$$

This estimate gives typical angular velocity of precession due to S_L. This can be compared, e.g., with the relativistic precession due to $\mathbf{\Omega}_{\mathrm{iner}}$. It is easy to see that the precession due to S_L for $l \geq 2$ is at least a factor 10^5 smaller than the relativistic precession due to $\mathbf{\Omega}_{\mathrm{iner}}$ (i.e. than the geodetic precession). This implies that these terms for any $l \geq 2$ can be neglected at the accuracy level of 0.1 μas. This circumstance makes the assumption (10)–(11) for S_L, $l \geq 2$ superfluous.

- All external bodies are supposed to be mass-monopoles, that is point masses characterized only by their masses M^A and BCRS positions $\mathbf{x}_A(t)$, t=TCB. Since the multipole structure (e.g., oblateness) of external bodies is not taken into account in the modern Newtonian theories of nutation of the rigid Earth, such an assumption does not prevent us to achieve the required accuracy of 0.1 μas also in the relativistic framework. In the framework of this model one can derive explicit formulas for the external tidal moments G_L influencing the Earth (E). One has

$$G_L = \sum_{A \neq E} GM_A\, g^A_L, \tag{19}$$

where g^A_L are functions of i) the BCRS position $\mathbf{x}_E$, velocity $\mathbf{v}_E$ and acceleration $\mathbf{a}_E$ of the Earth, ii) the BCRS position $\mathbf{x}_A$, velocity $\mathbf{v}_A$ and acceleration $\mathbf{a}_A$ of other bodies, iii) the mass M_E of the Earth, iv) the masses M_A of other bodies, v) the higher-order multiple moments M_L, $l \geq 2$ of the Earth. Note that in Newtonian physics only the positions of

the Earth and body A ($\mathbf{x}_E$ and $\mathbf{x}_A$) appear in g_L^A. In the post-Newtonian approximation one has

$$g_L^A = \frac{(-1)^l\,(2l-1)!!}{r_{EA}^{l+1}}\left[\hat{n}_{EA}^L\left\{1+\frac{1}{c^2}\left(2\,v_{EA}^2-\frac{1}{2}\,\mathbf{a}_A\,\mathbf{r}_{EA}-l\,\overline{w}_E(\mathbf{x}_E)-\overline{w}_A(\mathbf{x}_A)\right.\right.\right.$$
$$\left.\left.\left.-\frac{1}{2}\,(2l+1)\,(\mathbf{v}_A\,\mathbf{n}_{EA})^2\right)\right\}$$
$$-\frac{1}{c^2}\,\frac{(l-1)\,(l-8)}{2\,(2l-1)}\;\;v_{EA}^{\langle i_l}\,v_{EA}^{i_{l-1}}\,n_{EA}^{L-2\rangle}+\frac{1}{c^2}\,\frac{1}{2l-1}\,r_{EA}\,a^{\langle i_l}\,n_{EA}^{L-1\rangle}$$
$$+\frac{1}{c^2}\,\frac{l}{2}\,(\mathbf{v}_E\,\mathbf{n}_{EA})\,v_E^{\langle i_l}\,n_{EA}^{L-1\rangle}-\frac{1}{c^2}\;(l\,\mathbf{v}_A\,\mathbf{n}_{EA}+4\mathbf{v}_{EA}\,\mathbf{n}_{EA})\;v_{EA}^{\langle i_l}\,n_{EA}^{L-1\rangle}\Big], \quad (20)$$

where

$$\mathbf{a}=\left(l^2-l+4\right)\,\mathbf{a}_E+\frac{1}{2}\,(l-8)\,\mathbf{a}_A, \quad (21)$$

$$\overline{w}_E(\mathbf{x}_E)=\sum_{B\neq E}\frac{GM_B}{r_{EB}}, \quad (22)$$

$$\overline{w}_A(\mathbf{x}_A)=\sum_{B\neq A}\frac{GM_B}{r_{AB}}+G\sum_{l=2}^{\infty}\frac{(-1)^l\,(2l-1)!!}{l!\,r_{EA}^{l+1}}\,M_L\,\hat{n}_{EA}^L, \quad (23)$$

and for any A and B one has $\mathbf{r}_{AB}=\mathbf{x}_A-\mathbf{x}_B$, $\mathbf{v}_{AB}=\mathbf{v}_A-\mathbf{v}_B$, $n_{AB}^L=\dfrac{r_{AB}^{a_1}\cdots r_{AB}^{a_l}}{r_{AB}^l}$.

6. REDUCED EQUATIONS OF MOTION

Taking into account all the components of the model and the simplifying assumptions the equation of rotational motion of the Earth with respect to the GCRS can be written as

$$\frac{d}{d\,TCG}\left(C^{ab}\,\omega^b\right)=\sum_{l=1}^{\infty}\frac{1}{l!}\,\varepsilon_{abc}\,M_{bL}\,G_{cL}+\varepsilon_{abc}\,\Omega_{\rm iner}^b\,C^{cd}\,\omega^d. \quad (24)$$

The GCRS is kinematically non-rotating and this is the reason why the post-Newtonian Coriolis force proportional to $\mathbf{\Omega}_{\rm iner}$ appears in the right-hand side of (24). The equations of rotational motion of the Earth relative to a dynamically non-rotating local geocentric reference system does not contain this additional torque. However, the use of a dynamically non-rotating reference system does not seem to be advantageous since the slow precession of its spatial axes relative to those of the BCRS must be taken into account while computing the external tidal moments G_L in the dynamically non-rotating coordinates, which is by no means simpler than using (24). Note also that the relative orientation of the GCRS and that local dynamically non-rotating reference system is well known (see, e.g., Brumberg, Bretagnon, Francou (1991)) and this can be used as a check of theories of precession and nutation constructed in these two reference systems. However, it does not mean that a theory of precession and nutation of the Earth in one of these two reference systems can be constructed in a purely Newtonian way, as it was assumed in all modern theories of Earth nutation, where a purely Newtonian theory was interpreted as a theory in dynamically non-rotating coordinates.

The quantities characterizing the Earth, C^{ab}, ω^a and M_L, are functions of TCG or TT while the quantities appearing in the external tidal moments G_L (e.g., the BCRS positions of the bodies) are functions of TCB or TDB (since BCRS Solar system ephemerides should be used here to evaluate those quantities). To avoid the recomputing of G_L from TCB (or TDB) to TCG (or TT) during the [numerical] integration one may want to use TDB as the independent variable in (24). This version of the equations of rotational motion reads

$$\frac{d}{dTDB}\left(C^{ab}\,\omega^b\right) = \left(\frac{dTCG}{dTDB}\right)\Big|_{\text{geocenter}} \cdot \sum_{l=1}^{\infty} \frac{1}{l!}\,\varepsilon_{abc}\,M_{bL}\,G_{cL} + \varepsilon_{abc}\,\Omega^b_{\text{iner}}\,C^{cd}\,\omega^d. \qquad (25)$$

A solution of this equation gives the Euler angles parametrizing the orthogonal matrix P^{ab} from (8)–(9) as functions of TDB which should be re-calculated as functions of TCG or TT afterwards.

The factor $\frac{dTCG}{dTDB}$ gives a scaling of the torque as well as additional periodic signal in the torque. Its practical importance should be further investigated.

Another important issue is that the equations (24) and the formulas (20)–(23) for G_L are valid only if both time and space coordinates are not scaled in both GCRS and BCRS. Since in practice one employs scaled time scales TT and TDB as well as associated scaled spatial coordinates, the corresponding scaling factors must be taken into account while computing G_L and using (24) or (25).

In a further publication the equations of rotational motion (25) will be re-written in a form which can be directly used for practical construction of a post-Newtonian theory of Earth's rotation along the lines of Bretagnon *et al.* (1997, 1998).

7. REFERENCES

Bretagnon, P., Francou, G., Rocher, P., Simon, J.L. (1997) Theory of the rotation of the rigid Earth *Astronomy & Astrophysics*, **319**, 305–317

Bretagnon, P., Francou, G., Rocher, P., Simon, J.L. (1998) SMART97: a new solution for the rotation of the rigid Earth *Astronomy & Astrophysics*, **329**, 329–338

Brumberg, V.A., Bretagnon, P., Francou, G. (1991) Analytical algorithms of relativistic reduction of astronomical observations. In: *Métrologie et Astrométrie*, edited by Capitaine, N., Proceedings of Journées'1991, Observatoire de Paris, Paris, 141–148

Damour, T., Soffel, M., Xu, C. (1993) General Relativistic Celestial Mechanics III. Rotation Equations of Motion *Phys. Rev. D*, **Vol. no. 47**, 3124–3135

Fock, V.A. (1955) *Teoria Prostranstva, Vremeni i Tyagoteniya*, Fizmatgiz, Moscow (translated into English as *Theory of space, time and gravitation*, Pergamon, Oxford, 1959)

IAU (2001) Information Bulletin No. 88, January 2001 (see also Erratum in Information Bulletin No. 89, June 2001 and the full text of the Resolution at `http://danof.obspm.fr/IAU_resolutions/Resol-UAI.htm`

Klioner S.A. (1996): Angular velocity of extended bodies in general relativity. In: S.Ferraz-Mello, B.Morando, J.E.Arlot (eds.), Dynamics, ephemerides and astrometry in the solar system, Kluwer, Dordrecht, 309–320

Soffel, M. (1994) The problem of rotational motion and rigid bodies in the post-Newtonian framework. *unpublished notes*

Thorne, K.S., Gürsel, Y. (1983) The free precession of slowly rotating neutron stars: rigid-body motion in general relativity, *Mon. Not. R astr. Soc.*, **205**, 809–817

Voinov, A.V. (1988) Motion and rotation of celestial bodies in the post-Newtonian approximation, *Celestial Mechanics*, **41**, 293–307

APPLICATION OF POINCARÉ'S FORMALISM TO THE FREE NUTATIONS OF A THREE-LAYER EARTH MODEL

A. ESCAPA[1], J. GETINO[2], J. M. FERRÁNDIZ[1]

[1] Dpto. Análisis Matemático y Matemática Aplicada
Universidad de Alicante. E-03080 Alicante. Spain
e-mail: Alberto.Escapa@ua.es; jm.ferrandiz@ua.es

[2] Grupo de Mecánica Celeste. Facultad de Ciencias
Universidad de Valladolid. E-47005 Valladolid. Spain
e-mail: getino@maf.uva.es

ABSTRACT. In this Investigation we work out the free rotational motion of a three-layer Earth model through the Poincaré's equations. In this way, we enlarge the previous works developed by Poincaré (1910) and Moritz (1982), which were concerned with a non-dissipative two-layer Earth model. In addition, we compare this treatment with the Hamiltonian and Transfer Function approaches to the problem, showing the equivalence between the three methods with respect to the free nutations.

1. INTRODUCTION

Currently, there are two main approaches to study the Earth nutational motion: the Transfer Function approach and the Hamiltonian approach. The Transfer Function approach, see, for example, Mathews (2000), is a linear method, based on convolving some existing rigid nutation series with the so-called transfer function. In this way, the problem is simplified solely to compute this function. With this aim, it is necessary to establish the angular momentum equation for each layer of the Earth using the vectorial equations of the Newtonian Mechanics. The Hamiltonian approach, see, for expample, Getino and Ferrándiz (2000), is based on the variational principles of Mechanics, and generalizes the previous work of Kinoshita (1977) to the non-rigid case. The skeleton of the method consists in constructing a Hamiltonian function, and a set of canonical forces to include the dissipative processes, which describe properly the dynamical evolution of the system. The analytical expressions for the nutation series are derived by applying some canonical perturbation method, like the Hori's one.

¿From our point of view, the Hamiltonian approach is more complete than the Transfer Function approach. First, because the Hamiltonian method can provide non linear terms whereas the Transfer Function is intrinsically a linear procedure. Second, the Hamiltonian approach can treat in a unified way the nutational and precessional motions, even the orbital motion, of

the Earth whereas the Transfer Function approach is, in its actual formulation, limited to the nutational motion. Third, the Hamiltonian approach is a self-contained theory which does not need the support of any external rigid model. However, the study of the rotational motion of the Earth through the Hamiltonian mechanics presents, as other methods of Celestial Mechanics, the difficulty that it is a formalism which is developed within a strong mathematical background. This fact is the responsible for losing some physical insight into the problem, as it is the case when using Andoyer canonical variables or constructing the generalized forces, but, at the same time, it is also responsible for the power of the method itself.

In this note, we recover a previous variational approach to the Earth rotation problem developed by Poincaré (1910). This approach shares all the advantages of the Transfer Function approach. Besides, it also presents some of the profits of the Hamiltonian approach, but with the advantage that the theory is formulated in a more simple mathematical frame, since in the Poincaré formulation the dynamical variables are made up of Euler sets and angular velocities, variables that have an immediate geometrical and kinematical meaning.

The Poincaré approach has already been applied to the study of the rotation of a two-layer Earth model. Poincaré (1910) worked out the nutations of a two-layer Earth model composed by a rigid mantle and a fluid core. Later, Moritz (1982) improved the model by including the elasticity of the mantle, recovering the equations derived by Sasao *et al* (1980) by means of the equations of Newtonian Mechanics. In this work, we enlarge the previous studies in two ways: first, we consider a three-layer Earth model composed of a rigid mantle, a fluid core and a rigid inner core; second, we incorporate the dissipative mechanisms which were not included, nor formulated, in the former studies. Therefore, we establish a general framework for the treatment of this problem by means of the Poincaré formulation. Once we have taken this step, it is possible to describe more realistic Earth models by considering the elasticity of the layers, some internal gravitational interactions,... within the developed framework.

2. POINCARÉ'S EQUATIONS: A THREE LAYER EARTH MODEL

Let us consider an Earth model composed by three layers which share a common barycenter. The outer layer, mantle, is a rigid body, the middle layer, FOC, is a fluid layer and the inner one, SIC, is also a rigid body. In addition, we assume that the three layers have mechanical symmetry, that is to say, their equatorial inertia moments are equal. It is expedient to define the following reference frames with origin in the barycenter of the system:

i) An inertial frame: $\mathsf{T}^0 \equiv \{\mathbf{E}_1, \mathbf{E}_2, \mathbf{E}_3\}$.

ii) A frame of principal axes of inertia of the mantle: $\mathsf{T}^m \equiv \{\mathbf{e}_1, \mathbf{e}_2, \mathbf{e}_3\}$.

iii) A Tisserand frame of the FOC: $\mathsf{T}^f \equiv \left\{\mathbf{e}_1^f, \mathbf{e}_2^f, \mathbf{e}_3^f\right\}$.

iv) A frame of principal axes of inertia of the SIC: $\mathsf{T}^s \equiv \{\mathbf{e}_1^s, \mathbf{e}_2^s, \mathbf{e}_3^s\}$.

In order to determine the orientation of the frames T^m, T^f and T^s we employ three sets of Euler angles. Namely

a) $\{\phi, \theta, \psi\} \equiv \{q_1,\ q_2,\ q_3\}$ defined through the rotation

$$T^m = \mathbf{R}_3(\psi)\mathbf{R}_1(\theta)\mathbf{R}_3(\phi)T^0 = \mathbf{R}(\psi, \theta, \phi)T^0, \tag{1}$$

with

$$\mathbf{R}_3(\alpha) = \begin{pmatrix} \cos\alpha & \sin\alpha & 0 \\ -\sin\alpha & \cos\alpha & 0 \\ 0 & 0 & 1 \end{pmatrix},\ \mathbf{R}_1(\alpha) = \begin{pmatrix} 1 & 0 & 0 \\ 0 & \cos\alpha & \sin\alpha \\ 0 & -\sin\alpha & \cos\alpha \end{pmatrix}. \tag{2}$$

b) $\left\{\phi^f, \theta^f, \psi^f\right\} \equiv \{q_4,\ q_5,\ q_6\}$ defined by means of

$$T^f = \mathbf{R}_3(\psi^f)\mathbf{R}_1(\theta^f)\mathbf{R}_3(\phi^f)T^m = \mathbf{R}(\psi^f, \theta^f, \phi^f)T^m. \tag{3}$$

c) $\{\phi^s, \theta^s, \psi^s\} \equiv \{q_7,\ q_8,\ q_9\}$ are given by

$$T^s = \mathbf{R}_3(\psi^s)\mathbf{R}_1(\theta^s)\mathbf{R}_3(\phi^s)T^m = \mathbf{R}(\psi^s, \theta^s, \phi^s)T^m. \tag{4}$$

We must underline that the orientation of T^m is given with respect to the inertial frame T^0, whereas the orientation of T^f and T^s is given with respect to the mantle frame T^m.

The dynamical evolution of our Earth model can be tackled through the classical Lagrange equations. So, besides the generalized coordinates, the former Euler angles in this case, we would have to employ the generalized velocities associated to these coordinates. However, these velocities do not fit properly to the symmetries of the system. This fact complicates the development of the problem. To solve this disadvantage, maintaining the Euler sets as generalized coordinates, one takes advantage of the Poincare's equations (Poincaré, 1910) or, equivalently, the Lagrange equations for quasi-coordinates (Whittaker, 1989). Basically, this approach consists in a modification of Lagrange equations in which, instead of the generalized velocities, a linear combination of these ones is employed.

In our case, the variables which substitute the generalized velocities are

$$\begin{aligned}
\omega &= \begin{pmatrix}\omega_1\\ \omega_2\\ \omega_3\end{pmatrix} = \begin{pmatrix}\sin\theta\sin\psi & \cos\psi & 0\\ \sin\theta\cos\psi & -\sin\psi & 0\\ \cos\theta & 0 & 1\end{pmatrix}\begin{pmatrix}\dot\phi\\ \dot\theta\\ \dot\psi\end{pmatrix} = \mathbf{M}\dot{\mathbf{q}},\\
\omega^f &= \begin{pmatrix}\omega_4\\ \omega_5\\ \omega_6\end{pmatrix} = \begin{pmatrix}0 & \cos\phi^f & \sin\theta^f\sin\phi^f\\ 0 & \sin\phi^f & -\sin\theta^f\cos\phi^f\\ 1 & 0 & \cos\theta^f\end{pmatrix}\begin{pmatrix}\dot\phi^f\\ \dot\theta^f\\ \dot\psi^f\end{pmatrix} = \mathbf{M}^f\dot{\mathbf{q}}^{\mathbf{f}},\\
\omega^s &= \begin{pmatrix}\omega_7\\ \omega_8\\ \omega_9\end{pmatrix} = \begin{pmatrix}0 & \cos\phi^s & \sin\theta^s\sin\phi^s\\ 0 & \sin\phi^s & -\sin\theta^s\cos\phi^s\\ 1 & 0 & \cos\theta^s\end{pmatrix}\begin{pmatrix}\dot\phi^s\\ \dot\theta^s\\ \dot\psi^s\end{pmatrix} = \mathbf{M}^s\dot{\mathbf{q}}^{\mathbf{s}}.
\end{aligned} \tag{5}$$

These variables define a set of quasi-coordinates, π_i, of the form $\omega_i = d\pi_i/dt$. The variables ω_i have a clear kinematical meaning: they are the components of the angular velocities of each layer expressed in the mantle frame. In particular, ω is the angular velocity of T^m with respect T^0 and $\boldsymbol{\omega}^{\mathbf{f}}$, $\boldsymbol{\omega}^{\mathbf{s}}$ are, respectively, the angular velocities of T^f, T^s with respect to T^m.

The Poincaré's equations for these variables are given by

$$\frac{d}{dt}\left(\frac{\partial L}{\partial \omega_i}\right) + \sum_{j=1}^{9}\sum_{k=1}^{9} c_{ijk}\omega_j\frac{\partial L}{\partial \omega_k} - \sum_{r=1}^{9}\beta_{ri}\frac{\partial L}{\partial q_r} = Q_i,\ i = 1, ..., 9. \tag{6}$$

These equations had been taken from Moritz (1982), though, following Whittaker (1989), we have performed some modification in order to include dissipative processes. L is the Lagrangian of the system, that is to say, the difference between the kinetic and the potential energy. Q_i are the generalized forces associated with the quasi-coordinates π_i. The inclusion of these forces is necessary when considering dissipative mechanisms which can not be derived from any potential energy function. The elements β_{ri} and c_{ijk} are given by

$$\beta = (\alpha^t)^{-1},\ c_{ijk} = \sum_{r=1}^{9}\sum_{s=1}^{9}\beta_{ri}\beta_{sj}\left(\frac{\partial \alpha_{rk}}{\partial q_s} - \frac{\partial \alpha_{sk}}{\partial q_r}\right)\ \text{with}\ \alpha = \begin{pmatrix}\mathbf{M} & \mathbf{0}_{3\times3} & \mathbf{0}_{3\times3}\\ \mathbf{0}_{3\times3} & \mathbf{M}^f & \mathbf{0}_{3\times3}\\ \mathbf{0}_{3\times3} & \mathbf{0}_{3\times3} & \mathbf{M}^s\end{pmatrix}. \tag{7}$$

Taking into account eqs. (4) and (6), see Escapa, Getino and Ferrándiz (2001b), it can be shown that the elements c_{ijk} take the values

$$c_{i+3m\ j+3n\ k+3p} = (-1)^{1-\delta_{0m}}\delta_{mn}\delta_{mp}\epsilon_{ijk} \text{ with } i,j,k = 1,2,3 \text{ and } m,n,p = 0,1,2, \tag{8}$$

with δ_{ij} noting the Kronecker delta and ϵ_{ijk} the Levi-Civita symbol.

3. EQUATIONS OF MOTION: FREE PROBLEM

In this section, we will construct the ten functions, the Lagrangian and the nine generalized forces, necessaries for the establishment of the equations of motion. Because of the fact that in this work we are concerned with the free motion, we do not include in the Lagrangian none potential energies coming from internal or external origin. So, the Lagrangian will coincide with the kinetic energy of the system.

The expression of the kinetic energy is comprehensively described in Escapa, Getino and Ferrándiz (2001a), so, we only sketch the main points of this construction. First, let us introduce the inertia tensors, in mantle frame, through the inertia matrices:

a) Mantle and SIC inertia matrices

$$\mathbf{\Pi}_m = \begin{pmatrix} A_m & 0 & 0 \\ 0 & A_m & 0 \\ 0 & 0 & C_m \end{pmatrix},\ \mathbf{\Pi}_s = [\mathbf{R}(\psi^s,\theta^s,\phi^s)]^t \begin{pmatrix} A_s & 0 & 0 \\ 0 & A_s & 0 \\ 0 & 0 & C_s \end{pmatrix} \mathbf{R}(\psi^s,\theta^s,\phi^s). \tag{9}$$

b) FOC inertia matrix

$$\mathbf{\Pi}_f = \begin{pmatrix} A_f & 0 & 0 \\ 0 & A_f & 0 \\ 0 & 0 & C_f \end{pmatrix} + [\mathbf{R}(\psi^s,\theta^s,\phi^s)]^t\, \mathbf{\Pi}_{as} \mathbf{R}(\psi^s,\theta^s,\phi^s) - \mathbf{\Pi}_{as}. \tag{10}$$

Here, $\mathbf{\Pi_{as}}$ is given by

$$\mathbf{\Pi}_{as} = \begin{pmatrix} A_{as} & 0 & 0 \\ 0 & A_{as} & 0 \\ 0 & 0 & C_{as} \end{pmatrix} \tag{11}$$

This matrix is the inertia matrix of an auxiliary body, see Escapa, Getino and Ferrándiz (2001a), introduced to facilitate the decomposition of the instantantaneous inertia tensor of FOC.

Finally, by assuming that the velocity field of each layer can be described by a rigid rotation, and taking into account eqs. (9) and (10), the kinetic energy of the system is written as

$$T = \frac{1}{2}\omega^t \mathbf{\Pi}_m \omega + \frac{1}{2}\left(\omega+\omega^f\right)^t \mathbf{\Pi}_m \left(\omega+\omega^f\right) + \frac{1}{2}\left(\omega+\omega^s\right)^t \mathbf{\Pi}_s \left(\omega+\omega^s\right). \tag{12}$$

Computing this expression, we obtain that

$$L = T = L(\omega,\omega^f,\omega^s,\phi^s,\theta^s). \tag{13}$$

To model the dissipative processes of electromagnetic and viscous origin taking place in the mantle-FOC and FOC-SIC boundaries, we follow the same guidelines given by Sasao *et al.* (1980). In this way, we assume that there are two torques acting on FOC, one due to the interaction with the mantle and the other one due to the interaction with SIC, of the form

$$\mathbf{t}_{m-f} = \begin{pmatrix} -R_m & R'_m & 0 \\ -R'_m & -R_m & 0 \\ 0 & 0 & -R^*_m \end{pmatrix} \omega,\ \mathbf{t}_{s-f} = \begin{pmatrix} -R_s & R'_s & 0 \\ -R'_s & -R_s & 0 \\ 0 & 0 & -R^*_s \end{pmatrix} \left(\omega^f - \omega^s\right). \tag{14}$$

The generalized forces are constructed through the virtual work done by the dissipative torques in a virtual displacement of the system. In this way, by expressing the virtual rotations in terms of the quasi-coordinates π_i, it can be shown, see Escapa, Getino and Ferrándiz (2001b), that the nine generalized forces Q_i are written as

$$\begin{pmatrix} Q_1 \\ Q_2 \\ Q_3 \end{pmatrix} = \mathbf{0}, \quad \begin{pmatrix} Q_4 \\ Q_5 \\ Q_6 \end{pmatrix} = \mathbf{t}_{m-f} + \mathbf{t}_{s-f}, \quad \begin{pmatrix} Q_7 \\ Q_8 \\ Q_9 \end{pmatrix} = -\mathbf{t}_{s-f}. \tag{15}$$

4. FREE PROBLEM SOLUTIONS. COMPARISONS

Once we have obtained the explicit form of the Lagrangian of the system and the generalized forces, we can construct, with the help of eqs. (5), the dynamical equations of the system. The procedure is involved, though straightforward. By so doing, we get nine differential equations which can be put into the form

$$\sum_{j=1}^{9} B_{ij}(\omega, \omega^f, \omega^s, \phi^s, \theta^s) \frac{d}{dt}\omega_j = F_i(\omega, \omega^f, \omega^s, \phi^s, \theta^s). \tag{16}$$

Instead of using the Euler angles ϕ^s and θ^s, it is convenient to introduce the variables m_1 and m_2. Both sets are related by means of

$$\sin\phi^s = \frac{m_1}{\Omega \sin\theta^s}, \cos\phi^s = -\frac{m_2}{\Omega \sin\theta^s}, \cos\theta^s = \sqrt{1 - \frac{m_1^2 + m_2^2}{\Omega^2}}, \tag{17}$$

The variables m_1 and m_2 have also a clear geometrical meaning; they are the xy components of the vector $\Omega\mathbf{e_3^s}$ in the mantle frame, being Ω the mean angular velocity of the Earth rotation. It is worthy to note that, by the moment, we have not performed any approximation in the mathematical procedure which leads to the obtention of eqs. (15).

To treat analytically the system (15), usually, a linearization of the variables $\omega, \omega^f, \omega^s, \mathbf{m}_1, \mathbf{m}_2$ about the point $(0, 0, \Omega, 0, 0, 0, 0, 0, 0)$ is performed. So, we obtain as a first result that

$$\omega_3 = \Omega, \ \omega_3^f = 0, \ \omega_3^s = 0. \tag{18}$$

The six remaining equations are completed by adding the two linearized kinematical relationships, see eqs. (4),

$$\frac{d}{dt}m_1 = \Omega\omega_2^s, \frac{d}{dt}m_2 = -\Omega\omega_1^s. \tag{19}$$

In this way, we can write a complex four dimensional linear differential equations system of the form

$$\frac{d}{dt}\begin{pmatrix} \omega_1 + i\omega_2 \\ \omega_1^f + i\omega_2^f \\ \omega_1^s + i\omega_2^s \\ m_1 + im_2 \end{pmatrix} = \mathbf{P}\begin{pmatrix} \omega_1 + i\omega_2 \\ \omega_1^f + i\omega_2 \\ \omega_1^s + i\omega_2 \\ m_1 + im_2 \end{pmatrix} = \mathbf{P}\,\mathbf{p}, \tag{20}$$

being $\mathbf{P}$ a 4×4 complex matrix. This matrix provides the well-known expressions for the four nutation normal modes of a three-layer Earth model.

Next, we will do a comparison between eqs. (18) and the equations of the free problem given by the transfer function, Mathews (2000), and the Hamiltonian, Getino and Ferrándiz (2000), approaches.

In the transfer function approach the equations of the free problem can be written as

$$\mathbf{M}_1 \frac{d\mathbf{x}}{dt} + \mathbf{M}_2 \mathbf{x} = \mathbf{0}. \tag{21}$$

Here, $\mathbf{M}_1$ and $\mathbf{M}_2$ are 4×4 complex matrices depending on several Earth parameters and $\mathbf{x}$ is a column matrix containing the dynamical variables of the problem. By considering the kinematical and geometrical meaning of these variables it is possible to establish a relationship of the type

$$\mathbf{x} = \mathbf{C}_1 \, \mathbf{p}, \tag{22}$$

being $\mathbf{C}_1$ a matrix of constant coefficients. From eqs. (18), (21) and (22) it can be derived that

$$\mathbf{P} = -\mathbf{C}_1^{-1} \left(\mathbf{M}_1^{-1} \mathbf{M}_2 \right) \mathbf{C}_1 \, . \tag{23}$$

So, the systems of differential equations (18) and (21) are equivalent.

In the case of the Hamiltonian approach, let us remember that the free problem is derived from the system of equations

$$\frac{d\mathbf{h}}{dt} = \mathbf{H} \, \mathbf{h}. \tag{24}$$

$\mathbf{H}$ is a 4×4 complex matrix, whereas $\mathbf{h}$ is a column matrix containing some combinations of the canonical Andoyer variables. These combinations can be related with the xy components, in the mantle frame, of the angular momentum of the whole Earth, FOC and SIC and of the vector $\mathbf{e}_3^s$. Through these relationships, it can be established that

$$\mathbf{h} = \mathbf{C}_2 \, \mathbf{p}, \tag{25}$$

being $\mathbf{C}_2$ a matrix of constant coefficients. Taking into account eqs. (18), (24) and (19) we have found that

$$\mathbf{P} = \mathbf{C}_2^{-1} \mathbf{H} \mathbf{C}_2, \tag{26}$$

therefore the systems (18) and (24) are also equivalent.

Finally, let us point out that we have shown, by an indirect way, that the free problem of the Hamiltonian and Transfer Function approaches are also equivalent because both of them are equivalent to the Poincaré approach.

5. ACKNOWLEDGMENTS

This work has been supported by Spanish Projects AYA 2000-1787, AYA 2001-0787, PNE-015/2001-C and VA11/99 of the *Junta de Castilla y León.*

6. REFERENCES

Escapa A., Getino, J. and Ferrándiz, J. M., Canonical approach to the free nutations of a three–layer Earth model, *J. Geophys. Res.*, 106, 11387-11397, 2001a.

Escapa A., Getino, J. and Ferrándiz, J. M., Study of the nutations of a three–layer Earth model through the Poincaré's equations, (in preparation), 2001b.

Getino, J., and J. M. Ferrándiz, Advances in the unified theory of the rotation of the non–rigid Earth, in *Proceedings of IAU Colloquium 180*, edited by K. J. Johnston, D. D. McCarthy, B. J. Luzum, and G. H. Kaplan, pp. 236-241, U.S. Nav. Obs., Washington, D. C. , 2000.

Kinoshita, H., Theory of the rotation of the rigid Earth, *Celest. Mech., 15,* 277-326, 1977.

Mathews, P. M., Improved model for precesion and nutation, in *Proceedings of IAU Colloquium 180*, edited by K. J. Johnston, D. D. McCarthy, B. J. Luzum, and G. H. Kaplan, pp. 212-222, U.S. Nav. Obs., Washington, D. C. , 2000.

Moritz, H., A Variational Principle for Molodensky's Liquid-Core problem, *Bull. Géod.*, 56, 364-380, 1982.

Poincaré, H., Sur la précession des corps deformables, *Bull. Astron., 27*, 321-356, 1910.

Sasao, T., S. Okubo, and M. Saito, A simple theory on the dynamical effects of a stratified fluid core upon nutational motion of the Earth, in *Proceedings of IAU Symposium 78*, edited by E. P. Federov, M. L. Smith, and P. L. Bender, pp. 165-183, D. Reidel, Norwell, Mass., 1980.

Whittaker, E. T., *A Treatise on the Analytical Dynamics of Particles and Rigid Bodies*, 4th. ed., Cambridge University Press, 1989.

HIGH-PRECISION NUMERICAL THEORY OF THE EARTH ROTATION: MAIN PRINCIPLES OF CONSTRUCTION AND RESULTS

V. V. PASHKEVICH AND G. I. EROSHKIN
Central Astronomical Observatory at Pulkovo of the Russian Academy of Science
Pulkovskoe Shosse 65/1, Saint Petersburg, 196140, Russia
e-mail: apeks@gao.spb.ru

ABSTRACT. The numerical investigation of the rigid Earth rotation, taking into account the geodetic perturbations is based on the following principles:

a) *Slow Rodrigues-Hamilton parameters,* in which the main part of the secular component of the angle of proper rotation of the Earth is excluded, are used.

b) The mathematical formulation of the problem *distinguishes* between the Earth's equator of rotation and the Earth's dynamical equator.

c) *The high-precision method of the numerical integration* is applied.

d) *The semi-analytical theory SMART97* is modified for the calculation of the initial conditions of the numerical theory.

The results of the comparison of the modified KINEMATICAL solution of SMART97 theory and the numerical theory do not reveal discrepancies more than $5\mu as$ over the 200 yr time interval.

1. INTRODUCTION

The construction of the high-precision numerical theory of Earth rotation is based on the following principles:

a) For the efficient numerical solution of the problem *slow Rodrigues-Hamilton parameters* are used, in which the main part of the secular component of the proper rotation angle of the Earth is excluded. The first derivatives of slow Rodrigues-Hamilton parameters are small quantities of the order 10^{-7}/day. These properties of the variables make the process of the numerical integration more stable.

b) The mathematical formulation of the problem *distinguishes* the Earth equator of rotation and the Earth dynamical equator. The rotation of the Earth about its center of masses is described as the rotation of its principal axes of inertia with respect to the non-rotating geocentric ecliptical coordinate system. The reference frame of the problem refers to the fixed ecliptic and vernal equinox J2000.0. The ephemeris DE403/LE403 (Standish et al., 1995) is used for the description of the orbital motions of the disturbing bodies. The reference frame of the ephemeris DE403/LE403 is the Earth's mean equator of rotation at the epoch J2000.0. The coordinate system of DE403/LE403 after two rotation (Bretagnon et al., 1998):

1) a rotation $R_3(-0.''05334)$ in the equatorial plain,

2) a rotation $R_1(23^\circ 26' 21.''40928)$

coincides with the ecliptical coordinate system of the problem. From the elementary kinematical relations one can derive that the angle between the dynamical Earth's equator and the Earth's mean equator of rotation is approximately $9mas$. Thus the inclination of the Earth mean dynamical equator to the mean ecliptic J2000.0 is $\theta_0 = 23^o26'21.''400567...$ and the longitude of the ascending node of the Earth dynamical equator at the epoch J2000.0 is $\psi_0 = -0.2895...\mu$as.

c) *The high-precision method of the numerical integration* HIPPI (Eroshkin, 2000) is applied. The integration of the problem is carried out over the time interval 2000 – 2199 years from the initial epoch JD 2451545.0 (January 1, 2000). The initial conditions of the numerical integration are determined by the semi-analytical theory SMART97. The numerical integration is performed with one day constant step size and Chebyshev polynomials of 32-th degree approximating the right-hand sides of the differential equations. The method of integration is based on the almost uniform interpolation of the right-hand sides of the differential equations. Thus the polynomials, representing variables and their first derivatives, describe fairly well the behavior of the solution over the whole interval of step size.

d) *The modified semi-analytical theory SMART97* is used for the calculation of the initial conditions of the numerical theory. First of all, the modification means taking into account principles formulated in b). Besides, the values of the mean motion of the major planets and the node the of lunar orbit are changed by the value of the geodetic precession. Some corrections to the secular and periodic terms of the SMART97 theory are found by the method proposed in (Pashkevich, 2000).

2. FUNDAMENTALS

Usually, as the variables of the problem, four Rodrigues-Hamilton parameters are taken. They are defined by Euler angles $\psi, \theta, \tilde{\phi}$:

$$\mu_0 = \cos\frac{\theta}{2}\cos\frac{\psi+\tilde{\phi}}{2}, \quad \mu_1 = \sin\frac{\theta}{2}\cos\frac{\psi-\tilde{\phi}}{2}, \quad \mu_2 = \sin\frac{\theta}{2}\sin\frac{\psi-\tilde{\phi}}{2}, \quad \mu_3 = \cos\frac{\theta}{2}\sin\frac{\psi+\tilde{\phi}}{2},$$

where ψ is the longitude of the ascending node of the dynamical Earth equator on the fixed ecliptic J2000.0; θ is the angle of the inclination of the dynamical Earth equator to the fixed ecliptic J2000.0; $\tilde{\phi}$ is the angle of the proper rotation of the Earth, which is counted from the ascending node of the Earth dynamical equator.

The differential equations of the problem are derived from the Lagrange differential equations of the second kind:

$$\frac{d}{dt}\frac{\partial L}{\partial \dot{\mu}_i} - \frac{\partial L}{\partial \mu_i} = 0, \quad i = 0, 1, 2, 3.$$

Here and further a dot over a letter means the differentiation with respect to time. The Lagrange function of the problem is

$$L = T + U + \Delta L.$$

Here T is the kinetic energy of the rotational motion, U is the force function of the gravitational interaction of the Earth with disturbing bodies (the Moon, Sun and major planets). ΔL is the additional part of Lagrange function, which generates approximately the geodetic perturbations in the Earth rotation (Eroshkin, Pashkevich, 1997):

$$\Delta L = \sum_{j\neq\oplus} \frac{Gm_j}{c^2}\{\frac{1}{r_{j\oplus}^3}\overline{H}\cdot[\overline{r}_{j\oplus}\times(\frac{3}{2}\overline{v}_\oplus - 2\overline{v}_j)]-$$
$$-\frac{3}{2r_{j\oplus}^3}\{(C-B)\Omega_1(z_{j\oplus}\dot{y}_{j\oplus}+y_{j\oplus}\dot{z}_{j\oplus})+(A-C)\Omega_2(x_{j\oplus}\dot{z}_{j\oplus}+z_{j\oplus}\dot{x}_{j\oplus})+$$
$$+(B-A)\Omega_3(y_{j\oplus}\dot{x}_{j\oplus}+x_{j\oplus}\dot{y}_{j\oplus})+$$
$$+\frac{\overline{r}_{j\oplus}\cdot\overline{v}_j}{r_{j\oplus}^2}[(C-B)\Omega_1 z_{j\oplus}y_{j\oplus}+(A-C)\Omega_2 x_{j\oplus}z_{j\oplus}+(B-A)\Omega_3 x_{j\oplus}y_{j\oplus}]\}\}.$$

The angular momentum vector of the Earth is $\overline{H} = A\Omega_1\overline{i}_1 + B\Omega_2\overline{i}_2 + C\Omega_3\overline{i}_3$; A, B and C are the Earth principal moments of inertia; $\Omega_1, \Omega_2, \Omega_3$ are the projections on the angular velocity vector of the Earth $\bar{\Omega}$ on the axes of the principal moments of inertia; $\overline{i}_1, \overline{i}_2, \overline{i}_3$ are the unit vectors; G is the square of the Gaussian gravitational constant; m_j is the mass of the j-th disturbing body; c is the velocity of light in vacuum; $r_{j\oplus} = \sqrt{x_{j\oplus}^2 + y_{j\oplus}^2 + z_{j\oplus}^2}$ and $x_{j\oplus}, y_{j\oplus}, z_{j\oplus}$ are the geocentric equatorial coordinates of the j-th disturbing body; $\overline{v}_\oplus$ and $\overline{v}_j$ are the vectors of the barycentric velocity of the Earth and the disturbing body M_j determined in the geoequatorial coordinate system.

The first line of ΔL is a dominant part. It can be expressed as $\bar{H}\cdot\bar{\sigma}$, where $\bar{\sigma} = \sum\limits_{j\neq\oplus}\frac{Gm_j}{c^2 r_{j\oplus}^3}\left\{\bar{r}_{j\oplus}\times(\frac{3}{2}v_\oplus - 2v_j)\right\}$ is the vector of the geodetic rotation of the Earth, which can be joined with the expression of the kinetic energy $T = \frac{1}{2}H\cdot\Omega$. Now kinetic energy of the rotational motion, taking into account essential part of the geodetic rotation, is:

$$T = \frac{1}{2}(A\Omega_{*1}^2 + B\Omega_{*2}^2 + C\Omega_{*3}^2),$$

where $\bar{\Omega}_* = \bar{\Omega} + \bar{\sigma}$.

The angular velocity vector of the Earth rotation is:

$$\begin{pmatrix} 0 \\ \Omega_{*1} \\ \Omega_{*2} \\ \Omega_{*3} \end{pmatrix} = \begin{pmatrix} 0 \\ \Omega_1+\sigma_1 \\ \Omega_2+\sigma_2 \\ \Omega_3+\sigma_3 \end{pmatrix} =$$

$$= 2\begin{pmatrix} -\mu_0 & -\mu_1 & -\mu_2 & -\mu_3 \\ -\mu_1 & \mu_0 & \mu_3 & -\mu_2 \\ -\mu_2 & -\mu_3 & \mu_0 & \mu_1 \\ -\mu_3 & \mu_2 & -\mu_1 & \mu_0 \end{pmatrix}\left[\begin{pmatrix} \dot{\mu}_0 \\ \dot{\mu}_1 \\ \dot{\mu}_2 \\ \dot{\mu}_3 \end{pmatrix} + \frac{1}{2}\begin{pmatrix} -\mu_0 & -\mu_1 & -\mu_2 & -\mu_3 \\ -\mu_1 & \mu_0 & \mu_3 & -\mu_2 \\ -\mu_2 & -\mu_3 & \mu_0 & \mu_1 \\ -\mu_3 & \mu_2 & -\mu_1 & \mu_0 \end{pmatrix}\begin{pmatrix} 0 \\ \sigma_X \\ \sigma_Y \\ \sigma_Z \end{pmatrix}\right].$$

Here $\sigma_1, \sigma_2, \sigma_3$ are projections of the vector $\bar{\sigma}$ on the axes of the Earth principle moments of inertia and $\sigma_X, \sigma_Y, \sigma_Z$ are projections of this vector on the axes of the non-rotating ecliptical reference frame.

The *slow* variable ϕ is introduced by the following relation:

$$\phi = \tilde{\phi} - 2\pi(1 + 1/365.25)t = \tilde{\phi} - \nu t,$$

where t is the time expressed in Julian days.

Slow Rodrigues-Hamilton parameters as follows:

$$\lambda_0 = \cos\frac{\theta}{2}\cos\frac{\psi+\phi}{2},\ \lambda_1 = \sin\frac{\theta}{2}\cos\frac{\psi-\phi}{2},\ \lambda_2 = \sin\frac{\theta}{2}\sin\frac{\psi-\phi}{2},\ \lambda_3 = \cos\frac{\theta}{2}\sin\frac{\psi+\phi}{2}.$$

The differential equations of the rotation in *slow* Rodrigues-Hamilton parameters have a form:

$$\begin{pmatrix}\ddot{\lambda}_0\\ \ddot{\lambda}_1\\ \ddot{\lambda}_2\\ \ddot{\lambda}_3\end{pmatrix} = \frac{1}{2}\begin{pmatrix}-\lambda_0 & -\lambda_1 & -\lambda_2 & -\lambda_3\\ -\lambda_1 & \lambda_0 & -\lambda_3 & \lambda_2\\ -\lambda_2 & \lambda_3 & \lambda_0 & -\lambda_1\\ -\lambda_3 & -\lambda_2 & \lambda_1 & \lambda_0\end{pmatrix}\begin{pmatrix}\frac{1}{2}\omega_*^2\\ \dot{\omega}_{*1}\\ \dot{\omega}_{*2}\\ \dot{\omega}_{*3}\end{pmatrix} -$$

$$- \begin{pmatrix}-\dot{\lambda}_0 & -\dot{\lambda}_1 & -\dot{\lambda}_2 & -\dot{\lambda}_3\\ -\dot{\lambda}_1 & \dot{\lambda}_0 & \dot{\lambda}_3 & -\dot{\lambda}_2\\ -\dot{\lambda}_2 & -\dot{\lambda}_3 & \dot{\lambda}_0 & \dot{\lambda}_1\\ -\dot{\lambda}_3 & \dot{\lambda}_2 & -\dot{\lambda}_1 & \dot{\lambda}_0\end{pmatrix}\begin{pmatrix}0\\ \sigma_X\\ \sigma_Y\\ \sigma_Z\end{pmatrix} - \frac{1}{2}\begin{pmatrix}-\lambda_0 & -\lambda_1 & -\lambda_2 & -\lambda_3\\ -\lambda_1 & \lambda_0 & \lambda_3 & -\lambda_2\\ -\lambda_2 & -\lambda_3 & \lambda_0 & \lambda_1\\ -\lambda_3 & \lambda_2 & -\lambda_1 & \lambda_0\end{pmatrix}\begin{pmatrix}0\\ \dot{\sigma}_X\\ \dot{\sigma}_Y\\ \dot{\sigma}_Z\end{pmatrix},$$

where $\omega_*^2 = \omega^2 + 2(\omega_X\sigma_X + \omega_Y\sigma_Y + \omega_Z\sigma_Z) + \sigma^2$ and the first derivatives of the angular velocity components are expressed by means of the following equations:

$$\begin{aligned}
\dot{\omega}_{*1} =& -\nu\omega_{*2} - \omega_{*2}(\omega_{*3}+\nu)(\alpha\cos^2\nu t + \beta\sin^2\nu t) + \omega_{*1}(\omega_{*3}+\nu)(\alpha-\beta)\sin\nu t\cos\nu t +\\
&+\left(\frac{\cos^2\nu t}{A} + \frac{\sin^2\nu t}{B}\right)\sum_{j\neq\oplus}\left(z_{j\oplus}\frac{\partial U_j}{\partial y_{j\oplus}} - y_{j\oplus}\frac{\partial U_j}{\partial z_{j\oplus}}\right) +\\
&+\left(\frac{1}{A}-\frac{1}{B}\right)\sin\nu t\cos\nu t\sum_{j\neq\oplus}\left(x_{j\oplus}\frac{\partial U_j}{\partial z_{j\oplus}} - z_{j\oplus}\frac{\partial U_j}{\partial x_{j\oplus}}\right),\\
\dot{\omega}_{*2} =& \ \nu\omega_{*1} + \omega_{*1}(\omega_{*3}+\nu)(\alpha\sin^2\nu t + \beta\cos^2\nu t) - \omega_{*2}(\omega_{*3}+\nu)(\alpha-\beta)\sin\nu t\cos\nu t +\\
&+\left(\frac{\sin^2\nu t}{A} + \frac{\cos^2\nu t}{B}\right)\sum_{j\neq\oplus}\left(x_{j\oplus}\frac{\partial U_j}{\partial z_{j\oplus}} - z_{j\oplus}\frac{\partial U_j}{\partial x_{j\oplus}}\right) +\\
&+\left(\frac{1}{A}-\frac{1}{B}\right)\sin\nu t\cos\nu t\sum_{j\neq\oplus}\left(z_{j\oplus}\frac{\partial U_j}{\partial y_{j\oplus}} - y_{j\oplus}\frac{\partial U_j}{\partial z_{j\oplus}}\right),\\
\dot{\omega}_{*3} =& -\gamma(\omega_{*1}\cos\nu t + \omega_{*2}\sin\nu t)(-\omega_{*1}\sin\nu t + \omega_{*2}\cos\nu t) +\\
&+\frac{1}{C}\sum_{j\neq\oplus}\left(y_{j\oplus}\frac{\partial U_j}{\partial x_{j\oplus}} - x_{j\oplus}\frac{\partial U_j}{\partial y_{j\oplus}}\right).
\end{aligned}$$

Here $\alpha = \dfrac{B-A}{C}$, $\beta = \dfrac{C-B}{A}$, $\gamma = \dfrac{C-A}{B}$, and

$$\begin{pmatrix}0\\ \omega_{*1}\\ \omega_{*2}\\ \omega_{*3}\end{pmatrix} = 2\begin{pmatrix}-\lambda_0 & -\lambda_1 & -\lambda_2 & -\lambda_3\\ -\lambda_1 & \lambda_0 & \lambda_3 & -\lambda_2\\ -\lambda_2 & -\lambda_3 & \lambda_0 & \lambda_1\\ -\lambda_3 & \lambda_2 & -\lambda_1 & \lambda_0\end{pmatrix}\left[\begin{pmatrix}\dot{\lambda}_0\\ \dot{\lambda}_1\\ \dot{\lambda}_2\\ \dot{\lambda}_3\end{pmatrix} + \frac{1}{2}\begin{pmatrix}-\lambda_0 & -\lambda_1 & -\lambda_2 & -\lambda_3\\ -\lambda_1 & \lambda_0 & \lambda_3 & -\lambda_2\\ -\lambda_2 & -\lambda_3 & \lambda_0 & \lambda_1\\ -\lambda_3 & \lambda_2 & -\lambda_1 & \lambda_0\end{pmatrix}\begin{pmatrix}0\\ \sigma_X\\ \sigma_Y\\ \sigma_Z\end{pmatrix}\right].$$

3. RESULTS

A comparison of the results of the numerical integration with the modified semi-analytical solution SMART97, as it was mentioned in b), is carried out for every day over all the interval of

integration. The following secular and periodical corrections to the modified KINEMATICAL solution SMART97 were found by the method proposed in (Pashkevich, 2000):

$$\begin{aligned}
\psi_{smart97} &= -0.2895 + 50384564881.3693T - 107194853.5817T^2 - 1143646.1500T^3 + \\
&\quad +1328317.7356T^4 - 9396.2895T^5 \\
d\psi &= 0.7_{\pm 0.1} + 338_{\pm 9}T + 1500_{\pm 200}T^2 - 17000_{\pm 1000}T^3 + 18000_{\pm 3000}T^4 \\
\omega_{smart97} &= 84381400567.4132 - 265011.2586T + 5127634.2488T^2 - 7727159.4229T^3 - \\
&\quad -4916.7335T^4 + 33292.5474T^5 \\
d\omega &= -2.84_{\pm 0.06} + 28_{\pm 5}T - 2300_{\pm 100}T^2 + 3800_{\pm 700}T^3 + 11000_{\pm 2000}T^4 \\
\phi_{smart97} &= 37658226149.3691 + 27824506304T - 98437693.3264T^2 - \\
&\quad -1217008.3291T^3 + 1409526.4062T^4 - 9175.8967T^5, \\
d\phi &= -3.2_{\pm 0.2} - 520_{\pm 10}T + 110600_{\pm 300}T^2 + 907000_{\pm 2000}T^3 + 66000_{\pm 5000}T^4,
\end{aligned}$$

$$\begin{aligned}
\Delta\psi = {} & (-0.38 - 64.1T + 277T^2)\sin(\lambda_3 + D - F) + (1.33 - 18.4T - 157T^2)\cos(\lambda_3 + D - F) + \\
& +(1.04 - 10.2T + 0T^2)\sin(2\lambda_3 - 3\lambda_5 + 2D - 2l) + \\
& +(-0.59 + 24.7T - 156T^2)\cos(2\lambda_2 - 3\lambda_5 + 2D - 2l) + \\
& +(0.27 - 12.1T + 37T^2)\sin(\lambda_6) + (0.60 + 6.6T - 42T^2)\cos(\lambda_6)\ ..., \\
\Delta\omega = {} & (0.423 - 8.9T - 77T^2)\sin(\lambda_3 + D - F) + (1.38 + 41.9T - 188T^2)\cos(\lambda_3 + D - F), \\
\Delta\phi = {} & (-6.40 - 65.3T + 291T^2)\sin(\lambda_3 + D - F) + (1.31 - 16.9T - 140T^2)\cos(\lambda_3 + D - F) + \\
& +(-0.17 + 6.3T - 30T^2)\sin(3\lambda_2 - 5\lambda_3) + \\
& +(-0.35 + 6.4T - 21T^2)\cos(3\lambda_2 - 5\lambda_3) + \\
& +(0.98 - 11.5T + 16T^2)\sin(2\lambda_3 - 3\lambda_5 + 2D - 2l) + \\
& +(-0.69 + 25.1T - 153T^2)\cos(2\lambda_2 - 3\lambda_5 + 2D - 2l) + \\
& +(0.22 - 11.5T + 35T^2)\sin(\lambda_6) + (0.48 + 7.7T - 48T^2)\cos(\lambda_6)\ ....
\end{aligned}$$

Here T is the time expressed in Julian thousand years, counted from the fundamental epoch J2000. The values of the coefficients are expressed in microarcseconds; $\lambda_3 + D - F = \Omega + 180^o$; $\lambda_2, \lambda_3, \lambda_5, \lambda_6$ are the mean longitudes of Venus, the Earth, Jupiter and Saturn respectively; D is the difference between the mean longitudes of the Moon and the Sun; Ω is the mean longitude of the ascending node of the lunar orbit; F is the mean argument of the Moon's latitude; l is the mean anomaly of the Moon. The values of the coefficients are expressed in microarcseconds. All these corrections were added to the modified KINEMATICAL solution SMART97 and the numerical integration was repeated anew with the modified initial conditions. The results of comparison are depicted in Fig.1.

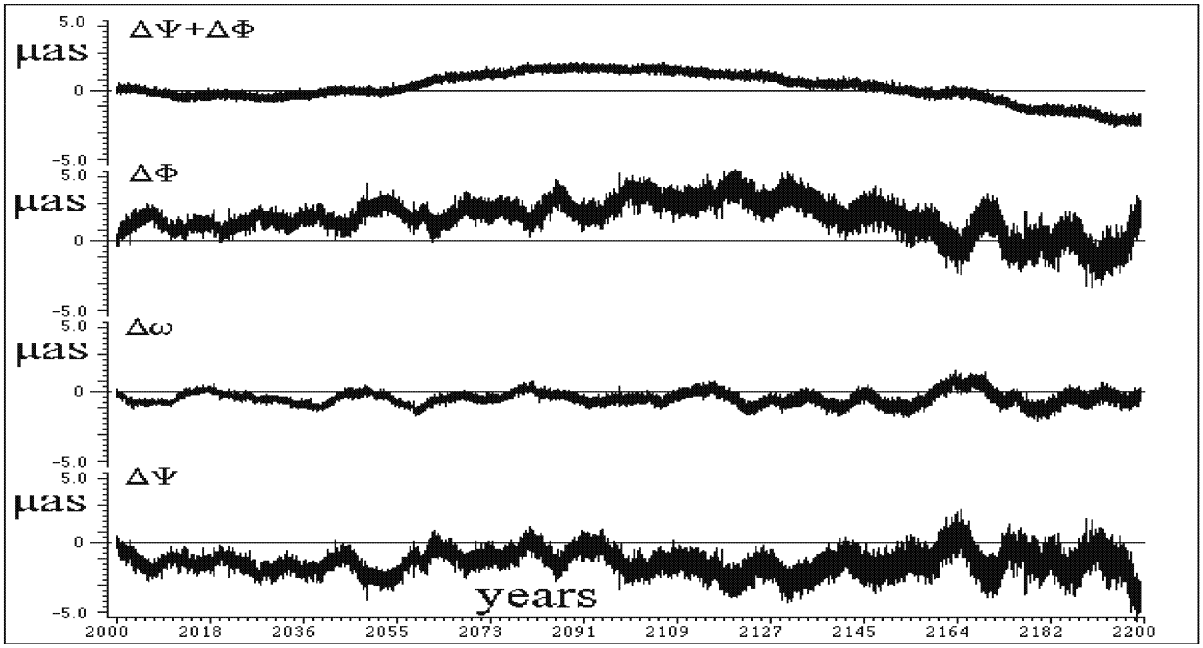

Figure 1: Numerical integration minus KINEMATICAL solution SMART97 in Euler angles

Fig. 1. Numerical integration minus KINEMATICAL solution SMART97 in Euler angles

4. CONCLUSION

The high-precision numerical theory of rotation of the rigid Earth rotation in *slow* Rodrigues-Hamilton parameters is constructed. The estimated accuracy of the numerical theory is of the order of several decimals of microarcsecond.

5. REFERENCES

Bretagnon P., Francou G., Rocher P., and Simon J. L., SMART97: A new solution for the rotation of the rigid Earth, *Astronomy and Astrophysics*, **329**, No.1, 329–338, 1998.

Eroshkin G. I., Pashkevich V. V.: 1997, "Numerical Simulation of the Rotational Motion of the Earth and Moon", *Dynamics and Astrometry of Natural and Artificial Celestial Bodies, IAU Colloquium 165* (I.M.Wytrzyszczak, J.H.Lieske, R.A.Feldman, eds), Kluwer, Dordrecht, pp. 275–280.

Eroshkin G. I., High-Precision method of the Numerical Solution of the Celestial Mechanic problems based on Chebishev Polynomial Interpolation, *Astrometry, Geodynamics and Celestial Mechanics at the turn of XXIth century, The Conference of the St.Petersburg in the IPA RAS, 19–23 June 2000* , pp. 229–230 (in Russian), 2000.

Pashkevich V. V.: 2000, "New development of the numerical theory of the earth rotation", In: Journees 2000: J2000, a fundamental epoch for origins of reference systems and astronomical models, (N.Capitaine, ed.), pp.169-176.

Standish E. M., Newhall X X, Williams J. G. and Folkner W. M.: 1995, "JPL Planetary and Lunar Ephemerides, DE403/LE403", *JPL IOM* 314.10-127.

THEORETICAL CONSIDERATIONS ON PRECESSION AND NUTATION REFERRED TO THE GCRS

N. CAPITAINE
SYRTE/UMR8630-CNRS
Observatoire de Paris, 61 avenue de l'Observatoire, 75014, Paris, France
e-mail: capitain@syrte.obspm.fr

ABSTRACT. IAU 2000 Resolutions bring significant improvement for precession and nutation. This concern definitions, theoretical models and parameters to be used. The celestial reference system is clearly specified in the framework of General Relativity, the definition of the pole to which the motion refers is extended to the high frequency domain (Celestial Intermediate Pole, CIP), the new theory (IAU 2000) for representing the motion is accurate at the level of 0.1 mas and the parameters to be used (celestial coordinates of the CIP) are close to the parameters to which the observations are sensitive. There is moreover a clear separation between Earth rotation and precession-nutation thanks to the use of the non-rotating origin on the moving equator (Celestial and Terrestrial Ephemeris Origins). This paper describes the consequences of these resolutions and show their corresponding improvements for precession-nutation.

1. INTRODUCTION

After the adoption of the International Celestial Reference System, ICRS, by the IAU in 1997, new IAU Resolutions have been adopted in 2000 that specify the new models and algorithms to be used in order to take advantage of the accuracy and the fundamental property of non-rotation of the ICRS. These resolutions bring significant improvements concerning definitions, theoretical models and parameters to be used and several of them concern more specifically precession and nutation. The first improvement is that the definition of the celestial reference system is now clearly specified in the framework of General Relativity and that the metric tensors are explicitely written both in the BCRS and in the GCRS in a compact and self-consistent form. Second, the definition of the pole to which the motion refers (Celestial Intermediate Pole, CIP) is sharpened in order to consider the non-negligible high frequency variations at the microarsecond level. Third, a new geophysically-based theory (IAU 2000) for representing precession and nutation is adopted that is accurate at the level of 0.1 mas. Fourth, the Earth Orientation Parameters to be used (celestial coordinates of the CIP and Earth Rotation Angle) are close to the parameters to which the observations are sensitive and the use of the non-rotating origin on the moving equator (Celestial and Terrestrial Ephemeris Origins) is recommended so that UT1 is directly proportional to the Earth Angle of Rotation resulting in a clear separation between Earth rotation and precession-nutation.

The following sections explain the consequences of the implementation (on 1 January 2003) of the IAU resolutions concerning precession and nutation and the corresponding improvements.

2. CONSEQUENCES OF THE IAU RESOLUTIONS OF THE XXIVth GA 2000 FOR PRECESSION AND NUTATION

2.1 IAU 2000 Resolutions concerning precession and nutation

The IAU resolutions of the XXIVth GA 2000 that have consequences for precession-nutation are the following: Resolution B1.3 on *Definition of BCRS and GCRS*, Resolution B1.6 on *IAU 2000 Precession-Nutation Model*, Resolution B1.7 on *Definition of Celestial Intermediate Pole* and Resolution B1.8 on *Definition and use of Celestial Ephemeris Origins and Terrestrial Ephemeris Origins.*

2.2 Consequences of IAU Resolution B1.3 for precession and nutation

Resolution B1.3 provides clarification of IAU's 1991 definition of the coordinate systems in the framework of GR for distinction between the celestial system for Solar Sytem or for the Earth. It specifies that the system of space-time coordinates within the framework of General Relativity be called the Barycentric Celestial Reference System (BCRS) for the Solar system and the Geocentric Celestial Reference System (GCRS) for the Earth and specify the metric to be used in these systems. The celestial reference system to refer precession nutation parameters and Earth's angle of rotation is thus changed from the FK5 to the GCRS.

2.3 Consequences of IAU Resolution B1.6 for precession and nutation

Resolution B1.6 describes the new IAU 2000 precession-nutation model which replaces the IAU 1976 Precession Model (Lieske *et al.* 1977) and IAU 1980 Theory of nutation (Seidelmann 1982). The IAU 2000 precession-nutation model (see IERS Conventions 2000) is based on (i) the rigid Earth nutation model (Souchay *et al.* 1999), (ii) the transfer function of Mathews *et al.* (2002) which is explicitly expressed as a function of basic Earth parameters that have been estimated from VLBI nutation offsets.

The model is IAU 2000A for 0.2 mas level (Mathews *et al.* 2002) or IAU 2000 B (its shorter version) for 1 mas level (McCarthy & Luzum 2003), with in both cases, associated precession and obliquity rates and associated celestial pole offsets. The 106 nutations of the IAU 1980 model is thus replaced by more than 1300 nutations with in-phase and out-of-phase components and the secular terms in longitude and obliquity of the IAU 1976 precession are revised.

2.4 Consequences of IAU Resolution B1.7 for precession and nutation

Resolution B1.7 recommends that the CIP be the pole, the motion of which is specified in the GCRS by the motion of the Tisserand mean axis of the Earth with periods greater than two days, and that it be realized by the IAU 2000A model for precession and forced nutation for periods greater than two days plus additional time-dependent corrections provided by the IERS through appropriate astro-geodetic observations. It also specifies that the motion of the CIP in the ITRS be provided by the IERS through appropriate astro-geodetic observations and models including high-frequency variations.

2.5 Consequences of IAU Resolution B1.8 for precession and nutation

Resolution B1.8 recommends that:

(i) UT1 be linearly proportional to the Earth Rotation Angle defined as the angle measured along the equator of the CIP between the unit vectors directed toward the Celestial Ephemeris Origin (CEO) and the Terrestrial Ephemeris Origin (TEO) (*i.e.* "non-rotating origin" as defined by Guinot, 1979),

(ii) the transformation between the ITRS and GCRS be specified by the position of the CIP in the GCRS, the position of the CIP in the ITRS.

This Resolution leads to abandon the current parameters in the FK5 System and especially the use of the true equinox to reckon the Earth Rotation Angle, and adopt instead the NRO (Guinot 1979) as the origin on the moving equator (CEO and TEO). It also leads to abandon the current formulation combining the motions of the equator and the ecliptic with respect to the ICRS and use instead parameters that include both precession and nutation.

3. IMPROVEMENTS OF THE IAU 2000 PRECESSION-NUTATION

3.1 Improvement in the reference system for precession-nutation

The FK5 was based on positions and proper motions of bright stars and was oriented so that at the "epoch", the positions are referred to the best estimate of the location of the mean pole and mean equinox. The proper motions of stars were evaluated so that, for the adopted model of precession, they provide the best access to the mean pole and mean equinox of epoch, at any other date. The direction of the mean pole and mean equinox of date, which had a major role in the realization of the FK5, were the natural directions of reference for the EOP. The FK5 System was composed of the FK5 catalog of positions and proper motions of fundamental stars and of the associated models: IAU1976 precession, IAU 1980 nutation and the conventional relationship between Greenwich sidereal time and UT1 (Aoki *et al.* 1981).

The ICRS, adopted by the IAU as the International Celestial Reference System since the 1st January 1998, is based on barycentric directions of distant extragalactic objects (Ma *et al* 1998) and its definition is independent of the models used for precession and nutation and of the relation between Earth Rotation Angle. Its fundamental property is that the barycentric directions of the extragalactic objects show no global rotation with respect to them. The GCRS follows the kinematical condition of absence of global rotation of geocentric directions w.r.t. the objects defining the ICRS. The ICRS was aligned with the FK5 at J2000.0 so that its x-axis is approximately directed to the J2000 dynamical mean equinox and its z-axis is approximately directed towards the J2000 mean pole. However, this was in order that the ICRS be consistent with the FK5, but no attempt has been made to refer the positions of the sources to the mean pole and mean equinox at J2000.0 and it was decided that further improvements of the ICRS will be accomplished without introducing any global rotation. This corresponds to a conceptual change, namely the abandonment of the link of the conventional celestial reference system with the precession-nutation model. The GCRS is independent from such models. Such a change requires to adopt a definition of the equatorial system without any relation to the orbital motion of the Earth and consequently to abandon the equinox as the origin on the equator. Moreover, as the mean pole is no more a fundamental point of the celestial frame of reference, precession has no reason to be considered separately from nutation, these two motions being observationally not separable.

3.2 Improvement in the precession-nutation theory

The new precession-nutation model (MHB2000) corresponds to an improvement both in the accuracy of the rigid Earth nutation (Bretagnon *et al.* 1998, Souchay *et al.* 1999, Roosbeck & Dehant 1999) and in the theoretical expression of the transfer function (Mathews *et al.* 2002) between rigid and non-rigid nutations. This transfer function is based on Basic Earth Parameters (BEP) which have been estimated from VLBI observations providing corrections to a number of prograde and retrograde nutations and to the precession rates in longitude and obliquity.

In addition to the MHB model for nutations of periods greater than two days, there are also recent models for polar motion which take account of the diurnal and sub-diurnal nutations for non-rigid Earth models (Bizouard *et al.* 2000, Brzezinski & Capitaine 2003, Mathews & Bretagnon 2003). Diurnal and sub-diurnal tidal variations in polar motion and Earth's rotation have also to be taken into account (Herring & Dong 1994).

3.3 Improvement of the pole of reference (CIP) for precession-nutation

The definition of the CIP sharpens the definition of the CEP by taking into account the high frequency variations of polar motion, that need to be considered in accurate theory and estimates (Brzeziński & Capitaine, 1993, Capitaine 2000a and 2000b). According to Resolution B1.7, the CIP is an intermediate pole separating, by convention, the motion of the pole of the TRS in the CRS into two parts (see the schematic representation below):

- the celestial motion of the CIP (precession/nutation), including all the terms with period greater than 2 days in the CRS (i.e. frequencies between -0.5 cpsd and $+0.5$ cpsd), plus the celestial pole offsets; the forced nutations with periods less than two days are, in contrast, included in the model for the motion of the CIP in the ITRS.

- the terrestrial motion of the CIP (polar motion), including all the terms outside the retrograde diurnal band in the TRS (i.e. frequencies lower that -1.5 cpsd or greater than $+0.5$ cpsd); the motion of the CIP in the ITRS is provided by observations taking into account a predictable part specified by a model including high frequency variations.

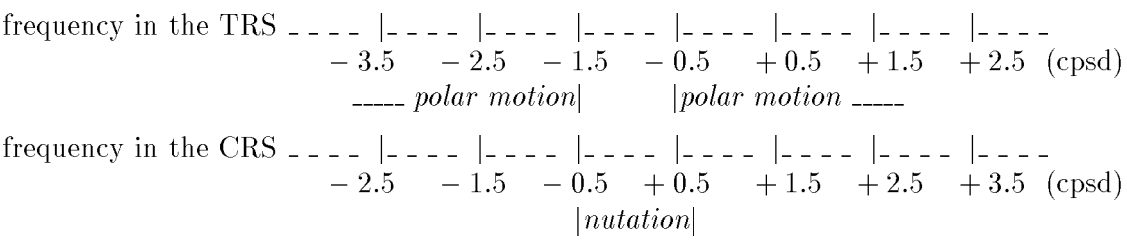

The pole is thus defined such that it can be realized by a model as accurately as necessary and be not dependent on the technique of observation. Note that the corrections to the model for the motion of the CIP in the ITRF may be estimated by extracting the high frequency signal in the pole coordinates. Note also that the forced nutations with periods less than two days (prograde diurnal and prograde semi-diurnal nutations) are not included in the nutation model, but is included in the model for the motion of the CIP in the TRS as follows:

- prograde diurnal terms in nutation are considered as long periodic prograde and retrograde variations of polar motion 27 d, ...) (amplitude of the order of 15 μas),

- prograde semi-diurnal terms in nutation are considered as prograde diurnal variations of polar motion (polar libration)(amplitude of the order of 15 μas).

3.4 Improvement in the parameters for precession-nutation

Resolution B1.8 introduces a change of parameters from the classical angles for precession (ϵ_A, ζ_A, z_A , θ_A, χ_A) and nutation ($\Delta\psi$, $\Delta\epsilon$) and the angle of Earth's rotation (GST) referred to the equinox of date γ in the FK5 to new parameters X, Y for positioning the CIP in the GCRS and the Earth Rotation Angle (ERA) as the angle from the CEO to the TEO on the equator of the CIP.

The new X,Y parameters for positioning the CIP are the x, y coordinates of the CIP unit vector in the GCRS (Capitaine 1990, McCarthy 1996). The change of origin for the Earth's angle of rotation from the classical equinox to the non-rotating origin (CEO) provides a clear separation between precession-nutation and Earth's rotation and a definition of UT1 as directly proportional to the ERA.

The use of an intermediate frame referred to the CIP and the new parameters clearly separate high frequency and low frequency motions and reduce to five the parameters for transformation between ITRF and GCRF:

- position of the CIP in the GCRS: E, d,
- position of the CIP in the ITRS : F, g,
- Earth's angle of rotation : θ.

There is thus a symmetric representation for the celestial and terrestrial parts of the motion: $PN(t) = R_3(-E).R_2(d).R_3(E)$ and: $W(t) = R_3(-F).R_2(g).R_3(F)$ (2) .

The coordinates of the CIP in the GCRS ($X = sind\cos E$ and $Y = sind\sin E$, E and d being the GCRS polar distance and azimuth of the CIP) provide the celestial position of the CIP; they include precession, nutation, the coupling effects between precession and nutation and the offsets ξ_o, η_o, $d\alpha_0$ of the precession-nutation models at J2000 with respect to the pole and equatorial origin of the GCRS. They fulfill all the requirements for EOP in the GCRS and can be derived from the precession and nutation model and developed as function of time (Capitaine *et al.* 2000). The position of the CEO in the GCRS is given by the quantity s, which can be given by a development as function of time (Capitaine *et al.* 2000).

4. FURTHER IMPROVEMENTS NEEDED

The future solutions of Earth rotation theory should be referred to the GCRS and not to the mean ecliptic of date as they are provided in the current expressions.

The use of the celestial coordinates X, Y of the CIP, which can be expressed as function of the precession and nutation angles referred to a fixed ecliptic, can provide solutions which would be closer to the observables and would therefore be more adequate than the current precession and nutation angles for estimating theoretical parameters from the observations.

This would contribute in the future improvement of the estimated amplitudes of the "geophysical" nutations from VLBI observations.

5. REFERENCES

Aoki, S., Guinot, B., Kaplan, G. H., Kinoshita, H., McCarthy, D. D., Seidelmann, P. K., 1982, *Astron. Astrophys.***105**, 359-361.

Bizouard, C., Folgeira, M., Souchay, J., 2000, in "Polar motion : Historical and scientific problems", ASP Conference series, Vol 208, S. Dick, D.D. McCarthy and B. Luzum eds, 613-617.

Bretagnon, P., Francou, G., Rocher P., and Simon J.-L., 1998, *Astron. Astrophys.***329**, 329-338.

Brzeziński A., Capitaine N., 1993, *J. Geophys. Res.***98**, No. B4, 6667-6675.

Brzezinski & Capitaine, 2003, this Volume, p 53.

Capitaine, N., 1990, *Celest. Mech. Dyn. Astr.***48**, 127-143.

Capitaine, N., 2000 a, in "Polar motion : Historical and scientific problems", ASP Conference series, Vol 208, S. Dick, D.D. McCarthy and B. Luzum eds, 573-584.

Capitaine, N., 2000 b, in "Towards Models and Constants for Sub-microarsecond Astrometry", K. Johnston, B. Luzum, D.D. McCarthy and G. Kaplan eds, 153-163.

Capitaine, N., Guinot, B., McCarthy, D.D., 2000, *Astron. Astrophys.***335**, 398-405.

Guinot, B., 1979, in *Time and the Earth's Rotation*, D.D. Mc Carthy, J.D. Pilkington (eds), D. Reidel Publishing Company, 7-18.

Herring, T.A. and D. Dong, 1994, *J. Geophys. Res.*, **99**, 18051-18071

Lieske, J. H., Lederle, T., Fricke, W., and Morando, B., 1977, *Astron. Astrophys.***58**, 1-16.

Ma, C.,Arias, E.F., Eubanks, M. Fey, A.L., Gontier, A.-M., Jacobs, C.S., Archninal, B.A., Charlot, P., 1998, *Astron. J.*, **116**, 516-546.

Mathews, P.M., Herring, T.A., Buffett B.A., 2002, *J. Geophys. Res.*, 107, B4, 10.1029/2001JB000165.

Mathews, P.M. and Bretagnon, 2003, this Volume, p 28.

McCarthy D.D., 1996, "IERS Conventions", IERS Technical Note 21, Observatoire de Paris.

McCarthy, D. D. and Luzum, B. J., 2003, *Celest. Mech.*, **85**, 35-49.

Roosbeek, F., and Dehant, V., 1998, *Celest. Mech.*, **70**, 215-253.

Seidelmann, P. K., 1982, *Celest. Mech.*, **27**, 79-106.

CONTRIBUTION OF LLR TO FUNDAMENTAL ASTRONOMY

J. CHAPRONT and G. FRANCOU
SYRTE - Observatoire de Paris - UMR 8630/CNRS
61, avenue de l'Observatoire 75014 Paris
e-mail: jean.chapront@obspm.fr

ABSTRACT. We briefly recall the principles of the analysis of the lunar laser ranging and the main results brought with this technique: Ephemeredes, gravitational physics, reference systems, geodynamics and selenophysics. We give a short description of the various perturbations acting on the Moon concerning its orbital motion and libration, and illustrate the amplitudes of several effects that have to be taken into account in order to reach the centimeter level in the models. A fundamental parameter for the orbital evolution of the Moon is the tidal acceleration in the lunar longitude. We summarize the results obtained since the nineties. Taking advantage of the long time range of observations, we show that we have a good convergence in the knowledge of this parameter with an uncertainty that should not be larger than 0.003 $''/\mathrm{cy}^2$.

1. SCIENTIFIC APPLICATIONS OF THE LUNAR LASER RANGING

Lunar Laser Ranging (LLR) covers a large domain of scientific applications. We list below a non-exhaustive list of applications which have been extensively developed after the deployment of the first reflector array by N. Armstrong on the lunar surface, in July 1969. Over the last thirty years the precision has regularly improved from the 0.25 m range in 1970 to an internal precision of the order of one centimeter today, and a post-fit accuracy of 2 to 3 cm.

• *Ephemeredes* The improvement of the orbital motion of the Moon has followed the accuracy in the LLR measurements. Several numerical integrations (Development Ephemeredes at JPL) and analytical solutions (ELP) have been constructed. The libration models (forced and free librations) have been elaborated in parallel.

• *Gravitational physics* A review of recent progresses in that field is given in (Williams et al., 2001). It concerns the verification of the equivalence principle, a determination of the PPN parameters β and γ , and the geodetic precession. Correlatively, precise boundaries of the rate of change of G (the gravitational constant) and of the solar J_2 have been also derived. Since 1996 (Williams et al., 1996) the uncertainties in gravitational physics parameters have been reduced by a factor 2 or more. It is mainly due to the data (an improved range accuracy and a longer time span), some additional solutions (plate motion and solid body tides on the Moon), a better determination of Earth Orientation Parameters, and finally, a modeling of the energy dissipation of the Moon.

• *Reference systems* The lunar motion defines intrinsically a dynamical system. It allows in particular a positioning of the dynamical reference frame in the ICRS (Chapront et al., 1999, Standish, 2000).

• *Geodynamics* The Moon is a main contributor in the improvement of various parameters of the Earth-Moon system. We shall mention in particular the determination of the lunar mass and the coefficients of the Earth potential when combined with SLR technique (Dickey et al., 1994). It contributes, complementary to VLBI, to a better knowledge of the precession constant and of few long-periodic terms in nutation (Chapront et al., 2000, Fukushima, 2000). A domain of excellence is a precise evaluation of the Earth tidal dissipation (Love numbers and time delay) due to the lunar action which induces a secular acceleration of the lunar longitude.
• *Lunar science and selenophysics* The Moon in rotation is submitted to two different effects: forced and free libration. Through the analysis of the lunar parameters, one derives an estimate of the principal moment of inertia, low degree gravitational harmonics, Love number k_2 and dissipation parameter Q (Dickey et al., 1994, Williams et al., 1996). LLR data are combined with lunar orbiting satellites data and result in a determination of the parameter C/MR^2 that is fundamental for the knowledge of the Moon's evolution. The free libration is implicit in the equations of motion. Once the total libration is known by the observations and the forced libration modeled, a frequency analysis of the difference: *Total Libration - Forced Libration*, exhibits 3 frequencies (Chapront et al., 1997) and 3 modes of libration: a wobble mode, a precession mode and a longitude mode (Newhall and Williams, 1997).

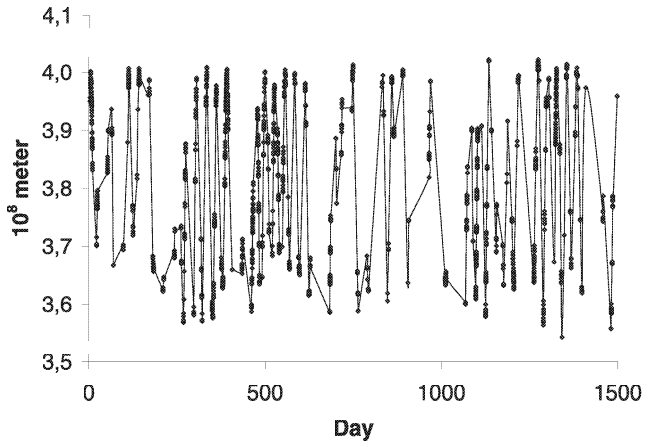

Figure 1: Absolute variation of the distance Observer-Reflector (CERGA-Apolo15), on the basis of real observations (1996-2000)

2. PRINCIPLES OF ANALYSIS OF LLR OBSERVATIONS

The analysis of the observations rests upon quite elementary principles. The main difficulty arises in the complexity of the models to render in account of the accuracy of the measurements. The measured quantity is the time of flight the light takes to make the round trip between the telescope and the lunar reflectors. The typical duration is 2.5 s. Converted in lunar distance, if an accuracy of 1 cm is aimed at, this means a relative accuracy of about 2.5×10^{-11}. This gives an idea of the precision that has to be reached to compare the observed time of flight Δt_O to the computed one Δt_C. To derive the computed time, several actors have to be considered: The Earth (E), the Moon (M), the observer (O) at the telescope, the reflector (R), the Earth-Moon barycenter (G), and the barycenter of the solar system (B). Δt_C depends on vectors computed in a celestial barycentric reference system:
EM (Earth-Moon) and **BG** (Solar system barycenter, Earth-Moon barycenter). The evaluation of these vectors requires lunar and planetary ephemeredes.
EO (Station of observation) which is computed on the basis of the Earth's rotation (precession, nutation, polar motion, Universal Time), and the position of the station in a terrestrial frame.

MR (Lunar reflector). Its evaluation requires an ephemeris of the lunar librations and selenocentric coordinates of the reflector.
The observed Δt_O is given in atomic time scale (TAI). All necessary transformations are done to compute the ephemeredes in TCB (Barycentric Coordinates Time). Besides, the coordinates of the station are given in the ITRF (International Terrestrial Reference Frame), referred in a GRS (Geocentric Reference System). Here again, all necessary relativistic transformations are done to compute the positions of the station in a BRS (Barycentric Reference System).
In the process of treatment of the data enters corrections of various types: local site displacements due to several causes (solid Earth tides, ocean loading, atmospheric pressure) and time propagation (relativistic curvature of the light beam and tropospheric perturbations). This last effect is very large (the equivalent distance correction varies between 2 to 9 meters) and badly modeled. They are many other causes which limit the quality of the models: the Earth Orientation Parameters, the plate motions, ...

3. A QUALITATIVE DESCRIPTION OF THE PERTURBATIONS

In order to give an idea about the complexity of the models, we shall briefly describe the various components which enter the lunar motion. Fig. 1 shows the variation of the distance between the Observer (O) and the Reflector (R). To illustrate the repartition of the data, we have used a sample of recent observations covering 4 years, (O) standing for the CERGA and (R) for Apollo 15. Fig. 2 shows the different components which enter the computation of the perturbations of the Moon's barycenter. Among the 3 variables (longitude, latitude and radius vector) we have selected the longitude. On a logarithmic scale, we see that the amplitudes of the perturbations cover a large domain between $10^5\,''$ and $10^{-5}\,''$. We recall that a displacement of $10^{-5}\,''$ in longitude corresponds to 2 cm which is around the lower limit in distance that we aim to reach. The Main Problem is the lunar motion restricted to the 3 bodies: Earth, Moon and Sun, the apparent motion of the Sun around G being keplerian. The planetary perturbations are divided in 2 groups: D, for direct perturbations of the planets acting on the Moon, I, for indirect ones, through the planetary perturbations of the Earth-Moon barycenter. Because of secular motion of the Earth-Moon elements (eccentricity, inclination,...) the perturbations are not only periodic, but also periodic with secular amplitudes (Poisson terms).

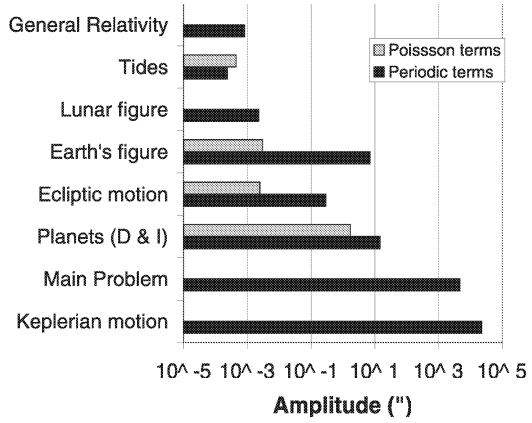

Figure 2: Lunar longitude. Amplitude of perturbations of various type. Units: $''$ for periodic terms, $''$/cy for Poisson terms.

The lunar libration is governed by Cassini's laws. The orbital plane of the Moon intersects

the ecliptic along the direction EN and the lunar equator along the direction MN' (N and N' are ascending nodes). Cassini's laws say that:
(1) the rotation period around its axis is identical to the circulation period along the orbit;
(2) the inclination of the lunar equator is a constant on the ecliptic;
(3) the secular motions of the nodes N and N' are identical, with a period of 18.6 yrs.
The libration is described by the motion of a selenodesic system materialized with the moments of inertia with respect to an ecliptic reference frame. The selenodesic system is referred by its Euler's angles φ, ψ, ϑ. The classical libration position angles in term of Euler's angles have the following definition: $p_1 = \sin\varphi \sin\vartheta$; $p_2 = \cos\varphi \sin\vartheta$; $\tau^* = \varphi + \psi$. The libration in longitude is the difference with the lunar mean longitude λ, i.e., $\tau = \tau^* - \lambda - 180°$. p_1 and p_2 are variables with monthly periods whose amplitudes reach $1.5°(\approx 6000'')$. This phenomenon is very large if we recall that a displacement of $1''$ on the lunar surface corresponds to 8.5 cm. The variation of the libration in longitude τ is illustrated on Fig. 3. This illustration covers a period of 4 years (1996-2000).

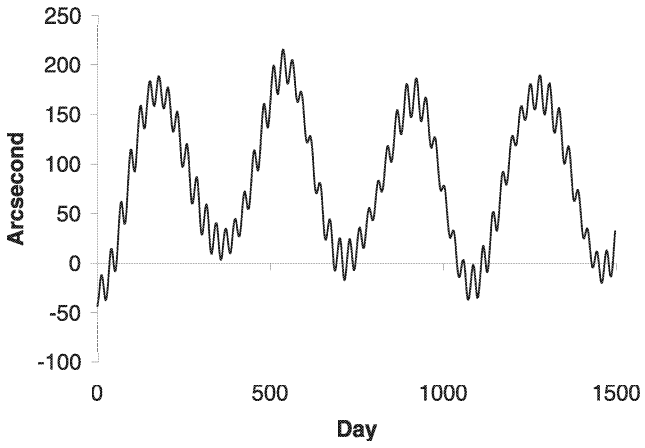

Figure 3: Libration in longitude over 4 years (1996-2000): variable τ

4. THE TIDAL ACCELERATION OF THE MOON The tidal component of the secular acceleration of the Moon's longitude is a fundamental parameter of the evolution of the Earth-Moon system. The tidal dissipation is due to a misalignment of the tidal bulge of the Earth relative to the Earth-Moon direction. This bulge exerts a secular torque and most of the effect comes from the ocean tides. It produces a secular acceleration of the Moon and a slowing Earth's rotation rate (length of the day). A consequence of the negative acceleration in the lunar longitude of approximately $-25.8''/\text{cy}^2$ is the well-known displacement of the Moon's barycenter which corresponds to an increasing Earth-Moon distance of 3.8 cm/year.
Let us examine the quadratic terms of the lunar mean longitude $W_1^{(2)}$ as it appears in the analytical lunar theory ELP2000-82 (Chapront et al., 1997). Here, the constants and parameters are those from the JPL ephemeris DE245, in particular the fitted value of the secular acceleration. It contains mainly 3 contributions expressed in $''/\text{cy}^2$ (these contributions have to be multiplied by 2 if we speak of the 'secular acceleration' component):

[1] Planetary perturbations:	5.8665
[2] Earth's figure perturbations:	0.1925
[3] Tides:	-12.8125

In [1] the main effect is due to the secular variations of the solar eccentricity. It represents in fact a Taylor's expansion of long periodic perturbations - called also 'secular perturbations' in

classical Celestial Mechanics, -with periods of revolution of the solar perigee and node covering several ten thousand years. In [2] the contribution is of the same nature. Hence, [1] and [2] are due to very long period effects. They have to be distinguished from the tides which induce dissipative forces. An analytical solution for the lunar motion (Chapront-Touzé and Chapront, 1988) provides also secular terms of higher degree in time (t^3-terms, t^4-terms, etc...). With the knowledge of all the secular components in the longitude, we are able to isolate the tidal acceleration from other perturbations. We gather in Table 1 a list of recent determinations of the secular acceleration of the lunar mean longitude with LLR observations. The solution S1998 is described in (Chapront et al., 1999). In S2000 (Chapront et al., 2000) several improvements have been introduced in the lunar ephemeredes, mainly in the libration model, and also in the program of reduction (an up-to-date nutation model) and in the statistical treatment of the data (an adequate distribution of weights among the various observing stations and periods of observations). Finally, in S2000 we introduce corrections in the position and motion of the stations. The total time span of the fit covers 1972-2001. We note that, for this type of determinations, a sensible improvement of the precision when accumulating the observations.

Table 1. Tidal acceleration of the lunar mean longitude. Determination with different models. Units:$''/cy^2$

Solution	Value	Publication
S1998	-25.782	1999
S2000	-25.836	2000
S2001 (this paper)	-25.858	
JPL Ephemeris		
DE200	-23.895	1982
DE245	-25.625	1990
DE403	-25.580	1995
DE405	-25.826	1998

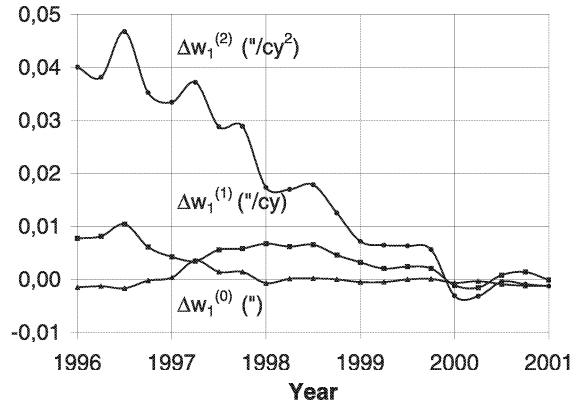

Figure 4: Time evolution of the corrections Δ to the secular components of the mean longitude of the Moon: $W_1 = W_1^{(0)} + W_1^{(1)}t + W_1^{(2)}t^2$ when increasing the set of LLR measurements.

It is interesting to bring closer the intrinsic value of this parameter in various JPL numerical integrations (DE: Development Ephemeris) gathered in the second part of Table 1. These values do not appear explicitly in the list of parameters which are provided with each lunar ephemeris. They are deduced from an analysis of the same nature as our determination of various parameters when using the LLR observations themselves. Hence, we consider a JPL ephemeris as an 'observational model' and isolate - as pointed out above - the tidal contribution.

The expression of the lunar mean longitude of the Moon W_1 has the following secular development: $W_1 = W_1^{(0)} + W_1^{(1)}t + W_1^{(2)}t^2 + ...$, where t is the time in century reckoned from J2000.0; $W_1^{(0)}$ is the origin of longitude for J2000.0; $W_1^{(1)}$ is the sidereal mean motion; $W_1^{(2)}$ is the total secular acceleration of the Moon. With the nominal values of these quantities resulting from our last fit to LLR observations (Solution S2001) we shall now investigate the evolution of the convergence to these values when increasing the time interval for the fit. Hence, we compute distant $\Delta W_1^{(0)}$, $\Delta W_1^{(1)}$ and $\Delta W_1^{(2)}$ apart the nominal values. In particular the variation of $\Delta W_1^{(2)}$ puts in evidence the time evolution of the correction to the tidal acceleration if we consider that this correction arises mainly from tides. On Fig. 4 we observe the evolution of this correction when using more and more recent LLR observations until 2001. This graph allows us to insure nowadays a precision in the knowledge of the secular acceleration better than 0.03 $''/cy^2$.

5. REFERENCES

Chapront-Touzé, M., Chapront, J.: 1988, ELP2000-85: a semi-analytical lunar ephemeris adequate for historical time, *Astron. Astrophys.*, **190**, 342

Chapront, J., Chapront-Touzé, M.: 1997, Lunar Motion: theory and observations, *Celest. Mech.*, **66**, 31

Chapront, J., Chapront-Touzé, M. and Francou, G.: 1999, Determination of the lunar orbital and rotational parameters and of the ecliptic reference system orientation from LLR measurements and IERS data, *Astron. Astrophys.*, **343**, 624

Chapront, J., Chapront-Touzé, M. and Francou, G.: 2000, Contribution of LLR to the reference systems and precession, in *Journées systèmes de référence spatio-temporels*, N. Capitaine Ed., Observatoire de Paris

Dickey, J.O., Bender, P.L., Faller, J.E., *et al.*: 1994, Lunar Laser Ranging: a continuing legacy of the Apollo program, *Science*, **265**, 482

Fukushima, T: 2000, Report on Astronomical Constants, in *IAU Colloquium 180: Towards Models and Constants for Sub-Microarcsecond Astrometry*, K.J. Johnston et al. Eds., Washington D.C.

Newhall, X X and Williams, J.G.: 1997, Estimation of the lunar physical librations, *Celest. Mech.*, **66**, 21

Standish, E.M.: 1982, *Astron. Astrophys.*, **114**, 297

Standish, E.M.: 1995, JPL Planetary and Lunar Ephemerides, DE403/LE403, IOM, 314.10-127, Pasadena

Standish, E.M.: 1998, JPL Planetary and Lunar Ephemerides, DE405/LE405, IOM, 312.F-98-048, Pasadena

Standish, E.M.: 2000, Dynamical Reference Frame - Current Relevance and Future Prospect, in *IAU Colloquium 180: Towards Models and Constants for Sub-Microarcsecond Astrometry*, K.J. Johnston et al. Eds., Washington D.C.

Williams, J.G., Newhall, X X and Dickey, J.O.: 1996, Relativity parameters determined from lunar laser ranging, *Phys. Rev. D*, **53**, 12, 6730

Williams, J.G., Newhall, X X and Dickey J.O.: 1996, Lunar moments, tides, orientation and coordinate frames, *Planet. Space Sci.*, **44**, 10, 1077

Williams, J.G., Boggs, D.H., Dickey, J.O. and Folkner W.M.: 2001, Lunar laser tests of gravitational physics, *World Scientific*, to be published

ANALYTICAL SOLUTION OF THE MARS MOTION

P. BRETAGNON
Institut de Mécanique céleste, UMR8028
Observatoire de Paris
77, avenue Denfert-Rochereau, 75014 PARIS, FRANCE
e-mail: pierre@bdl.fr

ABSTRACT. Taking into account the progress of the observations, in particular the distances Earth-planet, we undertook the construction of new analytical solutions of the motion of the planets. It is desirable to reach precisions, for the distance Earth-Mars for example, of about a few tens of meters. One of the difficulties of the study of the motion of Mars is the determination of the perturbations by the asteroids, the masses of which are badly known. We examine the most significant perturbations of the longitude of Mars by the asteroids in analytical form and in numerical form.

1. INTRODUCTION

The analytical theories VSOP of the motion of the planets were built at the Bureau des longitudes in the 1980's. The improvement of the techniques of observation and the needs for the spacecraft navigation make necessary the construction of new solutions of high accuracy. For example, the maximum uncertainty on the geocentric distance of Mars is expected to be a few tens of meters over short intervals of time about ten years.

Recently, the construction of such solutions was undertaken : VSOP2000 by Moisson (2000) and a new solution is under development by an iterative method. The integration constants of this last solution will be determined by adjustment with DE403 or DE405 (1995) and also by direct comparison with the observations.

In the VSOP2000 solution, the mutual Newtonian perturbations of the eight main planets were computed by an iterative method. The perturbations of the Earth-Moon barycenter by the Moon, the perturbations at the first order of the masses by the five asteroids Vesta, Iris, Bamberga, Ceres and Pallas, the perturbations due to Pluto (Simon, 2000) and the relativistic complements were added to the Newtonian solution.

In the new solution, we took care simultaneously of integrating all the effects by an iterative method.

2. COMPARISON WITH NUMERICAL INTEGRATIONS

To evaluate the accuracy of the solutions, we carried out comparisons of VSOP82 (1982) with DE200 and VSOP2000 with DE403. The table 1 gives the maximum differences over one century between VSOP2000 and DE403 for the semimajor axis a, the mean longitude λ, the

variables k and h related on the eccentricity and the longitude of the perihelion, the variables q and p related on the inclination and the longitude of the node. This comparison shows that VSOP2000 is 10 times more precise than VSOP82 for Venus and the Earth-Moon barycenter, 50 times for Jupiter, Saturn, Uranus and Neptune, 4 times for Mars. Actually, this difference of 3 mas in the longitude of Mars is due to the introduction into DE403 of the perturbations by 300 asteroids whereas currently, we disturbed the main planets only by five asteroids.

Table 2 gives the differences between DE403 and the new solution. This solution is in progress and the current lack of perturbations by Pluto gives errors on Uranus and Neptune of 3 mas and 5 mas. The maximum differences for the planets Jupiter and Saturn are 3 times smaller than for the VSOP2000 solution like for Mercury, Venus and the Earth. For Mars, the difference of 3 mas comes from the asteroids introduced into DE403.

Table 1: Maximum difference between the VSOP2000 solution and DE403 over one century

Planet	$\Delta a/a$	λ		k	h	q	p
	10^{-10}	10^{-10}	mas	10^{-10}	10^{-10}	10^{-10}	10^{-10}
Mercury	1.0	13	0.27	8	4	0.5	0.8
Venus	1.0	14	0.29	10	3	1.1	1.5
EMB	1.4	17	0.35	3	17	3.4	4.2
Mars	5.9	140	2.89	12	30	2.6	7.2
Jupiter	11.7	23	0.47	15	16	5.0	4.3
Saturn	47.4	85	1.75	19	35	7.8	8.1
Uranus	82.1	72	1.49	66	57	38.2	11.0
Neptune	104.4	90	1.86	61	68	4.1	11.3

Table 2: Maximum difference between the analytical solution and DE403 over one century

Planet	$\Delta a/a$	λ		k	h	q	p
	10^{-10}	10^{-10}	mas	10^{-10}	10^{-10}	10^{-10}	10^{-10}
Mercury	0.52	1.62	0.034	0.69	0.69	0.29	0.09
Venus	0.41	4.95	0.102	0.95	0.83	0.36	0.09
EMB	0.54	4.80	0.099	1.28	1.90	1.17	2.49
Mars	4.62	143.66	2.963	8.54	12.67	0.61	5.56
Jupiter	16.52	8.39	0.173	7.01	8.30	1.07	0.60
Saturn	258.18	30.71	0.633	11.13	13.25	2.60	1.30
Uranus	365.70	128.72	2.655	54.15	136.26	18.85	7.93
Neptune	295.94	258.10	5.324	159.12	149.85	1.88	11.61

Figure 1 gives the differences for the longitudes of Mercury, Venus, the Earth, and Mars. The unit is 10^{-12} radian. The maximum differences are, over one century, 12 meters for Mercury, 55 meters for Venus, 75 meters for the Earth and 3.5 kilometers for Mars.

The differences between the analytical solution of Mars and DE403 come mainly from the introduction of the perturbations by a great number of asteroids into DE403. As a test of the quality of the resolution of the equations, we compared the new solution with a numerical integration corresponding to the same physical model used in the analytical solution. Table 3 gives the heliocentric differences between the analytical solution and the numerical integration

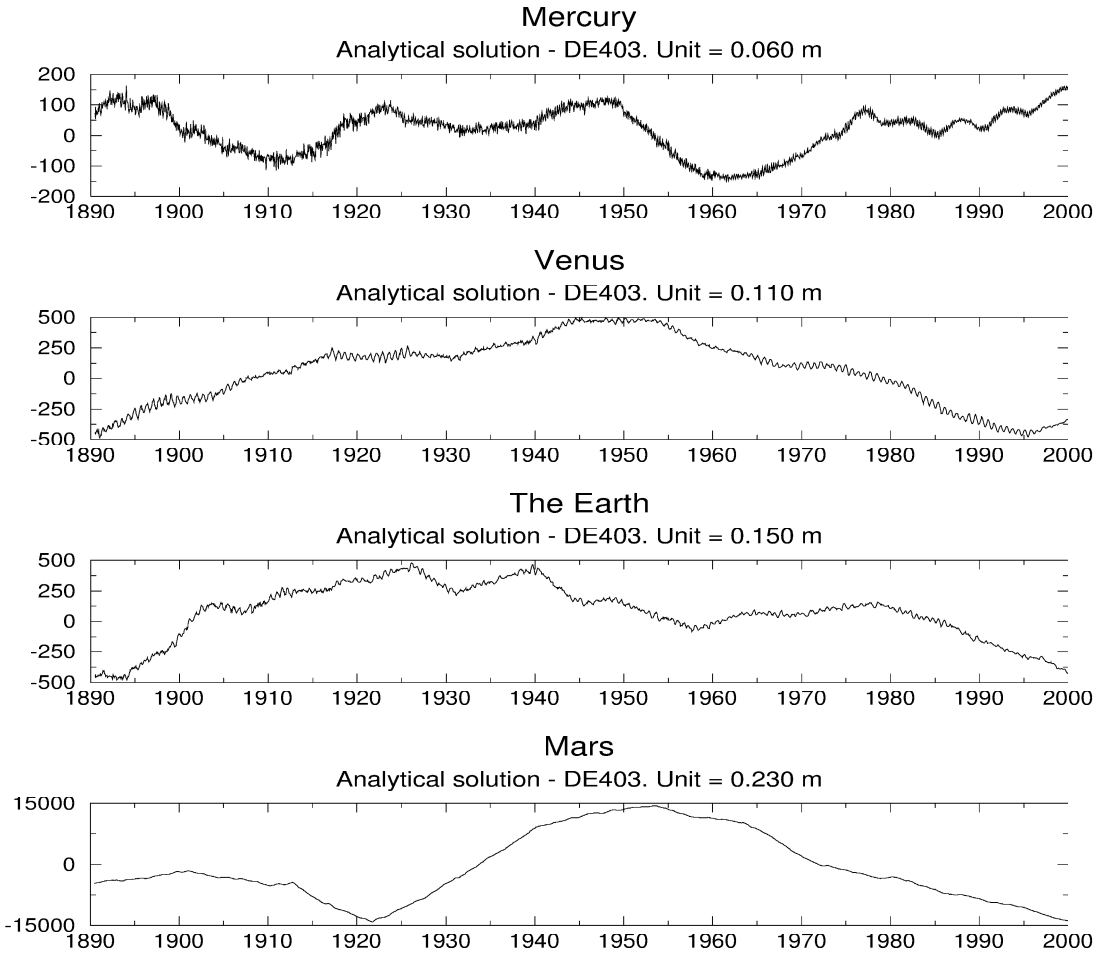

Fig. 1. Difference between the analytical solution and DE403 in 10^{-12} radian over [1891-2000].

over one century and over 10 years in mas and the corresponding values in meters. The impact of the asteroids on the motion of the Earth being not very significant, the residuals are similar to the previous ones : 63 meters instead of 75 meters in the comparison to DE403. For Mars, the residuals come from 3 mas to 0.4 mas. For the chosen model, the distance Earth-Mars can be given over 10 years with an accuracy of a few tens of meters. Figures 2 and 3 plot the differences between the analytical solution and the numerical integration over (1891-2000) (smaller than 500 meters) and over (1989-2000) (smaller than 17 meters).

3. PERTURBATIONS OF MARS BY THE ASTEROIDS

The accuracy of the position of Mars essentially depends on the computation of the perturbations by the asteroids. Table 4 gives, for the longitude of Mars, the number of terms of the perturbations by the five asteroids computed at the first order of the masses with an amplitude bigger than one meter. Many terms are produced at the higher orders mainly due to the resonance between Pallas and Jupiter. Tables 5 and 6 give the most important perturbations of the longitudes of the Earth and Mars with the amplitude in meters, the period in years and the corresponding argument. In the case of Mars, several terms have a period closed to 50 years. The perturbations of the longitude of Mars by Vesta, Iris, Bamberga, Ceres, and Pallas are plotted over one century in figure 4.

Table 3: Maximum difference of the longitude between the analytical solution and the numerical solution

Planet	over one century			over 10 years		
	10^{-10}	mas	meters	10^{-10}	mas	meters
EMB	4.20	0.087	63	0.50	0.010	8
Mars	20.92	0.431	477	0.75	0.015	17

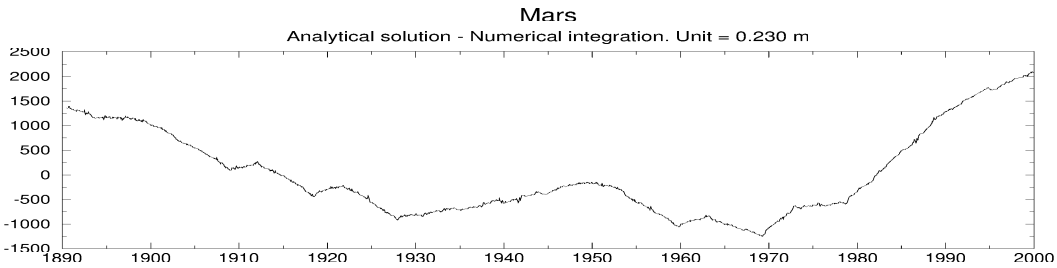

Fig. 2. Difference between the analytical solution and the numerical integration in 10^{-12} radian over [1891-2000].

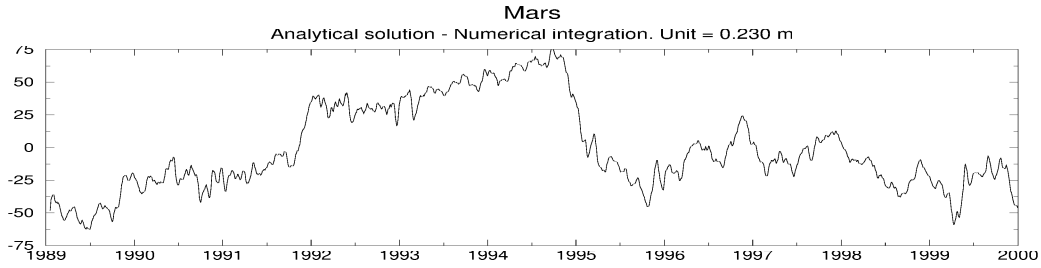

Fig. 3. Difference between the analytical solution and the numerical integration in 10^{-12} radian over [1989-2000].

Table 4: Number of terms due to the asteroids with an amplitude greater than 1 meter in the longitude

	Vesta	Iris	Bamberga	Ceres	Pallas
Mars first order solution	43	31	42	50	47
complete solution	67	44	56	83	500
Earth complete solution	12	2	7	8	32

4. MASS OF THE ASTEROIDS

We will now estimate the precision of this perturbation considering our present knowledge of the asteroid masses. The comparison between the asteroid masses determined by Fienga and Standish (2001) and by Krasinsky *et al.* (2001) shows important differences. Uncertainties on only the five used asteroids involve errors of about one kilometer over one century. For the 24

other asteroids with a mass higher than 5×10^{-12} solar mass, one can note that the sum of the differences of masses represents 75×10^{-12} solar mass and can produce, according to whether one uses one or the other set of masses, differences of several kilometers on the position of Mars over one century. Standish and Fienga (2001) showed that, over a shorter interval, about 10 years, uncertainties on the position of Mars could be limited to one kilometer.

Table 5: Most important perturbations of the Earth longitude by the asteroids

Origin	amplitude (in meters)	period (in years)	argument
Bamberga	33.6	292	5T − 22B
Ceres	13.1	1	2T − 2C
Vesta	6.8	1	2T − 2V
Bamberga	6.3	21	2T − 9B
Pallas	5.9	8	T − 4P
Pallas	5.8	12	T − 12P + 18J
Ceres	5.8	1	T − C
Pallas	5.8	12	T + 2P − 18J
Pallas	5.3	12	T − 5P
Vesta	5.1	6	T − 3V

Table 6: Most important perturbations of the Mars longitude by the asteroids

Origin	amplitude (in meters)	period (in years)	argument
Bamberga	12939	327	3M − 7B
Vesta	4683	52	M − 2V
Ceres	1968	44	2M − 5C
Pallas	1577	49	2M − 12P + 18J
Pallas	1540	49	2M + 2P − 18J
Bamberga	1258	164	6M − 14B
Pallas	1250	49	2M − 5P
Vesta	722	26	2M − 4V
Pallas	663	50	2M − 19P + 36J
Pallas	632	48	2M + 9P − 36J
Ceres	630	10	M − 2C
Iris	604	92	M − 2I
Pallas	558	119	2M − 3P − 5J
Pallas	540	492	M − 11P + 22J

5. CONCLUSION

The iterative process of integration of the equations will be continued for the model which we indicated at the introduction until reaching a precision of the solution of about one meter over 10 years.

The following step will consist in introducing the perturbations of Mars by the 180 asteroids

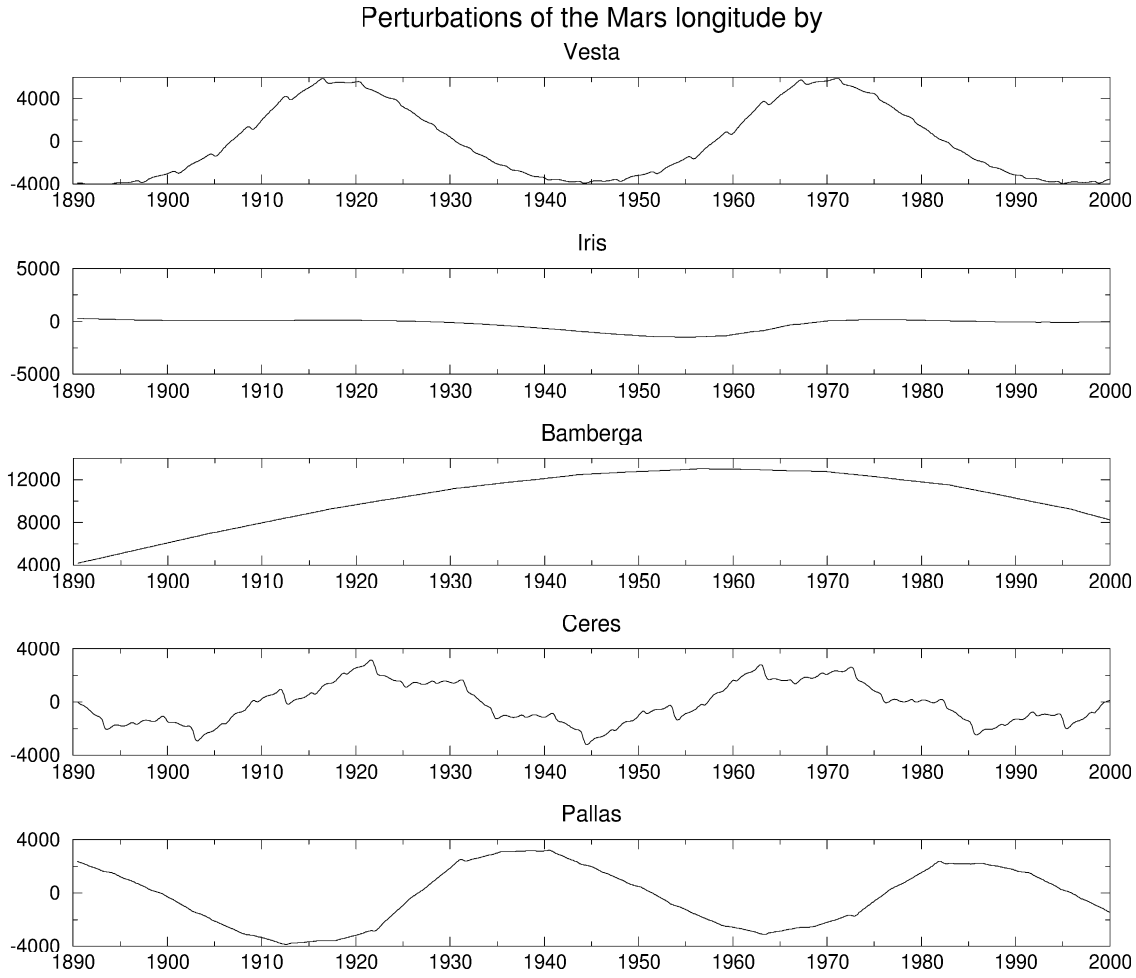

Fig. 4. Perturbations of Mars by the asteroids in meters over [1891-2000].

with a mass bigger than 10^{-12} solar mass. The precision of the solution will have to be about a few meters for the selected value of the masses but of course the accuracy of the solution could not be better than only a few hundred meters because of uncertainties on the mass of the asteroids. An internal precision about a few meters is however required to be certain that the difference between the observation and the analytical solution comes only from uncertainties on the mass of the asteroids.

Lastly, the integration constants will be determined by adjustment to the observations with the help of the methods developed by Fienga (1999).

6. REFERENCES

Bretagnon, P., 1982, *Astron. Astrophys.* 114, 278

Fienga, A., 1999, Thèse, Paris

Fienga, A., Standish, E. M., 2001, JPLIOM 312.F - 01 - 017

Krasinsky, G. A., Pitjeva, E. V., Vasilyev, M. V., Yagudina, E. I., 2001, Russian Academy of Sciences, Institute of Applied Astronomy, 139

Moisson, X., 2000, Thèse, Paris

Standish, E. M., 1998, JPLIOM 312.F - 98 - 048

Standish, E. M., Fienga, A., 1998, *Astron. Astrophys.* to be published

COMPACT REPRESENTATION OF SPHERICAL FUNCTIONS OF SUN/MOON COORDINATES BY FREQUENCY ANALYSIS

S.M. KUDRYAVTSEV
Sternberg Astronomical Institute of Moscow State University
13, Universitetsky Pr., Moscow, 119899, Russia
e-mail: ksm@sai.msu.ru

ABSTRACT. Spherical functions of celestial bodies coordinates are widely used in many topical applications of celestial mechanics and geodynamics, e.g. when studying the Earth rotation or physical libration of the Moon. This kind of functions also appears in expressions for effect of solid Earth tides and attraction of the third body (Sun/Moon) on satellite motion. Analytical methods of solving the above-mentioned tasks often need precise trigonometric series representing the values of spherical functions over a long-term interval. A way of getting the series is to numerically calculate the exact values of the functions over the interval with a small sampling step-size at first and then to perform a spectral analysis of the data. We employ and improve this approach by assuming the argument of the final series to be a high-degree polynomial of time as opposed to the classical Fourier analysis where the argument is a linear function. This leads to significant improvement in accuracy and compactness of the final series. We prove this by obtaining Poisson series precisely representing solid Earth tidal corrections to some geopotential coefficients which ensure the calculation of the latter to an accuracy of better than 3×10^{-12} over two thousands years.

1. INTRODUCTION

A number of important tasks of space dynamics and kinematics call for need of trigonometric series precisely representing spherical functions of coordinates of celestial bodies. For example, similar expansions are performed when developing analytical theories of the Earth rotation or physical libration of the Moon. These series are also required by precise analytical theories of satellite motion when calculating the satellite orbital perturbations due to the Sun/Moon attraction and expanding a perturbation function produced by solid Earth tides. The spherical functions of a perturbing body's coordinates are:

$$\left(\frac{R}{r}\right)^{n+1} P_{nm}\left(\sin\Phi\right) e^{-im\lambda} \tag{1}$$

where P_{nm} are associated Legendre functions of degree n and order m; r, Φ, and λ are distance to the body and its spherical latitude and longitude, respectively; $i \equiv \sqrt{-1}$; R is a constant.

One way to obtain the desired expansions is to take available trigonometric series for the Sun/Moon ecliptic coordinates and transform them to series for spherical functions (see, e.g. Kinoshita, 1977). For that one usually uses the accurate analytical theories of motion of the

Moon and planets by Eckert et al. (1954), Chapront-Touzé and Chapront (1983), Bretagnon and Francou (1988) as a source. However, in order to calculate precise values of spherical functions of the bodies' coordinates by means of those theories it is necessary to evaluate and transform a large number of terms of original analytical expressions. Last years such a bulky task is usually solved by employment of computer algebra tools or a Poisson processor (see, e.g. Emelianov, 1990). Nevertheless, the careful performance of all necessary steps is still a complex task. An important issue is the accuracy of the final results much depends on that of the initial analytical expressions for the Sun/Moon coordinates.

Another approach is to employ the most up-to-date numerical ephemerides of the Sun and Moon as the source. JPL planetary and lunar ephemerides DE 405/406 (Standish, 1998) can serve for this purpose now. Making use of those ephemerides we first calculate values of spherical functions of the bodies coordinates in a chosen reference frame at numerous epochs with a small sampling step-size over a long-term interval (several thousand years). Then a frequency analysis of such series is done. There are several technics for doing this. First, the classical fast Fourier transform (FFT) should be mentioned. However, it yields an enormous number of terms in the expansions because the frequencies of the resulting terms are often far apart from the real ones of the analyzed system. A more elegant way looks to define the real frequencies in advance and make the discrete Fourier transform just at them. As the extension of the latter approach Lascar (1990) has developed his NAFF method where the real (fundamental) frequencies are sought out in the analysis.

However, all the above-mentioned methods assume the argument of the resulting terms to be a linear function of time. This looks as a limitation of the approach as far as about all known fundamental frequencies of motion of the Moon, Sun and planets are high- degree time polynomials (like Delaunay variables, planetary and lunar mean longitudes). Thus in our work we propose to make the spectral analysis of the data by assuming just the polynomial form of the arguments in final expressions and suggest here an improved technique for calculating accurate amplitudes and phases of the series' terms. This approach leads to essential improvement in accuracy and compactness of the final series. The description of the technique and results obtained are presented in the following sections.

2. FOURIER ANALYSIS AT FREQUENCIES WITH NON-LINEAR ARGUMENT

Let us have a time-dependent function $f(t)$ sampled at numerous epochs within an interval $[-T, T]$. In the classical method of spectral analysis we assume $f(t) \approx \sum\limits_k a_k e^{i(\nu_k t + \varphi_k)}$ and look for amplitudes a_k and phases φ_k of the waves at frequencies ν_k. For that we find the projection of $f(t)$ on the space generated by functions $e^{i\nu_k t}$ by calculating a scalar product

$$I(\nu) \equiv < f, e^{i\nu t} > = \frac{1}{2T} \int_{-T}^{T} f(t) e^{-i\nu t} \left(1 + \cos\frac{\pi}{T} t\right) dt \tag{2}$$

where ν is consecutively taken equal to every ν_k and the Hanning window filter $1 + \cos\frac{\pi}{T}t$ is chosen as the weight.

If $f(t) \equiv a e^{i(\nu t + \varphi)}$, i.e. the function consists of just one wave at the frequency ν, then the analytical value $I_{an}(\nu)$ of the integral (2) is easily obtained:

$$I_{an}(\nu) = a e^{i\varphi}. \tag{3}$$

By using the known sampled values of $f(t)$ we can also calculate the complex value of the integral (2) numerically

$$I_{nu}(\nu) = A + iB. \tag{4}$$

Through equating (3) to (4) one finds both a and φ.

If the function $f(t)$ consists of two or more waves

$$f(t) \equiv a_1 e^{i(\nu_1 t+\varphi_1)} + a_2 e^{i(\nu_2 t+\varphi_2)} + \cdots + a_k e^{i(\nu_k t+\varphi_k)} \tag{5}$$

where $|a_1| \geq |a_2| \geq \cdots \geq |a_k|$ and the frequencies $\nu_1, \nu_2, \cdots, \nu_k$ are far apart then

$$I_{an}(\nu_1) = a_1 e^{i\varphi_1} + O\left(\frac{a_2}{(\nu_1-\nu_2)^3 T^3} + \cdots + \frac{a_k}{(\nu_1-\nu_k)^3 T^3}\right) \approx a_1 e^{i\varphi_1}, \tag{6}$$

so we are still able to rather accurately find the amplitude a_1 and phase φ_1 of the major term (Lascar et al., 1992).

Then the term $a_1 e^{i\varphi_1}$ is subtracted from the original $f(t)$ and the similar procedure is repeated to find the amplitudes and phases of other terms.

In order to make the spectral analysis of a sampled function f at a frequency with a non-linear argument $\omega(t) = \nu t + \nu_{(2)} t^2 + \nu_{(3)} t^3 + \cdots$ (where $\nu, \nu_{(2)}, \nu_{(3)}, \cdots$ are constants) one needs to find the projection of f on the function $\omega(t)$. This can be done by just substitution of the time polynomial $\omega(t)$ for the linear function νt in numerical calculation of the integral (2).

An alternative way is to take into account the non-linearity of the argument $\omega(t)$ when calculating the integral (2) analytically. At the same time the projection of f on the function $e^{i\nu t}$ is still calculated in numerical evaluation of the integral (2). Our tests prove the latter approach is more effective in the view of computation time.

Thus we assume $f(t) = a e^{i(\omega(t)+\varphi)}$ and need to find the amplitude a and phase φ at the frequency $\omega(t) = \nu t + \nu_{(2)} t^2 + \cdots + \nu_{(n)} t^n$ by using sampled values of f over the time interval $[-T, T]$. Here let us take $n = 4$ as this limit is set in the current expansions of Delaunay variables (Simon et al., 1996) which are widely used in further frequency analysis of spherical functions of Sun/Moon coordinates. In this case the analytical value of integral (2) is as follows

$$I_{an}\left(\nu, \nu_{(2)}, \nu_{(3)}, \nu_{(4)}\right) = \frac{a e^{i\varphi}}{2T} \int_{-T}^{T} e^{i\left(\nu_{(2)} t^2 + \nu_{(3)} t^3 + \nu_{(4)} t^4\right)} \left(1 + \cos\frac{\pi}{T} t\right)\, dt\,. \tag{7}$$

We evaluate (7) by expanding the exponent function to power series of t (the values of $\nu_{(2)}$, $\nu_{(3)}$, and $\nu_{(4)}$ in expansions of Delaunay variables and planetary/lunar mean longitudes are small but not negligible, so we had to perform the expansion up to the 12^{th} degree of time t inclusive).

As the result

$$I_{an}\left(\nu, \nu_{(2)}, \nu_{(3)}, \nu_{(4)}\right) = a e^{i\varphi}\left(1 + A^* + iB^*\right) \tag{8}$$

where

$$\begin{aligned} A^* = -\frac{1}{2}\nu_{(2)}^2 J_4 - \left(\nu_{(2)}\nu_{(4)} + \frac{1}{2}\nu_{(3)}^2\right) J_6 + \left(\frac{1}{24}\nu_{(2)}^4 - \frac{1}{2}\nu_{(4)}^2\right) J_8 + \\ \left(\frac{1}{6}\nu_{(2)}^3\nu_{(4)} + \frac{1}{4}\nu_{(2)}^2\nu_{(3)}^2\right) J_{10} + \\ \left(\frac{1}{2}\nu_{(2)}\nu_{(3)}^2\nu_{(4)} + \frac{1}{4}\nu_{(2)}^2\nu_{(4)}^2 + \frac{1}{24}\nu_{(3)}^4 - \frac{1}{720}\nu_{(2)}^6\right) J_{12}, \end{aligned} \tag{9}$$

$$\begin{aligned} B^* = \nu_{(2)} J_2 + \nu_{(4)} J_4 - \frac{1}{6}\nu_{(2)}^3 J_6 - \frac{1}{2}\left(\nu_{(2)}^2\nu_{(4)} + \nu_{(2)}\nu_{(3)}^2\right) J_8 - \\ \left(\frac{1}{2}\nu_{(2)}\nu_{(4)}^2 + \frac{1}{2}\nu_{(3)}^2\nu_{(4)} - \frac{1}{120}\nu_{(2)}^5\right) J_{10} + \\ \left(\frac{1}{12}\nu_{(2)}^3\nu_{(3)}^2 + \frac{1}{24}\nu_{(2)}^4\nu_{(4)} - \frac{1}{6}\nu_{(4)}^3\right) J_{12}, \end{aligned}$$

and

$$J_l \equiv \frac{1}{2T}\int_{-T}^{T} t^l \left(1+\cos\frac{\pi}{T}t\right)\,dt = T^l\left(\frac{1}{l+1}-\sum_{m=0}^{l-2} i^l \frac{l!}{(l-m-1)!\pi^{m+2}}\right) \tag{10}$$

where l and m are even ($J_l = 0$ if l is odd).

One sees the expression (8) differs from (3) by two additional summands A^* and iB^*, so by equating (8) to (4) we come to new values for the amplitude a and phase φ in the case of non-linear argument.

If now we assume the function f to be a Poisson series

$$f(t) = ae^{i(\omega(t)+\varphi)} + \dot{a}te^{i(\omega(t)+\varphi_1)} + \ddot{a}t^2e^{i(\omega(t)+\varphi_2)} + \cdots \tag{11}$$

the procedure of finding the coefficients a, φ, $\dot{a}$, φ_1, $\ddot{a}$, φ_2 can be as follows. (For clarity of presentation let us hereafter restrict the Poisson series up to the terms proportional to t^2; a similar procedure can be applied to find the coefficients of terms of higher degrees, if necessary).

First, we tabulate the function f over three time intervals of the length $[-T,T]$ each, and let $\Delta T'$ and $\Delta T''$ be the differences between the central epochs of the first and second intervals and of the first and third intervals, respectively. Then we calculate both analytically and numerically the value of the integral (2) at all three intervals where take into account the shifts in ν, $\nu_{(2)}$, $\nu_{(3)}$ due to the differences $\Delta T'$, $\Delta T''$ and get eventually to the following equations

- at the first time interval:

$$a_0\left[(1+A_0^*+iB_0^*)+\frac{a_1}{a_0}(A_1^*+iB_1^*)+\frac{a_2}{a_0}(J_2+A_2^*+iB_2^*)\right] = A+iB \tag{12}$$

where $a_0 \equiv ae^{i\varphi}$, $a_1 \equiv \dot{a}e^{i\varphi_1}$, $a_2 \equiv \ddot{a}e^{i\varphi_2}$, and $A_m^*+iB_m^*$ are originated by the non-linear part of the argument $\omega(t)$ of the m-degree Poisson term in (11). A_0^*, B_0^* are calculated according to (9),

$$A_1^* = -\nu_{(2)}\nu_{(3)}J_6 - \nu_{(3)}\nu_{(4)}J_8 + \frac{1}{6}\nu_{(2)}^3\nu_{(3)}J_{10} + \left(\frac{1}{2}\nu_{(2)}^2\nu_{(3)}\nu_{(4)} + \frac{1}{6}\nu_{(2)}\nu_{(3)}^3\right)J_{12},$$

$$B_1^* = \nu_{(3)}J_4 - \frac{1}{2}\nu_{(2)}^2\nu_{(3)}J_8 - \left(\nu_{(2)}\nu_{(3)}\nu_{(4)} + \frac{1}{6}\nu_{(3)}^3\right)J_{10} + \left(\frac{1}{24}\nu_{(2)}^4\nu_{(3)} - \frac{1}{2}\nu_{(3)}\nu_{(4)}^2\right)J_{12}, \tag{13}$$

$$A_2^* = -\frac{1}{2}\nu_{(2)}^2J_6 - \left(\nu_{(2)}\nu_{(4)} + \frac{1}{2}\nu_{(3)}^2\right)J_8 + \left(\frac{1}{24}\nu_{(2)}^4 - \frac{1}{2}\nu_{(4)}^2\right)J_{10} + \left(\frac{1}{4}\nu_{(2)}^2\nu_{(3)}^2 + \frac{1}{6}\nu_{(2)}^3\nu_{(4)}\right)J_{12},$$

$$B_2^* = \nu_{(2)}J_4 + \nu_{(4)}J_6 - \frac{1}{6}\nu_{(2)}^3J_8 - \frac{1}{2}\left(\nu_{(2)}\nu_{(3)}^2 + \nu_{(2)}^2\nu_{(4)}\right)J_{10} + \left(\frac{1}{120}\nu_{(2)}^5 - \frac{1}{2}\nu_{(2)}\nu_{(4)}^2 - \frac{1}{2}\nu_{(3)}^2\nu_{(4)}\right)J_{12};$$

- at the second time interval:

$$a_0'e^{i\Delta'}\left[\left(1+A_0'^*+iB_0'^*\right)+\frac{a_1'}{a_0'}\left(A_1'^*+iB_1'^*\right)+\frac{a_2'}{a_0'}\left(J_2+A_2'^*+iB_2'^*\right)\right] = A'+iB' \tag{14}$$

where $a_0' \equiv ae^{i\varphi} + \dot{a}e^{i\varphi_1}\Delta T' + \ddot{a}e^{i\varphi_2}(\Delta T')^2$, $a_1' \equiv \dot{a}e^{i\varphi_1} + 2\ddot{a}e^{i\varphi_2}\Delta T'$, $a_2' = a_2$; $A_0'^*$, $B_0'^*$, $A_1'^*$, $B_1'^*$, $A_2'^*$, $B_2'^*$ are calculated according to (9) and (13) with use of shifted values for $\nu_{(2)}$ and $\nu_{(3)}$ for the epochs difference $\Delta T'$; Δ' is the change in the phase φ caused by the shift in ν, $\nu_{(2)}$, $\nu_{(3)}$ for $\Delta T'$;

- at the third time interval:

  an equation similar to (14) is obtained; one has just to substitute the epochs difference $\Delta T''$ for $\Delta T'$ there.

The derived system of the three equations can be solved iteratively. Assuming $|\dot{a}| \ll |a|$ and $|\ddot{a}| \ll |a|$ at the first iteration we can neglect the second and third summands in the square brackets in the left-hand side of equations (12), (14) (and the other one built at the third interval). Thus initial approximations of complex values for a_0, a'_0, and a''_0 (the analog of a'_0 obtained at the third interval) can be found, and parameters a, φ, $\dot{a}$, φ_1, $\ddot{a}$, φ_2 derived from them. At the second iteration we employ the latter parameters in calculating improved values for the left-hand side of the equations and repeat the process till convergence of the results.

The algorithm has been employed for representing the solid Earth tidal corrections to some geopotential coefficients by accurate Poisson series. (The original expressions for calculating the effect of solid Earth tides include spherical functions of Sun/Moon instant coordinates.)

3. EXPANSION OF SOLID EARTH TIDES EFFECT TO POISSON SERIES

The IERS Conventions (McCarthy, 1996) express the effect of solid Earth tides on the geopotential through variations in normalized gravity coefficients $\Delta\bar{C}^{ST}_{nm}$, $\Delta\bar{S}^{ST}_{nm}$ of degree n, order m

$$\Delta\bar{C}^{ST}_{nm} - i\Delta\bar{S}^{ST}_{nm} = \frac{k_{nm}}{2n+1}\sum_{j=2}^{3}\frac{\mu_j}{\mu_E}\left(\frac{R_E}{r_j}\right)^{n+1}\bar{P}_{nm}\left(\sin\Phi_j\right)e^{-im\lambda_j} \qquad (15)$$

where k_{nm} are complex Love numbers; R_E, μ_E are the Earth's equatorial radius and gravitational parameter; μ_j, r_j, Φ_j and λ_j are respectively the gravitational parameter, geocentric distance, latitude and longitude (from Greenwich) of the Moon ($j = 2$) and Sun ($j = 3$) at epoch; $\bar{P}_{nm}$ are the normalized associated Legendre functions. We shall calculate the corrections by substituting to (15) the body right ascension α_j for the longitude λ_j . The expressions for solid Earth tidal corrections changed in such a way are simpler for use in analytical theories of satellite motion and, if necessary can be easily transformed to the original ones through multiplication by e^{imW} where W is Greenwich true sidereal time (which to sufficient accuracy can be approximated by Greenwich mean sidereal time here).

By using JPL ephemerides DE/LE 406 we calculated numerical values for solid Earth tidal corrections to several gravity coefficients: $\Delta\bar{C}^{ST}_{20}$, $\Delta\bar{C}^{ST}_{21}$, and $\Delta\bar{C}^{ST}_{22}$, over three time intervals: [3000BC, 1000BC], [1000BC, 1000AD], [1000AD, 3000AD] with a sampling step-size of one day. Then the following approximation of the data by Poisson series has been done

$$\Delta\bar{C}^{ST}_{nm} = \sum_k \left[A_k\cos\left(\omega_k(t)+\varphi_k\right) + A'_k t\cos\left(\omega_k(t)+\varphi'_k\right) + A''_k t^2\cos\left(\omega_k(t)+\varphi''_k\right)\right] \qquad (16)$$

where the arguments $\omega_k(t)$ are combination of multipliers of Delaunay variables, lunar and planetary longitudes (Simon et al., 1996). In our study they are polynomials of the fourth degree of time.

We get expansions on functions $\cos\omega_k(t)$ in order to have real values of the desired corrections. It is easy to show that terms of the cosine-series expansions can be derived from the relevant terms of the exponent-series expansions by halving amplitudes of the latter, except the constant term which is taken unchanged. The error introduced by such a procedure is as small as the inverse cube of the product of the term main frequency and the length of the time interval (two thousands years in our case).

By employing the algorithm above described we come to compact representation of the corrections by Poisson series in the form (16). The main characteristics of the series are given in Table 1.

Table 1: MAJOR TERMS OF EXPANSIONS & THE TOTAL NUMBER OF TERMS

Correction	Multipliers of					Period	$A \times 10^9$	$A' \times 10^{12}$	$A'' \times 10^{15}$	The number
	l	l'	F	D	Ω	(days)				of terms, k
	0	0	0	0	0	-	4.201	1.41	3.5	
$\Delta\bar{C}_{20}^{ST}$	0	0	2	0	2	13.66	0.889	0.97	4.9	187
	1	0	0	0	0	27.55	0.469	0.16	1.1	
	0	0	2	0	2	13.66	2.551	1.38	12.3	
$\Delta\bar{C}_{21}^{ST}$	0	0	2	-2	2	182.62	1.187	0.64	1.7	178
	0	0	0	0	1	-6798.35	0.534	0.05	0.2	
	0	0	2	0	2	13.66	5.960	0.55	2.6	
$\Delta\bar{C}_{22}^{ST}$	0	0	2	-2	2	182.62	2.773	0.28	1.6	226
	1	0	2	0	2	9.13	1.141	0.11	7.7	

The last column of Table 1 indicates the number of terms k included to the final expansions (16) which ensures calculation of the solid Earth tidal corrections to the normalized gravity coefficients with the maximal error of less than 3×10^{-12}. (Such level of accuracy is recommended by the IERS Conventions (McCarthy, 1996) for calculating the ocean tidal corrections to the gravity coefficients.) The archived accuracy is valid over the time interval of two thousands years lenght, [1000AD, 3000AD].

We could not reach such a result by using the classical spectral analysis method or NAFF.

4. ACKNOWLEDGEMENT

The work was supported in part by the Russian Foundation for Basic Research.

5. REFERENCES

Bretagnon, P. and Francou, G. (1988) Planetary theories in rectangular and spherical variables. VSOP87 solution, *Astron. Astrophys.*, **202**, 309-315.

Chapront-Touzé, M. and Chapront, J. (1983) The lunar ephemeris ELP 2000, *Astron. Astrophys.*, **124**, 50-62.

Eckert, W.J. et al. (1954) Construction of the Lunar ephemeris. Improved Lunar ephemeris 1952-1959, US Gov. Printing Office, Washington DC, 283-363.

Emelianov, N.V. (1990) A method of expansion of coordinates of the perturbing body in studies about satellite motion, the Earth and Moon rotation, *Kinematics and physics of celestial bodies*, **6**, 68-73 (in Russian).

Kinoshita, H. (1977) Theory of rotation of the rigid Earth, *Celest. Mech.*, **15**, 277-326.

Lascar, J. (1990) The chaotic behaviour of the Solar system: a numerical estimate of the size of the chaotic zones, *Icarus*, **88**, 266-291.

Lascar, J. et al. (1992) The measure of chaos by the numerical analysis of the fundamental frequencies. Application to standard mapping, *Physica D*, **56**, 253-269.

McCarthy, D.D., ed. (1996) IERS Conventions (1996), *IERS Technical Note 21*, Observatoire de Paris.

Simon, J.L. et al. (1996) Numerical expressions for the precession formulae and mean elements for the Moon and the planets, *Astron. Astrophys.*, **282**, 663-683.

Standish, E.M. (1998) JPL Planetary and Lunar Ephemerides, DE405/LE405, *JPL IOM 312.F-98-048*, Pasadena.

INFLUENCE OF THE TRIAXIALITY OF THE NON-RIGID EARTH ON THE J_2 FORCED NUTATIONS

A. ESCAPA[1], J. GETINO[2], J. M. FERRÁNDIZ[1]
[1] Dpto. Análisis Matemático y Matemática Aplicada
Universidad de Alicante. E-03080 Alicante. Spain
e-mail: Alberto.Escapa@ua.es; jm.ferrandiz@ua.es
[2] Grupo de Mecánica Celeste. Facultad de Ciencias
Universidad de Valladolid. E-47005 Valladolid. Spain
e-mail: getino@maf.uva.es

ABSTRACT. This note deals with the effects of the triaxiality of a two-layer Earth model on the nutations caused by the zonal harmonic of the second degree J_2. In particular, applying a Hamiltonian formalism, we calculate the analytical expressions of the forced nutations when considering the triaxiality in the kinetic energy of the model. The most relevant fact is the appareance of semidiurnal nutations. We evaluate their amplitudes, discussing their dependence as a function of the triaxiality of the fluid core.

1. INTRODUCTION

Usually, Hamiltonian studies of the rotation of the rigid and non-rigid Earth (for example, Souchay *et al.*, 1999; Getino, Ferrándiz and Escapa, 2001) include the triaxiality of the Earth solely by incorporating the non-zonal harmonics in the geopotential expansion. These terms give rise to the so-called short period nutations (diurnal and subdiurnal), which reach amplitudes at the level of a few microarcseconds. This kind of influence is called direct effect of the triaxiality (Escapa, Getino and Ferrándiz, 2001). However, the triaxiality of the Earth also modifies the kinetic energy of the system and, therefore, changes the analytical expression of the unperturbed, or zero order, Hamiltonian. So, when performing a canonical perturbation method, which depends on the differential equations generated by the unperturbed Hamiltonian, all the terms of the geopotential (zonal and non-zonal terms) are indirectly affected by the triaxiality. This effect is called indirect effect of the triaxiality.

In the case of the Hamiltonian theory for the rigid Earth, the indirect effect has been worked out by Escapa, Getino and Ferrándiz (2001) by expressing the potential energy in terms of the action-angle variables of the system. Here, we study the influence of this effect when considering a two-layer Earth model. In this way, we complete a set of works (González and Getino, 1997; Getino, González and Escapa, 2000; Getino, Ferrándiz and Escapa, 2001) in which the triaxiality of the non-rigid Earth is investigated by means of a Hamiltonian approach. As far we know, this is the only approach dealing with the two kinds of effects of the triaxiality (direct and indirect) of the non-rigid Earth.

2. HAMILTONIAN FOR THE PROBLEM

In this note, we will consider an Earth model composed by two layers: a non-symmetrical rigid mantle which encloses a fluid core. Both layers share a common barycenter. The kinetic energy of the system is given (González and Getino, 1997) by

$$2T = (\mathbf{L} - \mathbf{L}_c)^t \mathbf{\Pi}_m^{-1} (\mathbf{L} - \mathbf{L}_c) + \mathbf{L}_c \mathbf{\Pi}_c^{-1} \mathbf{L}_c. \tag{1}$$

$\mathbf{L}$ is the total angular momentum of the Earth, $\mathbf{L_c}$ is the angular momentum of the fluid core. In the principal frame of the mantle the inertia tensors of the mantle and of the core have the expressions

$$\mathbf{\Pi}_m = \begin{pmatrix} A - A_c & 0 & 0 \\ 0 & B - B_c & 0 \\ 0 & 0 & C - C_c \end{pmatrix}, \mathbf{\Pi}_c = \begin{pmatrix} A_c & 0 & 0 \\ 0 & A_c & 0 \\ 0 & 0 & C_c \end{pmatrix}, \tag{2}$$

being A, B and C the principal moments of inertia of the Earth and A_c, B_c and C_c the principal moments of inertia of the fluid core. To facilitate the computations, it is useful to introduce the adimensional parameters

$$e = \frac{C - A}{A},\ e_c = \frac{C_c - A_c}{A_c},\ d = \frac{1}{2}\left(1 - \frac{A}{B}\right),\ d_c = \frac{1}{2}\left(1 - \frac{A_c}{B_c}\right),\ r_{cm} = \frac{A_c}{A_m}. \tag{3}$$

e and e_c are the dynamical ellipticities of the Earth and of the core; d and d_c are related with the triaxiality of the model. From now on, we call them triaxiality parameters. It is worthy to note that for a symmetrical model the equatorial moments of inertia of the layer are equal and, therefore, the triaxiality parameters are equal to 0. In the case of the Earth, e, e_c, d and d_c are small quantities, hence, in the calculations we only retain first order terms with respect to these parameters. So, the kinetic energy of the model can be written as

$$T = T_s + \Delta_{Tr} T, \tag{4}$$

being T_s the kinetic energy corresponding to the symmetrical case and $\Delta_{Tr}T$ the contribution due to the triaxiality of the model, which, accordingly to the previous comments, will be proportional to d and d_c. This splitting of the kinetic energy will help us to isolate the influence of the non-symmetry on the nutational motion of the model.

Next, to construct a Hamiltonian theory, it is necessary to express the kinetic energy as a function of a canonical set. With this aim, we employ the canonical variables of Andoyer: M, N, Λ, M_c, N_c, Λ_c, μ, ν, λ, μ_c, ν_c, λ_c, (Getino, 1995). In terms of this set, the components of the angular momenta in the mantle frame are written as

$$\mathbf{L} = (M \sin\sigma \sin\nu, M \sin\sigma \cos\nu, N)^t,\ \mathbf{L}_c = (M_c \sin\sigma_c \sin\nu_c, -M_c \sin\sigma_c \cos\nu_c, N_c)^t, \tag{5}$$

with $N = M\cos\sigma$, $N_c = M_c \cos\sigma_c$. Hence, the kinetic energy is a function of the canonical set of the form

$$T = T_s(M, M_c, N, N_c, \nu, \nu_c) + \Delta_{Tr} T(M, M_c, N, N_c, \nu, \nu_c). \tag{6}$$

With regard to the potential energy of the system, arising from the gravitational interaction with the Moon and the Sun, let us remember that its analytical expresion is given by a sum of spherical harmonics (Kinoshita, 1977), known as geopotential expansion. In this expansion there are two kinds of terms: the zonal terms and the non-zonal terms. The last ones arise when the perturbed body is non-symmetrical. In this way, the potential energy of the system can also be written as

$$V = V_s\,(M, N, \Lambda, \mu, \lambda) + \Delta_{Tr} V\,(M, N, \Lambda, \mu, \nu, \lambda)\,. \tag{7}$$

The explicit expression of the different parts of the geopotential in terms of the Andoyer canonical variables is worked out in detail in Kinoshita (1977).

From eqs.(6) y (7), it is possible to construct the Hamiltonian of the system. It turns out to be

$$H = T(M, M_c, N, N_c, \nu, \nu_c) + V\,(M, N, \Lambda, \mu, \lambda)\,. \tag{8}$$

Strictly speaking, we should add to this expression a term due to the movement of the ecliptic. Anyway, this term only affects, at the first order, the preccesional motion. Because in this work we are focused on the nutational motion, we can disregard it without harm.

3. FIRST ORDER INTEGRATION

To solve analitically the equations of motion generated by the Hamiltonian H, we take advantage of the Horis's canonical perturbation method (Hori, 1966). To this end, we decompose the Hamiltonian as a sum of the form

$$H = H_0 + H_1 + ..., \text{ with } H_0 = T_s + \Delta_{Tr}T,\ H_1 = (V_2)_s + \Delta_{Tr}\,(V_2)\,. \tag{9}$$

V_2 is the second degree part of the geopotential. It gives the main contribution to the potential energy of the system. The former decomposition verifies that the zero order part of the Hamiltonian is biggest than the first order part. We can achive a more simplified form by considering that, in this work, we are investigating the influence of the triaxiality part of the kinetic energy on the nutations. Since, the triaxiality of the Earth is small, the combined effect of the triaxiality of the Earth on the kinetic energy, $\Delta_{Tr}T$, and on the potential energy, $\Delta_{Tr}\,(V_2)$, will be very small. Due to this fact, we will neglect the term $\Delta_{Tr}\,(V_2)$ in H_1.

The first step to apply the Hori's method is to find a solution of the differential equations generated by H_0. This one turns out to be

$$M = c_1,\ \Lambda = c_2,\ \lambda = c_3,\ M_c = c_4,\ \Lambda_c = c_5,\ \lambda_c = c_6, \tag{10}$$

where c_i are integration constants. The remaining solutions are derived with the help of the system

$$\frac{d}{dt}\begin{pmatrix} iM\sin\sigma e^{-i\nu} \\ -iM_c\sin\sigma_c e^{i\nu_c} \\ -iM\sin\sigma e^{i\nu} \\ iM_c\sin\sigma_c e^{-i\nu_c} \end{pmatrix} = i\Omega\mathbf{J}\begin{pmatrix} iM\sin\sigma e^{-i\nu} \\ -iM_c\sin\sigma_c e^{i\nu_c} \\ -iM\sin\sigma e^{i\nu} \\ iM_c\sin\sigma_c e^{-i\nu_c} \end{pmatrix}. \tag{11}$$

being $\mathbf{J} = (\mathbf{J})_s + \Delta_{Tr}\,(\mathbf{J})$. The first part of this matrix is the same as the obtained for the symmetrical case. The last one is due to the triaxiality of the model. The eigenvalues of $\mathbf{J}$ are given, at first order in e, e_c, d and d_c, by

$$m_1 = (1 + r_{cm})\sqrt{e^2 - 2ed},\ m_2 = -\left[1 + (1 + r_{cm})\,(e_c - d_c)\right],\ -m_1,\ -m_2. \tag{12}$$

$\pm m_1$ are related with the Chandler wobble, whereas $\pm m_2$ are related with the Free Core Nutation. It is worthy to note that the triaxiality modifies the analitycal expressions of both modes with respect to the symmetrical case. Eqs.(12) are equivalent to those ones obtained by González and Getino (1997).

Once we have found the solutions of the zero order part, the analytical expressions of the periodic part of the motion (forced nutations) are computed through the generating function, W. In our case, it is given by

$$W = \int H_{1\,per}\,dt = \int (V_2)_{s\,per}\,dt, \tag{13}$$

where the subscript *per* notes the periodic part. For our purposes, this term can be described properly by the expression (Getino and Ferrándiz, 2001)

$$(V_2)_{s\,per} = k' \sum_{i \neq 0} B_i \cos \Theta_i - k' \sin \sigma \sum_{i,\tau=\pm 1} C_i(\tau) \cos(\mu - \tau \Theta_i) . \tag{14}$$

k' is a numerical constant depending on the perturbing body (the Moon or the Sun in this case). B_i y $C_i(\tau)$ are functions of I ($\Lambda = M \cos I$), and Θ_i depends on λ and on the Delaunay variables of the Sun and the Moon. A precise definition of these functions is given in Kinoshita (1977).

The computation of the integral (13) along the solutions (10) and (11) is involved. Anyway, by performing a procedure similar to the described in Getino and Ferrándiz (2001), we have obtained

$$\begin{aligned} W = W_1 + W_2 + W_3 + \ldots = k' \sum_{i \neq 0} \frac{B_i}{n_i} \cos \Theta_i - k' \sin \sigma \sum_{i,\tau=\pm 1} C_i(\tau) R_{11} \cos(\mu - \tau \Theta_i) + \\ + k' \sin \sigma \sum_{i,\tau=\pm 1} C_i(\tau) R_{13} \cos(\mu + 2\nu - \tau \Theta_i) + \ldots . \end{aligned} \tag{15}$$

R_{ij} denotes the ij element of the matrix $[(\Omega - \tau n_i)\,\mathbf{1} + \Omega \mathbf{J}]^{-1}$, being Ω the mean angular velocity of the Earth and $n_i = d\Theta_i/dt$.

As it can be seen, the generating function is composed of three relevants parts: W_1, W_2 and W_3. With respect to the first part, let us point out that the expression of W_1 is not affected by the triaxiality of the model. Moreover, this term is exactly the same that the obtained in Getino (1995). It produces the so-called Poisson terms of the long-period nutations. The second part W_2 is slightly affected by the triaxiality through the matrix $\mathbf{J}$. Anyway, its functional dependence is the same as the corresponding part of the generating function of the symmetrical case (Getino, 1995). It gives rise to the Oppolzer terms of the long-period nutations. The third part, W_3, is completely new, and it is enterely due to the triaxiality of the model. We will show below that it gives rise to forced nutations of short period. We will focus our attention in this part of the generating function.

4. SEMIDIURNAL TERMS: NUMERICAL REPRESENTATION

Let us remember that the periodic variation, at the first order, of any function of the canonical variables is given by $\Delta f = \{f, W\}$, where $\{,\}$ denotes the Poisson bracket of the system. In particular, the longitude of the node, $-\epsilon_f$, and the obliquity, $-\psi_f$, of the plane perpendicular to the figure axis can be written in terms of the Andoyer variables (Kinoshita, 1977) as

$$\psi_f = -\lambda - \frac{\sigma}{\sin I} \sin \mu, \;\; \epsilon_f = -I - \sigma \cos \mu. \tag{16}$$

So, by computing the Poisson bracket of these equations with $W = W_3$ we can derive that

$$\begin{aligned} \Delta \epsilon_f &= -k \sum_{i,\tau} \{[C_i(\tau) R_{13} \cos g] \cos(2\phi - \tau \Theta_i) - [C_i(\tau) R_{13} \sin g] \sin(2\phi - \tau \Theta_i)\} , \\ \Delta \psi_f &= -\frac{k}{\sin I} \sum_{i,\tau} \{[C_i(\tau) R_{13} \cos g] \sin(2\phi - \tau \Theta_i) + [C_i(\tau) R_{13} \sin g] \cos(2\phi - \tau \Theta_i)\} . \end{aligned} \tag{17}$$

$\phi = \mu + \nu - g/2$ is the sidereal time, which is referred to the Greenwich meridian and $k'/M = k$. The explicit expression of R_{13} is given by

$$R_{13} = \frac{\Omega(1 + r_{cm}) \left[d_c r_{cm} (\tau n_i - \Omega)^2 - d(1 + r_{cm})(\tau n_i - 2\Omega) \tau n_i \right]}{(\Omega - \tau n_i - \Omega m_1)(\Omega - \tau n_i + \Omega m_1)(\Omega - \tau n_i - \Omega m_2)(\Omega - \tau n_i + \Omega m_2)} . \tag{18}$$

The nutations given by eq. (17) are short period nutations, or semidiurnal, because the argument 2ϕ-$\tau\Theta_i$ has a period of about a half of a sidereal day. Besides, it is interesting to note that, unlike the semidiurnal nutations coming from the non-zonal parts of the geopotential of the second degree (Getino, Ferrándiz and Escapa, 2001), the amplitude of the nutations presents a resonance when n_i is equal to the Free Core Nutation. That is to say, this effect is strongly dependent on the Earth model considered.

To evaluate numerically the amplitudes of the nutations we will employ the following values for the parameters appearing in (17): $k_{moon} = 7567.870647''$/Jcy, $k_{sun} = 3474.613746''$/Jcy, $CW = 400.7$ sidereal days, $FCN = 432.94$ sidereal days (Getino and Ferrándiz, 2001); $I = -.4090926298$, $\Omega = 230121.6483$ rd/Jcy (IERS, 1996); $g/2 = -.2605521212$ rd, $\bar{C}_{22} = 2.4386 \times 10^{-6}$, $\bar{S}_{22} = -1.400 \times 10^{-6}$ (Bretagnon *et al.*, 1997); $(\bar{C}_{22})_c = 2.400 \times 10^{-6}$, $(\bar{S}_{22})_c = -1.191 \times 10^{-6}$ (González and Getino, 1997); $A = 8.0115 \times 10^{37}\,\mathrm{kg{\cdot}m^2}$, $A_c = 9.1168 \times 10^{36}\,\mathrm{kg{\cdot}m^2}$, $M = 5.9732 \times 10^{24}\,\mathrm{kg}$, $M_c = 1.9395 \times 10^{24}\,\mathrm{kg}$ (PREM, taken from Mathews *et al.*, 1991). The moment of inertia B is obtained through the non-zonal harmonics of the second degree, by means of the relationship

$$B = A + 4Ma^2\sqrt{\frac{5}{12}}\sqrt{(\bar{C}_{22})^2 + (\bar{S}_{22})^2}. \tag{19}$$

An analagous expression is valid for the core. From these considerations we get that $d = 1.09856 \times 10^{-5}$, $d_c = 8.91125 \times 10^{-6}$, $m_1 = 2.4956 \times 10^{-3}$ and $m_2 = -1.002309789$.

By substituting the former numerical values in (17), we determine the amplitudes of the forced nutations due to the inclusion of the triaxiality in the kinetic energy. The results are presented below, where only the terms greater than .1 μas (microarcsecond) have been displayed.

Table I: Figure axis nutations (Unit=μas)

Period	Alias	Longitude				Obliquity			
(days)	(days)	sin		cos		sin		cos	
		IT	NZ	IT	NZ	IT	NZ	IT	NZ
.498634	∞	-5.304	35.944	3.044	-20.632	1.211	-8.207	2.110	-14.297
.498598	-6798.36	-.765	4.872	.439	-2.796	.175	-1.112	.304	-1.938
.500000	182.62	.585	-11.987	-.336	6.881	-.134	2.737	-.233	4.768
.517526	13.66	.333	-28.622	-.191	16.430	-.076	6.535	-.132	11.385
.498671	6798.36	.099	-.712	-.057	.408	-.023	.162	-.039	.283
.497955	-365.26	.215	.281	-.123	-.161	-.049	-.064	-.085	-.112

In Table I, IT notes the values obtained in this work, whereas NZ denotes the values obtained by Getino, Ferrándiz and Escapa (2001) when evaluating the semidiurnal nutations of a two-layer Earth model coming from the non-zonal harmonics of the second degree. As it can be seen, the amplitude of the obtained nutations obtained are small. Anyway, some of them reach a few microarcseconds. It is also important to note that, due to the resonance, for the argument alias -365.26 the value of the amplitude is of the same order of magnitude as the value corresponding to NZ.

Finally, it is interesting to evaluate the variation of the amplitudes with respect to d_c. Let us point out, that there is a great uncertainty in the value of this parameter (see, for example, Brzezinski and Capitane, 2001). With this aim, and as a qualitative example, we have recomputed the amplitudes for the values $d_c = a = 1.7823 \times 10^{-6}$, $d_c = b = 8.91125 \times 10^{-6}$ and $d_c = c = 4.4556 \times 10^{-5}$, assuming that the other parameters remain constant. In the next table, we show the amplitudes obtained for the sin component of the nutation in longitude of the figure axis.

Table II: Variation with d_c (Unit=μas)

Argument						Period	Longitude (sin)			Alias
ϕ	l_M	l_S	F	D	Ω	(days)	a	b	c	(days)
2	0	0	0	0	0	.498634	-1.061	-5.304	-26.519	∞
2	0	0	0	0	-1	.498598	-.151	-.765	-3.836	-6798.36
2	0	0	-2	2	-2	.500000	.167	.585	2.677	182.62
2	0	0	-2	0	-2	.517526	.237	.333	.813	13.66
2	0	0	0	0	1	.498671	.020	.099	.494	6798.36
2	0	-1	0	0	0	.497955	.032	.215	1.127	-365.26

As it can be checked in Table II, a variation in the value of d_c affects almost linearly to the nutation amplitudes, in this sense, it would be important to determine with greater accuracy the value of d_c. On the other hand, we can see that in the case c the amplitude of the argument alias -365.26 is much greater than the obtained one from NZ (Table I). This fact might provide some help to estimate d_c from observational data.

5. ACKNOWLEDGMENTS

This work has been supported by Spanish Projects AYA 2000-1787, AYA 2001-0787, PNE-015/2001-C and VA11/99 of the *Junta de Castilla y León.*

6. REFERENCES

Bretagnon, P., Rocher, P. and Simon, J. L., Theory of the rotation of the rigid Earth, *Astron. Astrophys.*, 319, 305-317, 1997

Brzezinski, A. and Capitaine, N., Lunisolar perturbations in Earth rotation due to the triaxial figure of the Earth: geophysical aspects, in *Abstracts of the Journées 2001*, p. 18, Royal Observatory of Belgium, Brussels, Belgium, 2001

Escapa, A., Getino, J. and Ferrándiz, J. M., Indirect effects of the triaxiality in the Hamiltonian theory for the rigid Earth nutations, submitted to *Astron. Astrophys.*, 2001

Getino, J.: Forced nutation of a rigid mantle-liquid core Earth model in canonical formulation, *Geophys. J. Int.*, 122, 803-814, 1995

Getino, J. and Ferrándiz, J. M., Forced nutations of a two layers Earth model, *Mon. Not. R. Astr.Soc.*, 322, 785-799, 2001

Getino, J., Ferrándiz, J. M. and Escapa, A., Hamiltonion Theory of the Non-rigid Earth: Semidiurnal Terms,*Astron. Astrophys.*, 370, 330-341, 2001.

Getino, J., González, A. B. and Escapa, A., The rotation of a Non–rigid, Non–symmetrical Earth II: Free nutations and dissipative effects, *Celest. Mech.*, 76, 1-21, 2000.

González, A. B. and Getino, J., The Rotation of a Non-rigid, Non-symmetrical Earth I: Free Nutations, *Celest. Mech.*, 68, 139-149, 1997.

Kinoshita, H., Theory of the rotation of the rigid Earth, *Celest. Mech.*, 15, 277-326, 1977.

Hori, G.,Theory of General Perturbations with Unspecified Canonical Variables, *Publ.Astron. Soc. Japan*, 18, 287-296, 1966

Mathews, P. M., B. A. Buffet, T. A. Herring, and I. I. Shapiro, Forced nutations of the Earth: Influence of inner core dynamics, 2, Numerical results and comparisons, *J. Geophys. Res.*, 96, 8243-8257, 1991

McCarty, D. D., IERS Conventions, *IERS Tech. Note 21*, 1996

Souchay, J., Losley, B., Kinoshita, H. and Folgueira, M., Corrections and new developments in rigid earth nutation theory, *Astron. Astrophys. Suppl. Ser.,* 135, 111-131, 1999

POSTFACE

JOURNÉES 2002 SYSTÈMES DE RÉFÉRENCE SPATIO-TEMPORELS
"Astrometry from ground and from space"

Scientific Organizing Committee :
N. Capitaine, France (Chair), A. Brzeziński, Poland, P. Defraigne, Belgium, J. Kovalevsky, France, M. Soffel, Germany, J. Vondrák, Czech R., Ya. Yatskiv, Ukraine

Local Organizing Committee :
V. Mioc, P. Popescu, M. Stavinschi (Chair)

Conference location : Institut français, 77 Boulevard Dacia, Bucharest

The Journées 2002 "Systèmes de référence spatio-temporels", with the sub-title "Astrometry from ground and from space ", will be held from 25 to 28 September 2002 in Bucharest, at Institut Français, organized jointly by the Astronomical Institute of the Romanian Academy and Paris Observatory. This reflects the long term tradition of cooperation between Romanian and French astronomers. These Journées will be the fourteen conferences in this series of which the purpose is to discuss the problems, from the concepts and realizations of space and time reference systems to the scientific interpretations of precise observations referred to these systems.

The problems to be discussed within Journées 2002 are related to the reference systems and also, more generally, to astrometry from ground and from space. These Journées will thus include, as usual, sessions related to space and time reference systems and Earth rotation and to space and ground-based astrometry. It will moreover include an open meeting of the IAU Division 1 Working Group "The Future Development of Ground-Based Astrometry" with a special round table to discuss the scientific programs that can still be successfully performed with ground-based instruments.

The programme of the Journées 2002 includes the five following sessions :

Session 1a : Kinematical and dynamical celestial reference systems

Session 1b : Celestial and terrestrial reference systems

Session 2 : Theory of Earth rotation

Session 3 : Space and ground-based astrometry

Session 4 : Time, time transfer and Earth rotation

For helping this meeting we are especially grateful to Service culturel de l'Ambassade de France en Roumanie, Minister of Education and Research, Observatoire de Paris, Astronomical Institute of the Romanian Academy.

Contact : Magda Stavinschi, Astronomical Institute of the Romanian Academy, Str.Cutitul de Argint 5, Bucharest, RO-75212, Romania, phone : +401 335 68 92, +401 335 80 10, fax : +401 337 33 89 ; e-amil: magda@aira.astro.ro

Or see : http://astro.ro/journees2002